UNIVERSITY OF SOUTHAMPTON

FACULTY OF NATURAL AND ENVIRONMENTAL SCIENCES

School of Chemistry

The Synthesis of Mechanically Planar Chiral Rotaxanes and their Application to Enantioselective Catalysis

by

Andrew W. Heard

Thesis for the degree of Doctor of Philosophy

February 2021

UNIVERSITY OF SOUTHAMPTON

ABSTRACT

FACULTY OF NATURAL AND ENVIRONMENTAL SCIENCE

Chemistry

Thesis for the degree of Doctor of Philosophy

The Synthesis of Mechanically Planar Chiral Rotaxanes and their Application to Enantioselective Catalysis

Andrew W. Heard

Mechanically interlocked molecules have been of interest to chemists since the 1960s. Recent synthetic advances have made the investigation of the mechanical bond more accessible, with most applications of interlocked molecules in molecular machines. The field of interlocked molecules was acknowledged by the Nobel committee in 2016, with the prestigeous prize being awarded to Sir J. Fraser Stoddart, Jean-Pierre Sauvage and Ben Feringa for their contribution to *"the design and synthesis of molecular machines"*.

This thesis discusses mechanical planar chirality, the challenging synthesis of interlocked molecules displaying this type of chirality, and the first application of this type of chirality in enantioselective catalysis. Finally this thesis presents a new, general approach to the synthesis of interlocked molecules displaying this type of chirality, allowing unprecedented access to enantiopure rotaxanes and a library of ligands for catalysis by application of this methodology.

Table of Contents

DECLARATION OF AUTHORSHIP

I, ANDREW HEARD

declare that this thesis and the work presented in it are my own and has been generated by me as the result of my own original research.

THE SYNTHESIS OF MECHANICALLY PLANAR CHIRAL ROTAXANES AND THEIR APPLICATION TO ENANTIOSELECTIVE CATALYSIS

I confirm that:

1. This work was done wholly or mainly while in candidature for a research degree at this University;
2. Where any part of this thesis has previously been submitted for a degree or any other qualification at this University or any other institution, this has been clearly stated;
3. Where I have consulted the published work of others, this is always clearly attributed;
4. Where I have quoted from the work of others, the source is always given. With the exception of such quotations, this thesis is entirely my own work;
5. I have acknowledged all main sources of help;
6. Where the thesis is based on work done by myself jointly with others, I have made clear exactly what was done by others and what I have contributed myself;
7. Parts of this work have been published as: "*Simplicity in the Design, Operation, and Applications of Mechanically Interlocked Molecular Machines*" A. W. Heard, S. M. Goldup, A*CS Cent. Sci.*, **2020**, *6*, 117-128; "*Synthesis of a Mechanically Planar Chiral Rotaxane Ligand for Enantioselective Catalysis*" A. W. Heard, S. M. Goldup, *Chem*, **2020**, *6*, 994-1006; "*A Chiral Interlocking Auxiliary Strategy for the Synthesis of Mechanically Planar Chiral Rotaxanes*" A. de Juan, D. Lozano, A. W. Heard, M. A. Jinks, J. Meijide Suarez, S. M. Goldup, *ChemRxiv*, doi: 10.26434/chemrxiv.13553996.v1

Signed: .....

Date: .....

Acknowledgements

I would like to thank past and present members of the Goldup group who helped guide my research throughout my PhD, and who provided a fun environment to work in. Thanks to Prof. Goldup for his excellent mentorship, for allowing me to travel to international conferences to present my work, and for providing a pressure free environment where his students are free to explore their own ideas.

Jack, ShuShuBaoBao, and Poom who started alongside me in 2017. Matt who regularly kept me full of croissants before the pandemic. Alberto and David, who provided a delightful, fun and knowledgeable Spanish sandwich to work between; and for tolerating me for three years. Peggy for indulging my absurd sense of humour and being a happy force in the lab. Andrea for his hilarious alternative abbreviations, most notably NMR. Arnau and Florian for being the best synthetic chemists I've worked alongside, I hope some of this has rubbed off on me. Neil, Julie and Graham for NMR, MS and crystallography assistance respectively. I would also like to thank Amanda, Ellen, Federica, Jorge, Lorenzo, Mathieu, Mike, Noel, and Peter.

I would like to thank my friends, family, and the great sea demon Sharktopus, for spiritual guidance.

Does this count Callum?

Definitions and Abbreviations

δ	Chemical Shift
AT-CuAAC	Active Template Copper Alkyne Azide Cycloaddition
BINAP	2,2′-bis(diphenylphosphino)-1,1′-binapthyl
BINOL	1,1′-bi-2-naphthol
CD	Circular Dichroism
CD_X	Cyclodextrin
CIP	Cahn-Ingold-Prelog
COSY	Correlation Spectroscopy
CSP-HPLC	Chiral Stationary Phase High-Performance Liquid Chromatography
DCE	1,2-dichloroethane
de	Diastereoisomeric Excess
DFT	Density Functional Theory
DMAP	4-(dimethylamino)pyridine
DMF	*N*,*N*′-Dimethylformamide
DMSO	Dimethylsulfoxide
dr	Diastereoisomeric Ratio
DTBM	3,5-di-*tert*-butyl-4-methoxyphenyl
ee	Enantiomeric Excess
EDC-HCl	*N*-(3-Dimethylaminopropyl)-*N*′-ethylcarbodiimide hydrochloride
EDTA	*N*,*N*,*N*′,*N*′-Ethylenediaminetetraacetate
EI	Electron Impact Ionisation
Eq.	Equivalents
er	Enantiomeric Ratio
ESI	Electrospray Ionisation
GCMS	Gas Chromatography Mass Spectrometry
h	hours
HMBC	Heteronuclear Multiple Bond Correlation
HOMO	Highest Occupied Molecular Orbital
HPLC	High-Performance Liquid Chromatography
HRMS	High Resolution Mass Spectrometry

HSQC	Heteronuclear Single Quantum Coherence
J	Coupling Constant
JMOD	J-Modulated Spin Echo
LCMS	Liquid Chromatography Mass Spectrometry
LRMS	Low Resolution Mass Spectrometry
LUMO	Lowest Unoccupied Molecular Orbital
MP	Melting point
MPC	Mechanically Planar Chirality
MTC	Mechanically Topologically Chiral
NHC	*N*-Heterocyclic Carbene
NMR	Nuclear Magnetic Resonance
NOESY	Nuclear Overhauser Effect Spectroscopy
PMB	4-methoxybenzyl
Quant.	Quantitative
R_{mp}	*R*-enantiomer (mechanically planar chiral)
rt	Room Temperature
SCXRD	Single Crystal X-Ray Diffraction
S_{mp}	*S*-enantiomer (mechanically planar chiral)
TBA	Tetrabutylammonium
TCA	Trichloroacetic acid
TFA	Trifluoroacetic acid
THF	Tetrahydrofuran
TLC	Thin Layer Chromatography
TMSA	Trimethylsilylacetylene
TOF	Time of Flight
UHPLC	Ultra-High-Performance Liquid Chromatography

Chapter 1: Introduction

Abstract: Mechanically interlocked molecules have been of interest to chemists since the 1960s. Recent synthetic advances have made the investigation of the mechanical bond more accessible, with most applications of interlocked molecules in molecular machines. The field of interlocked molecules was acknowledged by the Nobel committee in 2016, with the prestigeous prize being awarded to Sir J. Fraser Stoddart, Jean-Pierre Sauvage and Ben Feringa for their contribution to *"the design and synthesis of molecular machines"*. This chapter introduces the mechanical bond, and discusses the key synthetic advances making their synthesis more facile. It then details consequences of the mechanical bond, the interesting chirality it offers, and finally a brief overview of applications of the mechanical bond in materials chemistry and sensing.

Prior Publication: "*Simplicity in the Design, Operation, and Applications of Mechanically Interlocked Molecular Machines*" – A. W. Heard, S. M. Goldup, A*CS Cent. Sci.*, **2020**, *6*, 117-128.

1.1. Introduction to the Mechanical Bond

Mechanically interlocked molecules are those in which a macrocycle is trapped encircling another molecule due to steric constraints and the inability of covalent bonds to pass through each other (Figure 1).[1] A rotaxane is a molecule in which a macrocycle is trapped on a dumb-bell shaped axle, unable to dissociate due to the steric constraints of bulky stoppers. A catenane is a molecule with one macrocycle trapped encircling another macrocycle, akin to links in a chain.[1]

These interlocked molecules have progressed significantly in the last 60 years, from an intellectual curiosity and a synthetic challenge, to being a whole field of chemistry in their own right, with the 2016 Nobel Prize in Chemistry being awarded for "*the design and synthesis of molecular machines*".[2,3] Most applications of interlocked molecules are in molecular machines, where chemists have used the large amplitude conformational changes to achieve switchable properties, complex motion,[4] and to mediate complex synthesis.[5] Molecular machines are often inspired by natural processes, such as the synthesis of proteins by ribosomes, or catalysis achieved by enzymes. This chapter introduces mechanically bonded structures and the key advances in their syntheses. Then it will discuss examples of applications of the mechanical bond.

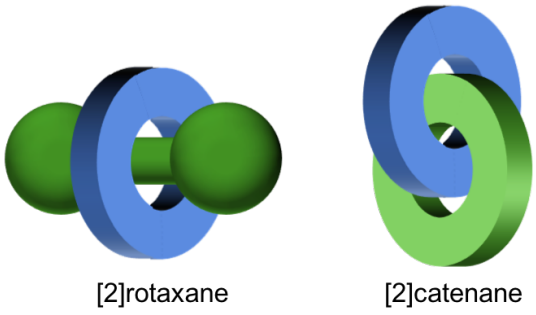

Figure 1: Schematic showing a [2]rotaxane and a [2]catenane.[1]

1.1.1. Advances in the Synthesis of Rotaxanes and Catenanes

In 1960, Wasserman published the first [2]catenane **4** (Figure 2), achieving approximately 1% yield during the cyclisation of **1** in the presence of 100 equivalents of **3**.[6–8] The statistical threading approach of Wasserman was the first system of a mechanically interlocked molecule. However, the low yields and purification difficulties made this discovery nothing more than an academic curiosity.[6] Yields were determined by the C-

D stretching frequency in the IR spectrum of the isolated product, which gave primarily **3** upon oxidative cleavage.[1]

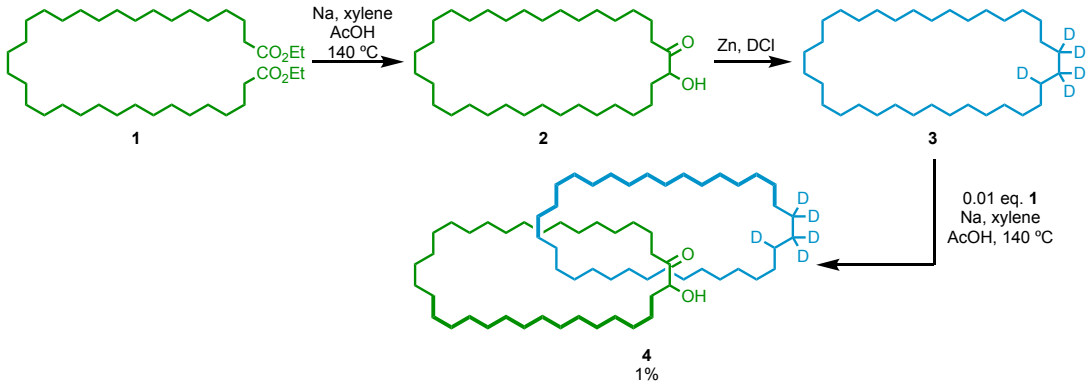

Figure 2: Wasserman's statistical synthesis of the first hetero[2]catenane **4**.[6] DCl refers to deuterated hydrochloric acid.

In 1967, Harrison and Harrison synthesised the first [2]rotaxane through repetitive (70 times) treatment of a resin-bound macrocycle **7**, with **8** and **9** (Figure 3).[9] They commented in the initial publication, that **11** was topologically trivial, and suggested the new class of compound be called a *'hooplane'*.[9] Fortunately Schill's terminology, the rotaxane, is now in common parlance (from *rotor* and *axle*). High concentrations and large macrocycles increase the probability of a threaded structure forming when using a statistical approach, provided the stoppering units are large enough.[1]

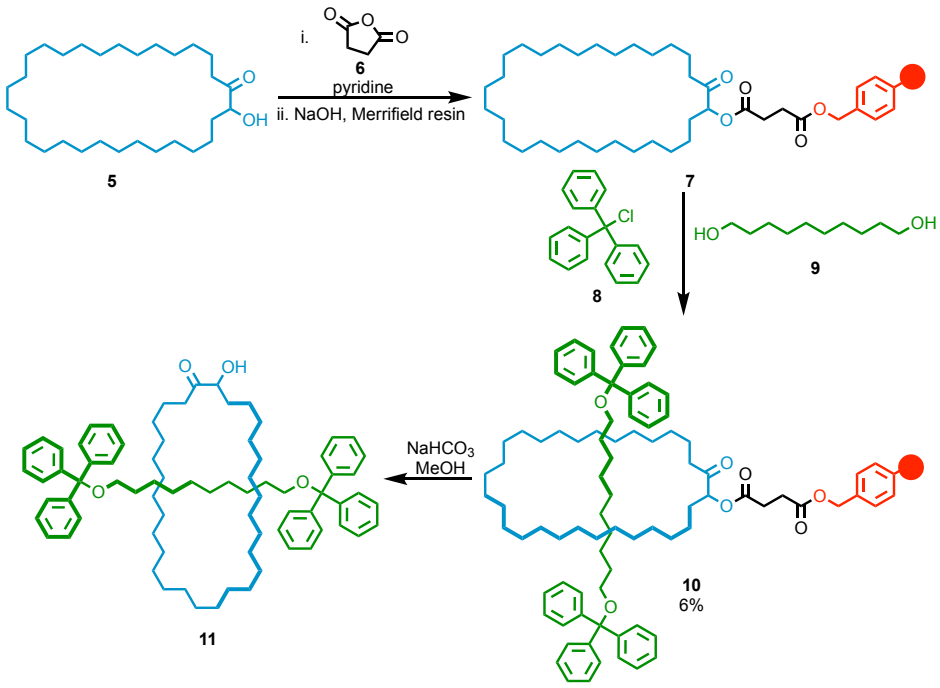

Figure 3: Harrison and Harrison's solid phase synthesis of [2]rotaxane **11**.[9]

In 1964, Lüttringhaus and Schill developed a covalent template approach to improve the synthetic accessibility of catenanes, achieving 5% yield over the longest linear sequence (Figure 4).[7,10,11] The *N*- and *C*-tethering centres increased the accessibility of catenanes significantly, through a rational synthetic approach. However this approach still required numerous synthetic modifications and harsh conditions. [10,11]

Schill synthesised many interlocked structures through this directed covalent templating approach, including [3]catenanes, [2]rotaxanes, and even attempted the synthesis of knotted structures;[10–12] however by this time metal-templated syntheses had surpassed this approach in efficiency and provided a simpler route to knotted structures.[7,8] During his studies, Schill found that if the macrocycle was shorter than 20-atoms in circumference, then the C_{aryl}-*N* bond could not be cleaved. This stability demonstrated the first potentially useful property resulting as a consequence of the mechanical bond.[10,11]

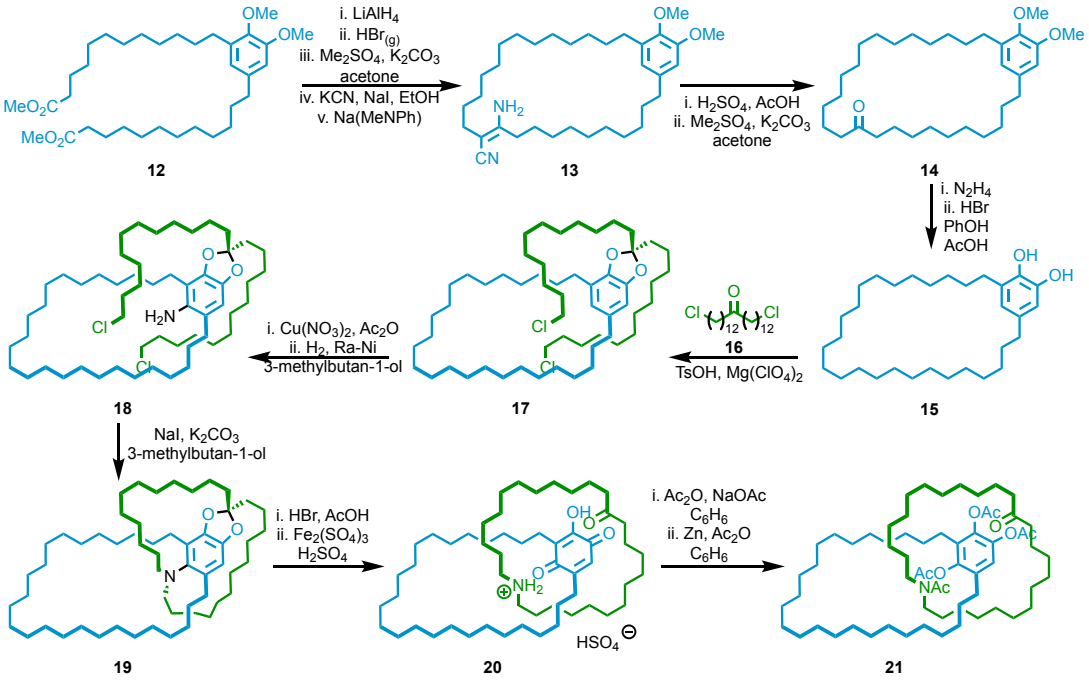

Figure 4: Lüttringhaus and Schill's covalent templated synthesis of hetero[2]catenane **21**.[10,11]

Although the covalent directed synthesis of interlocked molecules, pioneered by Schill, was surpassed in efficiency relatively quickly, the technique has been used since. In 2004, Hiratani and co-workers synthesised rotaxane **26** through this approach with moderate yields (Figure 5a),[13] and Kawai and co-workers utilised reversible imine formation to synthesise rotaxane **33** (Figure 5b).[14]

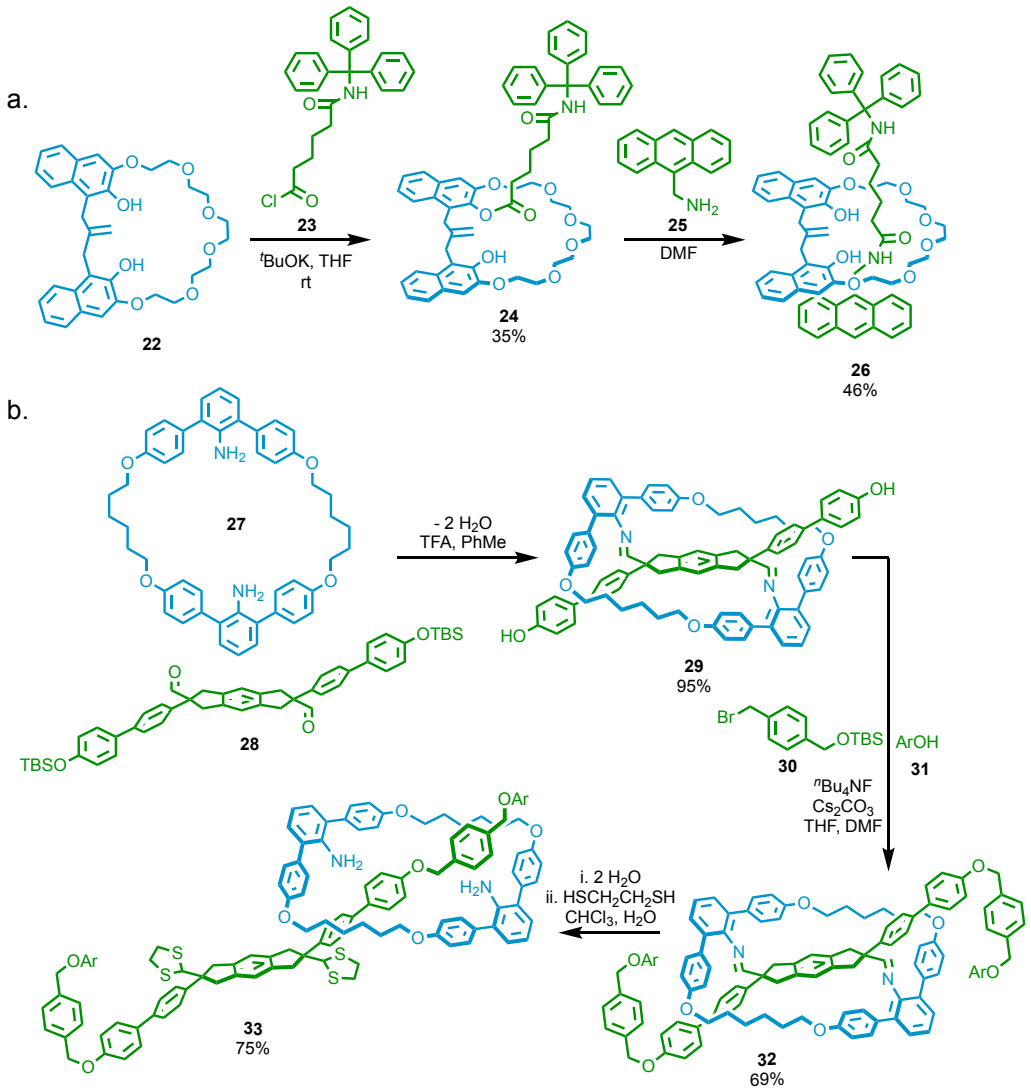

Figure 5: (a) Hiritani and co-workers' covalent directed [2]rotaxane **26** synthesis,[13] and (b) Kawai and co-workers' directed [2]rotaxane **33** synthesis.[14] Ar = $C_6H_4C(C_6H_4C_6H_4\text{-t-Bu})_3$.

Maarseveen and co-workers used a similar approach to synthesise spirocyclic *quasi*[1]catenanes, joined at a central fluorene carbon (Figure 6).[15] They demonstrate inverted spirocycles, with interlocking rings rather than typical fused spirocyclic bicycles. Topologically these are similar to Sauvage's revolutionary Cu^{I}-catenates.[16] Maarseveen and co-workers have used similar approaches to synthesise hetero[n]rotaxanes[17] and all-carbon-ring [2]rotaxanes.[18]

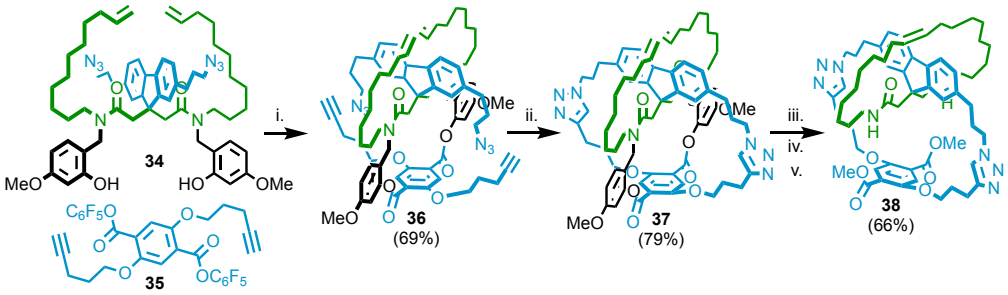

Figure 6: Maarseveen and co-workers' covalent directed synthesis of *quasi*[1]catenane **38**.[15] i. Cs_2CO_3, MeCN, 60 °C; ii. $[Cu(MeCN)_4]BF_4$, base, CH_2Cl_2; iii. Grubbs II, CH_2Cl_2 30 °C; iv. NaOMe, THF-MeOH; v. TFA, CH_2Cl_2, Et_3SiH.

Itami and co-workers used a similar covalent template technique to synthesise an all-benzene catenane **43** and a trefoil knot (Figure 7a).[19] This fully aromatic nanocarbon catenane had a ring diameter of 16.6 Å, and a dihedral angle of 15.9° between each benzene ring (Figure 7b).[19] The use of tetrahedral Si template and cleavable *C-Si* bonds, removed the requirement of heteroatoms in the core structure, thus allowing a traceless synthesis of nanocarbon structures.[19]

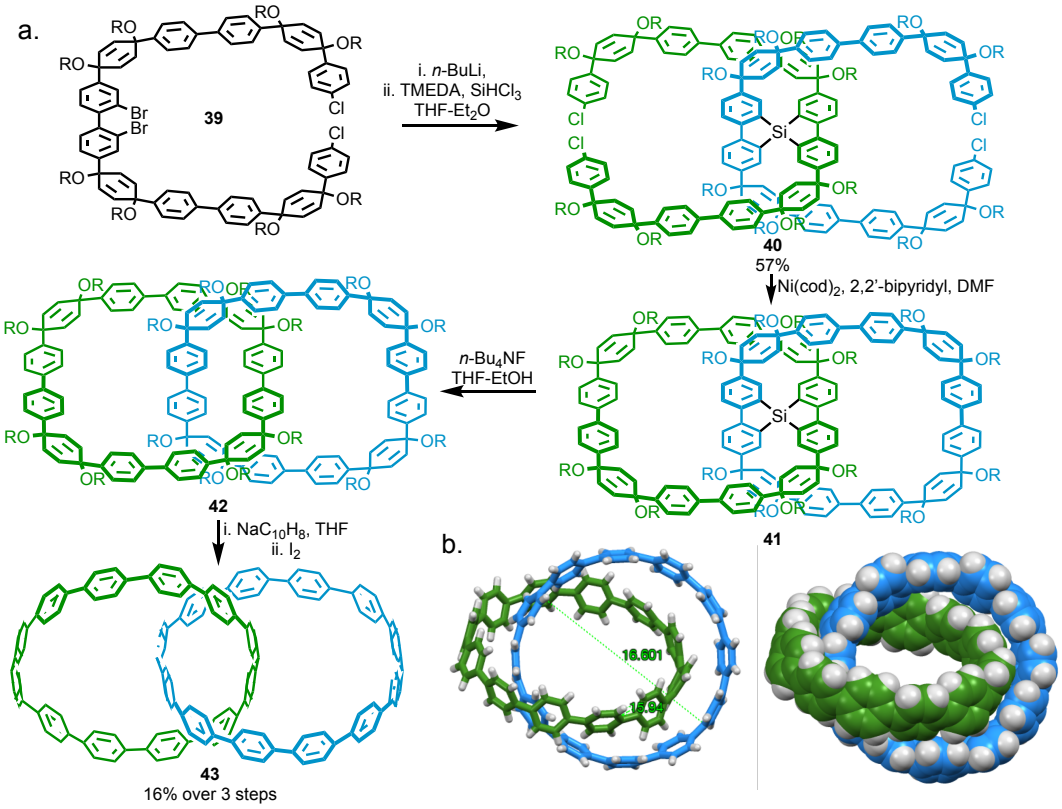

Figure 7: Itami and co-workers' (a) covalent templated all-benzene-ring [2]catenane **43** synthesis and (b) single crystal X-ray diffraction structure of **43** $C_{144}H_{96}$ (solvent molecules omitted for clarity).[19] R = *n*-Bu.

1.2. Passive Metal Template

A big leap forwards in the synthesis of interlocked molecules was achieved in 1983 by Sauvage and co-workers.[20,21] By coordinating two bidentate 2,9-diphenyl-1,10-

phenanthroline ligands around a tetrahedral Cu^{I}-ion (Figure 8), Sauvage and co-workers managed to synthesise interlocked [2]catenanes with relative ease and in much higher yields than achieved before.[20,21] The requirements for passive template synthesis of interlocked molecules, are that the intermediate **46** formation must be thermodynamically favourable and the templating interaction must be stable to the ring-closing methodology.[8,22] In the synthesis of rotaxanes, this approach can be realised by capping the axle-macrocycle complex, or clipping a macrocycle around an axle.

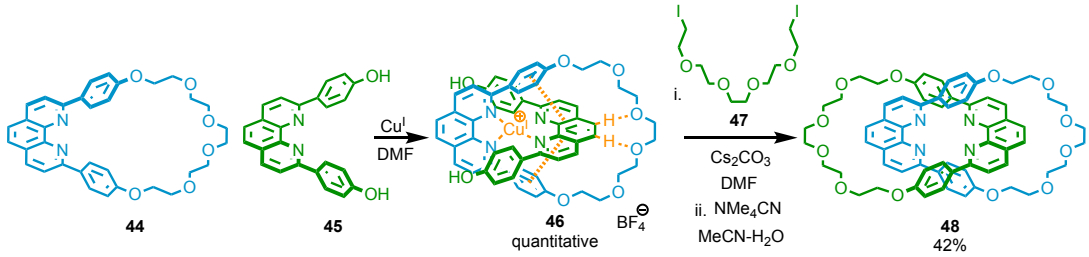

Figure 8: Sauvage and co-workers' first passive template synthesis of [2]catenane **48**.[20,21] Cu^{I} = $[Cu(MeCN)_4]BF_4$ Key secondary non-covalent interactions are shown in orange in **46**.

Besides the Cu^{I} template in **46**, secondary non-covalent interactions are also important for the passive template methodology.[23] Typically π-π stacking between the 4-alkoxyphenyl substituent of one ligand, and the 1,10-phenanthroline moiety of another ligand; and H-bonding between the polyethylene glycol ring and aromatic C-H bonds (Figure 8).[23] These secondary interactions increase the rigidity of the intermediate and increasing the efficiency of ring-closure.

Sauvage and co-workers achieved 90% yield of **50** with ring-closing alkene metathesis as the cyclisation step (Figure 9a).[24] These interlocked structures were made even more accessible by Leigh and co-workers, when they applied Sauvage's passive template technique to more general tridentate ligands **51**, with meridional coordination across a range of octahedral M^{II} ions (Figure 9b).[25] Leigh and co-workers' have also developed a linear Au^{I}-complex for passive template synthesis of catenane **54** (Figure 9c).[26]

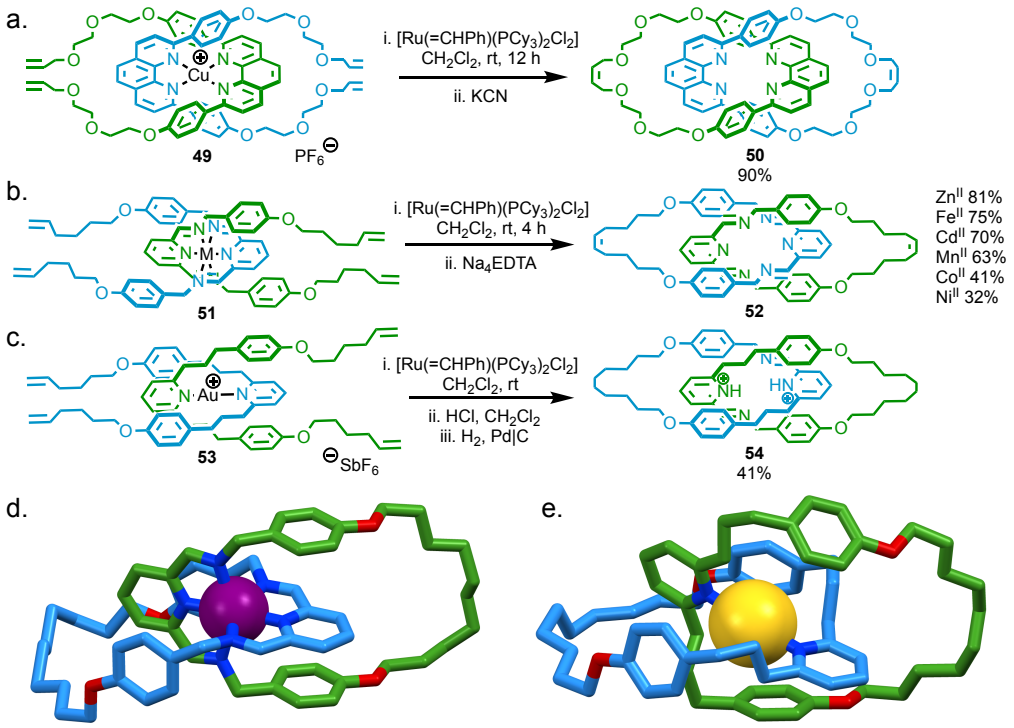

Figure 9: (a) Sauvage and co-workers' ring-closing metathesis synthesis of [2]catenane **50**,[24] (b) Leigh and co-workers' octahedral templated [2]catenane **52** synthesis,[25] and (c) Leigh and co-workers' linear Au(I) passive template synthesis of [2]catenane **54**.[26] Single crystal X-ray structures of (d) catenate **52**-Zn^{II} ($[C_{62}H_{72}N_6O_4Zn](ClO_4)_2$) and (e) catenate **54**-Au^{I} ($[C_{64}H_{82}N_4O_4Au](SbF_6)$). Counter ions and solvent molecules omitted for clarity.

Sauvage's passive template synthesis of rotaxanes could be achieved by capping (Figure 10a) or clipping (Figure 10b) an intermediate complex. However, these approaches had several limiting requirements.[20,21,23] Primarily, the passive template relies of the formation of a thermodynamically favourable pre-organised intermediate **III**, prior to the mechanical-bond forming step of capping the axle or clipping the macrocycle. The less favourable the pre-organised intermediate, the lower the yield of interlocked compound **IV**, due to the similar rate of capping the free axle **II** (Figure 10). Other limitations of the passive template include: the requirement of stoichiometric metal-ions to form the intermediate complex, requirement of two recognition sites, and a template that is stable to the ring closing methodology. Furthermore, secondary interactions are required to rigidify the complex making the interlocked molecule preferable to linear oligomers.

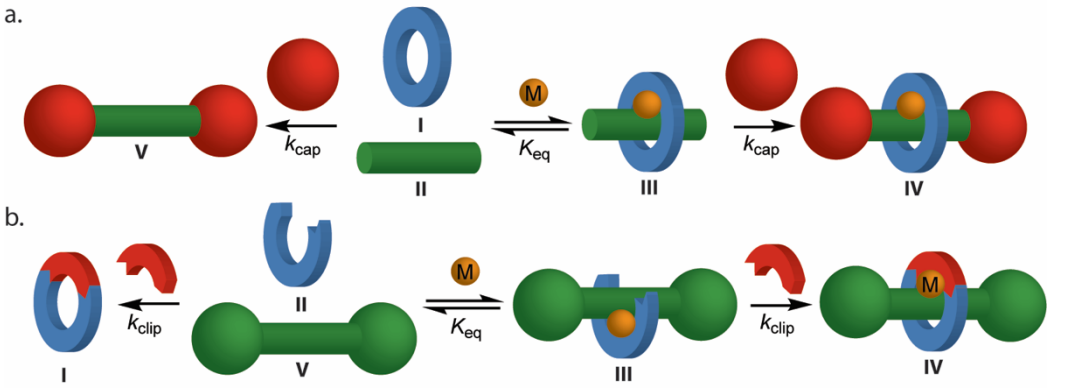

Figure 10: Schematic of Sauvage's passive template rotaxane synthesis through (a) capping approach and (b) clipping approach.[22] **I** macrocycle with metal binding recognition site, **II** precursor with metal binding recognition site, **III** pseudorotaxane inclusion complex with metal **M**, **IV** metallo-rotaxane product, **V** non-interlocked stoppered axle.[22]

1.3. Non-Covalent Interaction Templates

1.3.1. Solvophobic Interactions

In 1981, Ogino synthesised the first rotaxane from a non-covalent template in up to 19% yield.[27] The hydrophobic cavity of **55** allows an enthalpically favourable inclusion complex with 1,12-diaminododecane to form with α- or β-cyclodextrins (CD_X). The pseudorotaxane inclusion complex was then stoppered by reaction with *cis*-$[Co(en)_2Cl_2]Cl$.[27]

CD_X **55**, cucurbit[n]urils **56**, pillar[n]arenes **57**, and other readily available macrocycles have been used routinely to synthesise rotaxanes through weak intermolecular solvophobic interactions (Figure 11). Rotaxane **58** is an example of a pillar[5]arene rotaxane synthesised in 92% yield (Figure 11).[28]

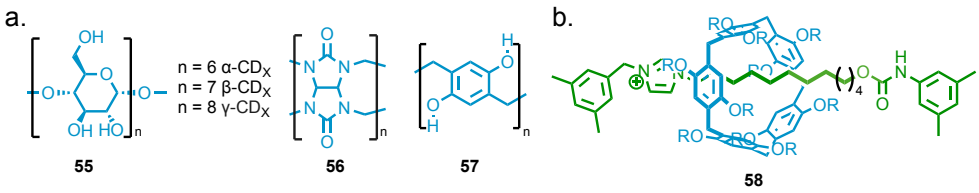

Figure 11: (a) Cyclodextrin **55**, cucurbit[n]uril **56**, pillar[n]arene **57** macrocycles. (b) Huang and co-workers' pillar[5]arene-imidazolium [2]rotaxane **58**, R = Et.[28] Counter-ion omitted for clarity.

1.3.2. π-π Interactions

In 1989, Stoddart and co-workers reported facile catenane **64** synthesis, through cyclising a π-donor-π-acceptor inclusion complex.[29] In this seminal work, Stoddart exploited the 1 : 1 inclusion complex of a paraquat dication with **59**, to synthesise [2]catenane **64** in a single step with high yield (Figure 12a).[29] These π-donor-π-acceptor

interactions have been used since to synthesise a range of interlocked molecules with relative synthetic simplicity, with the electrochemical properties of the viologen units allow easy shuttling between stations.[1,30] The high yielding synthesis of interlocked molecules from a wide range of readily available and cheap crown ethers gives this synthetic route greater versatility than many others.

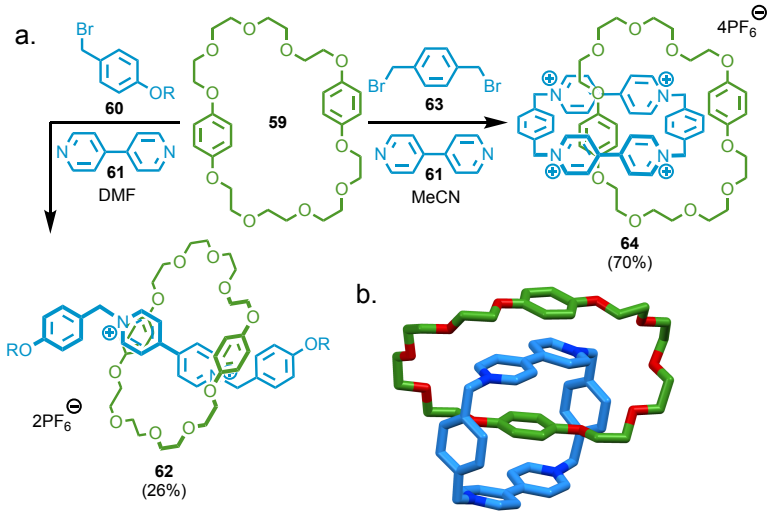

Figure 12: (a) Stoddart and co-workers' π-donor-π-acceptor [2]rotaxane **62**, and [2]catenane **64** synthesis.[29] R = $(CH_2)_2O(CH_2)_2OC_6H_4C(C_6H_4$-*t*-$Bu)_3$. (b) Single crystal X-ray structure of **64** $[C_{64}H_{72}N_4O_{10}](PF_6)_4$ (counter ions and solvent molecules omitted for clarity).

In 1994, Stoddart and co-workers applied this methodology to synthesise a [5]catenane, Olympiadane **68**, resembling the 5 interlocked rings in the symbol of the International Olympic Committee (Figure 13).[31]

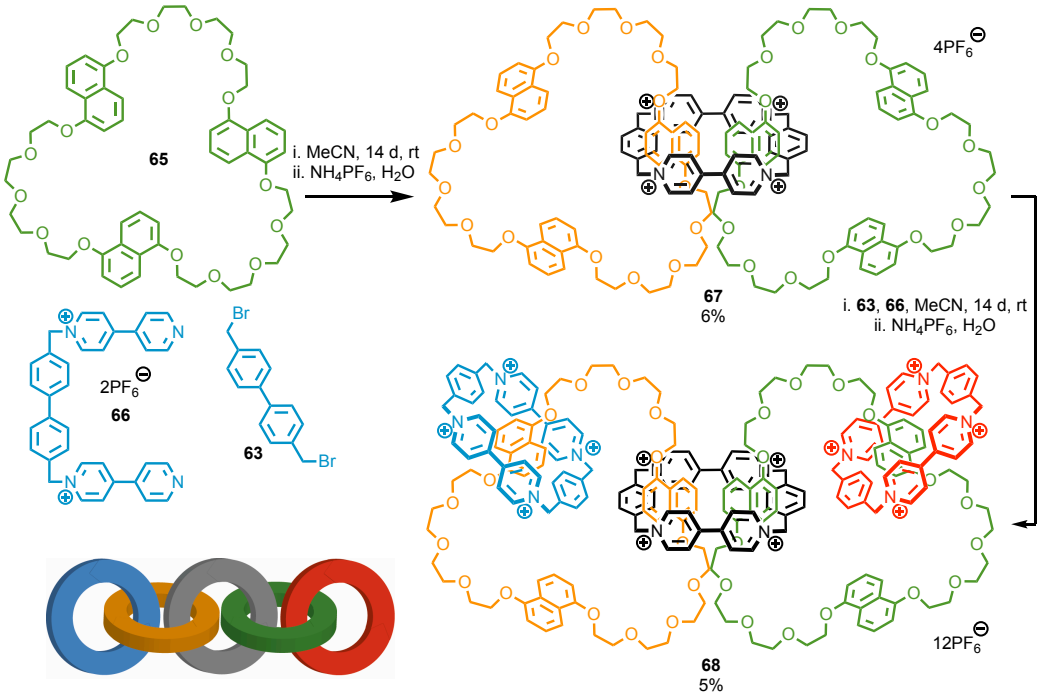

Figure 13: Stoddart and co-workers' [5]catenane 'Olympiadane' **68** synthesis.[31]

The viologen units of Stoddart's 'blue box' **69** are known to form a stable, singly reduced radical-cation upon reduction.[32,33] It was observed that the singly reduced viologen units had strong affinity for other singly reduced radical cations, paving the way for the radical pair template (Figure 14a).[32] Upon reoxidation the tetracationic macrocycle is electrostatically repelled from the dicationic station, but trapped due to the bulky stoppers (Figure 14b).[32,33]

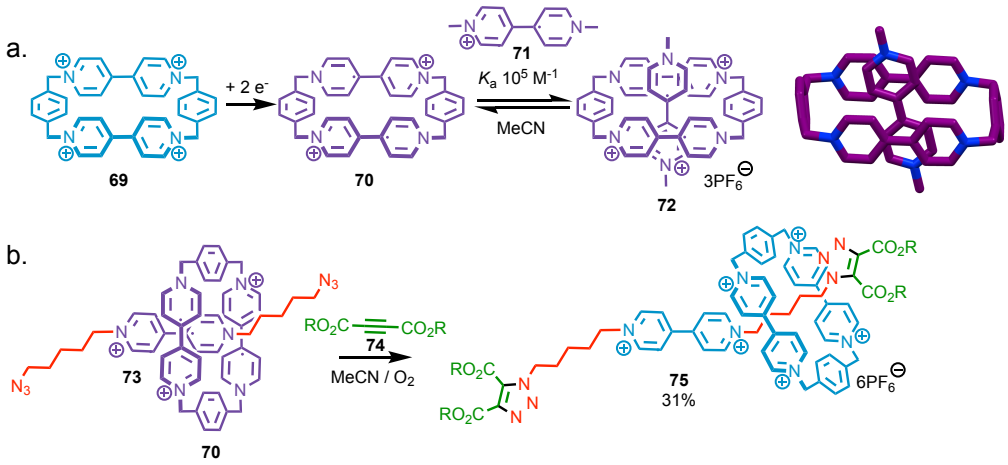

Figure 14: (a) Stoddart and co-workers' radical pair inclusion complex **72** and single crystal X-ray structure of **72** $[C_{36}H_{34}N_4]^{2+\bullet}[C_{12}H_{12}N_2]^{+\bullet}(PF_6)_3$ (counter-ions and solvent molecules omitted for clarity). (b) Application to template [2]rotaxane **75** synthesis.[32,33] R = CH_2-^{t}Bu.

1.3.3. Hydrogen-Bonding Template

Leigh and co-workers have assembled a tetralactam macrocycle around a fumaramide axle template **76**, achieving high yields of interlocked molecules in a single step (Figure 15).[34] The condensation reaction between **77** and **78** around axle **76**, yields rotaxane **79** in 97% yield in a single step, with the macrocycle adopting a chair-like conformation.[34]

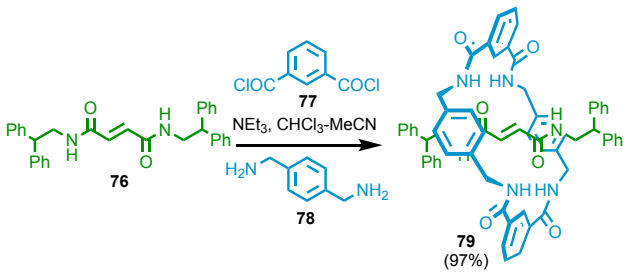

Figure 15: Leigh and co-workers' H-bond templated tetralactam [2]rotaxane **79** synthesis.[34]

Beer and co-workers have developed numerous systems of passive templated rotaxanes and catenanes, using non-covalent hydrogen- or halogen-bonding motifs bound around

an anion to template the mechanical bond formation (Figure 16).[35–37] These numerous examples of non-covalent templated synthesis of interlocked molecules demonstrate the significant advancement in understanding of the secondary interactions present in interlocked molecules, and the increase in synthetic accessibility since the first statistical interlocked compounds.[2,21,24,29,38,39] Systems templated around unusual guests, are typically highly selective for binding the template guest, therefore these rotaxanes have been used as selective sensors for anions.[36]

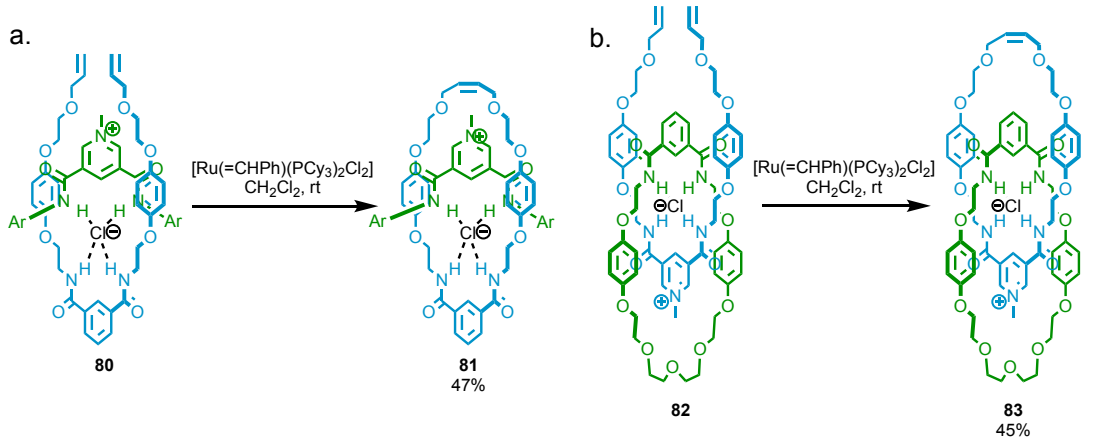

Figure 16: Beer and co-workers' chloride templated (a) [2]rotaxane **81** synthesis and (b) [2]catenane **83** synthesis.[35] Ar = $C_6H_4C(C_6H_4$-t-Bu$)_3$.

In 2017, Tian and co-workers demonstrated that through combining multiple non-covalent templating techniques, it was possible to synthesise hetero[6]rotaxane **88** in a one-pot reaction (Figure 17).[40] The macrocycles in this rotaxane cannot change order or pass over each-other, therefore the smaller, terminal macrocycles behave as stoppers for the larger central macrocycles. Without the small macrocycles, the larger macrocycles would dissociate easily.[40]

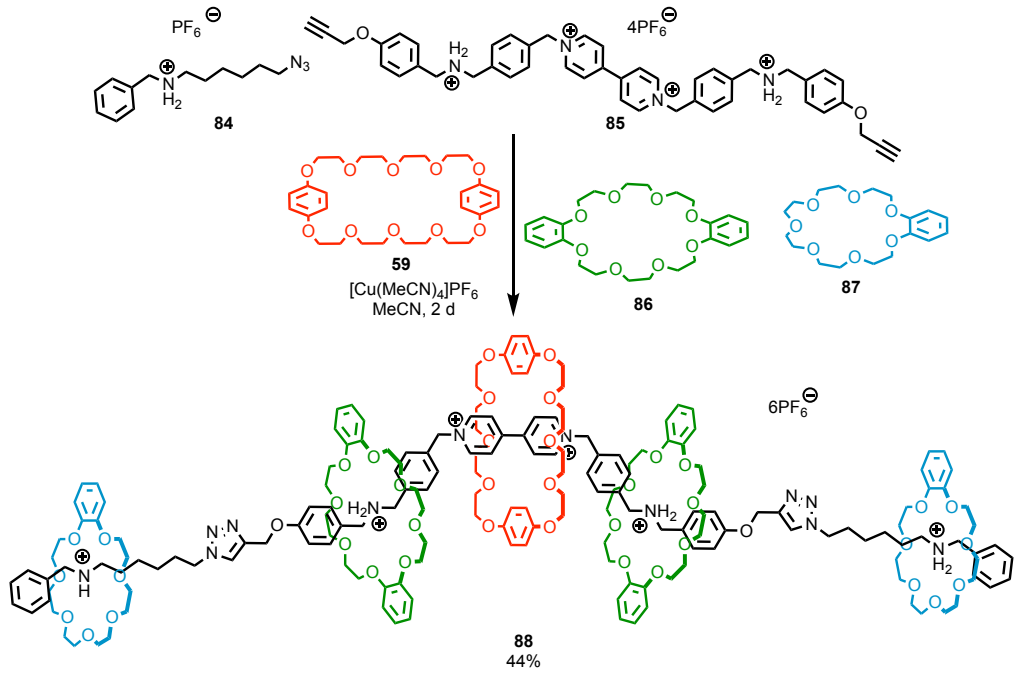

Figure 17: Non-covalent one-pot assembly of hetero[6]rotaxane **88**, through the combination of π-donor-π-acceptor, H-bonding and charge stabilising templates.[40]

Yields of interlocked molecules have improved from < 1% of chemically simple molecules over many steps, to almost quantitative yields of functional interlocked molecules.[8–11,16] The statistical and covalent directed syntheses of the 1960s produced simple compounds, with purification difficulties. The evaluation of the properties of the mechanical bond was impossible. Recent advances enable investigation of the properties of these interlocked molecules, approaching useful applications and allowing investigation of the properties of the mechanical bond.[41]

1.4. Active Template Synthesis

Sauvage's passive template revolutionised the synthesis of interlocked molecules, and the non-covalent template techniques above were inspired and conceptually similar to Sauvage's initial system.[2,16,24] While the passive template was a huge synthetic achievement, and continues to be used regularly to this day, it fails to take advantage of a key property of transition metals – their ability to catalyse reactions.

In 2006, Leigh and co-workers made a significant leap forwards in the synthesis of mechanically interlocked molecules, through development of the active template approach.[42] In the active template approach, a metal ion bound within a macrocycle ligand mediates the formation of a new covalent bond through the centre of the macrocycle, forming a rotaxane (Figure 18). The benefits of the active template

approach include a single recognition site, and sub-stoichiometric metal template.[22] Furthermore, whereas the passive template approach was primarily a thermodynamically driven process, the active template approach is a kinetic method allowing the synthesis of otherwise impossible structures. The yield of rotaxane, **IX**, depends on the relative rate at which it is produced compared to non-interlocked axle **XI**.[22]

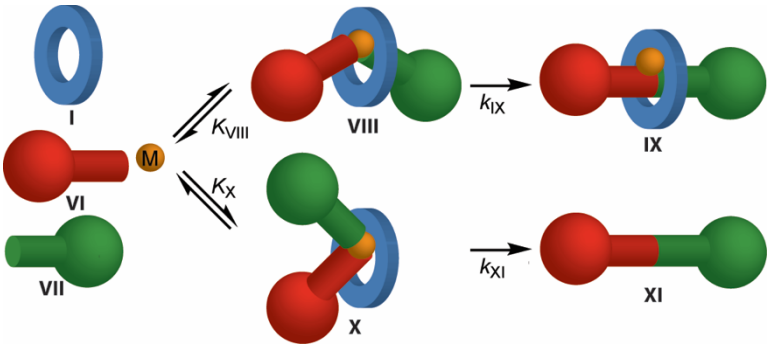

Figure 18: Schematic of Leigh's active template rotaxane synthesis.[22] **I** macrocycle with metal binding recognition site, **VI** stopper, **VII** stopper, **M** transition metal catalyst, **VIII** interlocked intermediate, **IX** interlocked product, **X** non-interlocked intermediate, **XI** non-interlocked product.[22]

In Leigh and co-workers' seminal publication, they describe a high yielding rotaxane synthesis through an active template Cu^{I}-catalysed alkyne azide cycloaddition (AT-CuAAC) approach (Figure 19).[42] With an equal ratio of **89**, **90**, **91** and Cu^{I}, a high 57% yield was achieved with the simple pyridine macrocycle **91**. The 57% yield implied 43% non-interlocked macrocycle remained in the reaction mixture, therefore with 5 equivalents of **89** and **90**, the remaining **91** from unproductive CuAAC reactions (Figure 18) was recycled, giving 94% yield of rotaxane **92**.[42,43]

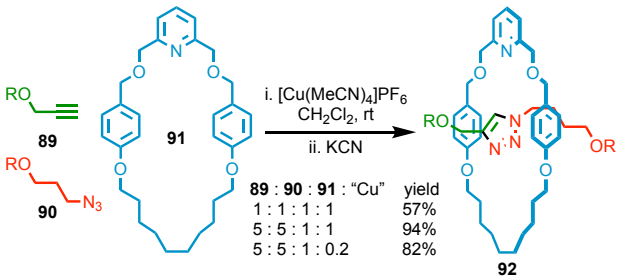

Figure 19: Leigh and co-workers' original active template [2]rotaxane **92** synthesis.[42] R = $C_6H_4C(C_6H_4$-*t*-$Bu)_3$. The Cu^{I} catalyst binds to the pyridine ligand and mediates the alkyne azide cycloaddition through the macrocycle.

Saito and co-workers' developed the active template approach independent of Leigh, using pre-formed **93**-CuI complex (Figure 20).[44,45] Saito used Glaser homocoupling to

form rotaxane **95** in 72% yield. In 2009, Saito used the same technique to demonstrate the first active template synthesis of [2]catenane **97**.[46]

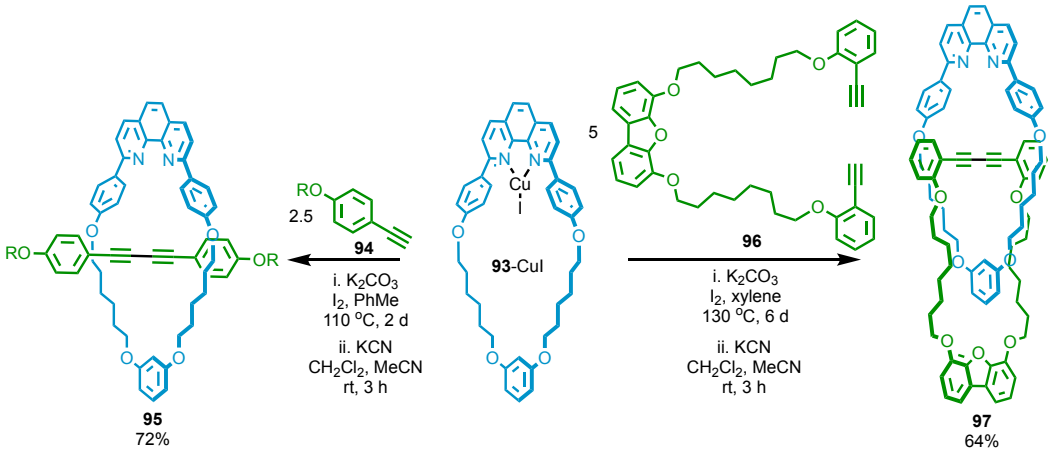

Figure 20: Saito and co-workers' active template [2]rotaxane **95**,[44] and [2]catenane **97** syntheses.[46] R = $(CH_2)_6C(C_6H_4Ph)_3$.

Since the initial active template publications, many different transition metal catalysed reactions have been used to synthesise interlocked molecules. A large range of coupling reagents and macrocycle designs are possible. Figure 21 summarises the types of macrocycles and active template reactions possible.[22,47] Despite the range of different active template approaches, the most commonly used is still the AT-CuAAC with pyridine derived macrocycle ligands.[22,43,47]

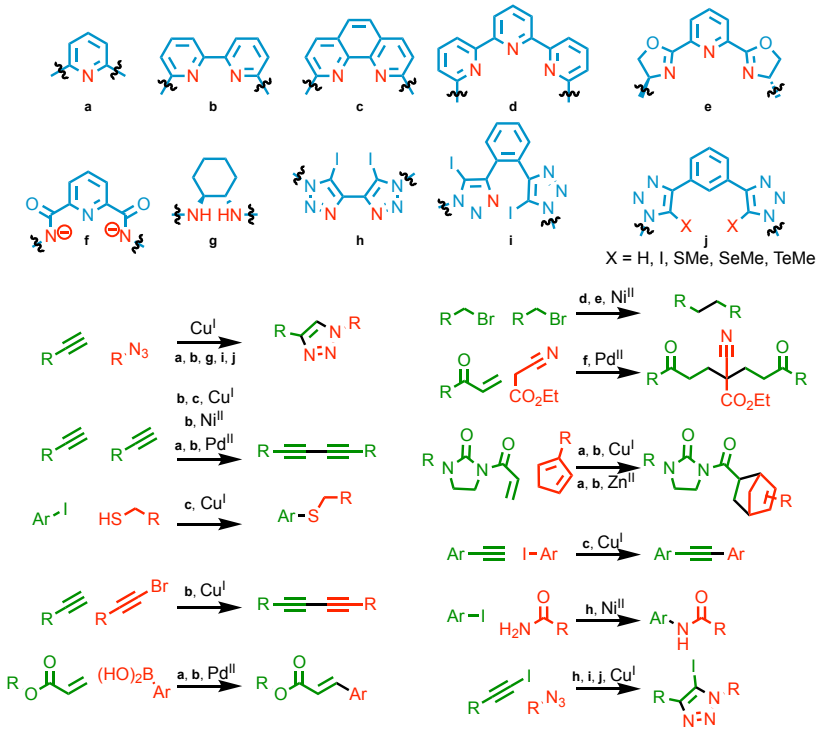

Figure 21: Summary of macrocycle ligand types, and metal catalysed active template reactions.[22,47]

The active template approach has made interlocked molecules much more synthetically accessible.[22,47–52] However, the main limitations of this approach are the use of transition metal catalysts, and the synthetically complex macrocycles, especially compared to the non-covalent assembly with crown ethers, cucurbit[n]urils, CD_X, pillar[n]arenes.[1]

In 2017, Leigh and co-workers further advanced the active template approach, through metal-free transition state stabilisation.[53] Leigh reported the metal-free synthesis of [2]rotaxanes, from readily accessible macrocycles, in up to 70% conversion (Figure 22a). More recently, Leigh and co-workers have shown that simple, commercially available crown ethers can be used for the active template synthesis of rotaxanes *via* transition state stabilisation (Figure 22b-c).[54] The compatibility of the transition state stabilisation active template with crown ethers solves the initial limitations of macrocycle availability. In the passive template approach, crown ether rotaxanes assemble *via* a *pseudo*rotaxane intermediate. However, in the active template approach, H-bonding in the transition state allows rotaxane formation in a single step without requiring a *pseudo*rotaxane intermediate.

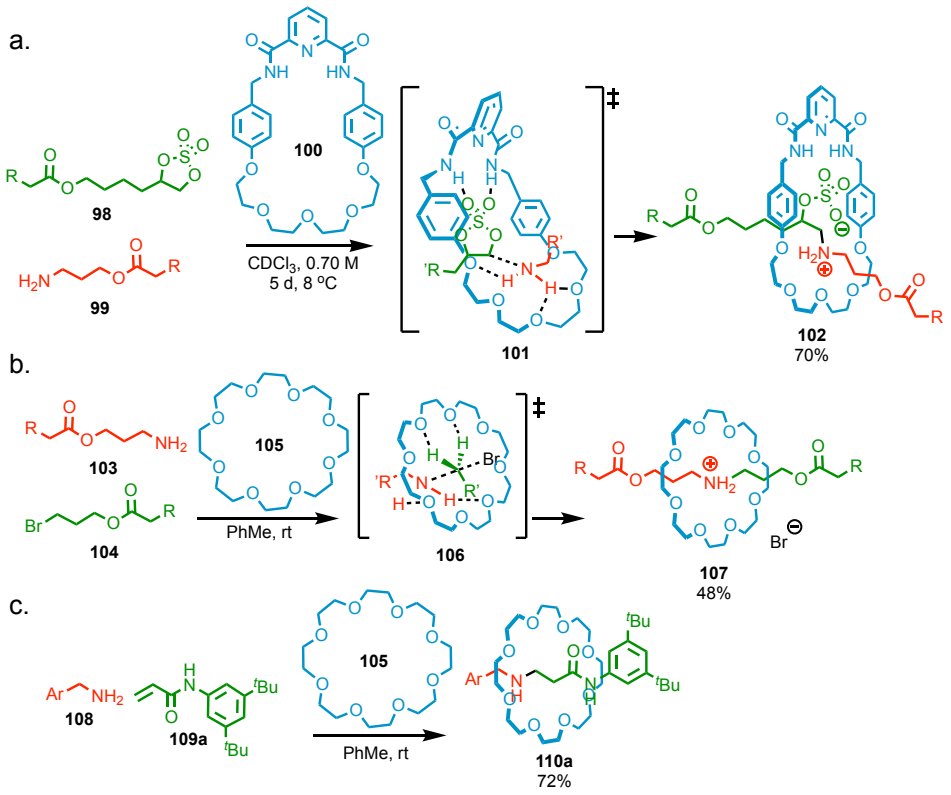

Figure 22: (a) Leigh and co-workers' initial transition state stabilisation active template approach,[53] and (b) and (c) the crown ether modification.[54] R = $C(C_6H_4Cl)_3$. Ar = 3,5-di-*t*-Bu-C_6H_3.

Subsequent work by Leigh and co-workers has evaluated the scope of the electrophilic coupling partner in this metal-free active template.[55] 11 different examples were demonstrated (**110b**-**110l**), including C=O, C=S, P=O and SO_2 electrophiles. Good yields of interlocked molecules were achieved with one equivalent of each coupling partner, from commercially available starting materials (Figure 23).[55]

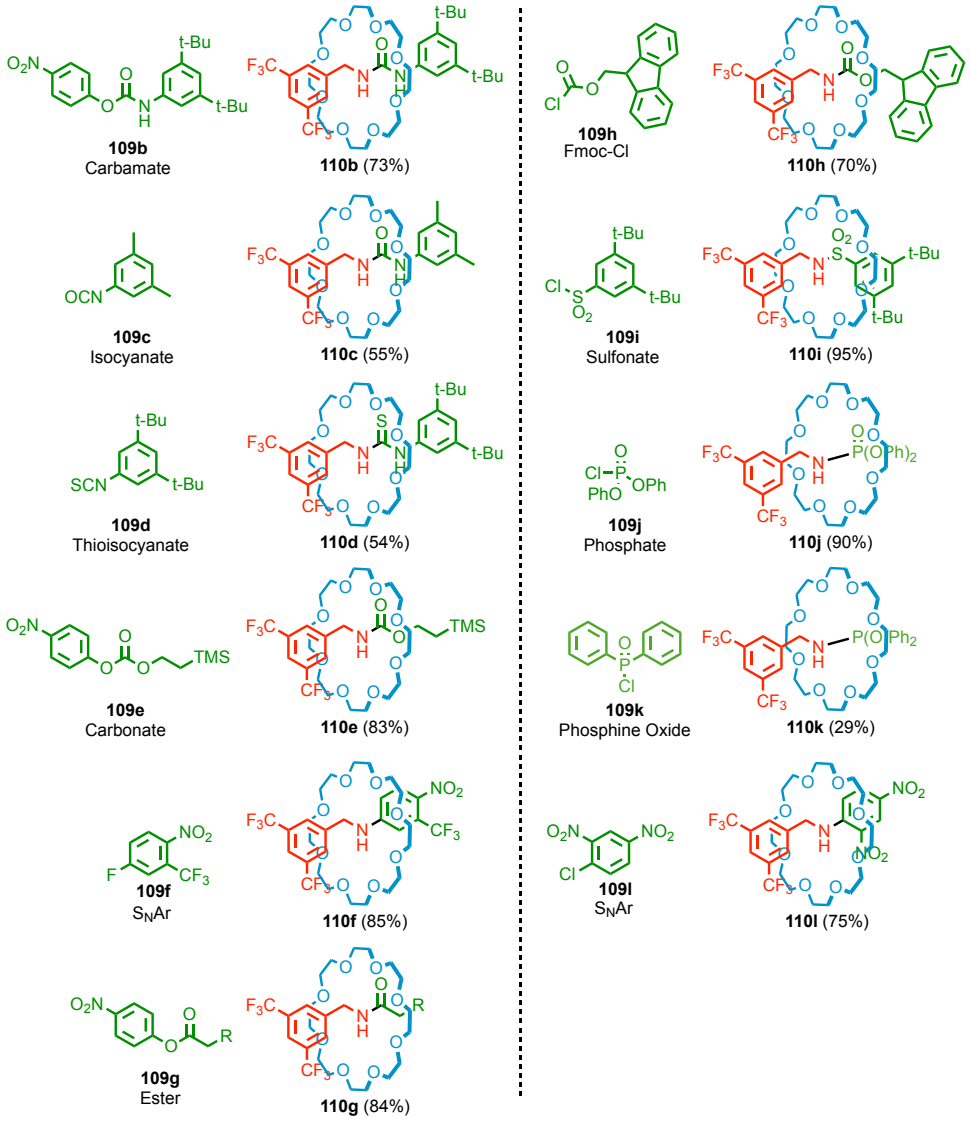

Figure 23: Leigh and co-workers' metal-free active template electrophile scope.[55] Nucleophile-Electrophile-macrocycle 1 : 1 : 1, PhMe, rt. R = $C(C_6H_4Cl)_3$.

Goldup and co-workers modified the AT-CuAAC reaction with small 2,2′-bipyridine containing macrocycles. The use of a bidentate macrocycle with a tetrahedral catalyst, meant that the two stopper units were forced to be oriented either-side of the macrocycle plane, **113**, reducing the number of unproductive product cycles. Application of this gave impressive 95% yields of rotaxane **117** with only 1 equivalent

of **114** and **115**, a significant improvement on Leigh's 57% yield (Figure 24a-d).[42,56] The rigidity of the bidentate 2,2′-bipyridine coordination unit, which occupies one plane of the tetrahedral Cu^{I}-ion made this motif especially effective for the active template.

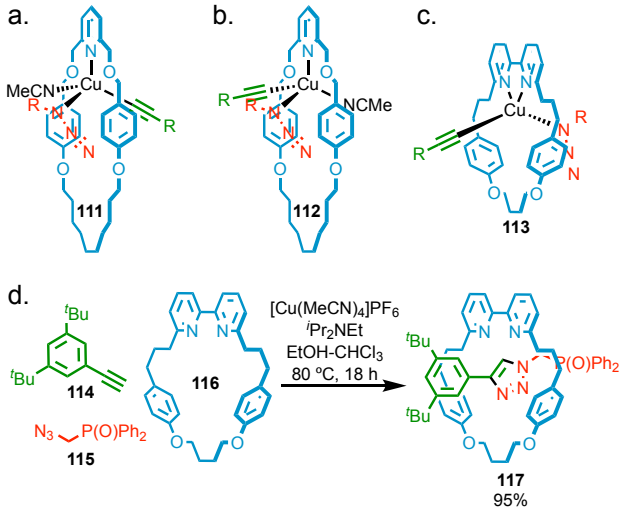

Figure 24: (a) productive and (b) unproductive intermediates in Leigh and co-workers' original active template rotaxane synthesis.[42] (c) the tetrahedral intermediate of Goldup and co-workers' small 2,2′-bipyridine macrocycles and (d) high yielding rotaxane synthesis with 1 equivalent of stoppers **114** and **115**.[56]

Goldup and co-workers noted that the large pyridyl macrocycles used for the active template approach generally relied on large substituted trityl stoppers, undermining the synthetic utility of the approach due to the limited commercial availability of the stoppering units.[57] Furthermore, larger macrocycles are conformationally flexible and can result in fewer productive CuAAC reactions. Goldup reasoned that the shielded local environment of the axle would be enhanced with smaller, tighter macrocycles (Figure 25).[57] This would result in the smaller macrocycle transferring information more efficiently to the axle, making the mechanical bond more effective for prodrugs, insulated wires, protected dyes, sensing and catalysis.[57] Using macrocycles **116**, Goldup and co-workers achieved highly efficient AT-CuAAC reactions using smaller stoppers (**121** and **122**) which were achieved in one high yielding step from commercially available starting materials.[57] It was also discovered, that smaller macrocycles, **119a-d**, were more efficient for the AT-CuAAC reaction, giving higher yields of the interlocked product **120a-d**, due to a higher proportion of productive AT-CuAAC reactions occurring within the macrocycle cavity (Figure 25). Larger macrocycles gave lower yields due to conformational flexibility resulting fewer productive CuAAC reactions.[57]

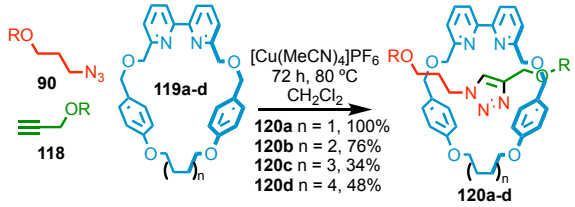

Figure 25: Goldup and co-workers' small macrocycle modification of the AT-CuAAC reaction.[57] R = $C_6H_4C(C_6H_4$-t-$Bu)_3$.

1.5. Consequences of the Mechanical Bond

Using their small macrocycle approach, Goldup and co-workers were able to isolate a water-stable Cu^I-triazolide intermediate **123** of the CuAAC reaction (Figure 26a).[58] The crystal structure of **123** showed that the macrocycle fitted around the axle closely, stabilising the intermediate (Figure 26b). Prior to this publication, the only reported isolable Cu^I-triazolide was complex **128** which was synthesised in aprotic conditions (Figure 26c).[59] This demonstrated the previously unprecedented stability of complex intermediates, resulting from the mechanical bond. Isolating the Cu^I-triazolide intermediate **123** demonstrates the power of the mechanical bond for mechanism elucidation. Goldup's interlocked Cu^I-triazolide stability[59] builds upon Schill's early observation that the C_{aryl}-*N* bond in **19** was inert when crowded by macrocycles shorter than 20-atoms in circumference (Figure 4).[10,11]

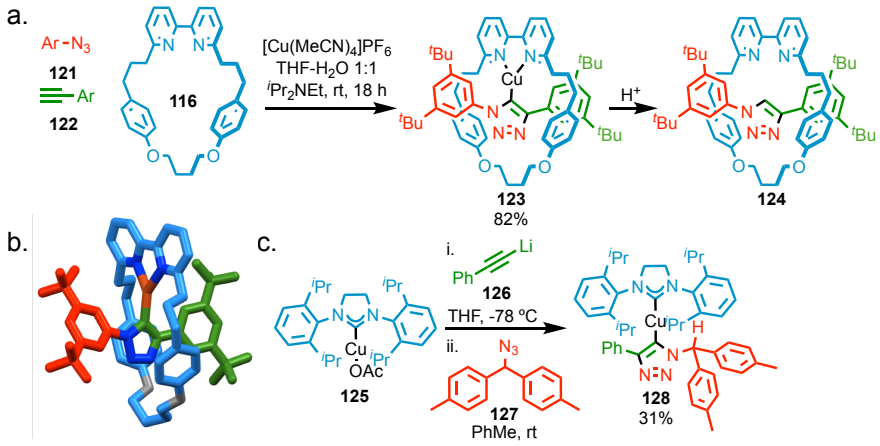

Figure 26: (a) Goldup and co-workers' water tolerant Cu^I-triazolide rotaxane **123**,[58] (b) X-ray crystal structure of rotaxane **123**,[58] and (c) Straub and co-workers' isolated Cu^I-triazolide **128**.[59] Ar = 3,5-di-*t*-Bu-C_6H_3.

1.6. Complex Interlocked Architectures

Goldup and co-workers managed to optimise the AT-CuAAC reaction conditions to yield up to 50% [3]rotaxane **130** in a single, four-component coupling reaction (Figure 27a).[60] The optimisation of [2]rotaxane synthesis to >95% for a range of macrocycles

demonstrates the significance of the 2,2′-bipyridine modification to the AT-CuAAC reaction. Furthermore, further optimisation towards the [3]rotaxane **130** product provides interesting mechanistic insight. The benzylic ether oxygen atoms of the macrocycle played a key role in assembling the intermediate yielding the [3]rotaxane **130** product; when these were replaced with methylene groups the [3]rotaxane **130** yield dropped to < 2 %. The coordination of the benzylic ether oxygen atom to the Cu^{I} centres in the intermediate was essential to supporting the bimetallic pathway and thus formation of the [3]rotaxane **130** (Figure 27b).[60]

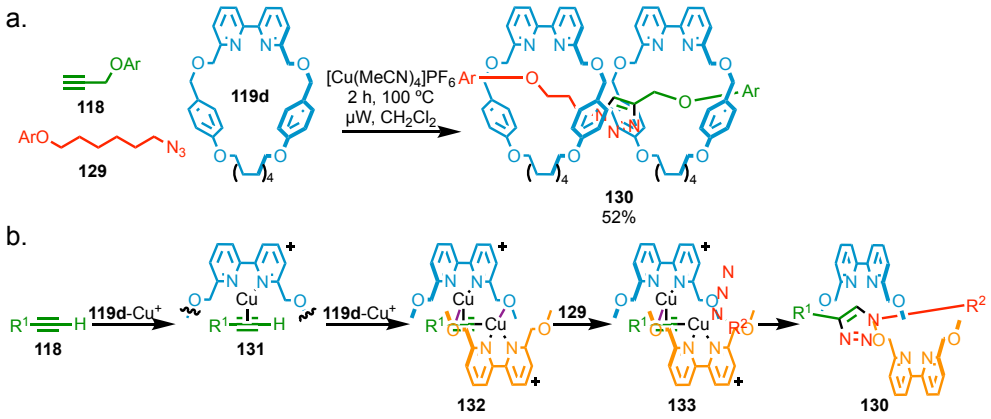

Figure 27: (a) Goldup's [3]rotaxane **121** formation and (b) the coordination of benzylic ethers that stabilises the bimetallic intermediate.[60] PF_6^- counter-ions omitted for clarity. Ar = $C_6H_4C(C_6H_4$-t-$Bu)_3$. R^1 = CH_2OAr. R^2 = $(CH_2)_6OAr$. Complete macrocycle structure is omitted from **131**-**133** for clarity.

Goldup and co-workers expanded this further to create a kinetic self-sorting hetero[3]rotaxane.[61] Provided that two different rings cannot pass through each other, a hetero[3]rotaxane with a non-centrosymmetric axle can form as two isomers. The formation of hetero[n]rotaxanes had previously been achieved thermodynamically with a stepwise approach. Goldup achieved a kinetic self-sorting approach governed by the stability of the products (Figure 28). By using two macrocycles of differing diameters, and two stoppers of differing size, it was possible to achieve a hetero[3]rotaxane with specific order of macrocycles, with other products dissociating to form axle or a [2]rotaxane side product.

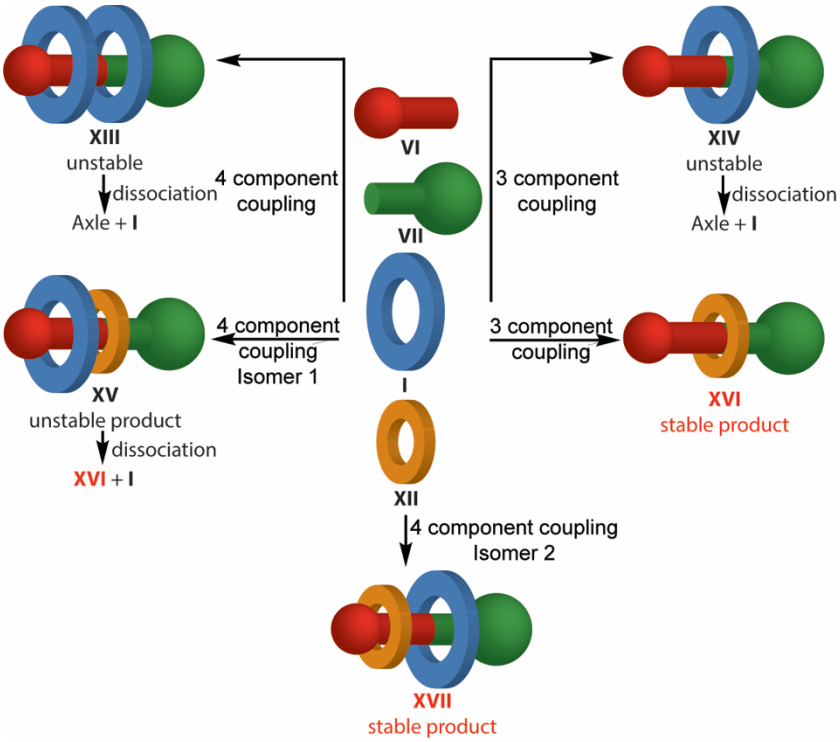

Figure 28: Schematic of Goldup and co-workers' self-sorting hetero[3]rotaxane. **I** large macrocycle, **VI** stopper, **VII** stopper, **XII** small macrocycle, **XIII XIV XV** unstable intermediates, **XVI** stable side product, **XVII** stable [3]rotaxane.[61]

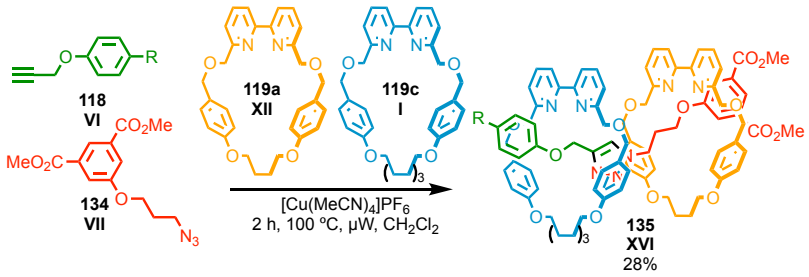

Figure 29: Goldup and co-workers' self-sorting hetero[3]rotaxane **135**.[61] R = $C(C_6H_4\text{-}t\text{-}Bu)_3$.

The high efficiency of Goldup's modified AT-CuAAC reaction, combined with the small macrocycles and stoppers, enabled the operationally simple synthesis of oligo[n]rotaxanes iteratively. With over 90% yield for each mechanical bond forming step, Goldup and co-workers achieved 67% yield of a [6]rotaxane **138** (Figure 30).[62]

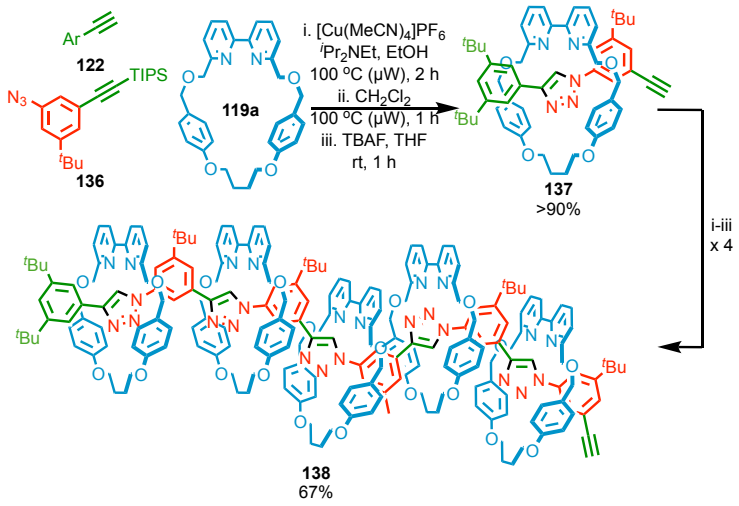

Figure 30: Goldup and co-workers' iterative oligo[n]rotaxane procedure.[62] Ar = 3,5-di-*t*-Bu-C_6H_3.

As well as stabilising the Cu^{I}-triazolide intermediate of the CuAAC reaction, Goldup and co-workers discovered that the mechanical bond was also responsible for a rearrangement of the 1,2,3-triazolide **141** to form acrylamide rotaxane **140** (Figure 31).[63] This demonstrates the ability of the mechanical bond to augment chemical reactivity to produce unusual reaction outcomes. The bulky environment surrounding the Cu^{I}-triazolide hindered proto-demetallation and promoted the protonation of the less basic hydroxy group, allowing the elimination of H_2O to occur. Demetallation and N_2 elimination formed the less crowded propa-1,2-dien-1-imine moiety which is hydrolysed to form acrylamide **140**.

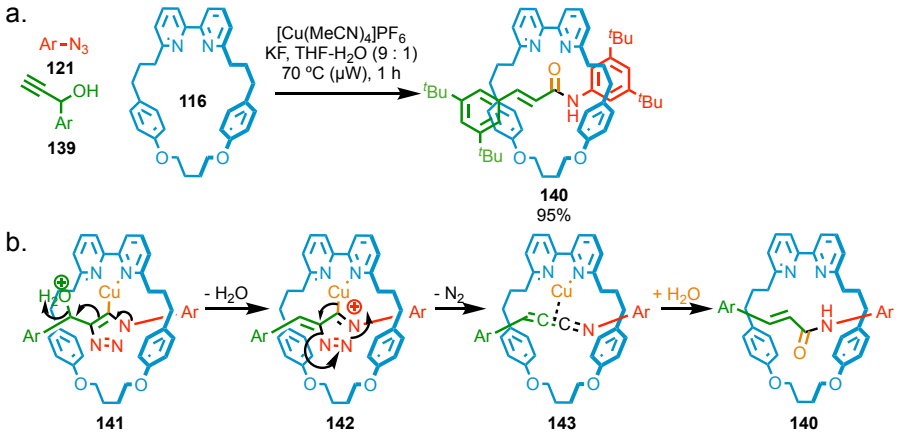

Figure 31: (a) Goldup and co-workers' 1,2,3-triazolide rearrangement to produce acrylamide rotaxane **140** and (b) the proposed mechanistic route.[63] Ar = 3,5-di-*t*-Bu-C_6H_3.

Application of the small macrocycle modification to the AT-CuAAC also enabled the high yielding synthesis of tight catenanes, utilising a single bipyridine macrocycle and a pre-macrocycle with an alkyne and azide moiety (Figure 32a). Utilisation of readily

available bis-alkynes and bis-azides enabled a high yielding multi-component approach to catenane synthesis **146**-**148** *via* an alkyne-azide bearing pre-macrocycle intermediate (Figure 32b).[64]

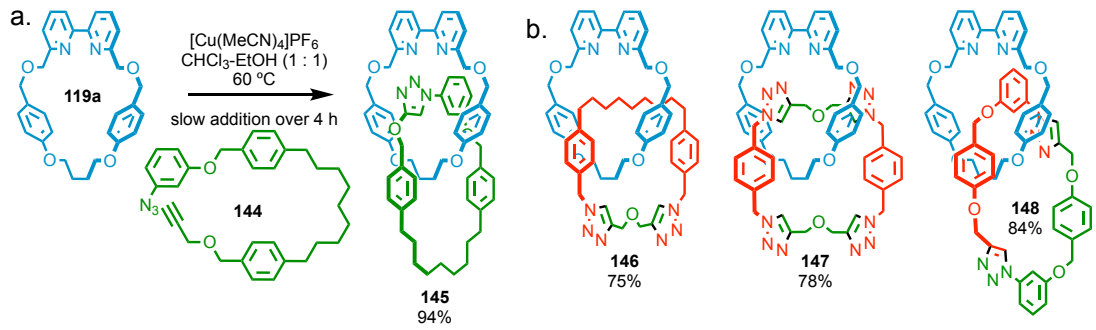

Figure 32: (a) Goldup and co-workers' small macrocycle catenane synthesis,[64] (b) multi-component [2]catenanes.[64]

1.7. Mechanical Stereogenic Elements

1.7.1. Mechanical Planar Chirality

An interesting and underexploited property of the mechanical bond is its ability to form chiral molecules from the combination of two achiral sub-components. Mechanically planar chiral (MPC) rotaxanes result from the threading of an achiral C_{nv} axle through an achiral C_{nh} macrocycle, leading to two enantiomers resulting from the orientation of the macrocycle around the axle (Figure 33). The mechanical bond de-symmetrises the macrocycle σ_h-plane and axle σ_v-planes, resulting in an interlocked molecule without any internal planes of symmetry.

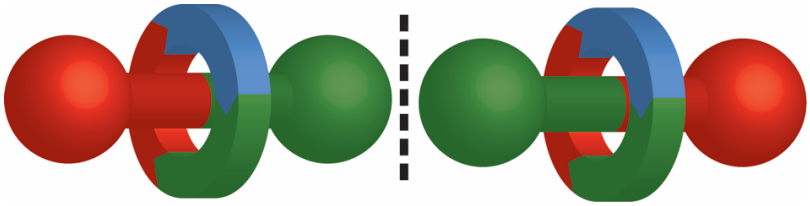

Figure 33: Two enantiomers of a MPC rotaxane from two achiral components.[65]

This enantiomerism was first described by Schill (as *'cyclochirality'*),[12] but not achieved until Vögtle and Okamoto used preparative chiral stationary phase HPLC to separate two enantiomers (Figure 34). When enantiopure, Vögtle showed that the mechanical bond led to a strong circular dichroism (CD) response.[66]

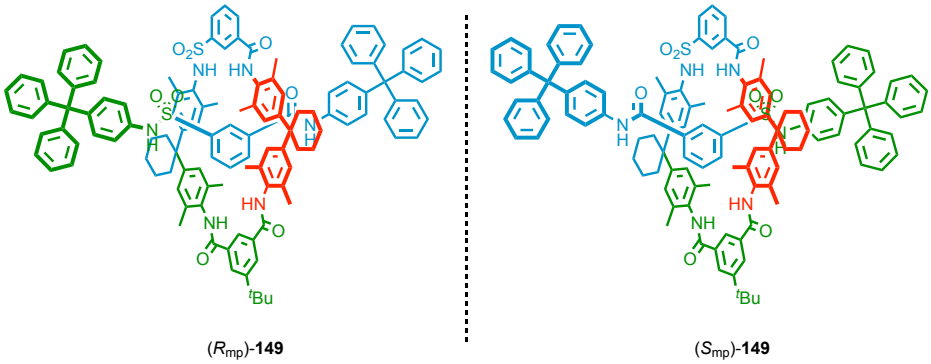

Figure 34: Vögtle and co-workers' enantiopure MPC [2]rotaxanes (R_{mp})-**149** and (S_{mp})-**149**, separated with preparative chiral stationary phase HPLC.[66]

The reliance of preparative chiral stationary phase HPLC significantly limited the scalability of these compounds. Until recently the investigation of the properties of this type of chirality had been underexplored. In 2014, Goldup and co-workers used a D-glucose derived chiral auxiliary to separate mechanically planar chiral diastereoisomers with standard preparative chromatographic techniques. Cleavage of the sugar auxiliary by ester aminolysis achieved enantiopure MPC rotaxane **153** (Figure 35).

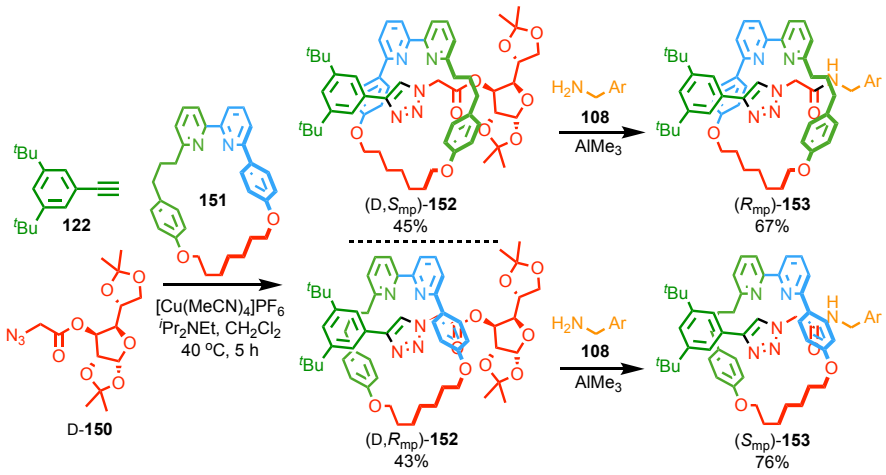

Figure 35: Synthesis of separable MPC diastereoisomers with a chiral auxilliary D-**150**.[67] Ar = 3,5-di-*t*-Bu-C_6H_3.

Recently, Goldup and co-workers have reported the diastereoselective synthesis of MPC rotaxanes. A simple stereo-directing azide (*S*)-**154** was used to induce up to 96% *de* with alkyne **122** and macrocycle **151** in the AT-CuAAC reaction (Figure 36), with the lowest reported *de* being 44% for the longer, more flexible alkyne **155**.[68] This high yielding and highly diastereoselective approach, with removable axle stereochemistry, was a huge leap forward in the synthesis of MPC rotaxanes and will make investigating their properties much more accessible.

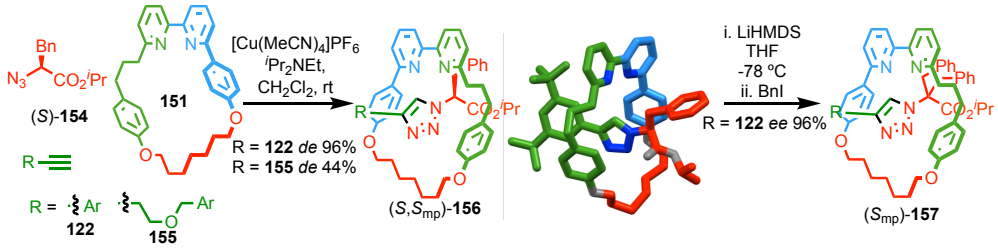

Figure 36: Goldup and co-workers' chiral directing azide (*S*)-**154** enabling up to 96% *de* of (S,S_{mp})-**156**, with subsequent alkylation erasing the covalent stereogenic centre enabling up to 96% *ee* of (S_{mp})-**157**.[68] Ar = 3,5-di-*t*-Bu-C_6H_3. Single crystal X-ray structure of (S,S_{mp})-**156** (R = 3,5-di-*t*-Bu-C_6H_3) ($C_{60}H_{71}N_5O_4$).

Goldup's chiral auxiliary D-**150** and chiral directing group (*S*)-**154** methodologies enable the synthesis of these MPC rotaxanes in high yield through accessible general synthetic techniques such as flash chromatography.[67,68] Now these MPC rotaxanes can be made on larger scales, the exploration of the properties of MPC rotaxanes can now be investigated, although no applications of MPC rotaxanes had been reported prior to the publication of elements of this thesis.[69]

Recently, Leigh and co-workers have reported the synthesis of MPC rotaxane **161** in 50% *ee* (Figure 37). This was achieved in a single step with a C_s-symmetric crown ether **160**, and an ester bearing a chiral leaving group (+)-**159**,[70] building upon previous metal-free active templates (Figure 22a).[53–55] The scalability of this approach makes it promising. However, the low *ee* and limited functionality reduce the scope of this approach, especially in comparison to Goldup's chiral auxiliary and diastereoselective approaches, which allow access to higher enantiopurity structures.[67,68] The stereoselectivity was attributed to the π-π interaction between the macrocycle naphthyl group and the 3,5-*di*-CF_3-C_6H_3 stopper enhancing steric clashes in the diastereoisomeric tetrahedral intermediate (Figure 22b).

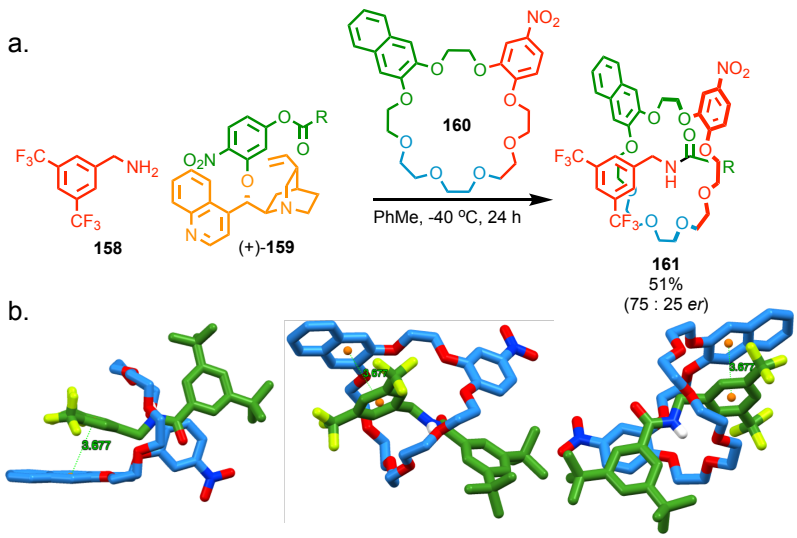

Figure 37: Leigh and co-workers' (a) chiral leaving group approach to the synthesis of MPC rotaxanes.[70] **161a** R = $CH_2C(C_6H_4Cl)_3$. (b) X-ray crystal structure of **161b** where R = 3,5-di-*t*-Bu-C_6H_3. π-π interaction between centroids of 3.677 Å.

1.7.2. Co-Conformational Mechanical Planar Chirality

In co-conformational MPC,[65] the motion of a C_{nh}-symmetric macrocycle on a D_{nh}-symmetric axle can generate two enantiomers depending on the location of the macrocycle. When the macrocycle moves away from the central position, it removes the σ_h symmetry element, generating a stereocentre (Figure 38).[65,71] Without a chiral input, this dynamic stereocentre remains racemic, due to the two enantiomeric co-conformations having equal energies and thus equal population.

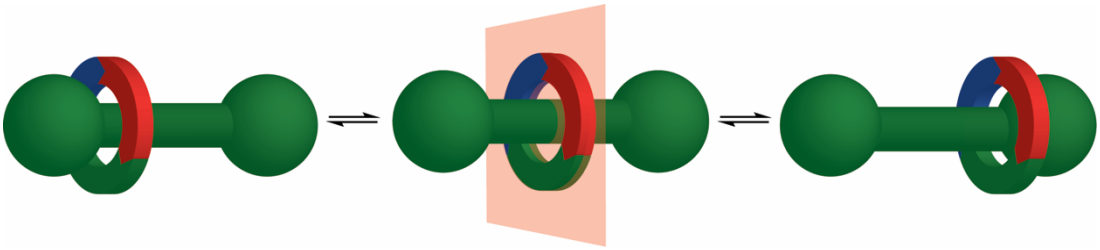

Figure 38: Co-conformational mechanically planar chirality.[65]

Credi and co-workers demonstrated a rotaxane which can generate selective co-conformation MPC on response to addition of (*S*)-camphor sulfonate guests (Figure 39).[72] It is hypothesised that the chiral anion binds preferentially to one of the exposed triazolium stations, biasing macrocycle occupation to one side and generating a diastereoisomeric complex (*dr* 85 : 15) exhibiting a co-conformational MPC stereogenic element. This was demonstrated by ^{1}H NMR, although the major diastereomer was not elucidated in this study.[71,72]

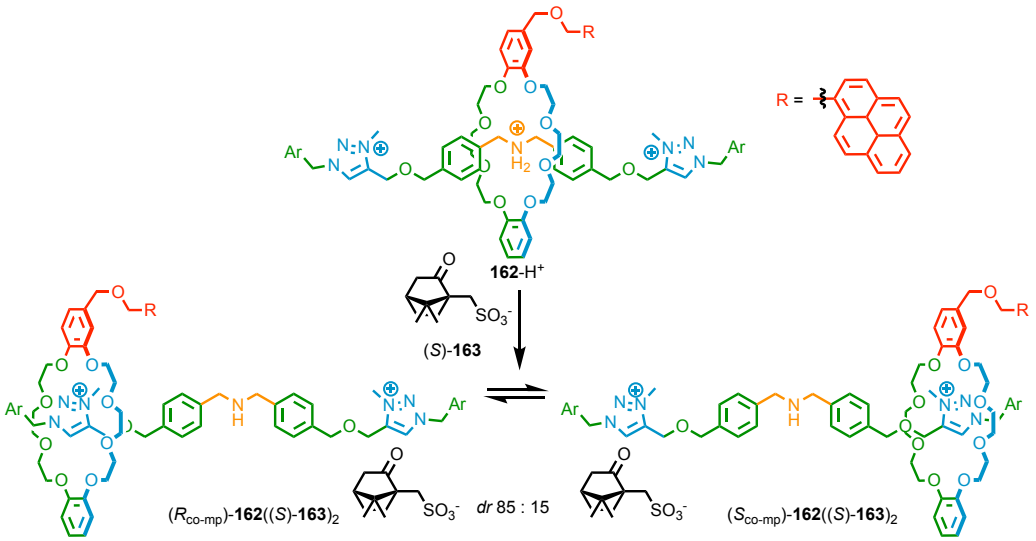

Figure 39: Credi and co-workers' diastereoselective co-conformational MPC rotaxane **162**.[72] Ar = 3,5-di-*t*-Bu-C_6H_3.

1.7.3. Topological Chiral Catenanes

[2]Catenanes consisting of two C_{nh}-symmetric macrocycles can also be chiral, despite both component parts possessing a σ_h-plane (Figure 40a).[65] Interestingly Wasserman acknowledged the topological isomerism in his initial catenane **4** from 1960, but it wasn't until 2019 when Goldup and co-workers isolated these using accessible chromatographic techniques (Figure 41).[6] [2]Catenanes can also display (non-topological) mechanical axial chirality, arising through the interlocking of two C_{nv} macrocycles (Figure 40b).[65]

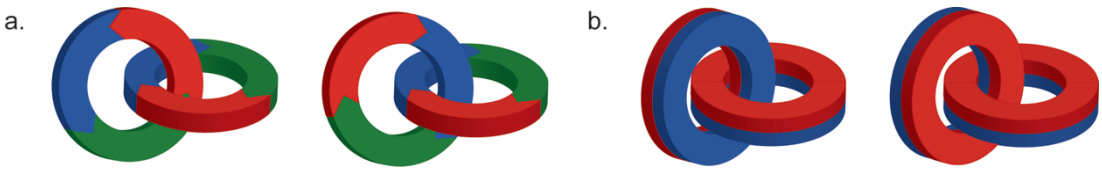

Figure 40: Cartoons depicting (a) mechanically topologically chiral [2]catenanes from the interlocking of two C_{nh} macrocycles, and (b) mechanically axial chiral [2]catenanes resulting from the interlocking of two C_{nv} macrocycles.[65]

Similar to Goldup and co-workers' application of chiral auxiliaries to separate MPC diastereoisomers (Figure 35),[67] mechanically topologically chiral (MTC) [2]catenanes were isolated by utilising a cleavable chiral auxiliary pre-macrocycle[73] in Goldup's small macrocycle catenane AT-CuAAC.[64] This allowed access to topologically chiral enantiomers of catenane **167** after Swern oxidation and hydrolysis (Figure 41).[73] Goldup and co-workers' chiral auxiliary approach to synthesising mechanically topological catenane **167**[73] is conceptually similar to the chiral auxiliary synthesis of MPC rotaxane **153**.[67]

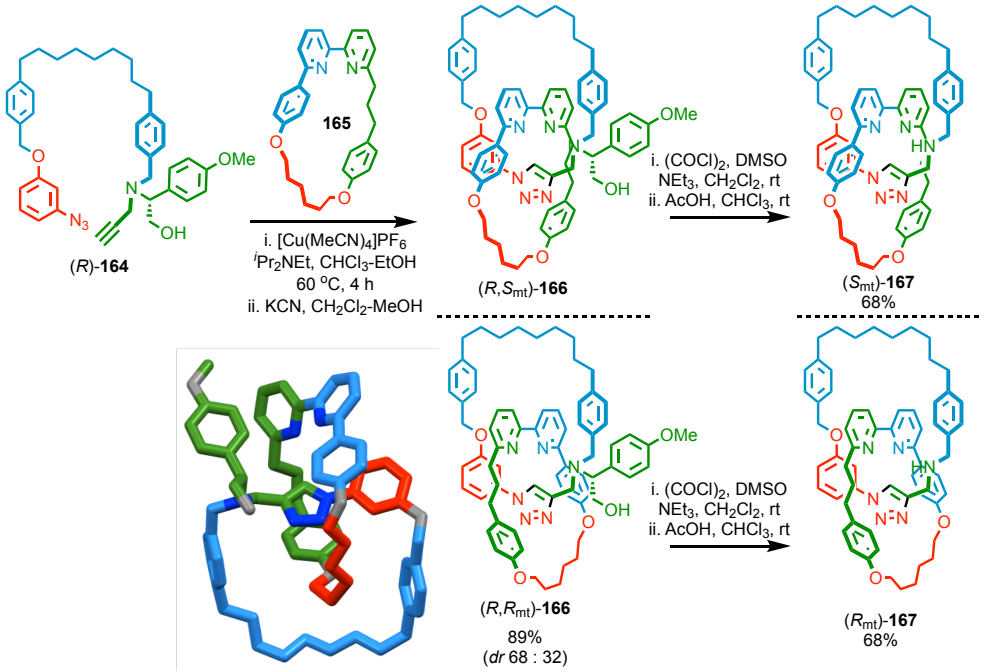

Figure 41: Goldup and co-workers' auxiliary approach to mechanically topologically chiral [2]catenane **167**.[73] Single Crystal X-ray structure of (*R*,*R*$_{mt}$)-**166** ($C_{72}H_{80}N_6O_5$).

1.8. Applications of Mechanically Interlocked Molecules

The synthesis of mechanically interlocked molecules has progressed significantly since their initial discovery. Attention has now turned to the application of these interlocked molecules. The easily induced, large amplitude conformational changes make interlocked molecules ideal for specific applications, mostly involving shuttling and switching.

It should be noted that the following sections are to demonstrate a range of applications of interlocked molecules and how the synthetic advances above are used in their applications. This is by all means not a thorough review of the applications of interlocked molecules, this will be completed as the introduction to chapter 2 with a focus on interlocked molecules for catalysis, and as the introduction to chapter 3 focussing on molecular shuttles.

1.8.1. Interlocked Molecules in Materials Chemistry

The large amplitude movement possible in interlocked molecules lends them to materials chemistry, and have been used in the development of stimuli responsive materials, self-healing materials and stress dissipating materials.[74] Here examples of polymer rotaxanes will be discussed, exemplifying the application of large amplitude movement in materials chemistry.

1.8.1.1. Slide Ring Polymers

The six, seven and eight membered cyclic oligoglucose, α, β, and γ-CD_X, have inner diameters of 0.44 nm, 0.58 nm and 0.74 nm respectively, and are highly biocompatible making them ideal for materials applications.[75,76] The amphiphilicity of CD_X results in polymer chains threading through the hydrophobic core, leaving only the hydrophilic outer surface in contact with aqueous solvent. Supramolecular cross-linking techniques of these inclusion complexes, have enabled slide-ring materials to be developed.[75,76] Ito and co-workers have used linked α-CD_X as figure of eight cross-links, resulting in materials with high elasticity (over 20 times their length) and solvent absorption (absorbing 24000 times their dry mass). Upon tensile deformation, the material readjusts, distributing the energy across the material.[76]

Takata and co-workers have synthesised rotaxane **168** bearing methacrylate groups on both the stopper and macrocycle, and used these methacrylate rotaxanes as cross-linkers in a butyl methacrylate polymerisation (Figure 42).[77] The rotaxane cross-linked polymers were much tougher than their covalent analogues, with much higher fracture energies (stress and strain). The mechanical properties were also dependent upon axle thickness and mobility of the interlocked cross-link, with the thickest axle (R = Et) having the lowest mobility and lower stretch-ability.

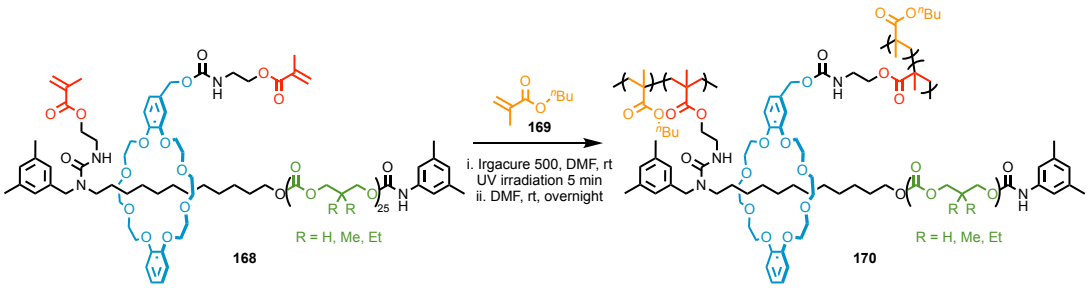

Figure 42: Takata and co-workers' rotaxane cross-linked polymer **170**.[77]

1.8.1.2. Switchable Polymer Morphology

Takata and co-workers have used macromolecular Lariat knots (Figure 43a)[78] and [c2]daisy chains (Figure 43b)[79] to make switchable polymer morphologies. In Figure 43a, protection of the secondary ammonium station causes the macrocycle to shuttle to the more favourable position,[78] resulting in a linear polymer chain. However, upon deprotection and protonation the macrocycle shuttles, bringing the two polymer ends together.[74,78] In Figure 43b, protection of both secondary ammonium stations causes

the [c2]daisy chain to swell as the macrocycles position themselves over the amide units at the end of the polymer chains.[74,79] These Lariat knots and [c2]daisy chains are distinguishable from the cyclic and linear polymers of the same molecular weight by size exclusion chromatography.[74]

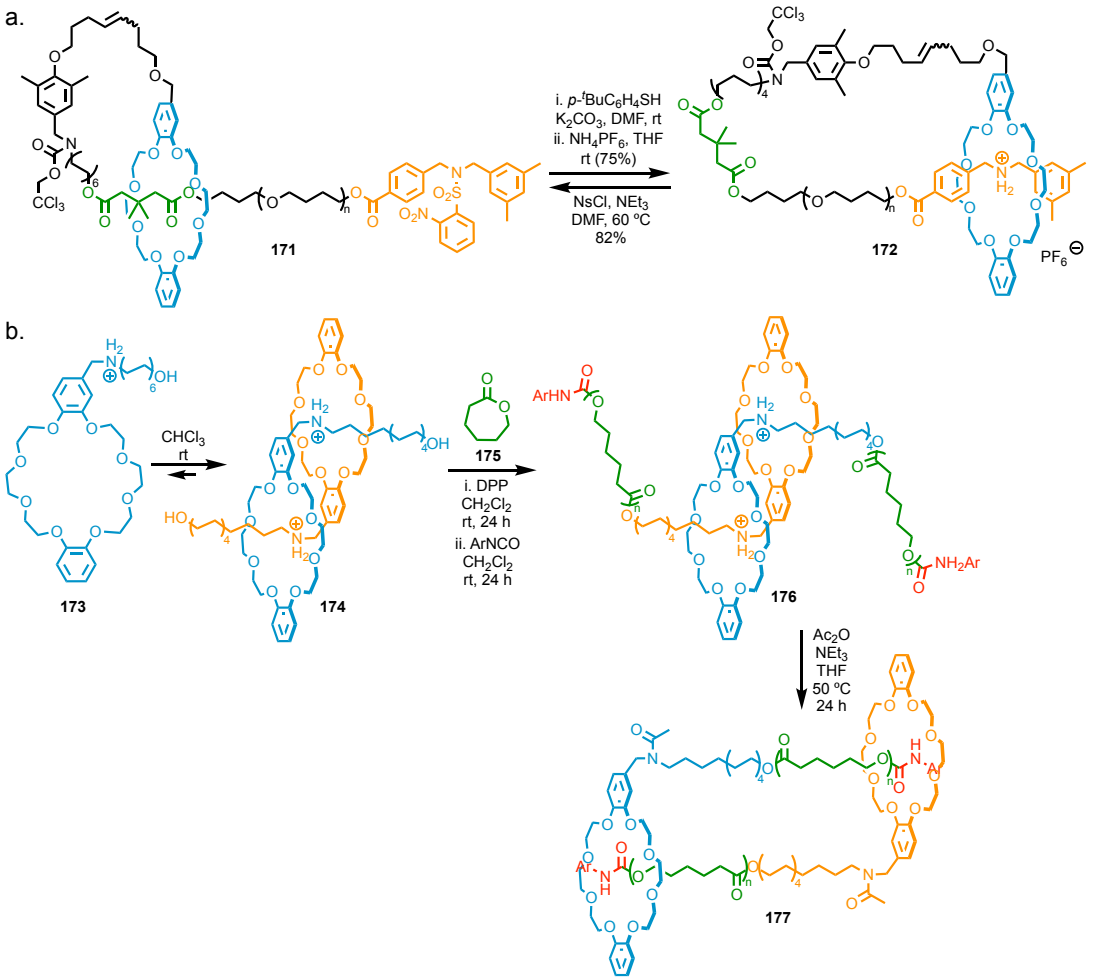

Figure 43: Takata and co-workers' (a) Lariot knot and (b) [c2]daisy chain stimuli responsive polymers. DPP refers to Diphenyl phosphoric acid, Ar = 3,5-di-CF_3-C_6H_3.[74,80]

1.8.1.3. Stress-Dispersing Groups

Ito and co-workers have used CD_X mechanical cross-links to dissipate energy throughout the structure, allowing greater elasticity and strength of their polymers.[75,76,81] De Bo and co-worker have studied the mechanical bond as a protecting group for mechanophore groups (Figure 44). The large amplitude movement of pirouetting in the catenane diverts tension away from a mechanophore, allowing greater control of the mechanical activity of the mechanophore.[82,83] The mechanophore included within the catenane was

protected due to the ability of the mechanical bond to undergo large amplitude conformational changes to remove tensile stress.

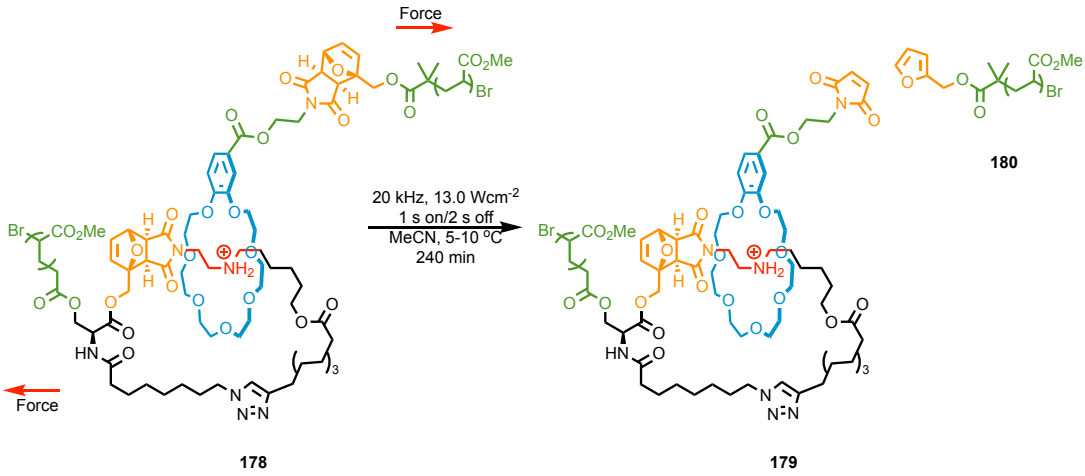

Figure 44: De Bo and co-worker's mechanical protecting group.[83]

1.8.1.4. Isoreticular Interlocked Materials

Beyond polymers, isoreticular materials such as MOFs have been fabricated from rotaxane carboxylate and pyridine ligands. Cucurbit[6]uril pseudorotaxanes have been crystallised into a 2D Cd-MOF structure with cucurbit[6]uril macrocycles aligned in one dimension (Figure 45).[84] The photoluminescent properties of these MOFs were studied for their application as metal sensors (Cd^{II}, Fe^{III}, Co^{II}, Zn^{II}, Ni^{II}, and Cu^{II}). It was found that the Cd^{II} ions enhanced photoluminescence, and Fe^{III} ions quenched it almost completely.[84]

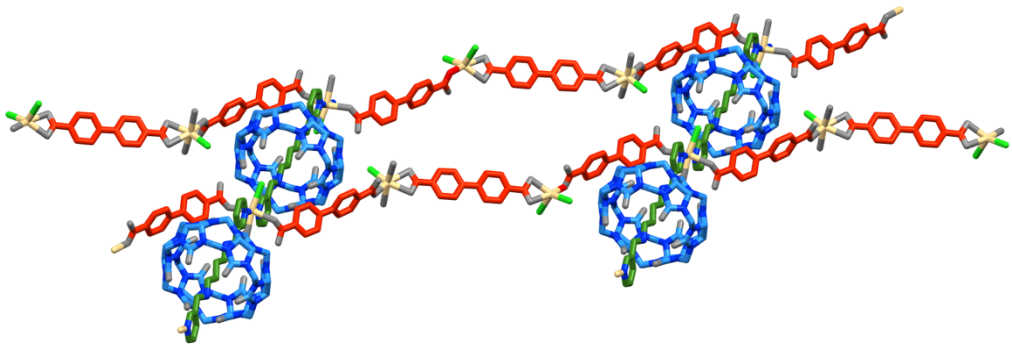

Figure 45: 2D MOF rotaxane with cucurbit[6]uril, $C_{146}H_{164}Cd_3Cl_4N_{56}O_{49}$.[84] An extended series of the asymmetric units are shown to demonstrate the isoreticular structure.

Although rotaxanes are predominantly applied in molecular machines, they are being incorporated into a wide range of materials and offer material properties that were not accessible before.[85]

1.8.2. Interlocked Molecular Sensors

Binding of specific ions is a key component of chemically stimulated shuttling in molecular machines. However, the large change in structure associated with binding often has a change in fluorescence resulting from it.[86] Furthermore, the tight but flexible environment of the mechanical bond makes it ideal for binding unusual guests, such as anions, as the system can reorganise itself to fit the guest.[35,36] Because of these properties, hosts and sensors are being developed from rotaxanes.[87–89] There are numerous examples where the mechanical bond has been used to bind simple cations,[90] anions,[86,91] and lanthanides, through charged interactions,[92] H-bonding,[86,87,89,93] halogen-bonding,[36,88,91,94–97] and chalcogen-bonding.[87–89]

Most notably, Beer and co-workers have exploited highly directional halogen-[36,91,94,95,97] and chalcogen-bonding[95,96] motifs to bind anionic guests. By using anionic templates to synthesise rotaxanes and catenanes, Beer and co-workers have made perfectly sized cavities to bind specific anions with high selectivity.[35]

Beer and co-workers have used a neutral halogen bonding rotaxane, **181**, to create a host with pH switchable binding (Figure 46).[92] When neutral, **181** has strong binding of metal cations. However, when protonated **181** has a strong binding affinity for anions. With cationic guests the binding sites are the basic triazole *N*, whereas when protonated, the anion binding results from halogen bonding and electrostatic attraction.[92]

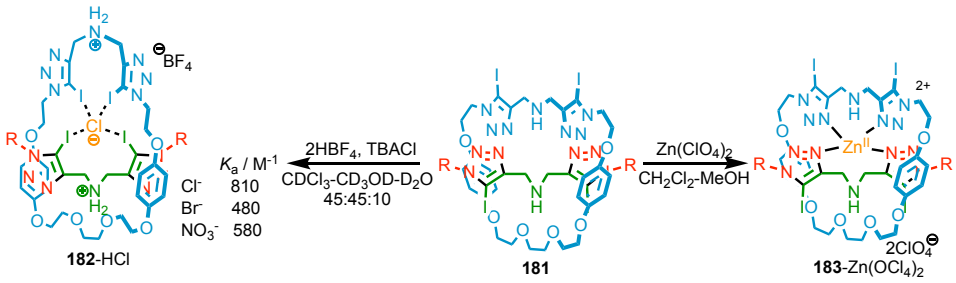

Figure 46: Beer and co-workers' acid-switchable cation/anion host **181**.[92] Association constants were determined in $CDCl_3$-CD_3OD-D_2O 45:45:10. R = $(CH_2)_3OC_6H_4C(C_6H_4$-*t*-$Bu)_3$.

The strong halogen-bonding rotaxanes **184** and **185** have been used to enantioselectively bind chiral anion guests, with up to 3 : 1 selectivity.[91] The chiral axle had significant effects, causing the preferentially bound enantiomer to change. However the axle and macrocycle alone had low selectivity.[91]

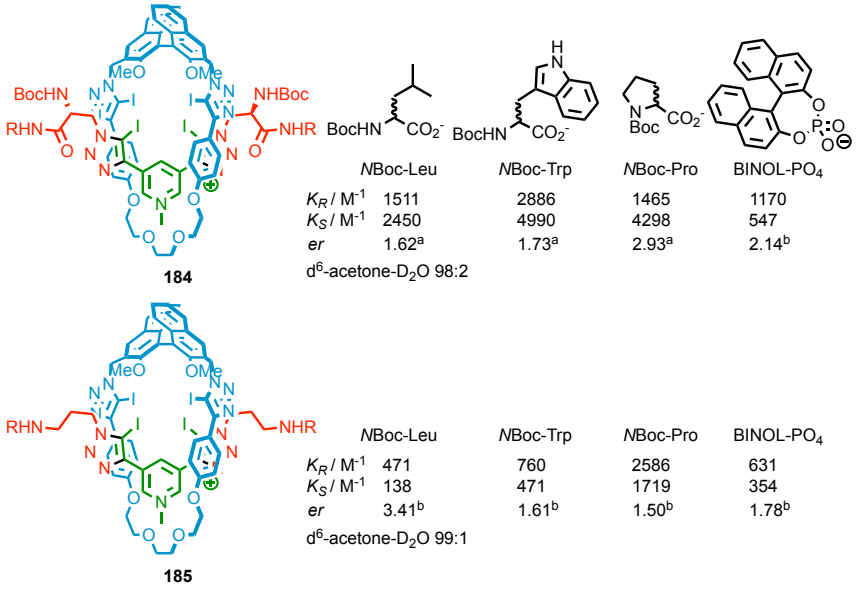

Figure 47: Beer and co-workers' enantioselective anion host **184** and **185**. Association constants determined in d^6-acetone-D_2O 98:2 and 99:1.[91] [a]*er* refers to K_S/K_R, [b]*er* refers to K_R/K_S. R = $C_6H_4C(C_6H_4$-*t*-Bu$)_3$.

Goldup and co-workers have used the mechanical bond to alter the properties of naphthalimide urea to bind anions.[98] This binding moiety plays no role in the synthesis of rotaxane **186**. The cavity of **186** was not designed for the guest, which played no role in the host synthesis. The rotaxane framework was activated allosterically by protonation, thus acting as a ditopic host for an HX ion pair.[98] Applications of the mechanical bond towards binding and sensing take advantage of the unique structural aspects of the supramolecular system and allow binding of otherwise unusual guests.

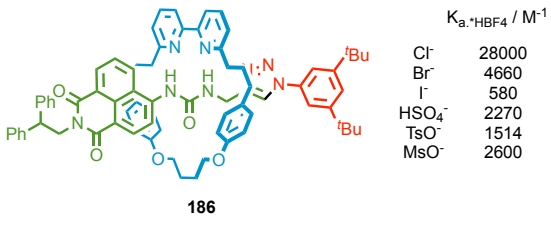

Figure 48: Goldup and co-workers' fluorescent ditopic HX ion sensor. Tetrabutyl ammonium salts of each anion were added to **186**-HBF_4. Association constants determined in $CDCl_3$-CD_3CN 1 : 1.[98]

1.9. Conclusions

The synthesis of mechanically interlocked molecules has made huge progress since the first examples in the 1960s.[6,9,12] Sauvage's passive template,[2,21,24] non-covalent templates,[1,8,29] and Leigh's active template[22,47,51] have increased the synthetic accessibility of these interlocked compounds from approximately 1% yield over may steps, to quantitative yield in a single bond-forming step. The modern, relatively trivial, synthesis of interlocked compounds has enabled their application in molecular machines,[99] and investigation of the fundamental properties of the mechanical bond. Although molecular machines and material applications[74–77,100] of the mechanical bond have been explored extensively,[2,80,99,101–105] one of the most interesting aspects of the mechanical bond, its ability to express chirotopic elements from the assembly of two achiral sub-components, remains under-explored.[65] Recent advances in the synthesis of MPC rotaxanes[67,68] have made these molecules more accessible. This thesis will discuss the synthesis of enantiopure MPC ligands, and the first applications of MPC rotaxanes.

1.10. Bibliography

[1] C. J. Bruns, J. F. Stoddart, *The Nature of the Mechanical Bond - From Molecules to Machines*, John Willey & Sons, Hoboken, New Jersey, **2017**.

[2] J. P. Sauvage, *Angew. Chem. Int. Ed.* **2017**, *56*, 11080–11093.

[3] D. A. Leigh, *Angew. Chem. Int. Ed.* **2016**, *55*, 14506–14508.

[4] D. A. Leigh, J. K. Y. Wong, F. Dehez, F. Zerbetto, *Nature* **2003**, *424*, 128–132.

[5] B. Lewandowski, G. De Bo, J. W. Ward, M. Papmeyer, S. Kuschel, M. J. Aldegunde, P. M. E. Gramlich, D. Heckmann, S. M. Goldup, D. M. D'Souza, *Science* **2013**, *339*, 189–193.

[6] E. Wasserman, *J. Am. Chem. Soc.* **1960**, *82*, 4433–4434.

[7] R. Brückner, *Eur. J. Org. Chem.* **2019**, 3289–3319.

[8] G. Gil-Ramirez, D. A. Leigh, A. J. Stephens, *Angew. Chem. Int. Ed.* **2015**, *54*, 6110–6150.

[9] I. T. Harrison, S. Harrison, *J. Am. Chem. Soc.* **1967**, *89*, 5723–5724.

[10] G. Schill, A. Lüttringhaus, *Angew. Chem. Int. Ed.* **1964**, *13*, 567–568.

[11] G. Schill, *Chem. Ber.* **1967**, *100*, 2021–2037.

[12] G. Schill, *Catenanes, Rotaxanes and Knots*, Academic Press, New York, **1971**.

[13] N. Kameta, K. Hiratani, Y. Nagawa, *Chem. Commun.* **2004**, *4*, 466–467.

[14] H. Kawai, T. Umehara, K. Fujiwara, T. Tsuji, T. Suzuki, *Angew. Chem. Int. Ed.* **2006**, 4281–4286.

[15] L. Steemers, M. J. Wanner, M. Lutz, H. Hiemstra, J. H. Van Maarseveen, *Nat. Commun.* **2017**, *8*, 15392.

[16] C. O. Dietrich-Buchecker, J. P. Sauvage, J. M. Kern, *J. Am. Chem. Soc.* **1984**, *106*, 3043–3045.

[17] M. D. Cornelissen, S. Pilon, L. Steemers, M. J. Wanner, S. Fro, E. Zuidinga, S. I. Jørgensen, J. I. Van Der Vlugt, J. H. Van Maarseveen, *J. Org. Chem.* **2020**, *85*, 3146–3159.

[18] L. Steemers, M. J. Wanner, A. W. Ehlers, H. Hiemstra, J. H. Van Maarseveen, *Org. Lett.* **2017**, *19*, 2342–2345.

[19] Y. Segawa, M. Kuwayama, Y. Hijikata, M. Fushimi, T. Nishihara, J. Pirillo, J. Shirasaki, N. Kubota, K. Itami, *Science* **2019**, *365*, 272–276.

[20] C. O. Dietrich-Buchecker, J. P. Sauvage, *Tet. Lett.* **1983**, *24*, 5091–5094.

[21] C. O. Dietrich-Buchecker, J. P. Sauvage, J. M. Kern, *J. Am. Chem. Soc.* **1984**, *106*, 3043–3045.

[22] M. Denis, S. M. Goldup, *Nat. Rev.* **2017**, *1*, 1–18.

[23] J. E. Beves, B. A. Blight, C. J. Campbell, D. A. Leigh, R. T. Mcburney, *Angew. Chem. Int. Ed.* **2011**, *50*, 9260–9327.

[24] B. Mohr, M. Weck, J. P. Sauvage, R. H. Grubbs, *Angew. Chem. Int. Ed.* **1997**, *36*, 1308–1310.

[25] D. A. Leigh, P. J. Lusby, S. J. Teat, A. J. Wilson, J. K. Y. Wong, *Angew. Chem. Int. Ed.* **2001**, *40*, 1538–1543.

[26] S. M. Goldup, D. A. Leigh, P. J. Lusby, R. T. Mcburney, A. M. Z. Slawin, *Angew. Chem. Int. Ed.* **2008**, *47*, 6999–7003.

[27] H. Ogino, *J. Am. Chem. Soc.* **1981**, *103*, 1303–1304.

[28] S. Dong, J. Yuan, F. Huang, *Chem. Sci* **2014**, *5*, 247–252.

[29] B. P. R. Ashton, T. T. Goodnow, A. E. Kaijer, M. I. Reddington, A. M. Z. Slawin, N. Spencer, J. F. Stoddart, C. Vicent, D. J. Williams, *Angew. Chem. Int. Ed.* **1989**, *28*, 1396–1399.

[30] R. A. Bissell, E. Cordova, A. E. Kaifer, J. F. Stoddart, *Nature* **1994**, *369*, 133–137.

[31] D. B. Amabilino, P. R. Ashton, N. Spencer, J. F. Stoddart, *Angew. Chem. Int. Ed.* **1994**, *33*, 1286–1290.

[32] I. Aprahamian, J. Olsen, A. Trabolsi, J. F. Stoddart, *Chem. Eur. J.* **2008**, *14*, 3889–3895.

[33] Y. Wang, M. Frasconi, J. F. Stoddart, *ACS Cent. Sci.* **2017**, *3*, 927–935.

[34] D. A. Leigh, A. Venturini, A. J. Wilson, J. K. Y. Wong, F. Zerbetto, *Chem. Eur. J.* **2004**, *10*, 4960–4969.

[35] M. S. Vickers, P. D. Beer, *Chem. Soc. Rev.* **2007**, *36*, 211–225.

[36] T. A. Barendt, A. Docker, I. Marques, V. Felix, P. D. Beer, *Angew. Chem. Int. Ed.* **2016**, *55*, 11069–11076.

[37] J. E. M. Lewis, S. M. Goldup, P. D. Beer, S. J. Loeb, *Chem. Soc. Rev.* **2017**, *46*, 2577–2591.

[38] F. Stoddart, *Chem. Soc. Rev.* **2009**, *38*, 1802–1820.

[39] J. E. M. Lewis, J. Winn, S. M. Goldup, *Molecules* **2017**, *22*, 1–12.

[40] S.-J. Rao, Q. Zhang, J. Mei, X.-H. Ye, C. Gao, Q.-C. Wang, D.-H. Qu, H. Tian, *Chem. Sci.* **2017**, *8*, 6777–6783.

[41] E. A. Neal, S. M. Goldup, *Chem. Commun.* **2014**, *50*, 5128–5142.

[42] V. Aucagne, K. D. Hanni, D. A. Leigh, P. J. Lusby, D. B. Walker, *J. Am. Chem. Soc.* **2006**, *128*, 2186–2187.

[43] V. Aucagne, J. Berna, J. D. Crowley, S. M. Goldup, K. D. Hanni, D. A. Leigh, P. J. Lusby, V. E. Ronaldson, A. M. Z. Slawin, A. Viterisi, *J. Am. Chem. Soc.* **2007**, *129*, 11950–11963.

[44] S. Saito, E. Takahashi, K. Nakazono, *Org. Lett.* **2006**, *8*, 5133–5136.

[45] S. Saito, *J. Incl. Phenom. Macrocycl. Chem.* **2015**, *82*, 437–451.

[46] Y. Sato, R. Yamasaki, S. Saito, *Angew. Chem. Int. Ed.* **2009**, *48*, 504–507.

[47] J. D. Crowley, S. M. Goldup, A. L. Lee, D. A. Leigh, R. T. McBurney, *Chem. Soc. Rev.* **2009**, *38*, 1530–1541.

[48] J. D. Crowley, S. M. Goldup, N. D. Gowans, D. A. Leigh, V. E. Ronaldson, A. M. Z. Slawin, *J. Am. Chem. Soc.* **2010**, *132*, 6243–6248.

[49] V. Aucagne, J. D. Crowley, S. M. Goldup, K. D. Ha, D. A. Leigh, P. J. Lusby, V. E. Ronaldson, A. M. Z. Slawin, D. B. Walker, *J. Am. Chem. Soc.* **2007**, *129*, 11950–11963.

[50] P. E. Barran, H. L. Cole, S. M. Goldup, D. A. Leigh, P. R. Mcgonigal, M. D. Symes, J. Wu, M. Zengerle, *Angew. Chem. Int. Ed.* **2011**, *50*, 12280–12284.

[51] S. M. Goldup, D. A. Leigh, T. Long, P. R. Mcgonigal, M. D. Symes, J. Wu, *J. Am. Chem. Soc.* **2009**, *131*, 15924–15929.

[52] C. Romuald, F. Coutrot, *Angew. Chem. Int. Ed.* **2012**, *51*, 2544–2545.

[53] G. De Bo, G. Dolphijn, C. T. Mcternan, D. A. Leigh, *J. Am. Chem. Soc.* **2017**, *139*, 8455–8457.

[54] S. D. P. Fielden, D. A. Leigh, C. T. Mcternan, B. Perez-Saavedra, I. J. Vitorica-yrezabal, *J. Am. Chem. Soc.* **2018**, *140*, 6049–6052.

[55] C. Tian, S. D. P. Fielden, G. F. S. Whitehead, I. J. Vitorica-Yrezabal, D. A. Leigh, *Nat. Commun.* **2020**, *11*, 1–10.

[56] J. E. M. Lewis, R. J. Bordoli, M. Denis, C. J. Fletcher, M. Galli, E. A. Neal, E. M. Rochette, S. M. Goldup, *Chem. Sci.* **2016**, *7*, 3154–3161.

[57] H. Lahlali, K. Jobe, M. Watkinson, S. M. Goldup, *Angew. Chem. Int. Ed.* **2011**, *50*, 4151–4155.

[58] J. Winn, A. Pinczewska, S. M. Goldup, *J. Am. Chem. Soc.* **2013**, *135*, 13318–13321.

[59] C. Nolte, P. Mayer, B. F. Straub, *Angew. Chem. Int. Ed.* **2007**, *46*, 2101–2103.

[60] E. A. Neal, S. M. Goldup, *Chem. Sci.* **2015**, *6*, 2398–2404.

[61] E. A. Neal, S. M. Goldup, *Angew. Chem. Int. Ed.* **2016**, *55*, 12488–12493.

[62] J. E. M. Lewis, J. Winn, L. Cera, S. M. Goldup, *J. Am. Chem. Soc.* **2016**, *138*, 16329–16336.

[63] F. Modicom, E. M. G. Jamieson, E. Rochette, S. M. Goldup, *Angew. Chem. Int. Ed.* **2019**, *58*, 3875–3879.

[64] J. E. M. Lewis, F. Modicom, S. M. Goldup, *J. Am. Chem. Soc.* **2018**, *140*, 4787–4791.

[65] E. M. G. Jamieson, F. Modicom, S. M. Goldup, *Chem. Soc. Rev.* **2018**, *47*, 5266–5311.

[66] C. Yamamoto, Y. Okamoto, T. Schmidt, R. Jager, F. Vogtle, *J. Am. Chem. Soc.* **1997**, *119*, 10547–10548.

[67] R. J. Bordoli, S. M. Goldup, *J. Am. Chem. Soc.* **2014**, *136*, 4817–4820.

[68] M. A. Jinks, A. De Juan, M. Denis, C. J. Fletcher, M. Galli, E. M. G. Jamieson, F. Modicom, Z. Zhang, S. M. Goldup, *Angew. Chem. Int. Ed.* **2018**, *57*, 14806–14810.

[69] A. W. Heard, S. M. Goldup, *Chem* **2020**, *6*, 994–1006.

[70] C. Tian, S. Fielden, B. Pérez-saavedra, I. J. Vitorica-yrezabal, D. A. Leigh, *J. Am. Chem. Soc.* **2020**, *142*, 9803–9808.

[71] E. M. G. Jamieson, S. M. Goldup, *Nat. Chem.* **2019**, *11*, 765–767.

[72] S. Corra, C. De Vet, J. Groppi, M. La Rosa, S. Silvi, M. Baroncini, A. Credi, *J. Am. Chem. Soc.* **2019**, *141*, 9129–9133.

[73] M. Denis, J. E. M. Lewis, F. Modicom, S. M. Goldup, *Chem* **2019**, *5*, 1512–1520.

[74] T. Takata, *ACS Cent. Sci.* **2020**, *6*, 129–143.

[75] K. Ito, *Chem. Pharm. Bull.* **2017**, *65*, 326–329.

[76] J. Araki, K. Ito, *Soft Matter* **2007**, *3*, 1456–1473.

[77] J. Sawada, D. Aoki, H. Otsuka, T. Takata, *Angew. Chem. Int. Ed.* **2019**, *58*, 2765–2768.

[78] K. Nakazono, T. Ogawa, T. Takata, *Mater. Chem. Front.* **2019**, *3*, 2716–2720.

[79] D. . Aoki, G. . Aibara, S. . Uchida, T. A. Takata, *J. Am. Chem. Soc.* **2017**, *139*, 6791–6795.

[80] A. W. Heard, S. M. Goldup, *ACS Cent. Sci.* **2020**, *6*, 117–128.

[81] A. S. D. Sandanayaka, G. Pagona, J. Fan, N. Tagmatarchis, M. Yudasaka, S. Iijima, Y. Araki, O. Ito, *J. Mater. Chem.* **2007**, *17*, 2540.

[82] M. Zhang, G. De Bo, *J. Am. Chem. Soc.* **2018**, *140*, 12724–12727.

[83] M. Zhang, G. De Bo, *J. Am. Chem. Soc.* **2020**, *142*, 5029–5033.

[84] X. Wu, J. Liang, X. Hu, X. Wang, B. Song, Y. Jiao, Z. Su, *Cryst. Growth Des.* **2015**, *15*, 4311–4317.

[85] S. Mena-Hernando, E. M. Perez, *Chem. Soc. Rev.* **2019**, *48*, 5016–5032.

[86] M. Denis, J. Pancholi, K. Jobe, M. Watkinson, S. M. Goldup, *Angew. Chem. Int. Ed.* **2018**, *57*, 5310–5314.

[87] R. Hein, P. D. Beer, J. J. Davis, *Chem. Rev.* **2019**, *120*, 1888–1935.

[88] J. Y. C. Lim, P. D. Beer, *Chem* **2018**, *4*, 731–783.

[89] K. M. Bak, K. Porfyrakis, J. J. Davis, P. D. Beer, *Mater. Chem. Front.* **2020**, *4*, 1052–1073.

[90] M. Denis, J. Pancholi, K. Jobe, S. M. Goldup, *Angew. Chem. Int. Ed.* **2018**, *57*, 5310–5314.

[91] J. Y. C. Lim, I. Marques, V. Felix, P. D. Beer, *J. Am. Chem. Soc.* **2017**, *139*, 12228–12239.

[92] X. Li, J. Y. C. Lim, P. D. Beer, *Chem. Eur. J.* **2018**, *24*, 17788–17795.

[93] M. S. Vickers, P. D. Beer, M. S. Vickers, *Chem. Soc. Rev.* **2007**, *36*, 211–225.

[94] A. Borissov, J. Y. C. Lim, A. Brown, K. E. Christensen, A. L. Thompson, M. D. Smith, P. D. Beer, *Chem. Commun.* **2017**, *53*, 2483–2486.

[95] A. Borissov, I. Marques, J. Y. C. Lim, V. Felix, M. D. Smith, P. D. Beer, *J. Am. Chem. Soc.* **2019**, *141*, 4119–4129.

[96] A. J. Y. C. Lim, J. Y. Liew, P. D. Beer, *Chem. Eur. J.* **2018**, *24*, 14560–14566.

[97] T. Bunchuay, A. Docker, A. J. Martinez-, P. D. Beer, *Angew. Chem. Int. Ed.* **2019**, *58*, 13823–13827.

[98] M. Denis, L. Qin, P. Turner, K. A. Jolliffe, S. M. Goldup, *Angew. Chem. Int. Ed.* **2018**, *57*, 5315–5319.

[99] S. Erbas-cakmak, D. A. Leigh, C. T. Mcternan, A. L. Nussbaumer, *Chem. Rev.* **2015**, *115*, 10081–10206.

[100] T. Kureha, D. Aoki, S. Hiroshige, K. Iijima, D. Aoki, T. Takata, D. Suzuki, *Angew. Chem. Int. Ed.* **2017**, *56*, 1–5.

[101] E. R. Kay, D. A. Leigh, F. Zerbetto, *Angew. Chem. Int. Ed.* **2007**, *46*, 72–191.

[102] J. F. Stoddart, *Angew. Chem. Int. Ed.* **2017**, *56*, 11094–11125.

[103] I. Aprahamian, *ACS Cent. Sci.* **2020**, *6*, 347–358.

[104] J. Collin, C. Dietrich-buchecker, M. C. Jimenez-molero, J. Sauvage, *Acc. Chem. Res.* **2001**, *34*, 477–487.

[105] R. D. Astumian, *Phys. Chem. Chem. Phys.* **2007**, *9*, 5067–5083.

Chapter 2: Synthesis of A Mechanically Planar Chiral Rotaxane Ligand for Enantioselective Catalysis

Abstract: Enantiopure mechanically interlocked Au^{I}-complexes with a single chirotopic element, originating from the orientation of the macrocycle in the mechanical bond, have been synthesised. These enantiopure complexes have been used to mediate Au^{I}-catalysed cyclopropanation reactions of 2-methyl-3-butyn-2-yl esters with alkenes.

Optimisation of catalytic reaction conditions and substrate screening has achieved enantiomeric excesses of up to 79%. Although mechanically planar chiral Au^{I}-catalysts lack generality, and their synthesis is challenging, this initial study demonstrates exciting potential of a new class of chiral ligand.

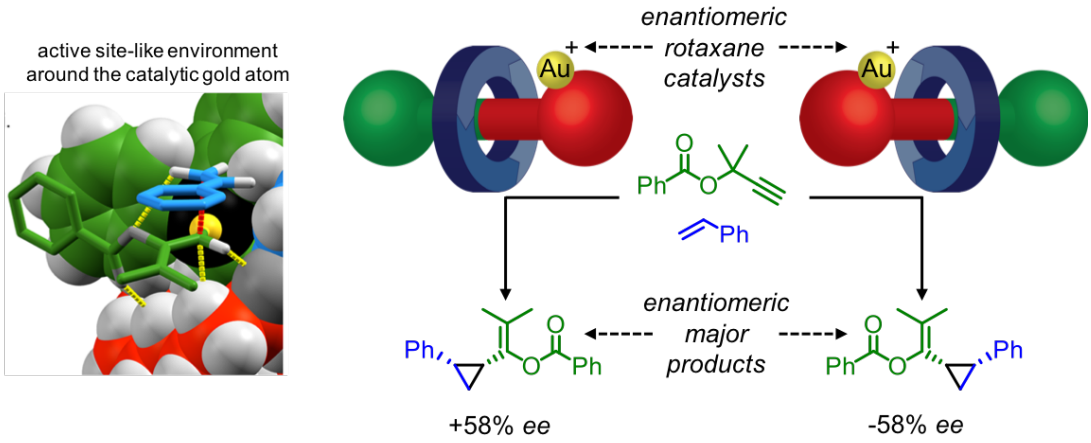

Computational modelling was completed by S. M. Goldup, all other work in this chapter was completed by the author.

Prior publication: A. W. Heard, S. M. Goldup, *Chem*, **2020**, *6*, 994-1006.

2.1. Introduction: Interlocked Molecules in Catalysis

This chapter details the synthesis of rotaxanes displaying mechanically planar chirality (MPC), and the application of these molecules to Au^{I}-catalysis. Due to the broad nature of the project, the introduction below covers: applications of mechanically interlocked molecules in catalysis; an overview of asymmetric Au^{I}-catalysis; and supramolecular strategies in Au^{I}-catalysis. As Au^{I}-catalysis is such an extensive field in itself, the introduction aims to explain the underlying relativistic effects which make Au interesting, and why enantioselective Au^{I}-catalysis is challenging. Notable examples of enantioselective Au^{I}-catalysts are discussed, to highlight the prominent approaches to asymmetric Au^{I}-catalysis. However, this is by no means an extensive review of enantioselective Au^{I}-catalysis.

2.1.1. Mechanically Interlocked Catalysts

As a result of recent advances in the synthesis of mechanically interlocked molecules (detailed in Chapter 1), attention has turned towards the applications of these compounds, typically in molecular machines,[1–7] host-guest chemistry,[8,9] catalysis,[10] and in materials chemistry.[11–15] Closely bound interlocked systems with two sub-components are attractive for molecular machines and switchable catalysis because of the large amplitude conformational changes that shuttling can induce.[16–18] In rotaxanes, activity and selectivity can be regulated by the position of a bulky ring.[19] The unique crowded environment at the centre of the mechanical bond allows different reactivities, chemo-, and stereoselectivities to be achieved.

The first demonstration of rotaxanes being used as catalysts was developed by Rowan, Nolte and co-workers.[20] Inspired by nature's ability to manipulate biopolymers, they developed a Mn^{III}-porphyrin epoxidation catalyst that traverses a polybutadiene axle modifying each repeat unit.[20] A glycoluril cavity, capped with a Mn^{III}-porphyrin, could bind the polybutadiene substrate through solvophobic interactions. With a bulky axial ligand on the opposite face of the porphyrin, the complex could preferentially oxidise the axle within the cavity (80%) (Figure 49a). However, at this point it was unclear as to whether the catalyst was proceeding randomly or in sequentially processive manner.[20] The exterior axial ligand was essential to inhibiting the exterior catalytic turnover and

increasing interior-selectivity. Subsequent studies indicated that the mechanism was most likely to be a random sliding process.[21]

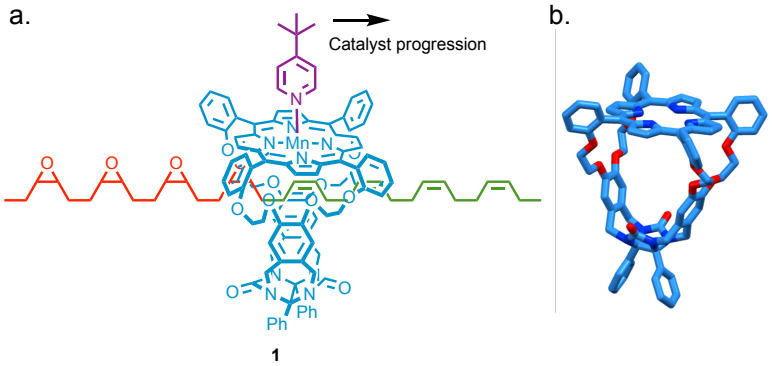

Figure 49: (a) Rowan and Nolte and co-workers' polybutadiene epoxidation catalyst **1**. The Mn bearing macrocycle traverses the polybutadiene axle, oxidising alkene functional groups as it progresses.[22] (b) X-Ray crystal structure of porphyrin macrocycle.[22]

In later studies, polymers with terminal viologen trapping units followed by a bulky stopper were synthesised. One end of the polymer remained unstoppered, allowing the macrocycle to thread onto the polymer *in situ*, then travels along the polymer until reaching the thermodynamic trap. Kinetic studies, realised by complex-induced quenching of the porphyrin fluorescence,[21] indicated velocities of 14 pm.s^{-1} for polybutadiene and 750 pm.s^{-1} for polytetrahydrofuran, implying a random oxidation process as velocity exceeded turnover frequency.[20,21]

The work of Rowan, Nolte and co-workers was the first example of a catalytic application of rotaxanes, and demonstrates the proximity effects and mobility that the mechanical bond has to offer. Although epoxidation is not a ground-breaking modification to the backbone, it demonstrated the fundamental properties of interlocked catalysis, and provided a useful technique to study polymer properties and traversing rates.[20,21,23,24]

Takata and co-workers have used Pd^{II}-bearing macrocycles to catalyse the rearrangement of propargyl and allyl urethanes in the axle (Figure 50).[25] The successive cyclisation of the propargyl ureas transported the Pd^{II}-macrocycle along the axle to the next pyridine station.[25] In addition, this reaction was quantitative with a non-stoppered axle and catalytic amount of Pd^{II}-macrocycle.

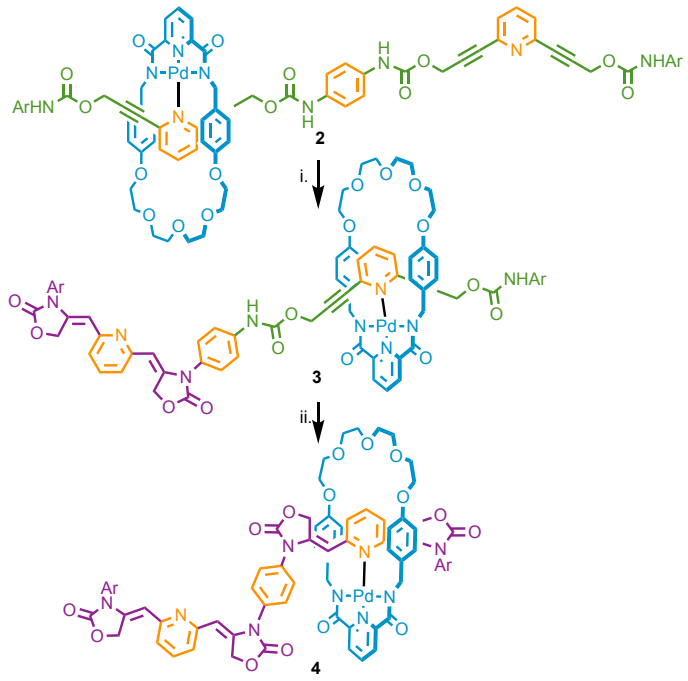

Figure 50: Takata and co-workers' Pd^{II}-catalyzed oxazolidinone formation.[25] i. $Mg(OMe)_2$ (0.4 M), MeOH-THF, reflux, 1 min (16%). ii. $Mg(OMe)_2$ (0.4 M), MeOH-THF, reflux, 90 min (99%). Ar = $C_6H_4C(C_6H_4$-*t*-$Bu)_3$.

2.1.2. Asymmetric Interlocked Catalysts

Takata and co-workers have synthesised chiral rotaxanes with (*R*)-1,1'-bi-2-naphthol (BINOL) macrocycles and axles bearing pendant thiazolium moieties.[11] (*R*)-**6** mediated asymmetric benzoin condensations achieving modest *ee* of up to 32% (Figure 51a).[11] The enantioselectivity decreased as the distance between the macrocycle and the thiazolium unit increased. This work demonstrated that the close proximity provided by the mechanical bond was useful for transferring chiral information to an achiral catalytic centre on the axle. Longer axles increased the distance between the chiral macrocycle and the catalytic axle moiety, resulting in decreased enantioselectivity.

Takata and co-workers later demonstrated highly enantioselective acylation of *meso*-diols, catalysed by an achiral pyridine-bearing axle threaded through the same atropisomeric C_2-symmetric crown ether (Figure 51b).[12] By bringing the catalytic pyridine moiety closer to the mechanical bond, and with a more rigid axle, (*R*)-**10** achieved >99% yield and 98% *ee* at -80 °C.[12] At room temperature (*R*)-**10** achieved >99% yield and 78% *ee*, whereas the non-interlocked analogue only achieved 46% yield and 8% *ee*.[12] Furthermore, by changing the orientation of the pyridine moiety, different enantioselectivities were observed. The enantioselectivity dropped off as the pyridine

was oriented away from the mechanical bond, demonstrating that subtle modifications to the active site alter the chiral environment of the mechanical bond.[12]

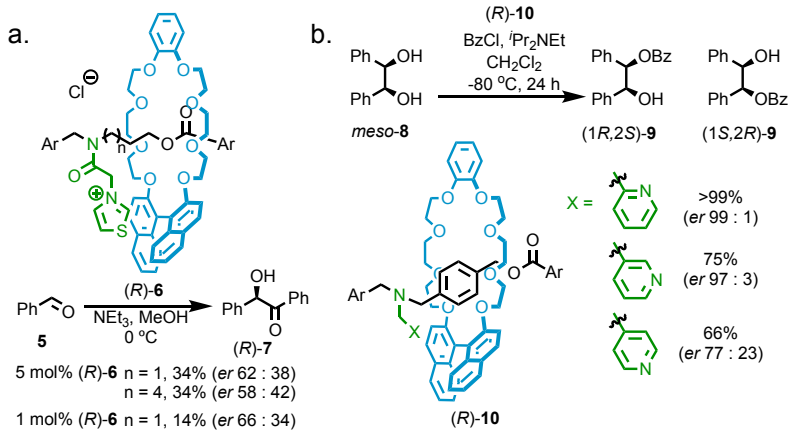

Figure 51: Takata and co-workers' (a) enantioselective rotaxane benzoin condensation catalyst (*R*)-**6**, demonstrating proximity effects related to axle length,[11] and (b) enantioselective acyl transfer catalyst (*R*)-**10**.[12] Ar = 3,5-di-*t*-Bu-C_6H_3.

Leigh and co-workers have reported a Goldberg active template rotaxane synthesis using a C_2-symmetric cyclohexyldiamine macrocycle (Figure 52).[26] The chiral rotaxane ligand (*R*,*R*)-**11** mediated asymmetric Michael additions to β-nitrostyrene with 86% *ee* of (*S*)-**15**. The enantioselectivity was significantly enhanced compared to the non-interlocked ligand (*R*,*R*)-**12**, 36% *ee*.[26] The increased steric bulk of the interlocked ligand improved enantioselectivity, however decreased catalytic activity significantly with time required for complete conversion increasing from 2 d to 27 d. This example demonstrates that the mechanical bond is a useful motif for increasing the steric bulk surrounding the ligand, however as a result of this is decreased catalyst turnover frequency.[26]

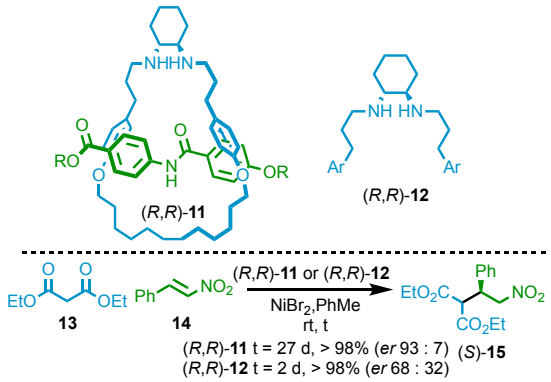

Figure 52: Leigh and co-workers' enantioselective mechanically interlocked ligand (*R*,*R*)-**11** for Ni catalysed Michael addition.[26] R = $(CH_2)_3OC_6H_4C(C_6H_4$-*t*-$Bu)_3$. Ar = C_6H_4OMe.

Niemeyer and co-workers have developed chiral homo[2]catenanes containing (*S*)-BINOL derived phosphoric acids. (*S*,*S*)-**17** was used in combination with Hantzsch ester **18**, for enantioselective transfer hydrogenation of quinoline **16** (Figure 53). (*S*,*S*)-**17** achieved good yields of **19** and up to 84% *ee*, far exceeding the non-interlocked analogues.[10]

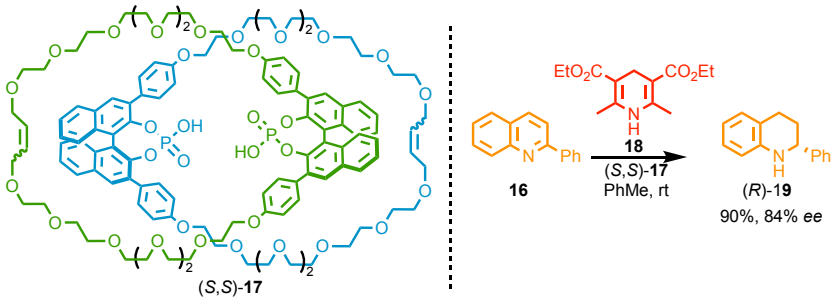

Figure 53: Niemeyer and co-workers' mechanically interlocked phosphoric acid co-catalysts for asymmetric reductions of **16**.[10]

Experimentally it was observed that the non-interlocked macrocycle gave 44 : 56 *er* ((*R*)-**19** : (*S*)-**19**) at 2.5 mol% catalyst loading, but at higher catalyst loading 55 : 45 *er* was observed.[10] The inverted selectivity at higher catalytic loading was attributed to the dimeric complex becoming the dominant pathway at higher catalyst concentration (Figure 54). The interlocked catalyst (*S*,*S*)-**17**, which prefers the dimer pathway, had 92 : 8 *er* at 2.5 mol% loading. Calculations further confirmed that the selectivity of the interlocked catalyst originates from the dimer complex, and therefore the much higher enantioselectivity is attributed to the higher local catalyst concentration and favoured dimer formation resulting from the mechanical bond.[10] The mechanical bond provides a bulkier chiral environment, enhancing enantioselectivity. However, it also changes the dominant mechanism from unimeric to dimeric, causing a change in the dominant enantiomer of product.

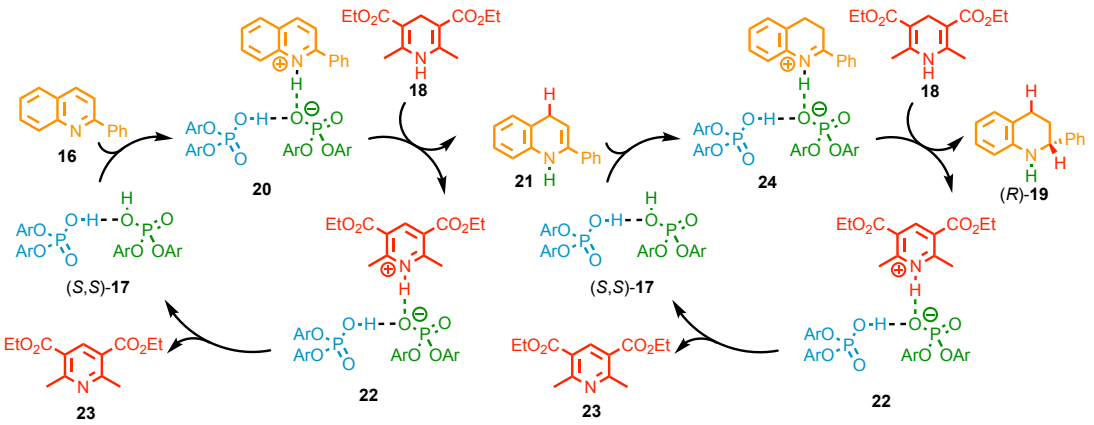

Figure 54: Mechanism of favourable dimeric pathway of enantioselective reduction.[10]

Niemeyer and co-workers have reported a bifunctional rotaxane organocatalyst (Figure 55).[27] The utilisation of the mechanical bond to bind both catalytic components together enhances both enantioselectivity and turnover frequency. This methodology capitalises on the mechanical bond to improve stereoselectivity up to 53% *ee*, but also to enhance otherwise slow reactions.[27] The non-interlocked axle-macrocycle catalytic mixture achieved consistently lower yields and enantioselectivities, demonstrating the ability of the mechanical bond to bind two catalytic units together and enhance their catalytic activity.[27]

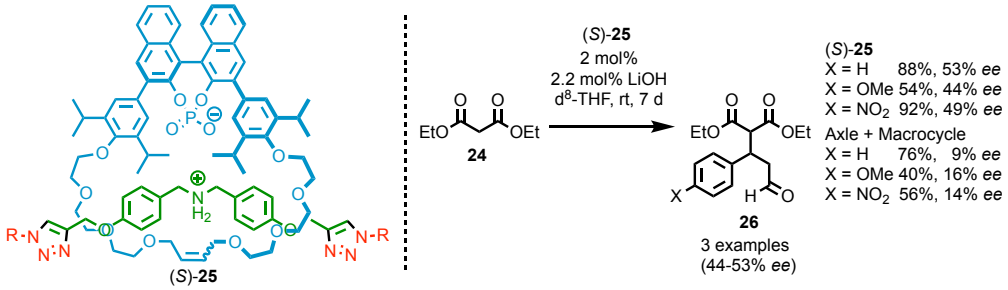

Figure 55: Niemeyer and co-workers' bifunctional rotaxane organocatalyst (*S*)-**25**.[27] R = $C_6H_4C(C_6H_4Ph)_3$.

Berná and co-workers reported a prolinamide axle **27** and rotaxane **28** which showed opposite enantioselectivity for the Michael addition of ketones to β-nitrostyrene, despite containing the same absolute stereochemistry of the covalent stereogenic element (Figure 56).[28] The presence or absence of the macrocycle encircling the catalytic prolinamide centre resulted in enantio-divergent products. Although not a general observation, the influence of the mechanical bond on transition state and chiral induction is so significant as to give the opposite selectivity.[28] The accompanying DFT calculations showed 7.0 kJ.mol^{-1} *Si*-face and 7.3 kJ.mol^{-1} *Re*-face energy difference upon approach of β-nitrostyrene for **27** and **28** respectively. The preference for *Si*-face attack

with **27** was attributed to an NH-ONO H-bond to the fumaramide N-H, whereas the *Re*-face preference with **28** was attributed to an NH-ONO H-bond to the macrocycle amide. The mechanical bond fundamentally changes the enantiocontrol, forming enantio-divergent products. By incorporating a lactam macrocycle around an amide stabilised transition state, the absolute stereochemical outcome is switched.[28]

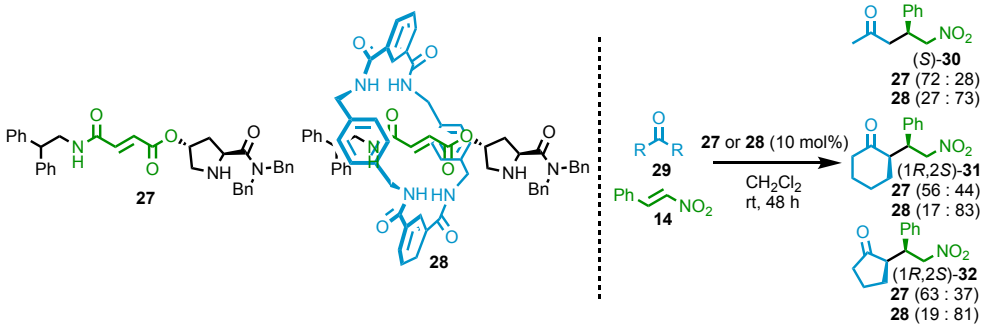

Figure 56: Berná and co-workers' enantio-divergent Michael addition catalysts.[28] Major *syn*-diastereoisomer products shown. Complete conversion of starting material was observed for all substrates.

Berná and co-workers have used the mechanical bond to alter the chiral environment and enhance enantioselectivity of prolinamide organocatalysts (Figure 57).[29] The mechanical bond itself had only a small effect on the enantioselectivity, compared to the non-interlocked axle. However, the diacyl pyridine template also behaves as a H-bond donor-acceptor-donor (DAD) host for acceptor-donor-acceptor (ADA) guests.[29] The binding of organic co-factors significantly changes the chiral environment which the catalytic unit occupies, causing changes in activity and enantioselectivity. Catalyst **34b** only achieved 8% *ee* for Michael addition across β-nitrostyrene. However, upon binding the organic co-factor, enantioselectivity increased to 82% *ee* of (*R*)-**30** (catalyst **35b**). With the other screened reactions, the co-factor caused a reduction in enantioselectivity. However, scope for multiple imide co-factors is large and the regulation of enantioselectivity through guest binding is an exciting facet of these interlocked catalysts.[29]

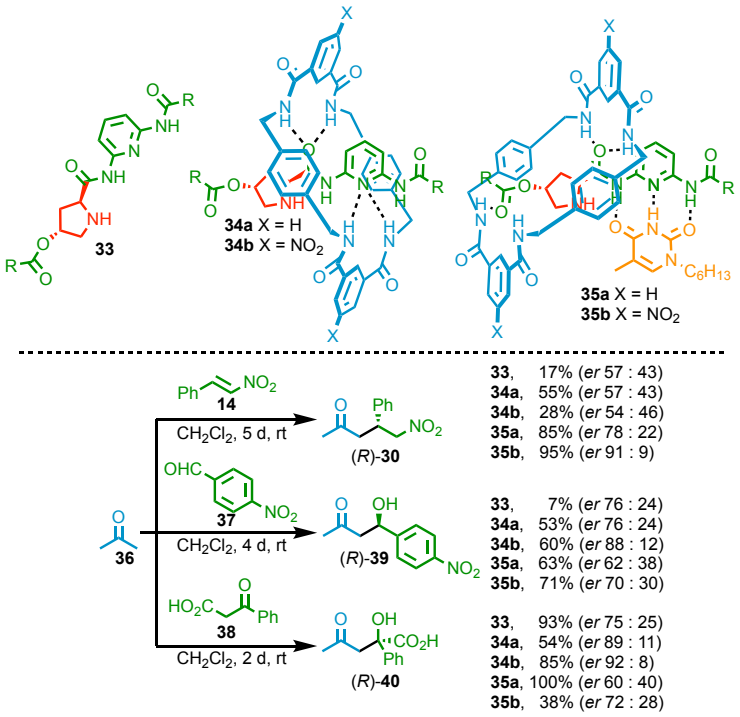

Figure 57: Berná and co-workers' organic substrate regulated enantioselective prolinamide catalyst.[29] R = CH_2CHPh_2.

Loeb and co-workers have developed a frustrated Lewis base for the activation of hydrogen in the presence of a borane Lewis acid.[30] The mechanical bond plays a dual role in the stability of the frustrated Lewis pair, both increasing the basicity of the secondary amine, and sterically protecting the secondary ammonium **42**. This activation of hydrogen demonstrates some of the potential benefits of including mechanical bonds in catalyst structure design, although this system is not catalytic itself.[30]

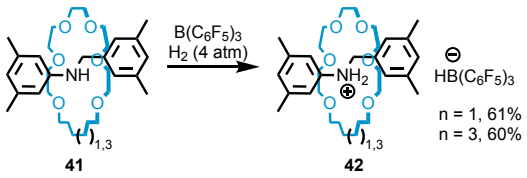

Figure 58: Loeb and co-workers' frustrated Lewis Base Rotaxane **41** for H_2 activation.[30]

Nishibayashi and co-workers reported an asymmetric hydrogenation catalyst with an atropisomeric BINOL component as well as an interlocked stereogenic element (Figure 59).[31] The C_1-symmetric crown ether ligand contains both a chiral phosphite ligand, and a non-centrosymmetric macrocycle. When the protonated ligand is complexed to Rh^I, a *pseudo*-Lariat knot forms. In the original report it is commented that when the two ligands are mixed, a mixture of two mechanical planar diastereoisomers form in the *pseudo*-rotaxane. However upon $[Rh(cod)_2]PF_6$ addition, the *pseudo*-rotaxane forms one

diastereoisomer of the *pseudo*-Lariat knot.[31] This Rh^{I}-complex mediated the hydrogenation of **43** in an impressive 77% *ee* and full conversion. However, when deprotonated, only 6% conversion was achieved. At 0 °C, 10 substrates were reported with full conversion and 90-96% *ee*. It is unclear as to whether the chiral induction is a result of the phosphite ligand or the MPC stereogenic element.

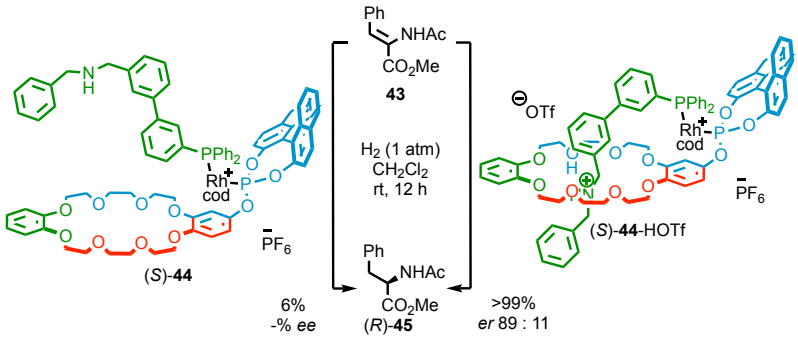

Figure 59: Nishibayashi and co-workers' chiral interlocked Rh^{I}-ligand.[26] cod = 1,5-cyclooctadiene.

2.1.3. Switchable Mechanically Interlocked Catalysts

Molecules which can reversibly change structure or conformation on application of an external stimulus (light, temperature, chemical, electrochemical or entropic) are attractive for molecular machines, switches, logic gates and memory devices.[32] Rotaxanes are attractive for stimuli driven switch applications, because of the relative ease by which a macrocycle can shuttle from one binding site to another.

Leigh and co-workers have developed a pH-switchable rotaxane organocatalyst **48** that mediates the Michael addition of **47** to **46** (Figure 60).[18] The crown ether macrocycle has highest affinity for the secondary ammonium station. However, when deprotonated, it shuttles to the cationic triazolium station. The dicationic rotaxane **48** mediated the iminium organocatalysis, with 83% yield after 5 d. Upon protonation, the ^{1}H NMR spectrum demonstrated characteristic increased shift of the benzylamine aromatic signals, indicating movement of the macrocycle to the ammonium station. When the macrocycle occupies the ammonium station, no conversion was observed, whereas the protonated axle itself mediated the reaction in 49% yield. The switchable rotaxane shuttle demonstrates activity regulation through chemical stimuli, drawing the comparison to enzymes.[18] Here the mechanical bond plays a key role in activity regulation, concealing the catalytic unit effectively. An additional effect of the mechanical bond is an increase in the basicity of the secondary amine.

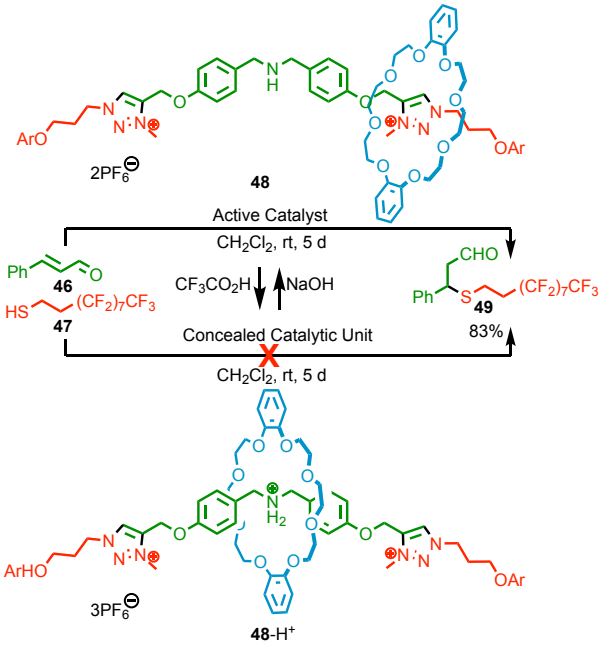

Figure 60: Leigh and co-workers' switchable organocatalyst.[18] Ar = 3,5-di-*t*-Bu-C_6H_3.

Cheng, Chui and co-workers have also developed an on-off switchable rotaxane catalyst (Figure 61).[33] It was hypothesised that the on-off activity came from macrocycle pirouetting, achieving 66% yield for the Michael addition of diethyl malonate to β-nitrostyrene. Only 2% yield was observed for the non-interlocked axle, macrocycle and Na^+ ion. Molecular dynamics simulations calculated that **49**-Na^+ could accommodate both enolate and β-nitrostyrene within 5 Å.[33] The pirouetting, rather than shuttling, mode of switchable catalysis exploits the rotational flexibility of the mechanical bond and removes the requirement of complex catalyst synthesis. Pirouetting switchable catalysts are yet to display the same broad scope as shuttling interlocked molecules.

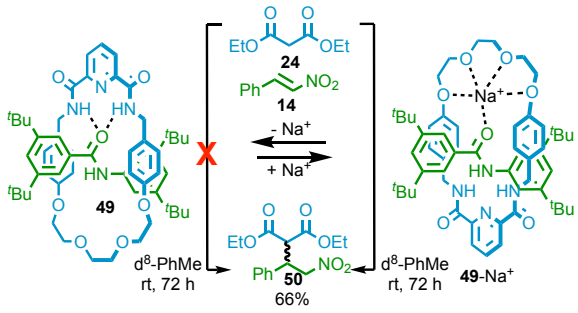

Figure 61: Cheng, Chui and co-workers' pirouetting Lewis acid catalyst.[33]

Leigh and co-workers have used rotaxane **52** to catalyse the decarboxylative decomposition of Cl_3CCO_2H, with one of the two rotaxane states catalysing the hydrogenation of β-nitrostyrene (Figure 62).[34] Rotaxane **52** is a pulsed switchable

catalyst, activated in the protonated state, slowly relaxing to the deactivated state as the chemical input is consumed. The trivial decarboxylation catalysis occurring allows pulsed switching between two states.

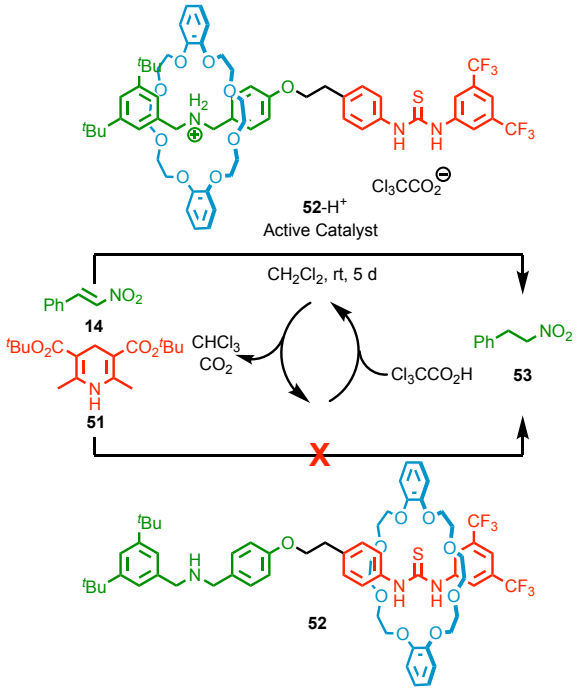

Figure 62: Leigh and co-workers' pulsed on-off switchable catalyst.[34]

Subsequent to the initial switchable catalyst **48** (Figure 60), a chiral analogue with a stereogenic centre next to the secondary amine (**56**, Figure 63), led to 80-84% *ee* of **57**. This was comparable to the non-interlocked axle, 70% *ee*.[17] Furthermore, the non-interlocked catalyst showed 50% conversion when protonated, whereas the interlocked catalyst showed 0% conversion, demonstrating the significance of the macrocycle for switchable catalytic activity as well as enantioselectivity.[17,35,36]

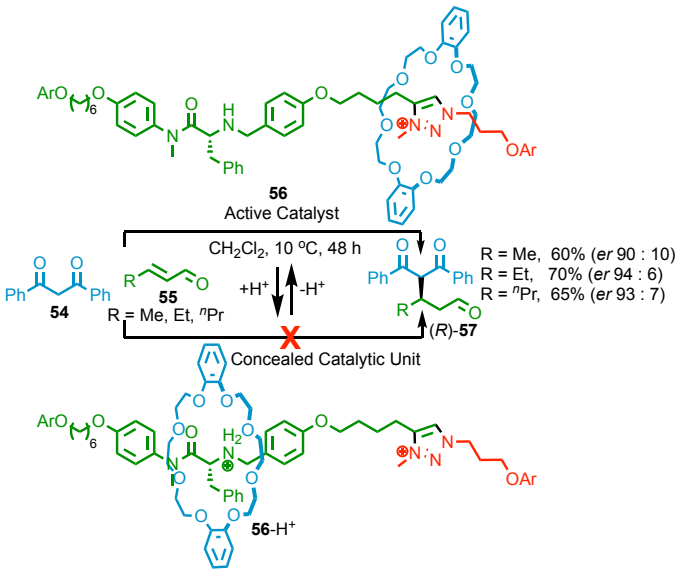

Figure 63: Leigh and co-workers' switchable asymmetric organocatalyst.[17] Ar = 3,5-di-*t*-Bu-C_6H_3. Counter-ion omitted for clarity.

Leigh and co-workers have reported a rotaxane catalyst which can be switched between two modes of organocatalysis, and is thus able to select reagents from a mixture depending on its state (Figure 64).[36] Rotaxane **58** consisted of a secondary ammonium station and a squaramide station. When protonated, the macrocycle occupies the ammonium station, leaving the squaramide catalytic unit free to act as a catalyst. However, when deprotonated, the macrocycle occupies the squaramide station, allowing the secondary amine to mediate the iminium catalysis.[36] The switchable substrate selectivity, through iminium or H-bond catalytic modes, demonstrates control of chemical synthesis by artificial catalysts.

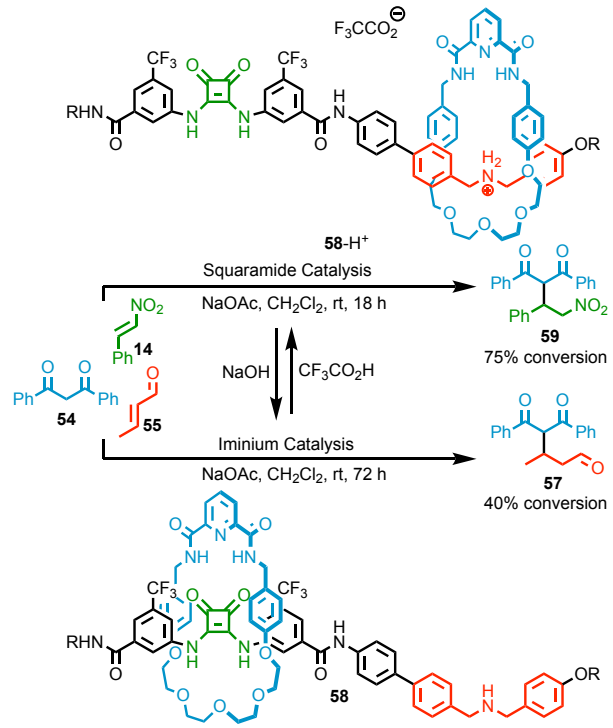

Figure 64: Leigh and co-workers' H-bond iminium switchable organocatalyst.[36] R = $(CH_2)_3OC_6H_4C(C_6H_4\text{-}t\text{-}Bu)_3$.

Leung and co-workers developed a similar system, with a thiourea H-bond activation catalyst and secondary amine catalyst, to mediate switchable Michael additions with similar results (Figure 65).[37] Where this system differs from Leigh and co-workers', is that it was coupled to an anthracene fluorophore. This catalyst mediates Michael additions depending on solution pH, whilst it is also possible to monitor the macrocycle position by fluorescence.[37] The anthracene fluorescence intensity was enhanced when the macrocycle occupied the closer ammonium station (**60**-HPF_6), thereby indicating when thiourea H-bond activated catalysis is possible. Leung and co-workers combined switchable catalysis and switchable fluorescence to make a system whereby the state of the catalyst was visible by fluorescence spectroscopy.[37]

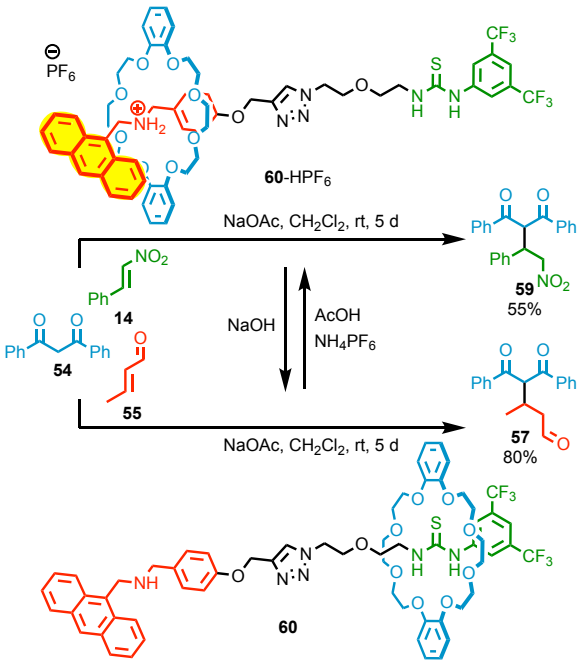

Figure 65: Leung and co-workers' substrate selective dual organocatalyst.[37]

Leigh and co-workers have developed a switchable, dual-function rotaxane catalyst with anion-binding catalytic moieties.[38] The rotaxane **62**-H^+ promoted bromide anion abstraction through H-bonding to the triazolium C-H bonds. **62**-H^+ catalysed the Ritter reaction in 69% conversion. However, **62** was catalytically inactive due to the macrocycle occupying the triazolium station and preventing H-bonded halide stabilisation (Figure 66). The inactive rotaxane **62** could be switched on by addition of CF_3CO_2H, and **62**-H^+ could be switched off by addition of NaOMe. The axle alone was catalytically active in both the protonated and deprotonated state. **62**-H^+ was also catalytically active for chloride abstraction of **64**, yielding **66** in 76% conversion by reaction with **65**. Similar conversions were observed with free axle in protonated or deprotonated states. Finally, it was demonstrated that after **62**-H^+ catalysed formation of **68**, and after *in situ* deprotonation, **62** was active for the enamine catalysis, forming **70**.[38] The shuttling of the macrocycle allows two modes of organocatalysis to be switched on and off, thereby completing cascade catalysis of two different functional groups in the molecule by anion-binding, then enamine catalysis.

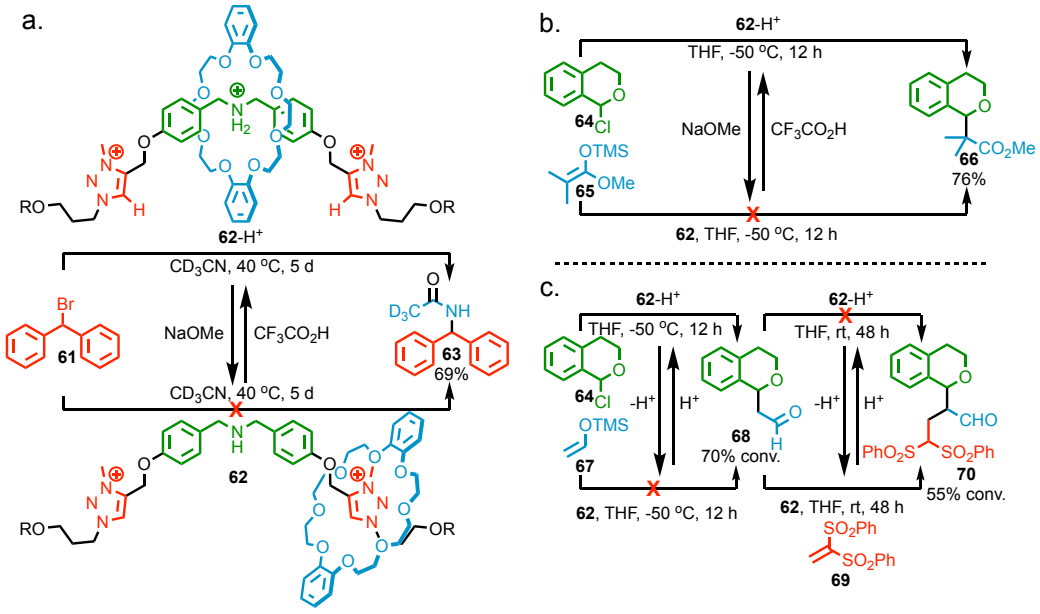

Figure 66: Leigh and co-workers' switchable dual function anion-binding and amine catalyst mediating (a) the Ritter reaction, (b) Mukaiyama aldol reaction, and (c) successive halide-abstraction and enamine catalytic modes.[38] R = 3,5-di-*t*-Bu-C_6H_3.

Goldup and co-workers developed an achiral Au^{I}-rotaxane catalyst **73** (Figure 67a).[19] **73** was not catalytically active on abstraction of the chloride ligand alone. This was because the bipyridine macrocycle coordinated to vacant Au^{I}-coordination site, inhibiting catalysis. On addition of H^+, Cu^{I}, Zn^{II} or Cd^{II} cofactors, the Au^{I} was displaced from the macrocycle and the rotaxane became catalytically active. **73** achieved up to 93% yield and 16 : 1 diastereoselectivity for the *cis*-**74a**.[19] **73** demonstrated the potential for stimuli-responsive transition metal catalysts, with stereoselectivity tuneable with additive choice. The active site of this Au^{I}-catalyst is achiral, thus there was no enantioselectivity.[19]

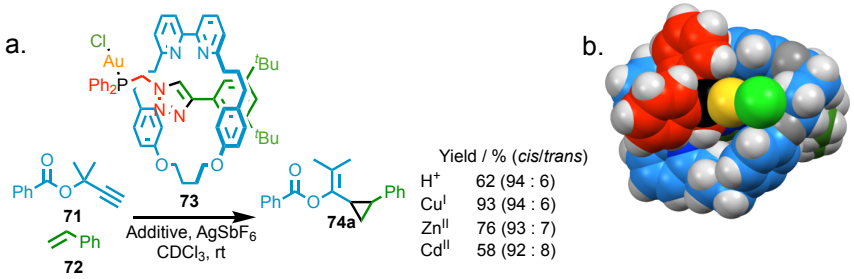

Figure 67: Goldup and co-workers' (a) stimuli responsive rotaxane catalyst and (b) X-Ray crystal structure.[19] H^+ = $TsOH.H_2O$, Cu^{I} = $[Cu(MeCN)_4]PF_6$, Zn^{II} = $Zn(OTf)_2$, Cd^{II} = $Cd(OTf)_2$.

Thus far, all examples discussed of enantioselective catalysis using interlocked molecules, have resulted from the incorporation of traditional covalently chiral stereogenic centres into an interlocked motif.[10–12,39] Although in some of the discussed

examples, the mechanical bond increases the enantioselectivity or alters the dominant pathway of catalysis,[10] none of them have achieved chiral induction from the mechanical bond itself, merely enhanced through proximity effects. Chirality resulting from the mechanical bond is one of the most interesting aspects of mechanical bonding, and the uniquely crowded chiral environment could be used to achieve asymmetric catalysis.[40] Co-conformational point-chirality occurs when a symmetrical D_{nh}-symmetric axle is desymmetrised by a macrocycle lying one side of the central σ_h-plane, crucially the macrocycle cannot cross the central plane due to a bulky substituent (Figure 68).[35,40,41]

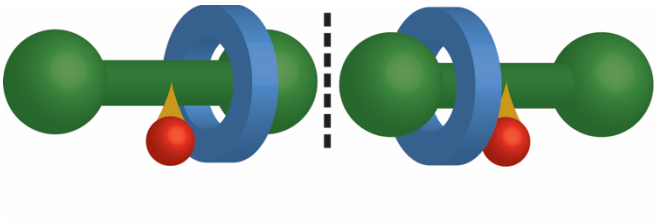

Figure 68: Co-conformational point-chiral rotaxane enantiomers.[40]

Leigh and co-workers synthesised enantioenriched rotaxane (*S*)-**75** in 84% *ee* (Figure 69a).[42] The secondary amine catalytic centre was then used to mediate iminium and enamine catalysis, achieving 36% and 42% *ee* respectively. The achiral axle alone produced racemic products as expected. This was the first example of a rotaxane with only co-conformational stereogenic units being used to mediate reactions asymmetrically.[42]

Leigh and co-workers then developed a dynamic switchable organocatalyst, whereby the macrocycle position breaks local symmetry (Figure 69b).[43] The central 2,5-disubstituted pyrrolidine unit had similar groups on both sides, giving it a *pseudo*-plane of symmetry. One arm of the central unit held a pyridyl-acyl hydrazone binding site, and the other arm held a simple glycyl amide group. When the hydrazone C=N bond is (*E*), the macrocycle preferentially binds to the hydrazone station. Upon irradiation with UV light, the (*Z*) stereoisomer forms, and the macrocycle preferentially binds to the glycyl amides. Addition of acid and subsequent neutralisation causes hydrazone epimerisation and thus the macrocycle returns to the (*E*)-hydrazone binding site.[43] The symmetry breaking associated with macrocycle location was then used to mediate asymmetric enamide catalysis. In (*E*)-**80**, with the macrocycle desymmetrising the *pseudo*-plane through hydrazone binding, the product (*S*)-**81** was obtained in 40% *ee*. After UV

irradiation, when the macrocycle occupies the glycyl amide, the product (*R*)-**81** was obtained in 20% *ee*. The (*E*)- and (*Z*)-axle however both gave *ee*s 34% lower (6% *ee* (*S*)-**81**, and 14% *ee* (*S*)-**81**).

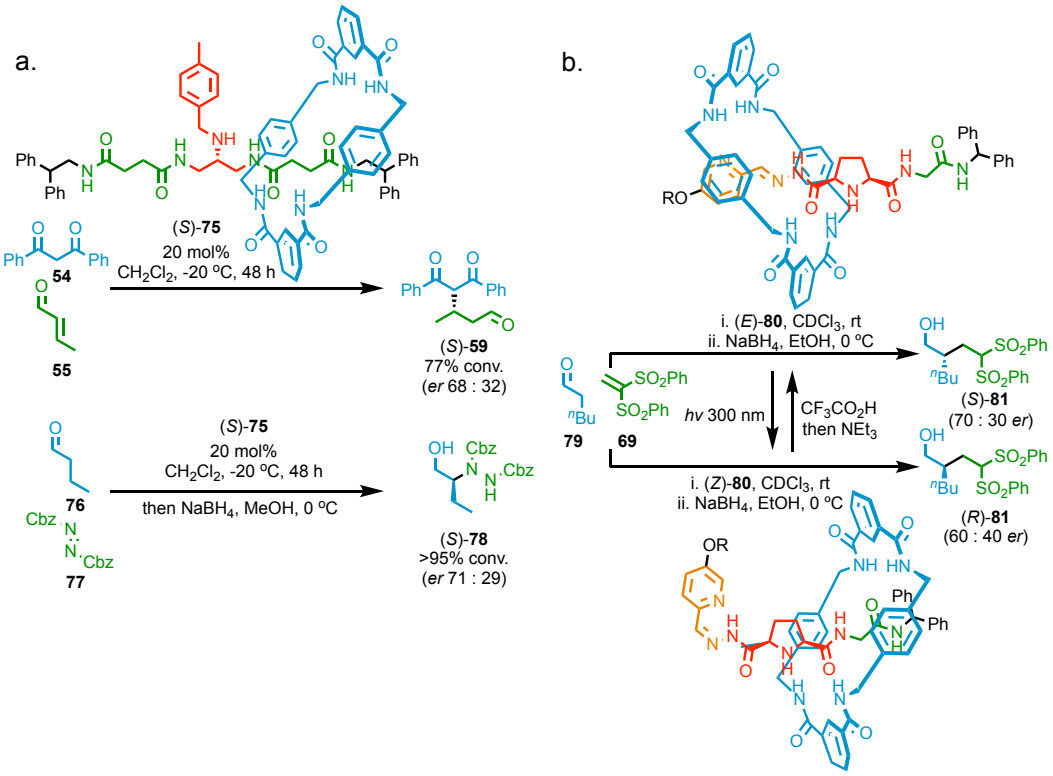

Figure 69: Leigh and co-workers' (a) mechanical point chiral enantioselective Michael addition catalyst,[42] and (b) switchable *pseudo*-mechanical point chiral catalyst.[43] R = $(CH_2)_2CHPh_2$.

2.1.4. Non-Interlocked Switchable Asymmetric Catalysts

Leigh and co-workers have previously developed a complementary pair of switchable squaramide organocatalysts.[44] These two catalysts were developed so that the conditions required to switch catalyst **82** on, would switch the other catalyst **83** off (Figure 70).[44] These switches achieve 98 : 2 (Figure 70a) and 1 : 99 (Figure 70b) on : off ratios. In theory, a mixture of these catalysts would provide a handle to switch the enantiomer of product being produced. However, this was unsuccessful.[44] Conversions of 95% and 93% respectively and *er* of 95 : 5 and 7 : 93 were achieved with catalyst (*E*)-**82** and (*Z*)-**83** (Figure 70c).[44]

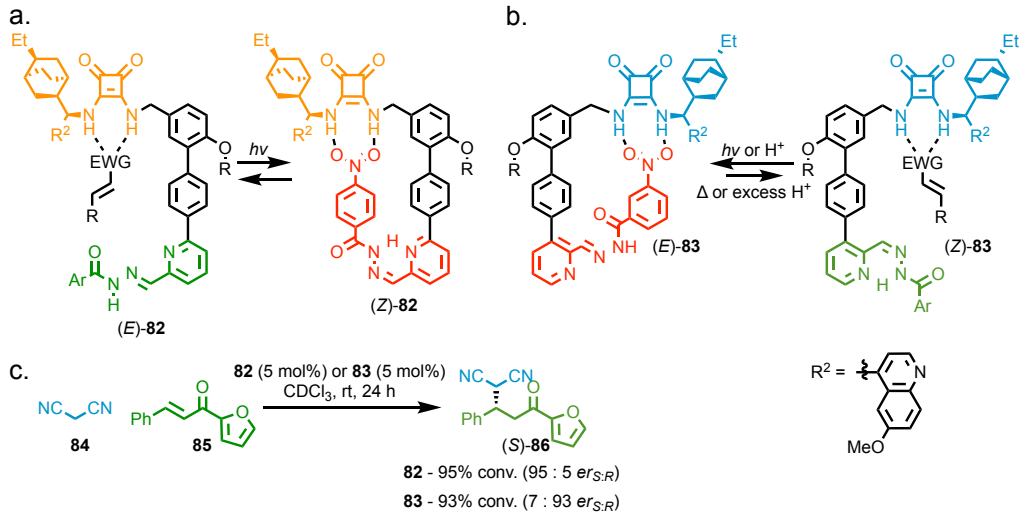

Figure 70: Leigh and co-workers' complementary enantioselective squaramide organocatalysts (a) 98 : 2 (*E*)-**82** : (*Z*)-**82** produces (*S*)-**86** in 90% *ee*. (b) 99 : 1 (*Z*)-**83** : (*E*)-**83** produces (*R*)-**86** in 86% *ee*. (c) summary of the most selective example.[44] R = $C_{10}H_{21}$. R^2 = 4-(6-methoxy-quinoline). Ar = $C_6H_4NO_2$.

Leigh and co-workers have developed a programmable molecular machine that can synthesise each of four stereoisomers from the tandem iminium catalysed Michael addition of a thiol to an α,β-unsaturated aldehyde, and subsequent enamine catalysed attack of an alkene (Figure 71).[45] The substrate (loaded by alkene metathesis) is attached to the machine and initial position is controlled by a pH-responsive rotary switch, locating the substrate close to either enantiomers of the prolinol silyl ether motif. Addition of the nucleophilic thiol initiates the first stereocontrolled iminium catalysed addition to the α,β-unsaturated aldehyde. Modification of the pH can be used to control the second stereocentre, prior to addition of the electrophile.[45] Finally cleavage of the substrate gives the programmed product. This simple single pot, pH-programmed molecular machine can produce any of the four stereoisomers, demonstrating the impressive synthetic capabilities of these machines. Furthermore, this machine allows access to two stereoisomers which are not accessible by normal iminium-enamine catalysis (2*S*,3*R*)-**90** and (2*S*,3*S*)-**89**, demonstrating the synthetic power of this approach, albeit with low selectivity.[45]

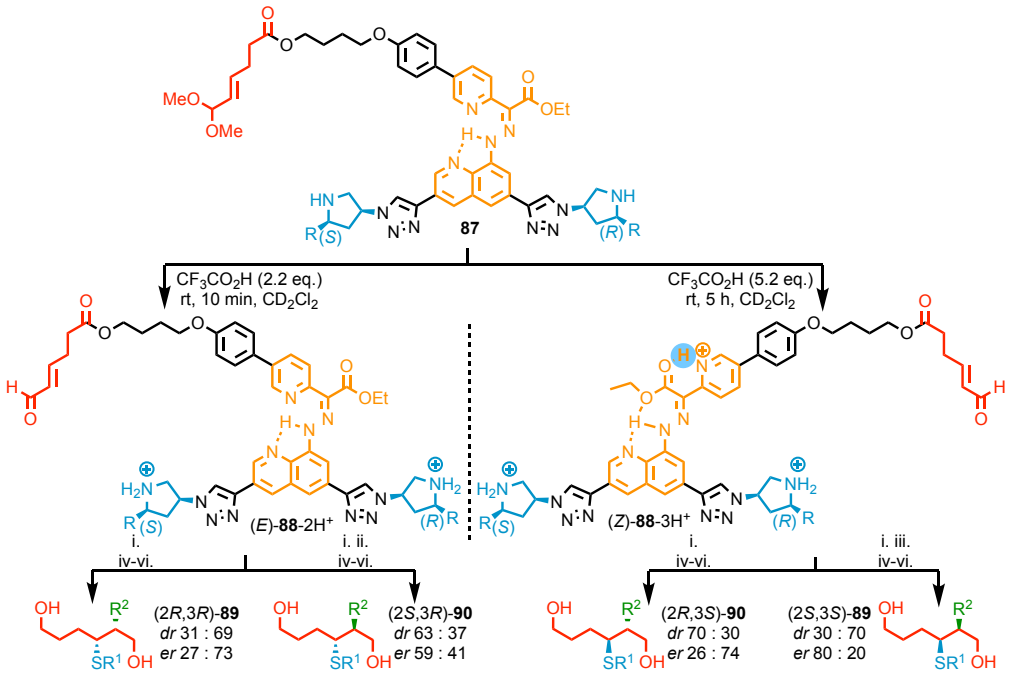

Figure 71: Leigh and co-workers' stereodivergent synthesis with a programmable molecular machine.[45] Counter-ions omitted for clarity. R = CPh_2OSiEt_3. R^1 = $(CH_2)_2(CF_2)_7CF_3$. R^2 = $CH_2CH(SO_2Ph)_2$. i. R^1SH, CD_2Cl_2, 0 °C, 30-41 h; ii. CF_3CO_2H, CD_2Cl_2, 0 °C, 20 h; iii. NEt_3, CD_3CN, CD_2Cl_2, 0 °C, 6 h; iv. $CH_2C(SO_2Ph)_2$, 0 °C, 24 h; v. $NaBH_4$, MeOH, CD_2Cl_2, 0 °C, 2h; vi. $LiAlH_4$, THF, -78 °C, 1 h.

2.1.5. Topological Interlocked Catalysts

Knots have been essential to the evolution of our species, both on a macroscopic scale for tool creation and on a molecular scale where knots exist in DNA and proteins.[46] Artificial knots exist spontaneously in tangled polymer chains, or can be assembled through the directed synthesis pioneered by Sauvage, Leigh and Itami.[46–53] Leigh and co-workers have synthesised a pentafoil knot that allosterically regulates a reaction upon addition of a metal co-factor (Figure 72).[53] The Fe^{II} templated knot has strong chloride and bromide binding affinity, through CH-X H-bonds and long range electrostatic interactions. The $[Zn^{II}_5(\mathbf{91})](BF_4)_{10}$ complex had strong affinity for bromide anions, catalysing alkyl halide hydrolysis. Furthermore, the complex abstracted bromide from trityl bromide, generating triyl carbocations which mediated Michael addition and Diels-Alder reactions.[53] The utilization of knots to restrict conformational freedom and encourage halide binding allows application in catalysis.

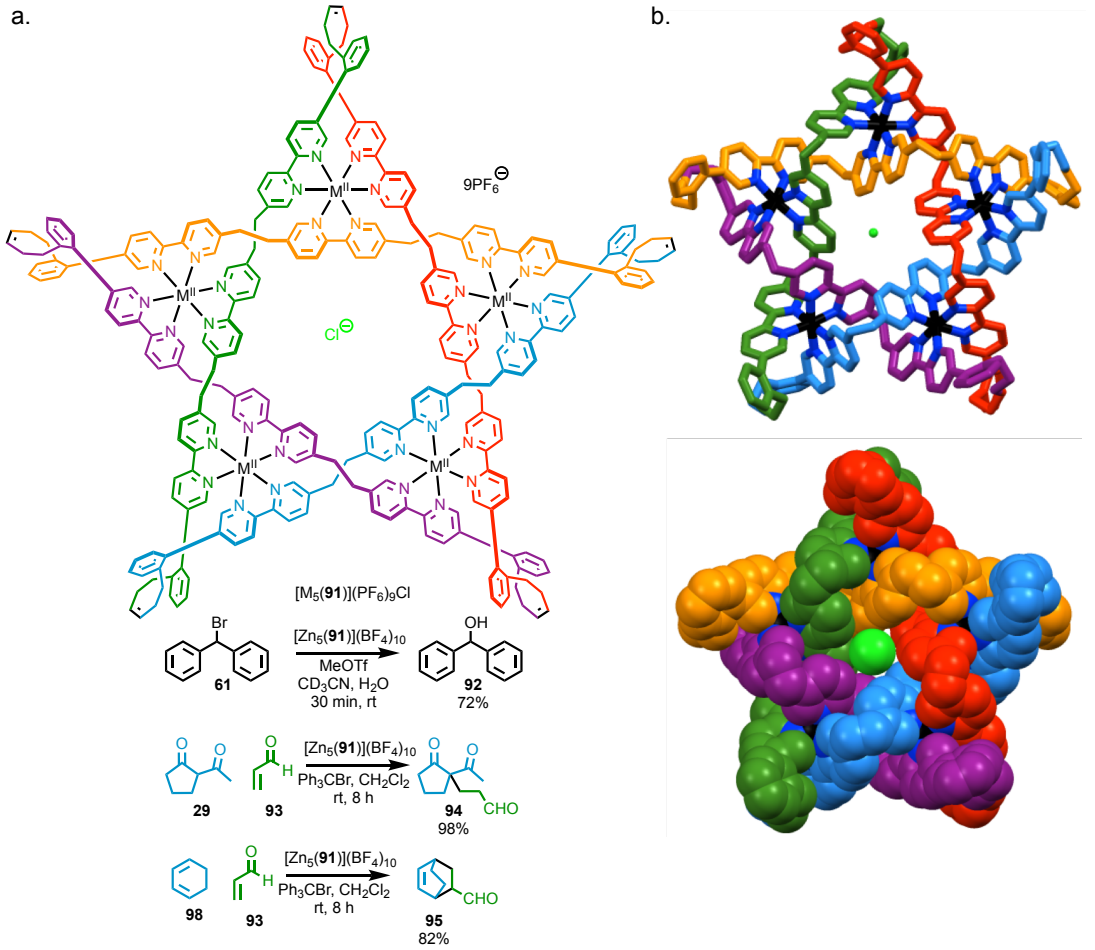

Figure 72: Leigh and co-workers' (a) molecular knot catalyst.[53] (b) Capped stick and spacefill X-Ray crystal structure of [Fe_5(**91**)](PF_6)$_9$Cl. Counter-ions and solvent molecules omitted for clarity.

Leigh and co-workers have reported the asymmetric La^{III}-templated synthesis of a *pseudo*-D_3-symmetric trefoil knot.[48] The chiral knot was coordinated to Eu^{III}, and catalysed the Mukaiyama aldol reaction achieving 66% *ee* (Figure 73).[48] The trefoil catalyst [Eu(Λ-(*R*^{6})-**96**)] has both covalent and topological chirotopic elements, thus demonstrating chiral induction through a topological stereogenic element for the first time.[48]

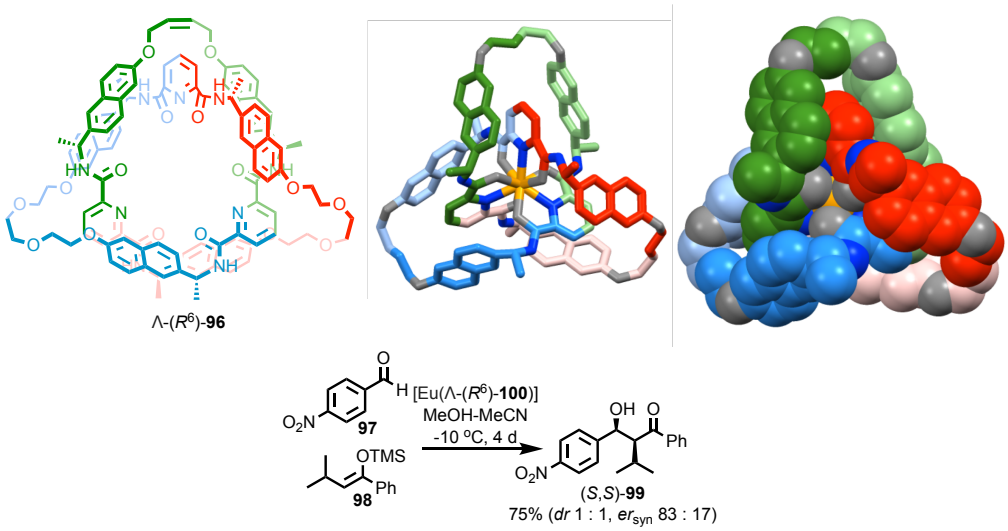

Figure 73: Leigh and co-workers' molecular knot catalyst.[48] X-Ray crystal structure of [Eu(Λ-(R^6)-**96**)].

2.1.6. Motion with Interlocked Catalysts

Many molecular machines utilise an interlocked catalyst to mediate conversion of an excess of fuel. Orenes and coworkers synthesised a rotaxane containing an azodicarboxamide station, and a succinamide station (Figure 74).[54] Upon addition of Ph_3P, the macrocycle shuttles to the succinimide station. By coupling a Mitsunobu reaction with an external oxidant, a continuous shuttle was achieved until all of the fuel was depleted. The successive affinities of dihydroazocarboxamide < succinimide < azodicarboxamide stations is essential for continuous shuttling to occur. Although the reaction itself is trivial, it demonstrates an important application of the catalytic ability of rotaxanes towards continuous motion in molecular shuttles and machines.[54]

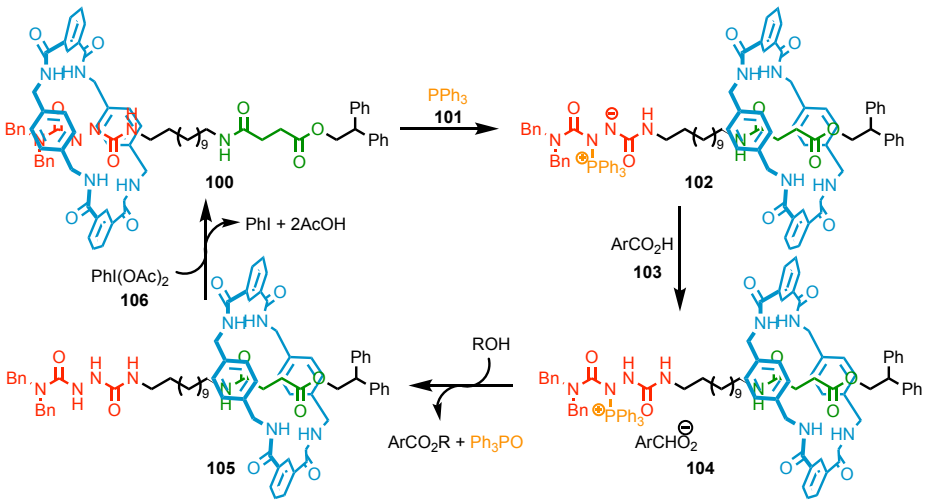

Figure 74: Mitsunobu esterification catalysed by a mechanically interlocked molecular shuttle.[54]

Di Stefano and co-workers have used catenane catalysed decarboxylation of 2-cyano-2-arylpropanoic acids to drive time dependent conformational switching.[55] Leigh and co-workers have demonstrated automated unidirectional motion of one ring around another through information ratchet[56] and energy ratchet mechanisms,[57] catalysing simple reactions such as Fmoc + NEt_3→ dibenzofulvene + CO_2 + NEt_3.HCl, and decarboxylation of trichloroacetic acid. The work of Orenes,[54] Di Stefano,[55] and Leigh[56,57] demonstrate the interlocked molecule undergoing structural changes between two states continuously upon addition of the chemical input. These are by different fundamental mechanisms but achieve similar outcomes. These examples are discussed amongst molecular machines chapter 3. Although they are interlocked catalysts, their primary function is as molecular machines and therefore will not be discussed in depth here.

2.2. Introduction: Gold Catalysis

2.2.1. Au and Special Relativity

Despite originally being considered inert, Au has been shown to be a highly active transition metal in both homogenous and heterogeneous catalysis, as well as for sensors as nanoparticles exploiting the surface plasmon resonance phenomenon.[58] Au^{I}-catalysts are excellent π-Lewis acids, owing to relativistic effects resulting from its positioning in the periodic table.[59] An in-depth overview of the relativistic origins of gold's interesting properties is rarely completed in reviews of its catalytic chemistry,[60–62] often covered independently in largely theoretical texts.[59,63–69] In light of this, a brief overview at an appropriate level is presented below, followed by relevant synthetic highlights of Au^{I}-catalysis.

Special relativity dictates that the momentum of an object must increase as it approaches the speed of light (*c*).[68] Relativistic effects result when the electrons in an atom travel close to *c*. Electrons travel at low speeds for the majority of elements, so the mass correction due to special relativity is negligible. The inner electrons of heavy elements travel much faster, therefore special relativity must be considered to fully explain the properties of these elements.[63–70] Relativistic effects are most extreme for Pt, Au and Hg (period 6, groups 10-12) which lie after the lanthanide series in the periodic table.[64,68]

The *s*- and *p*-electrons of heavy elements travel at speeds closer to *c*, resulting in increases in their mass, and in turn, a decrease in the Bohr radius. The contracted *s*- and *p*-orbitals more effectively screen the *d*- and *f*-orbitals from nuclear attraction, causing expansion and destabilisation. The non-relativistic Lanthanide contraction cannot fully explain these observations (contraction of *s*- and *p*-orbitals due to higher relative nuclear attraction resulting from diffuse 4*f*-orbitals).[64,68]

Relativistic effects cause characteristic variations in electron configuration, energy levels and periodic properties.[68] Properties affected include: preferred oxidation states, ionisation enthalpy and electron affinity, hydration energies, electronegativity, absorption spectra, bond lengths and strengths, and crystal polymorphism.[63,69,70] Relativistic effects increase spin-orbit coupling; the relaxation of spin selection rules is observed spectroscopically.[68]

Although there are many different embodiments of relativistic effects on atomic behaviours, the most relevant to catalysis, is the change in orbital energy levels.[59,60] Au's low energy 6*s*-orbital and diffuse 5*d*-orbitals, result in Au^{I} species having a low lying lowest unoccupied molecular orbital (LUMO) 6*s*-orbital. This makes Au^{I} an unusually strong π-Lewis acid. Furthermore, the LUMO lies at a comparable energy level to the π-orbitals of alkynes and allenes, making alkynes very aurophilic and often the preferred binding site in a molecule with extended π-networks. Because of the extraordinary π-Lewis acidic nature of Au^{I}, it can mediate many rearrangements under relatively mild conditions. [59,71]

Au^{I} species do not easily undergo oxidative addition to Au^{III}, therefore do no generally mediate traditional transition metal catalysed coupling reactions.[72–74] Some alternative strategies have been employed to allow Au to change oxidation state and mediate traditional couplings.[72–74] The benefit of the disfavoured oxidation of Au^{I}, is that rigorous inert atmospheres excluding oxygen are not always necessary.[59]

Descending group 11, Cu^{I} and Ag^{I} species typically form tetrahedral and trigonal planar complexes.[59,62] The only accessible orbital for bonding in Au^{I}, is the unoccupied 6*s*-orbital. Most LAuX complexes are linear with a three-centre four-electron (3c-4e) bond (Figure 75).[60,75] The LUMO energy level of LAu^{+} complexes is comparable to the highest occupied molecular orbital (HOMO) of an alkyne and allene, thus Au^{I} shows selectivity for alkyne complexation over other Lewis basic groups. This alkyne- and allene-philicity is exploited in Au^{I}-catalysed nucleophilic additions across these functional groups.[60,61,76] The minimal back-bonding from the diffuse Au^{I} 5*d*-orbitals into π-accepting ligands, results in more electron deficient ligands, thus explaining why Au^{I} species are such good catalysts for nucleophilic addition across alkynes.[75]

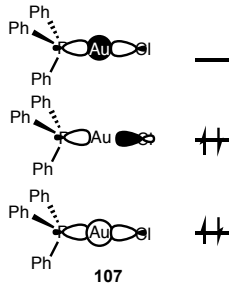

Figure 75: 3-centre-4-electron linear coordination modes of Au^{I} complexes (C_{3v}-symmetric $(Ph_3P)AuCl$).

The major challenge in achieving enantioselectivity with linear complexes, is that there is only one coordination site for ligand binding, the other being required for substrate coordination. The rotation of the L-Au bond and lack of a rigid coordination sphere reduces chiral induction. Furthermore, bimolecular Au^{I} catalysed reactions involve outer-sphere processes, thus chiral information is poorly transferred from a chiral ligand to the transition state.

2.2.2. Au^{I}-Catalysis

There are many in-depth reviews of catalytic activity of Au^{0}, Au^{I} and Au^{III} species.[60] Figure 76 displays a representative array of Au^{I}-catalysed π-system rearrangements, highlighting the aurophilicity of alkynes and demonstrating examples of Au^{I}-catalysed rearrangements in natural product syntheses.[77] Nucleophilic addition across alkynes and allenes are the most common Au^{I}-catalysed reaction,[78] some of which are possible reaction candidates to be enhanced by a MPC rotaxane catalyst.[60]

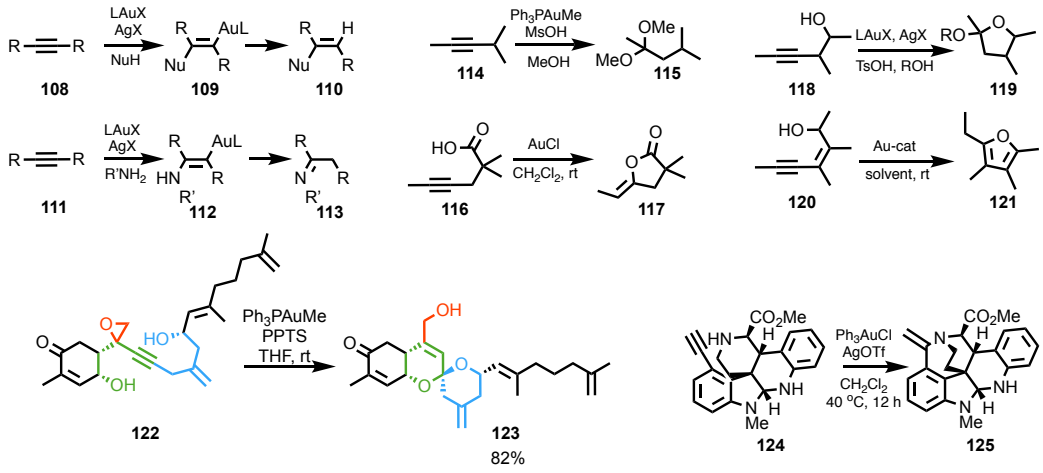

Figure 76: Examples of Au^{I}-catalysed reactions demonstrating alkyne-philicity.[60,77] PPTS = pyridinium *p*-toluenesulfonate.

2.2.3. Enantioselective Au^{I}-Catalysis

2.2.3.1. Chiral Induction by Chiral Counter-Ions

Most early investigations into enantioselective Au^{I}-catalysis were with *bis*(phosphine Au) complexes with axial chiral frameworks.[79] Subtle effects of ligand and counter-ion structure had significant effects on enantioselectivity, with the chiral counter-ion (*R*)-**127** inducing 48% *ee* in the hydroalkoxylation of allene **126** and 96% *ee* for the intramolecular hydroamination of allene **129** (Figure 77).[79,80]

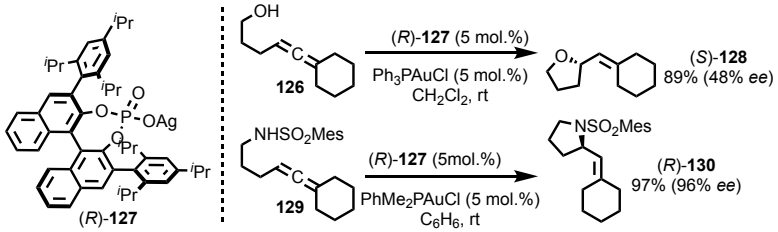

Figure 77: Toste and co-workers' enantioselective hydroalkoxylation of allenes with chiral counter-ion (*R*)-**127**.[79]

These early examples demonstrated that the secondary coordination sphere and surrounding environment were important to mediate enantioselective Au^{I}-catalysis. This approach was generally more successful than direct ligand modification of the linear monophosphine Au^{I}-complex, although excellent examples of this approach have been reported by Echavarren and co-workers.[81]

Recently, Marinetti and Guinchard have reported asymmetric catalysis mediated by complex (*S*)-**131** bearing a tethered chiral counter-ion.[82] Non-coordinating counter-ions led to the weak coordination between the phosphate anion and the Au^{I}-centre upon chloride abstraction ((*S*)-**132**). Tethered counter-ion directed catalysis is an exciting new approach to asymmetric Au^{I}-catalysis, increasing chiral induction through counter-ion coordination and rigidifying the Au^{I}-complex. This approach develops from the early chiral counter-ion studies in combination with the traditional rigidification approach through utilisation of bimetallic Au^{I}-complexes.

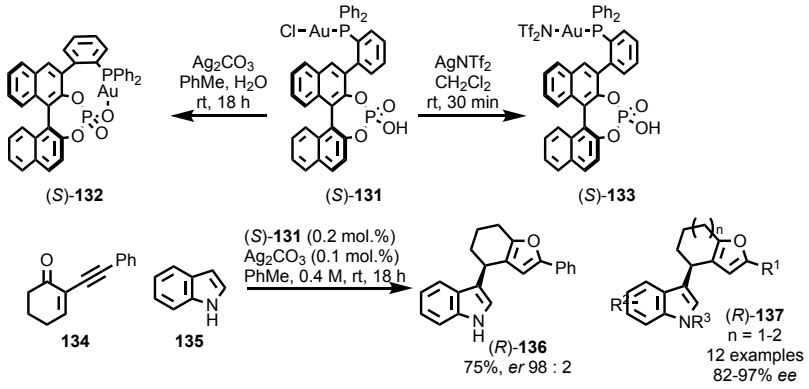

Figure 78: Marinetti and Guinchard and co-workers' asymmetric catalyst (*S*)-**131** bearing a chiral counter-ion moiety.[82]

2.2.3.2. Chiral Induction by Ligand Design

Initial research into enantioselective Au^{I}-catalysis was dominated by bimetallic catalysts with axially chiral components, rigidified by an Au^{I}-Au^{I} interaction (Figure 79a). Mononuclear enantioselectivity was achieved with phosphite and phosphoramidite

ligands, with carefully designed substituents to cradle the Au^{I} active site within a rigid, chiral environment (Figure 79b).[79]

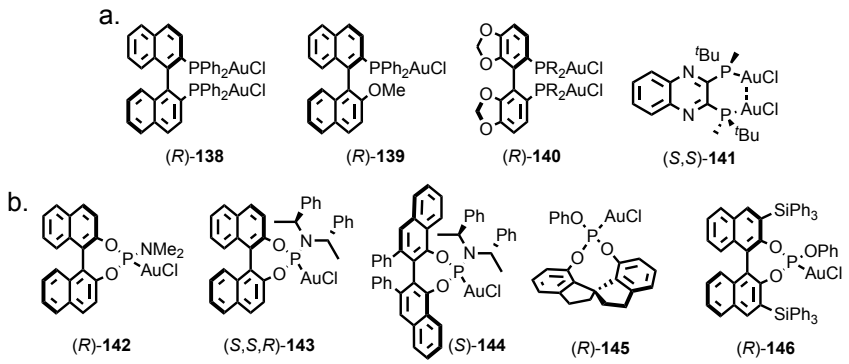

Figure 79: Common axially chiral (a) phosphine (b) phosphite and phosphoramidite pre-catalysts for enantioselective Au^{I}-catalysis.[62] R = 3,5-di-*t*-Bu-4-MeO-C_6H_2

Enantioselective Au^{I}-catalysed rearrangements of alkynes and allenes have been achieved,[83] initially through chirality transfer from the starting material, however now more generally using bimetallic species.[83]

An archetypical Au^{I}-catalysed reaction that will be studied in this report, is the anchimerically assisted cyclopropanation of a 2-methyl-3-butyn-2-yl ester (Figure 80a).[75] Toste and co-workers' achieved high *cis*-diastereoselective cyclopropanations with triphenylphosphine Au^{I} complexes. With (*R*)-**140** good chiral induction of 60-94% *ee* were reported for a series of 9 examples.[75] An interesting point to note is that in this landmark publication, several different chiral phosphine ligands were screened, with minimal enantioselectivity, and that the trends in structure to enantioselectivity were not immediately obvious and seemed difficult to predict.

The anchimeric effect of the 2-methyl-3-butyn-2-yl ester is key to generation of the Au^{I}-stabilised carbene (Figure 80b). Although addition of carbenes across alkenes is normally a concerted process, due to the minimal backbonding from Au^{I} and thus the low carbene nucleophilicity, this is a stepwise process, where the ring closure step typically takes place faster than the bond rotation in the intermediate (Figure 80c).

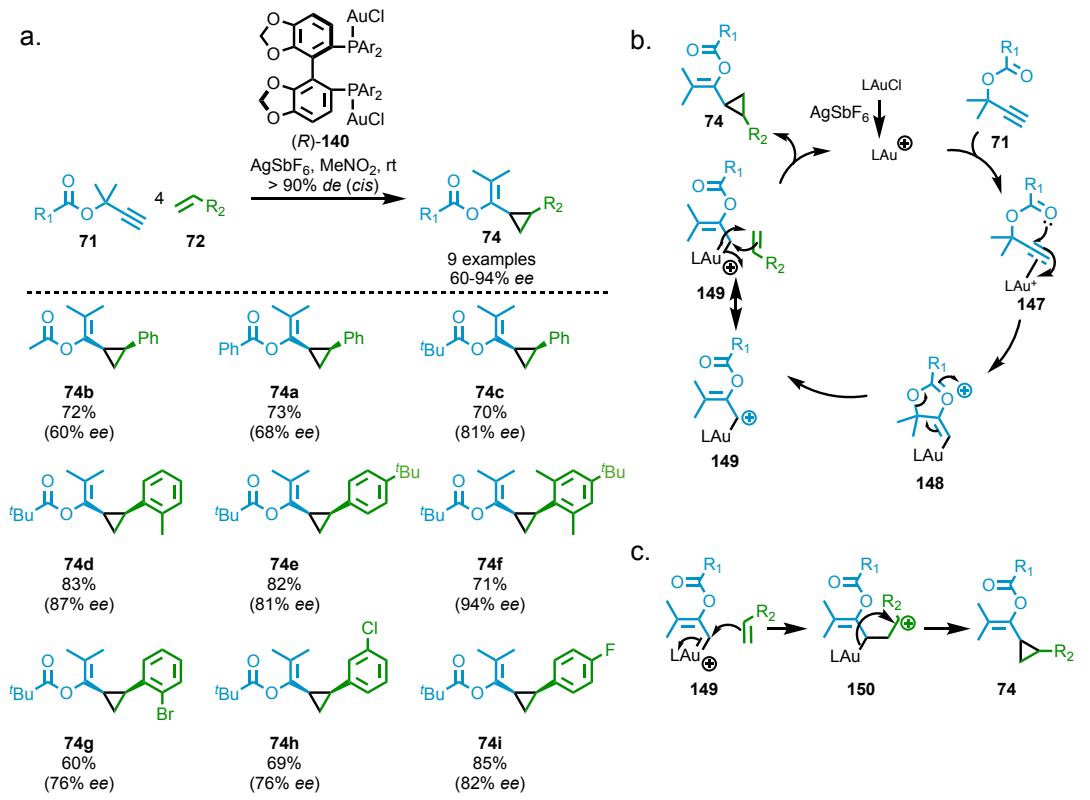

Figure 80: (a) Toste and co-workers' enantioselective Au^{I}-catalysed cyclopropanation. (b) The concerted mechanism of Au^{I}-catalysed cyclopropanations *via* a linear Au^{I}-supported carbene. (c) stepwise alternative addition of styrene to the Au^{I}-stabilised carbene.[75] Ar = 3,5-di-*t*Bu-4-OMe-C_6H_2

The *cis*-diastereoselectivity of Fischer (singlet)-carbene addition to alkenes, can be explained through orbital symmetry arguments. The Newman-projection of the transition states gives counter-intuitive diastereoselectivity. For best orbital overlap, the carbene must approach the alkene side-on (Figure 81a), before finally twisting in the transition state (Figure 81b). The disfavoured side-on approach yields the minor *trans*-**74** (Figure 81d), whereas the favoured side-on approach yields *cis*-**74** (Figure 81e).[75] The linear Au^{I}-complex has the ligand projected far away from the substrate, thus *Re* and *Si* facial differentiation is difficult with a chiral ligand, hence the challenging enantioselectivity in Au^{I}-catalysis. Facial selectivity was best achieved previously with bimetallic atropisomeric catalysts, where an aurophilic Au^{I}-Au^{I} **δ**-bonding interaction (Figure 81f) rigidifies the catalyst. (*R*)-**140** gave Toste and co-workers impressive enantioselectivity of 94% *ee* for **74f** (Figure 80a, Figure 81g).[75]

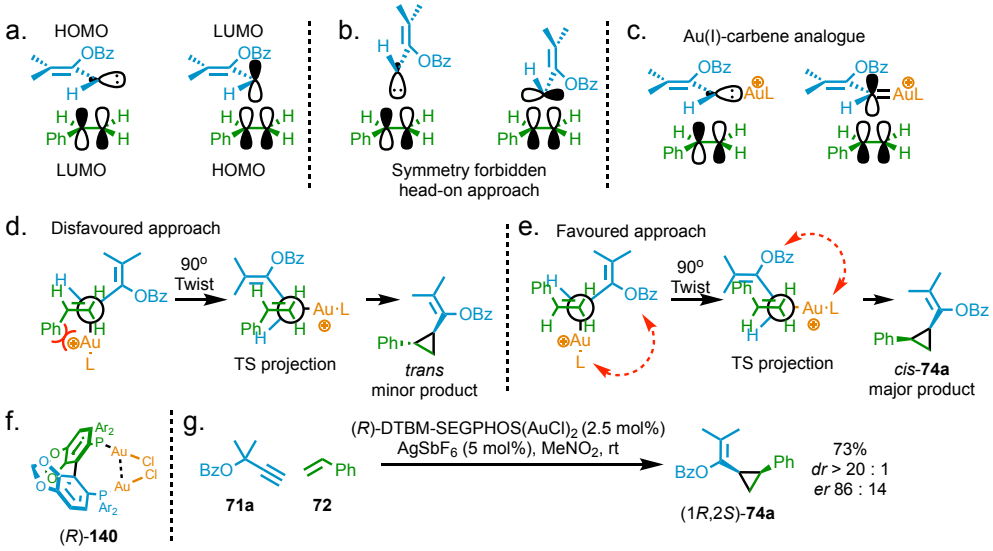

Figure 81: (a) Orbitally allowed side-on approach of Fischer-carbene (b) Orbitally forbidden head-on carbene approach (c) Orbitally allowed side-on approach of Au^{I}-stabilised carbenes (d) Newmann projection of the disfavoured approach resulting in the minor *trans*-cyclopropane (e) Newmann projection of the favoured approach resulting in the major *cis*-cyclopropane (f) The chiral environment rigidified with an Au^{I}-Au^{I} interaction present in (*R*)-**140**, Ar = 3,5-di-*t*-Bu-4-MeO-C$_6$H$_2$ (g) Toste and co-workers' asymmetric cyclopropanation reaction.[75]

Echavarren and co-workers have achieved impressive diastereoselectivity of similar aryl-vinyl cyclopropane **156**, *via* carbene generation from a retro-Buchner reaction of a 1,3,5-cycloheptatriene.[84,85] The Au^{I}-catalysed retro-Buchner reaction generates an Au^{I}-carbene **154**,[85] which subsequently forms a cyclopropane on reaction with an **72b** (Figure 82).[84] Calculations showed the diastereoselectivity originating from favourable π-π stacking interaction between aromatic components in the *cis*-transition state **155**.

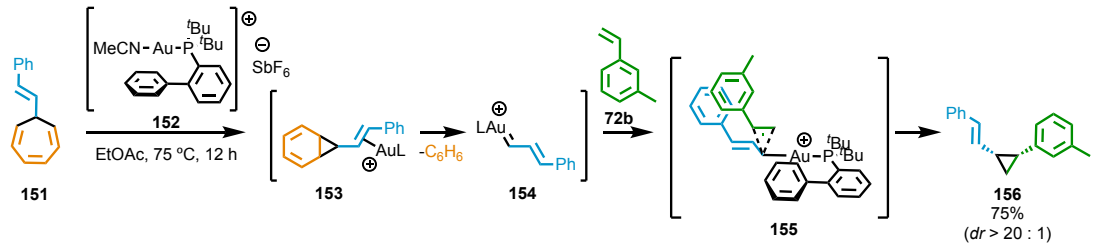

Figure 82: Echavarren and co-workers' cyclopropanation from a retro-Buchner carbene formation step.[84]

Au^{I}-catalysed oxidative cyclisations of 7-ethynyl-1,3,5-cycloheptatrienes have achieved the shortest synthesis of bullvalene derivative **165** (Figure 83).[86] The low energy [3,3]-sigmatropic rearrangements of bullvalene **167**, can lead to 1 209 600 degenerate tautomers,[86] making them an interesting molecule class. This elegant Au^{I}-catalysed synthesis removed the need for toxic, explosive reagents such as diazomethane, and increases the overall yield significantly.

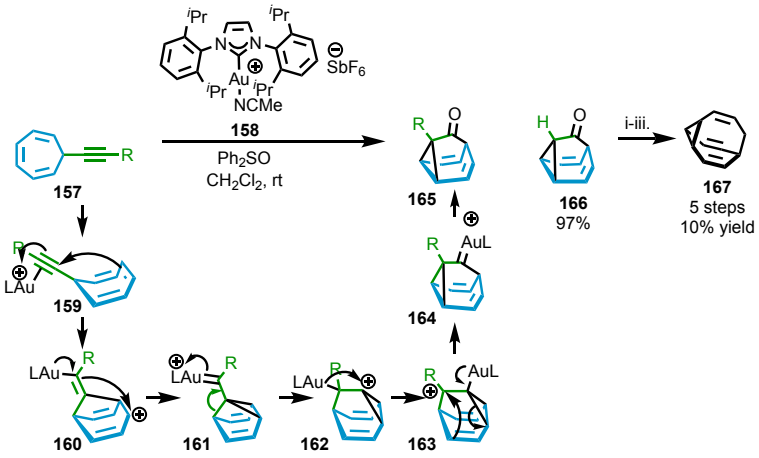

Figure 83: Echavarren and co-workers' Barbaralone **166** (R = H) and Bullvalene **167** synthesis.[86] i. $THMSCH_2N_2$, *n*-BuLi, MeOH, SiO_2, THF, Et_2O, -78 °C→rt (37%); ii. LiHMDS, $PhNTf_2$; iii. *N*-Bu_3SnH, LiCl, $Pd(PPh_3)_4$ (44%).

The [2,3]-sigmatropic rearrangement of **168** was achieved with impressive enantioselectivities, with bimetallic **174**$(AuCl)_2$ (94% *ee* of **172**, Figure 84),[87] and with BINOL derived phosphoramidite ligand **173** (97% *ee* of **172**, Figure 84).[88] The steric bulk surrounding the nitrogen atom in **173**, in combination with the rigid BINOL motif, resulted in a very crowded Au^I-environment, and thus good chiral induction to the substrate. This enantioselective addition across an aldehyde in another examples of the dominant bimetallic approach to enantioselective Au^I-catalysis.

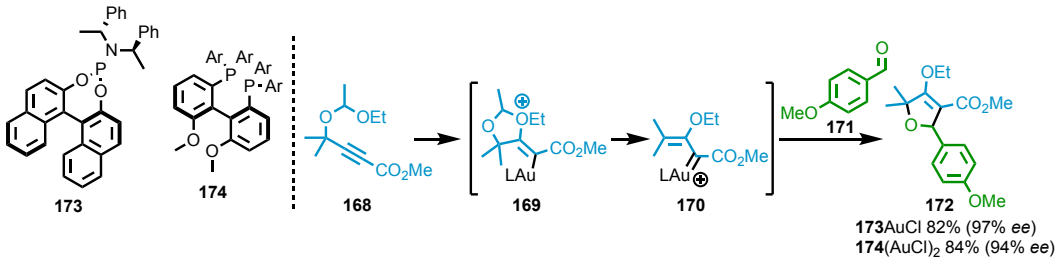

Figure 84: [2,3]-Sigmatropic rearrangement of **168**, impressive enantioselectivities were achieved with BINAP and BINOL phosphoramidite ligands. Ar = 3,5-di-^{t}Bu-4-MeO-C_6H_2.[83,87,88]

The Au^I-stabilised carbene reactions have been achieved enantioselectively in the past, utilising bimetallic species.[75,84,85,89] The Rautenstrauch rearrangement had initially only been achieved enantioselectively through chirality transfer from enantioenriched starting material.[83] However, Toste and co-workers achieved good enantioselectivity by utilising acetal anchimeric effects (Figure 85),[90] rather than propargylic esters.[75] Excellent enantioselectivities were achieved for a range of substrates, with little effect from variation of R_1 and R_2. The high enantioselectivities were dependent on an electron-withdrawing substituent, R_3, and indole assisted charge delocalisation, ensuring a planar achiral intermediate.[83,90] Although high enantioselectivities were

achieved, the substrate scope of this reaction is low, requiring the indole motif and electron-withdrawing groups. Furthermore, the enantioselectivity achieved required extremely bulky, bimetallic phosphine ligands, demonstrating the limited ligand scope for enantioselective Au^{I}-catalysis with phosphine ligand classes.[90]

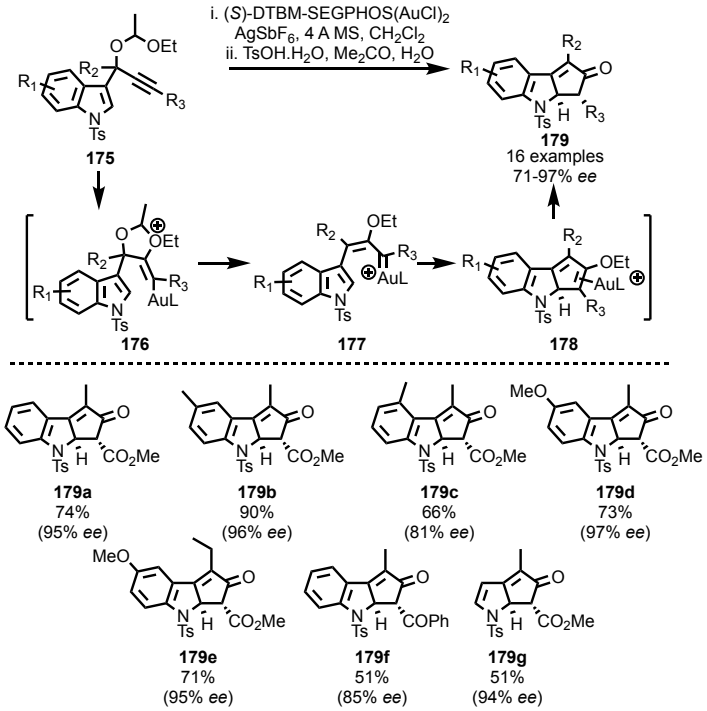

Figure 85: Toste and co-workers' enantioselective Rautenstrauch rearrangement of **175**.[90]

The cycloisomerisation of 1,5- and 1,6-enynes have been another successful reaction class catalysed by Au^{I} (Figure 86, Figure 87).[61,62,76] The 6-*endo-dig* cyclisation of enyne **180**,[91] was achieved with excellent 90-98% *ee*, for a range of substrates **183**. This was achieved with another bimetallic axially chiral catalyst with (*R*)-**184**$(AuCl)_2$ (Figure 86).

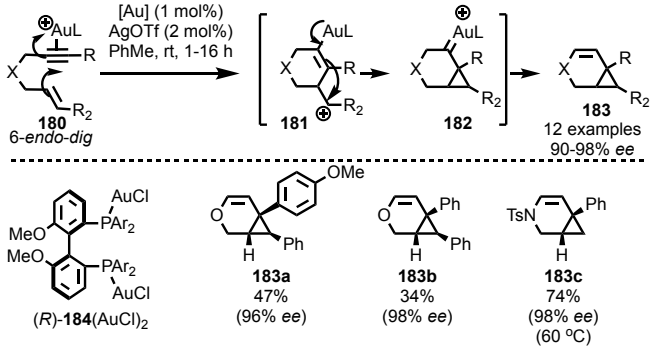

Figure 86: Michelet and co-workers' enantioselective cycloisomerisations of enynes with (*R*)-**184**$(AuCl)_2$ ligands. Ar = 3,5-di-*t*-Bu-4-MeO-C_6H_2.[91]

Michelet and co-workers also achieved enantioselectivity with (*R*)-**174**$(AuCl)_2$ in 5-*exo*-*dig* rearrangements of enyne **180**, with a range of aryl nucleophilies (Figure 87).[92] Interestingly, the enantioselectivity with (*R*)-BINAP$(AuCl)_2$ and (*R*)-MeOBIPHEP$(AuCl)_2$ were low (12-54% *ee* depending on conditions), whereas (*R*)-**174**$(AuCl)_2$ achieved much higher enantioselectivities (74-80% *ee*) due to the bulky DTBM (3,5-di-^{t}Bu-4-MeOC_6H_2) substituents. This demonstrates that the bimetallic axially chiral motif requires large steric bulk to achieve good chiral induction.[92] This built on work by Echavarren and co-workers, who reported these rearrangements with alcohol nucleophiles, catalysed by Au^I and Pt^{II}, with modest *ee*s.[93]

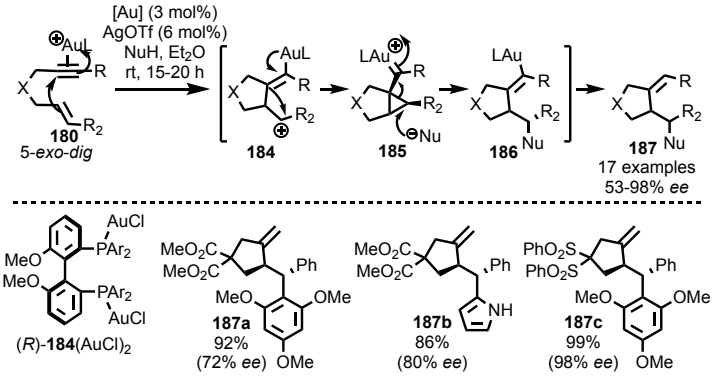

Figure 87: Michelet and co-workers' enantioselective 5-*exo*-dig rearrangement. Ar = 3,5-di-*t*-Bu-4-MeO-C_6H_2.[92,93]

Slaughter and co-workers have developed diaminocarbene Au^I ligands, yielding impressive enantioselectivities for a mono-metallic species (Figure 88).[94] The weak Au^I-naphthyl interaction gave an 8 kJmol^{-1} enthalpic preference for one rotamer (Figure 88). These dynamic chiral pockets are analogous to the bimetallic species which preceded them, relying on atropisomerism. This innovative ligand class were very selective for these isochromene derivatives, although had low substrate scope beyond these.[94]

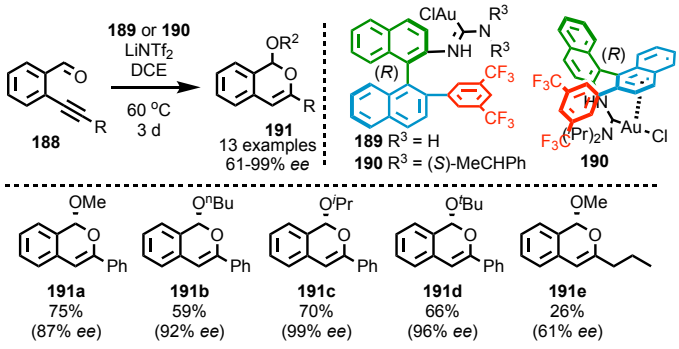

Figure 88: Slaughter and co-workers' enantioselective diaminocarbene Au^I complex, and a 3D projection of **190** displaying the Au^I-naphthyl interaction.[94] DCE refers to 1,2-dichloroethane.

Allenes, like alkynes, are aurophilic functional groups. Au^{I} π-catalysts are very good for nucleophilic addition across an allene, *via* a vinyl Au^{I}-intermediate. These vinyl Au^{I}-intermediates typically then undergo proto-demetallation, although halo-demetallation has also been reported in bromoamination reactions (Figure 89).[95] In this work, good enantioselectivities were achieved with previously established axially chiral bimetallic complexes, in combination with chiral counter-ion (*S*)-**127**.

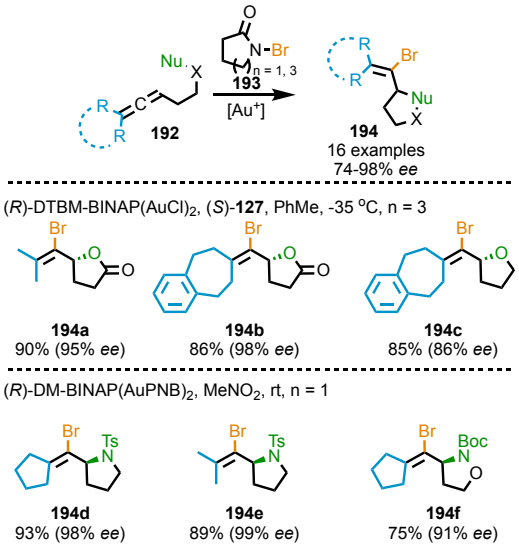

Figure 89: Toste and co-workers' catalytic enantioselective bromoamination of allenes with atropisomerically chiral Au^{I}-complexes.[95]

Intramolecular hydroamination is an attractive route to *N*-heterocycles, in an atom economical fashion.[96] One major challenge to hydroamination of allenes, is the regioselectivity between the two C=C bonds, limiting substrates to intramolecular cyclisations.[97] Regioselectivity has been achieved before with NHC-Au^{I} complexes. However, enantioselectivity remained challenging in intermolecular hydroaminations.[98] Widenhoefer and co-workers have achieved enantioselective intermolecular hydroaminations, with excellent regioselectivity with a terminal CHMe allene.[97]

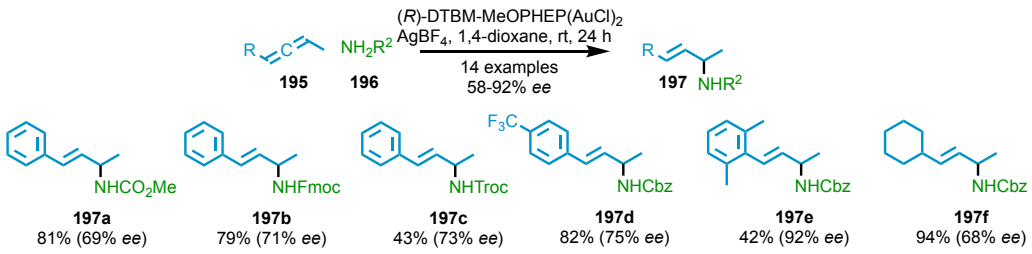

Figure 90: Widenhoefer and co-workers' intermolecular regioselective enantioselective hydroamination of allenes.[97]

High enantioselectivity in intramolecular hydroaminations has been achieved by Toste and co-workers, with good enantiomeric excesses (Figure 91). However the reaction did not tolerate terminal allenes (R cannot be H).[99] This further demonstrates the progress in enantioselective Au^{I} catalysis since its beginnings. Numerous other examples of enantioselective intramolecular additions across allenes can be found in relevant reviews.[80]

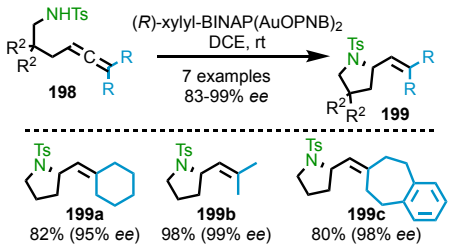

Figure 91: Toste and co-workers' intramolecular hydroamination of allenes.[99]

Tanaka and co-workers have achieved the highly enantioselective synthesis of azahelices and double azahelices with bimetallic axially chiral Au^{I} catalysts (Figure 92).[100] The simple $BINAP(AuCl)_2$ complex mediated sequential enantioselective hydroarylations across diyne to form the azahelicene **202a** and double azahelicene **202b** in good enantiopurity.

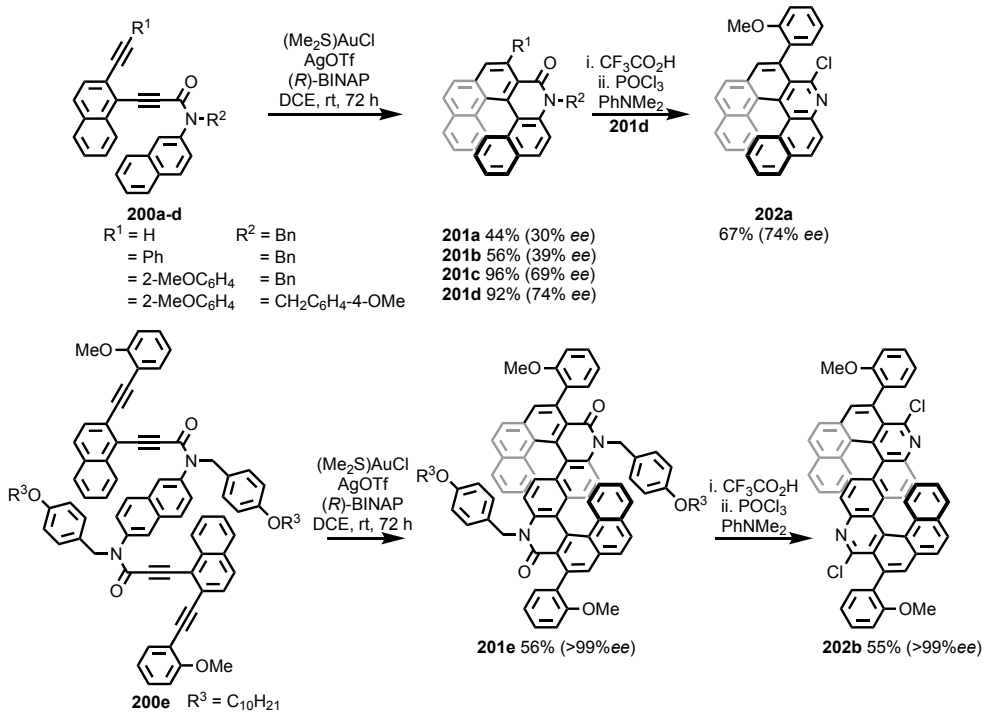

Figure 92: Tanaka and co-workers' enantioselective Au^{I}-catalysed azahelicene synthesis.[100]

Echavarren and co-workers have developed Au^{I}-ligands from variations of Buchwald's JohnPhos ligand **203b**.[101,102] Echavarren's arsenic analogue of JohnPhos(AuCl) **203c** was shown to be more electrophilic (determined by ^{31}P chemical shift of a bound Ph_2MePO guest). The As-analogue behaved similarly to JohnPhos(AuCl), whereas the indazole analogue **203a** had catalytic behaviour comparable to an NHC(AuCl) complexes.[102] The similar behaviour demonstrates that the As-analogue **203c** could be a phosphine alternative.

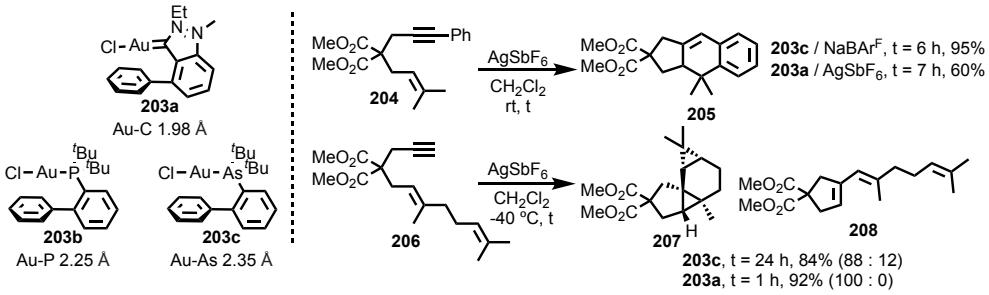

Figure 93: Echavarren and co-workers' As and indazole analogues of JohnPhos(AuCl).[102]

Echavarren and co-workers have recently incorporated a distant C_2-symmetric element into phosphine ligand (*R*,*R*)-**203d**, achieving asymmetric Au^{I} catalysis with high enantioselectivities and impressive reaction generality.[81] In this landmark publication, not only do they show that their catalyst had impressive enantioselectivity in a range of enyne reactions, but also screened 80 previously published chiral ligands for these reactions, reporting low enantioselectivity for most complexes. This demonstrates that despite many publications showing good enantioselectivity, scope is still a problem in Au^{I}-catalysis and is very reaction dependent.[81] Furthermore, this simple ligand demonstrated that monodentate phosphine ligands can induce good enantioselectivity generally across Au^{I} catalysed reactions. Echavarren's folding catalyst (*R*,*R*)-**208** showed excellent generality and advances the field of enantioselective Au^{I}-catalysis.[81] This report is significant because it simultaneously demonstrates that bimetallic axially chiral motifs are not necessary, and highlights that reaction scope and generality remains a challenge. It still remains difficult to predict a successful catalyst structure.

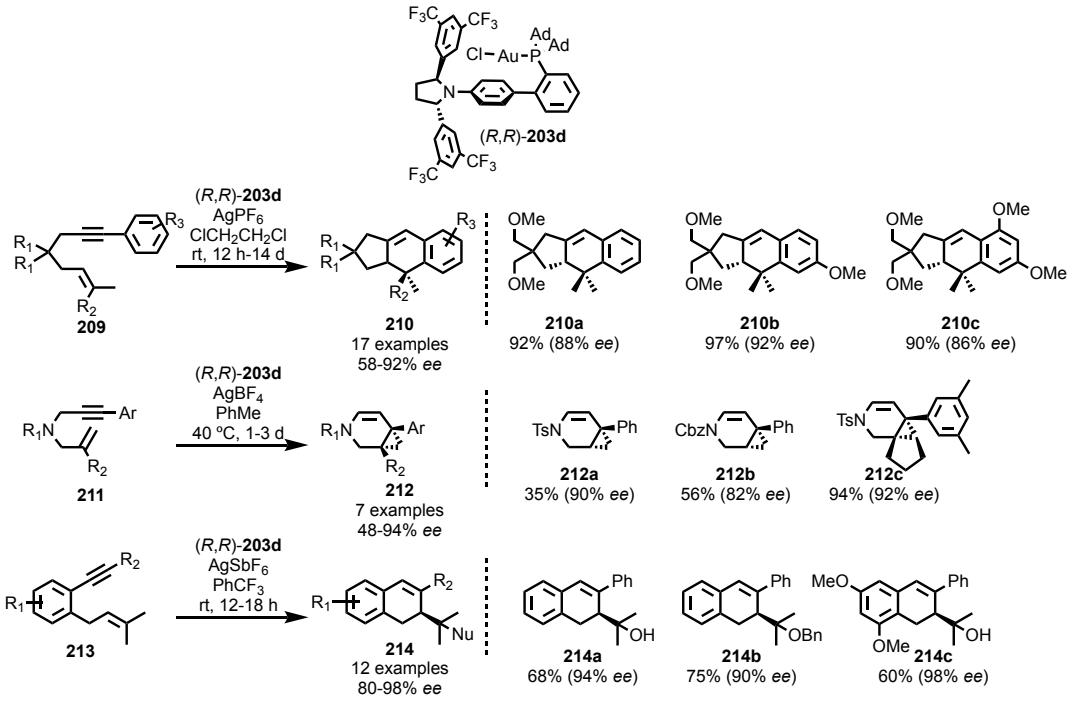

Figure 94: Echavarren and co-workers' impressive Au^{I} catalyst (*R*,*R*)-**203d**.[81]

Beyond axially chiral ligands, Marinetti and co-workers have developed chiral ligands (*R*$_P$,*P*)**-216** and (*R*$_P$,*P*)**-220** with helicene moieties. These catalysts achieved good enantioselectivities for enyne cycloisomerisations (84-86% *ee*, Figure 95a), and intramolecular allene addition (85-88% *ee*, Figure 95b).[103] These complexes utilise chirality not previously explored in Au^{I}-catalysis, which had been limited to axially chiral bimetallic complexes, NHCs and phosphoramidites. These ligands produce good enantioselectivity. However these are synthetically less accessible than Echavarren's monophosphine (*R*,*R*)-**208**,[81] limiting the impact of these monophosphine helicenes.[103]

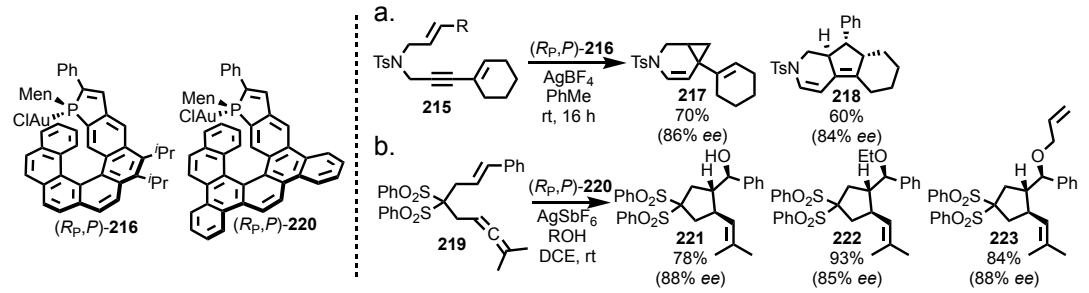

Figure 95: Marinetti and co-workers' helicene phosphine ligands for asymmetric Au^{I}-catalysis of (a) enyne cycloisomerization and (b) intramolecular addition across allenes.[103]

Toste and co-worker have also developed a complicated monophosphine ligand to mediate Au^{I}-catalysed reactions.[104] This bifunctional catalyst included a monophosphine and hydrogen-bond donor, to mediate acetylide addition to imines and

a three component coupling to form cyclic carbamimidates in good *ee* (Figure 96).[104] **226** is relatively straightforward to synthesise, by addition of 2-(diphenylphosphine)cyclohexanamine to an isocyanate, and subsequent coordination to Au^{I}.

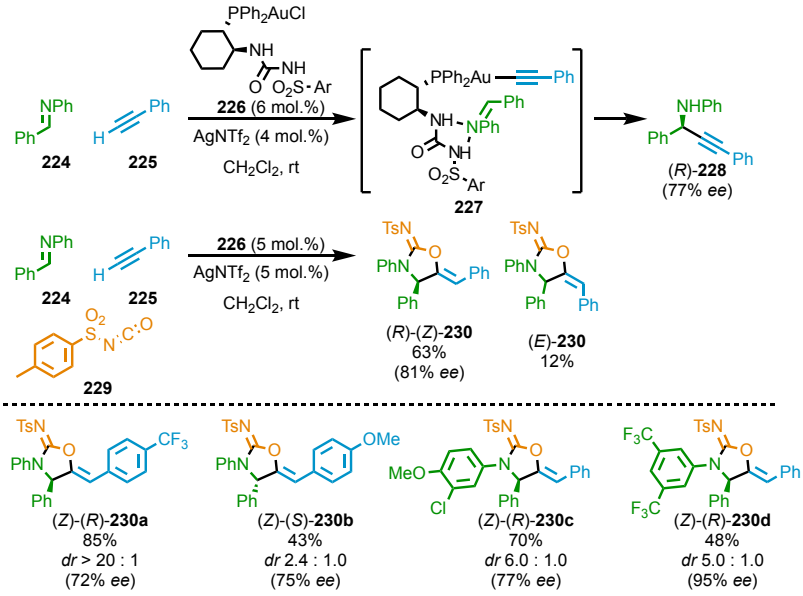

Figure 96: Toste and co-workers' bifunctional monophosphine Au^{I} catalyst.[104] Ar = 2,4,6-tri-*i*-Pr-C_6H_2.

From surveying the Au-catalysis literature, impressive enantioselectivities have been achieved. Reports often show vast and unpredictable differences in enantioselectivity between structurally similar bimetallic complexes; predictability is still an important limitation of enantioselective Au-catalysis.

2.2.4. Supramolecular Strategies for Au^{I} Catalysis

Sollogoub and co-workers have synthesised a series of cyclodextrin-carbene ligands to project Ag, Au or Cu catalytic centres into the chiral cavity of the cyclodextrin (Figure 97).[105] With A,D-β cyclodextrins, Sollogoub and co-workers achieved up to 80% *ee* for a simple Au^{I} catalysed cycloisomerisation.[105] The use of cyclodextrins as a chiral cavity is very exciting, demonstrating that enantioselective Au^{I}-catalysis can be achieved with accessible ligands, as opposed to complex phosphines, NHCs or phosphoramidites. Sollogoub, Fensterbank, Mouries-Mansuy and co-workers further developed this A,D-β-cyclodextrin-Au^{I} catalyst, to demonstrate highly enantioselective mediation of alkoxycyclisations (Figure 97b).[106]

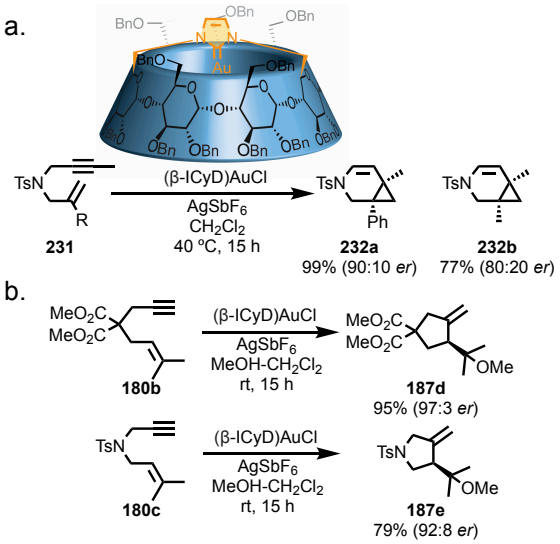

Figure 97: Sollogoub and coworkers' chiral A,D-β-cyclodextrin cavity.[105]

Atwood and co-workers' self-assembling cubic resorcin[4]arene cage (**233**$_6$(H$_2$O)$_8$, Figure 98b),[107] as predicted in their initial publication, has been used to encapsulate NHC Au^I-catalysts by Reek and co-workers (Figure 98).[108] The hydrophobic effect drives catalyst encapsulation and limits the hydration sphere of the catalyst. Using the free catalyst **234** in water yielded ketone **237** quantitatively, with traces of aldehyde **238** and rearrangement product **239**. The encapsulated catalyst was significantly slower and gave a product distribution of **237** : **238** : **239** 3 : 1 : 3, demonstrating that the encapsulated catalyst in a less solvated environment favoured the intramolecular rearrangement.[108]

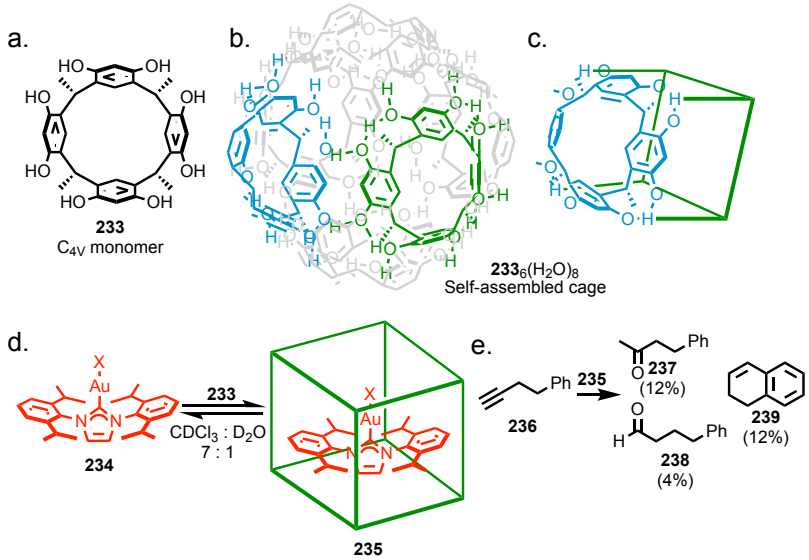

Figure 98: (a-c) Atwood and co-workers' self-assembling resorcinarene cage,[107] and (d) Reek and co-workers' Au^I catalyst encapsulation and (e) intramolecular biased product distribution.[108] In **233**$_6$(H$_2$O)$_8$ and **235** each face represents **233** and each node represents H$_2$O.

Reek and co-workers then expanded this work to make a stimuli responsive Au^{I}-catalyst.[109] When encapsulated, the Au^{I}-catalyst was inert and no activity was observed over a 24 h period. However, upon addition of NEt_4^+, the Au^{I}-catalyst was displaced from the cavity and mediated nucleophilic addition of phenol across diphenylacetylene, quantitatively within 1 h.[109]

In the same year as Reek and co-workers' initial publication of an encapsulated Au^{I}-catalyst,[108] Toste and co-workers demonstrated that the catalytic activity of Me_3PAuBr was increased 8-fold for the hydroalkoxylation of allenes when encapsulated within a tetrahedral L_6Ga_4 cage, due to dramatic increases in local substrate concentration.[110] This enhanced catalyst lifetime and turnover (Figure 99).[111] These cationic guests have large association constants due to electrostatic enthalpic attraction to the 12^- charged cage, and entropically favoured solvent displacement.[110] Neutral guests are bound primarily due to the hydrophobic effect.[110]

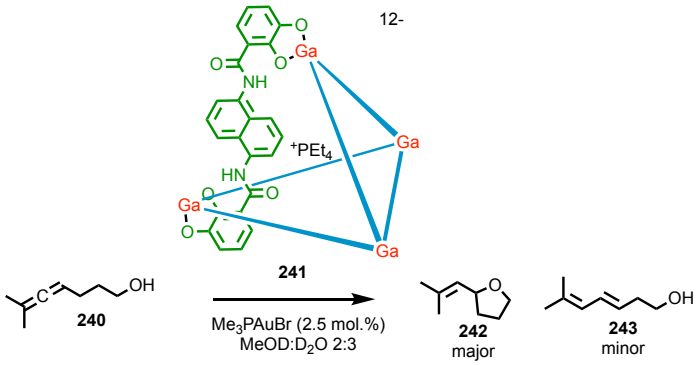

Figure 99: Toste and co-workers' encapsulated allene hydroalkoxylation catalyst.[111] Counter-ions removed for clarity.

In 2013, Toste and co-workers used these encapsulated catalysts to couple achiral Au^{I}-catalysis with an enantioselective enzyme-mediated acetate hydrolysis, giving an enantioenriched substrate for the Au^{I}-catalysed cyclisation (Figure 100).[112] In the absence of the cage, the Au^{I} catalyst isn't compatible with the enzyme mediated reaction. This impressive kinetic resolution using of cages to allow compatibility of enzymatic hydrolysis and Au^{I}-catalysis, yielded 96% *ee* of the major diastereoisomer.[112] It was not commented on as to whether the ΔΔΔΔ-**246** or ΛΛΛΛ-**246** inclusion complexes gave different reactivities or selectivities for the cyclisation of (*R*)-**245**.[110,112]

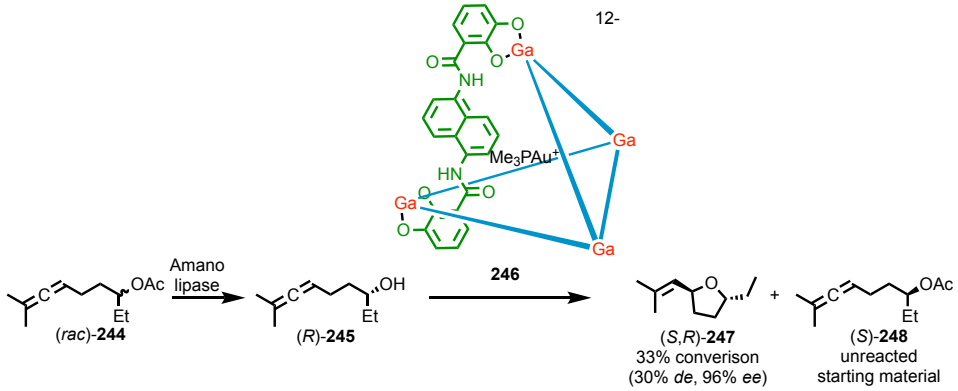

Figure 100: Toste and co-workers' orthogonal enzyme and encapsulated Au^{I} catalysis.[112] Counter-ions removed for clarity.

2.2.5. Oxidative Addition to Au^{I}

Au^{III} complexes are also excellent Lewis acid catalysts. $AuCl_3$ (D_{3h}-symmetric) with a low energy $2a'_1$ LUMO (Figure 101a), catalyses many of the same reactions as Au^{I}.[116] Occupation of this $2a'_1$ orbital by donation from a Lewis base (Figure 101a) leads to a stable square planar complex (Figure 101b). Ligand design to force trigonal planar (D_{3h}) Au^{I} geometry (filled $2a'_1$ orbital, Figure 101a) with bipyridyl ligands,[72] have enabled Au^{I}-Au^{III} oxidative addition (Figure 104).[74] Similarly, oxidative addition of a linear Au^{I} complex has been achieved with pendant tertiary amine groups adjacent to the phosphine ligand, to stabilise the resulting Au^{III}-complex enough to mediate oxidative addition (Figure 103),[71,72,117] but not so much as to inhibit potential reductive elimination.[72]

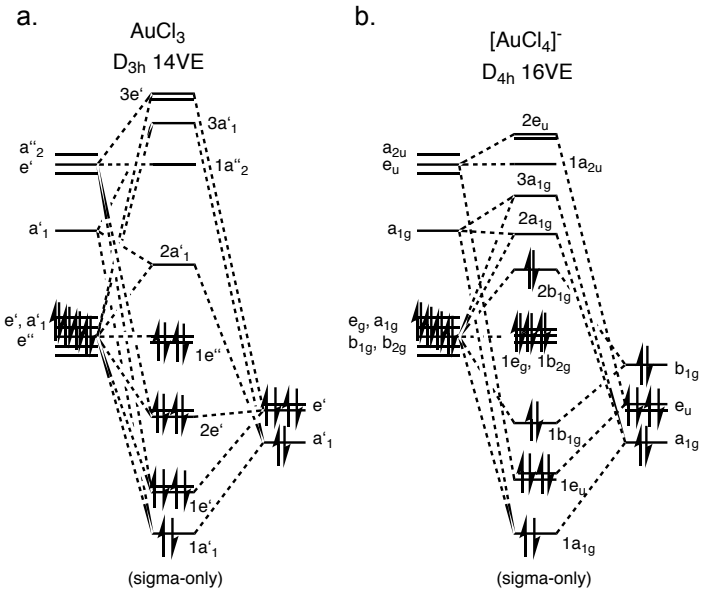

Figure 101: Sigma-bonding only molecular orbital energy level diagram of (a) Au^{III} D_{3h} and (b) D_{4h} complexes explaining the excellent Lewis acid nature of Au^{III}.

Nevado and co-workers' have developed a Suzuki-*like* Au^{I} catalysed cross-coupling, whereby the transmetallation occurs onto the Au^{I} species **107**, followed by oxidation to Au^{III} **251** by an external oxidant, **106**. Finally, an electrophilic aromatic substitution formed a C-Au^{III} bond, **253**, which readily eliminated the coupled product **254** (Figure 102).[73] This route simulates an oxidative addition and aromatic auration by using a strong external oxidant. The facile reductive elimination results from a much less stable Au^{III} complex (Figure 101).

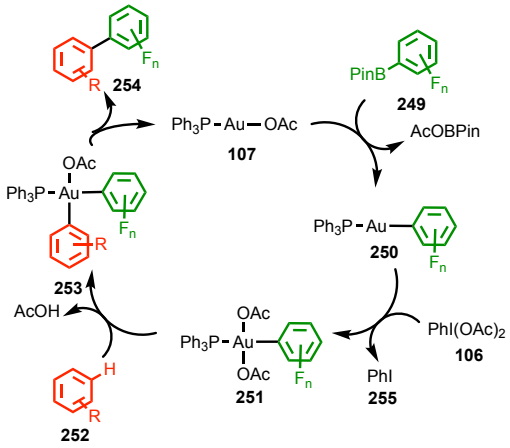

Figure 102: Au^{I} catalysed Suzuki-*like* cross couplings.[73]

Despite the reluctance of Au^{I} to participate in oxidative addition reactions, Bourissou and co-workers have developed an Au^{I}/Au^{III} catalytic cycle whereby Au^{I} oxidative addition occurs with C_{sp}^{2}-X species (Figure 103a), and is *pseudo*-transmetallated by electrophilic aromatic auration of the C_{sp}^{2}-H bond. Finally a reductive elimination results in the overall effect of C-H activation coupling by gold.[72] The linear Au^{I} complex underwent oxidative addition with **255**, due to the tertiary amine component of Me-Dalphos stabilising the Au^{III} intermediate **256**, allowing oxidative addition whilst remaining active to *pseudo*-transmetallation (see molecular orbital energy level diagram Figure 101). Ligand choice is key to achieving both oxidative addition and reductive elimination. Too strong donor in this position would inhibit reductive elimination, thus the tertiary amine donor is fundamental to mediation of Au^{I}-Au^{III} transitions reversibly.[72] Once this balance of secondary donor strength was established, Bourissou and co-workers demonstrated π-alkene complexation and a low-energy rearrangement prior to reductive elimination (Figure 103b).[117] Furthermore, this reaction was highly efficient with a range of electron poor, rich and *ortho*-substituted aryliodides, as well as substituted alkene coupling partners.[117]

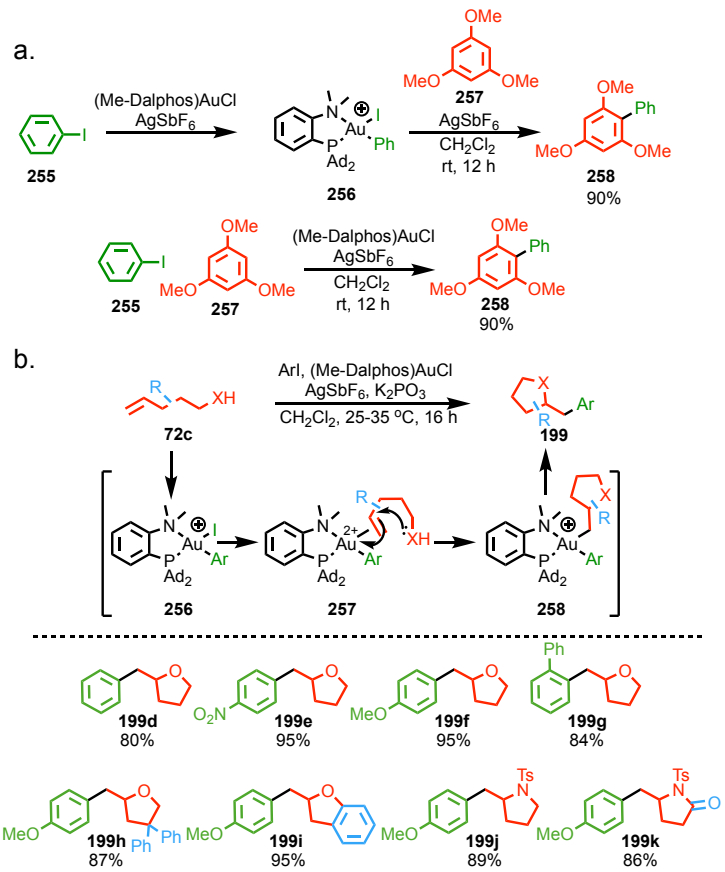

Figure 103: Bourissou and co-workers' Au^{I}/Au^{III} catalytic coupling with (a) C-H auration, and (b) alkene rearrangement transmetallation processes.[72,117]

Russell and co-workers managed to produce a high yielding catalytic Negishi-*like* coupling using Au^{I} in place of Pd^{0}. Bipyridyl ligands forced Au^{I} into a trigonal planar geometry (**261** Figure 101a), encouraging oxidative addition of aryl iodides to form a square planar Au^{III} species **263** (Figure 101b). These Au^{III} species rapidly underwent transmetallation and reductive elimination in a Negishi-*like* manner.[74] The trigonal planar nature of the Au^{I} species **261** (Figure 101) enabled oxidative addition to a stabilised Au^{III} species, analogous to that of Bourissou and co-workers.[72]

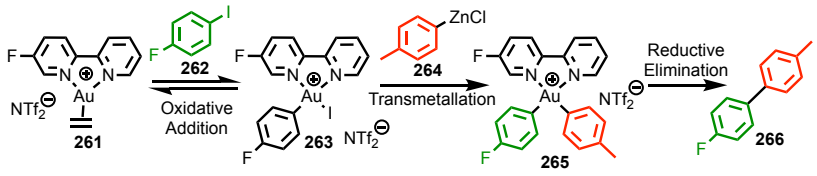

Figure 104: Negishi-*like* Au^{I}-catalysed cross-coupling. Trigonal planar Au^{I} species enabled oxidative addition to occur more easily than in linear Au^{I}-complexes.[74]

2.3. Project Aims

The aim of this project is the synthesis and isolation of enantiopure phosphine ligands displaying MPC stereogenic units. Application of this under-utilised type of chirality, will then be investigated towards the challenging field of enantioselective Au^{I}-catalysis. The hypothesis is that the uniquely crowded chiral environment of a small macrocycle MPC rotaxane, will enable good chiral induction into Au^{I}-catalytic reactions, providing a new approach to asymmetric catalysis.

Previously in the group, Goldup and co-worker[19] synthesised an achiral mechanically interlocked phosphine ligand. This was then coordinated to Au^{I} and used to mediated diastereoselective cyclopropanation reactions of 2-methyl-3-butyn-2-yl esters. The serendipitous discovery of this study was its stimuli-responsive nature. It was found that without an additive, the macrocycle would bind to the cationic Au^{I}-centre, inhibiting catalysis. However, on addition of an acid or metal ion, the bipyridine macrocycle binds to this, freeing the Au^{I} coordination site to mediate catalysis. Achieving asymmetric catalysis with a MPC stereogenic element would demonstrate the first application of this type of mechanical chirality, a significant milestone for the field. Furthermore, stimuli regulated enantioselectivity is desired as this would add to the potential of MPC ligands and improve tuneability.

2.4. Results and Discussion

In order to achieve an enantioselective interlocked catalyst displaying MPC, careful design of the catalyst was key. Previously in the group, the small chiral azide (*S*)-**269** enabled access to up to 96% *de* rotaxanes displaying a MPC stereogenic element. The interlocked catalyst was designed to be compatible with azide (*S*)-**269**, with the aim of utilising this methodology to achieve an interlocked phosphine ligand with 96% *de* (Figure 105).

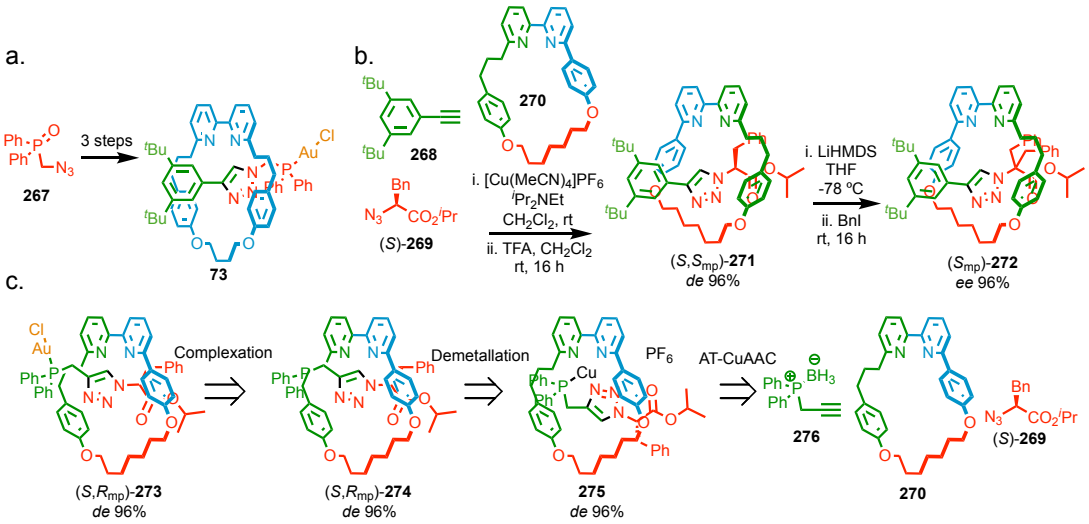

Figure 105: (a) Goldup and co-worker's diastereoselective Au^{I} catalyst. (b) Goldup and co-workers' diastereoselective AT-CuAAC reaction to MPC rotaxanes. (c) Planned retrosynthetic route to 96% *de* Au^{I} rotaxane incorporating a simple chiral directing group.

The initial difference between this catalyst design and rotaxane **73**,[19] is that to use the chiral directing azide (*S*)-**269**, the phosphorous containing component must be bound to the alkyne **276**, as opposed to the azide **267**.[115] Therefore, an initial study was required to establish whether the Au^{I} complex remained catalytically active with the inverted triazole. An achiral analogue of this system was designed to test the new proposed triazole orientation.

2.4.1. Synthesis of an Achiral Au^{I} Rotaxane Catalyst

The C_{2v}-symmetric macrocycle **278** was synthesised, following literature procedures,[19] and used in an AT-CuAAC reaction with alkyne **276** and an azide **277**, yielding the achiral C_s-symmetric rotaxane **279**. Subsequent complexation to Au^{I} yielded the achiral Au^{I} complex **281**, containing the new triazole orientation (Scheme 1).

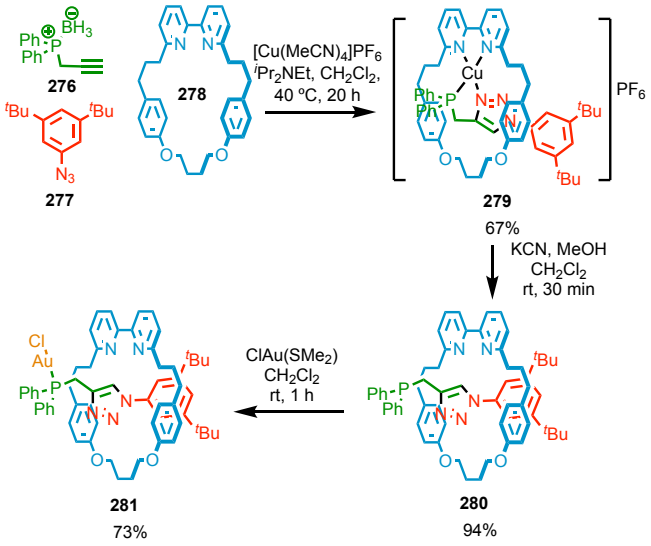

Scheme 1: Synthesis of an achiral, C_s-symmetric, mechanically interlocked Au^{I} complex **281**.

Pre-catalyst **281** was used to mediate the cyclopropanation of **71a** with **72a**. An additive screen showed that complex **281** was active with Cu^{I} (61% NMR yield). However, **281** was much less active with Zn^{II} (2% NMR yield), and completely inactive in the absence of an additive. This result was contrary to the published rotaxane **73**, which was active with Cu^{I}, Zn^{II}, Cd^{II} or H^{+} additives.[19]

With the Cu^{I} additive, **281** achieved 90% *de* of **74a**, comparable to **107** (89% *de*) and the previously published rotaxane **73** (89% *de*).[19] The activity and comparable diastereoselectivity of **281** showed that the triazole inversion would be tolerated in the proposed catalyst retrosynthesis (Figure 105).

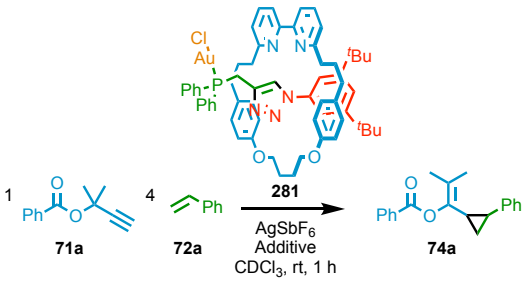

Entry	Catalyst	Additive	Yield **74a** (%) (*cis* : *trans*)	Entry	Catalyst	Additive	Yield **74a** (%) (*cis* : *trans*)
1	$(Ph_3P)AuCl$	None	69 (94 : 6)	4	**281**	Cu^{I}	62 (95 : 5)
2	**281**	None	0	5	**281**	Zn^{II}	2
3	**281**	H^+	0				

Table 1: NMR yields and *dr* of cyclopropanations of **71a** with **72a**. Solvent $CDCl_3$, temperature 25 °C, time 1 h. All experiments were performed in triplicate, average values shown. Catalytic loading was 5 mol%. NMR yields were determined relative to a $C_2H_2Cl_4$ internal standard. H^+ refers to $HOTs.H_2O$, Cu^{I} refers to $[Cu(MeCN)_4]PF_6$, Zn^{II} refers to $Zn(OTf)_2$.

2.4.2. A Covalent Chiral Rotaxane Au^{I} Complex

As the proposed catalyst structure (*S*,R_{mp})-**273** involves a covalent stereogenic centre, it was important to establish the effect of this on the reaction activity and selectivity before applying it to more synthetically-involved structures. Azide (*S*)-**269** was synthesised by diazotisation of (*S*)-**282** with *ee* > 99.5%.[115]

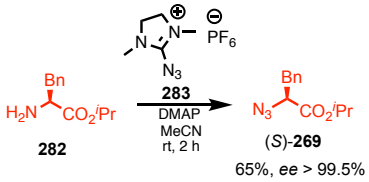

Scheme 2: Synthesis of (*S*)-**269**. DMAP refers to 4-(dimethylamino)pyridine

Azide (*S*)-**269** and alkyne **276** were reacted with the C_{2v}-symmetric macrocycle **278** in an AT-CuAAC reaction to make the C_1-symmetric Au^{I}-complex (*S*)-**285** (Scheme 3). (*S*)-**285** contains a covalent stereogenic centre on the opposite side of the macrocycle to the Au atom. Interlocked catalysts demonstrating enantioselectivity due to a covalent stereogenic centre in the axle or macrocycle have been shown before (Figure 51-53). However, this work is key for testing the catalyst activity with azide (*S*)-**269**, and for establishing the extent of chiral induction of the covalent centre through the macrocycle.

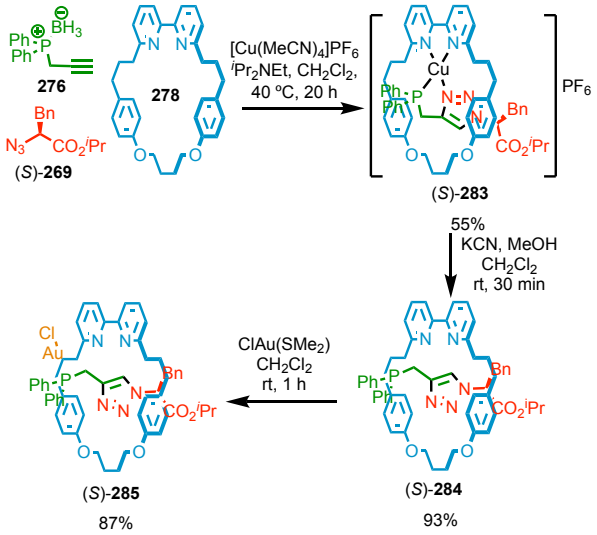

Scheme 3: Synthesis of a C_1-symmetric (*S*)-**285** with a conventional covalent stereogenic centre.

(*S*)-**269** was used to mediate the cyclopropanation of **71a** and **72a** with a Cu^{I} additive (Scheme 4), demonstrating an 87% *de* comparable to **73**, **107**, and **281**. Notably (*S*)-**285** also achieved an *ee* of 5% for the major *cis*-**74a**. This demonstrates that the chirality transfer of the covalent stereogenic centre through the achiral ring is of minimal significance, resulting from the stereo-shielding macrocycle, and the distance between the Au^{I} atom and the stereo-directing group. Therefore the macrocycle was shown to separate the catalytic and chiral components of the rotaxane effectively.

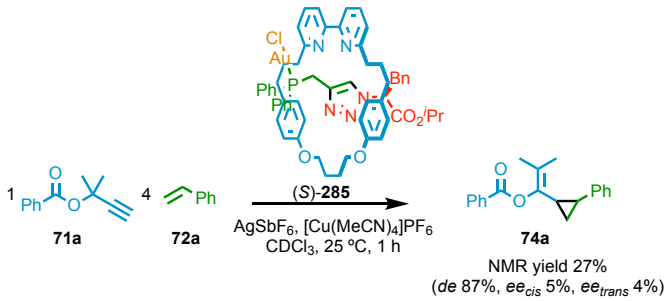

Scheme 4: Cyclopropanation of **71a** with **72a** with catalyst (*S*)-**285**, performed in triplicate.

The chiral inducing behaviour of the chiral stopper should be minimal compared to the MPC directing stereogenic centre in the designed catalyst. From here onwards an MPC analogue was developed to assess the chiral induction from this new stereogenic element.

2.4.3. Interlocked Catalyst Displaying Mechanically Planar Chirality

The AT-CuAAC reaction of (*S*)-**269**, **270** and **276** (Scheme 5) gave a lower than expected 35% *de* of **288** with respect to the mechanical bond. The previously lowest reported *de* with azide (*S*)-**269** was 44%.[115] The 35% *de* of **288** was attributed to the more flexible methylene group adjacent to the alkyne **276**. Demetallation and complexation to Au^{I} achieved a 35% *de* pre-catalyst mixture **289**. The diastereoisomeric mixture of **289** was used to mediate **71a** cyclopropanations with **72a**, achieving 84% *de* and 25% *ee* of *cis*-**74a** (Scheme 6).

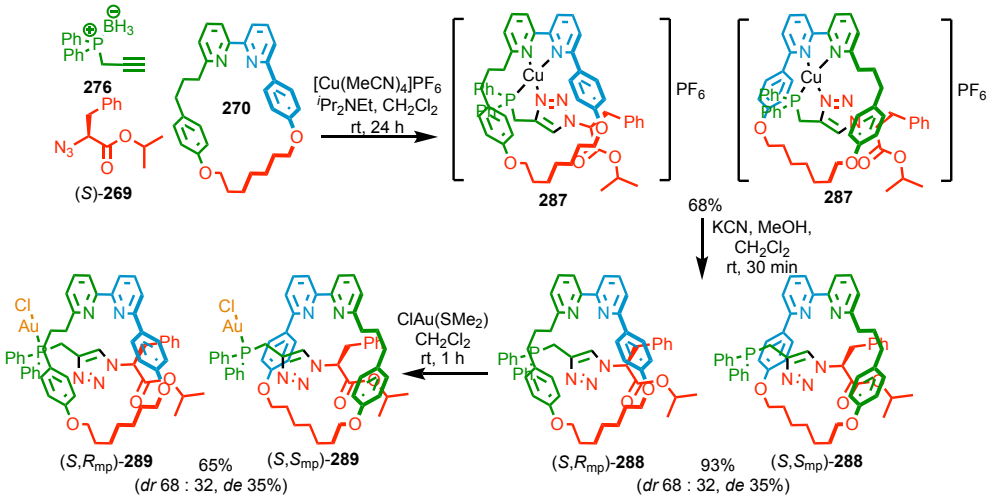

Scheme 5: Synthesis of a C_1-symmetric **289** with both covalent and mechanically planar stereogenic centres.[115]

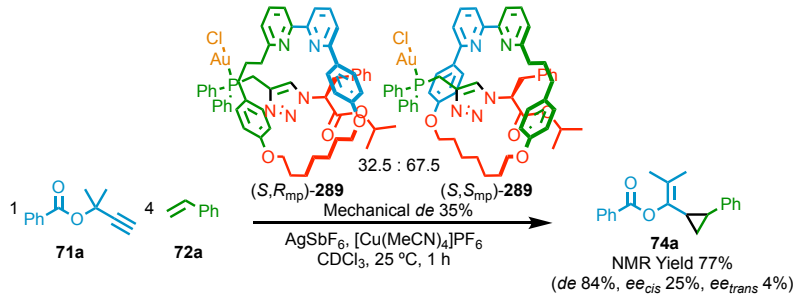

Scheme 6: Cyclopropanation of **71a** with **72a**, mediated by diastereoisomer mixture **289**, performed in duplicate.

It was assumed that the two diastereoisomers (*S*,*R*$_{mp}$)-**289** and (*S*,*S*$_{mp}$)-**289** were equally active and had equal but opposite selectivity, due to the covalent chiral group being far from the Au^{I} centre. The 5% *ee* of analogous catalyst (*S*)-**285**, without an MPC stereogenic unit, suggests this is reasonable.

The promising initial 25% *ee* selectivity resulting from the 35% *de* **289**, confirmed that the investigation of MPC was worthwhile. Separation of the (S,R_{mp})-**289** and (S,S_{mp})-**289** (or intermediates **287**, or **288**) would enable access to a pre-catalyst with one mechanical configuration. This is necessary to fully investigate the chiral induction resulting from the mechanical bond. Furthermore, this would allow evaluation of the activity and selectivities of the two diastereoisomeric catalysts present in the 35% *de* mixture of **289**.

2.4.4. Diastereoisomer Separation

Despite many attempts at separation of **289** and its intermediates **287** and **288** (Scheme 5), the diastereoisomer mixtures were inseparable and unstable on normal (SiO_2 and Al_2O_3) and reverse phase column chromatography (C_{18}-SiO_2). As separation was key to evaluating the chiral induction of MPC rotaxanes, a new route was developed to achieve separable, diastereoisomerically pure rotaxanes (Scheme 7). Oxidation of **288** to the stable phosphine oxide **294** enabled more facile separation, as decomposition was prevented.

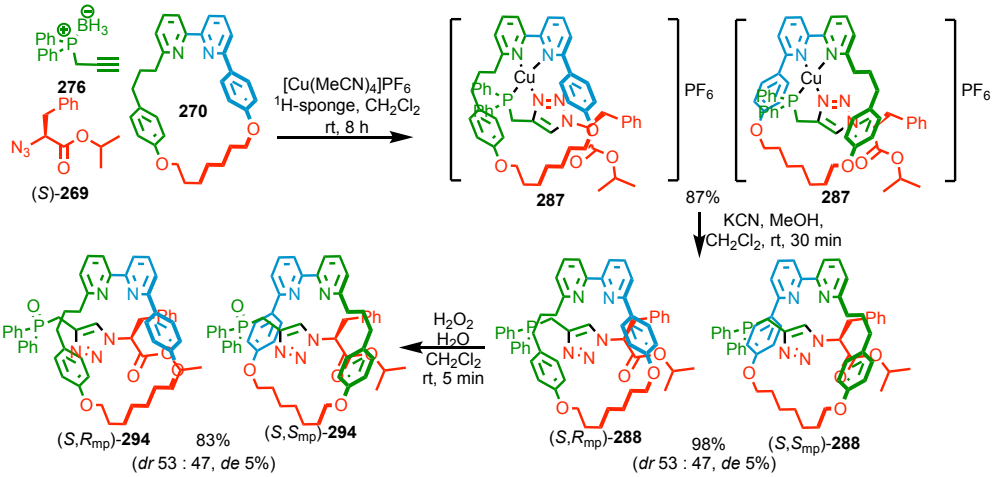

Scheme 7: Synthesis of a stable C_1-symmetric **294**, whose diastereoisomers were separable by normal phase column chromatography (pre-treated SiO_2 with water saturated petrol-Et_2O-EtOAc 5 : 3 : 2).

Stable rotaxanes (S,R_{mp})-**294** and (S,S_{mp})-**294** were analysed by chiral stationary phase HPLC before and after diastereoisomer separation, and it was noticed that epimerisation of the covalent stereocentre was occurring during the three step synthetic process (Scheme 7). Screening bases and solvents for the AT-CuAAC step revealed that epimerisation was occurring during this step. The epimerisation was exacerbated by the polar protic co-solvent EtOH. Screening demetallation and oxidation procedures

revealed that no epimerisation was occurring during these steps, despite the hard nucleophilic nature of KCN. Alternative demetallation conditions such as TFA were significantly slower and showed increased epimerisation.

The $^{i}Pr_2NEt$ base used in the AT-CuAAC step was changed to ^{1}H-sponge (1,8-*bis*(dimethylamino)naphthalene) in anhydrous dichloromethane solvent to minimise epimerisation. Unfortunately, this also reduced the *de* further from 35% to 5%.[115]

Separation of the diastereoisomers by normal phase column chromatography enabled isolation of rotaxanes (*S*,R_{mp})-**294** and (*S*,S_{mp})-**294** in excellent enantiopurity (98% *ee* by CSP-HPLC). However, this process was not reproducible; epimerisation of the covalent stereocentre was also occurring during the chromatography. This was minimised by switching to an automated chromatography system, as this reduced the time the compound spent on silica.

Reproducibility was improved further by equilibration of the column with water saturated eluent before sample addition. Ultimately we were able to reproducibly isolate (*S*,R_{mp})-**294** and (*S*,S_{mp})-**294**. Figure 106 displays 98% *ee* (*S*,R_{mp})-**294** (top) stacked against a racemate of each diastereoisomer.

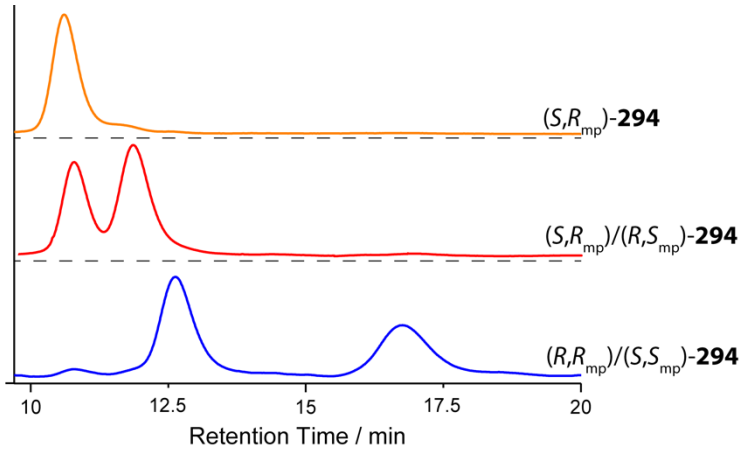

Figure 106: Chiral stationary phase HPLC trace of (*S*,R_{mp})-**294** (top), racemate (*S*,R_{mp})-**294** (10.3 min), (*R*,S_{mp})-**294** (11.4 min) (middle), and the racemate (*R*,R_{mp})-**294** (12.1 min), (*S*,S_{mp})-**294** (16.3 min) (bottom), and. Column: (*S*, *S*)Whelk, Eluent: isocratic *n*-hexane-isopropanol 25-75, flowrate 1 mLmin^{-1}.

2.4.5. Assignment of Absolute Stereochemistry

Single crystals of (*S*,R_{mp})-**294** and (*S*,S_{mp})-**294** were grown by vapour diffusion (see experimental for details) from diastereoisomerically pure samples. The absolute stereochemical assignment of the first eluting diastereoisomer was (*S*,R_{mp})**-294**. Therefore it was known that the species eluting at 10.3 min and 11.4 min in the HPLC

chromatogram corresponded to (*S*,R_{mp})-**294** and (*R*,S_{mp})-**294** respectively. The absolute stereochemical assignment of the second eluting diastereoisomer **294** was (*S*,S_{mp}). Therefore it was now known that the species eluting at 12.1 min and 16.3 min in the HPLC chromatogram corresponded to (*R*,R_{mp})-**294** and (*S*,S_{mp})-**294** respectively.

The mechanical stereogenic centre is assigned by viewing the rotaxane from the highest priority axle element (P_A) to its highest priority substituent (O_B), and determining whether the rotation from the highest priority macrocycle element (O_C) to its highest priority substituent (Ar_D) is clockwise (R_{mp}) or anticlockwise (S_{mp}).[40]

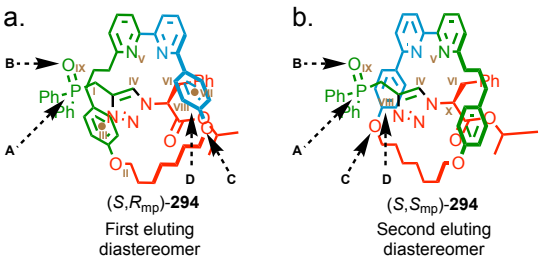

Figure 107: Assigned diastereoisomers (a) (*S*,R_{mp})-**294**, and (b) (*S*,S_{mp})-**294**.

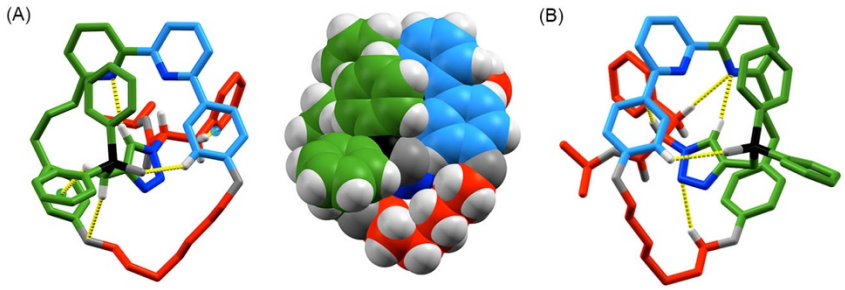

Figure 108: (A) Capped sticks and space fill representations of the solid state structure of (*S*,R_{mp})-**294** with selected intercomponent interactions highlighted (atom labels and colours (O = dark grey, N = dark blue) as in Scheme 1, selected distances (Å): H_I•••O_{II} = 2.4, H_I•••centroid$_{III}$ = 2.6, H_{IV}•••N_V = 2.5, H_{VI}•••centroid$_{VII}$ = 3.2, H_{VIII}•••O_{IX} = 2.5). (B) Solid state structure of (*S*,S_{mp})-**294** with selected intercomponent interactions (atom labels and colours (O = dark grey, N = dark blue), selected distances (Å): H_{IV}•••N_V = 2.4, H_X•••C = 2.6, H_{VI}•••N_V = 2.7, H_{VIII}•••O_{IX} = 2.7). It should be noted that the asymmetric unit contains an oxidised derivative of (*S*,S_{mp})-**294** as a disordered impurity. The figure depicts the component of the unit cell that is unaffected by this disorder.

2.4.6. Catalysis with a Single MPC Stereogenic Element

After managing to isolate, and unambiguously assign enantiopure (*S*,R_{mp})-**294** and (*S*,S_{mp})-**294**, all that remained to access the initial catalyst design (*S*,R_{mp})-**273** was reduction of the P^V=O and complexation to Au^I. Unfortunately, attempts to reduce P^V=O of each diastereoisomer resulted in epimerisation of the covalent stereogenic centre, resulting in a near 1 : 1 diastereoisomeric mixture of phosphines (*S*/*R*,R_{mp})-**288** (*de* 5%, Scheme 8), seen by ^{1}H and ^{31}P{^{1}H} NMR. This epimerisation was due to the harsh reduction conditions and extensive work up procedure required to remove all

triethylammonium chloride salt from the rotaxane (*S*/*R*,R_{mp})-**288**. Fortunately, the MPC stereogenic unit could not epimerise. Catalyst (*S*/*R*,R_{mp})-**273** (*de* 5%, R_{mp}:S_{mp} 95 : 5) was used to mediate an Au^{I}-catalysed cyclopropanation, achieving 13% ee_{cis} of **74a**, (Figure 109).

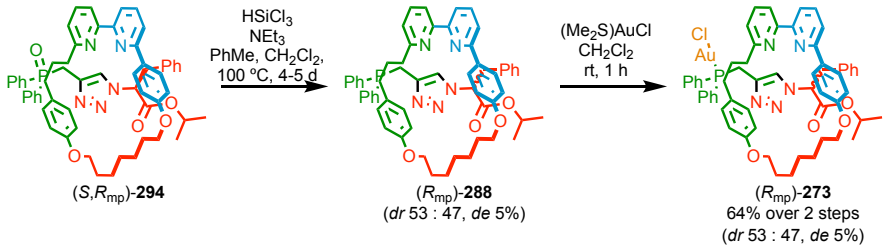

Scheme 8: Reduction of (*S*,R_{mp})-**294**, resulting in epimerisation, and subsequent complexation to Au^{I}.

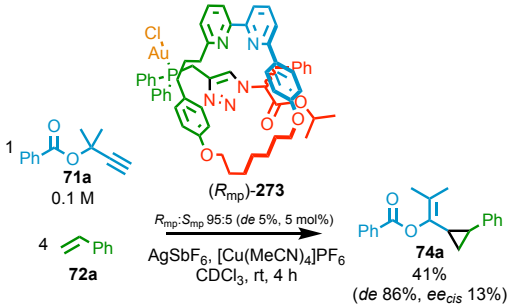

Scheme 9: Cyclopropanation results with (R_{mp})-**273**. This experiment was performed in duplicate.

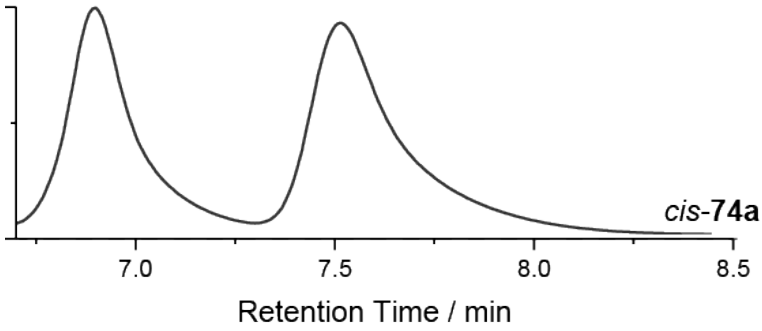

Figure 109: Chiral Stationary Phase HPLC trace of the *cis*-**74a** of the cyclopropane detailed above in Scheme 9, RegisPack, isocratic hexane-isopropanol 99 : 1, 1 mgmL-1, 5 µL injection, 0.75 mLmin^{-1}. 6.4 min (694157, 43.6%), 7.0 (898454, 56.4%)

The enantioselectivity of (R_{mp})-**273** was lower than anticipated. The inconsistency of this result with the initial lead 25% *ee* from the diastereoisomeric mixture suggests that the two diastereoisomers (*S*,R_{mp})-**273** and (*R*,R_{mp})-**273** have different activities and selectivities. Unfortunately, as these could not be isolated on their own, this wasn't evaluated. Thus, it cannot be assumed that the mechanical chirotopic element is the dominant one in directing stereoselectivity.

2.4.7. Au^{I} Complex with a Single Mechanically Planar Chirotopic Element

To avoid the issue of epimerisation during the P^{V}=O reduction, the enantiopure rotaxane (S,R_{mp})-**294** was alkylated prior to reduction (Scheme 10). The alkylated rotaxane (R_{mp})-**295** had only one chirotopic element (the mechanical bond). The bulkier stopper was expected to enhance chiral induction from the mechanical bond, by forcing the macrocycle closer to the Au^{I} catalytic centre.

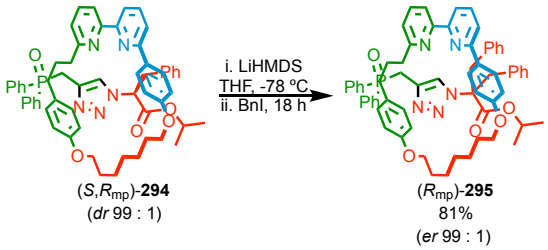

Scheme 10: Alkylation of (S,R_{mp})-**294**, symmetrising the covalent stereogenic centre to give 98% *ee* (R_{mp})-**295**.

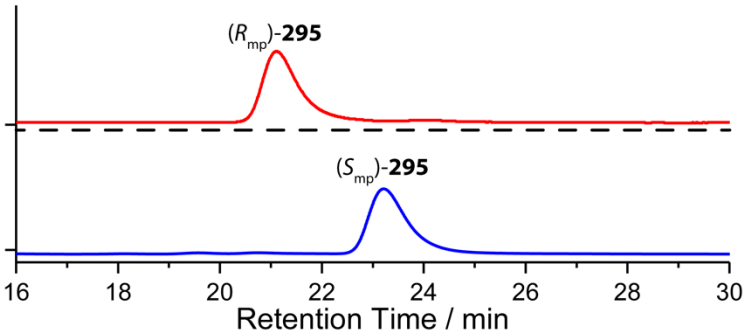

Figure 110: Chiral Stationary Phase HPLC ((*S*,*S*)Whelk, isocratic *n*-hexane-isopropanol 70 : 30, 303 K, load solvent Et_2O, 5 µL injection, flowrate 0.75 $mLmin^{-1}$) of 99 : 1 *er* (R_{mp})-**295** (red). Retention times (min): (R_{mp})-**295** 21.6 (379266, 98.9%), (S_{mp})-**295** 25.2 (4118, 1.1%). 1 : 99 *er* (S_{mp})-**295** (blue). Retention times (min): (R_{mp})-**295** 20.9 (185193, 1.2%), (S_{mp})-**295** 24.2 (15419194, 98.8%).

Using catalysts derived from (R_{mp})-**295**, it is clear that any chiral induction is a result of the mechanical bond, as no other chirotopic elements are present. No alkylation of the methylene adjacent to the phosphine oxide was observed. Reduction and complexation to Au^{I} yielded pre-catalyst (R_{mp})-**296** in 98% *ee* (Scheme 11).

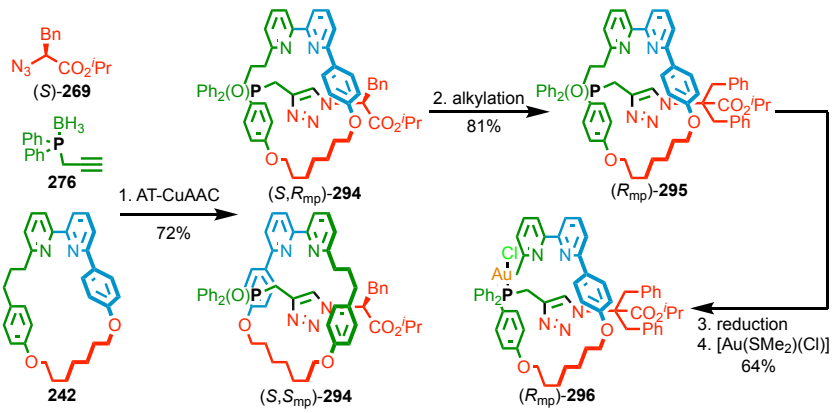

Scheme 11: Full synthesis of (R_{mp})-**296**. Reagents and conditions: 1. (i) $[Cu(MeCN)_4]PF_6$, ^{1}H-sponge®, CH_2Cl_2, rt, 8 h; (ii) KCN, MeOH-CH_2Cl_2 (1 : 1), rt, 30 min; (iii) H_2O_2 (35% w/w in H_2O), CH_2Cl_2, rt, 5 min. 72% combined yield over 3 steps prior to separation of diastereomers. (*S*,R_{mp})-**294**: 30%, 98% *ee*, >99 : <1 *dr*; (*S*,S_{mp})-**294**-(*R*,S_{mp})-**294**-(*S*,R_{mp})-**294** = 98.4 : 1.0 : 0.6. 2. LiHMDS, THF, –78 °C then, BnI, –78 °C to rt, 18 h. (R_{mp})-**295**: 81% (98% *ee*). (S_{mp})-**295** 63% (98% *ee*; not shown, see ESI). 3. $HSiCl_3$, NEt_3, PhMe, CH_2Cl_2, 100 °C, 3 d. 4. $(Me_2S)AuCl$, CH_2Cl_2, rt, 1 h. (R_{mp})-**295**: 64% yield over two steps (98% *ee*). (S_{mp})-**296**: 62% (98% *ee*; not shown).

This pre-catalyst mediated the cyclopropanation reaction of **71a** with **72a**, achieving an impressive ee_{cis} of 62% for cyclopropane *cis*-**74a** (Scheme 12, Figure 111). Thus, work was continued to screen solvents, additives, temperatures and substrates to optimise enantioselectivity.

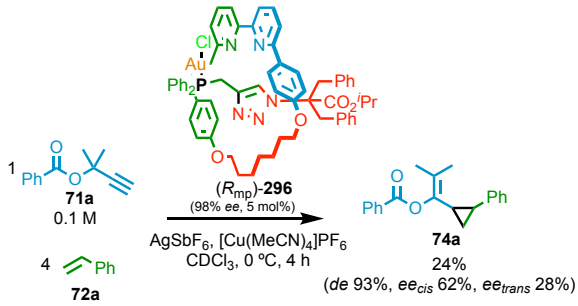

Scheme 12: Cyclopropanation results with the 98% *ee* (R_{mp})-**296**.

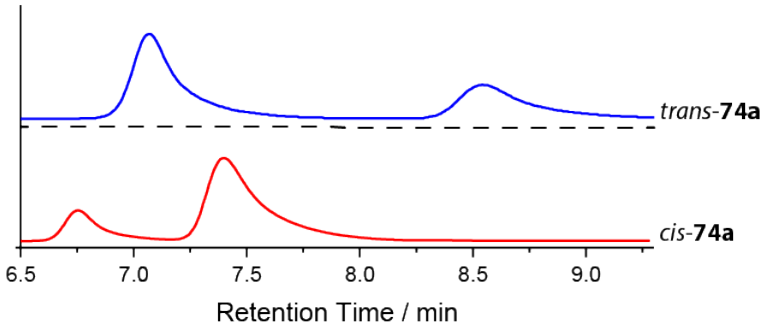

Figure 111: Chiral Stationary Phase HPLC trace of the *cis*-**74a** (red 6.3 min (2728957, 19.1%), 6.90 (11535412, 80.9%)) and *trans*-**74a** (blue 6.3 min (953580, 63.8%), 6.90 (541727, 36.2%)) diastereoisomer of the cyclopropane. RegisPack, isocratic *n*-hexane-isopropanol 99-1, 1 $mgmL^{-1}$, 5 µL injection, 0.75 $mLmin^{-1}$.

2.4.8. Optimisation of Reaction Conditions

In order to optimise the reaction conditions to maximise the enantioselectivity of (R_{mp})-**296**, a solvent screen with **107** was completed showing that CCl_4, $CDCl_3$, CD_2Cl_2, $MeNO_2$ and PhMe allowed high conversion after only 1 h (entries **1**-**4**, **6**, Table 2). These solvents were chosen to apply to (R_{mp})-**296**. EtOAc, Et_2O, THF, and 1,4-dioxane (entries **8**-**11**) were low yielding so were not used for the interlocked catalyst.

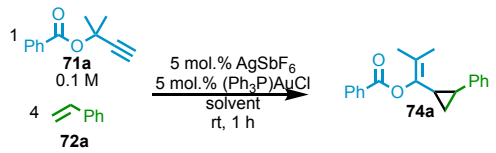

Entry	Solvent	Yield **74a** (%)[a] (*cis* : *trans*)	Entry	Solvent	Yield **74a** (%)[a] (*cis* : *trans*)	Entry	Solvent	Yield **74a** (%)[a] (*cis* : *trans*)
1	CCl_4	45 (90 : 10)	**5**	*n*-hexane	47 (89 : 11)	**9**	Et_2O	22 (94 : 6)
2	$CDCl_3$	63 (90 : 10)	**6**	PhMe	45 (94 : 6)	**10**	THF	12 (89 : 11)
3	CH_2Cl_2	73 (90 : 10)	**7**	C_6D_6	32 (92 : 8)	**11**	1,4-dioxane	22 (94 : 6)
4	$MeNO_2$	71 (89 : 11)	**8**	EtOAc	31 (94 : 6)			

Table 2: Results from the solvent screen of **107** catalysed synthesis of **74a**. [a]NMR yields were determined relative to an internal standard $C_2H_2Cl_4$.

*2.4.8.1. Optimisation of Reaction Conditions for (R_{mp})-**296***

The first variable screened for catalyst (R_{mp})-**296** was the reaction solvent. At room temperature after 1 h, (R_{mp})-**296** achieved 72 : 28 er_{cis} in $CDCl_3$ (entry **2**, using 94% *ee* (R_{mp})-**296**). $MeNO_2$ (entry **4**), and CD_2Cl_2 (entry **5**) gave low enantioselectivities (53 : 47 er_{cis} and 64 : 36 er_{cis} respectively). No improvement was observed with other solvents in the screening (entries **2**-**7**). Because of the higher yields, lower toxicity and lower price of $CDCl_3$ compared to CCl_4 and PhMe (entries **6**-**7**, 71 : 29 er_{cis} and 69 : 31 er_{cis}), this was the solvent used for the rest of the study.

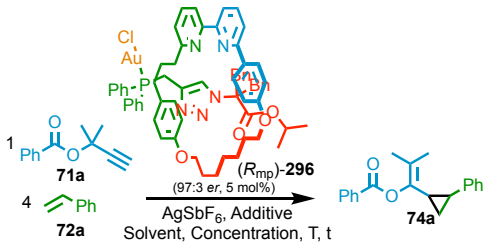

Entry[a]	Solvent	T (°C)	Additive	t (h)	Yield 74a (%) (*cis* : *trans*[b])	*e.r.*$_{cis}$[c]	*e.r.*$_{trans}$[c]
1	$CDCl_3$	25	-	1	-	-	-
2	$CDCl_3$	25	Cu^{I}	1	42 (95 : 5)	72 : 28	58 : 42
3[d]	$CDCl_3$	25	Cu^{I}	1	35 (95 : 5)	29 : 71	42 : 58
4	$MeNO_2$	25	Cu^{I}	1	69 (87 : 13)	53 : 47	65 : 35
5	CD_2Cl_2	25	Cu^{I}	1	13 (83 : 17)	64 : 36	66 : 34
6	CCl_4	25	Cu^{I}	1	46 (86 : 14)	71 : 29	58 : 42
7	PhMe	25	Cu^{I}	1	17 (85 : 15)	69 : 31	56 : 44
8[e]	$CDCl_3$	0	-	6	-	-	-
9[e]	$CDCl_3$	0	Cu^{I}	6	86 (94 : 6)	79 : 21	62 : 38
10[e]	$CDCl_3$	0	Zn^{II}	6	0 (-)	-	-
11[e]	$CDCl_3$	0	H^+	6	1 (-)	-	-
12[e]	$CDCl_3$	0	-	6	0 (-)	-	-
13	$CDCl_3$	-35	Cu^{I}	24	25 (96 : 4)	79 : 21	61 : 39
14[f]	$MeNO_2$	25	-	0.5	73 (>20 : 1)	16 : 84	-

Table 3: [a](R_{mp})-**296** with e.r. = 97 : 3 stereopurity was used for screening experiments unless otherwise stated. [b]Determined by ^{1}H NMR analysis of the crude reaction product using $C_2H_2Cl_4$ as an internal standard for yield determination. [c]Determined by HPLC. [d]Reaction conducted with (S_{mp})-**296** of 3 : 97 *er*. [e]Reaction conducted with (R_{mp})-**296** with *er* = 99 : 1 stereopurity. Cu^{I} refers to $[Cu(MeCN)_4]PF_6$, Zn^{II} refers to $Zn(OTf)_2$, H^+ refers to $HOTs.H_2O$, Ag^{I} refers to $AgSbF_6$. [f]Reaction outcome reported by Toste and co-workers for (*R*)-DTBM-SEGPHOS®$(AuCl)_2$.

Cooling the reaction from room temperature to 0 °C improved the enantioselectivity of **74a** from 72 : 28 to 79 : 21 *er*$_{cis}$ (entries **2** and **9**). However, further cooling to -35 °C (entry **13**) did not increased the enantioselectivity further. All additives besides Cu^{I} showed negligible conversion (entries **10**-**11**).

One potential explanation for the enhanced enantioselectivity at 0 °C, is that under these conditions the formation of Au nanoparticles is reduced; the reaction mixture did

not darken significantly at lower temperatures, implying greater catalyst stability. Given that Au nanoparticles can be catalytically active and are expected to be unselective, minimising this second pathway would enhance the enantioselectivity. Furthermore, this explains why the enantioselectivity did not increase any further at -35 ˚C, as would be expected if there was a significant difference in activation energies of the two pathways.

The stimuli-responsive rotaxane **73** could be activated with Cu^{I}, H^{+}, Zn^{II} or Cd^{II}.[19] However, as neither **281** or (R_{mp})-**296** showed conversion with Zn^{II} and H^{+}, it was assumed that this reduced activity resulted from the inverted triazole.

The final variable screened for effects on the reaction enantioselectivity was reaction concentration. Concentration screening (entries **15**-**17**) showed no significant change in er_{cis} with concentration, therefore 0.10 M was continued with as optimum conditions.

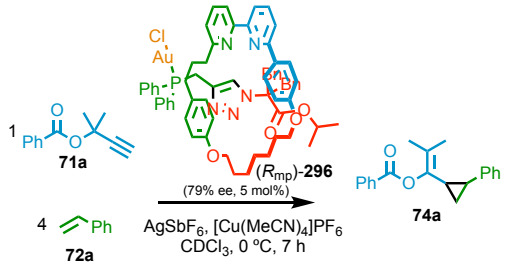

Entry[a]	Solvent	Concentration (M)	Additive	Yield **74a** (%) (*cis* : *trans*[b])	*e.r.*$_{cis}$[c]	*e.r.*$_{trans}$[c]
15	$CDCl_3$	0.10	Cu^{I}	77 (95 : 5)	76 : 24	61 : 39
16	$CDCl_3$	0.05	Cu^{I}	68 (95 : 5)	76 : 24	61 : 39
17	$CDCl_3$	0.20	Cu^{I}	86 (93 : 7)	73 : 27	-

Table 4: [a] (R_{mp})-**296** with *e.r.* = 90 : 10 stereopurity was used for screening experiments unless otherwise stated. [b]Determined by ^{1}H NMR analysis of the crude reaction product using $C_2H_2Cl_4$ as an internal standard for yield determination. [c]Determined by HPLC. Cu^{I} refers to $[Cu(MeCN)_4]PF_6$.

Finally, the absolute stereochemistry of cyclopropanes **74a** produced by catalyst **296** was determined by comparing the HPLC chromatogram of the major *cis*-**74a** produced by **296** (entries **2**-**3**), with that produced using (*R*)-DTBM-SEGPHOS®$(AuCl)_2$ (entry **14**) under conditions reported by Toste and co-workers, the stereochemical outcome is known to be (1*R*,2*S*)-**74a**. Using this approach, the reactions mediated by (R_{mp})-**296** and (S_{mp})-**296** (entries 2 and 3) were shown to yield (1*S*,2*R*)-**74a** and (1*R*,2*S*)-**74a** respectively as their major products (**Figure 112**).

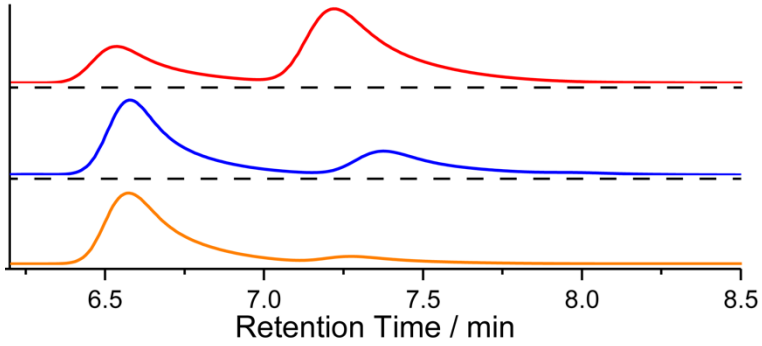

Figure 112: Chiral Stationary Phase HPLC (RegisPack, *n*-hexane-isopropanol 99 : 1, 303 K, load Et_2O, flowrate 0.75 $mLmin^{-1}$) (*red*, *top*) 72 : 28 *er cis*-**74a** produced using (R_{mp})-**296** (97 : 3 er). Retention times (min): (1*R*,2*S*)-**74a** 6.6 (28.4%), (1*S*,2*R*)-**74a** 7.4 (71.6%). (*blue*, *middle*) 29 : 71 *er cis*-**74a** produced using (S_{mp})-**296** (3 : 97 er). Retention times (min): (1*R*,2*S*)-**74a** 6.6 (71.0%), (1*S*,2*R*)-**74a** 7.4 (29.0%). (*orange*, *bottom*) *cis*-**74a** produced using (*R*)-DTBM-SEGPHOS®$(AuCl)_2$ in according to literature conditions to determine absolute stereochemistry. Retention times (min): (1*R*,2*S*)-**74a** 6.6 (88.0%), (1*S*,2*R*)-**74a** 7.4 (12.0%).

2.4.9. Substrate Scope

After determining optimum conditions for catalyst **296**, substrates were screened to establish the generality of the catalyst, and whether steric or electronic effects of the substrates would influence the reaction selectivity.

It was not possible to develop HPLC conditions to separate the stereoisomers of all cyclopropane products. To determine the stereochemical outcome of these reactions, the inseparable cyclopropane products were reduced to the corresponding ketone which was separable by HPLC, as previously reported by Toste and co-workers' (Scheme 13).[75] It was confirmed that there was no epimerisation of ketone **297** by monitoring the *de* of the cyclopropanes *cis*-**74a** and *trans*-**74a**, before and after reduction. The absence of epimerisation is to be expected due to the highly strained sp^2 cyclopropane of the enol intermediate. No change in *de* implied that $LiAlH_4$ reductions were an adequate method to determine the *ee* of compounds (varied R_1) which could not otherwise be separated by HPLC.[75] Although this approach would reduce the number of HPLC conditions required for cyclopropanes (as it only contains R_2), this approach was not used generally, due to the requirement of additional small scale reaction reactions.

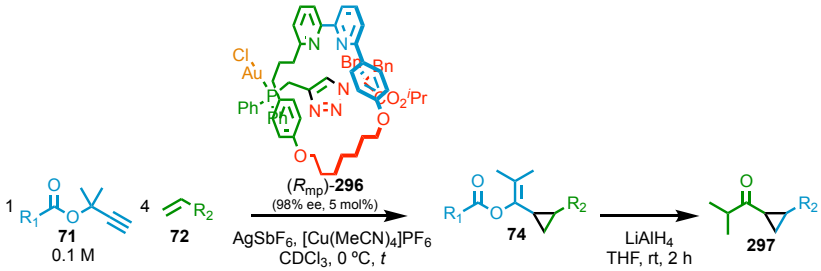

Scheme 13: Cyclopropanation scheme for substrate screen. Optimised conditions 5 mol% (R_{mp})-**296**, $[Cu(MeCN)_4]PF_6$ and $AgSBF_6$. 1 eq. **71** (0.1 M in $CDCl_3$), 4 eq. **72**, 0 °C.

In Toste and co-workers' previous work,[75] varying carboxylate R_1 (Scheme 13) significantly improved the enantioselectivity of (*R*)-DTBM-SEGPhos(AuCl)$_2$, with the best R_1 being a *t*-Bu group and best R_2 being mesityl group. With catalyst (R_{mp})-**296**, pivaloate ester **71** (R_1 = ^{t}Bu), was reacted with a variety of alkenes to give the corresponding cyclopropanes in low enantioselectivity. *Cis*-**74c** 10% *ee* (Figure 113) had been previously reported at 81% *ee*.[75]

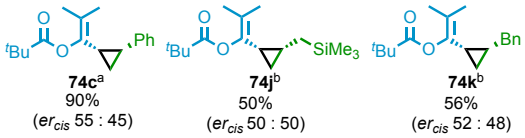

Figure 113: Substrate screen of pivaloate ester **71** with styrene, allyltrimethylsilane and allylbenzene. [a]completed with 99 : 1 *er* (R_{mp})-**296**. [b]completed with 95 : 5 *er* (R_{mp})-**296**, the normalised *ee*s are shown.

From screening substituted variations of 2-methyl-3-butyn-2-yl esters, it was discovered that the er_{cis} increased significantly from 79 : 21 with *cis*-**74a**, to 87 : 13 with *cis*-**74n**, and to 89 : 11 with *cis*-**74m**. As expected, the increased steric bulk enhanced enantioselectivity. However, mesityl *cis*-**74l** had low 53 : 47 er_{cis}. (R_{mp})-**296** gave similar enantioselectivities for *cis*-**74a** and *cis*-**74w**.

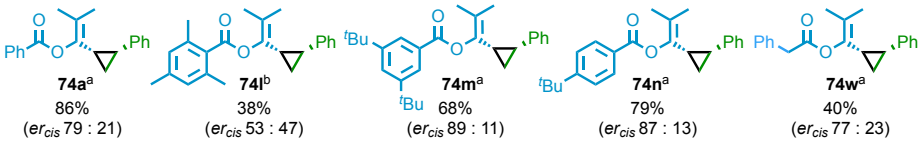

Figure 114: Alkyne substrate screen with styrene. [a]completed with 99 : 1 *er* (R_{mp})-**296**. [b]completed with 95 : 5 *er* (R_{mp})-**296**, the normalised *ee* is shown.

Screening alkenes with 2-methyl-3-butyn-2-yl benzoate revealed promising enantioselectivities for *cis*-**74o** (er_{cis} 72 : 28), *cis*-**74u** (er_{cis} 75 : 25), and *cis*-**74v** (er_{cis} 73 : 27). This implies a good scope with regards to the alkene component.

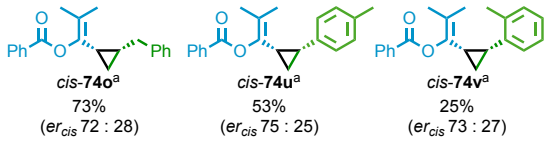

Figure 115: Alkene scope of benzoate esters . [a]completed with 99 : 1 *er* (R_{mp})-**296**.

The 4-substituted position on ester **71** was investigated to determine whether electron donating and withdrawing groups had an effect on enantioselectivity (Scheme 14). The steric bulk of *cis*-**74n** (X = *t*-Bu) gave high er_{cis} 87 : 13. However, other π-electron donating groups in *cis*-**74p** (X = OMe) decreased enantioselectivity (er_{cis} 71 : 29). Similar selectivities were observed for *cis*-**74q** (X = F) and *cis*-**74r** (X = Cl). π-electron withdrawing groups in *cis*-**74s** (X = CF_3) also gave lower enantioselectivity (er_{cis} 73 : 27). *Cis*-**74t** also gave lower enantioselectivity, however with low conversion. This substrate series revealed that only the steric bulk influenced the enantioselectivity.

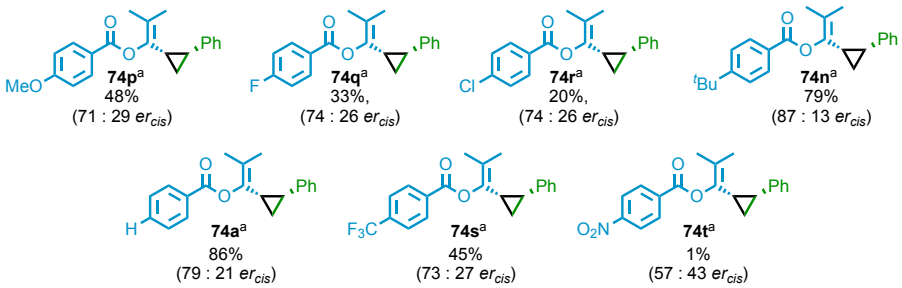

Scheme 14: Investigation of electron donating/withdrawing effects on enantioselectivity. [a]completed with 99 : 1 *er* (R_{mp})-**296**.

2.4.10. Origin of Stereoselectivity in the Au^{I}-Mediated Cyclopropanation Reaction

The calculations in this section were completed by Prof. S. M. Goldup. What follows is a short summary included for completeness.

The size and flexibility of interlocked molecules makes their detailed modelling difficult. The 68% *ee* of *cis*-**74a** implies a small energy difference in activation barrier of 3.0 $kJmol^{-1}$. Computational models of the reaction between **71a** and **72a**, mediated by (R_{mp})-**296**, were completed to determine the origin of the chiral induction from the catalyst to the transition state.

It should be noted that modifications to the axle or macrocycle can change the mechanical stereodescriptor despite maintaining the same orientation. This is not the case when adding Au^{I} to the free phosphine ligand, because the highest priority atom becomes Au_A and the second Cl_B, therefore the orientation of the macrocycle relative

to the axle remains the same as when the highest priority atom was P_A and then O_B. It should also be noted that upon chloride abstraction by Ag^I, the absolute MPC stereodescriptor changes as the highest priority atom Au_A is now bound only to P_B. In calculations, the stereodescriptor of the catalytically active cationic Au^I complex is labelled the same as the pre-catalyst, to avoid confusion of alternating stereodescriptors throughout the reaction mechanism.

The lowest energy transition state for the stereo-defining step for the reaction of **71a** and **72a**, mediated by **107**, was located (CAM-B3LYP/6-31G*/SDD(Au)) reproduced from by Echavarren and co-workers. The reaction of the carbene derived from **71a** with **72a** was found to be a two-step process. A similar pathway for catalyst **296** was assumed. The Cu^I coordination and Cl abstraction give rise to the active catalyst metallo-rotaxane [Cu(**296**)]$^{2+}$. Reaction of [Cu(**296**)]$^{2+}$ with **71a** gave complex **I**. An anchimeric rearrangement follows, forming Au-carbene **II**. Stepwise addition of styrene gives carbocation **III** *via* **TS1**, determining the product stereochemistry. Fast ring closure gives final product cyclopropane **74a** and regenerates [Cu(**296**)]$^{2+}$.

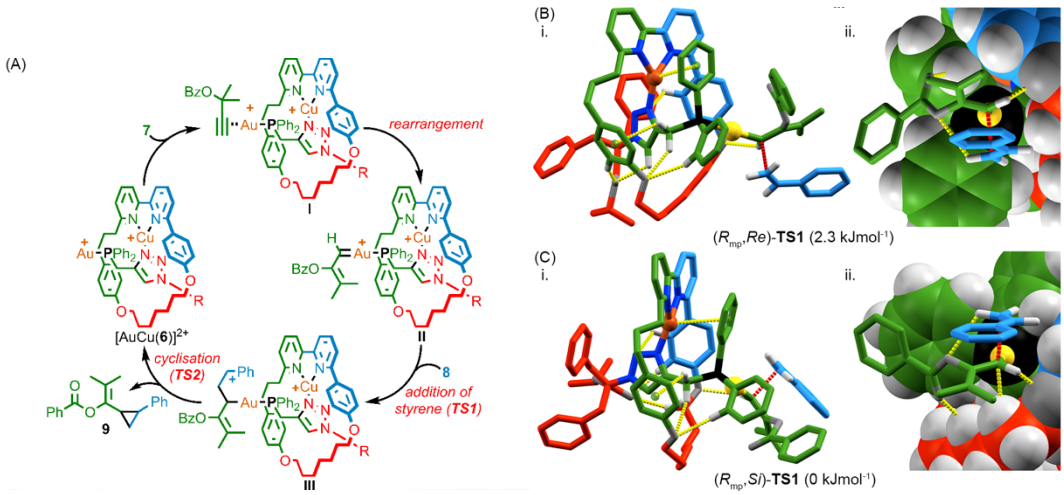

Figure 116: (A) Reaction pathway based on molecular modelling of the reaction of **71a** and **72a**, mediated by **296**. R = $C(Bn)_2CO_2{}^iPr$. (B) Modelling of transition state structure leading to minor enantiomer (1*R*,2*S*)-**74a**. (C) Modelling of transition state leading to major enantiomer (1*S*,2*R*)-**74a.**

Models (R_{mp},*Re*)-**TS1** and (R_{mp},*Si*)-**TS1** (Figure 116) reveal that the rotaxane framework is relatively rigid due to steric crowding combined with the coordination of the Cu^I ion. This is surprising given the size and large number of rotatable bonds in **296**. The transition state rigidity originates from a series of short intra- and inter-molecular interactions (CH hydrogen bonds, CH-π interactions and cation-π interactions between the Cu^I ion and a phosphine Ph substituent). These interactions stabilise the transition

state and project the reactive Au^{I}-carbene moiety towards the macrocycle, close to one of the phenoxy ether groups. The projection of the Au^{I}-carbene moiety towards the macrocycle is observed in the spacefill models of (R_{mp},*Re*)-**TS1** and (R_{mp},*Si*)-**TS1**. The macrocycle blocks one face of the carbene and restricts the rotation of the Au-P bond. A CH-$C_{carbene}$ interaction in the favoured (R_{mp},*Si*)-**TS1** between the substrate and rotaxane stabilises the transition state further.

The MPC stereogenic element allows good chiral induction from catalyst to substrate, resulting in a rigid chiral environment for the catalysis to take place within. (R_{mp},*Si*)-**TS1** was stabilised by an additional 2.3 $kJmol^{-1}$, corresponding to an $er_{cis\mathbf{74a}}$ of 74 : 26 (experimental 3.0 $kJmol^{-1}$ $er_{cis\mathbf{74a}}$ 79 : 21) in favour of the observed major product (1*S*,2*R*)-**74a**.

2.4.11. Catalyst Generality

Two cycloisomerisation reactions and an intramolecular hydroamination reaction were performed to compare the enantioselectivity of (R_{mp})-**296** with (*R*)-DTBM-SEGPHOS®$(AuCl)_2$. Unfortunately no notable enantioselectivity was observed with (R_{mp})-**296**. However, similar results were also obtained for (*R*)-DTBM-SEGPHOS$(AuCl)_2$. The first cycloisomerisation attempted was that of Echavarren and co-workers[81] who achieved an impressive *er* of 97 : 3 with their ligand (*R*,*R*)-**208**.

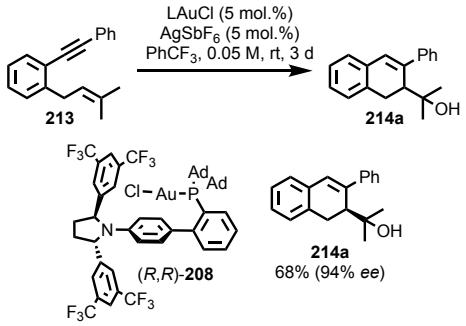

Entry	Catalyst	Yield (%)	*er*
1	Ph_3PAuCl	25	50 : 50
2[a]	(R_{mp})-**296**	18	48 : 52
3[b]	(*R*)-DTBM-SEGPHOS$(AuCl)_2$	9	57 : 43

Table 5: [a]Reaction uses 5 mol.% $[Cu(MeCN)_4]PF_6$ additive. [b]Reaction uses 10 mol.% Ag salt

Although this lack of catalyst generality is disappointing, it is not unexpected given that many highly selective Au^{I}-catalysts are limited to one reaction only. This is demonstrated by the low selectivity of Toste and co-workers' (*R*)-DTBM-SEGPHOS$(AuCl)_2$ in this cycloisomerization.

Sollogoub and co-workers have used their functionalised cyclodextrin NHC-Au^{I} catalysts to mediate an ene-yne cycloisomerisation.[105] Substrate **231b** was synthesised according to literature procedures.[105] Sollogoub and co-workers achieved a best *er* of 80 : 20. However, MPC rotaxane (R_{mp})-**296** catalyst did not induce any enantioselectivity. It is important to note that (*R*)-DTBM-SEGPHOS$(AuCl)_2$ was also used to mediate this reaction and gave no selectivity either.

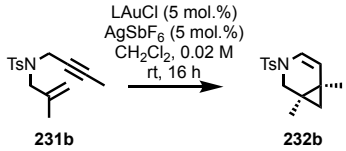

231b **232b**

Entry	Catalyst	Yield (%)	*e.r.*
1	Ph_3PAuCl	76	50 : 50
2[a]	(R_{mp})-**296**	37	51 : 49
3[b]	(*R*)-DTBM-SEGPHOS$(AuCl)_2$	20	50 : 50

Table 6: [a]Reaction uses 5 mol.% $[Cu(MeCN)_4]PF_6$ additive. [b]Reaction uses 10 mol.% Ag salt

Finally Widenhoefer and co-workers' enantioselective hydroamination of an allene was attempted.[118] Substrate **300** was prepared following literature procedures.[118] Widenhoefer reported up to 91 : 9 *er* for this reaction with (*S*)-**174**$(AuCl)_2$, however only 83 : 17 *er* at room temperature. Following this procedure, we achieved no enantioselectivity. Although (*R*)-DTBM-SEGPHOS$(AuCl)_2$ achieved some enantioselectivity, it was much lower than Widenhoefer's catalyst, which is especially surprising given the structural similarity of the two catalysts.

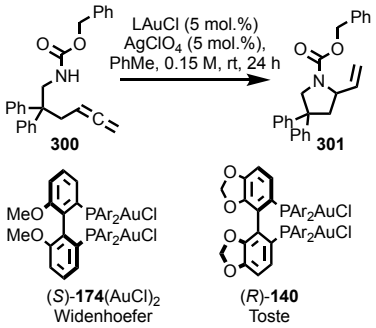

Entry	Catalyst	Yield (%)	*e.r.*
1	Ph_3PAuCl	5	50 : 50
2[a]	(R_{mp})-**296**	51	50 : 50
3[b]	(*R*)-**140**	38	67 : 33

Table 7: [a]Reaction uses 5 mol.% $[Cu(MeCN)_4]PF_6$ additive. [b]Reaction uses 10 mol.% Ag salt. Ar = 3,5-di-*t*-Bu-4-OMe-C_6H_2.

In conclusion, four Au^I-catalysed reactions were screened for both (R_{mp})-**296** and (*R*)-**140**, however no enantioselectivity was observed for the three additional reactions. This low generality was not unexpected and highlights the need for Au^I-catalysts to be screened for multiple reaction types. Echavarren and co-workers' automated screening of 80 ligands for cycloisomerization reactions further highlights the lack of transferability between reaction types.[81]

2.5. Conclusions and Future Work

The synthesis of an enantiopure Au^I-complex with only one stereogenic centre corresponding to the mechanical bond is in itself an achievement as these molecules are still inherently difficult to synthesise. Current work has shown for the first time that chiral induction from MPC is significant for asymmetric catalysis and can result in enantiomeric ratios of up to 9 : 1 in Au^I-catalysed cyclopropanation reactions. This is a promising initial study into mechanically interlocked catalysts and future work on different metal catalysts is currently underway. Second generation MPC catalysts will involve a streamlined synthesis and attempts at a broader range of catalysis to investigate structural relationships to enantioselectivity. The study into triazole orientation and co-factor response will be studied further in later chapters to investigate allosteric regulation of enantiomeric excesses with the co-factor.

2.6. Bibliography

[1] J. P. Sauvage, *Angew. Chem. Int. Ed.* **2017**, *56*, 11080–11093.

[2] E. R. Kay, D. A. Leigh, F. Zerbetto, *Angew. Chem. Int. Ed.* **2007**, *46*, 72–191.

[3] A. W. Heard, S. M. Goldup, *ACS Cent. Sci.* **2020**, *6*, 117–128.

[4] J. F. Stoddart, *Angew. Chem. Int. Ed.* **2017**, *56*, 11094–11125.

[5] I. Aprahamian, *ACS Cent. Sci.* **2020**, *6*, 347–358.

[6] S. Erbas-cakmak, D. A. Leigh, C. T. Mcternan, A. L. Nussbaumer, *Chem. Rev.* **2015**, *115*, 10081–10206.

[7] W. R. Browne, B. L. Feringa, *Nat. Nanotechnol.* **2006**, *1*, 25–35.

[8] T. A. Barendt, A. Docker, I. Marques, V. Felix, P. D. Beer, *Angew. Chem. Int. Ed.* **2016**, *55*, 11069–11076.

[9] M. Denis, J. Pancholi, K. Jobe, M. Watkinson, S. M. Goldup, *Angew. Chem. Int. Ed.* **2018**, *57*, 5310–5314.

[10] R. Mitra, H. Zhu, S. Grimme, J. Niemeyer, *Angew. Chem. Int. Ed.* **2017**, *56*, 11456–11459.

[11] Y. Tachibana, N. Kihara, T. Takata, *J. Am. Chem. Soc.* **2004**, *126*, 3438–3439.

[12] K. Xu, K. Nakazono, T. Takata, *Chem. Lett.* **2016**, *45*, 1274–1276.

[13] T. Kureha, D. Aoki, S. Hiroshige, K. Iijima, D. Aoki, T. Takata, D. Suzuki, *Angew. Chem. Int. Ed.* **2017**, *56*, 1–5.

[14] E. A. Neal, S. M. Goldup, *Chem. Commun.* **2014**, *50*, 5128–5142.

[15] J. Sawada, D. Aoki, H. Otsuka, T. Takata, *Angew. Chem. Int. Ed.* **2019**, *58*, 2765–2768.

[16] V. Blanco, D. A. Leigh, V. Marcos, *Chem. Soc. Rev.* **2015**, *44*, 5341–5370.

[17] V. Blanco, D. A. Leigh, V. Marcos, J. A. Morales-Serna, A. L. Nussbaumer, *J. Am. Chem. Soc.* **2014**, *136*, 4905–4908.

[18] V. Blanco, A. Carlone, K. D. Hänni, D. A. Leigh, B. Lewandowski, *Angew. Chem. Int. Ed.* **2012**, *51*, 5166–5169.

[19] M. Galli, J. E. M. Lewis, S. M. Goldup, *Angew. Chem. Int. Ed.* **2015**, *54*, 13545–13549.

[20] P. Thordarson, E. J. A. Bijsterveld, A. E. Rowan, R. J. M. Nolte, *Nature* **2003**, *424*, 915–918.

[21] R. G. E. Coumans, J. A. A. W. Elemans, R. J. M. Nolte, A. E. Rowan, *Proc. Natl. Acad. Sci.* **2006**, *103*, 19647–19651.

[22] P. H. Ramos, R. G. E. Coumans, A. B. C. Deutman, J. M. M. Smits, R. De Gelder, J. A. A. W. Elemans, R. J. M. Nolte, A. E. Rowan, *J. Am. Chem. Soc.* **2007**, *129*, 5699–5702.

[23] A. B. C. Deutman, C. Monnereau, J. A. A. W. Elemans, G. Ercolani, R. J. M. Nolte, A. E. Rowan, *Science* **2008**, *322*, 1668–1672.

[24] C. Monnereau, P. H. Ramos, A. B. C. Deutman, J. A. A. W. Elemans, R. J. M. Nolte, A. E. Rowan, *J. Am. Chem. Soc* **2010**, *132*, 1529–1531.

[25] N. Miyagawa, M. Watanabe, T. Matsuyama, Y. Koyama, T. Moriuchi, T. Hirao, Y. Furusho, T. Takata, *Chem. Commun.* **2010**, *46*, 1920–1922.

[26] S. Hoekman, M. O. Kitching, D. A. Leigh, M. Papmeyer, D. Roke, *J. Am. Chem. Soc.* **2015**, *137*, 7656–7659.

[27] N. Pairault, H. Zhu, D. Jansen, A. Huber, C. G. Daniliuc, S. Grimme, J. Niemeyer, *Angew. Chem. Int. Ed.* **2020**, *59*, 5102–5107.

[28] A. Martinez-Cuezva, M. Marin-Luna, D. A. Alonso, D. Ros-Niguez, M. Alajarin, J. Berna, *Org. Lett.* **2019**, *21*, 5192–5196.

[29] M. Calles, J. Puigcerver, D. A. Alonso, M. Alajarin, A. Martinez-Cuezva, J. Berna, *Chem Sci* **2020**, *11*, 3629–3635.

[30] C. B. Caputo, K. Zhu, V. N. Vukotic, S. J. Loeb, D. W. Stephan, *Angew. Chem. Int. Ed.* **2013**, *52*, 960–963.

[31] G. Hattori, T. Hori, Y. Miyake, Y. Nishibayashi, *J. Am. Chem. Soc.* **2007**, *129*, 12930–12931.

[32] H. Tian, Q.-C. Wang, *Chem. Soc. Rev.* **2006**, *35*, 361–374.

[33] Y. Lee, K. Liu, C. Lai, Y. Liu, S. Peng, R. P. Cheng, S.-H. Chui, *Chem. Eur. J.* **2017**, *23*, 9756–9760.

[34] C. Biagini, S. D. P. Fielden, D. A. Leigh, F. Schaufelberger, S. Di Stefano, D. Thomas, *Angew. Chem. Int. Ed.* **2019**, *58*, 9876–9880.

[35] S. M. Goldup, *Nat. Chem.* **2016**, *8*, 404–406.

[36] J. Beswick, V. Blanco, G. De Bo, D. A. Leigh, U. Lewandowska, B. Lewandowski, K. Mishiro, *Chem. Sci.* **2015**, *6*, 140–143.

[37] C. Kwan, A. S. C. Chan, K. C. Leung, *Org. Lett.* **2016**, *18*, 976–979.

[38] K. Eichstaedt, J. Jaramillo-Garcia, D. A. Leigh, V. Marcos, S. Pisano, T. A. Singleton, *J. Am. Chem. Soc.* **2017**, *139*, 93676–9381.

[39] D. A. Leigh, V. Marcos, M. R. Wilson, *ACS Catal.* **2014**, *4*, 4490–4497.

[40] E. M. G. Jamieson, F. Modicom, S. M. Goldup, *Chem. Soc. Rev.* **2018**, *47*, 5266–5311.

[41] E. M. G. Jamieson, S. M. Goldup, *Nat. Chem.* **2019**, *11*, 765–767.

[42] Y. Cakmak, S. Erbas-cakmak, D. A. Leigh, *J. Am. Chem. Soc.* **2016**, *138*, 1749–1751.

[43] M. Dommaschk, J. Echavarren, D. A. Leigh, V. Marcos, T. A. Singleton, *Angew. Chem. Int. Ed.* **2019**, *58*, 14955–14958.

[44] G. De Bo, D. A. Leigh, C. T. Mcternan, S. Wang, *Chem. Sci.* **2017**, *8*, 7077–7081.

[45] S. Kassem, A. T. L. Lee, D. A. Leigh, V. Marcos, L. I. Palmer, S. Pisano, *Nature* **2017**, *549*, 374–378.

[46] S. D. P. Fielden, D. A. Leigh, S. L. Woltering, *Angew. Chem. Int. Ed.* **2017**, *56*, 11166–11194.

[47] J. E. Beves, B. A. Blight, C. J. Campbell, D. A. Leigh, R. T. Mcburney, *Angew. Chem. Int. Ed.* **2011**, *50*, 9260–9327.

[48] G. Gil-Ramirez, S. Hoekman, M. O. Kitching, D. A. Leigh, I. J. Vitorica-Yrezabal, G. Zhang, *J. Am. Chem. Soc.* **2016**, *138*, 13159–13162.

[49] T. Prakasam, A. Devaraj, R. Saha, M. Lusi, J. Brandel, C. Platas-iglesias, M. A. Olson, D. Esteban-Gomez, P. S. Mukherjee, A. Trabolsi, *ACS Catal.* **2019**, *9*, 1907–1914.

[50] Y. Segawa, M. Kuwayama, Y. Hijikata, M. Fushimi, T. Nishihara, J. Pirillo, J. Shirasaki, N. Kubota, K. Itami, *Science* **2019**, *365*, 272–276.

[51] P. E. Barran, H. L. Cole, S. M. Goldup, D. A. Leigh, P. R. Mcgonigal, M. D. Symes, J. Wu, M. Zengerle, *Angew. Chem. Int. Ed.* **2011**, *50*, 12280–12284.

[52] C. Romuald, F. Coutrot, *Angew. Chem. Int. Ed.* **2012**, *51*, 2544–2545.

[53] V. Marcos, A. J. Stephens, J. Jaramillo-garcia, A. L. Nussbaumer, S. L. Woltering, A. Valero, J.-F. Lemonnier, D. A. Leigh, *Science* **2016**, *352*, 1555–1560.

[54] J. Berná, M. Alajarín, R. Orenes, *J. Am. Chem. Soc.* **2010**, *132*, 10741–10747.

[55] C. Biagini, S. Albano, R. Caruso, L. Mandolini, J. A. Berrocal, S. Di Stefano, *Chem. Sci.* **2018**, *9*, 181–188.

[56] M. R. Wilson, J. Solà, A. Carlone, S. M. Goldup, N. Lebrasseur, D. A. Leigh, *Nature* **2016**, *534*, 235–240.

[57] S. Erbas-Cakmak, S. D. P. Fielden, U. Karaca, D. A. Leigh, C. T. Mcternan, D. J. Tetlow, M. R. Wilson, *Science* **2017**, *358*, 340–343.

[58] S. Horikoshi, N. Serpone, in *Microwaves Nanoparticle Synth. Fundam. Appl.*, **2013**, 1–24.

[59] D. J. Gorin, F. D. Toste, *Nature* **2007**, *446*, 395–403.

[60] A. S. K. Hashmi, *Chem. Rev.* **2007**, *107*, 3180–3211.

[61] C. Obradors, A. M. Echavarren, *Chem. Commun.* **2014**, *50*, 16–28.

[62] B. Ranieri, I. Escofet, A. M. Echavarren, *Org. Biomol. Chem.* **2015**, *13*, 7103–7118.

[63] H. Schmidbaur, S. Cronje, B. Djordjevic, O. Schuster, *Chem. Phys.* **2005**, *311*, 151–161.

[64] P. Pyykkö, *Inorganica Chim. Acta* **2005**, *358*, 4113–4130.

[65] J. P. Dognon, P. Pyykkö, *Angew. Chem. Int. Ed.* **2017**, *56*, 10132–10134.

[66] P. Pyykko, *J. Comput. Chem. Japan* **2014**, *13*, A2–A3.

[67] H. Tatewaki, S. Yamamoto, Y. Hatano, **2017**, *ASC Omega* **2017**, *2*, 6072-6080.

[68] K. B. Yatsimirskii, *Theor. Exp. Chem.* **1995**, *31*, 153–168.

[69] P. Pyykkö, *Chem. Soc. Rev.* **2008**, *37*, 1967.

[70] O. Crespo, *Modern Supramolecular Gold Chemistry*, **2008**.

[71] B. Huang, M. Hu, F. D. Toste, *Trends Chem.* **2020**, 1–14.

[72] A. Zeineddine, L. Estévez, S. Mallet-Ladeira, K. Miqueu, A. Amgoune, D. Bourissou, *Nat. Commun.* **2017**, *8*, 565.

[73] M. Hofer, A. Genoux, R. Kumar, C. Nevado, *Angew. Chem. Int. Ed.* **2017**, *56*, 1021–1025.

[74] M. J. Harper, C. J. Arthur, J. Crosby, E. J. Emmett, R. L. Falconer, A. J. Fensham-Smith, P. J. Gates, T. Leman, J. E. McGrady, J. F. Bower, *J. Am. Chem. Soc.* **2018**, *140*, 4440–4445.

[75] M. J. Johansson, D. J. Gorin, S. T. Staben, F. D. Toste, *J. Am. Chem. Soc.* **2005**, *127*, 18002–18003.

[76] P. Pérez-Galán, E. Herrero-Gómez, D. T. Hog, N. J. A. Martin, F. Maseras, A. M. Echavarren, *Chem. Sci.* **2011**, *2*, 141–149.

[77] J. Lee, J. Kim, H. Lee, *Org. lett.* **2020**, *22*, 4073-4077.

[78] Z. Zhang, C. Liu, R. E. Kinder, X. Han, H. Qian, R. A. Widenhoefer, N. Carolina, *J. Am. Chem. Soc.* **2006**, *128*, 9066–9073.

[79] Y. Wang, A. D. Lackner, F. D. Toste, *Acc. Chem. Res.* **2014**, *47*, 889–901.

[80] R. A. Widenhoefer, *Chem. Eur. J.* **2008**, *14*, 5382–5391.

[81] G. Zuccarello, J. G. Mayans, I. Escofet, D. Scharnagel, M. S. Kirillova, P. Calleja, J. R. Boothe, A. M. Echavarren, A. H. Pe, *J. Am. Chem. Soc.* **2019**, *141*, 11858–11863.

[82] Z. Zhang, V. Smal, P. Retailleau, A. Voituriez, G. Frison, A. Marinetti, X. Guinchard, *J. Am. Chem. Soc.* **2020**, *142*, 3797-3805.

[83] W. Zi, F. D. Toste, *Chem. Soc. Rev.* **2016**, *45*, 4567–4589.

[84] B. Herle, P. M. Holstein, A. M. Echavarren, *ACS Catal.* **2017**, *7*, 3668–3675.

[85] M. Mato, C. Garcia-Morales, A. M. Echavarren, *ChemCatChem* **2019**, *11*, 53–72.

[86] S. Ferrer, A. M. Echavarren, *Angew. Chem. Int. Ed.* **2016**, *55*, 11178–11182.

[87] C. Navarro, N. D. Shapiro, M. Bernasconi, T. Hirobe, F. D. Toste, *Tetrahedron* **2015**, *71*, 5800–5805.

[88] F. Liu, Y. Wang, W. Ye, J. Zhang, *Org. Chem. Front.* **2015**, *2*, 221–225.

[89] J. M. S. Toro, C. Garc, M. Raducan, E. S. Smirnova, A. M. Echavarren, *Angew. Chem. Int. Ed.* **2017**, *129*, 1885–1889.

[90] W. Zi, H. Wu, F. D. Toste, *J. Am. Chem. Soc.* **2015**, *137*, 3225–3228.

[91] C. Chao, D. Beltrami, P. Y. Toullec, V. Michelet, *Chem. Commun.* **2009**, 6988–6990.

[92] C. Chao, M. R. Vitale, P. Y. Toullec, J. Genþt, *Chem. Eur. J.* **2009**, *15*, 1319–1323.

[93] J. Adrio, J. C. Carretero, A. M. Echavarren, *Organometallics* **2005**, *24*, 1293–1300.

[94] S. Handa, L. M. Slaughter, *Angew. Chem. Int. Ed.* **2012**, *51*, 2912–2915.

[95] D. H. Miles, M. Veguillas, F. D. Toste, *Chem. Sci.* **2013**, *4*, 3427–3431.

[96] J. C. Timmerman, R. A. Widenhoefer, *Org. Lett.* **2017**, *19*, 1466–1469.

[97] K. L. Butler, M. Tragni, R. A. Widenhoefer, *Angew. Chem. Int. Ed.* **2012**, *51*, 5175–5178.

[98] R. E. Kinder, Z. Zhang, R. A. Widenhoefer, *Org. Lett.* **2008**, *10*, 3157–3159.

[99] R. L. Lalonde, B. D. Sherry, E. J. Kang, F. D. Toste, *J. Am. Chem. Soc.* **2007**, *129*, 2452–2453.

[100] K. Nakamura, S. Furumi, M. Takeuchi, T. Shibuya, K. Tanaka, *J. Am. Chem. Soc.* **2014**, *136*, 5555–5558.

[101] A. H. Christian, Z. L. Niemeyer, M. S. Sigman, F. D. Toste, *ACS Catal.* **2017**, *7*, 3973–3978.

[102] J. Carreras, A. Pereira, M. Zanini, A. M. Echavarren, *Organometallics* **2018**, *37*, 3588–3597.

[103] P. Aillard, P. Retailleau, A. Voituriez, A. Marinetti, *Chem. Eur. J.* **2015**, *21*, 11989–11993.

[104] M. J. Campbell, F. D. Toste, *Chem. Sci.* **2011**, *2*, 1369–1378.

[105] P. Zhang, C. Tugny, L. Fensterbank, P. Zhang, C. Tugny, J. Meijide Suarez, M. Guitet, E. Derat, M. Sollogoub, *Chem* **2017**, *3*, 174–191.

[106] C. Tugny, N. del Rio, M. Koohgard, N. Vanthuyne, D. Lesage, K. Bijouard, P. Zhang, J. Meijide Suarez, S. Roland, E. Derat, *ACS Catal.* **2020**, *10*, 5964–5972.

[107] L. R. Macgillivray, J. L. Atwood, *Nature* **1997**, *389*, 469–472.

[108] A. Cavarzan, A. Scarso, P. Sgarbossa, G. Strukul, J. N. H. Reek, *J. Am. Chem. Soc.* **2011**, *133*, 2848–2851.

[109] A. C. H. Jans, A. Gomez-Suarez, S. P. Nolan, J. N. H. Reek, *Chem. Eur. J.* **2016**, *22*, 14836–14839.

[110] C. M. Hong, R. G. Bergman, K. N. Raymond, F. D. Toste, *Acc. Chem. Res.* **2018**, *51*, 2447–2455.

[111] Z. J. Wang, C. J. Brown, R. G. Bergman, K. N. Raymond, F. D. Toste, *J. Am. Chem. Soc.* **2011**, *133*, 7358–7360.

[112] Z. J. Wang, K. N. Clary, R. G. Bergman, K. N. Raymond, F. D. Toste, *Nat. Chem.* **2013**, *5*, 100–103.

[113] M. Galli, S. M. Goldup, *Synthesis of Rotaxane Au Complexes and Application in Gold Catalysis*, **2016**.

[114] R. J. Bordoli, S. M. Goldup, *J. Am. Chem. Soc.* **2014**, *136*, 4817–4820.

[115] M. A. Jinks, A. De Juan, M. Denis, C. J. Fletcher, M. Galli, E. M. G. Jamieson, F. Modicom, Z. Zhang, S. M. Goldup, *Angew. Chem. Int. Ed.* **2018**, *57*, 14806–14810.

[116] B. F. Straub, *Chem. Commun.* **2004**, *13*, 1726–1728.

[117] M. Rigoulet, O. Thillaye du Boullay, A. Amgoune, D. Bourissou, *Angew. Chem. Int.*

Ed. **2020**, *59*, 16625-16630.

[118] Z. Zhang, C. F. Bender, R. A. Widenhoefer, *Org. Lett.* **2007**, *9*, 2887–2889.

[119] A. Pigorsch, M. Kockerling, *Cryst.Growth Des.* **2016**, *16*, 4240–4246.

[120] A. W. Heard, S. M. Goldup, *Chem* **2020**, *6*, 994–1006.

[121] J. E. M. Lewis, R. J. Bordoli, M. Denis, C. J. Fletcher, M. Galli, E. A. Neal, E. M. Rochette, S. M. Goldup, *Chem. Sci.* **2016**, *7*, 3154–3161.

[122] R. J. Detz, S. Are, R. De Gelder, P. W. N. M. Van Leeuwen, H. Hiemstra, J. N. H. Reek, J. H. Van Maarseveen, *Org. Lett.* **2006**, *8*, 3227–3230.

[123] M. Juríek, M. Felici, P. Contreras-Carballada, J. Lauko, S. R. Bou, P. H. J. Kouwer, A. M. Brouwer, A. E. Rowan, *J. Mater. Chem.* **2011**, *21*, 2104–2111.

[124] D. Zeng, R. Zhang, Q. Nie, L. Cao, L. Shang, Z. Yin, *ACS Med. Chem. Lett.* **2016**, *7*, 1197–1201.

[125] S. Thurow, A. A. G. Fernandes, Y. Quevedo-Acosta, M. F. De Oliveira, M. G. De Oliveira, I. D. Jurberg, *Org. Lett.* **2019**, *21*, 6909–6913.

[126] T. A. Bakka, M. B. Strøm, J. H. Andersen, O. R. Gautun, *Bioorg. Med. Chem. Lett.* **2017**, *27*, 1119–1123.

2.7. General Experimental Information

Unless otherwise stated, all reagents were purchased from commercial sources (Acros Organics, Alfa Aesar, Fisher Scientific, FluoroChem, Sigma Aldrich and VWR) and used without further purification. Styrene was purified by vacuum distillation prior to usage and stored under inert N_2 atmosphere. $[Cu(MeCN)_4]PF_6$ was prepared as described by Pigorsch and Köckerling.[119] Anhydrous solvents were purchased from Acros Organics. Petrol refers to the fraction of petroleum ether boiling in the range 40-60 °C. IPA refers to isopropanol. THF refers to tetrahydrofuran. EDTA-NH_3 solution refers to an aqueous solution of NH_3 (17% w/w) saturated with sodium-ethylenediaminetetraacetate. $CDCl_3$ (without stabilising agent) was distilled over $CaCl_2$ and K_2CO_3 prior to use. Unless otherwise stated, all reactions were performed in oven dried glassware under an inert N_2 atmosphere with purchased anhydrous solvents. Unless otherwise stated experiments carried out in sealed vessels were performed in CEM microwave vials, with crimped aluminium caps, with PTFE septa. Young's tap vessels and Schlenk techniques were used where specified.

Flash column chromatography was performed using Biotage Isolera-4 or Isolera-1 automated chromatography system. SiO_2 cartridges were purchased commercially from Teledyne Technologies, or Biotage (SNAP or ZIP, 50 μm irregular silica, default flow rates). Neutralised SiO_2 refers to ZIP cartridges which were eluted with petrol-NEt_3 (99 : 1, 5 column volumes), followed by petrol (5 column volumes). H_2O saturated SiO_2 refers to ZIP cartridges first eluted with H_2O saturated petrol-Et_2O-EtOAc (5 : 3 : 2 shaken with H_2O and the layers separated) followed by petrol-Et_2O-EtOAc (5 : 3 : 2) before loading the compound. Analytical TLC was performed on pre-coated silica gel plates on aluminum (0.25 mm thick, 60F254, Merck, Germany) and observed under UV light (254 nm) or visualised with $KMnO_4$ stain.

All melting points were determined using a Griffin apparatus and are uncorrected. NMR spectra were recorded on Bruker AV400 or AV500 instrument, at a constant temperature of 298 K. Chemical shifts are reported in parts per million from low to high field and referenced to residual solvent. Coupling constants (*J*) are reported in Hertz (Hz). Standard abbreviations indicating multiplicity were used as follows: m = multiplet,

quint = quintet, q = quartet, t = triplet, d = doublet, s = singlet, app. = apparent, br = broad, sept = septet. Signal assignment was carried out using 2D NMR methods (COSY, NOESY, TOCSY, HSQC, HMBC or ^{31}P-^{1}H HMBC) where necessary. In some cases, complex multiplets with multiple contributing proton signals, exact assignment was not possible. In interlocked compounds, all proton signals corresponding to axle components are in lower case, and all proton signals corresponding to the macrocycle components are in upper case. For mixtures of diastereomeric cyclopropanes, upper case is used to denote the major diastereoisomer, and lower case is used to denote the minor diastereoisomer.

Low resolution mass spectrometry was carried out by the mass spectrometry services at University of Southampton (Waters TQD mass spectrometer equipped with a triple quadrupole analyser with UHPLC injection [BEH C18 column; MeCN-H_2O gradient {0.2% formic acid}]). High resolution mass spectrometry was carried out either by the mass spectrometry service at the University of Edinburgh (ThermoElectron MAT 900) or by the mass spectrometry services at the University of Southampton (MaXis, Bruker Daltonics, with a Time of Flight (TOF) analyser; samples were introduced to the mass spectrometer via a Dionex Ultimate 3000 autosampler and UHPLC pump in a gradient of 20% MeCN in hexane to 100% acetonitrile (0.2% formic acid) over 5-10 min at 0.6 mL/min; column: Acquity UPLC BEH C18 (Waters) 1.7 micron 50 × 2.1mm). In HR-MS, the most abundant isotope is quoted. Where 1 Br atom is present, the HR-MS signal quoted corresponds to ^{79}Br. When m/z < 1000, HR-MS is quoted to 4 dp (within 5 ppm of calculated m/z). When m/z > 1000, HR-MS is quoted to 1 dp.

Circular dichroism spectra were acquired on an Applied Photo-physics Chirascan spectropolarimeter, recorded using Applied Photophysics software Ver. 4.2.0 in dried spectroscopic grade $CHCl_3$, following overnight desiccation of the sample, at a concentration range of 0.1-1 10^{-4} M, in a quartz cell of 1 cm path length, at a temperature of 293 K.

Stereochemical purity was determined by Chiral Stationary Phase HPLC on a Waters Acquity Arc Instrument at 303 K, with *n*-hexane-isopropanol isocratic eluents. Regis Technologies (*S*,*S*)-Whelk-O1 (1-(3,5-dinitrobenzamido)-1,2,3,4-tetrahydrophenanthrene stationary phase), RegisPack (tris-(3,5-dimethylphenyl)

carbamoyl amylose stationary phase) and RegisCell (tris-(3,5-dimethylphenyl) carbamoyl cellulose stationary phase) columns were used throughout (5 micron, column dimensions 25 cm x 4.6 mm). The absolute stereochemistry of mechanically planar chiral rotaxanes **294**-**296** was determined by X-ray crystallography of rotaxanes **294**, with the mechanical stereogenic unit assumed to be invariant through subsequent steps. Stereochemical labels were assigned using our established approach. The absolute stereochemistry of cyclopropanes **74a** was determined by comparison with the known stereochemical outcome of the reaction mediated by (*R*)-DTBM-SEGPHOS®(AuCl)$_2$.

Compounds **71a**,[75,120] **71c**,[75,120] **71w**,[125] **74a**,[75] **74c**,[75] **74l**,[75] **213**,[81] **214a**,[81] **231b**,[102] **232b**,[102] (*S*)-**269**,[115] **270**,[121] **276**,[122] **277**,[123] **278**,[121] (*S*)-**282**,[124] **294**-**296**,[120] **300**-**305**[118] were made according to literature procedures and matched literature characterisation. Procedures are included for these molecules if the procedure differs from the literature.

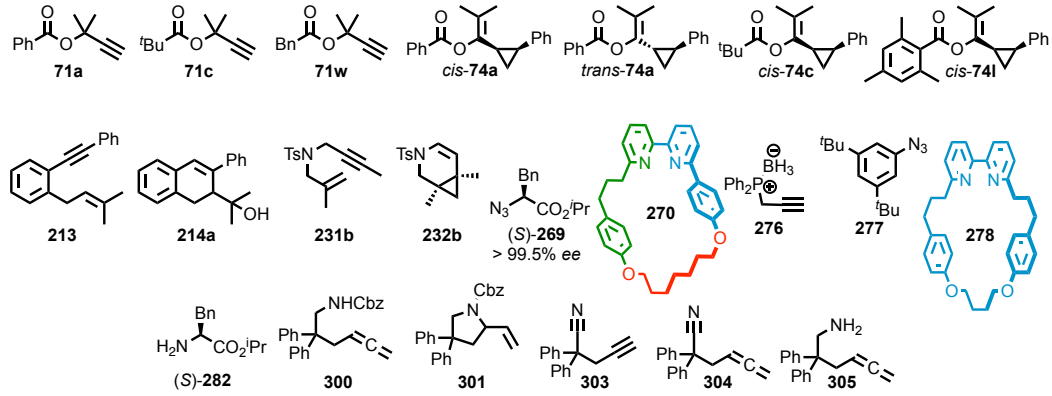

Compound **277**[123,126]

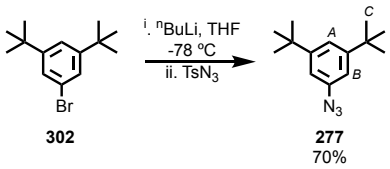

302 **277**
70%

302 (1.35 g, 5.0 mmol, 1.0 eq.) was flushed with N_2 and dissolved in anhydrous THF (50 mL). The solution was cooled to -78 °C in an acetone dry ice bath and stirred for 10 min. *n*-butyllithium (0.384 g, 6.0 mmol, 1.2 eq.) was added dropwise and the reaction mixture stirred for 20 min. TsN_3 (1.20 g, 6.0 mmol, 1.2 eq.) was then added slowly, changing from a white solution to orange and then deep red/purple, and the reaction stirred for 1 h. The mixture was left stirring overnight changing colour to orange, was washed with $NH_4Cl_{(aq)}$ (10 mL) and extracted in Et_2O (3 x 20 mL), dried over $MgSO_4$, filtered and solvent removed under reduced pressure. The crude product was purified by column chromatography (SiO_2, petrol) yielding a yellow oil **277** (0.798 g, 3.45 mmol, 70%). Spectra match literature.[126] δ_H (400 MHz, $CDCl_3$) 7.21 (1H, t, *J* = 1.5, ***H***$_A$), 6.88 (2H, d, *J* = 1.5, ***H***$_B$), 1.33 (18H, s, ***H***$_C$). δ_C ($CDCl_3$, 101 MHz) 152.7, 139.1, 119.3, 113.4, 35.1, 31.3. LR-GC-EI-MS $[M\text{-}N_2]^{+\cdot}$ m/z 203.2 (calc. for $C_{14}H_{21}N$ 203.2).[123,126]

Rotaxane **281**

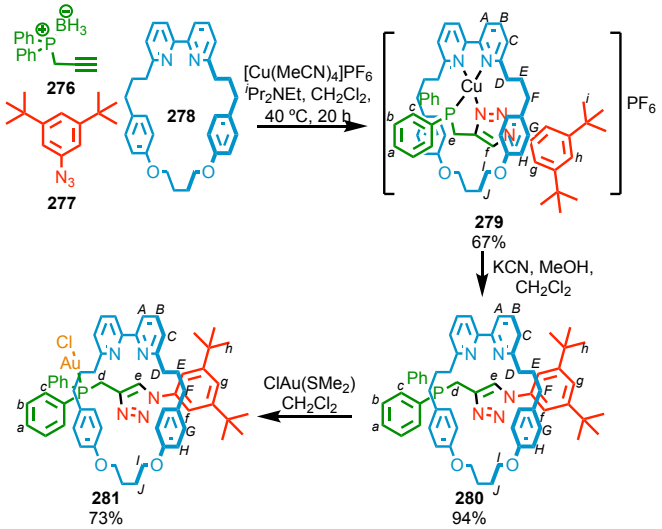

278 (48.0 mg, 0.100 mmol, 1.0 eq.), **276** (71.6 mg, 0.301 mmol, 3.0 eq.), **277** (69.6 mg, 0.301 mmol, 3.0 eq.), $[Cu(MeCN)_4]PF_6$ (35.9 mg, 0.096 mmol, 0.96 eq.) and *N,N*-diisopropylethylamine (0.17 mL, 1.30 g, 1.0 mmol, 10 eq.) were stirred in anhydrous CH_2Cl_2 (9 mL) at 40 °C for 16 h under N_2, quickly changing from orange to yellow. The solution was then diluted with CH_2Cl_2 (15 mL), washed with sat. EDTA-NH_3 (15 mL) and brine (15 mL), then extracted in CH_2Cl_2 (3 x 20 mL) and dried over $MgSO_4$. The solvent

was removed *in vacuo*. The residue was purified by column chromatography (neutralised SiO_2, petrol-CH_2Cl_2 1 : 1 with 0→2.5% MeOH) yielding an orange foam **279** (76.6 mg, 0.067 mmol, 67%). δ_H ($CDCl_3$, 400 MHz) 8.15 (2H, d, J = 7.8, H_C), 8.02 (2H, t, J = 7.8, H_B), 7.80 (4H, ddd, J = 10.9, 7.9, 1.5, H_c), 7.54 (1H, t, J = 1.8, H_h), 7.48 (2H, d, J = 7.8, H_A), 7.45 (2H, d, J = 1.8, H_g), 7.42 (4H, td, J = 7.0, 1.8, H_b), 7.38 (2H, td, J = 7.2, 1.8, H_a), 7.18 (1H, s, H_f), 6.49 (2H, d, J = 8.6, H_G), 6.11 (2H, d, J = 8.6, H_H), 4.38 (4H, br. t, J = 5.8, H_I), 3.54 (2H, d, J = 9.6, H_e), 2.59 (1H, ddd, J = 13.7, 6.0, 3.0, H_F), 2.44-2.23 (8H, m, H_D, H_J), 1.96-1.88 (1H, m, H_F), 1.88-1.79 (2H, m, H_E), 1.62-1.49 (2H, m, $H_{E'}$), 1.42 (18H, s, H_j). δ_C ($CDCl_3$, 101 MHz) 162.1, 157.7, 153.2, 152.4, 142.9 (d, J_{CP} = 10.9), 138.9, 136.7, 134.7 (d, J_{CP} = 31.0), 133.1 (d, J_{CP} = 17.1), 132.3, 130.8 (d, J_{CP} = 1.8), 129.2, 129.1 (d, J_{CP} = 9.6), 124.6, 123.2, 121.3 (d, J_{CP} = 8.3), 119.8, 115.3, 114.1, 65.8, 39.6, 35.5, 35.0, 31.6, 29.6, 24.5, 23.9 (d, J_{CP} = 22.5). $\delta_{31P\{1H\}}$ ($CDCl_3$, 202 MHz) 27.9 (P=O), -7.6 ($Ph_2\boldsymbol{P}CH_2$, broad), -143.4 ($\boldsymbol{P}F_6$, J_{PF} = 713.8). HR-ESI-MS $[M\text{-}PF_6]^+$ m/z 996.4399 (calc. $C_{61}H_{68}CuN_5O_2P$ 996.4401, calc. $C_{61}H_{68}CuN_5O_2P_2F_6$ 1141.404843)

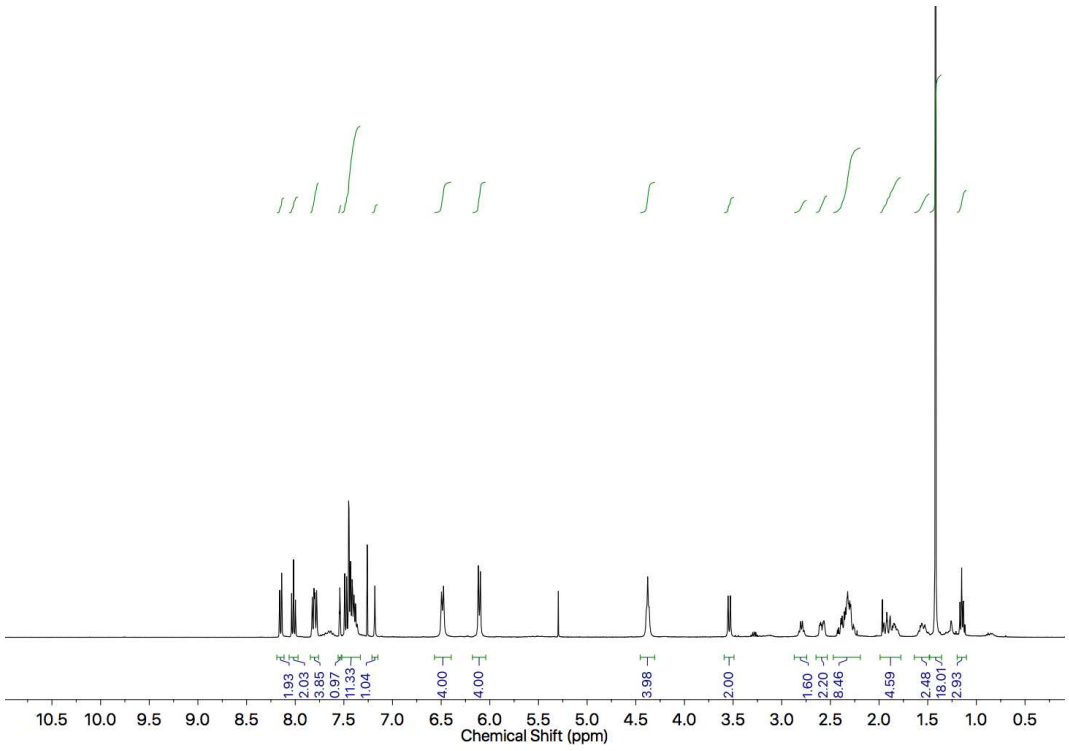

Figure 117: ^{1}H NMR (400 MHz, $CDCl_3$) of **279**.

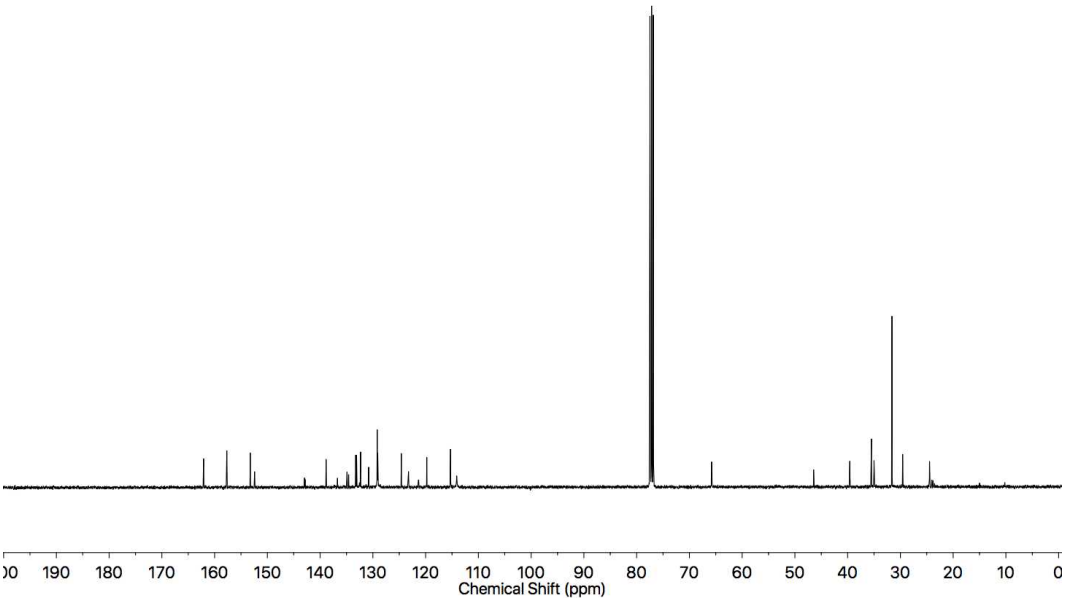

Figure 118: ^{13}C NMR (101 MHz, $CDCl_3$) of **279**.

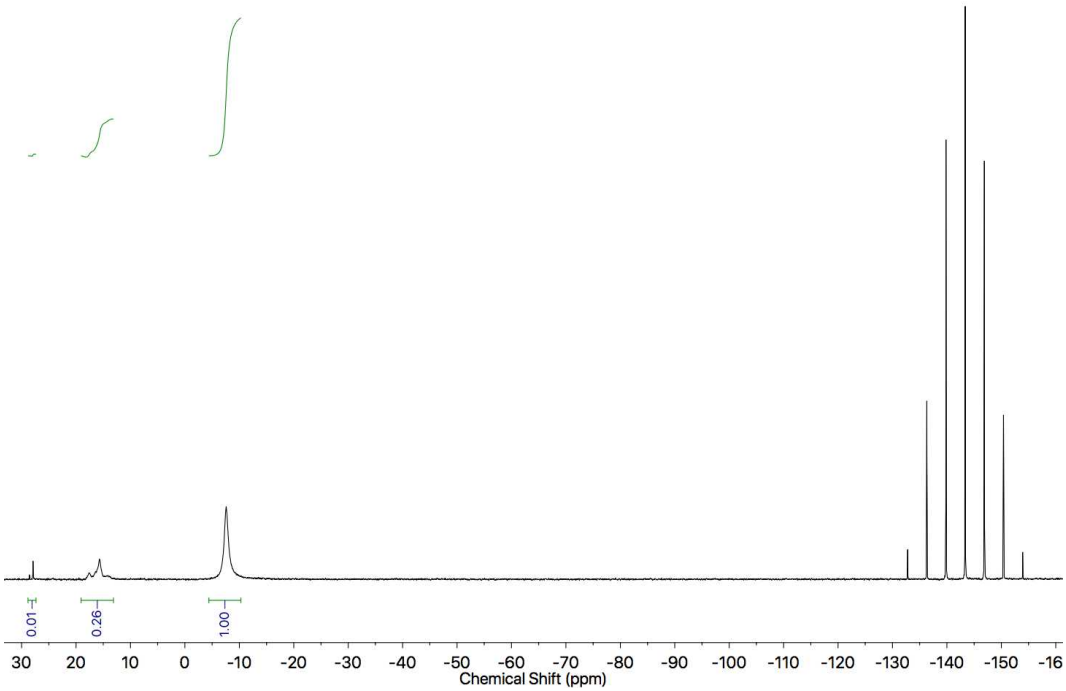

Figure 119: $^{31}P\{^1H\}$ NMR (202 MHz, $CDCl_3$) of **279**.

279 (76.6 mg, 0.067 mmol, 1.0 eq.) in anhydrous CH_2Cl_2 (2 mL) was added to an excess of potassium cyanide (20 mg, 0.31 mmol, 4.5 eq.) in anhydrous MeOH (1.0 mL) and stirred for 24 h at room temperature under N_2. The solution was washed with brine solution (15 mL), extracted in CH_2Cl_2 (3 x 20 mL). The combined organic layers were

dried over $MgSO_4$ and solvent removed *in vacuo*, yielding a white foam **280** (59.0 mg, 0.063 mmol, 94%). δ_H ($CDCl_3$, 400 MHz) 10.06 (1H, s, H_e), 7.67 (2H, t, J = 7.5, H_B), 7.55 (2H, d, J = 1.5, H_f), 7.51 (2H, d, J = 8.0, H_A), 7.28 (4H, dt, J = 7.0, 2.0, H_b), 7.20-7.13 (7H, m, H_a, H_c, H_g), 7.06 (2H, d, J = 8.0, H_C), 6.42 (4H, d, J = 8.5, H_G), 6.30 (4H, d, J = 8.5, H_H), 4.59 (2H, q (dt), J = 8.0, H_I), 4.20 (2H, q(dt), J = 8.0 Hz, $H_{I'}$), 3.02 (2H, s, H_d), 2.42-2.26 (4H, m, H_D, H_J), 2.25-2.10 (6H, m, $H_{D'}$, H_F, $H_{J'}$), 2.09-1.98 (2H, $H_{F'}$), 1.61-1.47 (4H, m, H_E), 1.16 (18H, s, H_h). δ_C ($CDCl_3$, 101 MHz) 163.5, 157.5, 157.3, 150.8, 139.6 (d, J_{CP} = 18.0), 139.5 (d, J_{CP} = 14.8), 137.3, 136.7, 132.7 (d, J_{CP} = 18.9), 132.0, 128.3 (d, J_{CP} = 4.4), 128.2, 123.5, 121.9, 120.9 (d, J_{CP} = 209), 120.7, 119.8, 115.2, 115.1, 66.8, 37.0, 35.3, 35.2, 31.3, 30.5, 25.2, 25.0. $\delta_{P\{1H\}}$ ($CDCl_3$, 202 MHz) -15.8. HR-ESI-MS $[M+H]^+$ m/z 934.5182 (calc. for $C_{61}H_{69}N_5O_2P$ 934.5183).

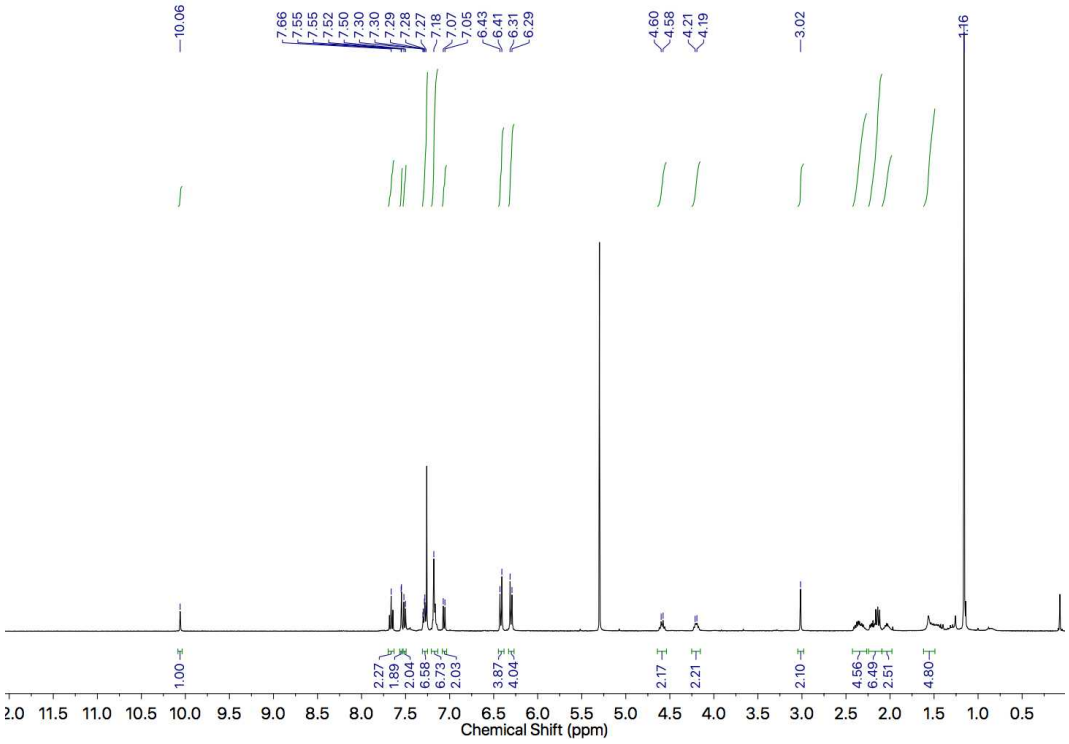

Figure 120: ^1H NMR (400 MHz, $CDCl_3$) of **280**.

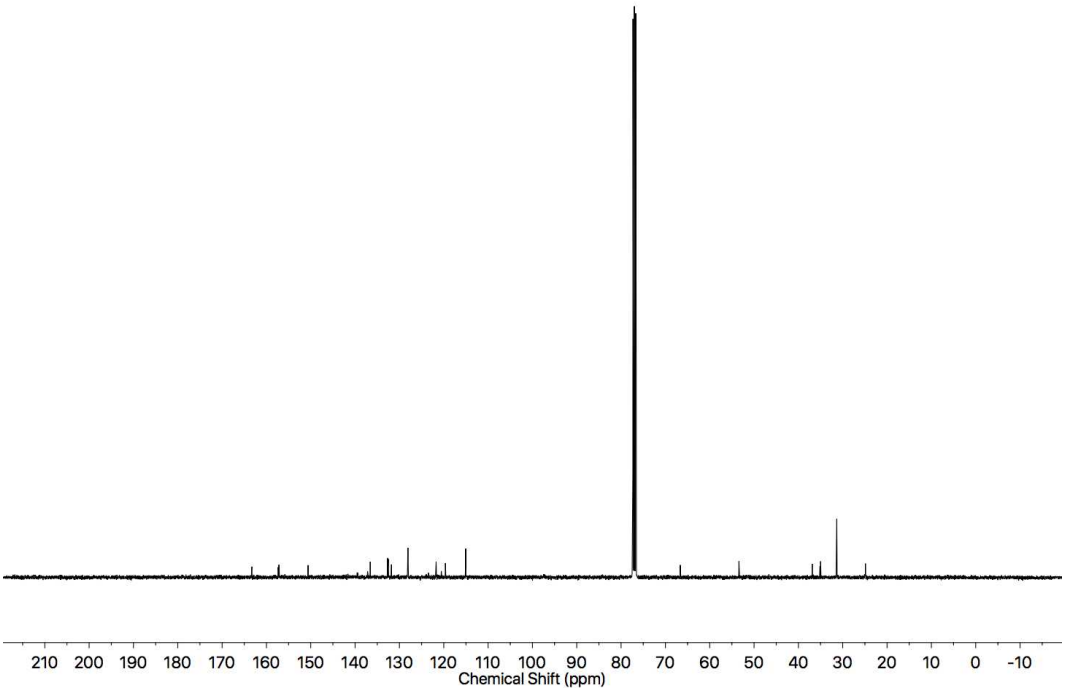

Figure 121: ^{13}C NMR (101 MHz, $CDCl_3$) of **280**.

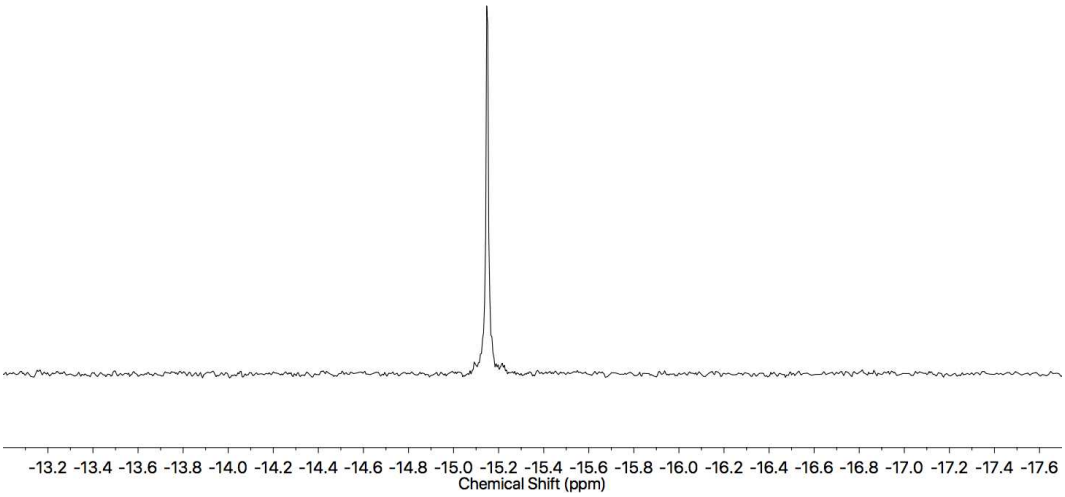

Figure 122: $^{31}P\{^1H\}$ NMR (202 MHz, $CDCl_3$) of **280**.

280 (59.0 mg, 0.063 mmol, 1.05 eq) was stirred for 2 h under N_2, in CH_2Cl_2 (4.5 mL) at room temperature with $(Me_2S)AuCl$ (17.7 mg, 0.060 mmol, 1.0 eq). The reaction mixture was then filtered through Celite and the solvent removed under reduced pressure. The crude product was purified by column chromatography (neutralised SiO_2, petrol-CH_2Cl_2

1:1 with 0→3% MeOH) yielding a white foam **281** (54.0 mg, 0.046 mmol, 73%). δ_H ($CDCl_3$, 400 MHz) 10.07 (1H, s, H_e), 7.71 (2H, t, J = 8.0, H_B), 7.66 (4H, ddd, J = 13.0, 6.5, 2.0, H_c), 7.56 (2H, d, J = 8.0, H_A), 7.46 (2H, d, J = 2.0, H_f), 7.42 (2H, ddd, J = 7.5, 3.5, 1.5, H_a), 7.34 (4H, td, J = 8.0, 2.0, H_b), 7.20 (1H, t, J = 2.0, H_g), 7.13 (2H, d, J = 8.0, H_C), 6.40 (4H, d, J = 8.0, H_G), 6.27 (4H, d, J = 8.0, H_H), 4.54 (2H, q (ddd), J = 7.5, H_I), 4.54 (2H, ddd, J = 9.5, 5.0, 2.0, $H_{I'}$), 3.40 (2H, d, J = 11.0, H_d), 2.40-2.29 (4H, m, H_D, H_J), 2.28-2.19 (2H, m, H_F), 2.19-2.12 (4H, m, $H_{D'}$, $H_{F'}$), 2.05-1.95 (2H, m, $H_{J'}$), 1.50 (2H, dq, J = 16.5, 7.0, H_E), 1.44 (2H, dq, J = 16.5, 7.0, $H_{E'}$), 1.16 (18H, s, H_h). δ_C ($CDCl_3$, 101 MHz) 163.4, 157.5, 157.4, 150.9, 137.0, 136.8, 135.7 (d, J_{CP} = 3.0), 133.4 (d, J_{CP} = 13.5), 131.8 (d, J_{CP} = 2.5), 131.7, 130.2 (d, J_{CP} = 59.0), 129.2 (d, J_{CP} = 11.5), 128.1, 124.4 (d, J_{CP} = 7.0), 122.2, 121.0, 120.0, 115.3, 114.7, 66.9, 37.0, 35.1 (d, J_{CP} = 1.5), 31.8, 31.4, 25.9, 25.7, 24.9. $\delta_{31P\{1H\}}$ ($CDCl_3$, 202 MHz) 27.7. RP-LCMS-ESI$^+$ m/z $[M\text{-}Cl]^+$ 1130.91. HR-ESI-MS $[M\text{-}Cl]^+$ m/z 1130.5 (calc. for $C_{61}H_{68}N_5O_4PAu$ m/z 1130.5).

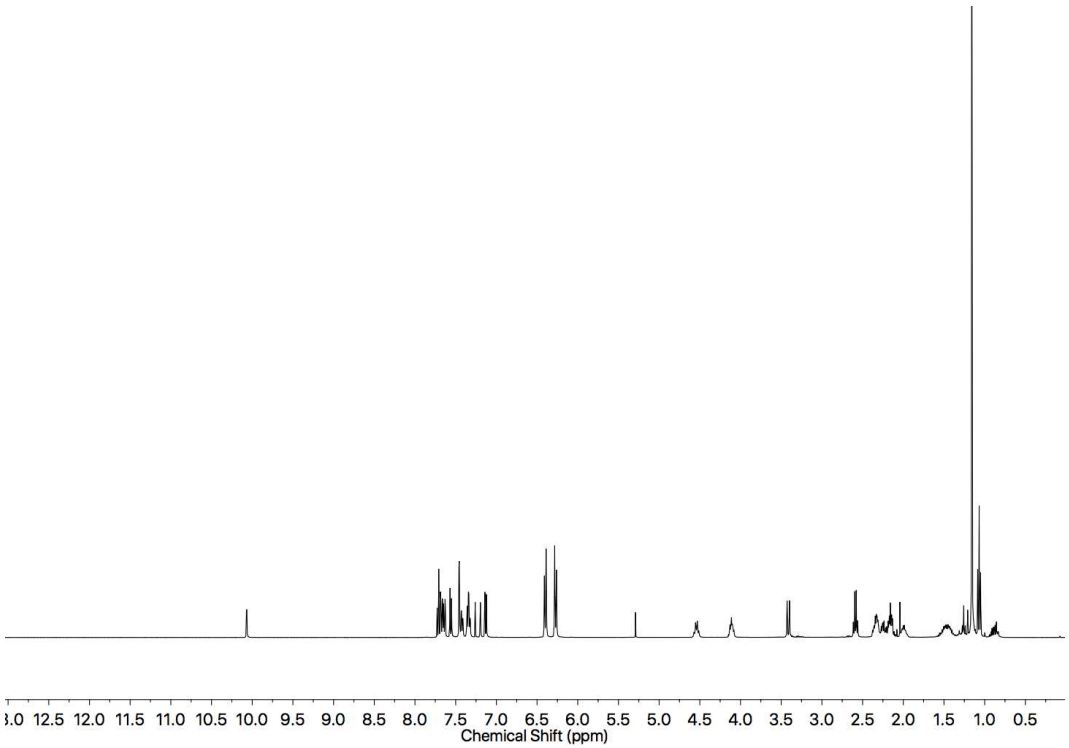

Figure 123: ^1H NMR (400 MHz, $CDCl_3$) of **281**.

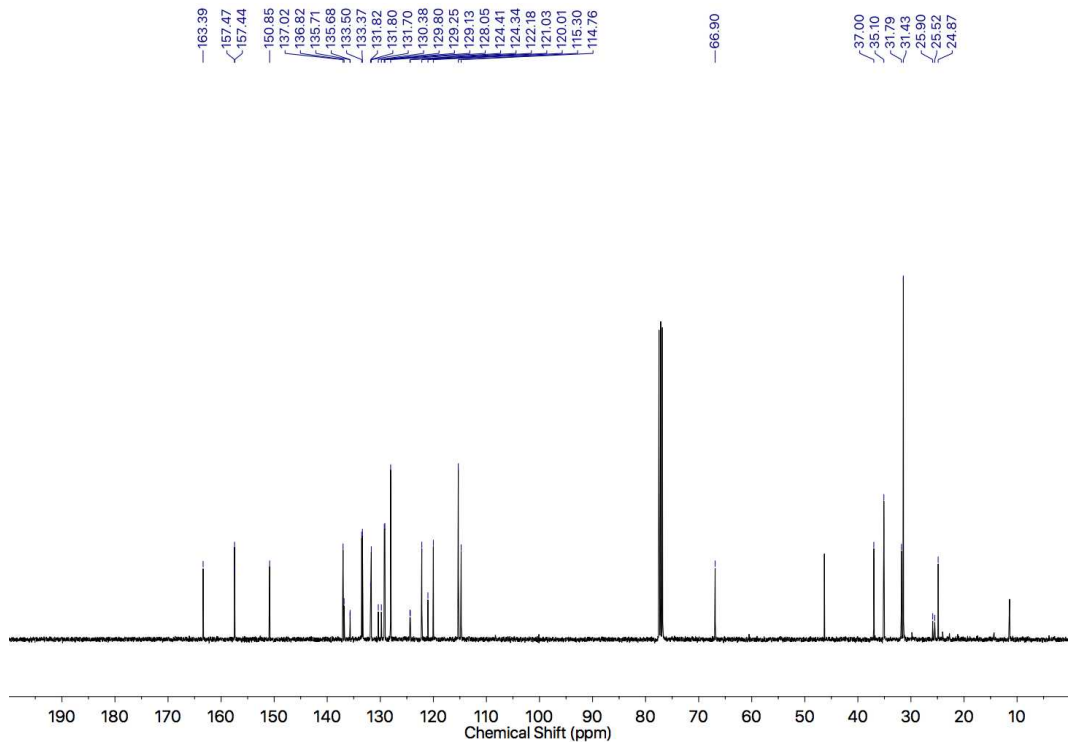

Figure 124: ^{13}C NMR (101 MHz, $CDCl_3$) of **281**.

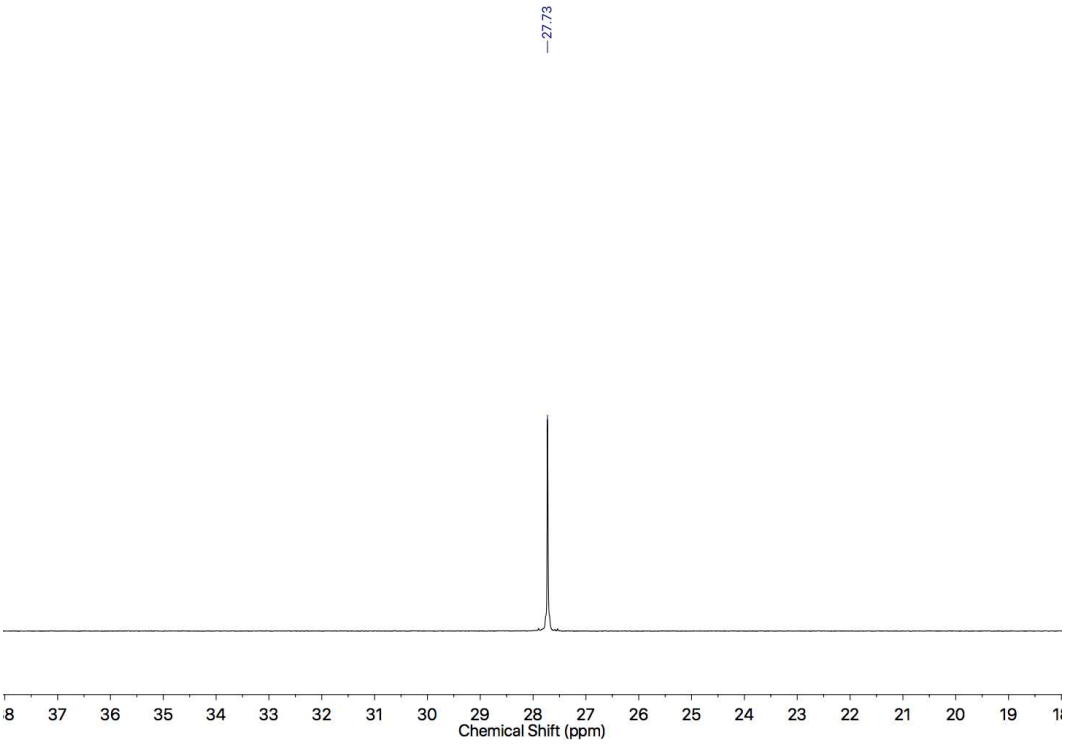

Figure 125: $^{31}P\{^1H\}$ NMR (202 MHz, $CDCl_3$) of **281**.

Rotaxane (*S*)-**285**

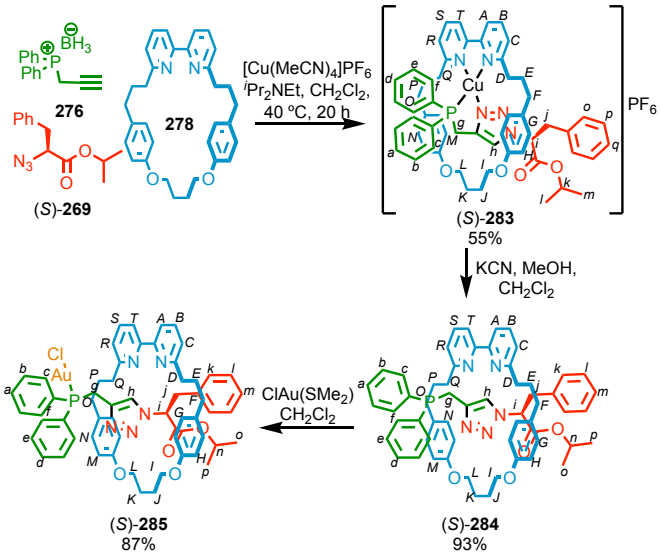

278 (48.0 mg, 0.100 mmol, 1.0 eq.), **276** (71.6 mg, 0.300 mmol, 3.0 eq.), (*S*)-**269** (70.2 mg, 0.300 mmol, 3.0 eq.), $[Cu(MeCN)_4]PF_6$ (35.9 mg, 0.096 mmol, 0.96 eq.) and *N,N*-diisopropylethylamine (0.17 mL, 1.00 mmol, 10 eq.) were stirred in anhydrous CH_2Cl_2 (9 mL) at 40 °C for 16 h under N_2, quickly changing from orange to yellow. The solution was then diluted with CH_2Cl_2 (10 mL), washed with sat. EDTA-NH_3 (15 mL), brine (15 mL), then extracted in CH_2Cl_2 (3 x 20 mL). The combined organic layers were dried over $MgSO_4$, and concentrated *in vacuo*. The residue was purified by column chromatography (neutralised SiO_2, petrol-CH_2Cl_2 with 0→2.5% MeOH) yielding a yellow foam (*S*)-**283** (63.2 mg, 0.055 mmol, 55%). δ_H ($CDCl_3$, 400 MHz) 8.16 (2H, dd, *J* = 8.0, 2.0, H_C, H_R), 8.03 (2H, dd, *J* = 7.5, 7.0, H_B, H_S), 7.69-7.52 (4H, m, H_c, H_f), 7.49 (2H, dd, *J* = 7.5, 5.5, H_A, H_T), 7.42-7.36 (7H, m, H_a, H_b, H_d, H_e, H_q), 7.34 (1H, s, H_h), 7.30-7.29 (4H, m, H_o, H_p), 6.65 (2H, d, *J* = 8.5, H_N), 6.47 (2H, d, *J* = 8.5, H_G), 6.18 (2H, d, *J* = 8.5, H_M), 5.77 (2H, d, *J* = 8.5, H_H), 5.47 (1H, t, *J* = 8.0, H_i), 5.03 (1H, sept., *J* = 6.0, H_k), 4.31 (4H, m, H_l), 3.53 (1H, dd, *J* = 14.0, 8.0, H_j), 3.43 (1H, dd, *J* = 14.0, 8.0, $H_{j'}$), 3.05 (1H, dd, *J* = 14.0, 8.0, H_g), 2.91 (1H, dd, *J* = 14.0, 8.0, $H_{g'}$), 2.53 (1H, ddd, *J* = 14.0, 6.5, 2.5, H_D), 2.42 (1H, ddd, *J* = 14.0, 6.5, 2.5, H_Q), 2.35-2.19 (8H, m, H_J, H_E, H_P), 2.10 (1H, *J* = 13.5, 9.0, 3.5, $H_{D'}$), 1.97 (1H, *J* = 13.5, 9.0, 3.5, $H_{Q'}$), 1.76-1.58 (4H, m, H_F, H_O), 1.29 (3H, d, *J* = 6.5, H_l), 1.01 (3H, d, *J* = 6.5, H_m). δ_C ($CDCl_3$, 101 MHz) 167.6, 162.4, 162.4, 157.3, 157.2, 152.5, 152.4, 142.7 (d) 138.8, 138.8, 135.0, 134.7, 134.6, 133.4 (d), 132.2, 132.1, 130.8, 129.4 (d), 129.1, 129.1, 129.0 (d), 127.8, 124.8 (d), 119.7 (d) 114.7, 114.3, 77.4, 70.8, 66.4, 66.4, 64.6, 64.5, 46.5, 40.0, 39.6, 38.1, 35.0, 30.1, 29.2, 25.0, 24.9, 23.1 (d), 21.7,

21.5, 11.1. 7 doublets identified. Overlapping environments of PPh_2 (not all 49 environments observable). $\delta_{31P\{1H\}}$ ($CDCl_3$, 202 MHz) -7.67 ($Ph_2\boldsymbol{P}CH_2$, br.), -143.27 ($\boldsymbol{P}F_6$, *J* 713.1 Hz). HR-ESI-MS $[M\text{-}PF_6]^+$ m/z 998.3825 (calc. $C_{59}H_{62}N_5O_4PCu$ 998.3840).

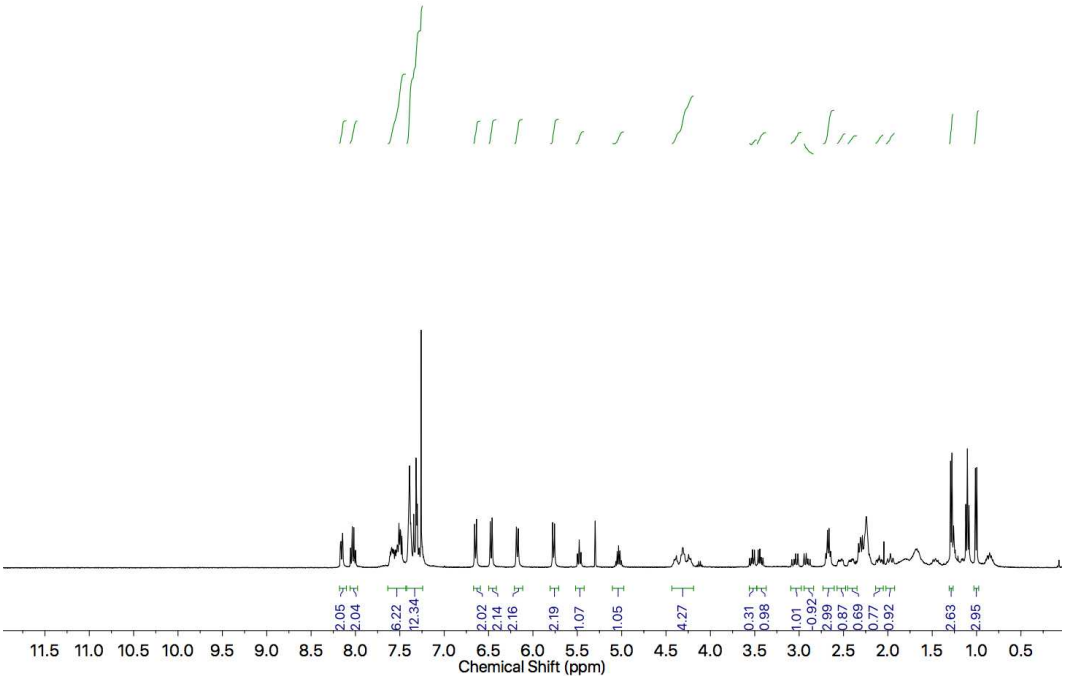

Figure 126: ^1H NMR (400 MHz, $CDCl_3$) of a (*S*)-**283**.

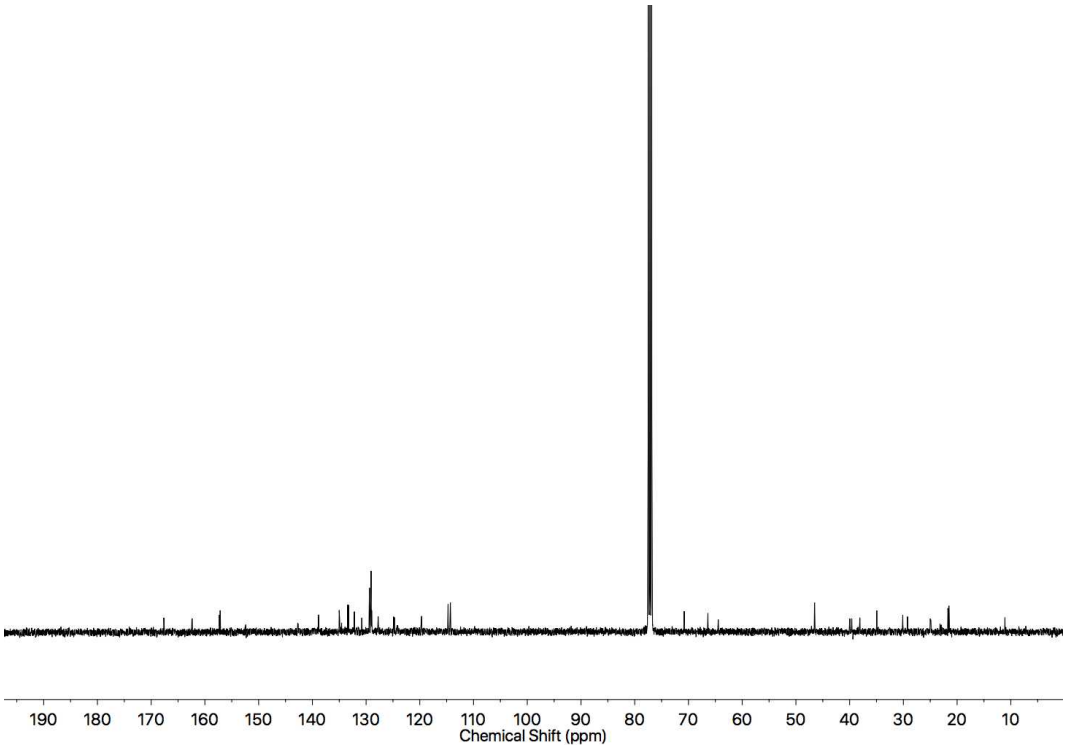

Figure 127: ^{13}C NMR (101 MHz, $CDCl_3$) of (*S*)-**283**.

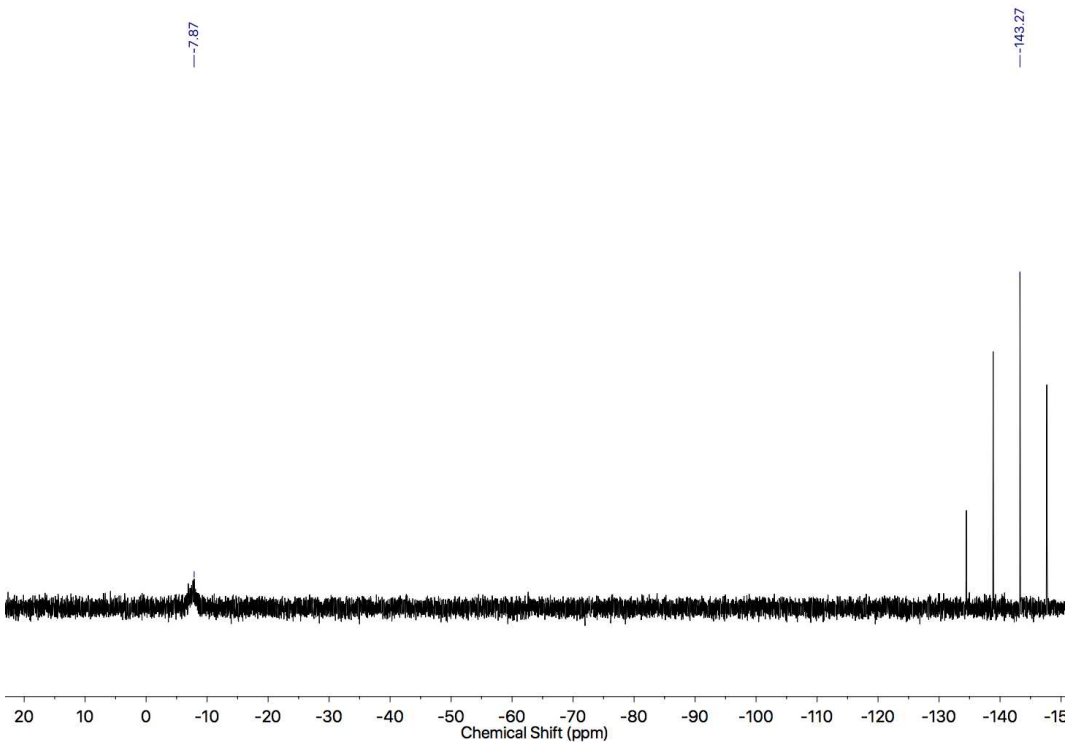

Figure 128: $^{31}P\{^{1}H\}$ NMR (202 MHz, $CDCl_3$) of (*S*)-**283**.

(*S*)-**283** (53.2 mg, 0.046 mmol, 1.0 eq.) in anhydrous CH_2Cl_2 (4 mL) was added to an excess of potassium cyanide (30 mg, 0.47 mmol, 10 eq.) in anhydrous MeOH (2.0 mL) and stirred for 24 h at room temperature under N_2. The solution was washed with brine solution (15 mL), extracted in CH_2Cl_2 (3 x 20 mL), dried over $MgSO_4$, and concentrated *in vacuo* yielding a white foam (*S*)-**284** (40.6 mg, 0.043 mmol, 93%). δ_H ($CDCl_3$, 400 MHz) 9.18 (1H, s, H_h), 7.71 (1H, t, *J* = 7.5, H_S), 7.66 (1H, t, *J* = 7.5, H_B), 7.51 (1H, d, *J* = 7.5, H_T), 7.49 (1H, d, *J* = 7.5, H_A), 7.20-7.15 (5H, m, H_R, H_b, H_e), 7.14-7.10 (3H, m, H_C, H_l), 7.07-6.96 (6H, m, H_a, H_c, H_d, H_f), 6.86 (2H, dd, *J* = 5.0, 3.0, H_k), 6.66 (2H, d, *J* = 8.0, H_G), 6.57 (2H, d, *J* = 8.0, H_H), 6.56 (2H, d, *J* = 9.0, H_N), 6.52 (2H, d, *J* = 9.0, H_M), 4.99 (1H, dd, *J* = 10.0, 6.5, H_i), 4.80 (2H, dt, *J* = 14.5, 6.5, H_l), 4.65 (1H, sept., *J* = 5.5, H_n), 4.11 (2H, ddd, *J* = 15.0, 4.5, 4.0, H_L), 3.27 (1H, dd, *J* = 13.5, 10.0, H_j), 3.18 (1H, dd, *J* = 13.5, 6.5, $H_{j'}$), 3.09 (1H, t(dd), *J* = 8.0, 8.0, H_g), 3.07 (1H, t(dd), *J* = 8.0, 8.0, $H_{g'}$), 2.65-2.49 (4H, m, H_D, H_Q), 2.40 (2H, ddd, *J* = 13.5, 9.0, 4.5, H_O), 2.32 (2H, ddd, *J* = 13.5, 8.5, 4.5, H_F), 2.25 (2H, dt(ddd), *J* = 18.0, 8.5, 8.0, H_J), 2.04 (2H, ddd, *J* = 18.0, 6.5, 4.5, H_K), 1.71-1.57 (4H, m, H_P), 0.84 (3H, d, *J* = 6.5 Hz, H_o), 0.79 (3H, d, *J* = 6.5, H_p). δ_C ($CDCl_3$, 101 MHz) 168.1, 163.4, 163.3, 157.3, 141.3, 140.3, 140.1, 136.7, 136.6, 133.2, 133.0, 132.8, 132.4, 132.4, 129.5, 129.3, 129.0, 128.3, 128.0, 127.9, 127.9, 127.8, 127.8, 125.6, 125.5, 121.5, 121.3,

119.9, 119.7, 115.0, 114.8, 68.8, 66.3, 66.2, 62.6, 46.0, 38.6, 36.8, 36.7, 35.3, 35.2, 30.4, 30.2, 29.9, 25.0, 25.0, 21.4, 14.3, 8.9. 49 signals. $\delta_{P\{1H\}}$ ($CDCl_3$, 202 MHz) -18.7 ($Ph_2\boldsymbol{P}CH_2$). HR-ESI-MS $[M+H]^+$ m/z 936.4614 (calc. for $C_{59}H_{63}N_5O_4P$ 936.4626).

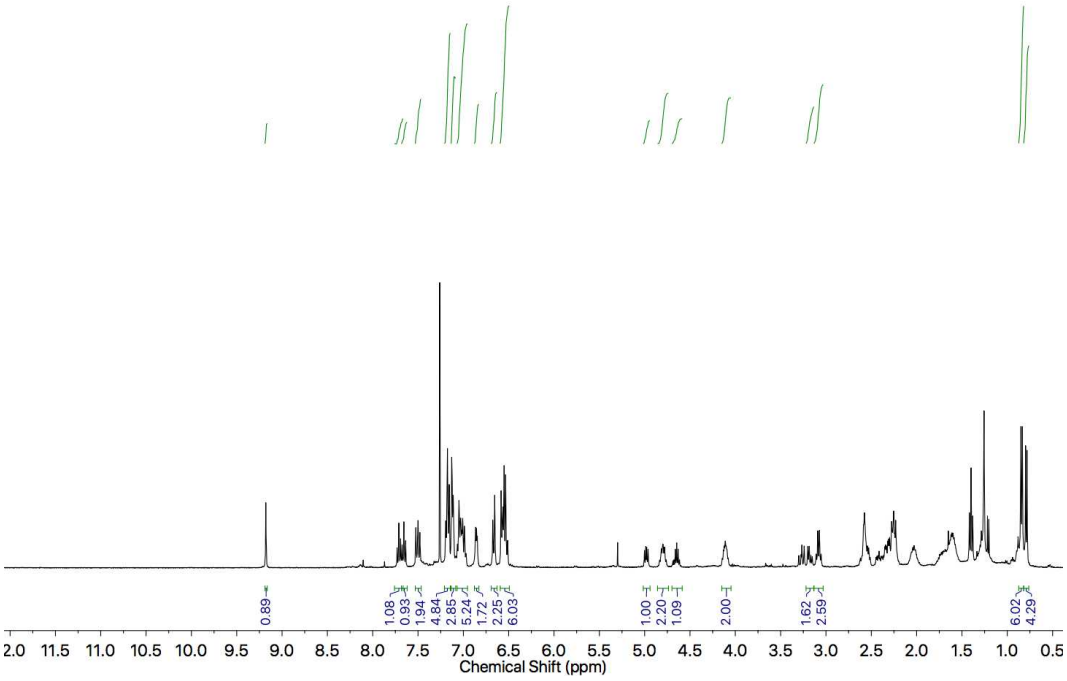

Figure 129: ^1H NMR (400 MHz, $CDCl_3$) of (*S*)-**284**.

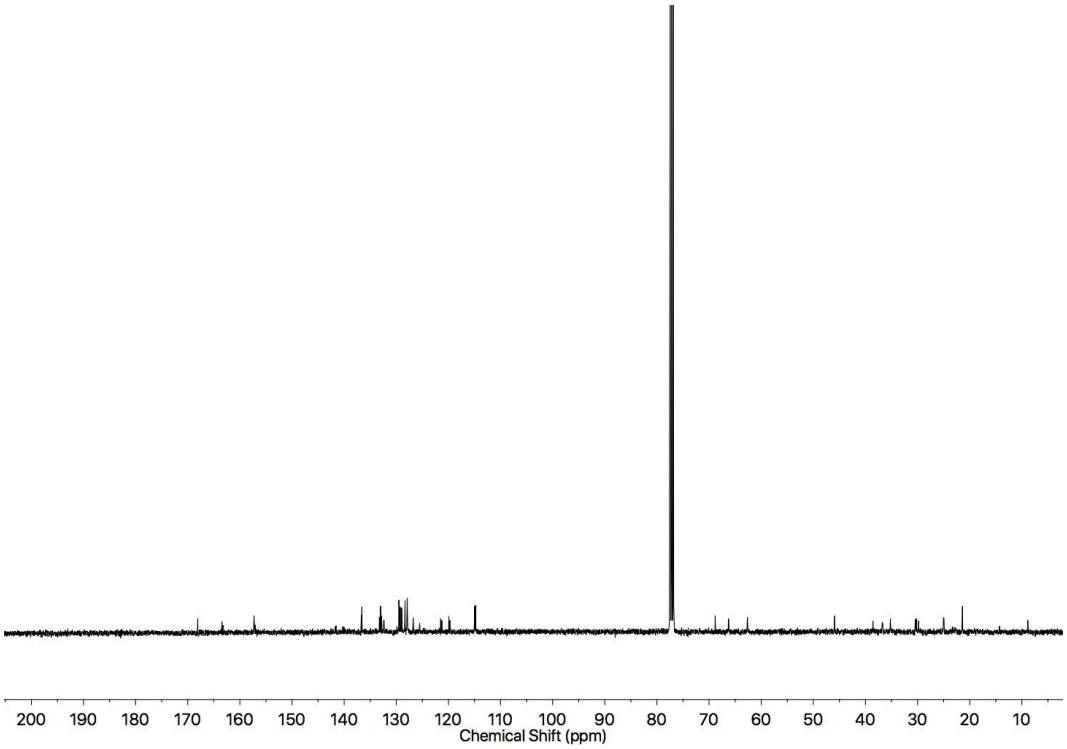

Figure 130: ^{13}C NMR (101 MHz, $CDCl_3$) of (*S*)-**284**.

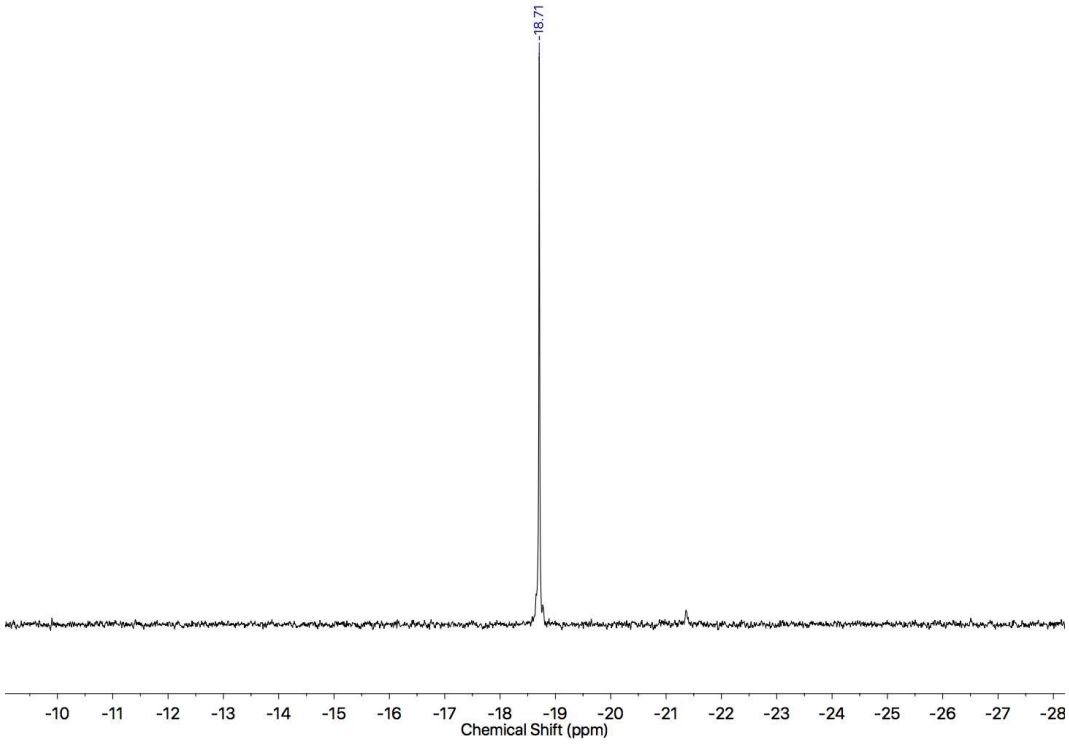

Figure 131: $^{31}P\{^{1}H\}$ NMR (202 MHz, $CDCl_3$) of (*S*)-**284**.

(*S*)-**284** (38.6 mg, 0.041 mmol, 1.05 eq) was stirred for 2 h under N_2, in CH_2Cl_2 (4.0 mL) at room temperature with $(Me_2S)AuCl$ (11.6 mg, 0.039 mmol, 1.0 eq). The reaction mixture was then filtered through Celite and the solvent removed under reduced pressure. The crude product was purified by column chromatography (neutralised SiO_2, petrol-CH_2Cl_2 1:1 with 0→3% MeOH) yielding a white foam, which was then dissolved in minimum CH_2Cl_2 and crystallised by hexane diffusion, yielding white prism crystals (*S*)-**285** (39.5 mg, 0.034 mmol, 87%). δ_H ($CDCl_3$, 400 MHz) 8.89 (1H, s, H_h), 7.71-7.62 (4H, m, H_S, H_B, H_c), 7.62-7.54 (2H, m, H_f), 7.51 (2H, d, *J* = 7.5, H_A, HT_D), 7.49-7.44 (1H, m, H_a), 7.43-7.36 (3H, m, H_b), H_d), 7.33 (2H, td, *J* = 7.5, 2.0, H_e), 7.23-7.16 (4H, m, H_l, H_m, H_R), 7.13 (1H, d, *J* = 8.0, H_C), 6.96 (2H, dd, *J* = 8.0, 2.0, H_k), 6.66-6.58 (6H, m, H_G, H_M, H_N), 6.55 (2H, d, *J* = 9.0, H_H), 4.67 (1H, dd, *J* = 12.0, 5.5, H_i), 4.49 (1H, sept., *J* = 7.0, H_n), 4.48 (1H, dd, *J* = 15.5, 6.5, H_l), 4.40 (1H, dd, *J* = 15.5, 7.5, H_L), 4.18 (2H, ddd, *J* = 14.0, 8.5, 5.0, $H_{K'}$, $H_{L'}$) 3.36 (1H, dd, *J* = 15.5, 12.5, H_g), 3.17 (1H, dd, *J* = 15.5, 12.5, $H_{g'}$), 2.86 (1H, dd, *J* = 13.0, 5.0, H_j), 2.73 (1H, t, *J* = 12.5, $H_{j'}$), 2.53-2.44 (2H, m, H_Q), 2.31 (2H, dd, *J* = 11.0, 4.5, H_D), 2.25-2.08 (2H, m, H_K), 2.07-1.94 (2H, m, H_J), 1.78-1.55 (8H, m, H_E, H_F, H_P, H_O), 0.86 (3H, d, *J* = 6.0, H_o), 0.52 (3H, d, *J* = 6.5, H_p). δ_C ($CDCl_3$, 101 MHz) 167.8, 163.1, 163.0, 157.9, 157.9, 157.6, 157.6, 137.0, 136.9, 135.8 (d, J_{CP} = 2.5), 135.9 (d, J_{CP} = 2.0),

133.6 (d, J_{CP} = 13.0), 132.0, 132.0, 131.7 (d, J_{CP} = 10.0), 131.6 (d, J_{CP} = 10.0), 130.9 (d, J_{CP} = 18.5), 130.3 (d, J_{CP} = 18.0), 129.4, 129.2, 129.1, 129.0, 128.8, 128.8, 128.5, 127.0, 124.8 (d, J_{CP} = 7.5), 121.7, 121.3, 120.2, 120.1, 115.1, 115.0, 68.9, 67.0, 66.8, 62.8, 38.4, 36.9, 36.7, 31.0, 30.8, 25.2, 25.0, 24.9, 21.4, 21.1. $\delta_{31P\{1H\}}$ ($CDCl_3$, 202 MHz) 25.9. HR-ESI-MS m/z $[M\text{-}Cl]^+$ 1132.5 (calc. for $C_{59}H_{62}N_5O_4PAu$ m/z 1132.5), $[M+H]^+$ 1168.5 (calc. for $C_{59}H_{63}N_5O_4PAuCl$ m/z 1168.4).

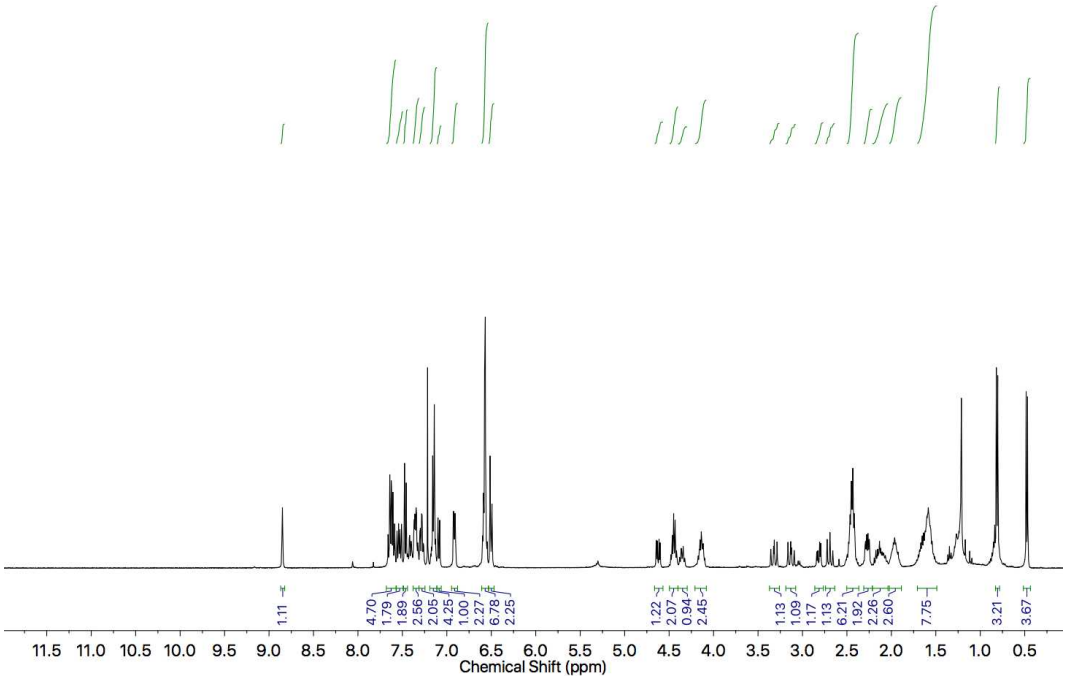

Figure 132: ^1H NMR (400 MHz, $CDCl_3$) of (*S*)-**285**.

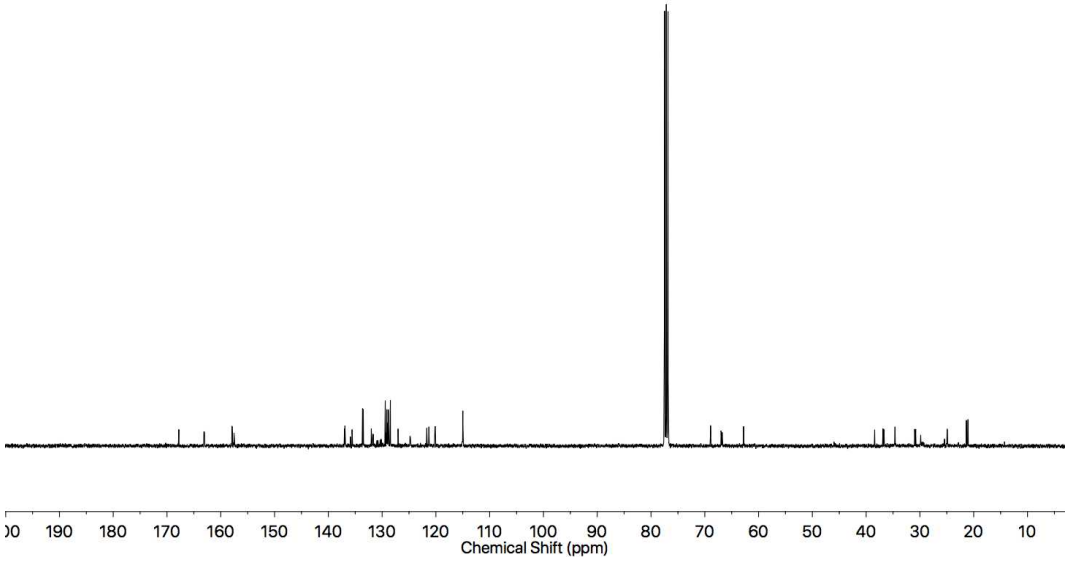

Figure 133: ^{13}C NMR (101 MHz, $CDCl_3$) of (*S*)-**285**.

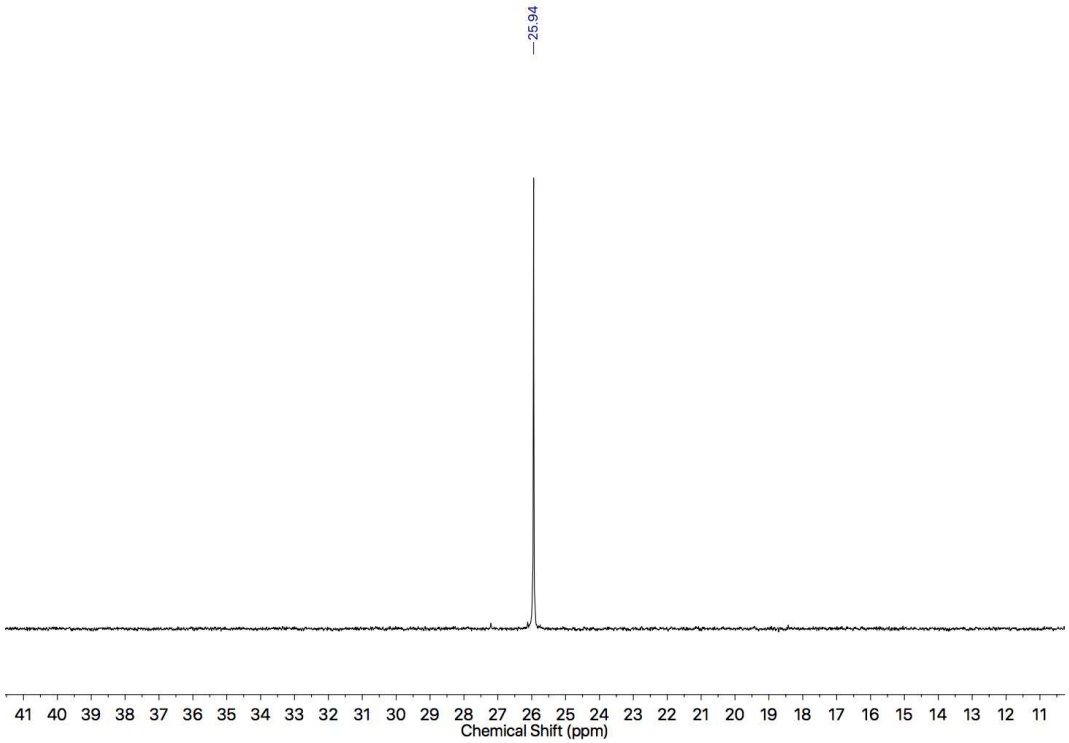

Figure 134: $^{31}P\{^1H\}$ NMR (202 MHz, $CDCl_3$) of (*S*)-**285**.

Rotaxane **289**

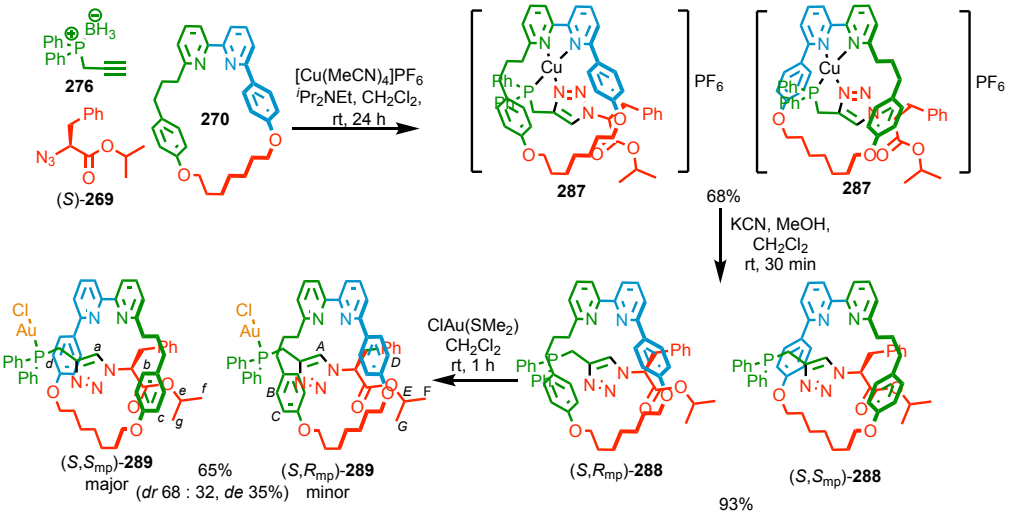

270 (48.0 mg, 0.100 mmol, 1.0 eq.), **276** (71.6 mg, 0.301 mmol, 3.0 eq.), (*S*)-**269** (70.2 mg, 0.301 mmol, 3.0 eq.), $[Cu(MeCN)_4]PF_6$ (35.9 mg, 0.096 mmol, 0.96 eq.) and *N,N*-diisopropylethylamine (0.17 mL, 1.30 g, 1.0 mmol, 10 eq.) were stirred in anhydrous CH_2Cl_2 (2.5 mL) at room temperature for 24 h under N_2. The orange solution was diluted with CH_2Cl_2 (10 mL), washed with sat. EDTA-NH_3 (15 mL), brine (15 mL), extracted in CH_2Cl_2 (3 x 20 mL). The combined organic phases were dried over $MgSO_4$,and concentrated *in vacuo*. The residue was purified by column chromatography (neutralised SiO_2 petrol-CH_2Cl_2 with 0→2.5% MeOH) yielding an orange foam **287** (77.6 mg, 0.068 mmol, 68%). **287** (66.2 mg, 0.058 mmol, 1.0 eq.) in anhydrous CH_2Cl_2 (2.0 mL) was added to an excess of potassium cyanide (3.8 mg, 0.0.058 mmol, 1.0 eq.) in anhydrous MeOH (2.0 mL) and stirred for 4 h at room temperature under N_2. The solution was washed with brine solution (15 mL), extracted in CH_2Cl_2 (3 x 20 mL). The combined organic phases were dried over $MgSO_4$ and concentrated *in vacuo*, yielding a pale yellow foam **288** (50.0 mg, 0.054 mmol, 93%). **288** (43.3 mg, 0.046 mmol, 1.05 eq) was stirred for 2 h under N_2, in CH_2Cl_2 (3.0 mL) at room temperature with $(Me_2S)AuCl$ (13.0 mg, 0.044 mmol, 1.0 eq). The reaction mixture was then filtered through celite and the solvent removed under reduced pressure. The crude product was purified by column chromatography (neutralised SiO_2 petrolCH_2Cl_2 1 : 1 with 0→3% MeOH) yielding a white foam (*S*,R_{mp})-**289** and (*S*,S_{mp})-**289** (34.5 mg, 0.030 mmol, 65%, *d.r.* 2.1:1.0 from ^1H and $^{31}P\{^1H\}$ NMR). δ_H ($CDCl_3$, 400 MHz) 9.71 (1H, d, *J* = 1.9, H_A), 9.68 (1H, d, *J* = 2.5, H_a), 7.87-7.00 (20H, m), 6.89 (2H), 6.82 (2H, dd, *J* = 8.2, H_b), 6.78 (2H, dd, *J* = 8.2, H_B), 6.58 (2H), 6.51 (2H, dd, *J* = 8.2, H_c), 6.45 (2H, dd, *J* = 8.2, H_C), 6.33 (2H, dd, *J* = 8.8, H_D), 6.24

(2H, dd, J = 8.8, $\boldsymbol{H}_d$), 4.64 (1H, sept., J = 6.2, $\boldsymbol{H}_e$), 4.53 (1H, sept., J = 6.2, $\boldsymbol{H}_E$), 0.98 (3H, d, J = 6.3, $\boldsymbol{H}_f$), 0.77 (3H, d, J = 6.4, $\boldsymbol{H}_F$), 0.62 (3H, d, J = 6.3, $\boldsymbol{H}_g$), 0.48 (3H, d, J = 6.4, $\boldsymbol{H}_G$). $\boldsymbol{\delta}_{31P\{1H\}}$ ($CDCl_3$, 202 MHz) 28.6 (major), 27.9 (minor). HR-ESI-MS $[M - Cl]^+$ 1132.4 (calc. for $C_{59}H_{62}N_5O_4PAu$ 1132.4). Full assignment was not possible due to the complexity of the diastereoisomeric mixture, these compounds were synthesised by a different route.

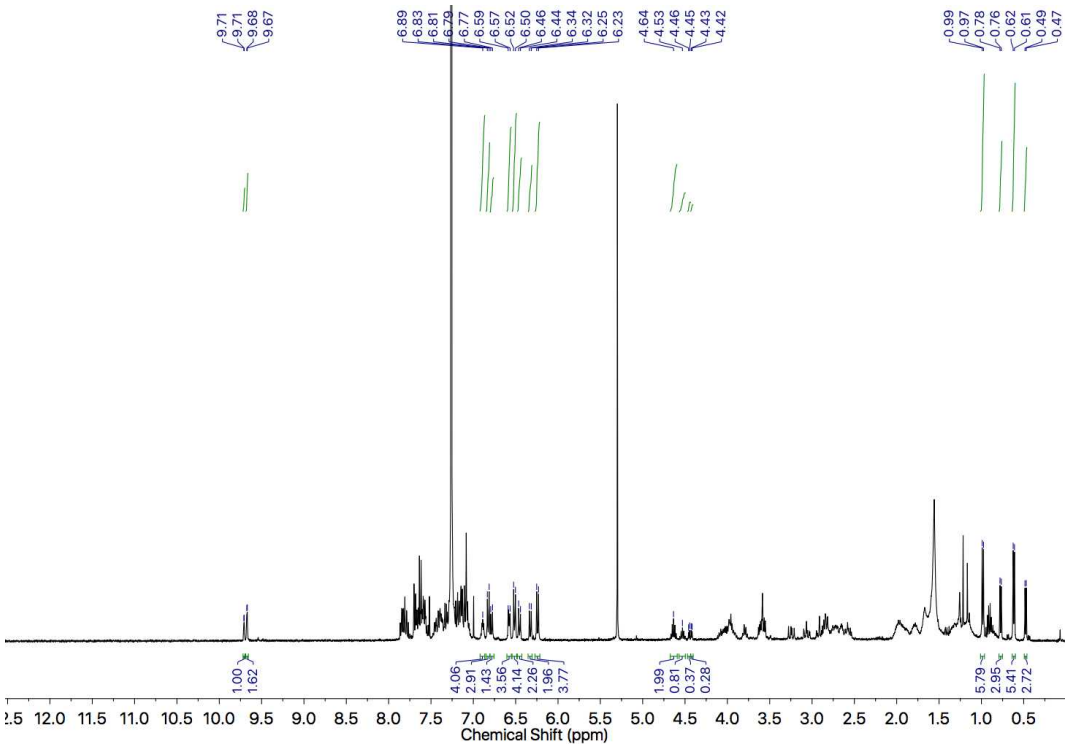

Figure 135: ^1H NMR (400 MHz, $CDCl_3$) of a diastereoisomeric mixture **289**.

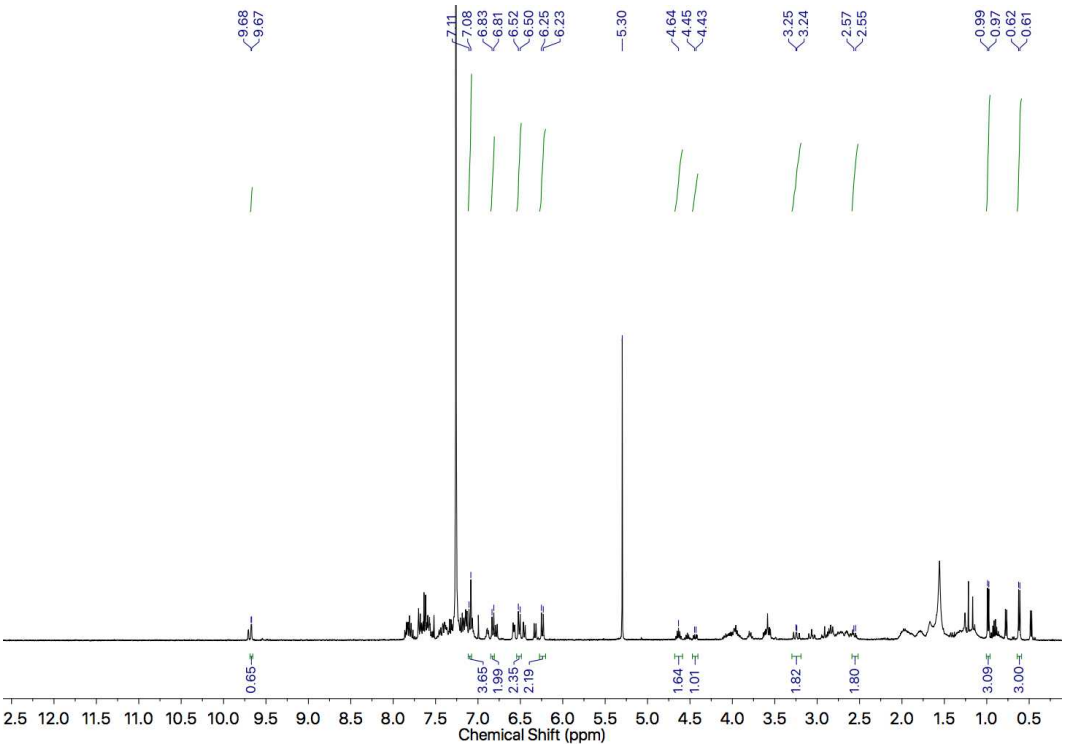

Figure 136: ^{1}H NMR (400 MHz, $CDCl_3$) of a diastereoisomeric mixture **289**.

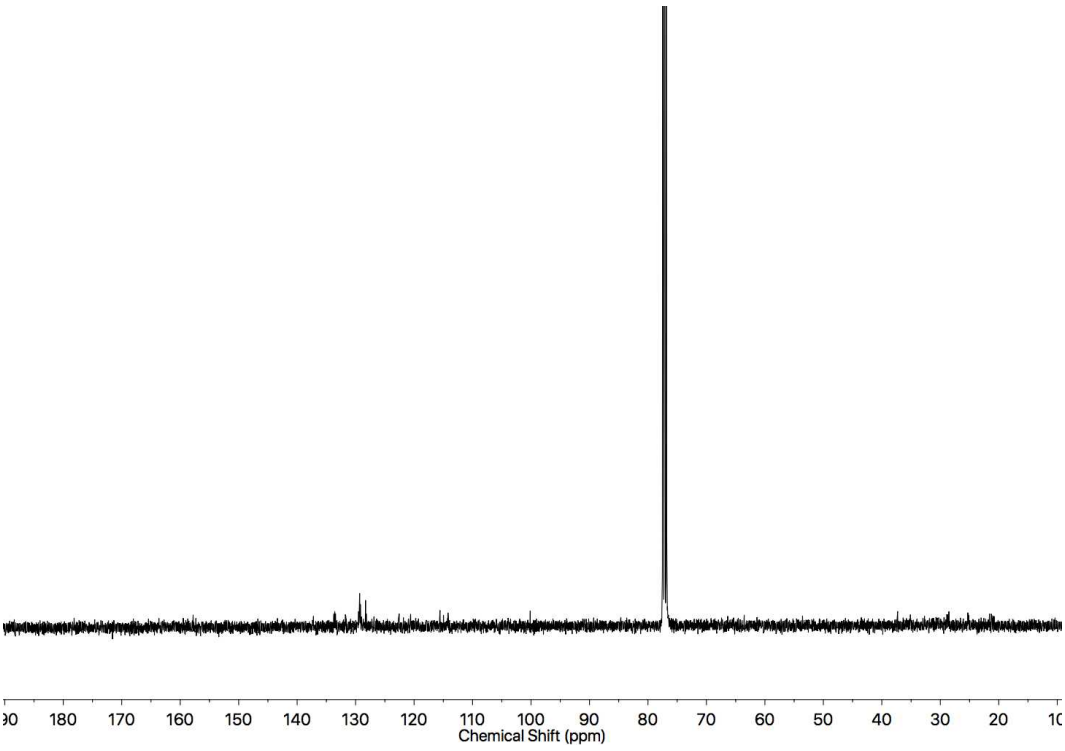

Figure 137: JMOD NMR (101 MHz, $CDCl_3$) of a diastereoisomeric mixture of **289**.

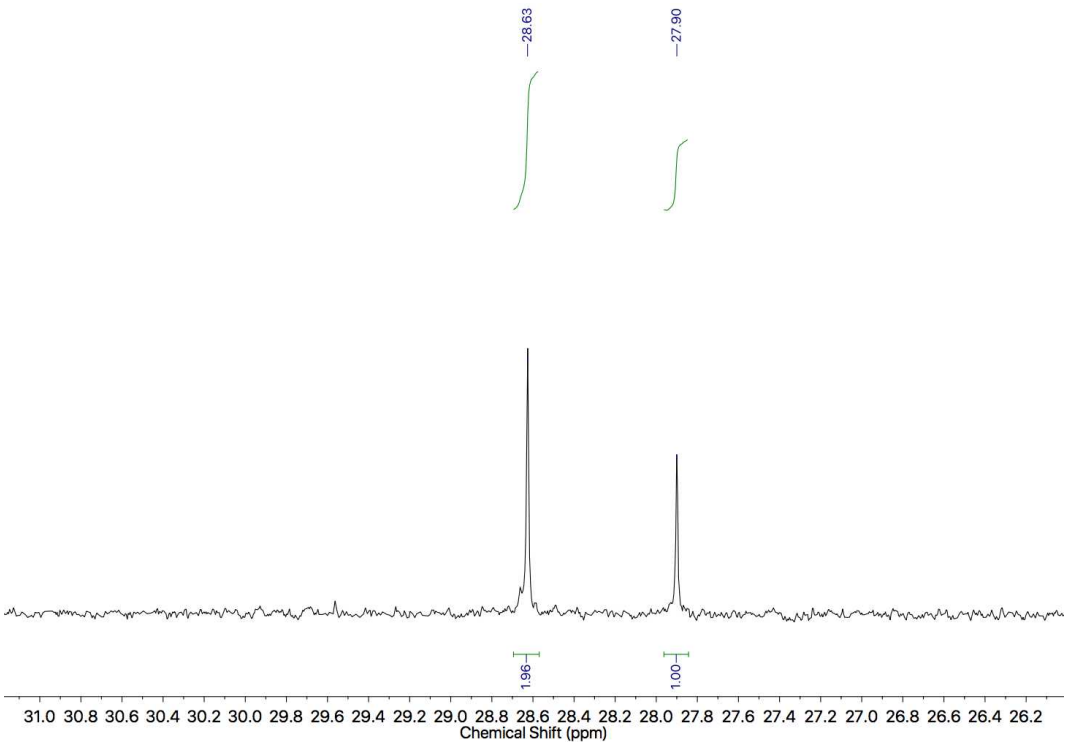

Figure 138: $^{31}P\{^{1}H\}$ NMR (202 MHz, $CDCl_3$) of a diastereoisomeric mixture **289**.

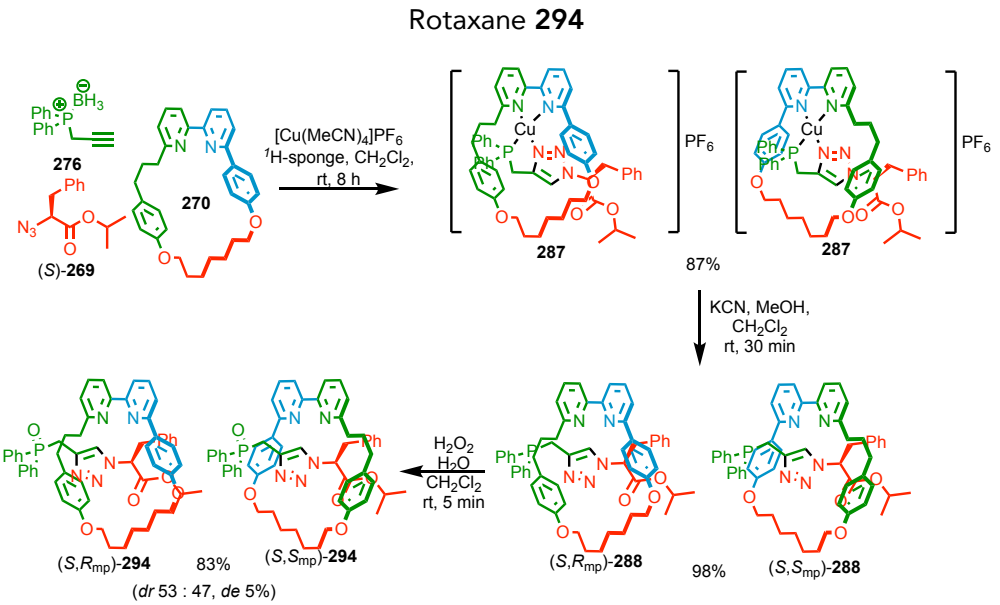

270 (200 mg, 0.418 mmol, 1.0 eq.), **276** (298 mg, 1.25 mmol, 3.0 eq.), (*S*)-**269** (292 mg, 1.25 mmol, 3.0 eq.), $[Cu(MeCN)_4]PF_6$ (150 mg, 0.401 mmol, 0.96 eq.) and ^{1}H-sponge (89.5 mg, 0.418 mmol, 1.0 eq.) were stirred in anhydrous CH_2Cl_2 (10 mL) at rt for 8 h under N_2. The orange solution was diluted with CH_2Cl_2 (10 mL), washed with sat. EDTA-NH_3 (25 mL) and then brine (25 mL). The combined aqueous washes were extracted with CH_2Cl_2 (3 x 25 mL). The combined organic extracts were dried ($MgSO_4$), and the solvent

removed *in vacuo*. The residue was purified by column chromatography (neutralised SiO_2 (see general experimental), petrol-CH_2Cl_2 1 : 1 with 0→5% MeOH gradient), yielding an orange foam containing both diastereoisomers of **287** (393 mg, 0.343 mmol, *dr* 1.0 : 1.1, 82%).[120]

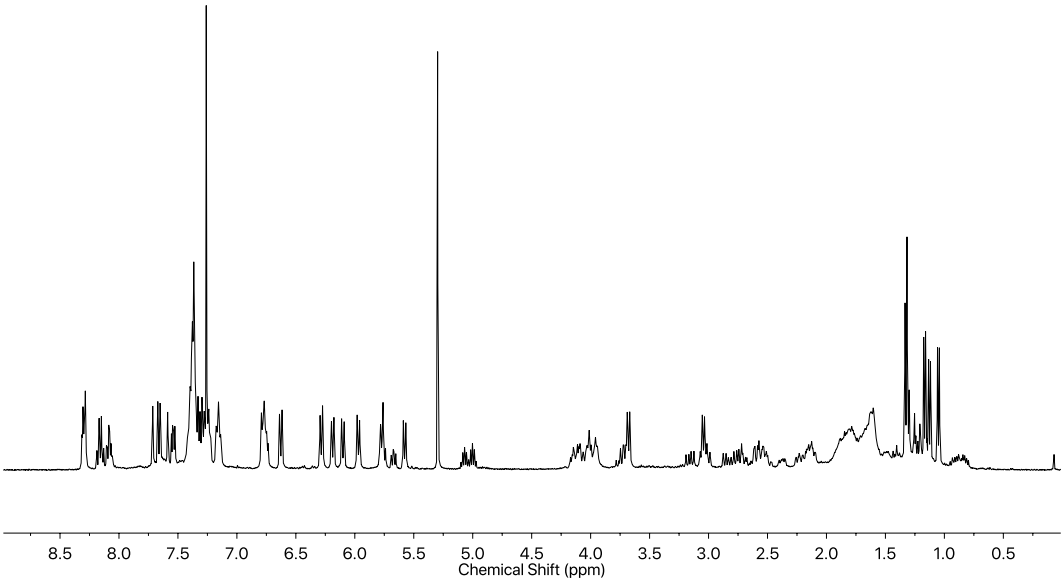

Figure 139: ^{1}H NMR (400 MHz, $CDCl_3$) of the diastereomeric mixture of Cu complexes **287**.

The diastereomeric mixture of **287** (393 mg, 0.343 mmol, 1.0 eq.) in CH_2Cl_2 (2.0 mL) was added to a solution of KCN (100 mg, 1.54 mmol, 4.5 eq.) in MeOH (2.0 mL), and the reaction mixture stirred for 30 min at rt. The solution was washed with brine (15 mL), aqueous H_2O_2 (35% w/w, 20 mL), brine (20 mL), and the combined aqueous washes were extracted with CH_2Cl_2 (3 x 15 mL). The combined organic phases were dried ($MgSO_4$) and the solvent removed *in vacuo* yielding a yellow foam (*S*,R_{mp})-**294**:(*S*,S_{mp})-**294** (295 mg, 0.309 mmol, *dr* 1.0 : 1.1, 90%). (*S*,R_{mp})-**294** and (*S*,S_{mp})-**294** were separated by column chromatography (H_2O saturated SiO_2, isocratic petrol-Et_2O-EtOAc 5 : 3 : 2) to give (*S*,R_{mp})-**294** (121 mg, 0.127 mmol, *er* = 99 : 1) and (*S*,S_{mp})-**294** (97 mg, 0.102 mmol, (*S*,R_{mp})-**294** : (*R*,S_{mp})-**294** : (*S*,S_{mp})-**294** = 0.6 : 1.0 : 98.4). The absolute stereochemistry of these products was determined by SC-XRD (*vide infra*) and the stereolabels assigned based on our established approach using the priority atoms A-D indicated below. Stereochemical purity was determined by HPLC using racemic samples of rotaxanes **294** (synthesised as above) for comparison (**Figure 143**, **Figure 144**). The stereochemical

purity of (S,R_{mp})-**294** was ultimately confirmed by analysis of its derivative, (R_{mp})-**295** (**Figure 154**), due to better HPLC peak separation, although it should be noted that direct HPLC analysis of (S,R_{mp})-**294** (**Figure 145**) is consistent with this value.[120]

Rotaxane (S,R_{mp})-**294**

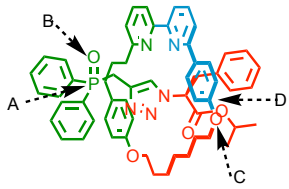

(S,R_{mp})-**294**

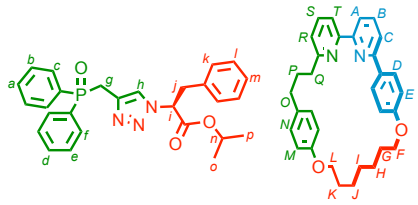

(S,R_{mp})-**294**

δ$_H$ ($CDCl_3$, 400 MHz) 9.49 (1H, d, J = 2.0, H_h), 7.81 (1H, t, J = 7.8, H_S), 7.77 (2H, td, J = 9.0, 1.4, H_f), 7.76 (1H, t, J = 7.8, H_B), 7.71 (2H, ddd, J = 11.4, 7.4, 1.5, H_c), 7.63 (1H, d, J = 7.8, H_R), 7.59 (1H, d, J = 7.8, H_T), 7.44 (2H, ddd, J = 8.3, 7.4, 1.4, H_e), 7.41 (1H, d, J = 7.7, H_C), 7.38 (1H, m, H_d), 7.32 (2H, dt, J = 8.8, 2.5, H_D), 7.28 (1H, d, J = 7.8, H_A), 7.20 (1H, td, J = 7.4, 1.4, H_a), 7.12 (2H, td, J = 7.4, 2.6, H_b), 6.80 (2H, dt, J = 8.7, 2.3, H_N), 7.08-7.02 (3H, m, H_l, H_m), 6.72 (2H, dd, J = 7.0, 2.4, H_k), 6.48 (2H, dt, J = 8.6, 2.0, H_M), 6.47 (2H, dt, J = 8.8, 2.4, H_E), 4.73 (1H, dd, J = 12.4, 4.7, H_i), 4.51 (1H, sept., J = 6.2, H_n), 4.32 (1H, app. q (ddd), J = 7.4, H_Q), 3.90 (2H, m, H_F, $H_{F'}$), 3.82 (1H, dt, J = 7.8, 4.1, $H_{Q'}$), 3.57 (1H, dd, J = 15.9, 13.6, H_g), 3.13 (1H, t(dd), J = 12.8, H_j), 2.99 (1H, dd, J = 15.9, 11.1, $H_{g'}$), 2.80-2.71 (2H, m, H_O, $H_{O'}$), 2.64 (2H, td, J = 8.6, 3.8, H_L, $H_{L'}$), 2.22 (1H, dd, J = 13.5, 4.7, $H_{j'}$), 2.07-1.95 (2H, m, H_P, H_K), 1.92-1.73 (4H, m, $H_{P'}$, $H_{K'}$, H_J, $H_{J'}$), 1.65-1.42 (2H, m, H_G, $H_{G'}$), 0.95-0.70 (4H, m, H_H, $H_{H'}$, H_I, $H_{I'}$), 0.69 (3H, d, J = 6.3, H_p), 0.44 (3H, d, J = 6.3, H_o). **δ**$_C$ ($CDCl_3$, 101 MHz) 169.0, 163.0, 159.2, 158.8, 157.7, 157.5, 157.0, 137.2, 137.0, 136.0, 135.6 (d, J = 7.2), 134.5 (d, J = 79.0), 132.5 (d, J = 78.8), 131.8, 131.5 (d, J = 2.6), 131.3 (d, J = 2.6), 131.2 (d, J = 3.4), 131.1 (d, J = 3.3), 130.6, 129.4, 129.3, 128.9, 128.7 (d, J = 11.6), 128.4 (d, J = 11.6), 128.1, 127.4 (d, J = 5.3), 126.5, 121.9, 120.3, 120.0, 119.5, 115.1, 114.3, 68.6, 67.9, 66.2, 62.3, 37.1, 36.4, 35.1, 31.3, 28.8, 28.7, 28.0 (d, J = 69.1), 25.5, 25.1, 24.0, 21.2, 20.9. **δ**$_{31P\{1H\}}$ ($CDCl_3$, 202 MHz) 28.7. HR-ESI-MS m/z = 952.4564 $[M + H]^+$ (calc. m/z for $C_{59}H_{62}N_5O_5P$ 952.4561).[120]

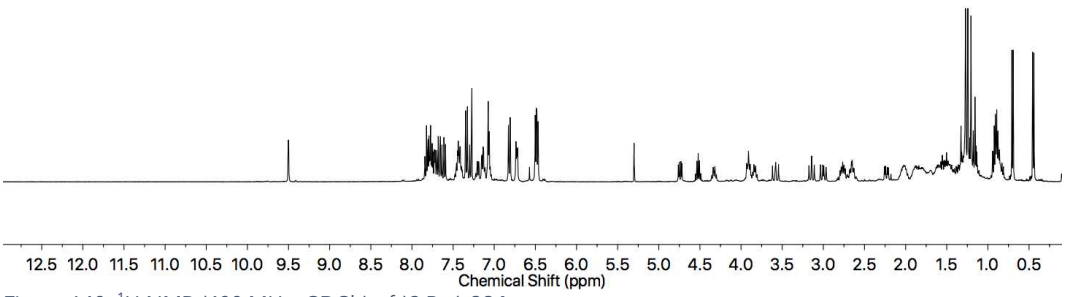

Figure 140: ^{1}H NMR (400 MHz, $CDCl_3$) of (*S*,R_{mp})-**294**.

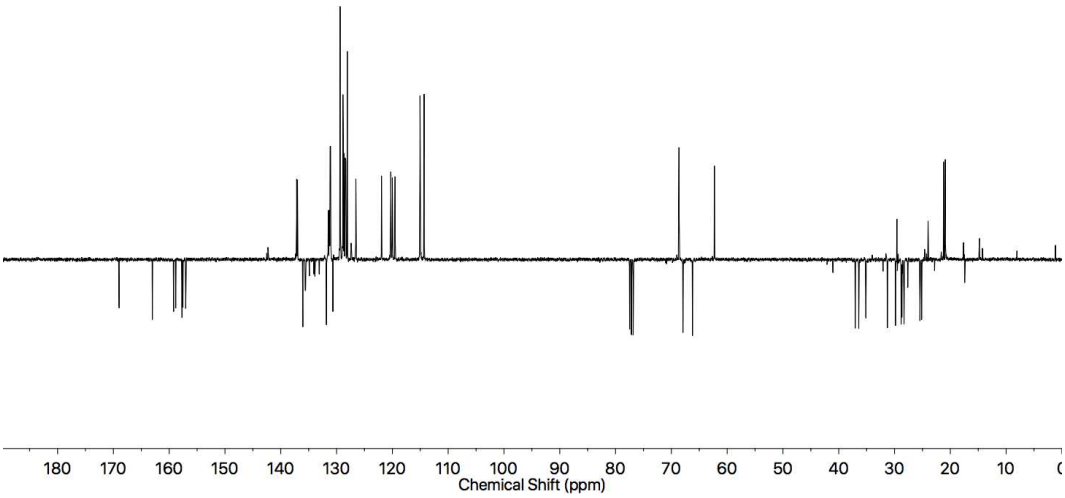

Figure 141: JMOD NMR (101 MHz, $CDCl_3$) of (*S*,R_{mp})-**294**.

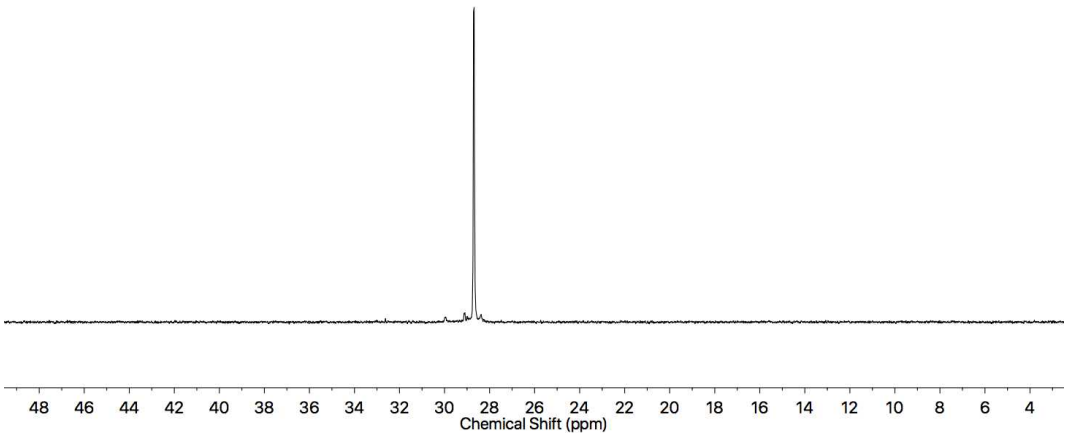

Figure 142: $^{31}P\{^{1}H\}$ NMR (202 MHz, $CDCl_3$) of (*S*,*R*$_{mp}$)-**294**.

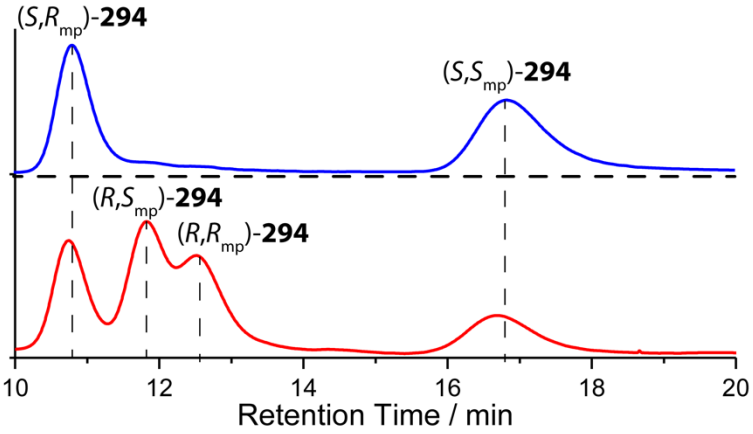

Figure 143: Chiral Stationary Phase HPLC ((*S*,*S*)Whelk, isocratic *n*-hexane-isopropanol 25 : 75, 303 K, load solvent Et_2O, 5 µL injection, flowrate 1 $mLmin^{-1}$) of the mixture of rotaxanes (*S*,*R*$_{mp}$)-**294** and (*S*,*S*$_{mp}$)-**294** (blue), and the equivalent racemate (red). Retention times (min): (*S*,*R*$_{mp}$)-**294** 10.7, (*R*,*S*$_{mp}$)-**294** 11.8, (*R*,*R*$_{mp}$)-**294** 12.5, (*S*,*S*$_{mp}$)-**294** 16.7.

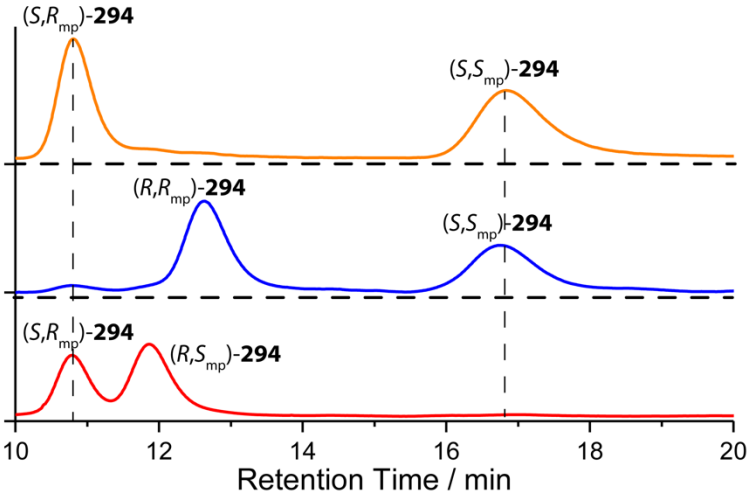

Figure 144: Chiral Stationary Phase HPLC ((*S*,*S*)Whelk, isocratic *n*-hexane-isopropanol 25 : 75, 303 K, load solvent Et_2O, 5 µL injection, flowrate 1 $mLmin^{-1}$) of the crude mixture of rotaxanes **294** (top) and the racemates of highly diastereomerically enriched samples (middle and bottom). Retention times (min): (*S*,R_{mp})-**294** 10.7, (*R*,S_{mp})-**294** 11.8, (*R*,R_{mp})-**294** 12.5, (*S*,S_{mp})-**294** 16.7.

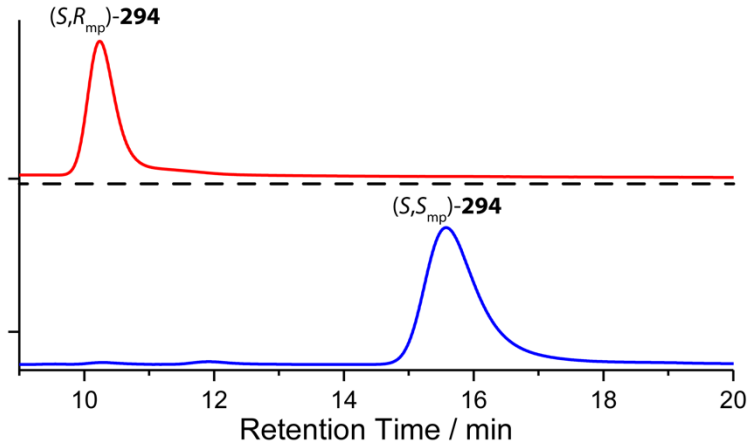

Figure 145: Chiral Stationary Phase HPLC ((*S*,*S*)Whelk, isocratic *n*-hexane-isopropanol 25 : 75, 303 K, load solvent Et_2O, 5 µL injection, flowrate 1 $mLmin^{-1}$) of 99 : 1 *er* (*S*,R_{mp})-**294** (red). Due to overlap of the peaks, the stereochemical purity is inferred from analysis of (R_{mp})-**295**. The HPLC trace shown here is consistent with this. (*S*,R_{mp})-**294** : (*R*,S_{mp})-**294** : (*S*,S_{mp})-**294**, 0.6 : 1.0 : 98.4 (blue). Mechanically planar stereogenic element ratio (R_{mp}) : (S_{mp}) 1 : 99.

Rotaxane (S,S_{mp})-**294**

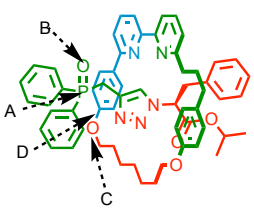

(S,S_{mp})-**294**

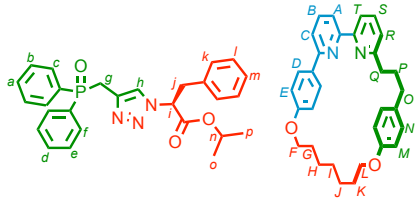

(S,S_{mp})-**294**

δ_H ($CDCl_3$, 400 MHz) 9.54 (1H, d, J = 1.8, H_h), 7.87-7.79 (4H, m, H_b, H_e), 7.83 (1H, t, J = 7.6, H_B), 7.75 (1H, t, J = 7.6, H_S), 7.65 (1H, d, J = 7.6, H_A), 7.62 (1H, d, J = 7.6, H_T), 7.59 (1H, d, J = 8.0, H_a or H_d), 7.44-7.35 (4H, m, H_c, H_f), 7.33 (1H, d, J = 7.7, H_C), 7.32 (2H, dt, J = 8.9, 2.4, H_D), 7.31-7.29 (1H, m, H_a or H_d), 7.27 (1H, d, J = 7.6, H_R), 6.91 (2H, d, J = 8.8, H_N), 7.08-7.01 (3H, m, H_l, H_m), 6.53 (2H, d, J = 8.9, H_M), 6.52 (2H, dd, J = 7.5, 1.9, H_k), 6.31 (2H, dt, J = 9.1, 2.2, H_E), 4.64 (1H, sept., J = 6.2, H_n), 3.96 (1H, app. q., J = 6.7, H_F), 3.82 (2H, t, J = 7.6, H_L), 3.74 (1H, t, J = 6.6, $H_{F'}$), 3.71 (1H, dd, J = 11.9, 4.3, H_i), 3.56 (1H, dd, J = 15.1, 12.0, H_g), 3.52 (1H, dd, J = 11.9, 4.3, H_j), 3.18 (1H, t, J = 15.1, $H_{g'}$), 2.92 (1H, t, J = 11.9, $H_{j'}$), 2.80 (2H, dt, J = 14.0, 3.6, H_Q, $H_{Q'}$), 2.73 (1H, dt, J = 13.6, 5.0, H_O), 2.58 (1H, dt, J = 13.6, 6.8, H_O'), 2.00-1.87 (3H, m, H_P, $H_{P'}$, H_G), 1.80-1.46 (5H, m, $H_{G'}$, H_J, $H_{J'}$), 1.31-1.10 (2H, m, H_K, $H_{K'}$), 0.94-0.79 (4H, m, H_H, $H_{H'}$, H_I, $H_{I'}$),0.99 (3H, d, J = 6.2, H_p), 0.63 (3H, d, J = 6.3, H_o). δ_C ($CDCl_3$, 101 MHz) 167.8, 163.1, 159.4, 158.9, 157.6, 157.2, 137.1 (d, J = 3.4), 135.7 (d, J = 7.4), 135.5, 134.3 (d, J = 11.8), 133.3 (d, J = 12.5), 131.5, 131.4, 131.3 (d, J = 2.7) 131.3, 131.1 (d, J = 9.8), 130.9, 129.1, 129.1, 128.5 (d, J = 7.4), 128.4 (d, J = 7.4), 128.3, 128.1, 126.5, 126.2 (d, J = 6.3), 122.5, 120.2 (d, J = 17.6), 119.4, 115.6, 114.0, 68.7, 68.3, 66.0, 63.3, 37.3, 37.3, 35.1, 32.6, 29.7, 29.4, 29.3, 28.5, 28.3 (d, J = 22.5), 27.8, 25.0, 24.7, 23.9, 21.5, 21.1. $\delta_{31P\{1H\}}$ ($CDCl_3$, 202 MHz) 29.8. HR-ESI-MS m/z = 952.4564 $[M + H]^+$ (calc. m/z for $C_{59}H_{62}N_5O_5P$ 952.4561).[120]

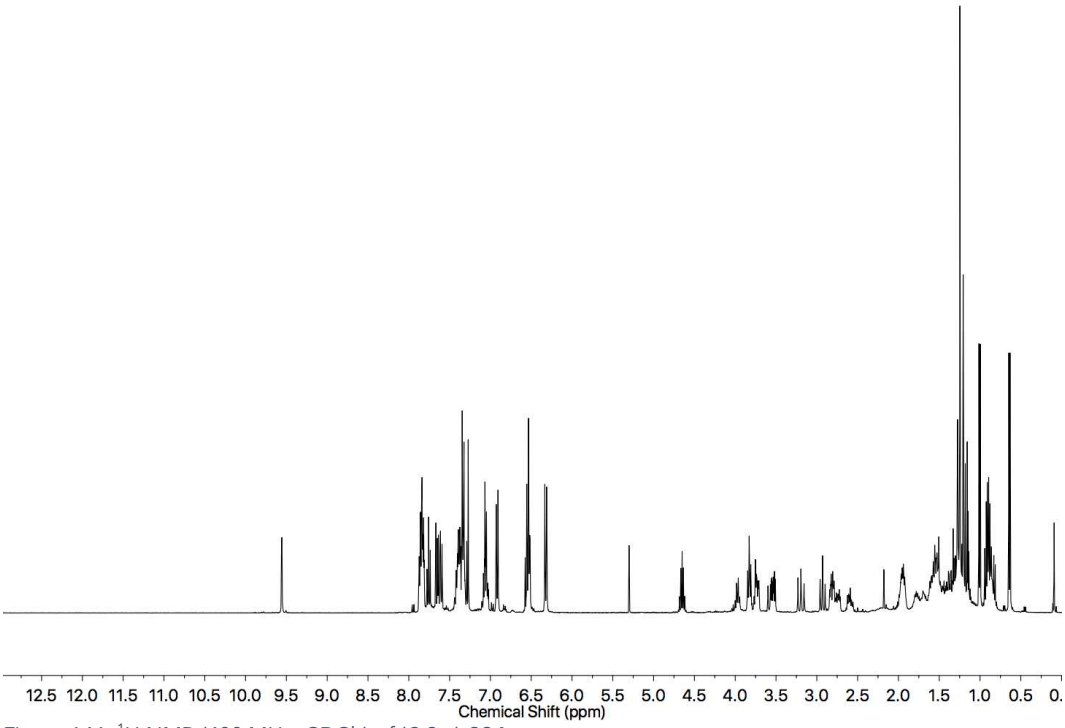

Figure 146: ^{1}H NMR (400 MHz, $CDCl_3$) of (S,S_{mp})-**294**.

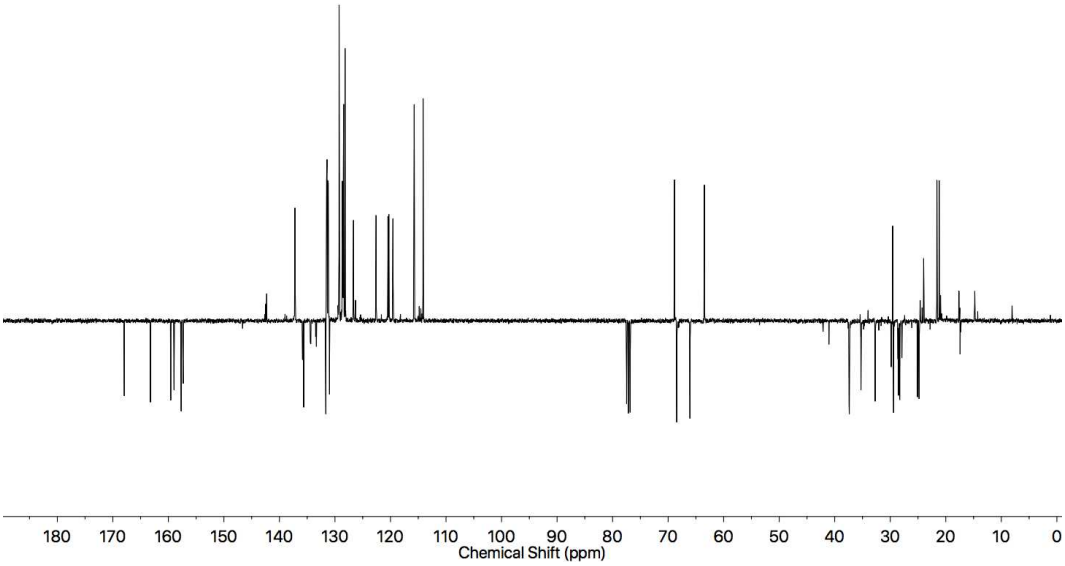

Figure 147: JMOD NMR (101 MHz, $CDCl_3$) of (S,S_{mp})-**294**.

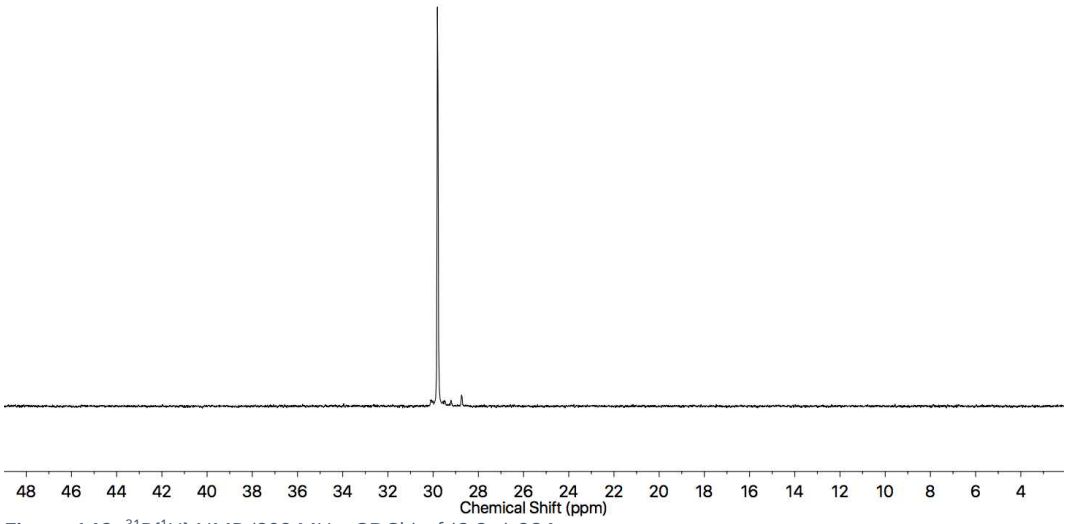

Figure 148: $^{31}P\{^{1}H\}$ NMR (202 MHz, $CDCl_3$) of (S,S_{mp})-**294**.

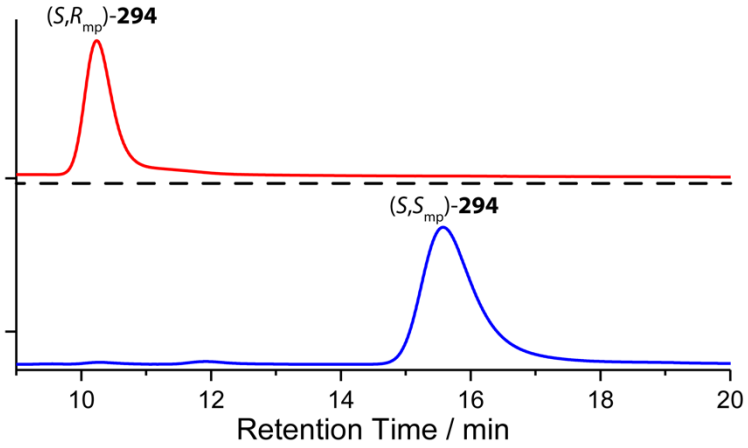

Figure 149: Chiral Stationary Phase HPLC ((*S*,*S*)Whelk, isocratic *n*-hexane-isopropanol 25 : 75, 303 K, load solvent Et_2O, 5 µL injection, flowrate 1 $mLmin^{-1}$) of 99 : 1 *er* (S,R_{mp})-**294** (red). Due to overlap of the peaks, the stereochemical purity is inferred from analysis of (R_{mp})-**295**. The HPLC trace shown here is consistent with this. (S,R_{mp})-**294** : (R,S_{mp})-**294** : (S,S_{mp})-**294**, 0.6 : 1.0 : 98.4 (blue). Mechanically planar stereogenic element ratio (R_{mp}) : (S_{mp}) 1 : 99.

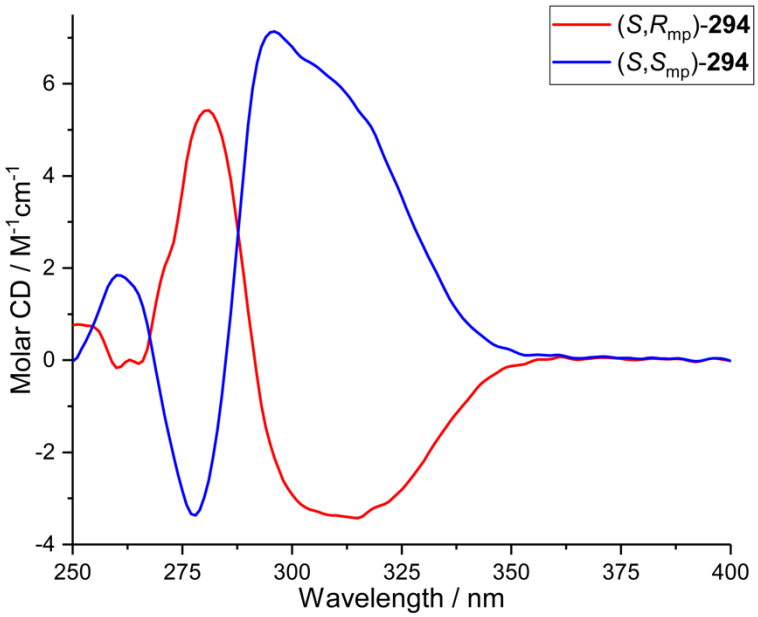

Figure 150: Circular Dichroism spectra of (*S*,R_{mp})-**294** (53.4 µM, 99 : 1 *er*) and (*S*,S_{mp})-**294** (58.8 µM, (*S*,S_{mp})-**294** : (*R*,S_{mp})-**294** : (*S*,R_{mp})-**294**, 98.4 : 1.0 : 0.6) at 293 K in $CHCl_3$.

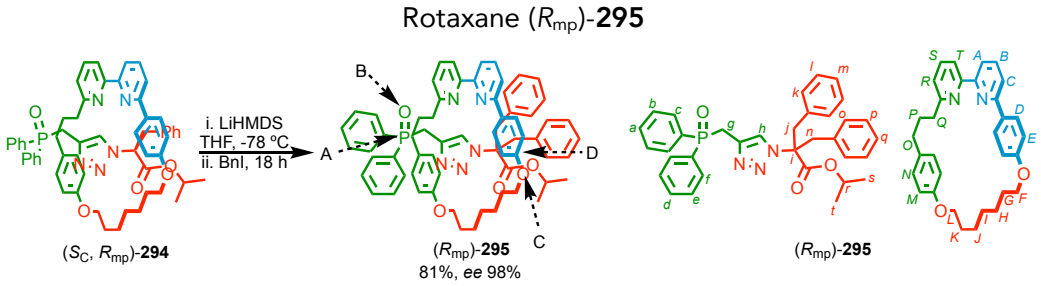

(*S*,R_{mp})-**294** (61.4 mg, 0.064 mmol, 1.0 eq.) was dissolved in anhydrous THF (3 mL) and transferred into a dry CEM MW vial under N_2. The solution was cooled to -78 °C and stirred for 20 min. Lithium bis(trimethylsilyl)amide (1 M in THF, 0.32 mL, 0.32 mmol, 5.0 eq.) was added to the reaction mixture and stirred for 10 min. Benzyl iodide (1 M in THF, 0.65 mL, 0.65 mmol, 10.0 eq.) was added. The reaction was allowed to warm to rt and stirred for 18 h. The reaction mixture was diluted with saturated NH_4Cl (30 mL) and extracted with CH_2Cl_2 (3 x 20 mL). The combined organic extracts were dried ($MgSO_4$) and solvent removed *in vacuo*. The residue was purified by column chromatography (SiO_2, petrol-EtOAc 0→50%) to give a yellow foam product (R_{mp})-**295** (53.7 mg, 0.051 mmol, 81%, *er* 99 : 1). *Enantiopurity was assessed by chiral stationary phase HPLC*. The absolute mechanical stereochemistry was inferred from that of the starting materials and the stereolabels assigned based on our established approach using the priority atoms indicated below.[120] δ_H ($CDCl_3$, 400 MHz) 9.48 (1H, d, *J* = 1.6, H_h), 7.77 (1H, t, *J* = 8.1, H_S), 7.74 (1H, t, *J* = 8.1, H_B), 7.64 (4H, ddd, *J* = 8.2, 7.7, 2.3, H_c, H_f), 7.58 (1H, d, *J* = 8.1, H_T), 7.54 (1H, d, *J* = 7.8, H_A), 7.52 (2H, d, *J* = 8.5, H_D), 7.36 (4H, td, *J* = 7.6, 2.7, H_b, H_e),

7.29-7.23 (4H, m, $\boldsymbol{H}_a$, $\boldsymbol{H}_d$, $\boldsymbol{H}_R$, $\boldsymbol{H}_C$), 7.14-7.09 (3H, m, $\boldsymbol{H}_k$, $\boldsymbol{H}_m$), 7.06-7.01 (3H, m, $\boldsymbol{H}_o$, $\boldsymbol{H}_q$), 6.90 (2H, d, J = 8.5, $\boldsymbol{H}_N$), 6.89 (2H, dd, J = 7.2, 2.1, $\boldsymbol{H}_l$), 6.79 (2H, dd, J = 7.1, 2.6, $\boldsymbol{H}_p$), 6.49 (2H, d, J = 8.5, $\boldsymbol{H}_E$), 6.35 (2H, d, J = 8.3, $\boldsymbol{H}_M$), 4.60 (1H, sept., J = 6.2, $\boldsymbol{H}_r$), 3.45 (1H, d, J = 15.0, $\boldsymbol{H}_g$), 3.93-3.81 (4H, m, $\boldsymbol{H}_L$, $\boldsymbol{H}_{L'}$, $\boldsymbol{H}_F$, $\boldsymbol{H}_{F'}$), 3.39 (1H, d, J = 14.8, $\boldsymbol{H}_j$), 3.09-2.97 (2H, m, $\boldsymbol{H}_Q$, $\boldsymbol{H}_{Q'}$), 2.92 (1H, d, J = 14.7, $\boldsymbol{H}_n$), 2.74 (1H, d, J = 15.2, $\boldsymbol{H}_g$), 2.68 (1H, br. d, J = 14.8, $\boldsymbol{H}_O$), 2.63-2.54 (1H, m, $\boldsymbol{H}_{j'}$), 2.38 (1H, d, J = 14.7, $\boldsymbol{H}_{n'}$), 2.02-1.89 (3H, m, $\boldsymbol{H}_P$, $\boldsymbol{H}_{P'}$, $\boldsymbol{H}_{O'}$), 1.87-1.77 (2H, m, $\boldsymbol{H}_J$, $\boldsymbol{H}_{J'}$), 1.75-1.62 (2H, m, $\boldsymbol{H}_G$, $\boldsymbol{H}_{G'}$), 1.61-1.48 (2H, m, $\boldsymbol{H}_K$, $\boldsymbol{H}_{K'}$), 1.47-1.36 (2H, m, $\boldsymbol{H}_l$, $\boldsymbol{H}_{l'}$), 0.94-0.86 (2H, m, $\boldsymbol{H}_H$, $\boldsymbol{H}_{H'}$), 0.71 (3H, d, J = 6.3, $\boldsymbol{H}_s$), 0.66 (3H, d, J = 6.3, $\boldsymbol{H}_t$). $\boldsymbol{\delta}_C$ ($CDCl_3$, 101 MHz) 169.1, 163.1, 159.4, 158.5, 158.1, 157.8, 157.7, 137.9 (d, J = 7.2), 137.0, 136.9, 136.5 (2C, d, J = 48.6), 132.0, 131.5, 131.2, 131.2, 131.1 (2C, d, J = 9.3), 130.6, 130.0, 129.9, 129.4, 128.4 (2C, d, J = 8.4), 128.3. (2C, d, J = 8.4), 127.7 (d, J = 6.4), 126.4, 126.1, 120.6, 120.4, 120.1, 119.0, 115.0, 114.6, 70.8, 69.7, 68.5, 66.9, 44.3, 42.7, 36.5, 34.7, 29.5, 28.9, 28.6, 28.1, 26.8 (d, J = 72.6), 25.5, 24.9, 24.0, 21.1, 21.0. $\boldsymbol{\delta}_{31P\{1H\}}$ ($CDCl_3$, 202 MHz) 28.1. HR-ESI-MS [M+H$^+$] m/z 1042.5 (calc. for $C_{66}H_{69}N_5O_5P$ m/z 1042.5).[120]

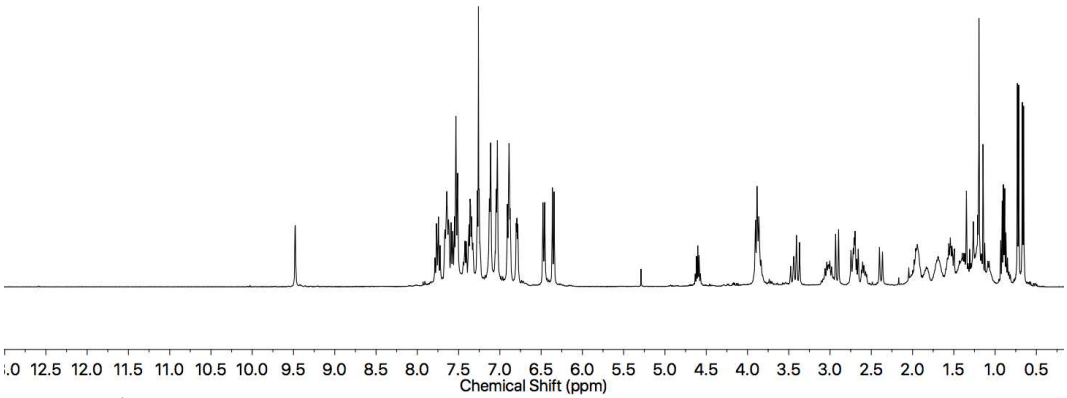

Figure 151: ^{1}H NMR (400 MHz, $CDCl_3$) of (R_{mp})-**295**.

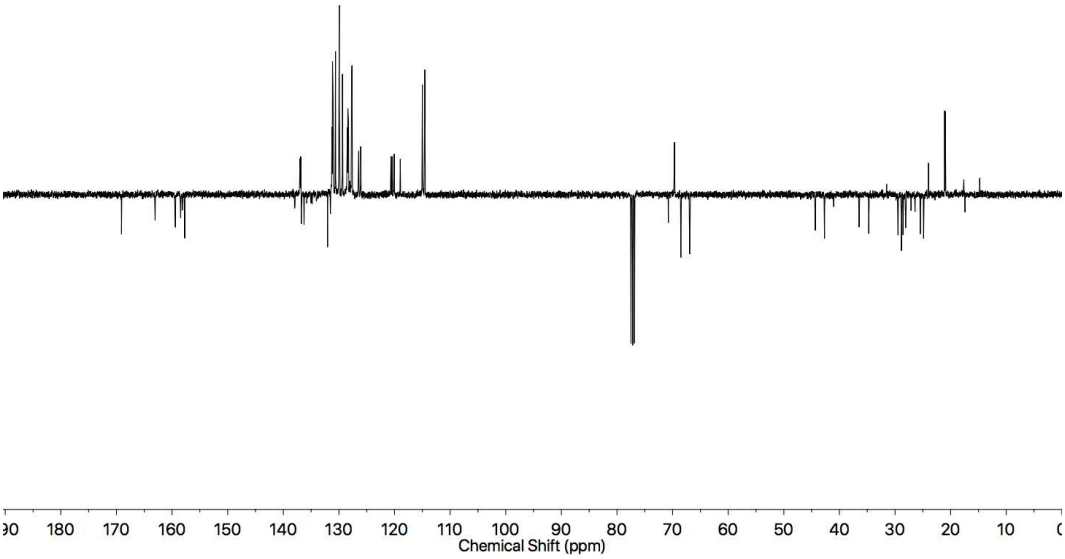

Figure 152: JMOD NMR (101 MHz, $CDCl_3$) of (R_{mp})-**295**.

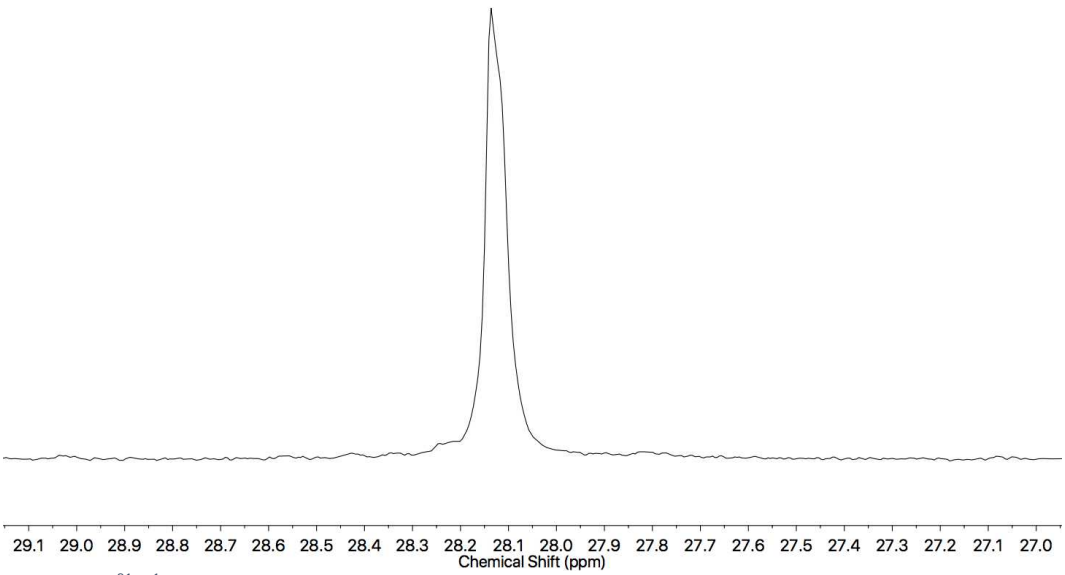

Figure 153: $^{31}P\{^1H\}$ NMR (202 MHz, $CDCl_3$) of (R_{mp})-**295**.

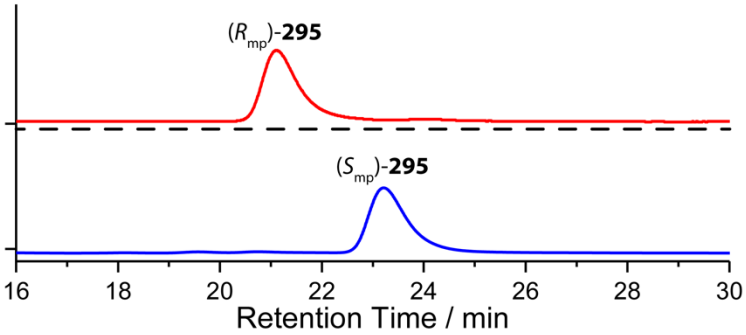

Figure 154: Chiral Stationary Phase HPLC ((*S*,*S*)Whelk, isocratic *n*-hexane-isopropanol 70 : 30, 303 K, load solvent Et_2O, 5 µL injection, flowrate 0.75 $mLmin^{-1}$) of 99 : 1 *er* (R_{mp})-**295** (red). Retention times (min): (R_{mp})-**295** 21.6 (379266, 98.9%), (S_{mp})-**295** 25.2 (4118, 1.1%). 1 : 99 *er* (S_{mp})-**295** (blue). Retention times (min): (R_{mp})-**295** 20.9 (185193, 1.2%), (S_{mp})-**295** 24.2 (15419194, 98.8%).

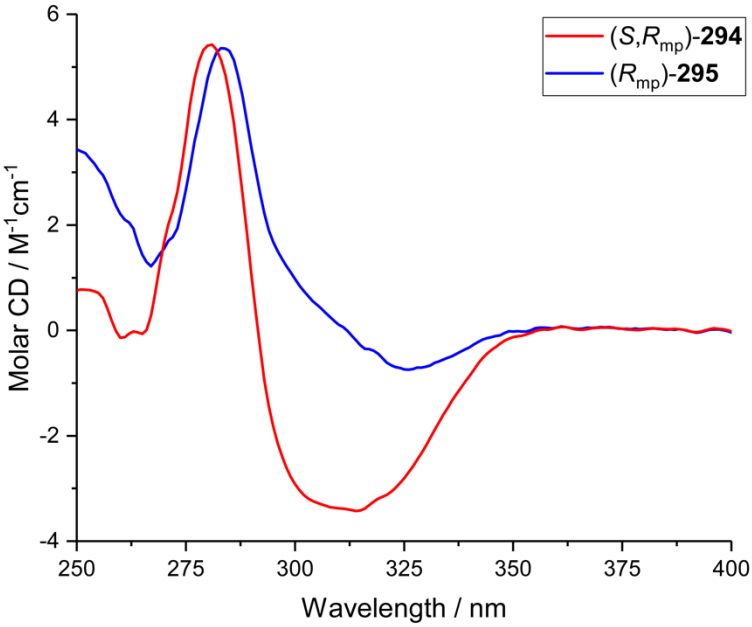

Figure 155: Circular Dichroism spectra of (*S*,R_{mp})-**294** (53.4 µM, 99 : 1 *er*) and (R_{mp})-**295** (66.2 µM, 99 : 1 *er*) at 293 K in $CHCl_3$.

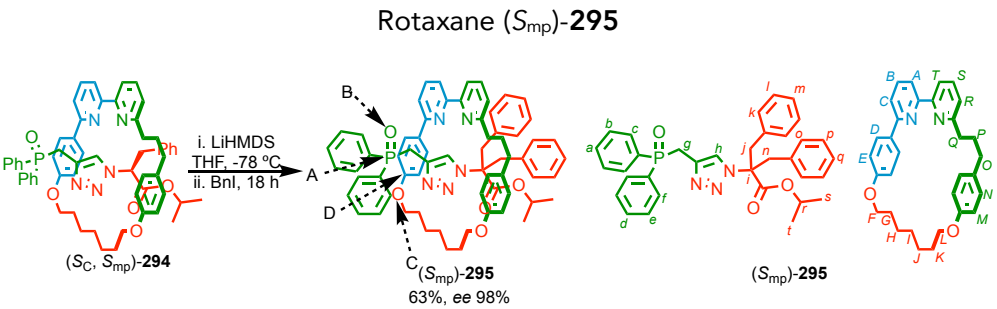

(*S*,S_{mp})-**294** (55.9 mg, 0.059 mmol, 1.0 eq.) was dissolved in anhydrous THF (3 mL) and transferred into a dry CEM MW vial under N_2. The solution was cooled to -78 °C and stirred for 20 min. Lithium bis(trimethylsilyl)amide (1 M in THF, 0.29 mL, 0.29 mmol, 5.0 eq.) was added to the reaction mixture and stirred for 10 min. Benzyl iodide (1 M in THF, 0.59 mL, 0.59 mmol, 10.0 eq.) was added. The reaction was allowed to warm to rt and

stirred for 18 h. The reaction mixture was diluted with saturated NH_4Cl (30 mL) and extracted with CH_2Cl_2 (3 x 20 mL). The combined organic extracts were dried ($MgSO_4$) and solvent removed *in vacuo*. The reidue was purified by column chromatography (SiO_2, petrol-EtOAc 0→50%) to give a yellow foam product (S_{mp})-**295** (38.4 mg, 0.037 mmol, 63%, 1 : 99 *er*). Enantiopurity was assessed by chiral stationary phase HPLC. The absolute mechanical stereochemistry was inferred from that of the starting material and the stereolabel assigned based on our established approach using the priority atoms indicated below.[120] (S_{mp})-**295** same as (R_{mp})-**295** above. δ_H ($CDCl_3$, 400 MHz) 9.48 (1H, d, J = 1.6, H_h), 7.77 (1H, t, J = 8.1, H_S), 7.74 (1H, t, J = 8.1, H_B), 7.64 (4H, ddd, J = 8.2, 7.7, 2.3, H_c, H_f), 7.58 (1H, d, J = 8.1, H_T), 7.54 (1H, d, J = 7.8, H_A), 7.52 (2H, d, J = 8.5, H_D), 7.36 (4H, td, J = 7.6, 2.7, H_b, H_e), 7.29-7.23 (4H, m, H_a, H_d, H_R, H_C), 7.14-7.09 (3H, m, H_k, H_m), 7.06-7.01 (3H, m, H_o, H_q), 6.90 (2H, d, J = 8.5, H_N), 6.89 (2H, dd, J = 7.2, 2.1, H_l), 6.79 (2H, dd, J = 7.1, 2.6, H_p), 6.49 (2H, d, J = 8.5, H_E), 6.35 (2H, d, J = 8.3, H_M), 4.60 (1H, sept., J = 6.2, H_r), 3.45 (1H, d, J = 15.0, H_g), 3.93-3.81 (4H, m, H_L, $H_{L'}$, H_F, $H_{F'}$), 3.39 (1H, d, J = 14.8, H_j), 3.09-2.97 (2H, m, H_Q, $H_{Q'}$), 2.92 (1H, d, J = 14.7, H_n), 2.74 (1H, d, J = 15.2, H_g), 2.68 (1H, br. d, J = 14.8, H_O), 2.63-2.54 (1H, m, $H_{j'}$), 2.38 (1H, d, J = 14.7, $H_{n'}$), 2.02-1.89 (3H, m, H_P, $H_{P'}$, $H_{O'}$), 1.87-1.77 (2H, m, H_J, $H_{J'}$), 1.75-1.62 (2H, m, H_G, $H_{G'}$), 1.61-1.48 (2H, m, H_K, $H_{K'}$), 1.47-1.36 (2H, m, H_I, $H_{I'}$), 0.94-0.86 (2H, m, H_H, $H_{H'}$), 0.71 (3H, d, J = 6.3, H_s), 0.66 (3H, d, J = 6.3, H_t). δ_C ($CDCl_3$, 101 MHz) 169.1, 163.1, 159.4, 158.5, 158.1, 157.8, 157.7, 137.9 (d, J = 7.2), 137.0, 136.9, 136.5 (2C, d, J = 48.6), 132.0, 131.5, 131.2, 131.2, 131.1 (2C, d, J = 9.3), 130.6, 130.0, 129.9, 129.4, 128.4 (2C, d, J = 8.4), 128.3. (2C, d, J = 8.4), 127.7 (d, J = 6.4), 126.4, 126.1, 120.6, 120.4, 120.1, 119.0, 115.0, 114.6, 70.8, 69.7, 68.5, 66.9, 44.3, 42.7, 36.5, 34.7, 29.5, 28.9, 28.6, 28.1, 26.8 (d, J = 72.6), 25.5, 24.9, 24.0, 21.1, 21.0. $\delta_{31P\{1H\}}$ ($CDCl_3$, 202 MHz) 28.1. HR-ESI-MS [M+H$^+$] m/z 1042.5 (calc. for $C_{66}H_{69}N_5O_5P$ m/z 1042.5).[120]

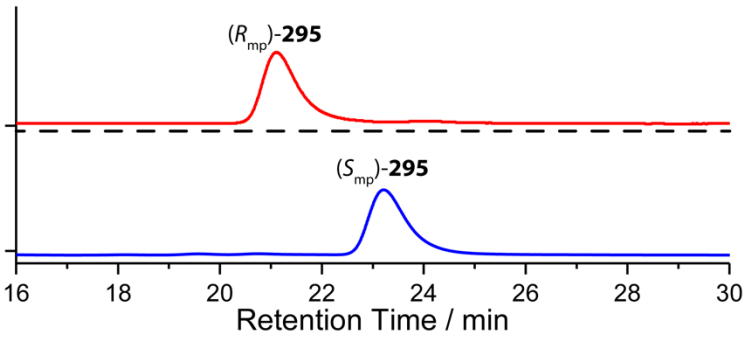

Figure 156: Chiral Stationary Phase HPLC ((*S*,*S*)Whelk, isocratic *n*-hexane-isopropanol 70 : 30, 303 K, load solvent Et_2O, 5 µL injection, flowrate 0.75 $mLmin^{-1}$) of 99 : 1 *er* (R_{mp})-**295** (red). Retention times (min): (R_{mp})-**295** 21.6 (379266, 98.9%), (S_{mp})-**295** 25.2 (4118, 1.1%). 1 : 99 *er* (S_{mp})-**295** (blue). Retention times (min): (R_{mp})-**295** 20.9 (185193, 1.2%), (S_{mp})-**295** 24.2 (15419194, 98.8%).

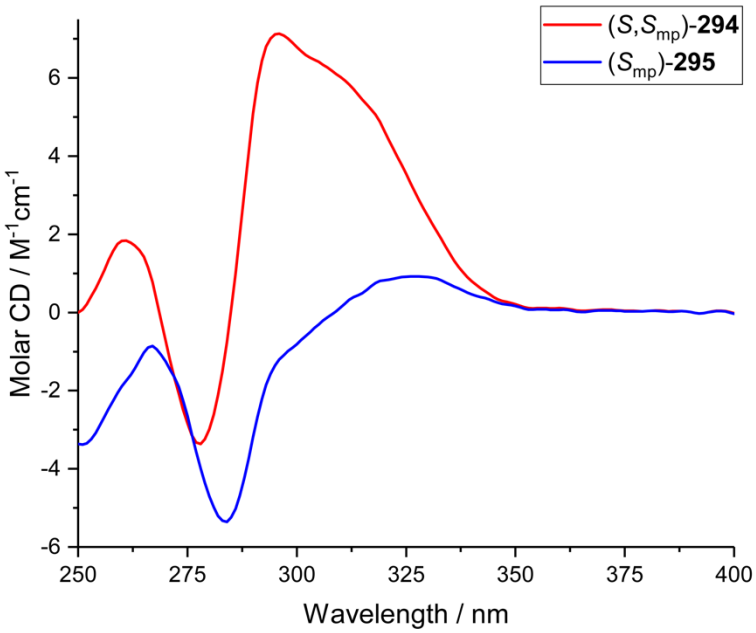

Figure 157: Circular Dichroism spectra of (S,S_{mp})-**294** (58.8 µM, (S,S_{mp})-**294** : (R,S_{mp})-**294** : (S,R_{mp})-**294**, 98.4 : 1.0 : 0.6) and (S_{mp})-**295** (54.7 µM, 99 : 1 *er*) at 293 K in $CHCl_3$.

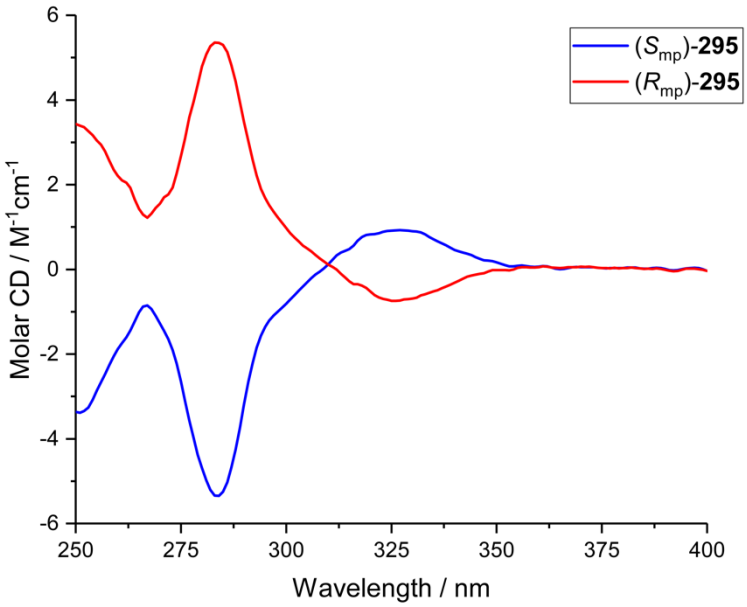

Figure 158: Circular Dichroism spectra of (R_{mp})-**295** (66.2 µM, 99 : 1 *er*) and (S_{mp})-**295** (54.7 µM, 99 : 1 *er*) at 293 K in $CHCl_3$.

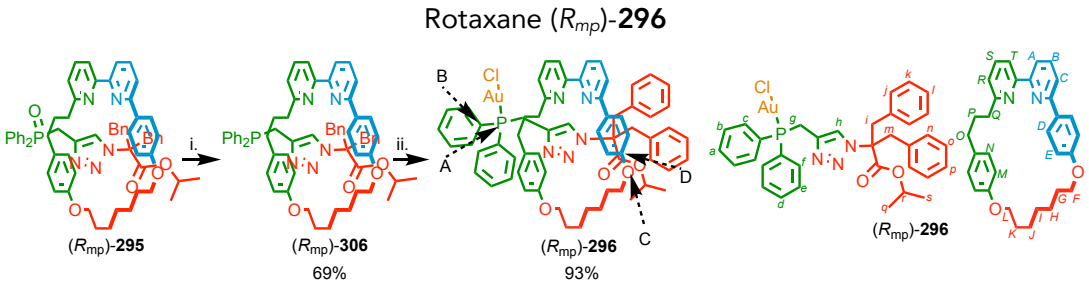

Scheme 15: Synthesis of (R_{mp})-**296**. i. $HSiCl_3$, NEt_3, PhMe, CH_2Cl_2, 100 °C, 3 d; ii. $(Me_2S)AuCl$, CH_2Cl_2, rt, 1 h.

A Young's tube was dried under reduced pressure with a heat gun three times and filled with nitrogen in-between each period, as per Schlenk technique. Under a high flow of nitrogen, anhydrous NEt_3 (3.0 mL, 21.5 mmol, 200 eq.) was added, followed by $HSiCl_3$ (1.1 mL, 10.7 mmol, 100 eq.) slowly. After 5 minutes, (R_{mp})-**295** (112 mg, 0.107 mmol, 1eq.) was transferred in anhydrous PhMe (5.5 mL) and then anhydrous CH_2Cl_2 (1.1 mL). The vessel was sealed and stirred at 100 °C for 3 days. After 3 days the solution was cooled to rt, washed with NaOH (1 M, 40 mL) and extracted in CH_2Cl_2 (4 x 30 mL). The combined organic phases were dried ($MgSO_4$), and the solvent removed *in vacuo*. This work up was repeated 4 times until NEt_3.HCl was absent from the ^1H NMR, yielding an orange oil (R_{mp})-**306** (76.2 mg, 0.074 mmol, 69%). A dry vial was charged with $(Me_2S)AuCl$ (22.1 mg, 0.074 mmol, 1.0 eq.) and (R_{mp})-**306** was transferred in anhydrous CH_2Cl_2 (1.5 mL). The solution was stirred at rt for 1 h. The solution was filtered through Celite® and eluted with Et_2O. The solvent was removed *in vacuo*. The residue was purified by column chromatography (SiO_2, petrol-Et_2O 0→100%) to give (R_{mp})-**296** as a

white foam (86.2 mg, 0.068 mmol, 93%), the enantiopurity of which (*er* = 99 : 1) was inferred from the enantiopurity of the (R_{mp})-**295** starting material and the stereolabel assigned based on our established approach using the priority atoms indicated above.[120] δ_H ($CDCl_3$, 400 MHz) 9.82 (1H, d, *J* = 2.3, H_h), 7.86 (1H, t, *J* = 7.8, H_S), 7.77 (1H, t, *J* = 7.7, H_B), 7.74 (2H, dd, *J* = 11.9, 5.0, H_f), 7.69 (1H, d, *J* = 7.7, H_T), 7.57 (1H, dd, *J* = 7.5, 0.7, H_A), 7.52 (1H, dd, *J* = 7.9, 0.7, H_C), 7.49 (1H, ddt (dq), *J* = 7.2, 1.3, H_d), 7.44 (2H, td, *J* = 7.9, 2.5, H_e), 7.37 (2H, ddd, *J* = 12.7, 7.9, 1.5, H_c) 7.33 (2H, d, *J* = 8.9, H_D), 7.31 (1H, d, *J* = 7.7, H_R), 7.29-7.27 (1H, m, H_a), 7.19 (2H, td, *J* = 7.9, 2.6, H_b), 7.16-7.10 (3H, m, H_o, H_p), 7.07-7.03 (3H, m, H_j, H_l), 6.94 (2H, dd, *J* = 7.5, 1.7, H_M), 6.76-6.71 (2H, m, H_k), 6.61 (2H, d, *J* = 8.4, H_N), 6.31 (2H, d, *J* = 8.4, H_n), 6.15 (2H, d, *J* = 8.9, H_E), 4.60 (1H, sept., *J* = 6.3, H_r), 3.17 (1H, d, *J* = 14.8, H_i), 3.04 (1H, d, *J* = 14.8, H_m), 3.01 (1H, dd, *J* = 14.8, 13.3, H_g), 2.94-2.85 (1H), 2.79 (1H, dd, *J* = 14.8, 12.0, $H_{g'}$), 2.75-2.65 (1H), 2.59 (1H, d, *J* = 14.8, $H_{i'}$), 2.54-2.44 (1H), 2.28 (1H, d, *J* = 14.8, $H_{m'}$), 2.18-1.88 (3H), 1.78-1.03 (14H), 0.68 (3H, d, *J* = 6.4, H_q), 0.63 (3H, d, *J* = 6.4, H_s). It was not possible to unambiguously assign alkyl region of macrocycle (H_F-H_L, H_O-H_Q). δ_C ($CDCl_3$, 101 MHz) 169.0, 162.3, 158.7, 158.5, 158.4, 157.9, 157.4, 137.9, 137.8, 137.1, 137.0, 136.6, 136.1, 134.4, 134.2, 133.3, 133.2, 132.0, 131.5, 131.5, 131.2, 131.1, 131.0, 130.9, 130.2, 129.9, 129.8, 129.6, 128.9, 128.8, 128.7, 128.6, 128.6, 127.7, 127.6, 126.2, 126.2, 121.8, 120.7, 120.4, 119.0, 114.5, 114.2, 70.6, 69.6, 68.0, 57.2, 65.9, 44.0, 42.8, 35.7, 34.2, 30.3, 29.5, 28.4, 28.2, 27.9, 25.4, 25.3, 25.0, 24.8, 20.8, 20.8, 15.3. 64 signals corresponding to all 53 environments (11 doublets coupling to ^{31}P). $\delta_{31P\{1H\}}$ ($CDCl_3$, 202 MHz) 26.2. δ_{31P} ($CDCl_3$, 202 MHz) 26.2 (1P, broad quin.d, *J* 12.6, 3.6). HR-ESI-MS [M-Cl] m/z 1222.5 (calc. for $C_{66}H_{68}N_5O_4PAu$ m/z 1222.5).[120]

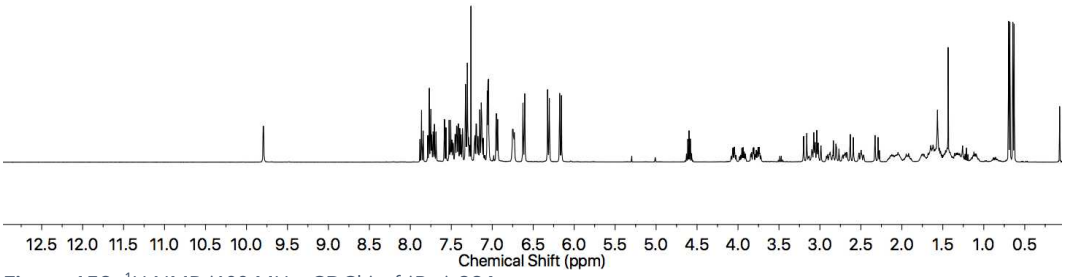

Figure 159: ^{1}H NMR (400 MHz, $CDCl_3$) of (R_{mp})-**296**.

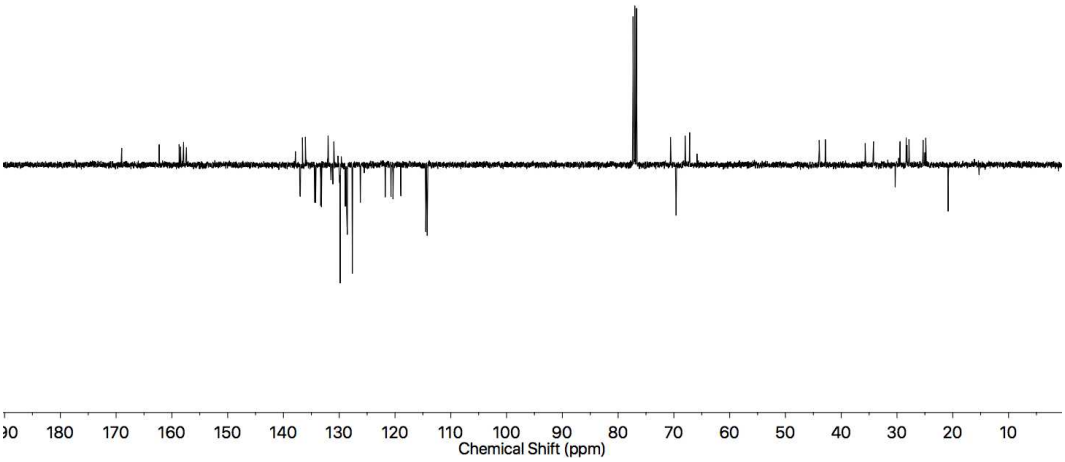

Figure 160: JMOD NMR (101 MHz, $CDCl_3$) of (R_{mp})-**296**.

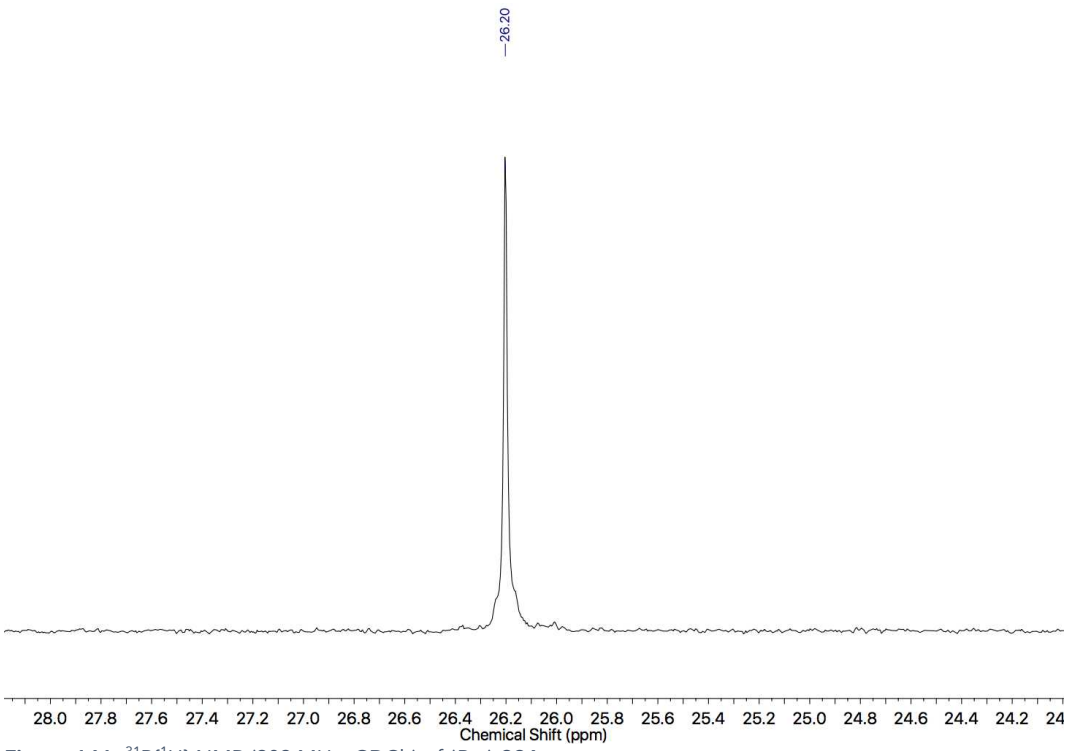

Figure 161: $^{31}P\{^{1}H\}$ NMR (202 MHz, $CDCl_3$) of (R_{mp})-**296**.

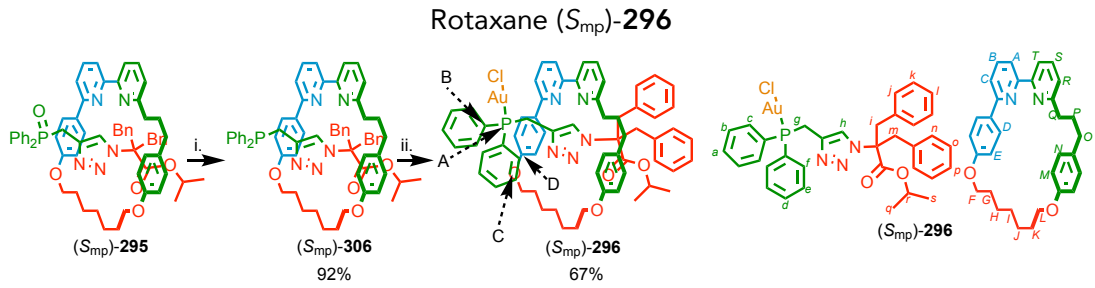

Scheme 16: Synthesis of (S_{mp})-**296**. i. $HSiCl_3$, NEt_3, PhMe, CH_2Cl_2, 100 °C, 3 d; ii. $(Me_2S)AuCl$, CH_2Cl_2, rt, 1 h.

A Young's tube was dried under reduced pressure with a heat gun three times and filled with nitrogen in-between each period, as per Schlenk technique. Under a high flow of nitrogen, anhydrous NEt_3 (2.5 mL, 17.9 mmol, 200 eq.) was added, followed by $HSiCl_3$ (0.9 mL, 8.95 mmol, 100 eq.) slowly. After 5 minutes, (S_{mp})-**295** (93.3 mg, 0.090 mmol, 1eq.) was transferred in anhydrous PhMe (4.6 mL) and then anhydrous CH_2Cl_2 (0.9 mL). The vessel was sealed and stirred at 100 °C for 3 days. After 3 days the solution was cooled to rt, washed with NaOH (1 M, 40 mL) and extracted in CH_2Cl_2 (4 x 30 mL). The combined organic phases were dried ($MgSO_4$), and the solvent removed *in vacuo*. This work up was repeated 4 times until NEt_3.HCl was absent from the ^{1}H NMR, yielding an orange oil (S_{mp})-**306** (85.3 mg, 0.083 mmol, 92%). A dry vial was charged with $(Me_2S)AuCl$ (24.4 mg, 0.083 mmol, 1.0 eq.) and (S_{mp})-**306** was transferred in anhydrous CH_2Cl_2 (2.0 mL). The solution was stirred at rt for 1 h. The solution was filtered through

Celite® and eluted with Et_2O. The solvent was removed *in vacuo*. The residue was purified by column chromatography (SiO_2, petrol-Et_2O 0→100%) to give (S_{mp})-**296** as a white foam (70.5 mg, 0.056 mmol, 67%, 62% yield over two steps), the enantiopurity of which (*er* = 99 : 1) was inferred from the enantiopurity of the (S_{mp})-**295** starting material and the stereolabel assigned based on our established approach using the priority atoms indicated above.[120] (S_{mp})-**296** same as (R_{mp})-**296** above. δ_H ($CDCl_3$, 400 MHz) 9.82 (1H, d, *J* = 2.3, H_h), 7.86 (1H, t, *J* = 7.8, H_S), 7.77 (1H, t, *J* = 7.7, H_B), 7.74 (2H, dd, *J* = 11.9, 5.0, H_f), 7.69 (1H, d, *J* = 7.7, H_T), 7.57 (1H, dd, *J* = 7.5, 0.7, H_A), 7.52 (1H, dd, *J* = 7.9, 0.7, H_C), 7.49 (1H, ddt (dq), *J* = 7.2, 1.3, H_d), 7.44 (2H, td, *J* = 7.9, 2.5, H_e), 7.37 (2H, ddd, *J* = 12.7, 7.9, 1.5, H_c) 7.33 (2H, d, *J* = 8.9, H_D), 7.31 (1H, d, *J* = 7.7, H_R), 7.29-7.27 (1H, m, H_a), 7.19 (2H, td, *J* = 7.9, 2.6, H_b), 7.16-7.10 (3H, m, H_o, H_p), 7.07-7.03 (3H, m, H_j, H_l), 6.94 (2H, dd, *J* = 7.5, 1.7, H_M), 6.76-6.71 (2H, m, H_k), 6.61 (2H, d, *J* = 8.4, H_N), 6.31 (2H, d, *J* = 8.4, H_n), 6.15 (2H, d, *J* = 8.9, H_E), 4.60 (1H, sept., *J* = 6.3, H_r), 3.17 (1H, d, *J* = 14.8, H_i), 3.04 (1H, d, *J* = 14.8, H_m), 3.01 (1H, dd, *J* = 14.8, 13.3, H_g), 2.94-2.85 (1H), 2.79 (1H, dd, *J* = 14.8, 12.0, $H_{g'}$), 2.75-2.65 (1H), 2.59 (1H, d, *J* = 14.8, $H_{i'}$), 2.54-2.44 (1H), 2.28 (1H, d, *J* = 14.8, $H_{m'}$), 2.18-1.88 (3H), 1.78-1.03 (14H), 0.68 (3H, d, *J* = 6.4, H_q), 0.63 (3H, d, *J* = 6.4, H_s). It was not possible to unambiguously assign the alkyl region of macrocycle (H_F-H_L, H_O-H_Q). δ_C ($CDCl_3$, 101 MHz) 169.0, 162.3, 158.7, 158.5, 158.4, 157.9, 157.4, 137.9, 137.8, 137.1, 137.0, 136.6, 136.1, 134.4, 134.2, 133.3, 133.2, 132.0, 131.5, 131.5, 131.2, 131.1, 131.0, 130.9, 130.2, 129.9, 129.8, 129.6, 128.9, 128.8, 128.7, 128.6, 128.6, 127.7, 127.6, 126.2, 126.2, 121.8, 120.7, 120.4, 119.0, 114.5, 114.2, 70.6, 69.6, 68.0, 57.2, 65.9, 44.0, 42.8, 35.7, 34.2, 30.3, 29.5, 28.4, 28.2, 27.9, 25.4, 25.3, 25.0, 24.8, 20.8, 20.8, 15.3. 64 signals corresponding to all 53 environments (11 doublets coupling to ^{31}P). $\delta_{31P\{1H\}}$ ($CDCl_3$, 202 MHz) 26.2. δ_{31P} ($CDCl_3$, 202 MHz) 26.2 (1P, broad quin.d, *J* 12.6, 3.6). HR-ESI-MS [M-Cl] m/z 1222.5 (calc. for $C_{66}H_{68}N_5O_4PAu$ m/z 1222.5).[120]

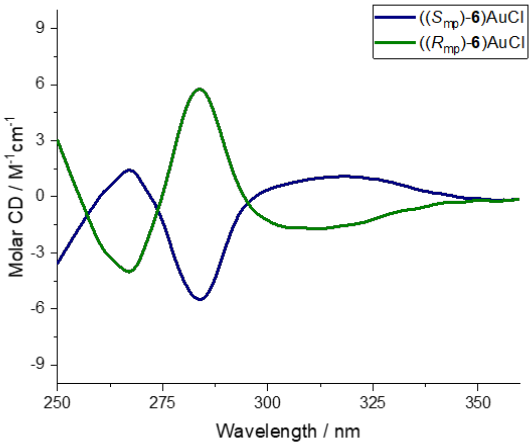

Figure 162: Circular Dichroism spectra of (R_{mp})-**296** (32.1 μM) and (S_{mp})-**296** (55.6 μM) at 293 K in $CHCl_3$. Both samples were 99 : 1 *er*.

^{1}H NMR Stack Plot Demonstrating the binding of Cu^I to the Rotaxane Framework

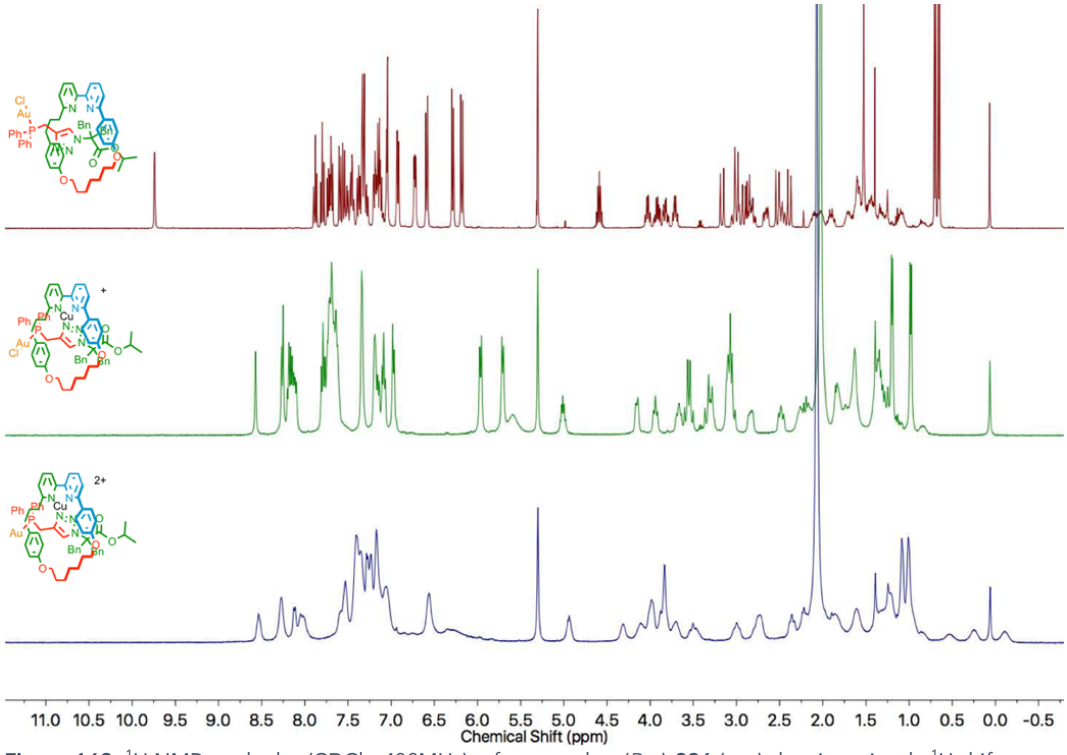

Figure 163: ^{1}H NMR stack plot ($CDCl_3$, 400MHz) of pre-catalyst (R_{mp})-**296** (top) showing triazole ^{1}H shift on addition of $[Cu(MeCN)_4]PF_6$ (middle), and further shift upon chloride abstraction on addition of $AgSbF_6$ to form the active catalyst (bottom). Counter-ions omitted for clarity.

Rotaxane (S,R_{mp})-**4** SCXRD Data

Enantiopure single crystals of (S,R_{mp})-**294** were grown from (S,R_{mp})-**94** (diastereomerically pure, er 99 : 1) by vapor diffusion of n-pentane into a saturated solution in CH_2Cl_2. Data was collected at 100 K using a Rigaku 007 HF diffractometer equipped with a HYPix6000 enhanced sensitivity detector. Cell determination, data collection, data reduction, cell refinement and absorption correction were performed with CrysAlisPro. The crystal structure was solved using Olex2 with SHELXT dual methods and refined against F^2 with SHELXL refinement package using anisotropic thermal displacement parameters for all non-hydrogen atoms. H atoms were placed in calculated position and refined using a riding model.

Note on the assignment of the absolute stereochemistry of (S,R_{mp})-**294**: SC-XRD analysis of (S,R_{mp})-**294** allows the relative covalent and mechanical stereochemistry to be directly determined as (S*,R*$_{mp}$). Furthermore, the absolute stereochemistry of the azide-derived stereocenter is known to be (S) due to the known stereochemistry of the starting material, (S)-**269**. This allows us to unambiguously assign the absolute stereochemistry of the sample to be (S,R_{mp})-**294**.

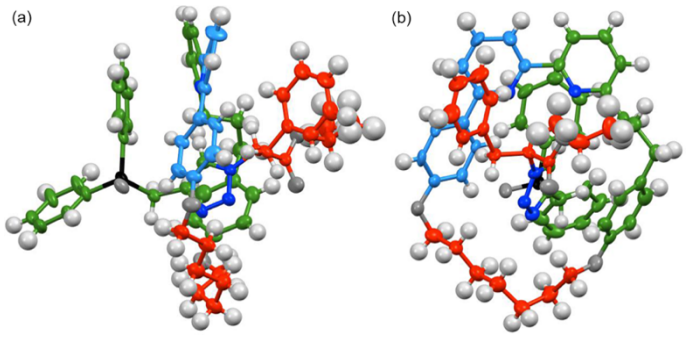

Figure 164: The SCXRD derived asymmetric unit of (S,R_{mp})-**294**, (crystallised from a (S,R_{mp})-**294** *er* 99 : 1, by vapour diffusion of *n*-pentane into CH_2Cl_2) in thermal elipsoid (50%) representation from the (a) side and (b) the front.

Table 8. Crystal Structure Parameters for (*S*,*R*$_{mp}$)-**294**

Empirical formula	$C_{59}H_{62}N_5O_5P$	μ/mm^{-1}	0.920
Formula weight	952.10	F(000)	2024.0
Temperature/K	100(2)	Crystal size/mm^3	0.05 × 0.05 × 0.05
Crystal system	orthorhombic	Radiation	CuK**α** (**λ** = 1.54184)
Space group	$P2_12_12_1$	2**Θ** range for data collection/°	6.274 to 140.93
a/Å	12.69420(10)	Index ranges	-15 ≤ h ≤ 15, -23 ≤ k ≤ 23, -25 ≤ l ≤ 24
b/Å	19.2864(2)	Reflections collected	96525
c/Å	20.6222(2)	Independent reflections	9590 [R_{int} = 0.0620, R_{sigma} = 0.0295]
α/°	90	Data/restraints/parameters	9590/3/633
β/°	90	Goodness-of-fit on F^2	1.083
γ/°	90	Final R indexes [I>=2**σ** (I)]	R_1 = 0.0462, wR_2 = 0.1146
Volume/Å^3	5048.84(8)	Final R indexes [all data]	R_1 = 0.0495, wR_2 = 0.1166
Z	4	Largest diff. peak/hole / e Å^{-3}	0.37/-0.25

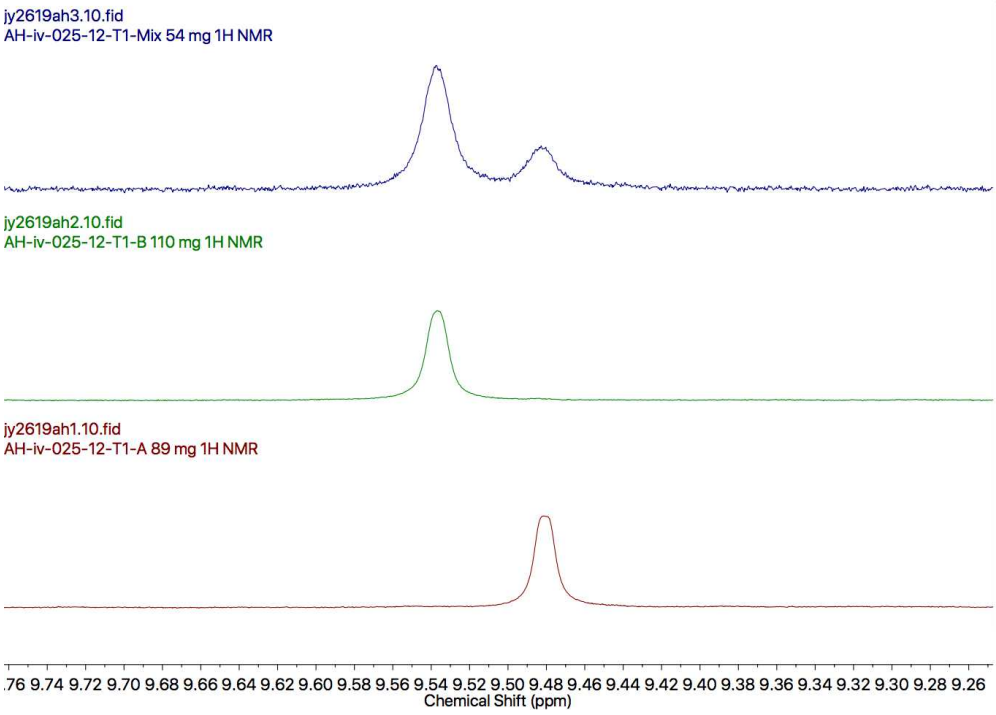

Figure 165: ^{1}H NMR (400 MHz, $CDCl_3$) of (*S*,*R*$_{mp}$)-**294** (bottom) used for crystallisation. Middle (*S*,*S*$_{mp}$)-**294** and top (*S*,*S*/*R**$_{mp}$)-**294** for reference.

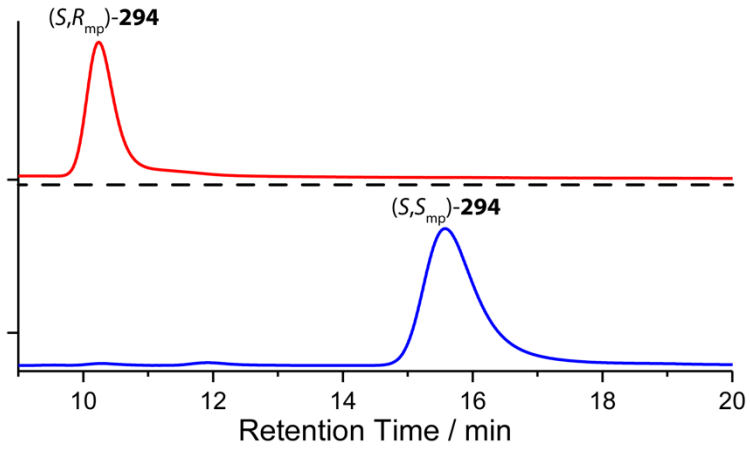

Figure 166: Chiral Stationary Phase HPLC ((*S*,*S*)Whelk, isocratic *n*-hexane-isopropanol 25 : 75, 303 K, load solvent Et_2O, 5 µL injection, flowrate 1 $mLmin^{-1}$) of 99 : 1 *er* (*S*,R_{mp})-**294** (red). Due to overlap of the peaks, the stereochemical purity is inferred from analysis of (R_{mp})-**295**. The HPLC trace shown here is consistent with this. (*S*,R_{mp})-**294** : (*R*,S_{mp})-**294** : (*S*,S_{mp})-**294**, 0.6 : 1.0 : 98.4 (blue). Mechanically planar stereogenic element ratio (R_{mp}) : (S_{mp}) 1 : 99.

Rotaxane (*S*,S_{mp})-**294** SCXRD Data

Racemic single crystals of (*S**,*S**$_{mp}$)-**294** were grown from a diastereomerically pure, scalemic sample of (*S*,S_{mp})-**294** (*er* 88 : 12) by vapor diffusion of n-pentane into a saturated solution in Et_2O. Data was collected at 100 K using a FRE+ HF diffractometer equipped with a Saturn 724+ enhanced sensitivity detector. Cell determination, data collection, data reduction, cell refinement and absorption correction were performed with CrysAlisPro. The crystal structure was solved using Olex2 with SHELXT dual methods and refined against F^2 with SHELXL refinement package using anisotropic thermal displacement parameters for all non-hydrogen atoms. H atoms were placed in calculated position and refined using a riding model.

Important Note: Although the bulk sample of (*S*,S_{mp})-**294** was of high purity, as judged by NMR and HPLC, SC-XRD analysis revealed additional electron density that could not be accounted for by solvent or other impurities. Ultimately, we found the data was consistent with 25% of the molecules in the unit cell being peroxide oxidation product X; modelling a 50% occupancy of an O_2 unit in which one O atom is situated 1.32 Å from the benzylic position of one of the two molecules in the asymmetric unit produced a solution that agrees well with the diffraction data. Importantly, this solution is also chemically reasonable – the position found to be oxidized is activated to radical pathways, although it is not clear if the oxidation takes place during the peroxide work up (vide supra), or during crystallization due to adventitious oxygen (Scheme S6). Regardless, oxidation product X is not observed as an impurity by HPLC, NMR or MS

analysis of bulk samples of either diastereomer of 4, or its derivatives, suggesting it is present only in trace quantities. Thus, it appears that X is incorporated selectively during the crystallization process, resulting in enrichment of the crystal obtained in this minor species. Although this complicates the SC-XRD analysis of the sample of (S*,S*$_{mp}$)-**294**, once this element of disorder is taken into consideration, the structure solution is of reasonable quality. Importantly, the data is consistent with the relative stereochemistry of the (S*,S*$_{mp}$)-**294** diastereomer being epimeric with that determined by SC-XRD for (S,R_{mp})-**294** (*vide supra*). Finally, the major enantiomer in the scalemic sample could be determined to be (S,S_{mp})-**294** based on the known covalent stereochemistry of azide (S)-**269** from which it is derived.

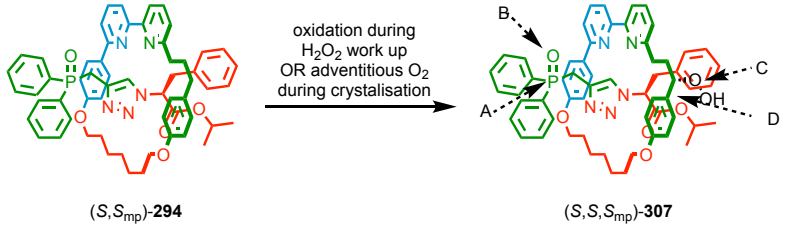

(S,S_{mp})-**294** (S,S,S_{mp})-**307**

Scheme S6: Oxidation of (S,S_{mp})-**294** to give peroxide **307**, which is observed as an impurity by SC-XRD

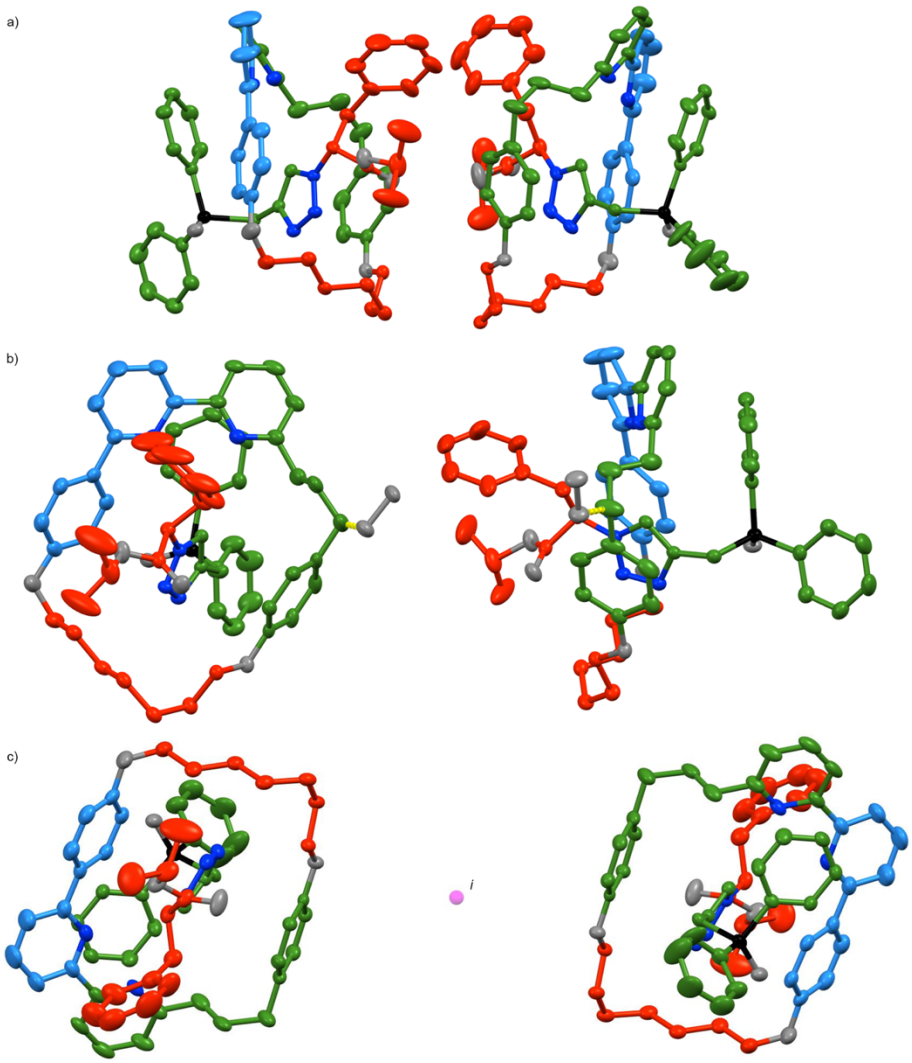

Figure 167: SCXRD structures of (*S**,*S**$_{mp}$)-**294** (crystallised from 88 : 12 *er* mixture, *n*-pentane vapour diffusion into Et_2O) in ellipsoid representation (50% probability, H atoms omitted for clarity). a) The asymmetric unit showing (*S**,*S**$_{mp}$)-**294** only (left hand molecule has 50% occupancy with peroxide **307**). b) Front and side views showing both (*S**,*S**$_{mp}$)-**294** and **307**, the latter being represented by the presence of an O_2 unit 1.32 Å from the benzylic C. c) An enantiomeric pair of (*S**,*S**$_{mp}$)-**294** related by an inversion centre, *i*, in the unit cell.

Table 9. X-ray diffraction data for (*S**,*S**$_{mp}$)-**294**

Empirical formula	$C_{118}H_{124}N_{10}O_{11}P_2$	μ/mm^{-1}	0.107
Formula weight	1920.20	F(000)	4080.0
Temperature/K	100.0(2)	Crystal size/mm^3	0.4 × 0.04 × 0.04
Crystal system	monoclinic	Radiation	Mo K**α** (**λ** = 0.71075)
Space group	$P2_1/n$	2**Θ** range for data collection/°	3.272 to 54.968
a/Å	21.0723(2)	Index ranges	-27 ≤ h ≤ 27, -24 ≤ k ≤ 24, -34 ≤ l ≤ 33
b/Å	18.6958(2)	Reflections collected	236269
c/Å	26.7361(2)	Independent reflections	24147 [R_{int} = 0.0733, R_{sigma} = 0.0432]
α/°	90	Data/restraints/parameters	24147/207/1330
β/°	90.9780(10)	Goodness-of-fit on F^2	1.071
γ/°	90	Final R indexes [I>=2**σ** (I)]	R_1 = 0.0770, wR_2 = 0.1780
Volume/Å^3	10531.51(17)	Final R indexes [all data]	R_1 = 0.1072, wR_2 = 0.1916
Z	4	Largest diff. peak/hole / e Å^{-3}	0.69/-0.51
ρ$_{calc}$g/cm^3	1.211	μ/mm^{-1}	0.107

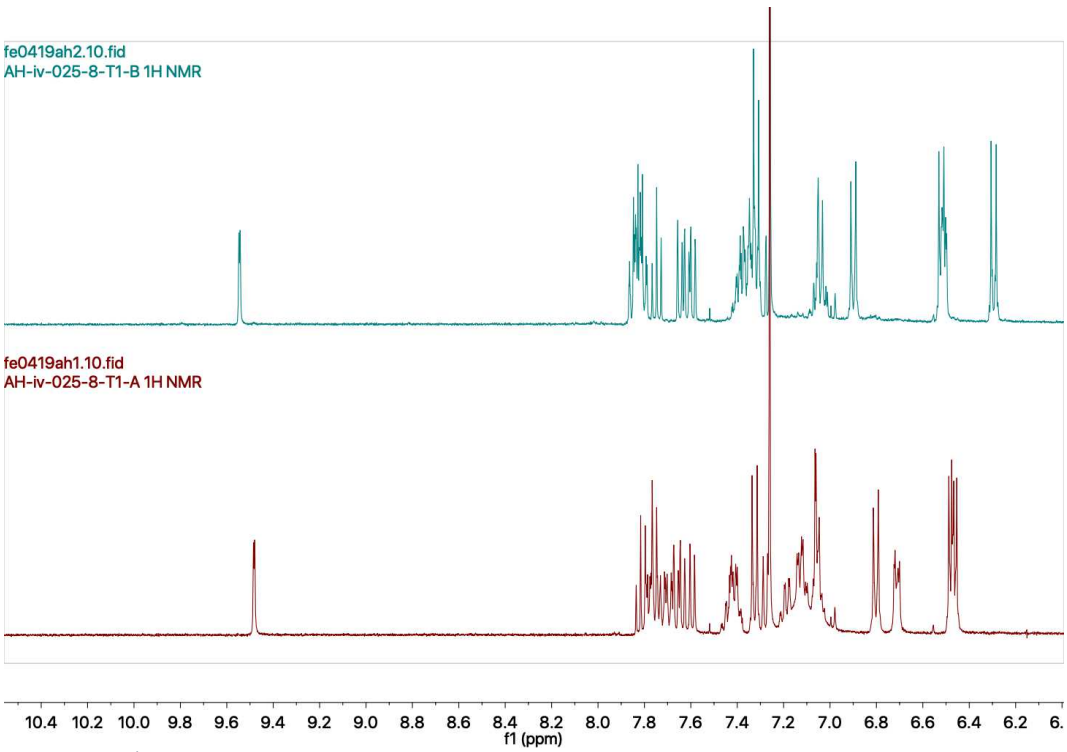

Figure 168: ^{1}H NMR (400 MHz, $CDCl_3$) of (*S*,*R*$_{mp}$)-**294** (bottom) and the sample of (*S*,*S*$_{mp}$)-**294** (top) used for crystallisation, demonstrating the diastereopurity of the sample.

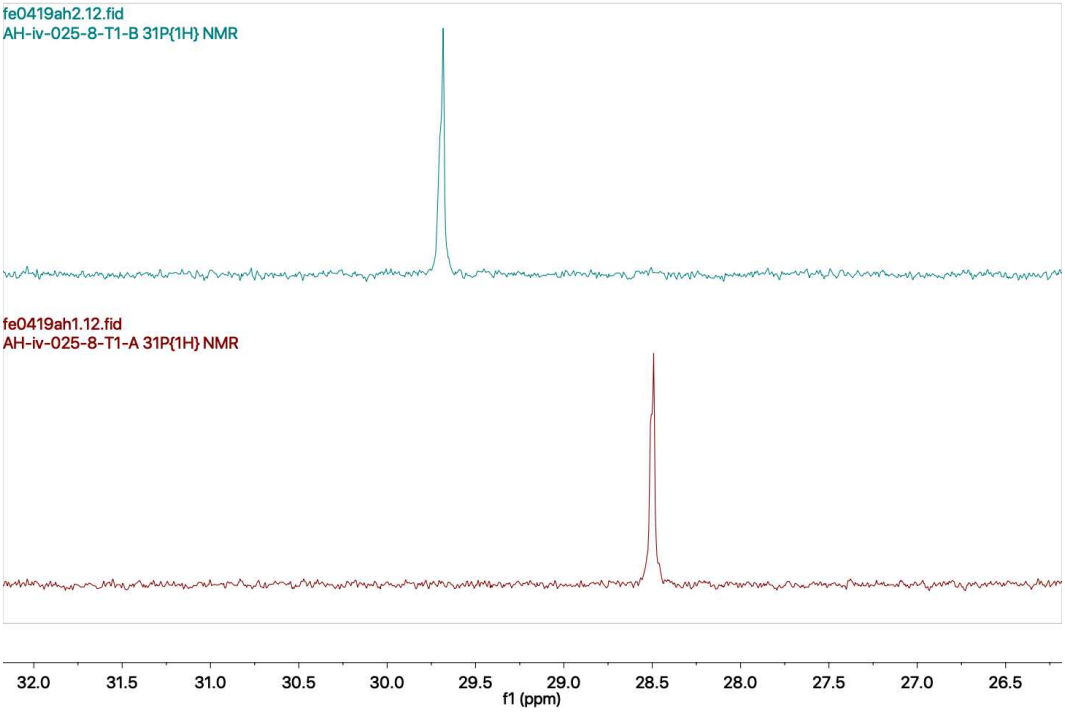

Figure 169: $^{31}P\{^{1}H\}$ (202 MHz, $CDCl_3$) NMR of (*S*,R_{mp})-**294** (bottom) and the sample of (*S*,S_{mp})-**294** (top) used for crystallisation, demonstrating the diastereopurity of the sample

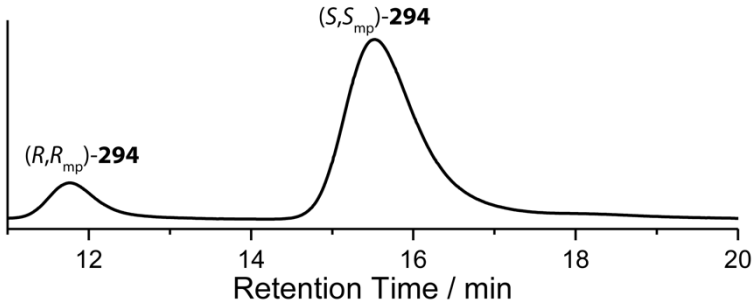

Figure 170: Chiral Stationary Phase HPLC ((*S*,*S*)Whelk column, isocratic *n*-hexane-isopropanol 25 : 75, 303 K, load solvent Et_2O, flowrate: 1.0 $mLmin^{-1}$) of the sample of (*S*,S_{mp})-**294** used for crystallisation demonstrating the enantiopurity of the sample to be 88 : 12 *er*. Retention times (min): (*R*,R_{mp})-**294** 11.3 (303685, 12.2%), (*S*,S_{mp})-**294** 15.0 (2185477, 87.8%).

Substituted 2-methyl-3-butyn-2-yl benzoate general procedure

Carboxylic acid (1.0 mmol, 1.0 eq.) was heated under reflux at 80 °C, under inert atmosphere, with $SOCl_2$ (0.58 mL, 8.0 mmol, 8.0 eq.) for 3 h. The reaction was cooled and excess $SOCl_2$ was removed *in vacuo*. The residue was cooled to 0 ˚C, and a solution of 2-methyl-3-butyn-2-ol (0.10 mL, 1.0 mmol, 1.0 eq.) and 4-(dimethylamino)pyridine (0.244 g, 2.0 mmol, 2.0 eq) in $CDCl_3$ (2.0 mL, 0.5 M concentration of 2-methyl-3-butyn-2-ol) was added dropwise. The resulting solution was stirred for 17 h at 35 ˚C. Solvent was removed under reduced pressure, and the residue was purified by column chromatography (SiO_2, petrol-Et_2O 0→5%).

Compound **71m**[75,120]

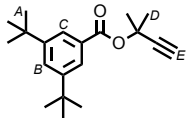

Colourless oil (188 mg, 0.626 mmol, 63%). δ_H ($CDCl_3$, 400 MHz) 7.88 (2H, d, J = 1.8, $\boldsymbol{H}_C$), 7.62 (1H, t, J = 1.8, $\boldsymbol{H}_B$), 2.58 (1H, s, $\boldsymbol{H}_E$), 1.83 (6H, s, $\boldsymbol{H}_D$), 1.34 (18H, s, $\boldsymbol{H}_A$). δ_C ($CDCl_3$, 101 MHz) 165.8, 151.1, 130.2, 127.3, 123.9, 85.1, 72.5, 72.1, 35.1, 31.5, 29.2. HR-EI-MS m/z 300.2080 $[M]^{+\cdot}$ (calc. m/z for $C_{20}H_{28}O_2$ 300.2084).[75,120]

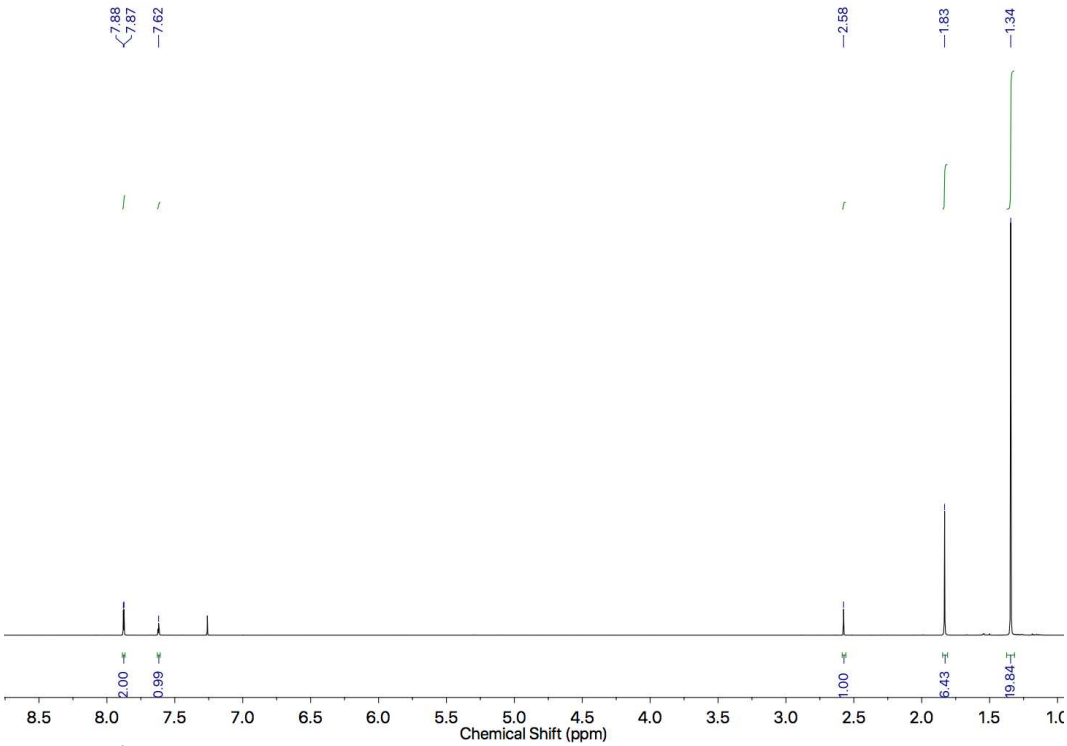

Figure 171: ^{1}H NMR (400 MHz, $CDCl_3$) of **71m**.

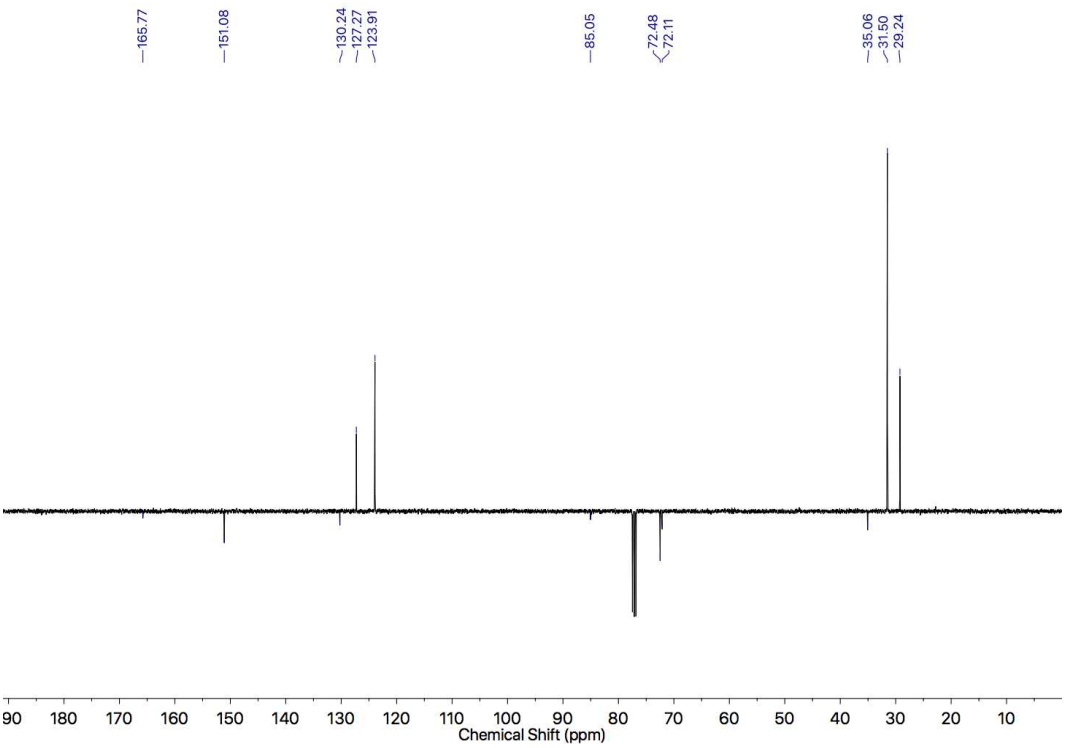

Figure 172: JMOD NMR (101 MHz, $CDCl_3$) of **71m**.

Compound **71n**[75,120]

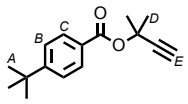

Colourless oil (240 mg, 0.982 mmol, 98%). δ_H ($CDCl_3$, 400 MHz) 7.95 (2H, dt, J = 8.8, 2.1, $\boldsymbol{H}_C$), 7.45 (2H, dt, J = 8.8, 2.1, $\boldsymbol{H}_B$), 2.57 (1H, s, $\boldsymbol{H}_E$), 1.81 (6H, s, $\boldsymbol{H}_D$), 1.33 (18H, s, $\boldsymbol{H}_A$). δ_C ($CDCl_3$, 101 MHz) 165.0, 156.7, 129.6, 128.2, 125.4, 85.0, 72.5, 72.1, 35.2, 31.3, 29.2. HR-EI-MS m/z 244.1457 $[M]^{+\cdot}$ (calc. m/z for $C_{16}H_{20}O_2$ 244.1458).[75,120]

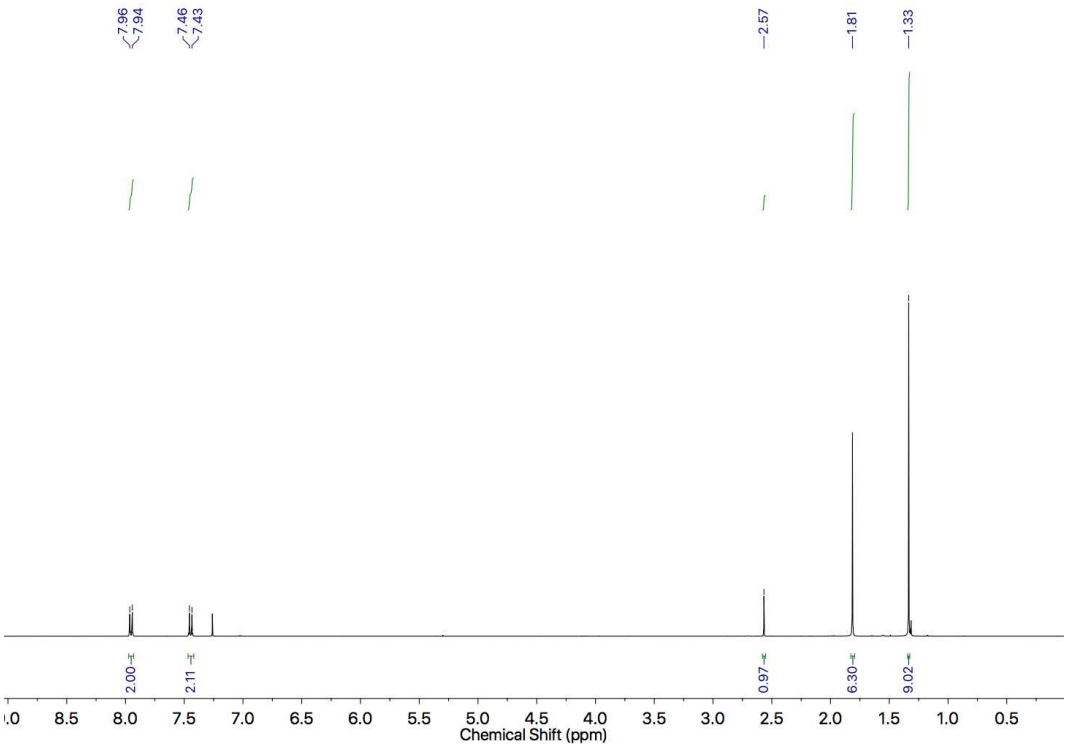

Figure 173: ^{1}H NMR (400 MHz, $CDCl_3$) of **71n**.

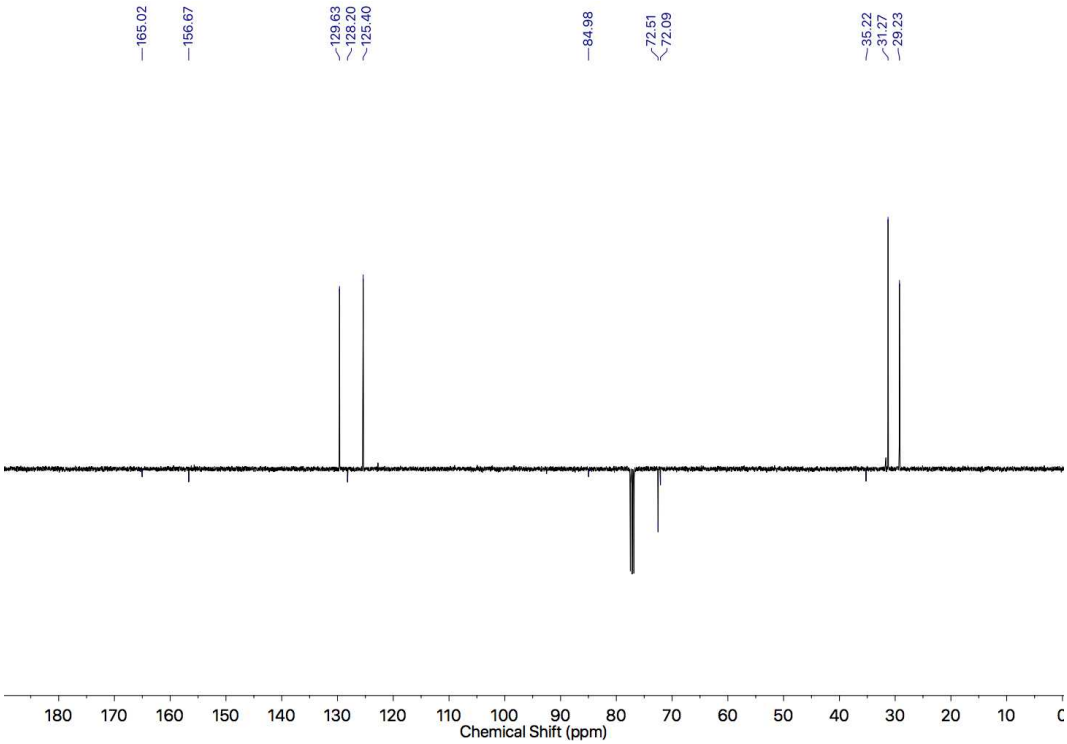

Figure 174: JMOD NMR (101 MHz, $CDCl_3$) of **71n**.

Compound **71p**

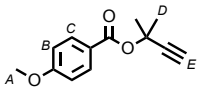

Colourless oil (209 mg, 0.96 mmol, 96%). δ_H ($CDCl_3$, 400 MHz) 7.98 (2H, dt, *J* = 9.1, 2.4, H_C), 6.91 (2H, dt, *J* = 9.1, 2.4, H_B), 3.86 (3H, s, H_A), 2.57 (1H, s, H_E), 1.81 (6H, s, H_D). δ_C ($CDCl_3$, 101 MHz) 164.8, 163.5, 131.8, 123.4, 113.7, 85.1, 72.5, 72.0, 55.6, 29.2. HR-EI-MS m/z 218.0933 $[M]^{+\cdot}$ (calc. m/z for $C_{13}H_{14}O_3$ 218.0937).

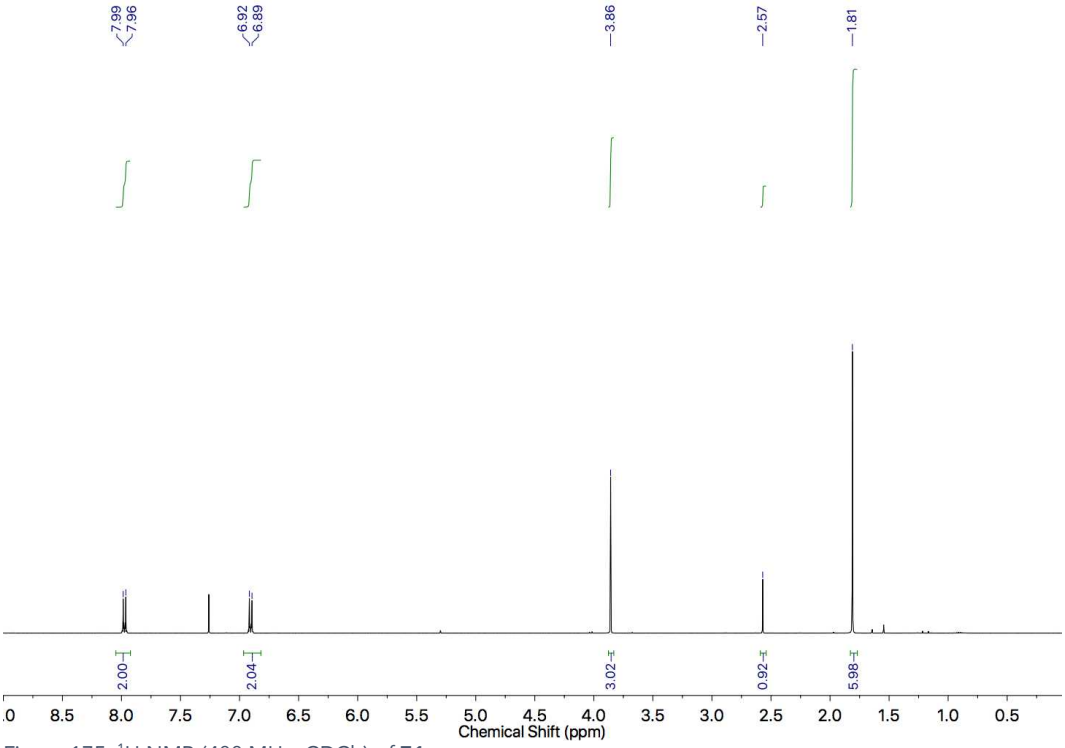

Figure 175: ^1H NMR (400 MHz, $CDCl_3$) of **71p**.

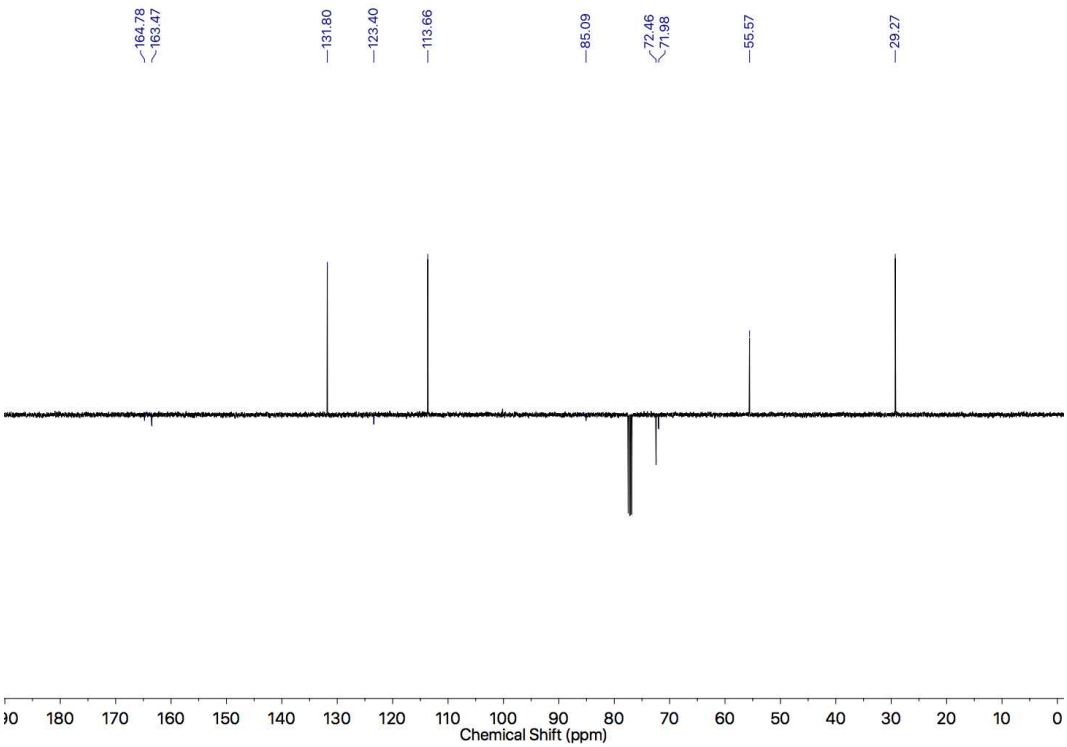

Figure 176: JMOD NMR (101 MHz, $CDCl_3$) of **71p**.

Compound **71q**

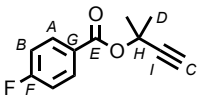

Colourless oil (143 mg, 0.69 mmol, 69%). $\boldsymbol{\delta}_H$ ($CDCl_3$, 400 MHz) 8.04 (2H, ddt, *J* 8.9, 5.4, 2.5 Hz, $\boldsymbol{H}_A$), 7.10 (2H, ddt, *J* 8.7, 8.7, 4.5, $\boldsymbol{H}_B$), 2.59 (1H, s, $\boldsymbol{H}_C$), 1.82 (6H, s, $\boldsymbol{H}_D$). $\boldsymbol{\delta}_C$ ($CDCl_3$, 101 MHz) 167.1 ($\boldsymbol{C}_E$), 164.3 (d, *J* 61.6 Hz, $\boldsymbol{C}_F$), 132.3 (d *J* 9.4 Hz $\boldsymbol{C}_A$), 127.2 (d, *J* 3.1 Hz, $\boldsymbol{C}_G$), 115.5 (d, *J* 22.0 Hz, $\boldsymbol{C}_B$), 84.7 ($\boldsymbol{C}_C$), 72.8 ($\boldsymbol{C}_H$), 72.6 ($\boldsymbol{C}_I$), 29.2 ($\boldsymbol{C}_D$). $\boldsymbol{\delta}_F$ ($CDCl_3$, 376 MHz) -106.1 (1F, tt, *J* 8.6, 5.7 Hz). $\boldsymbol{\delta}_{F\{H\}}$ ($CDCl_3$, 376 MHz) -106.1. HR GCMS [$M^{+\cdot}$] m/z 206.0735 (calc. m/z for $C_{12}H_{11}FO_2$ 206.0743).

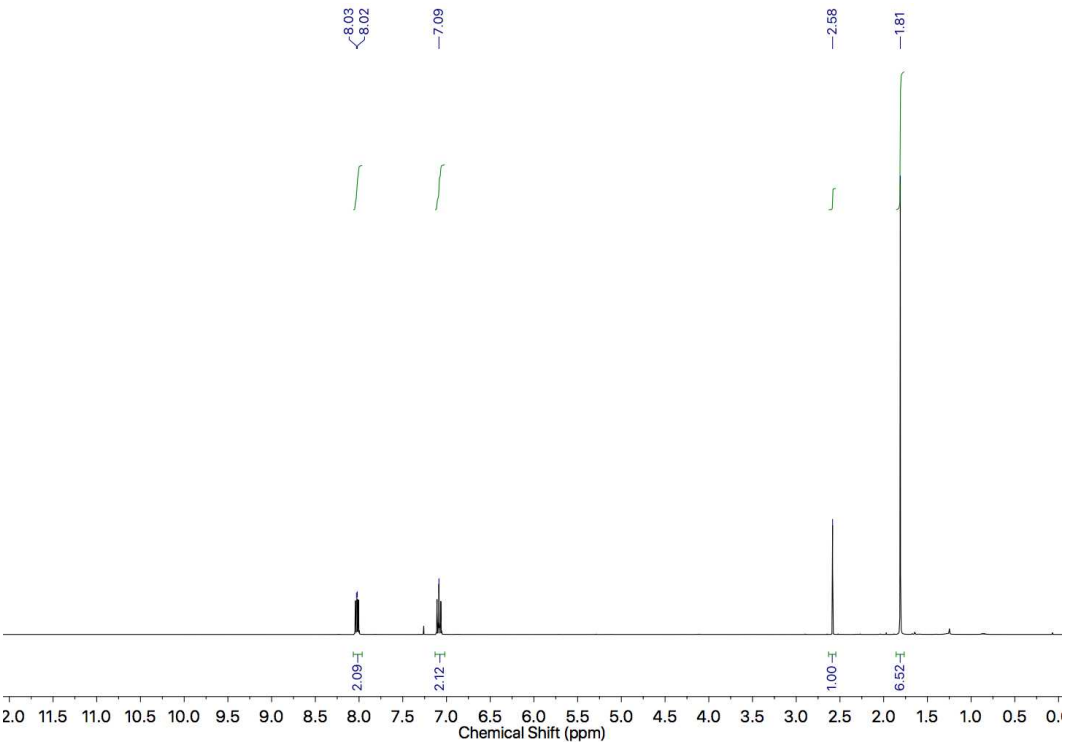

Figure 177: ^{1}H NMR (400 MHz, $CDCl_3$) of **71q**.

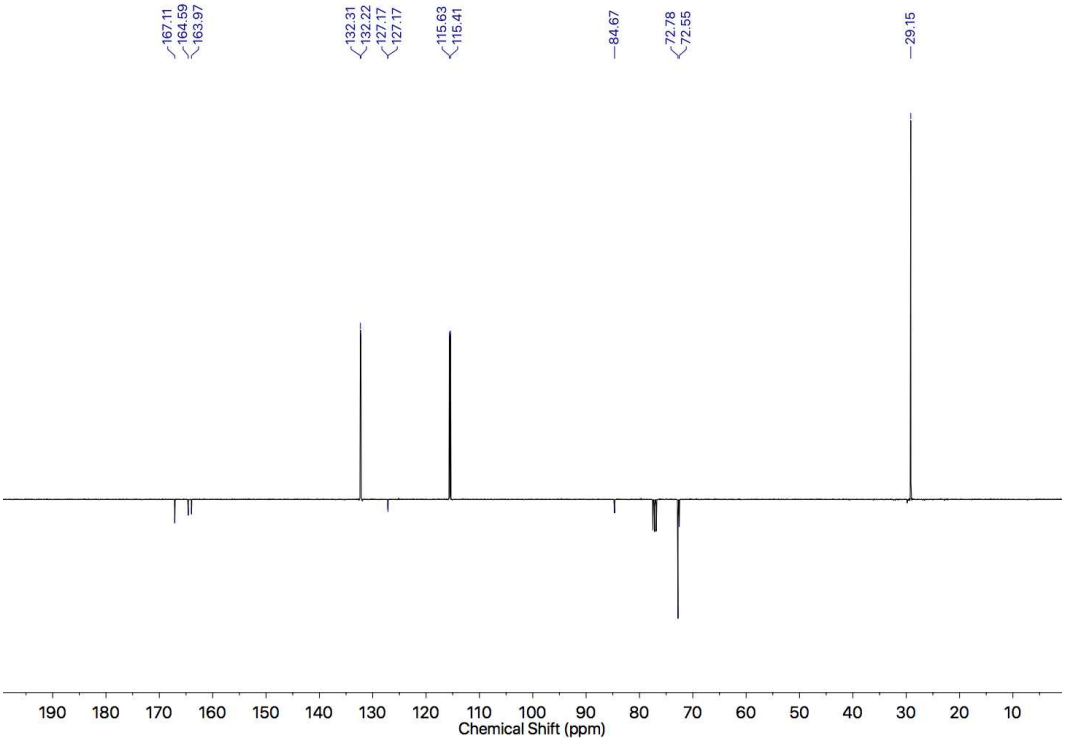

Figure 178: JMOD NMR (101 MHz, $CDCl_3$) of **71q**.

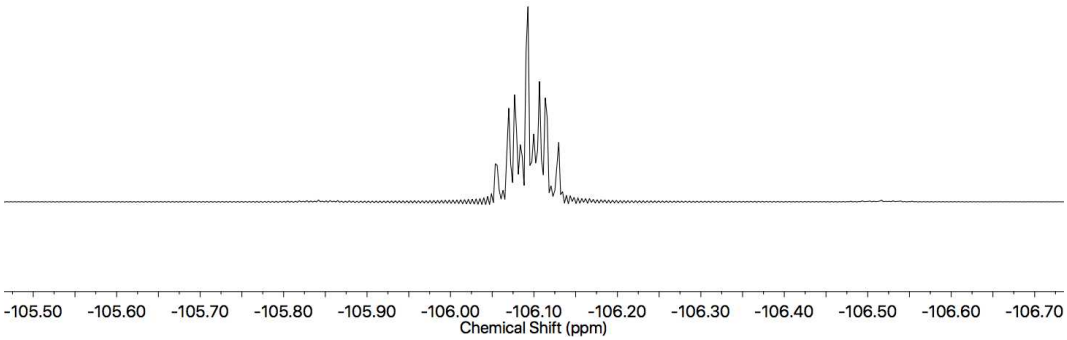

Figure 179: ^{19}F NMR (376 MHz, $CDCl_3$) of **71q**.

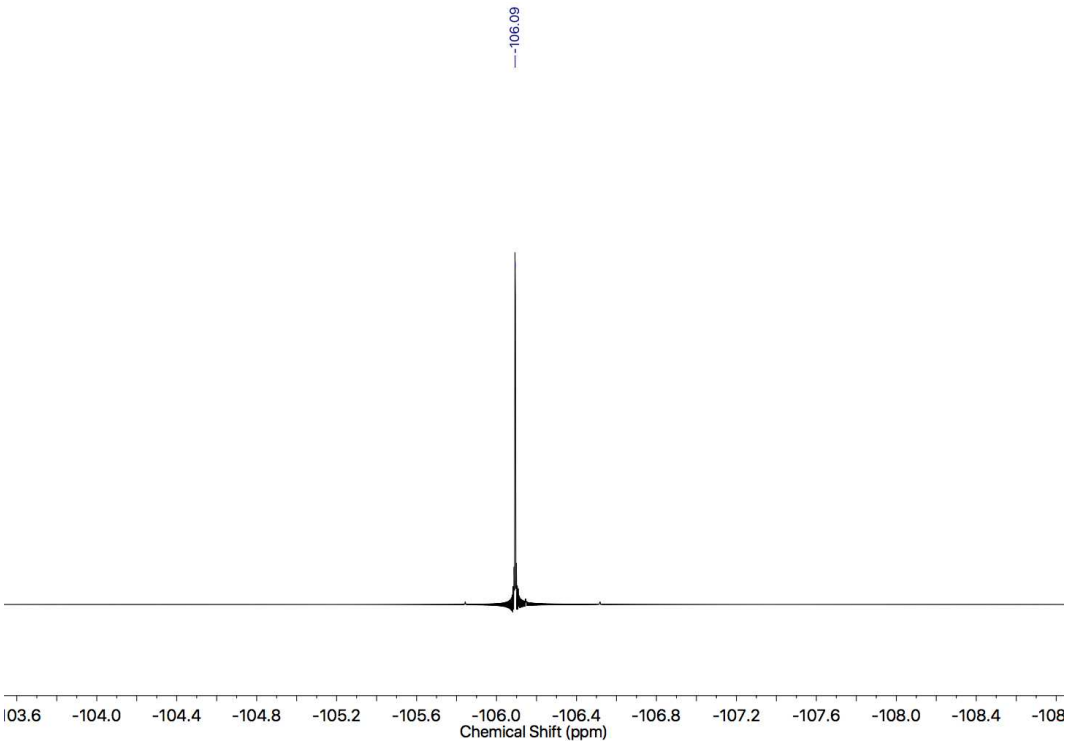

Figure 180: $^{19}F\{^1H\}$ NMR (376 MHz, $CDCl_3$) of **71q**.

Compound **71r**

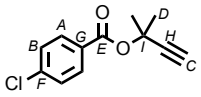

White solid (358 mg, 1.60 mmol, 80%), m.p. 33-35 °C. δ_H ($CDCl_3$, 400 MHz) 7.94 (2H, dt, *J* 8.7, 2.2 Hz, H_A), 7.39 (2H, dt, *J* 8.8, 2.2 Hz, H_B), 2.59 (1H, s, H_C), 1.81 (6H, s, H_D). δ_C ($CDCl_3$, 101 MHz) 164.1 (C_E), 139.5 (C_F), 131.1 (C_A), 129.4 (C_G), 128.8 (C_B), 84.6 (C_H), 72.9 (C_C), 72.7 (C_I), 29.1 (C_D). HR GCMS [$M^{+\cdot}$] m/z 222.0480 (calc. m/z for $C_{12}H_{11}ClO_2$ 222.0448).

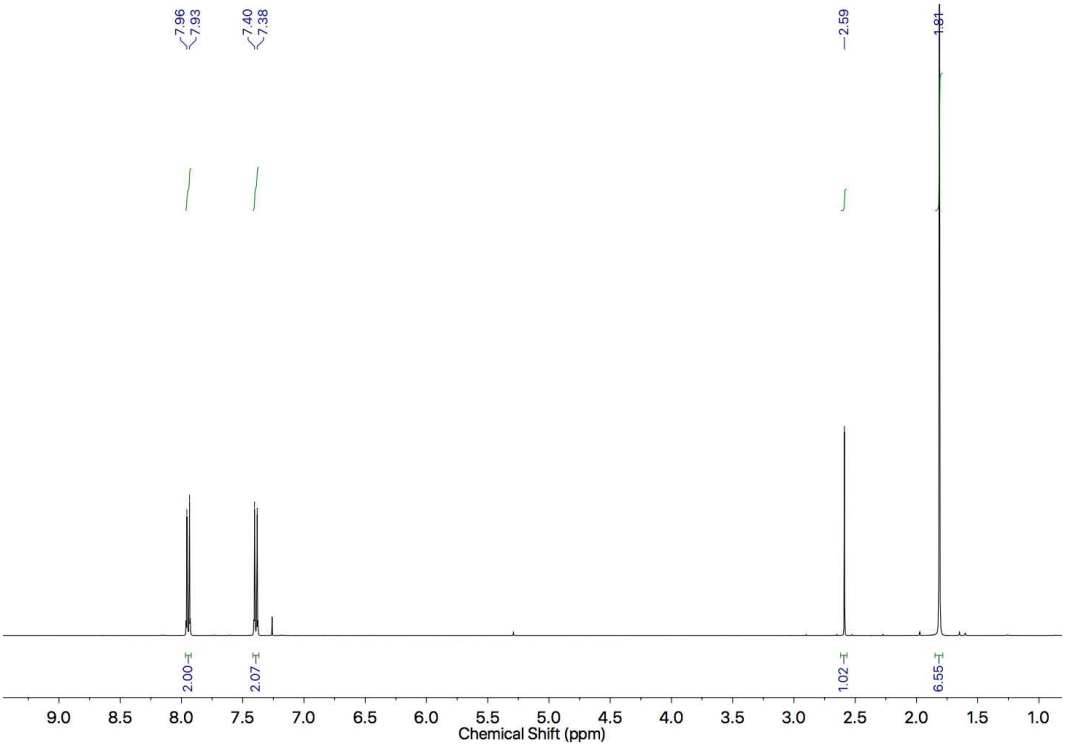

Figure 181: ^{1}H NMR (400 MHz, $CDCl_3$) of **71r**.

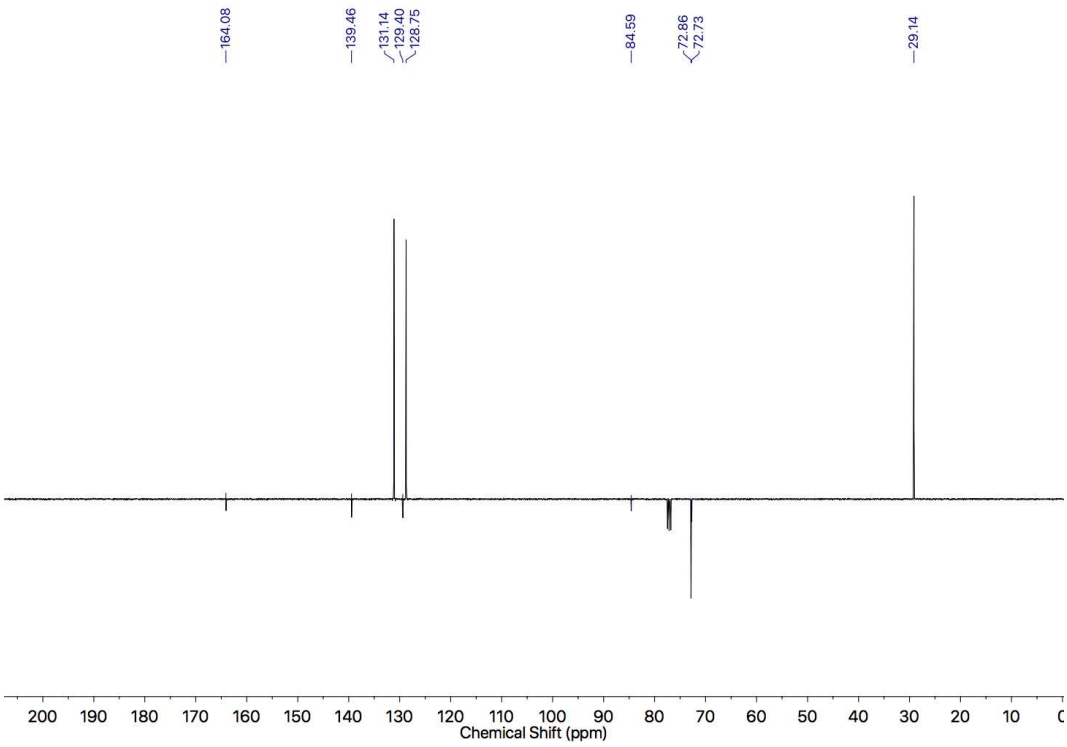

Figure 182: JMOD NMR (101MHz, $CDCl_3$) of **71r**.

Compound **71s**

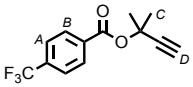

White solid (128 mg, 0.50 mmol, 50%) m.p. 32-34 °C. δ_H ($CDCl_3$, 400 MHz) 8.11 (2H, d, J = 8.1, H_B), 7.70 (2H, d, J = 8.2, H_A), 2.61 (1H, s, H_D), 1.84 (6H, s, H_C). δ_C ($CDCl_3$, 101 MHz) 163.7, 134.5 (q, J = 32.7), 134.3 (q, J = 18.2), 130.1, 125.4 (q, J = 3.7), 122.4, 84.4, 73.1, 73.2, 29.1. δ_F ($CDCl_3$, 376 MHz) 63.3 (s). $\delta_{F\{H\}}$ ($CDCl_3$, 376 MHz) 63.3. HR-EI-MS m/z 256.0701 [$M^{+\cdot}$] (calc. m/z for $C_{13}H_{11}O_2F_3$ 256.0706).

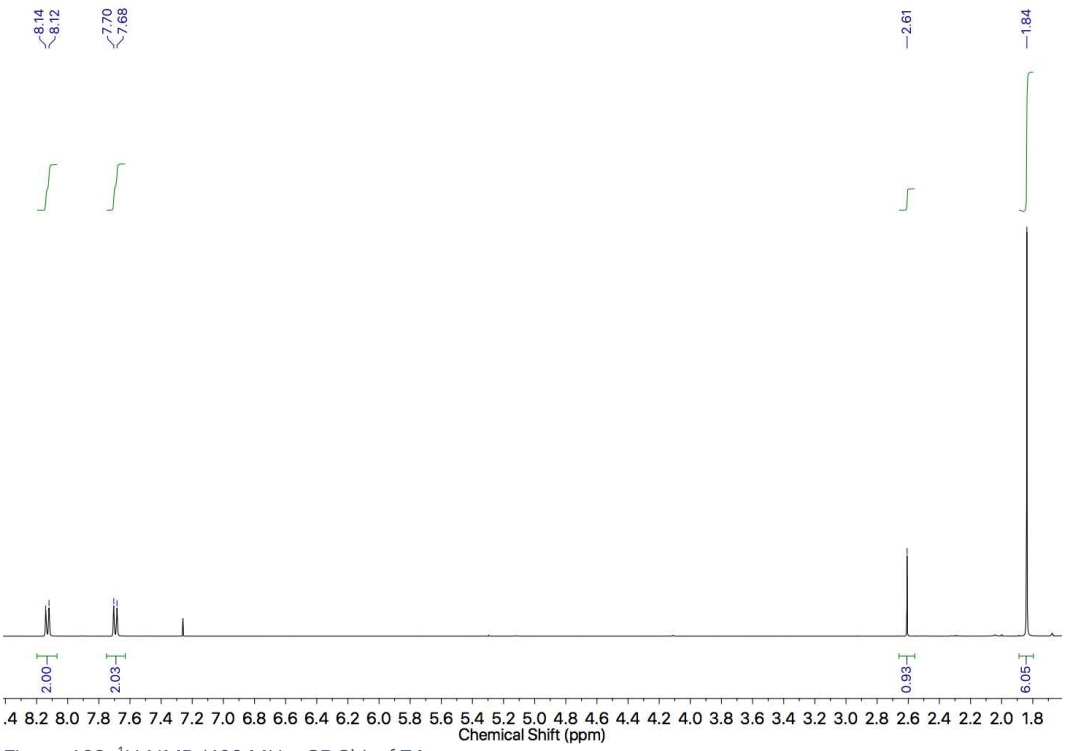

Figure 183: ^{1}H NMR (400 MHz, $CDCl_3$) of **71s**.

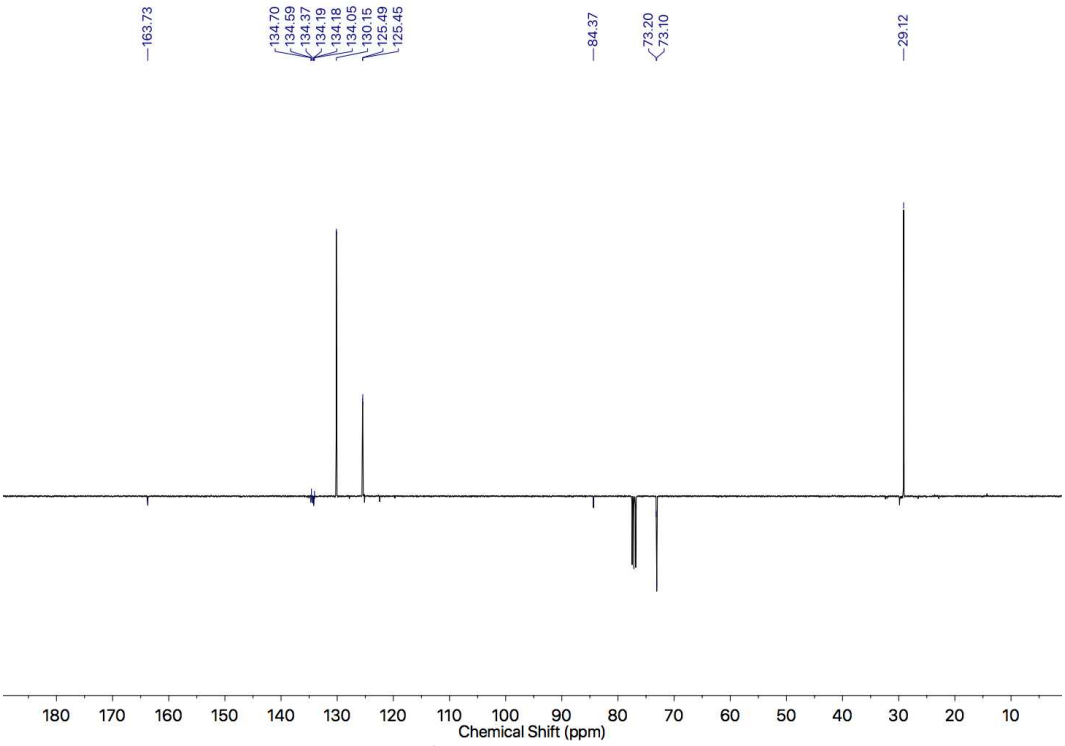

Figure 184: JMOD NMR (101 MHz, $CDCl_3$) of **71s**.

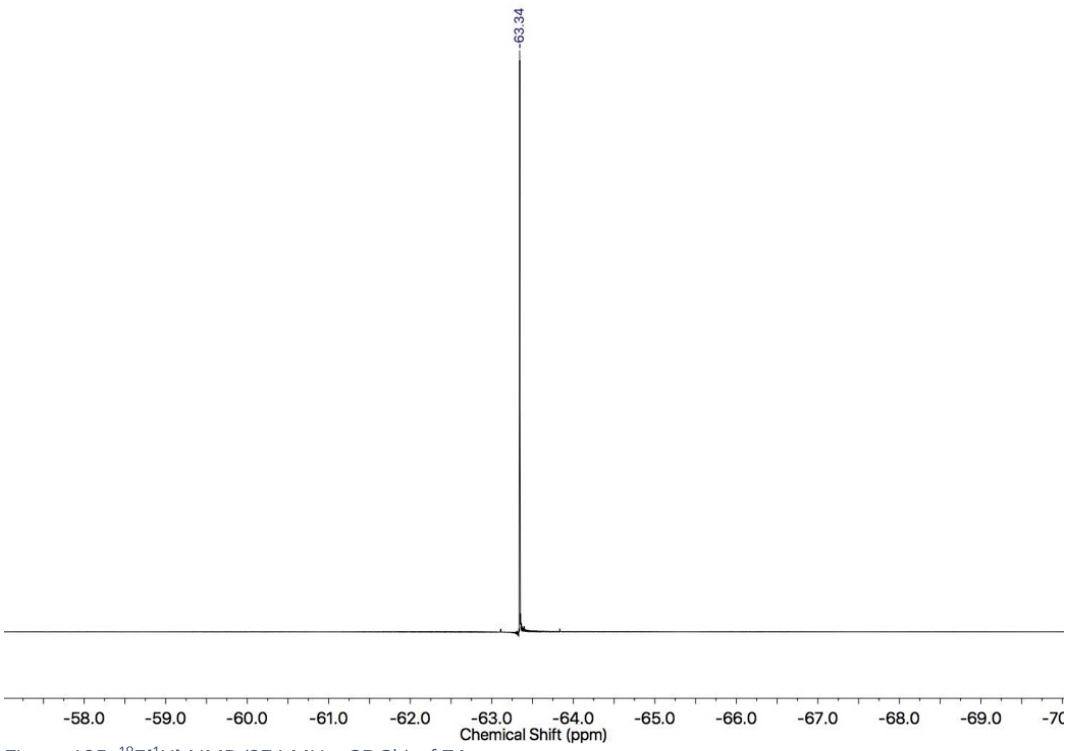

Figure 185: $^{19}F\{^{1}H\}$ NMR (376 MHz, $CDCl_3$) of **71s**.

Compound **71t**

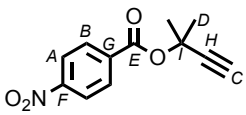

White solid (55 mg, 0.24 mmol, 12%) m.p. 121-124 °C. δ_H ($CDCl_3$, 400 MHz) 8.27 (2H, dt, *J* 9.0, 2.1 Hz, H_A), 8.17 (2H, dt, *J* 9.0, 2.1f Hz, H_B), 2.62 (1H, s, H_C), 1.84 (6H, s, H_D). δ_C ($CDCl_3$, 101 MHz) 163.0 (C_E), 150.6 (C_F), 136.3 (C_G), 130.8 (C_B), 123.6 (C_A), 84.1 (C_H), 73.7 (C_I), 73.4 (C_C), 29.1 (C_D). HR GCMS [$M^{+\cdot}$] m/z 233.0678 (calc. m/z for $C_{12}H_{11}NO_4$ 233.0688).

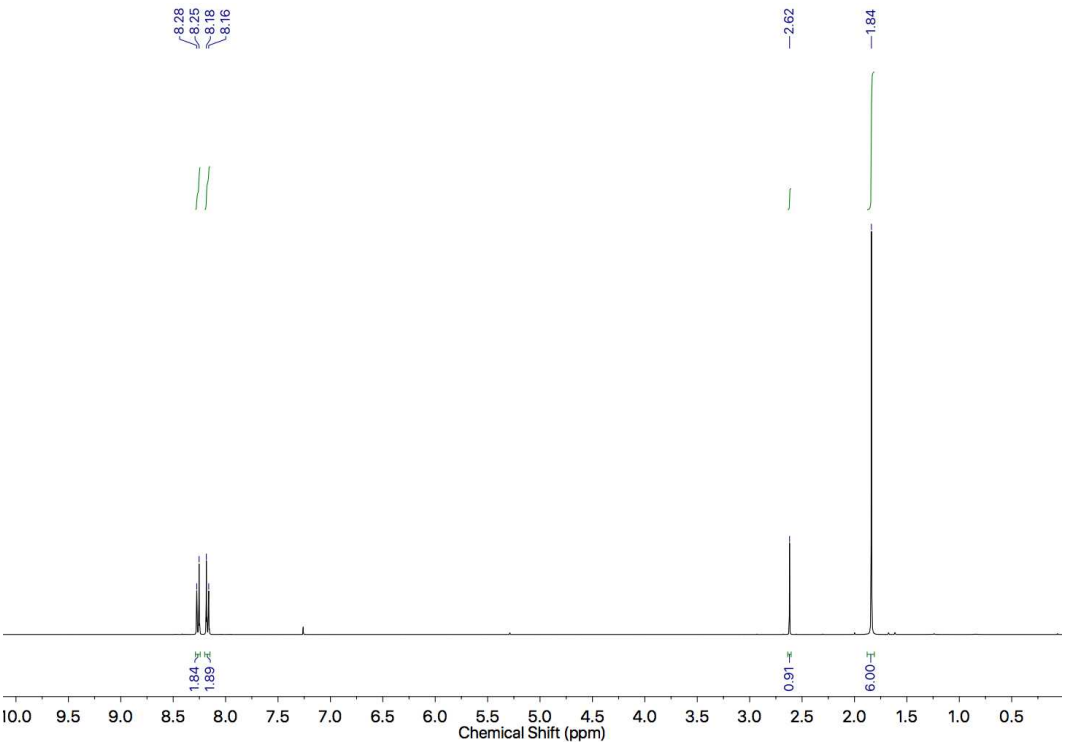

Figure 186: ^{1}H NMR (400 MHz, $CDCl_3$) of **71t**.

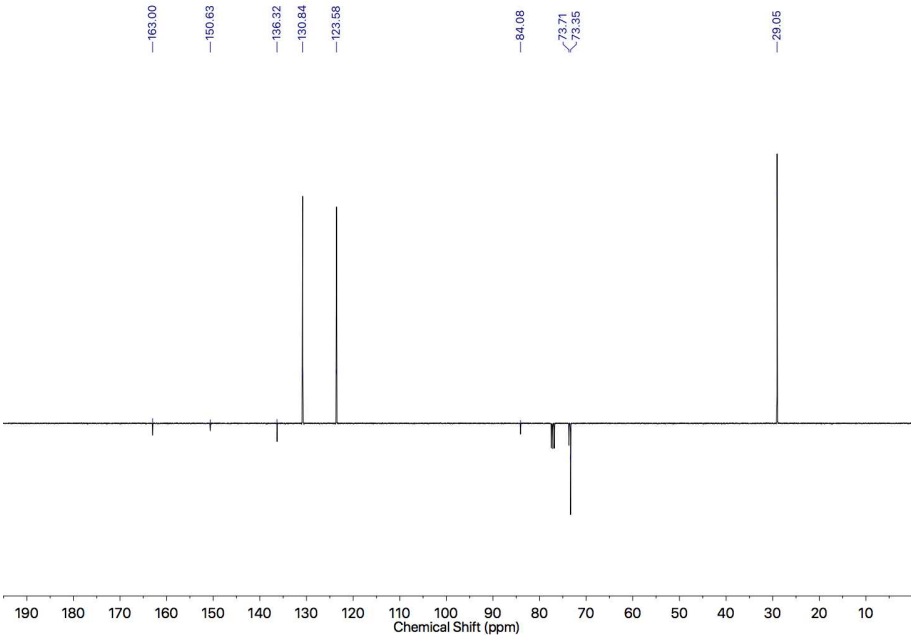

Figure 187: JMOD NMR (101 MHz, $CDCl_3$) of **71t**.

Compound **71x**

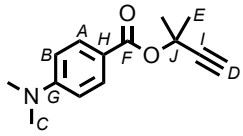

Colourless oil (46 mg, 0.20 mmol, 10%). δ_H ($CDCl_3$, 400 MHz) 7.88 (2H, dt, *J* 9.1, 2.4 Hz, H_A), 6.63 (2H, dt, *J* 9.1, 2.4 Hz, H_B), 3.02 (6H, s, H_C), 2.55 (1H, s, H_D), 1.80 (6H, s, H_E). δ_C ($CDCl_3$, 101 MHz) 165.4 (C_F), 153.4 (C_G), 131.4 (C_A), 117.7 (C_H), 110.7 (C_B), 85.5 (C_I), 72.1 (C_D), 71.2 (C_J), 40.2 (C_C), 29.3 (C_E). HR GCMS [$M^{+\cdot}$] m/z 222.1263 (calc. m/z for $C_{14}H_{17}NO_2$ 231.1259).

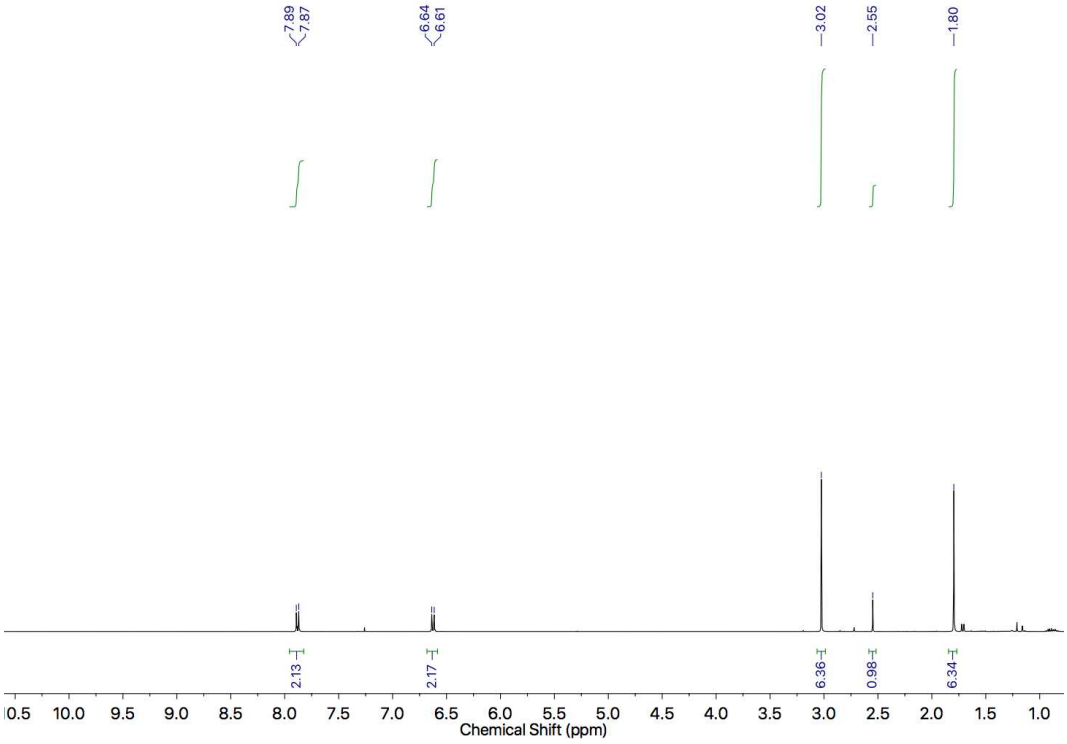

Figure 188: ^{1}H NMR (400 MHz, CDCl3) of **71x**.

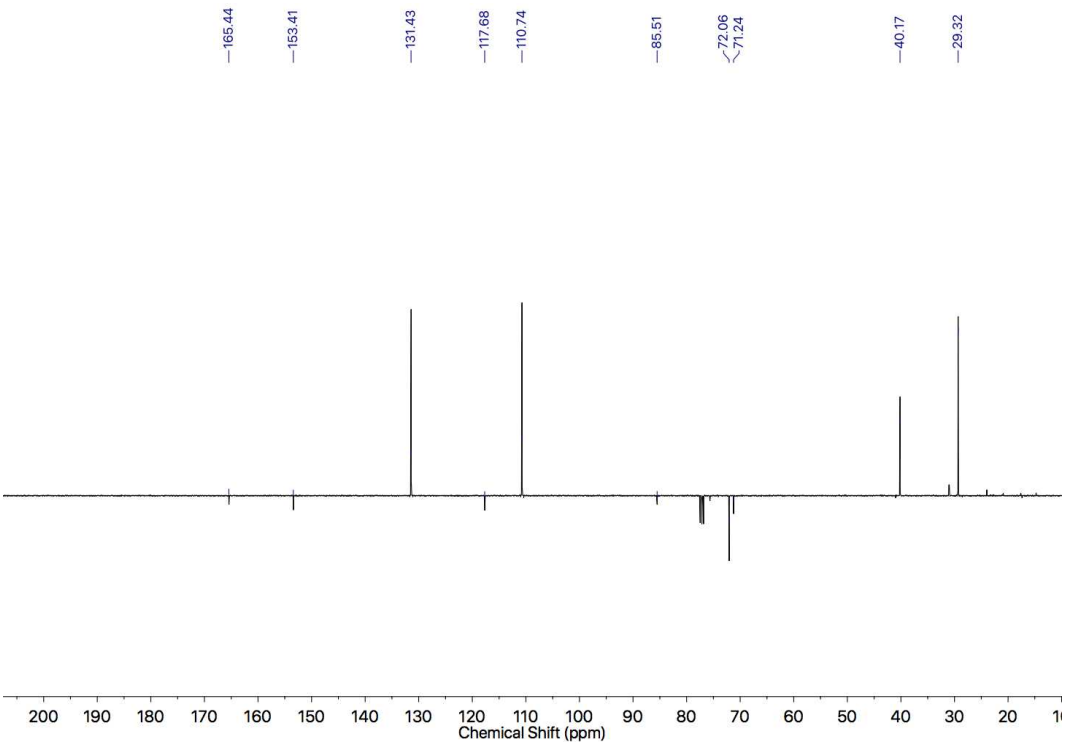

Figure 189: JMOD NMR (101 MHz, $CDCl_3$) of **71x**.

Cyclopropanation Reactions: Screening of reaction conditions

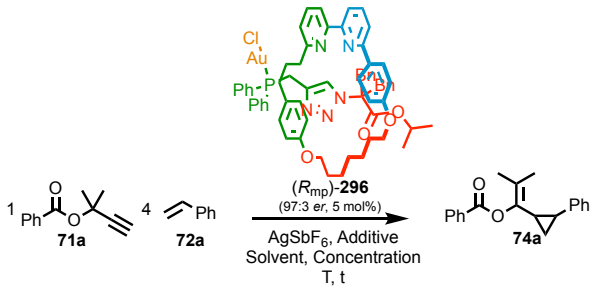

Optimum catalytic conditions were determined by screening the reaction of **71a** with **72a** mediated by **296** for a range of solvents, additives and temperatures. Unless otherwise stated, the stereopurity of the rotaxane catalyst used was 97 : 3 *er*. The best conditions (entry 9) obtained are given in the general procedure (*vide infra*) and were used throughout the experiments that follow.

Entry[a]	Solvent	T (°C)	Additive	t (h)	Yield 74a (%) (*cis* : *trans*[b])	*e.r.*$_{cis}$[c]	*e.r.*$_{trans}$[c]
1	$CDCl_3$	25	-	1	-	-	-
2	$CDCl_3$	25	Cu^{I}	1	42% (95 : 5)	72 : 28	58 : 42
3[b]	$CDCl_3$	25	Cu^{I}	1	35% (95 : 5)	29 : 71	42 : 58
4	$MeNO_2$	25	Cu^{I}	1	69% (87 : 13)	53 : 47	65 : 35
5	CD_2Cl_2	25	Cu^{I}	1	13% (83 : 17)	64 : 36	66 : 34
6	CCl_4	25	Cu^{I}	1	46% (86 : 14)	71 : 29	58 : 42
7	PhMe	25	Cu^{I}	1	17% (85 : 15)	69 : 31	56 : 44
8[e]	$CDCl_3$	0	-	6	-	-	-
9[e]	$CDCl_3$	0	Cu^{I}	6	86% (94 : 6)	79 : 21	62 : 38
10[e]	$CDCl_3$	0	Zn^{II}	6	0% (-)	-	-
11[e]	$CDCl_3$	0	H^{+}	6	1% (-)	-	-
12[e]	$CDCl_3$	0	-	6	0% (-)	-	-
13	$CDCl_3$	-35	Cu^{I}	24	25% (96 : 4)	79 : 21	61 : 39
14[f]	$MeNO_2$	25	-	0.5	73% (>20 : 1)	16 : 84	-

Table 10. Screening of conditions for the reaction of **71a** and **72a** mediated by **296** [a](R_{mp})-**296** with e.r. = 97 : 3 stereopurity was used for screening experiments unless otherwise stated. [b]Determined by ^{1}H NMR analysis of the crude reaction product using $C_2H_2Cl_4$ as an internal standard for yield determination. [c]Determined by HPLC. [d]Reaction conducted with (S_{mp})-**296** of 3 : 97 *er*. [e]Reaction conducted with **296** with e.r. = 99 : 1 stereopurity. [a] Cu^{I} refers to $[Cu(MeCN)_4]PF_6$, Zn^{II} refers to $Zn(OTf)_2$, H^+ refers to $HOTs.H_2O$, Ag^{I} refers to $AgSbF_6$. [f]Reaction outcome reported by Toste and co-workers for (*R*)-DTBM-SEGPHOS®$(AuCl)_2$.

Determination of the absolute stereochemistry of cyclopropanes **74a**

The absolute stereochemistry of cyclopropanes **74a** was determined by comparing the HPLC trace of the major *cis* diastereomer produced at room temperature by **296**, with that produced using (*R*)-DTBM-SEGPHOS®$(AuCl)_2$ under conditions reported by Toste and co-workers, the stereochemical outcome of which is known. Using this approach, the reactions mediated by (R_{mp})-**296** and (S_{mp})-**296** (Table S1, entries 2 and 3) yielded (1*S*,2*R*)-**74a** and (1*R*,2*S*)-**74a** respectively as the major products.

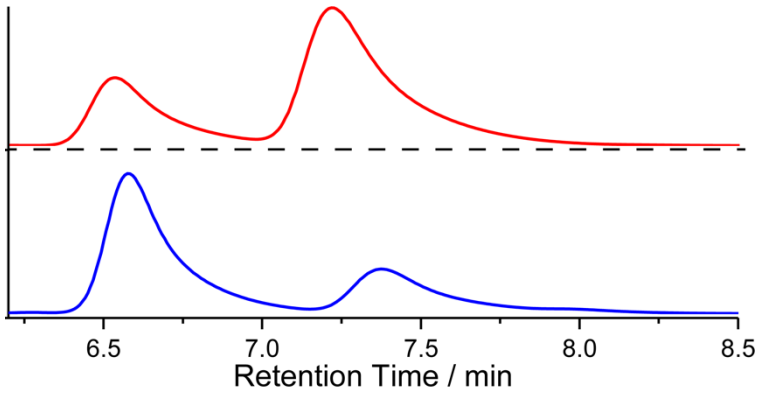

Figure 190: Chiral Stationary Phase HPLC (RegisPack, *n*-hexane-isopropanol 99 : 1, 303 K, load Et_2O, flowrate 0.75 $mLmin^{-1}$) (*red*, *top*) 72 : 28 *er cis*-**74a** produced using (R_{mp})-**296** (97 : 3 er). Retention times (min): (1*R*,2*S*)-**74a** 6.6 (28.4%), (1*S*,2*R*)-**74a** 7.4 (71.6%). (*blue*, *bottom*) 29 : 71 *er cis*-**74a** produced using (S_{mp})-**296** (3 : 97 er). Retention times (min): (1*R*,2*S*)-**74a** 6.6 (71.0%), (1*S*,2*R*)-**74a** 7.4 (29.0%).

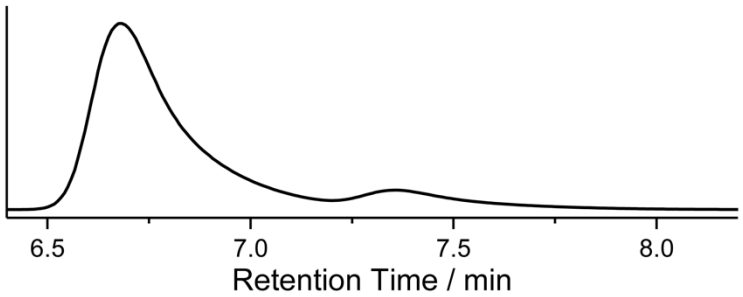

Figure 191: Chiral Stationary Phase HPLC (RegisPack, *n*-hexane-isopropanol 99 : 1, 303 K, load Et_2O, flowrate 0.75 $mLmin^{-1}$) of *cis*-**74a** produced using (*R*)-DTBM-SEGPHOS®$(AuCl)_2$ in according to literature conditions to determine absolute stereochemistry. Retention times (min): (1*R*,2*S*)-**74a** 6.6 (88.0%), (1*S*,2*R*)-**74a** 7.4 (12.0%).

Cyclopropanation General Procedures

Catalyst 296: A foil-covered, CEM MW vial was charged with $AgSbF_6$ (1.0 mg, 2.97 *μ*mol, 0.05 eq.) and $[Cu(MeCN)_4]PF_6$ (1.1 mg, 3.0 *μmol*, 0.05 eq.), then purged with N_2. LAuCl was added as solution in $CDCl_3$ (0.059 M, 50 *μL* 3.0 *μmol*, 0.05 eq.*)* and the solution cooled to 0 ˚C. After 5 minutes, 2-methyl-3-butyn-2-yl ester (59.4 *μmol*, 1.0 eq.) and alkene (238 *μ*mol, 4.0 eq.) were added in $CDCl_3$ (0.54 mL) (0.1 M with respect to the alkyne), and the solution stirred for 6 h at 0 ˚C . After 6 h, $C_2H_2Cl_4$ (20.0 *μL, 0.189 mmol)* was added, the solution was filtered through Celite®, and the yield and *dr* was determined by ^1H NMR. The reaction mixture was purified by column chromatography (SiO_2, petrol-Et_2O 0→10%) yielding isolated *cis* and *trans* cyclopropanes. Where possible, the enantiopurity of both diastereoisomers was determined by chiral stationary phase HPLC.

[Au(PPh$_3$)(Cl)]: Reactions with $[Au(PPh_3)(Cl)]$ were performed as per the general procedure at rt for 2 h in the absence of $[Cu(MeCN)_4]PF_6$ to provide racemic samples for HPLC method development.

(*R*)-DTBM-SEGPHOS®(AuCl)$_2$: Performed as per literature procedure (rt, $MeNO_2$, 2.5 mol% [Au(L)(Cl) (2.5 mol%), $AgSbF_6$ (5 mol%), benzoyl ester (1 eq., 0.05 M), alkene (4 eq.), $MeNO_2$, rt, 2 h).

Cyclopropanes **74a**[75]

Catalyst	Yield / %	*dr*	er_{cis}	er_{trans}
$(Ph_3P)AuCl$	96	89 : 11	1 : 1	1 : 1
(R_{mp})-**296**	86	94 : 6	78.5 : 21.5	62 : 38
(*R*)-DTBM-SEGPHOS®$(AuCl)_2$	73	>20 : 1	16 : 84	-

Cis-**74a**[75]

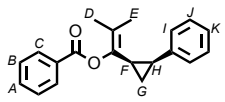

δ$_H$ ($CDCl_3$, 400 MHz) 7.88 (2H, d, *J* = 7.5, ***H***$_C$), 7.58 (1H, tt, *J* = 7.5, 1.5, ***H***$_A$), 7.43 (2H, tt, *J* = 7.5, 1.0, ***H***$_B$), 7.26 (2H, dd, *J* = 7.0, 6.5, ***H***$_J$), 7.20 (1H, tt, *J* = 7.0, 1.5, ***H***$_K$), 7.12 (2H, dd, *J* = 7.5, 1.5, ***H***$_I$), 2.43-2.28 (2H, m, ***H***$_H$, ***H***$_F$), 1.65 (3H, s, ***H***$_F$), 1.49 (3H, s, ***H***$_D$), 1.29 (1H, ddd (td), *J* = 9.0, 5.5, ***H***$_G$), 1.11 (1H, dt (ddd), *J* = 5.5, 5.5, ***H***$_{G'}$). **δ**$_C$ ($CDCl_3$, 101 MHz) 164.8, 139.5, 138.7, 133.2, 130.0, 129.9, 128.5, 127.8, 127.8, 125.7, 123.6, 23.9, 21.6, 18.8, 17.8, 11.9. HR-EI-MS m/z 292.1455 [$M^{+\cdot}$] (calc. m/z for $C_{20}H_{20}O_2$ 292.1458).

Trans-**74a**[75]

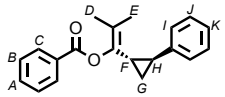

δ$_H$ ($CDCl_3$, 400 MHz) 8.13 (2H, dd, *J* = 8.1, 1.4, ***H***$_C$), 7.61 (1H, tt, *J* = 7.4, 2.7, ***H***$_A$), 7.49 (2H, app. t, *J* = 7.6, ***H***$_B$), 7.26 (2H, br. t, *J* = 7.5, ***H***$_J$), 7.16 (1H, tt, *J* = 7.4, 1.3, ***H***$_K$), 7.10 (2H, dd, *J* = 7.7, 1.5, ***H***$_I$), 7.28-7.18 (2H, m, ***H***$_F$, ***H***$_H$), 1.86 (3H, s, ***H***$_E$), 1.63 (3H, s, ***H***$_D$), 1.21 (1H, ddd, *J* = 8.7, 6.2, 4.9, ***H***$_G$), 1.16 (1H, ddd, *J* = 8.9, 6.0, 5.1, ***H***$_{G'}$). **δ**$_C$ ($CDCl_3$, 101 MHz) 164.9, 142.2, 141.0, 133.4, 130.1, 129,8, 128.7, 128.5, 126.1, 125.9, 121.1, 23.8, 23.5, 19.0, 18.3, 14.8. HR-EI-MS m/z 292.1455 [$M^{+\cdot}$] (calc. m/z for $C_{20}H_{20}O_2$ 292.1458).

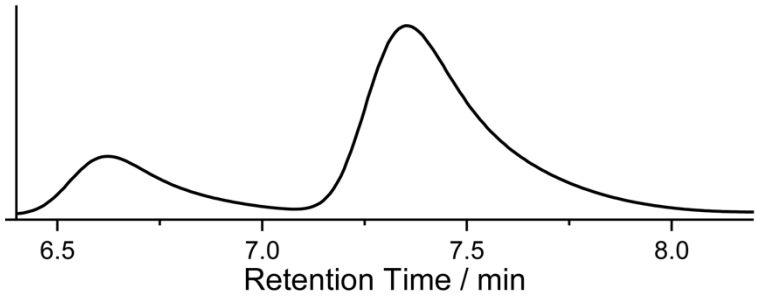

Figure 192: Chiral Stationary Phase HPLC (RegisPack, *n*-hexane-isopropanol 99 : 1, 303 K, load Et_2O, flowrate 0.75 $mLmin^{-1}$) of 78.5 : 21.5 *er cis*-**74a**. Retention times (min): (1*R*,2*S*)-**74a** 6.6 (21.5%), (1*S*,2*R*)- **74a** 7.4 (78.5%).

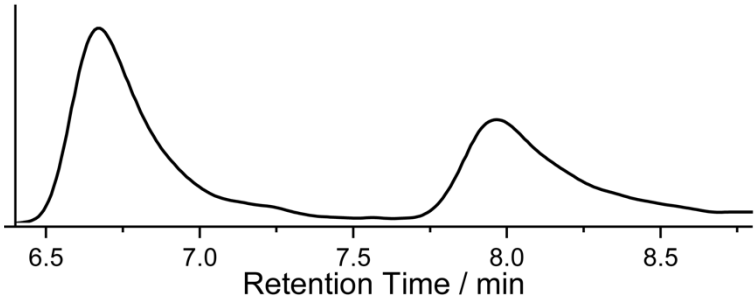

Figure 193: Chiral Stationary Phase HPLC (RegisPack, *n*-hexane-isopropanol 99 : 1, 303 K, load Et_2O, flowrate 0.75 $mLmin^{-1}$) of 62 : 38 *er trans*-**74a**. Retention times (min): 6.7 (61.9%), 8.0 (38.1%).

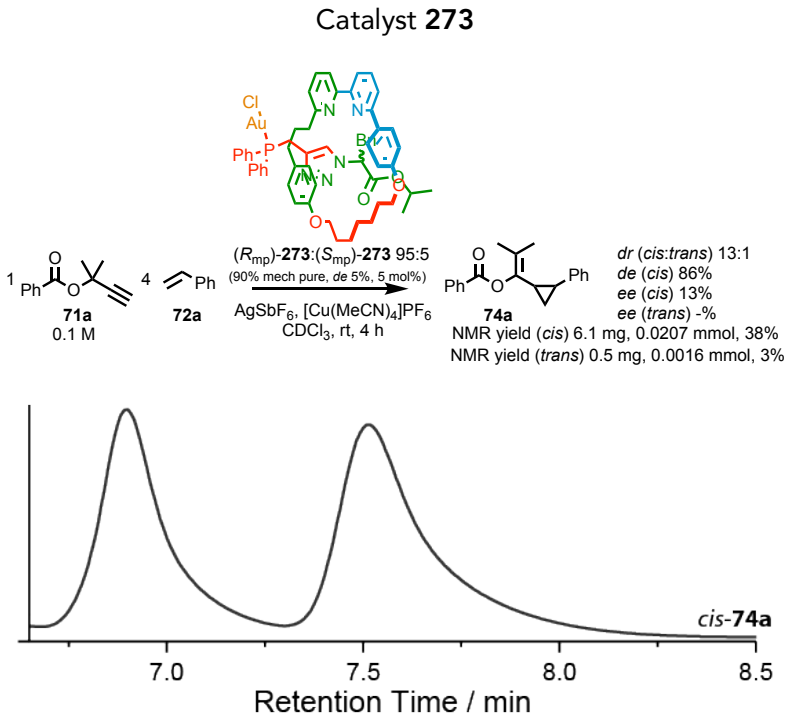

Figure 194: Chiral Stationary Phase HPLC trace of *cis*-**74a**. Retention times 6.4 min (694157, 43.6%), 7.0 min (898454, 56.4%). RegisPack, isocratic hexane-isopropanol 99-1, flowrate 0.75 $mLmin^{-1}$.

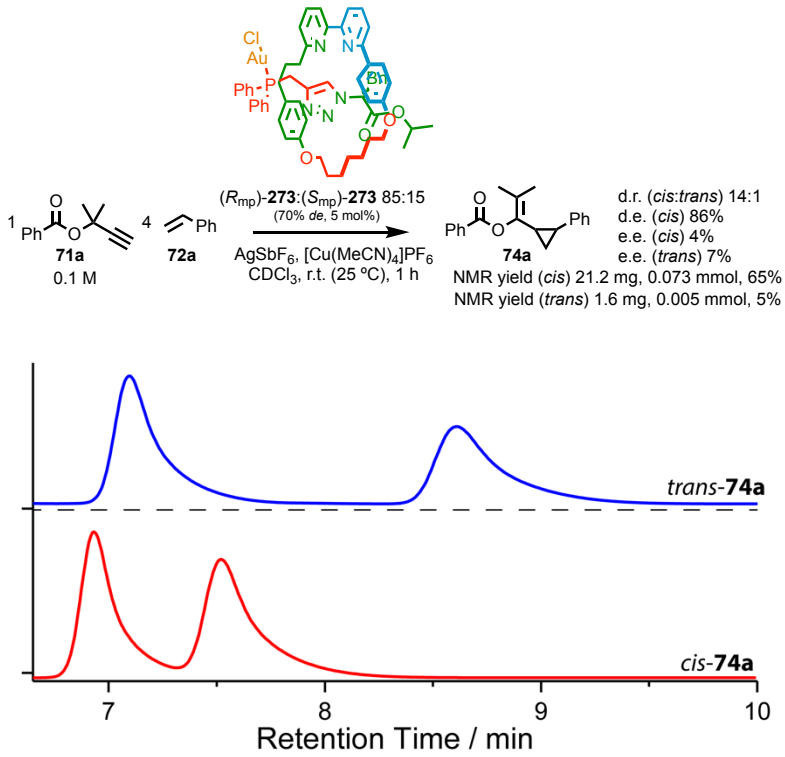

Figure 195: Chiral Stationary Phase HPLC trace of *cis*-**74a** (red) detailed in this scheme. Retention times 6.4 min (914177, 48.1%), 7.0 min (987433, 51.9%). *Trans*-**74a** (blue) 6.6 min (158230, 53.5%), 8.1 min (1345562, 46.5%). RegisPack, isocratic hexane-isopropanol 99-1, flowrate 0.75 mLmin^{-1}.

Cyclopropanes **74c**[75]

Catalyst	Yield / %	*dr*	er_{cis}	er_{trans}
$(Ph_3P)AuCl$	44	92 : 8	1 : 1	-
(R_{mp})-**296**	90	97 : 3	55 : 45	-
(*R*)-DTBM-SEGPHOS®$(AuCl)_2$	70	>20 : 1	91 : 9	-

Cis-**74c**[75]

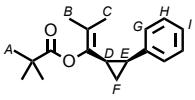

δ_H ($CDCl_3$, 400 MHz) 7.21 (2H, tt, *J* = 7.5, 1.6, $\boldsymbol{H}_H$), 7.14 (1H, tt, *J* = 7.4, 1.3, $\boldsymbol{H}_I$), 7.03 (2H, dd, *J* = 7.5, 1.3, $\boldsymbol{H}_G$), 2.28 (1H, d, *J* = 6.5, $\boldsymbol{H}_E$), 2.26 (1H, d, *J* = 6.5, $\boldsymbol{H}_D$), 1.48 (3H, s, $\boldsymbol{H}_C$), 1.41 (3H, s, $\boldsymbol{H}_B$), 1.26 (1H, m, $\boldsymbol{H}_F$), 1.22 (9H, s, $\boldsymbol{H}_A$), 1.00 (1H, dt, *J* = 6.0, 6.0, $\boldsymbol{H}_{F'}$). δ_C ($CDCl_3$, 101 MHz) 176.9, 139.6, 138.2, 127.6, 127.4, 125.6, 123.2, 39.0, 27.4, 24.1, 21.9, 18.7, 17.4, 11.9. HR-EI-MS m/z 272.1766 [$M^{+\cdot}$] (calc. m/z for $C_{18}H_{24}O_2$ 272.1771).

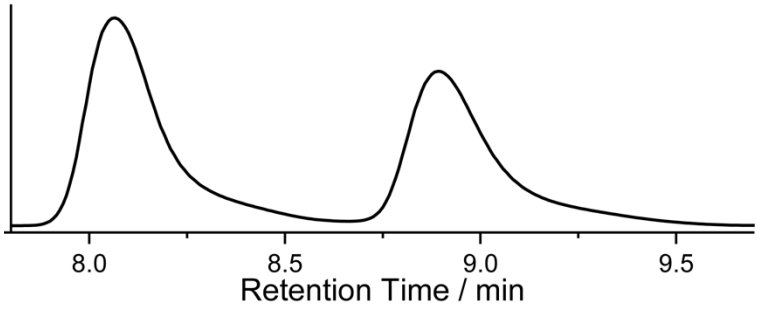

Figure 196: Chiral Stationary Phase HPLC (RegisCell, *n*-hexane-isopropanol 99.5 : 0.5, 303 K, load solvent Et_2O, flowrate 0.50 $mLmin^{-1}$) of 54 : 46 *er cis*-**74c**. Retention times (min): 8.1 (54.4%), 8.9 (45.6%). The absolute stereochemistry of the products was not determined. The (1*S*,2*R*)-**74c** isomer is shown for illustrative purposes only.

Cyclopropane *cis*-**74j**

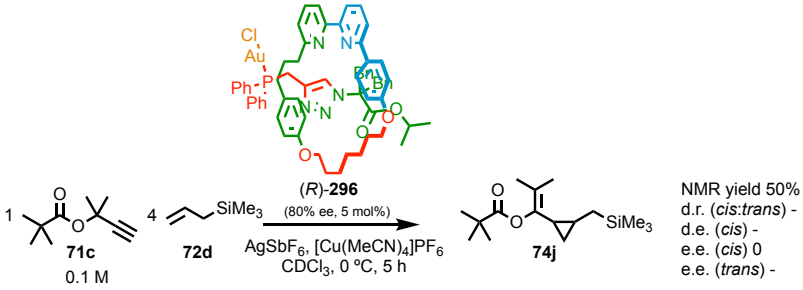

Characterisation data matched literature.[19,75]

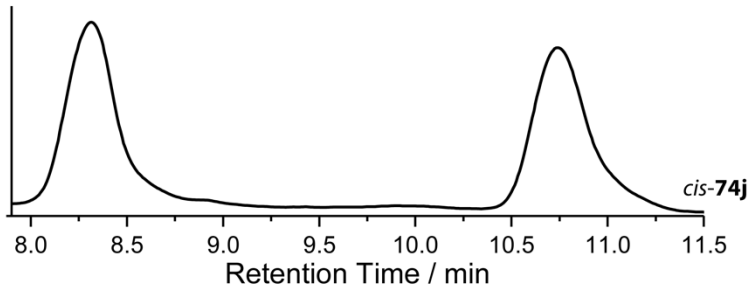

Figure 197: Chiral Stationary Phase HPLC separation achieved for *cis*-**74j** Retention times: 7.8 min (81519, 49.1%), 10.2 min (84390, 50.9%). (*S,S*)Whelk, isocratic hexane-isopropanol 99.9-0.1, flowrate 0.75 mLmin^{-1}.

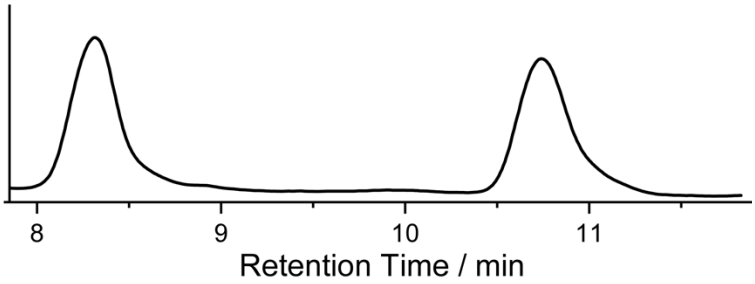

Figure 198: Chiral Stationary Phase HPLC separation achieved for *cis*-**74j** Retention times (7.8 min, 10.2 min) (*S,S*)Whelk, isocratic hexane-isopropanol 99.9-0.1, flowrate 0.75 mLmin^{-1}.

Compound **74k**

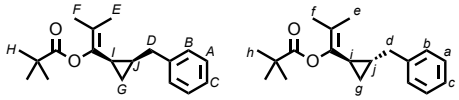

δ$_H$ ($CDCl_3$, 400 MHz) 7.31-7.26 (4H, m, ***H***$_A$, ***H***$_a$), 7.25-7.17 (6H, m, ***H***$_B$, ***H***$_C$, H$_b$, ***H***$_c$), 2.78 (1H, dd, *J* = 15.0, 5.7, ***H***$_D$), 2.73 (1H, dd, *J* = 14.7, 6.2, ***H***$_d$), 2.54 (1H, dd, *J* = 14.7, 7.4, ***H***$_{d'}$), 2.35 (1H, dd, *J* = 14.8, 9.1, ***H***$_{D'}$), 1.91 (1H, m, ***H***$_i$), 1.74 (3H, s, ***H***$_E$), 1.72 (3H, s, ***H***$_e$), 1.69-1.60 (1H, m, ***H***$_I$) 1.59 (3H, s, ***H***$_f$), 1.54 (1H, m, ***H***$_j$), 1.51 (3H, s, ***H***$_F$), 1.30 (9H, s, ***H***$_H$), 1.22 (9H, s, ***H***$_h$), 1.19-1.11 (1H, m, ***H***$_J$), 0.90 (1H, ddd, *J* = 8.8, 8.5, 5.5, ***H***$_g$), 0.73 (1H, dt, *J* = 8.6, 4.9, ***H***$_G$), 0.60 (1H, ddd, *J* = 8.7, 5.1, 5.1, ***H***$_{G'}$), 0.40 (1H, q, *J* = 5.6, ***H***$_{g'}$). **δ**$_C$ ($CDCl_3$, 100 MHz) 176.6, 176.6, 142.1, 141.3, 141.2, 139.8, 128.6, 128.5, 128.4, 128.4, 126.1,

125.9, 121.9, 119.6, 39.7, 39.1, 35.8, 27.5, 27.4, 19.6, 19.4, 18.9, 18.7, 18.7, 18.0, 17.8, 17.3, 12.2, 10.8. HR-GCMS [$M^{+\cdot}$] m/z 286.1923 (calc. for $C_{19}H_{26}O_2$ 286.1927).

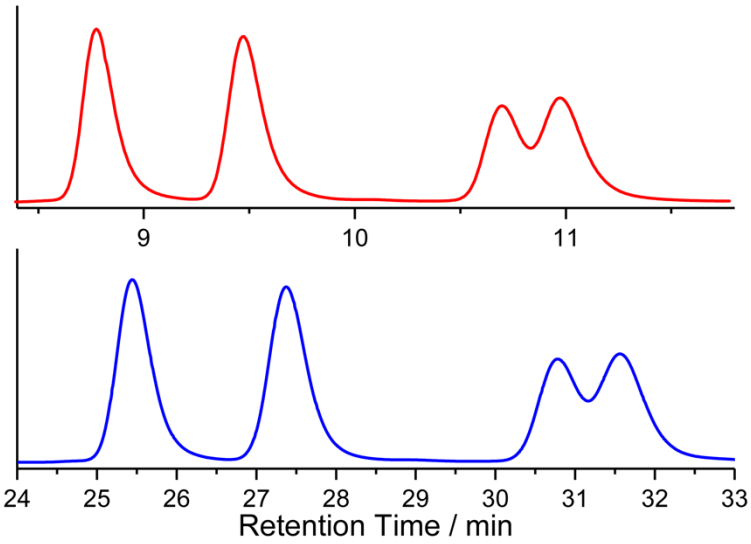

Figure 199: Chiral HPLC trace of **74k**. (blue) *cis* (25.0 min, 26.9 min) (S,S)Whelk, isocratic Hx-IPA 99.9-0.1, loading solvent petrol, 1 mgmL^{-1}, 5 µL injection, flowrate 0.25 mLmin^{-1}. (red) *cis* (8.3 min, 9.0min) *trans* (10.2 min, 10.5 min) (S,S)Whelk, isocratic Hx-IPA 99.9-0.1, loading solvent petrol, 1 mgmL^{-1}, 5 µL injection, flowrate 0.75 mLmin^{-1}.

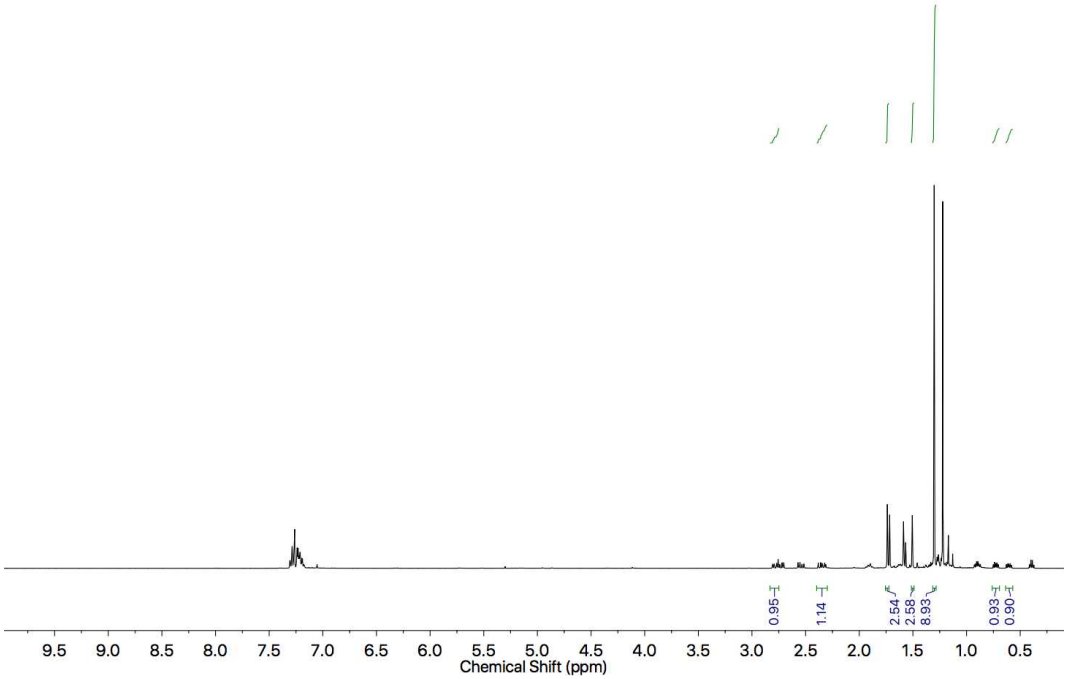

Figure 200: ^{1}H NMR of **74k**.

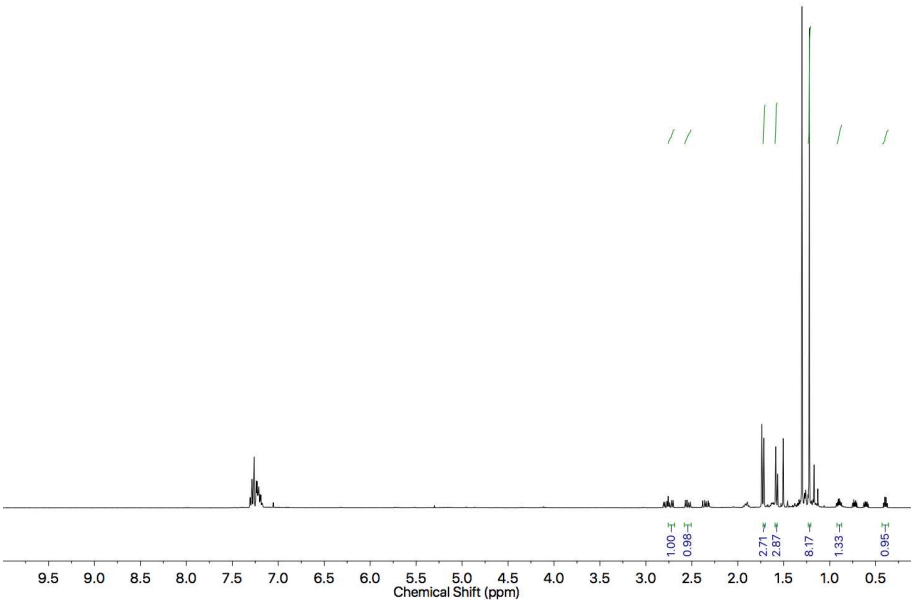

Figure 201: ^{1}H NMR (400 MHz, $CDCl_3$) of **74k**.

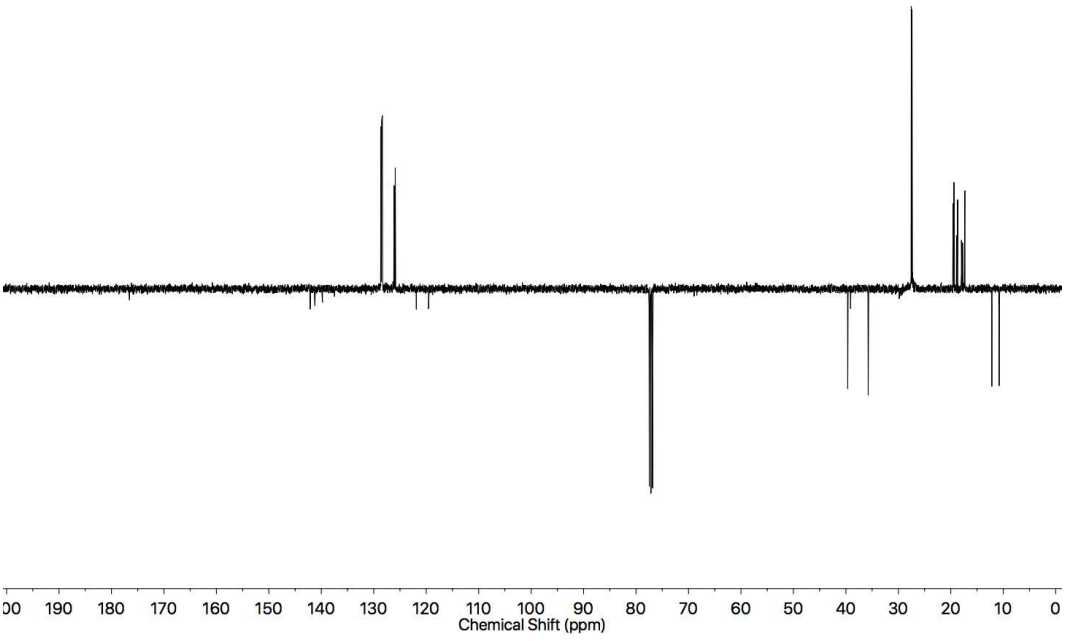

Figure 202: JMOD NMR (101 MHz, $CDCl_3$) of **74k**.

Cyclopropane **308**

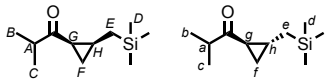

δ$_H$ ($CDCl_3$, 400 MHz) 2.72 (1H, sept., *J* = 6.8, ***H***$_A$), 2.71 (1H, sept., *J* = 6.8, ***H***$_a$), 2.08 (1H, ddd, *J* = 8.6, 7.5, 5.6, ***H***$_G$), 1.69 (1H, ddd, *J* = 8.1, 4.5, 4.0, ***H***$_g$), 1.39 (1H, ddddd, *J* = 15.0, 12.7, 7.3, 4.2, 1.8, ***H***$_h$), 1.33-1.24 (1H, m, ***H***$_H$), 1.13 (6H, d, *J* = 6.8, ***H***$_b$, ***H***$_c$), 1.12 (3H, d, *J* = 6.8, ***H***$_B$), 1.11 (3H, d, *J* = 6.8, ***H***$_C$), 1.02-0.95 (2H, m, ***H***$_F$), 0.89-0.80 (2H, m, ***H***$_f$), 0.64 (1H, dd, *J* = 14.5, 10.6, ***H***$_E$), 0.54 (1H, dd, *J* = 14.5, 4.2, ***H***$_{E'}$), 0.40 (1H, dd, *J* = 14.5, 8.6, ***H***$_e$), 0.40 (1H, dd, *J* = 14.5, 8.6, ***H***$_{e'}$), 0.02 (9H, s, ***H***$_d$), 0.01 (9H, s, ***H***$_D$). **δ**$_C$ ($CDCl_3$, 100 MHz) 214.2, 212.6, 42.4, 41.7, 29.1, 25.3, 22.3, 21.6, 21.6, 20.2, 18.4, 18.3, 18.2, 18.2, 15.6, 13.5, -1.3, -1.4. High Resolution APPI-MS [$M^{+\cdot}$] m/z 199.1510 (calc. for $C_{11}H_{23}OSi$ 199.1513)

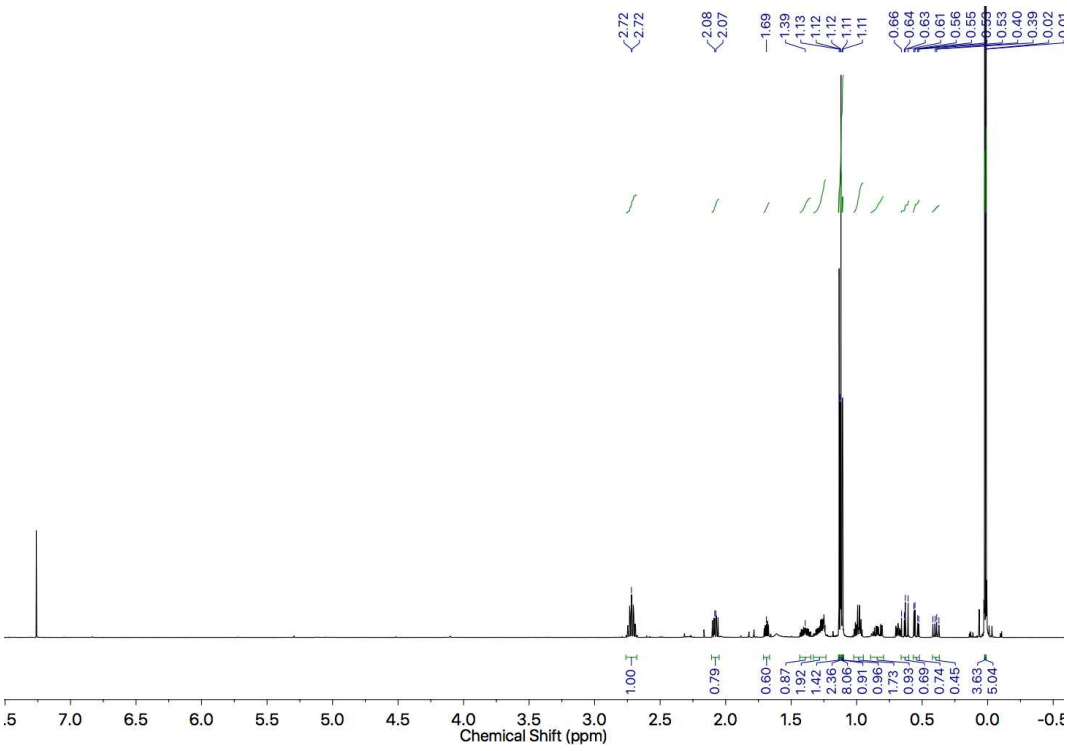

Figure 203: ^{1}H NMR (500 MHz, $CDCl_3$) of **308**.

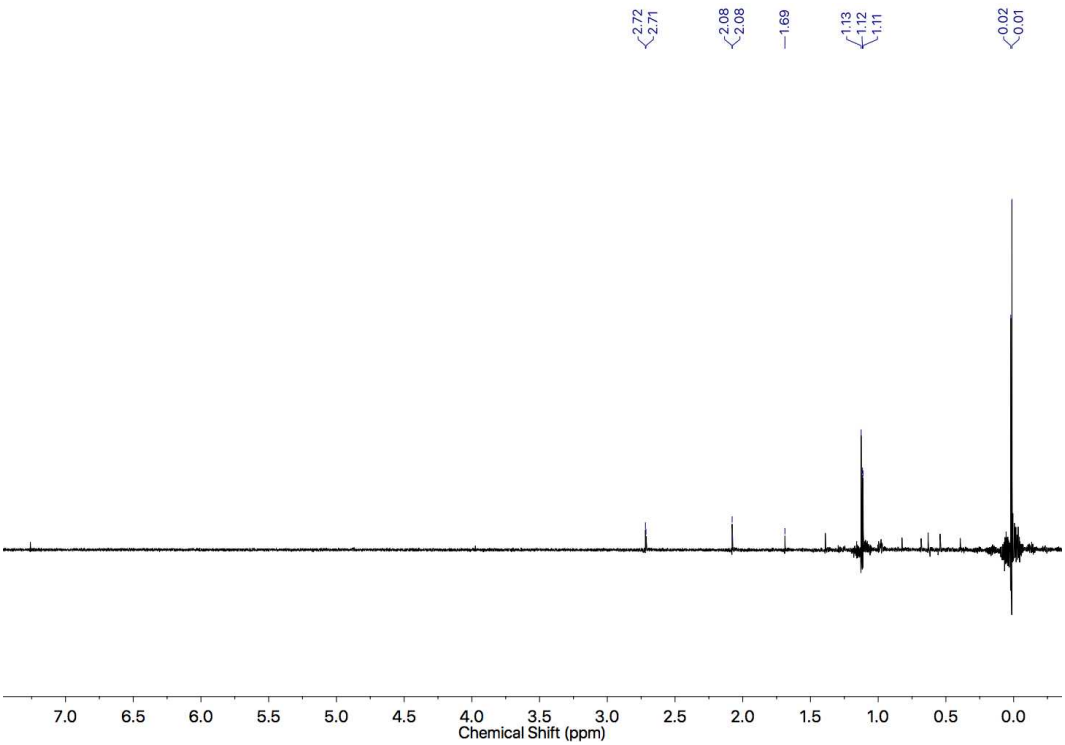

Figure 204: Pureshift ^{1}H NMR (500 MHz, $CDCl_3$) of **308**.

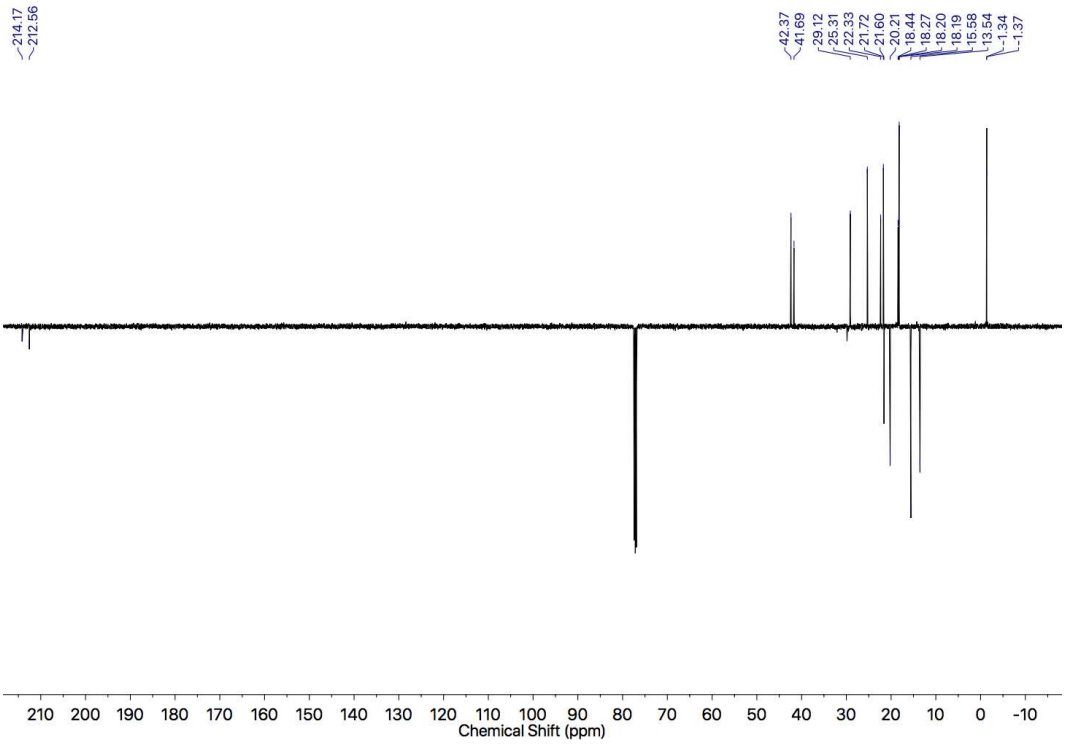

Figure 205: JMOD NMR (126 MHz, $CDCl_3$) of **308**.

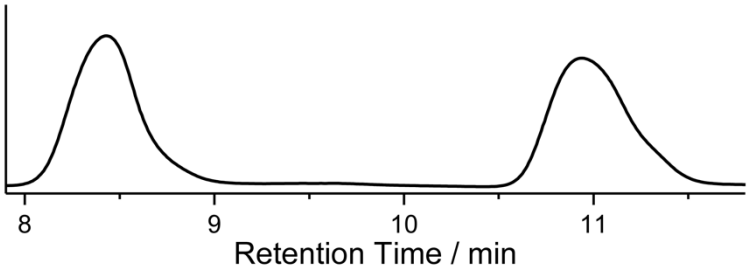

Figure 206: Chiral HPLC trace of racemate **308**. *Cis* 7.9 min (261377, 51.0%), 10.4 min (251501, 49.0%) (S,S)Whelk, isocratic Hx-IPA 99.8-0.2, loading solvent petrol, 1 mgmL^{-1}, 5 µL injection, flowrate 0.75 mLmin^{-1}.

Cyclopropanes **74l**[75]

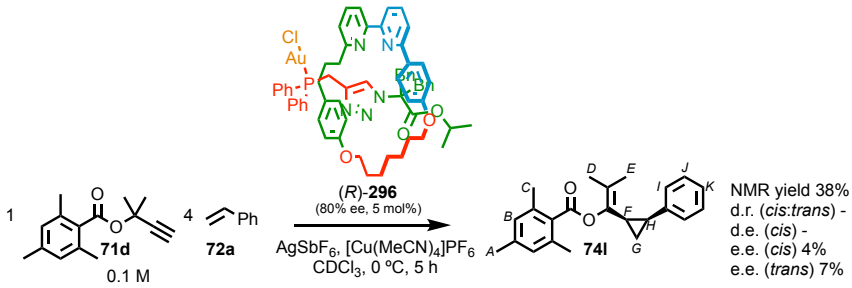

Characterisation data matches literature.[75]

δ$_H$ ($CDCl_3$, 400 MHz) 7.16 (2H, tt, *J* = 7.1, 1.7, ***H***$_J$), 7.11 (1H, tt, J = 7.0, 1.5, ***H***$_K$), 7.02-6.98 (2H, m, ***H***$_I$), 6.89 (2H, s, ***H***$_B$), 2.41 (6H, s, ***H***$_C$), 2.36 (1H, td, *J* = 8.6, 6.3, ***H***$_H$), 2.30 (3H, s, ***H***$_A$), 1.53 (3H, s, ***H***$_E$), 1.41 (3H, s, ***H***$_D$), 1.36 (1H, td, *J* = 9.1, 5.2, ***H***$_F$), 1.15 (1H, td, *J* = 6.4, 5.2, ***H***$_G$), 0.90-0.83 (1H, m, ***H***$_{G'}$). **δ**$_C$ ($CDCl_3$, 100 MHz) 168.9, 139.6, 139.5, 138.4, 135.6, 130.8, 128.9, 127.5, 127.2, 125.6, 124.6, 24.9, 22.5, 21.2, 20.6, 19.1, 18.1, 13.0. HR-APPI-MS [$M^{+\cdot}$] m/z 334.1925 (calc. of $C_{23}H_{26}O_2$ 334.1927).

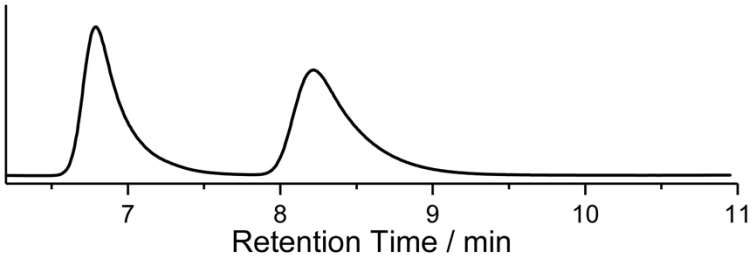

Figure 207: Chiral Stationary Phase HPLC trace of *cis*-**74l** detailed in this scheme. Retention times (6.3 min, 7.7 min). RegisPack, isocratic hexane-isopropanol 99-1, flowrate 0.75 mLmin^{-1}.

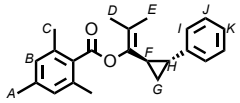

δ$_H$ ($CDCl_3$, 400 MHz) 7.27-7.24 (2H, m, ***H***$_J$), 7.19-7.14 (1H, m, ***H***$_K$), 7.12-7.09 (2H, m, ***H***$_I$), 6.87 (2H, s, ***H***$_B$), 2.39 (6H, s, ***H***$_C$), 2.29 (3H, s, ***H***$_A$), 2.19-2.12 (2H, m, ***H***$_F$, ***H***$_H$), 1.87 (3H, s, ***H***$_E$), 1.69 (3H, s, ***H***$_D$), 1.32-1.26 (1H, m, ***H***$_G$), 1.20-1.13 (1H, m, ***H***$_{G'}$).

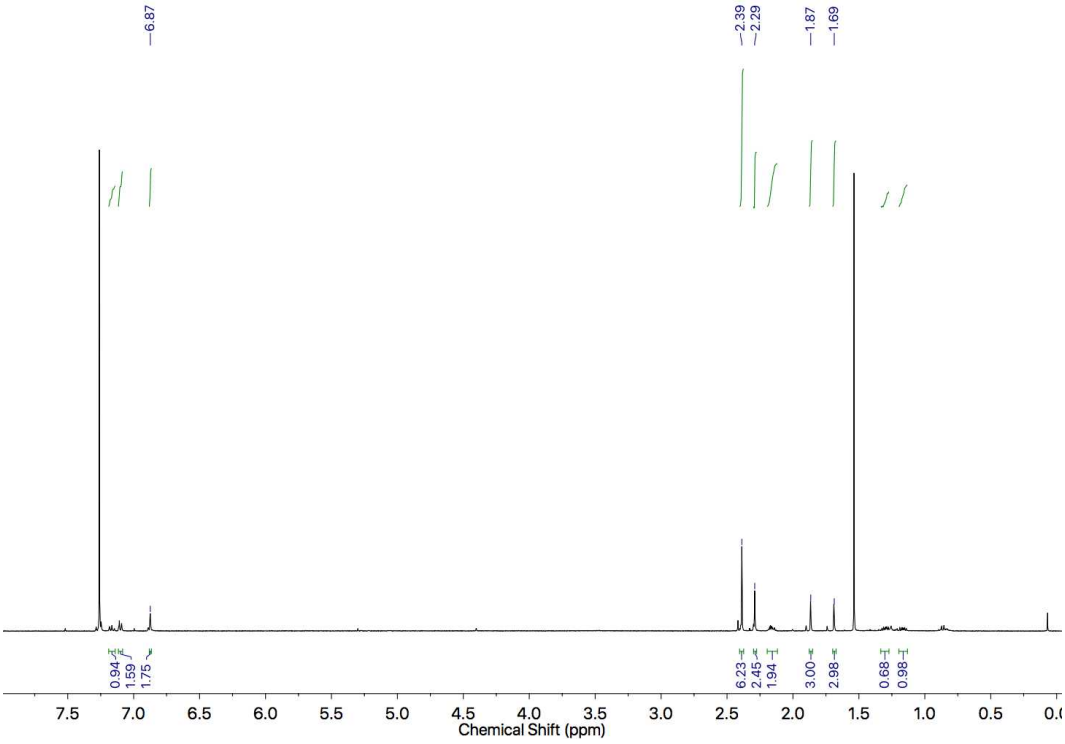

Figure 208: ^{1}H NMR (400 MHz, $CDCl_3$) of *trans*-**74l**.

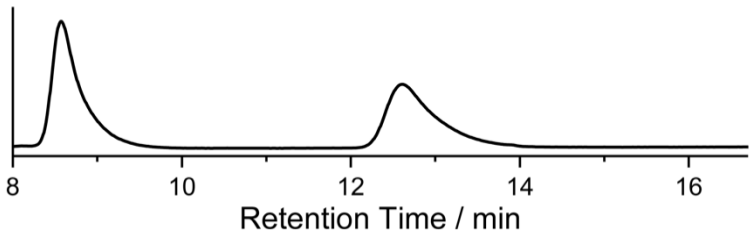

Figure 209: Chiral Stationary Phase HPLC trace of *trans*-**74l** detailed in this scheme. Retention times *trans* (8.1 min, 12.1 min). RegisPack, isocratic hexane-isopropanol 99-1, flowrate 0.75 mLmin^{-1}.

Cyclopropanes **74m**

Catalyst	**Yield / %**	***dr***	***er*$_{cis}$**	***er*$_{trans}$**
$(Ph_3P)AuCl$[a]	99	95 : 5	1 : 1	1 : 1
(R_{mp})-**296**	68	96 : 4	89 : 11	70 : 30

Cis-**74m**

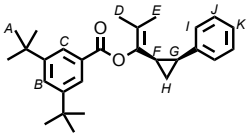

δ$_H$ ($CDCl_3$, 400 MHz) 7.84 (2H, d, *J* = 1.9, ***H***$_C$), 7.66 (1H, t, *J* = 1.9, ***H***$_B$), 7.25 (2H, t, *J* = 7.6, ***H***$_J$), 7.18 (1H, tt, *J* = 7.3, 2.0, ***H***$_K$), 7.15 (2H, d, *J* = 7.1, ***H***$_I$), 2.42-2.29 (2H, m, ***H***$_F$, ***H***$_G$), 1.67 (3H, s, ***H***$_E$), 1.49 (3H, s, ***H***$_D$), 1.37 (18H, s, ***H***$_A$) 1.32-1.26 (1H, m, ***H***$_H$), 1.15 (1H, dt, *J* = 6.1, ***H***$_H$). **δ**$_C$ ($CDCl_3$, 101 MHz) 165.5, 151.2, 139.5, 138.7, 129.3, 127.8, 127.8, 127.5, 125.8, 124.2, 123.3, 35.1, 31.5, 23.9, 21.8, 18.8, 17.9, 11.8. HR-EI-MS m/z 404.2703 [$MS^{+\cdot}$] (calc. m/z for $C_{28}H_{36}O_2$ 404.2710).

Trans-**74m**

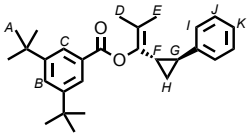

Colourless oil (*dr cis-trans* 95 : 5, NMR yield 94 mg, 0.232 mmol, 99%). **δ**$_H$ ($CDCl_3$, 400 MHz) 7.97 (2H, d, *J* = 1.9, ***H***$_C$), 7.68 (1H, t, *J* = 1.9, ***H***$_B$), 7.26 (2H, tt, *J* = 7.5, 1.3, ***H***$_J$), 7.15 (1H, tt, *J* = 7.4, 1.9, ***H***$_K$), 7.10 (2H, dd, *J* = 7.4, 1.5, ***H***$_I$), 2.19-2.07 (2H, m, ***H***$_F$, ***H***$_G$), 1.86 (3H, s, ***H***$_E$), 1.63 (3H, s, ***H***$_D$), 1.38 (18H, s, ***H***$_A$), 1.23 (1H, ddd, *J* = 11.1, 5.1, 6.0, ***H***$_H$), 1.15 (1H, ddd, *J* = 11.0, 5.7, 5.1, ***H***$_{H'}$). **δ**$_C$ ($CDCl_3$, 101 MHz) 165.6, 151.4, 142.0, 141.0, 129.1, 128.5, 127.7, 126.1, 125.9, 124.3, 120.9, 35.1, 31.5, 23.8, 23.7, 19.0, 18.4, 14.8. HR-EI-MS m/z 404.2711 [$M^{+\cdot}$] (calc. m/z for $C_{28}H_{36}O_2$ 404.2710).

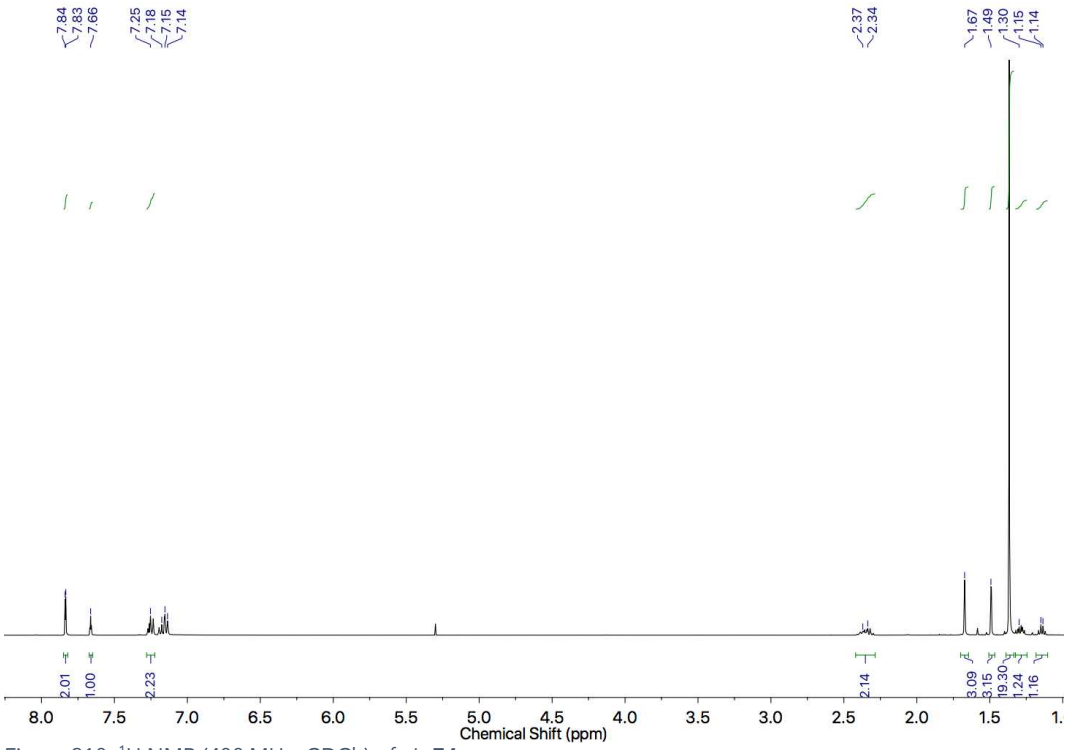

Figure 210: ^{1}H NMR (400 MHz, $CDCl_3$) of *cis*-**74m**.

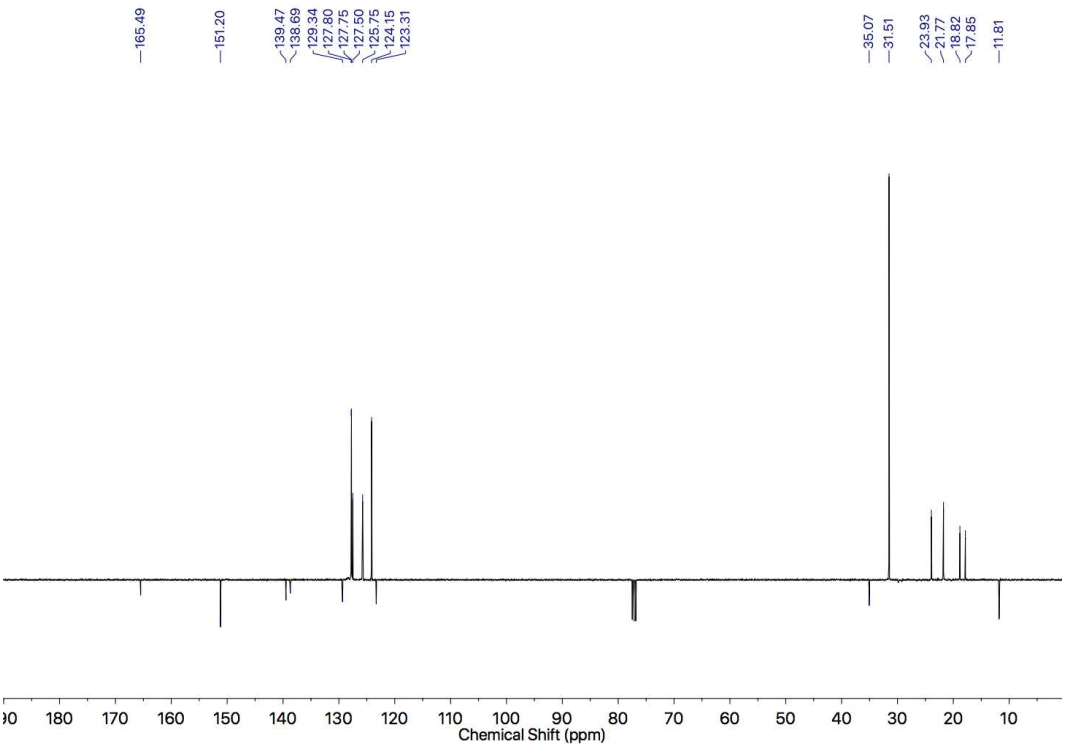

Figure 211: JMOD NMR (101 MHz, $CDCl_3$) of *cis*-**74m**.

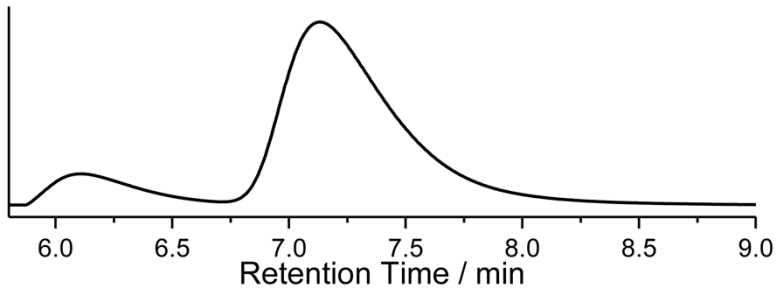

Figure 212: Chiral Stationary Phase HPLC (RegisPack, *n*-hexane-isopropanol 99.8 : 0.2, 303 K, load Et_2O, flowrate 0.75 $mLmin^{-1}$) of 88 : 12 *er cis*-**74m**. Retention times (min): 6.1 (11.7%), 7.1 (88.3%). The absolute stereochemistry of the products was not determined. The (1*S*,2*R*)-**74m** isomer is shown for illustrative purposes only.

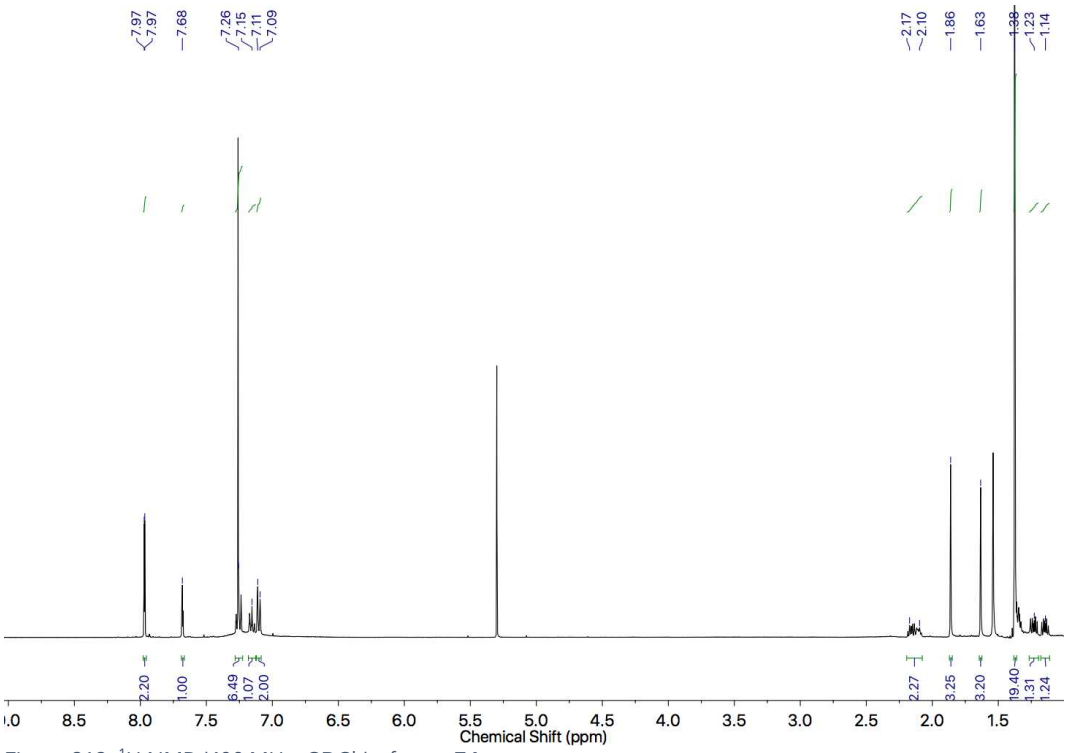

Figure 213: ^{1}H NMR (400 MHz, $CDCl_3$) of *trans*-**74m**.

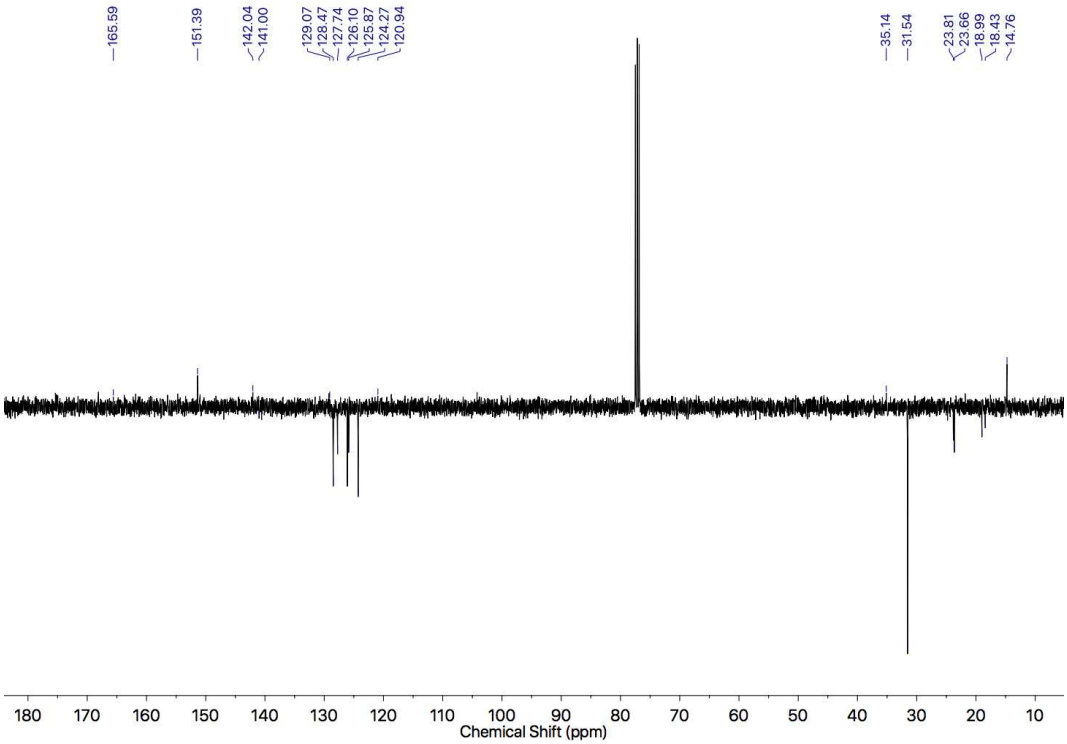

Figure 214: JMOD NMR (101 MHz, $CDCl_3$) of *trans*-**74m**.

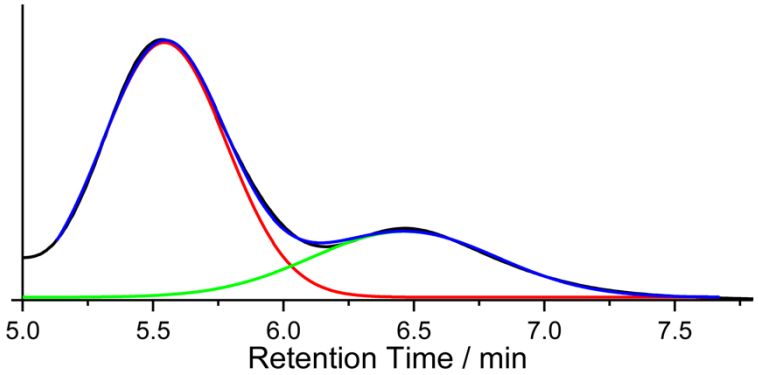

Figure 215: Chiral stationary phase HPLC (RegisPack, hexane-isopropanol 99.8 : 0.2, 303 K, load Et_2O, flowrate 0.75 $mLmin^{-1}$) of 70 : 30 *er trans*-**74m**. Retention times (min): 5.5 (69.8%), 6.5 (30.2%). The absolute stereochemistry of the products was not determined. The (1*S*,2*S*)-**74m** isomer is shown for illustrative purposes only.

Cyclopropanes **74n**

Catalyst	Yield / %	*dr*	er_{cis}	er_{trans}
$(Ph_3P)AuCl$	87	95 : 5	1 : 1	1 : 1
(R_{mp})-**296**	79	95 : 5	87 : 13[c]	65 : 35

Cis-**74n**

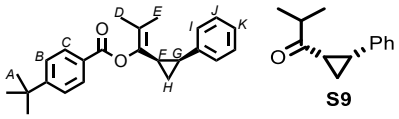

S9

Colourless oil (*dr cis-trans* 95 : 5, 71 mg, 0.202 mmol, 87%). δ_H ($CDCl_3$, 400 MHz) 7.84 (2H, dt, *J* = 9.2, 1.8, H_C), 7.45 (2H, dt, *J* = 9.1, 1.8, H_B), 7.26 (2H, tt, *J* = 7.1, 1.5, H_J), 7.19 (1H, tt, *J* = 7.2, 1.3, H_K), 7.12 (2H, dd, *J* = 7.5, 1.7, H_I), 2.42-2.28 (2H, m, H_F, H_G), 1.62 (3H, s, H_E), 1.47 (3H, s, H_D), 1.36 (9H, s, H_A), 1.30-1.24 (1H, m, H_H), 1.10 (1H, dt, *J* = 5.4, $H_{H'}$). δ_C ($CDCl_3$, 101 MHz) 164.8, 156.9, 139.5, 138.5, 129.9, 127.8, 127.7, 127.2, 125.7, 125.5, 123.5, 35.2, 31.3, 24.0, 21.7, 18.8, 17.7, 11.7. HR-EI-MS m/z 348.2081 [$M^{+\cdot}$] (calc. m/z for $C_{24}H_{28}O_2$ 348.2084). The enantiomers of *cis*-**74n** could not be separated and so were converted to ketone

Trans-**74n**

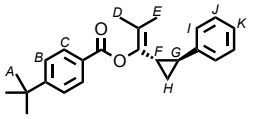

Colourless oil (*dr cis-trans* 95 : 5, NMR yield 71mg, 0.202 mmol, 87%). δ_H ($CDCl_3$, 400 MHz) 7.84 (2H, dt, *J* = 8.9, 2.0, H_C), 7.50 (2H, dt, *J* = 8.8, 2.0, H_B), 7.25 (2H, tt, *J* = 7.4, 1.2, H_J), 7.15 (1H, tt, *J* = 7.3, 1.9, H_K), 7.09 (2H, dd, *J* = 7.2, 1.5, H_I), 2.17-2.06 (2H, m, H_F, H_G), 1.85 (3H, s, H_E) 1.61 (3H, s, H_D), 1.36 (9H, s, H_A), 1.20 (1H, ddd, *J* = 11.1, 6.0, 5.0, H_H), 1.13 (1H, ddd, *J* = 11.1, 5.9, 5.0, $H_{H'}$). δ_C ($CDCl_3$, 101 MHz) 164.9, 157.2, 142.3, 130.0, 128.5, 127.0, 126.1, 125.9, 125.7, 122.8, 120.9, 35.3, 31.3, 23.8, 23.6, 19.0, 18.3, 14.7. HR-EI-MS m/z 348.2077 [$M^{+\cdot}$] (calc. m/z for $C_{24}H_{28}O_2$ 348.2089).

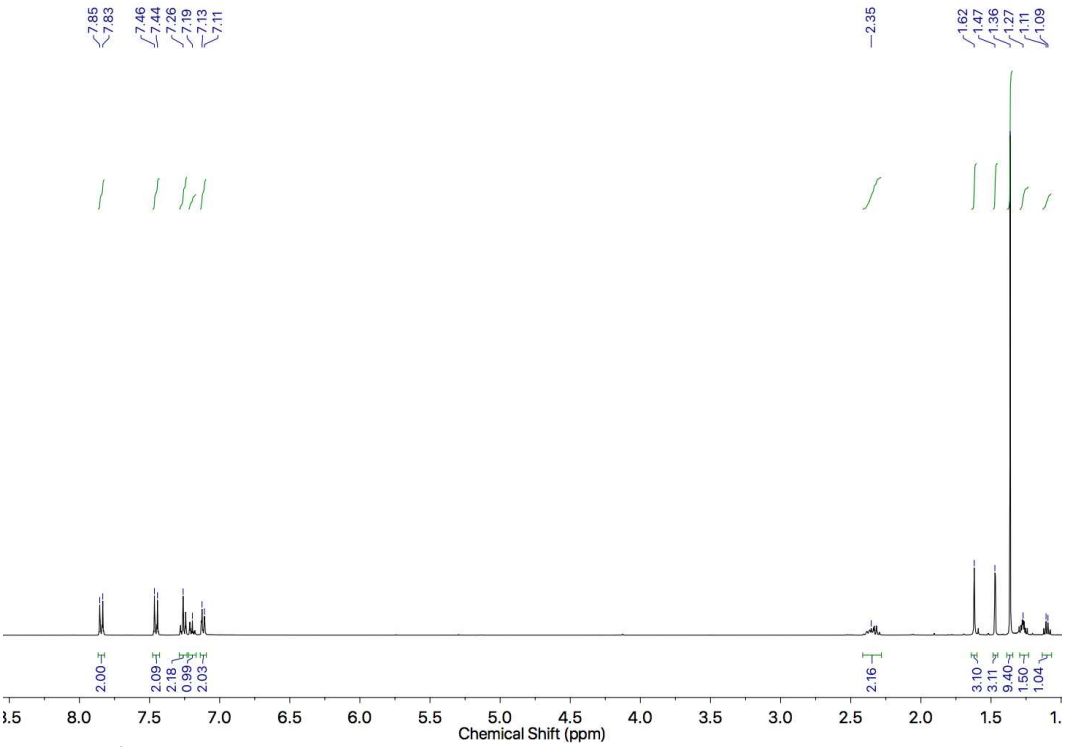

Figure 216: ^{1}H NMR (400 MHz, $CDCl_3$) of *cis*-**74n**.

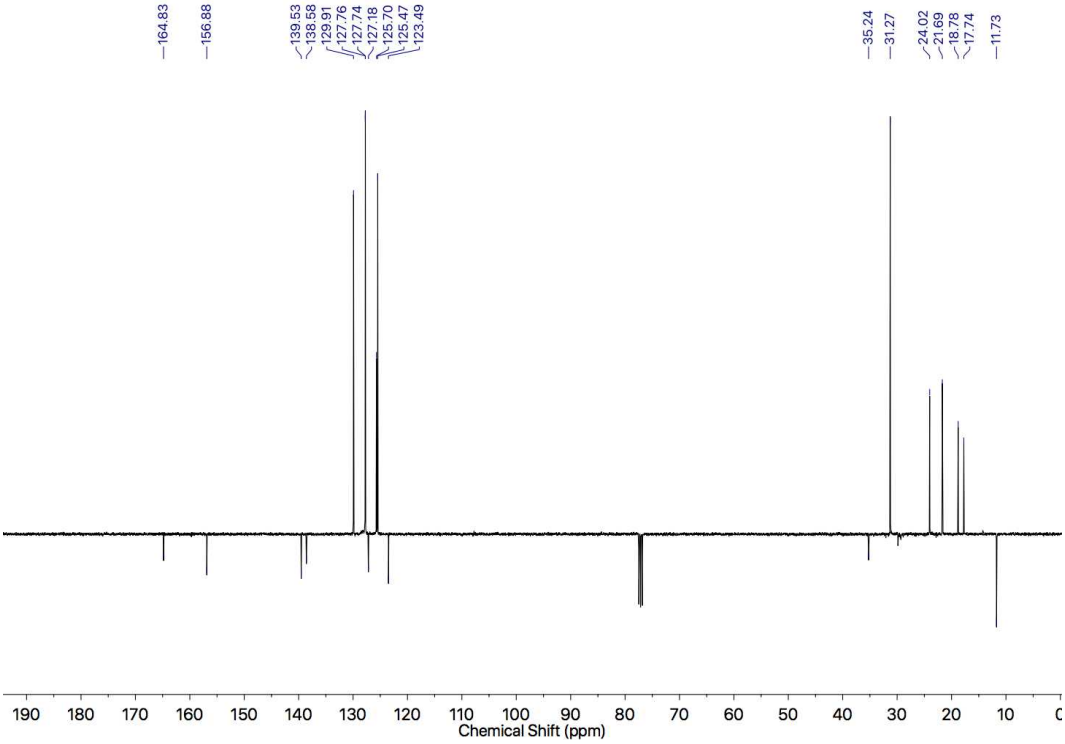

Figure 217: JMOD NMR (101 MHz, $CDCl_3$) of *cis*-**74n**.

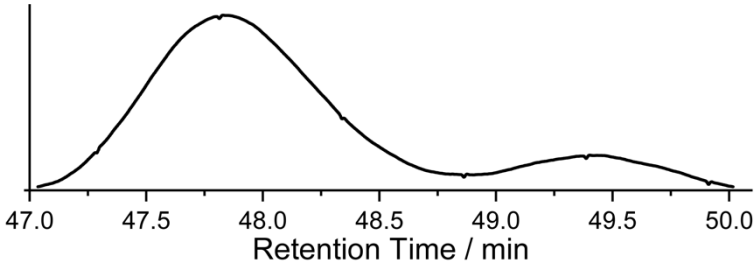

Figure 218: Chiral Stationary Phase HPLC ((*S*,*S*)Whelk, n-hexane-isopropanol 99.5 : 0.5, 303 K, load Et_2O, flowrate 0.25 mLmin^{-1}) of 83 : 17 *er cis*-**74n**. Retention times (min): 47.8 (87.2%), 49.4 (12.8%). The absolute stereochemistry of the products was not determined. The (1*S*,2*R*)-**74n** isomer is shown for illustrative purposes only.

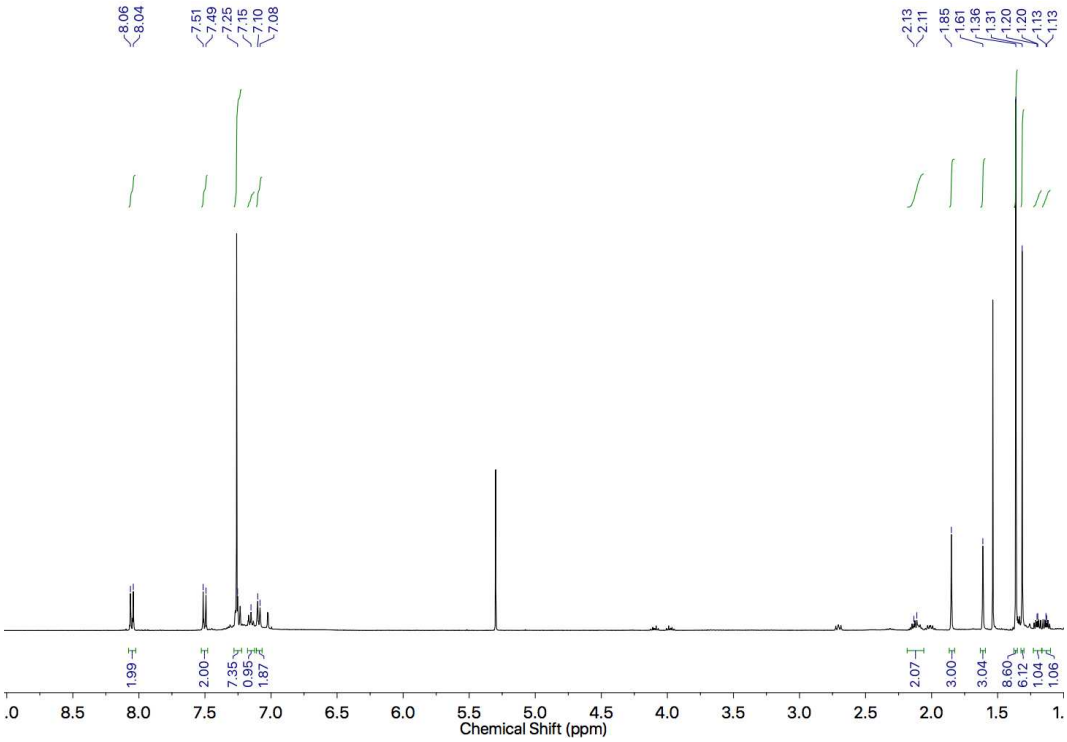

Figure 219: ^{1}H NMR (400 MHz, $CDCl_3$) of *trans*-**74n**.

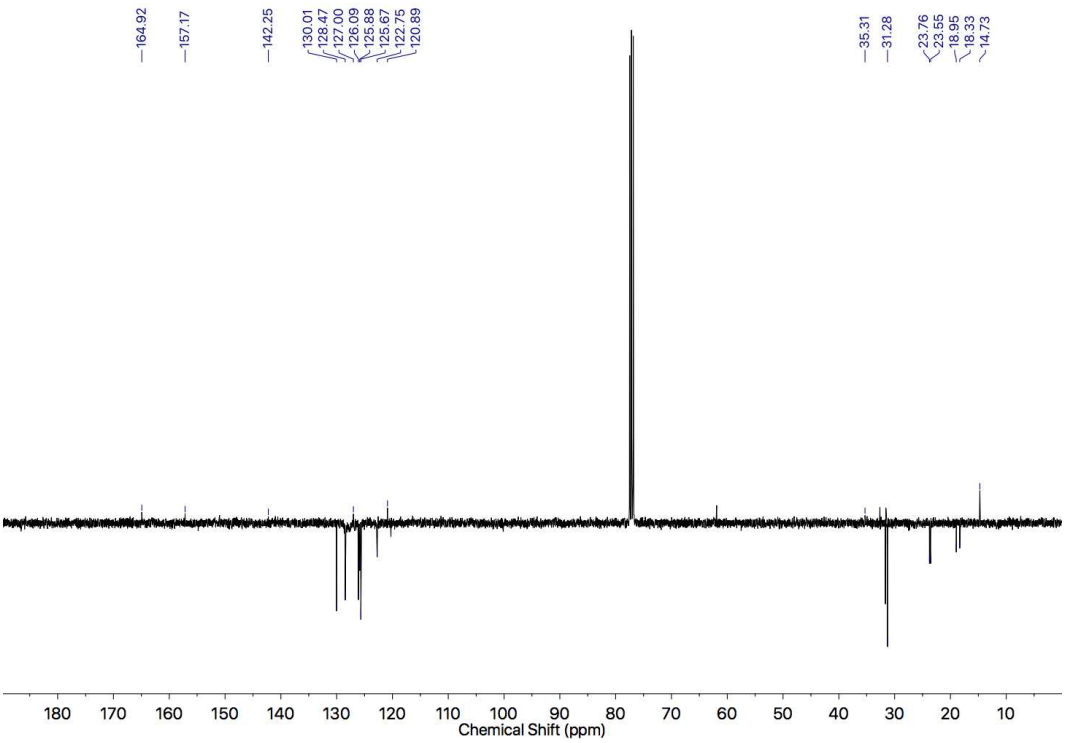

Figure 220: JMOD NMR (101 MHz, $CDCl_3$) of *trans*-**74n**.

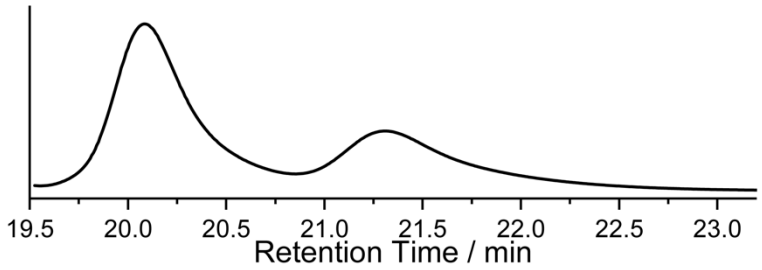

Figure 221: Chiral Stationary Phase HPLC (RegisPack, *n*-hexane-isopropanol 99 : 1, 303 K, load Et_2O, flowrate 0.25 $mLmin^{-1}$) of 65 : 35 *er trans*-**74n**. Retention times (min): 20.1 (64.7%), 21.3 (35.3%). The absolute stereochemistry of the products was not determined. The (1*S*,2*S*)-**74n** isomer is shown for illustrative purposes only.

Cyclopropanes **74o**

Catalyst	**Yield / %**	***dr***	***er*$_{cis}$**	***er*$_{trans}$**
$(Ph_3P)AuCl$[a]	77	56 : 44	1 : 1	1 : 1
(R_{mp})-**296**	73	82 : 18	71 : 29	53 : 47

cis-**74o** and *trans*-**74o** were not fully separated

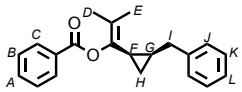

δ$_H$ ($CDCl_3$, 400 MHz) 8.04 (2H, dd, *J* = 8.5, 1.4, ***H***$_C$), 7.63-7.55 (1H, m, ***H***$_A$), 7.50-7.42 (1H, m, ***H***$_B$), 7.31-7.12 (5H, m, ***H***$_J$, ***H***$_K$, ***H***$_L$), 2.71 (1H, dd, *J* = 14.8, 6.5, ***H***$_I$), 2.59 (1H, dd, *J* = 14.7, 7.3, ***H***$_{I'}$), 1.82 (3H, s, ***H***$_E$), 1.76-1.70 (1H, m, ***H***$_F$), 1.58 (3H, s, ***H***$_D$), 1.31-1.25 (1H, m, ***H***$_G$), 0.84 (1H, dt, *J* = 8.5, 5.1, ***H***$_H$), 0.67 (1H, dt, *J* = 8.5, 5.1, ***H***$_{H'}$). **δ**$_C$ ($CDCl_3$, 101 MHz) 164.8, 141.6, 141.2, 133.2, 130.0, 129.9, 128.5, 128.4, 126.1, 122.7, 39.6, 19.8, 18.9, 18.8, 18.7, 18.3, 12.5. HR-EI-MS m/z 306.1607 [$M^{+\cdot}$] (calc. m/z for $C_{21}H_{22}O_2$ 306.1620).

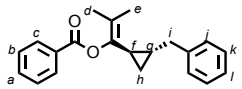

δ$_H$ ($CDCl_3$, 400 MHz) 8.11 (2H, dd, *J* = 8.4, 1.31, ***H***$_c$), 7.63-7.55 (1H, m, ***H***$_a$), 7.50-7.42 (1H, m, ***H***$_b$), 7.31-7.12 (5H, m, ***H***$_j$, ***H***$_k$, ***H***$_l$), 2.85 (1H, dd, *J* = 14.8, 6.1, ***H***$_i$), 2.50 (1H, dd, *J* = 15.0, 8.6, ***H***$_{i'}$), 2.07-1.99 (1H, m, ***H***$_f$), 1.79 (3H, s, ***H***$_e$), 1.66 (3H, s, ***H***$_d$), 1.40-1.31 (1H, m, ***H***$_g$), 0.96 (1H, ddd, *J* = 13.5, 8.8, 5.0, ***H***$_h$), 0.47 (1H, q, *J* = 5.6, ***H***$_{h'}$). **δ**$_C$ ($CDCl_3$, 101 MHz) 164.8, 142.1, 140.2, 133.3, 130.0, 129.9, 128.6, 128.5, 128.4, 125.9, 120.1, 35.9, 19.5, 18.7, 18.1, 17.4, 11.5. (***C***$_h$, ***C***$_j$, ***C***$_k$, ***C***$_l$ in 8 signal in the range 128.6-125.9). HR-EI-MS m/z 306.1607 [$M^{+\cdot}$] (calc. m/z for $C_{21}H_{22}O_2$ 306.1620).

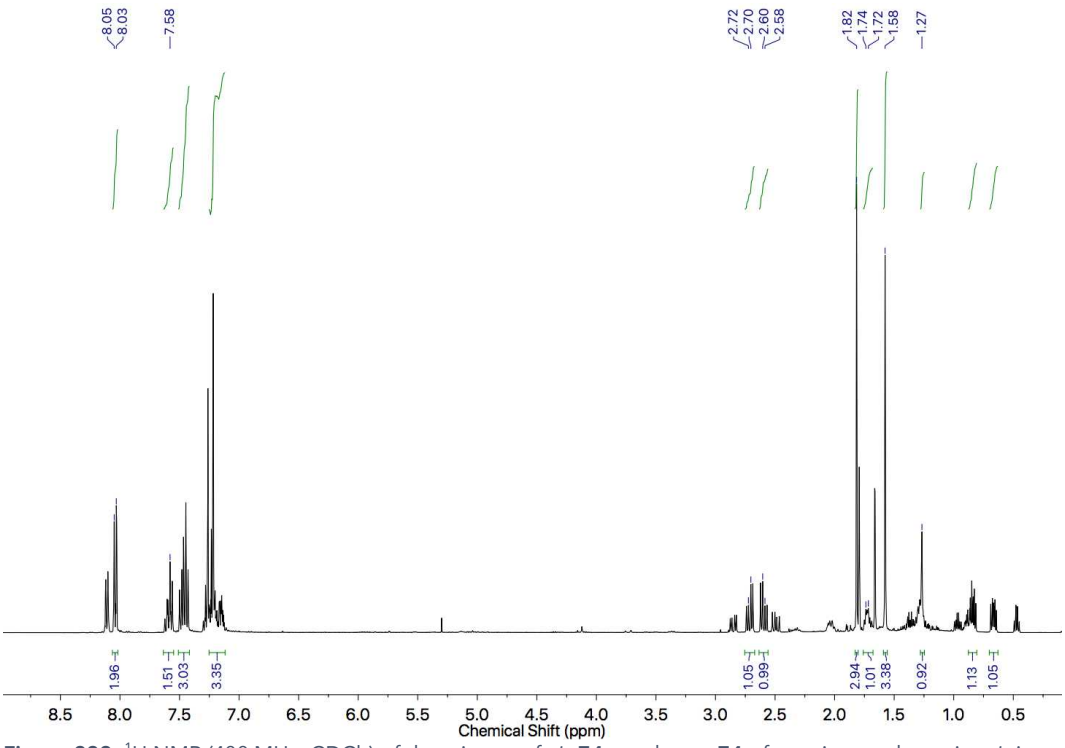

Figure 222: ^{1}H NMR (400 MHz, $CDCl_3$) of the mixture of *cis*-**74o** and *trans*-**74o** focussing on the major *cis* isomer.

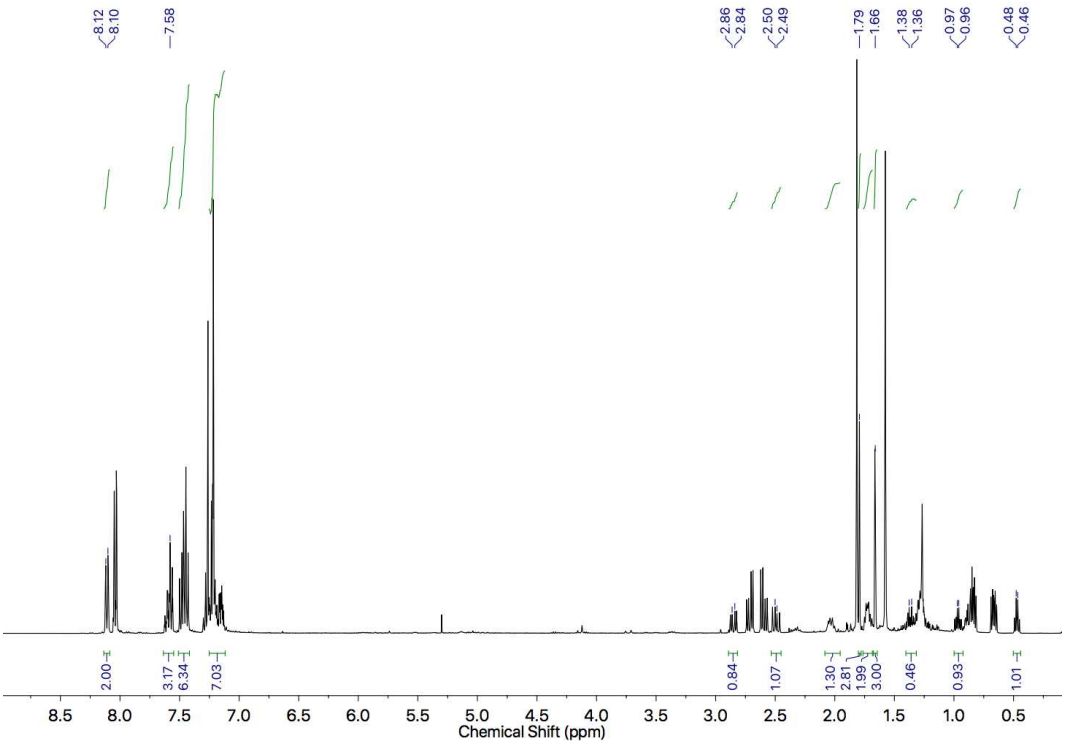

Figure 223: ^{1}H NMR (400 MHz, $CDCl_3$) of the mixture of *cis*-**74o** and *trans*-**74o** focussing on the minor *trans* isomer.

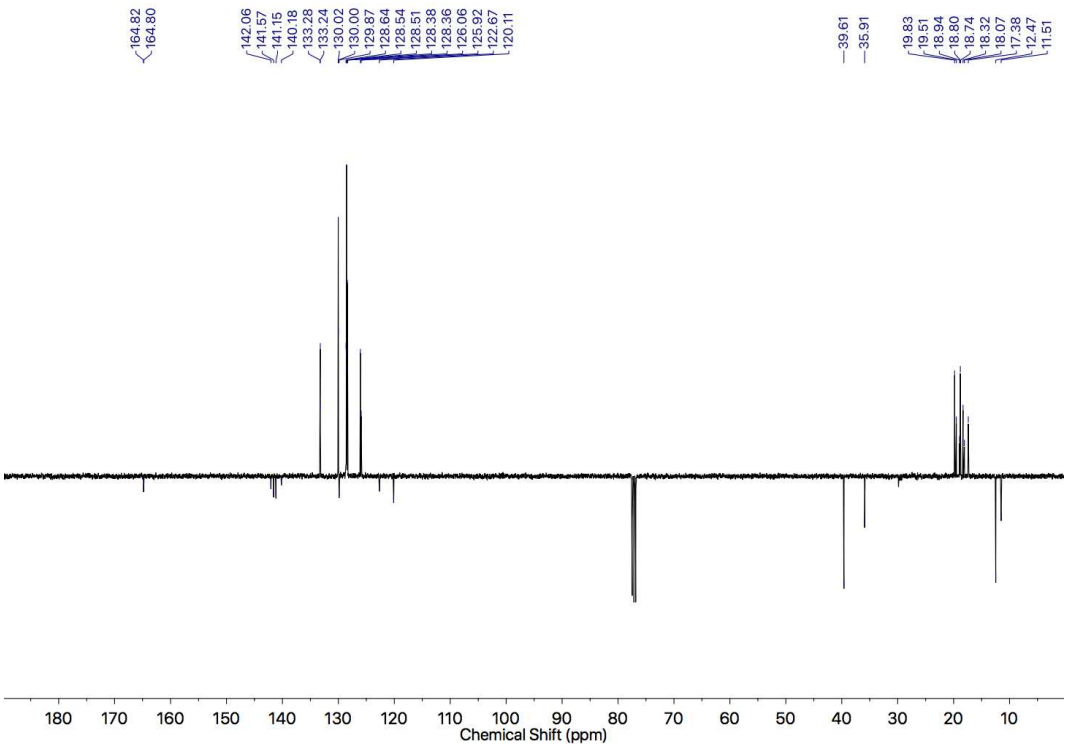

Figure 224: JMOD NMR (101 MHz, $CDCl_3$) of cyclopropanes **74o**.

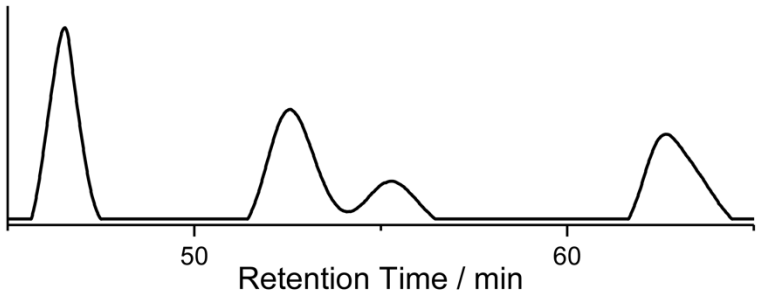

Figure 225: Chiral Stationary Phase HPLC ((S,S)Whelk, isocratic *n*-hexane-isopropanol 99.9 : 0.1, 303 K, loading solvent petrol, 5 µL injection, flowrate 0.25 $mLmin^{-1}$) 1 : 1 *er trans*-**74o** and 64 : 36 *er cis*-**74o** (*dr trans-cis* 1.8 : 1.0, not representative of the crude reaction product analysed by ^1H NMR). Retention times (min): *trans*-**74o** 46.5, *trans*-**74o** 52.6, (1*R*,2*R*)-*cis*-**74o** 55.3, (1*S*,2*S*)-*cis*-**74o** 62.6. The absolute stereochemistry of the products was not determined. (1*S*,2*R*)- **74o** is shown for illustrative purposes only.

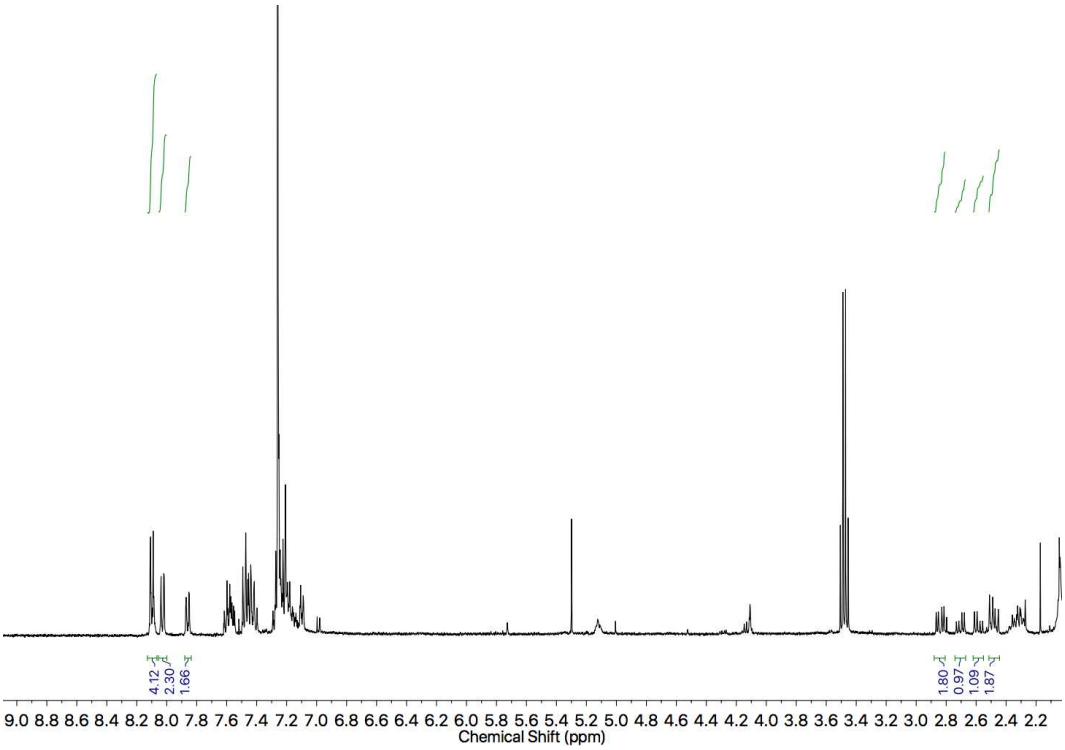

Figure 226: ^{1}H NMR (400 MHz, $CDCl_3$) of *trans*-**74o** and *cis*-**74o** diastereomer mixture (*dr* 1.8 : 1.0) from column chromatography fraction used for chiral HPLC.

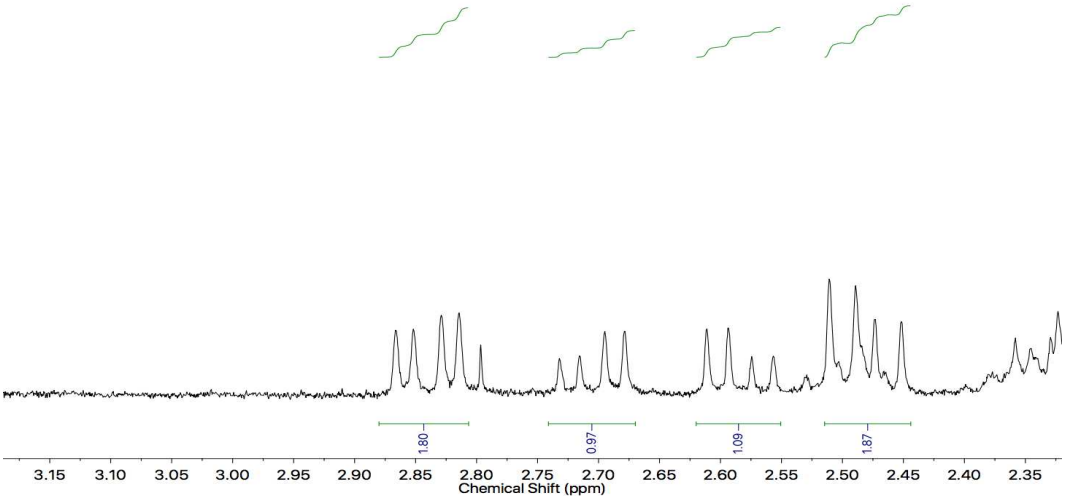

Figure 227: ^{1}H NMR (400 MHz, $CDCl_3$) of *trans*-**74o** and *cis*-**74o** diastereomer mixture (*dr* 1.8 : 1.0) from column chromatography fraction used for chiral HPLC.

Cyclopropanes **74p**

Catalyst	Yield / %	*dr*	er_{cis}	er_{trans}
$(Ph_3P)AuCl^a$	62	90 : 10	1 : 1	1 : 1
(R_{mp})-**296**	48	94 : 6	71 : 29	73 : 27

Cis-**74p**

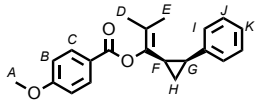

δ$_H$ ($CDCl_3$, 400 MHz) 7.81 (2H, dt, *J* = 9.0, 2.4, ***H***$_C$), 7.24 (2H, br. dd, *J* = 7.7, 7.2, ***H***$_J$), 7.18 (1H, tt, *J* = 7.2, 1.5, ***H***$_K$), 7.10 (2H, dd, *J* = 7.6, 1.6, ***H***$_I$), 6.89 (2H, dt, *J* = 9.0, 2.4, ***H***$_B$), 3.87 (3H, s, ***H***$_A$), 2.40-2.27 (2H, m, ***H***$_F$, ***H***$_G$), 1.63 (3H, s, ***H***$_E$), 1.46 (3H, s, ***H***$_D$), 1.26 (1H, ddd, *J* = 14.2, 8.8, 5.6, ***H***$_H$), 1.09 (1H, q, *J* = 5.9, ***H***$_{H'}$). **δ**$_C$ ($CDCl_3$, 101 MHz) 164.6, 163.6, 139.6, 138.6, 132.1, 127.8, 127.8, 125.7, 123.4, 122.3, 113.7, 55.6, 23.9, 21.6, 18.8, 17.8, 11.8. HR-EI-MS m/z 322.1556 [$M^{+\cdot}$] (calc. m/z for $C_{21}H_{22}O_3$ 322.1563).

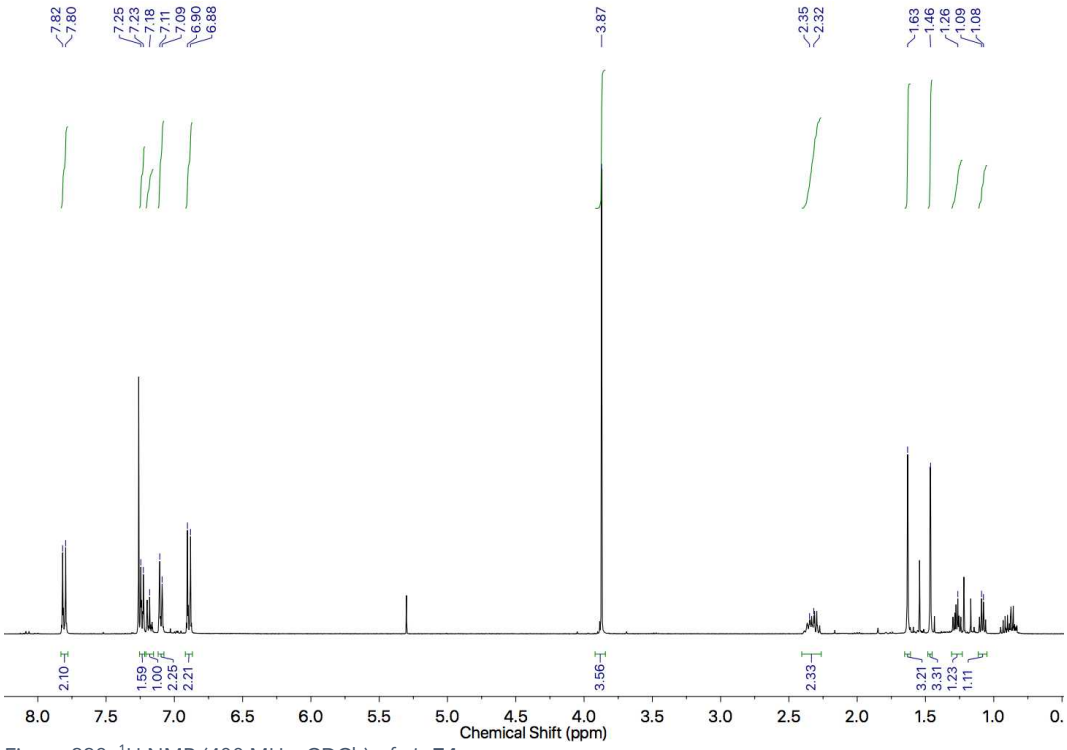

Figure 228: ^{1}H NMR (400 MHz, $CDCl_3$) of *cis*-**74p**.

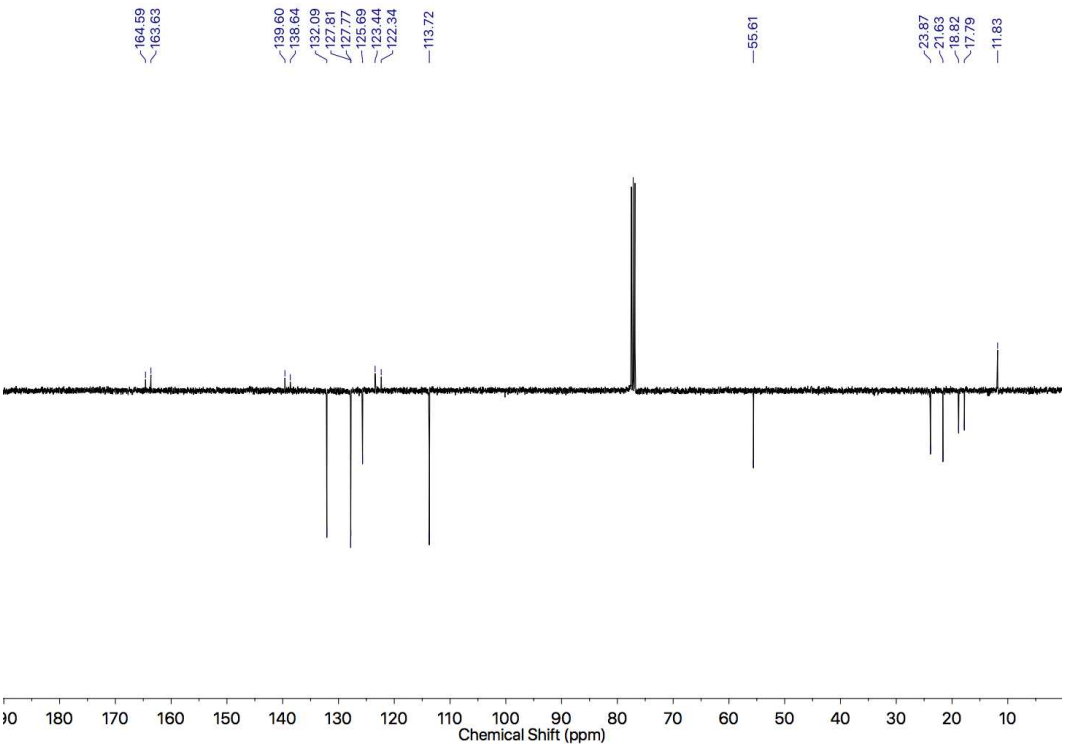

Figure 229: JMOD NMR (101 MHz, $CDCl_3$) of *cis*-**74p**.

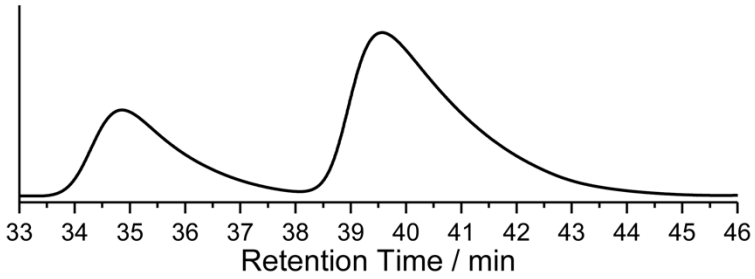

Figure 230: Chiral Stationary Phase HPLC (RegisPack, *n*-hexane-isopropanol 99 : 1, 303 K, load Et_2O, flowrate 0.25 $mLmin^{-1}$) of 70 : 30 *er cis*-**74p**. Retention times (min): 34.8 (29.6%), 35.6 (70.4%). The absolute stereochemistry of the products was not determined. The (1*S*,2*R*)-**74p** isomer is shown for illustrative purposes only.

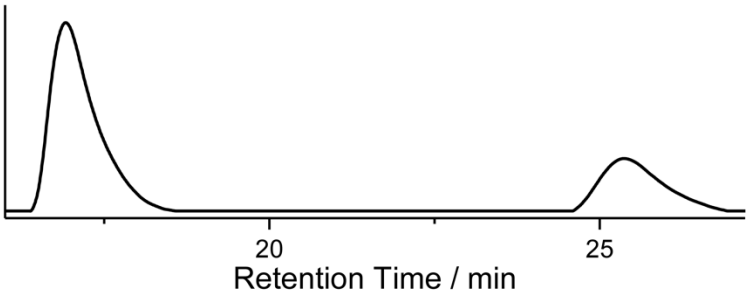

Figure 231: Chiral Stationary Phase HPLC (RegisPack, *n*-hexane-isopropanol 99 : 1, 303 K, load Et_2O, flowrate 0.25 $mLmin^{-1}$) of 72.5 : 27.5 *er trans*-**74p**. Retention times (min): 16.9 (72.5%), 25.4 (27.5%). The absolute stereochemistry of the products was not determined. The (1*S*,2*S*)-**74p** isomer is shown for illustrative purposes only.

Cis-**74q**

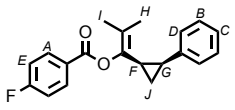

δ_H ($CDCl_3$, 400 MHz) 7.81 (2H, ddt, *J* = 8.9, 5.5, 2.5, H_A), 7.23 (2H, dd, *J* = 7.5, 1.6, H_B), 7.19 (1H, tt, *J* = 7.0, 1.5, H_D), 7.09 (2H, dd, *J* = 7.0, 1.6, H_D), 7.08 (2H, ddt, *J* = 8.8, 5.5, 2.4, H_E), 2.41-2.27 (2H, m, H_F, H_G), 1.67 (3H, s, H_H), 1.48 (3H, s, H_I), 1.30 (1H, ddd, *J* = 14.4, 8.7, 5.4, H_J), 1.09 (1H, q (ddd), *J* = 6.0, $H_{J'}$). δ_C ($CDCl_3$, 100 MHz) 167.3, 164.2 (d, *J* = 92.2), 139.5, 138.7, 132.6 (d, *J* = 9.0), 127.8, 127.8, 126.1, 125.8, 123.8, 115.6 (d, *J* = 21.9), 23.7, 21.3, 18.9, 17.8, 12.0. δ_F ($CDCl_3$, 376 MHz) -105.8 (1F, tt, *J* = 8.5, 5.5). $\delta_{F\{H\}}$ ($CDCl_3$, 376 MHz) -105.8. HR-GCMS [$M^{+\cdot}$] m/z 310.1359 (calc. for $C_{20}H_{19}FO_2$ 310.1364)

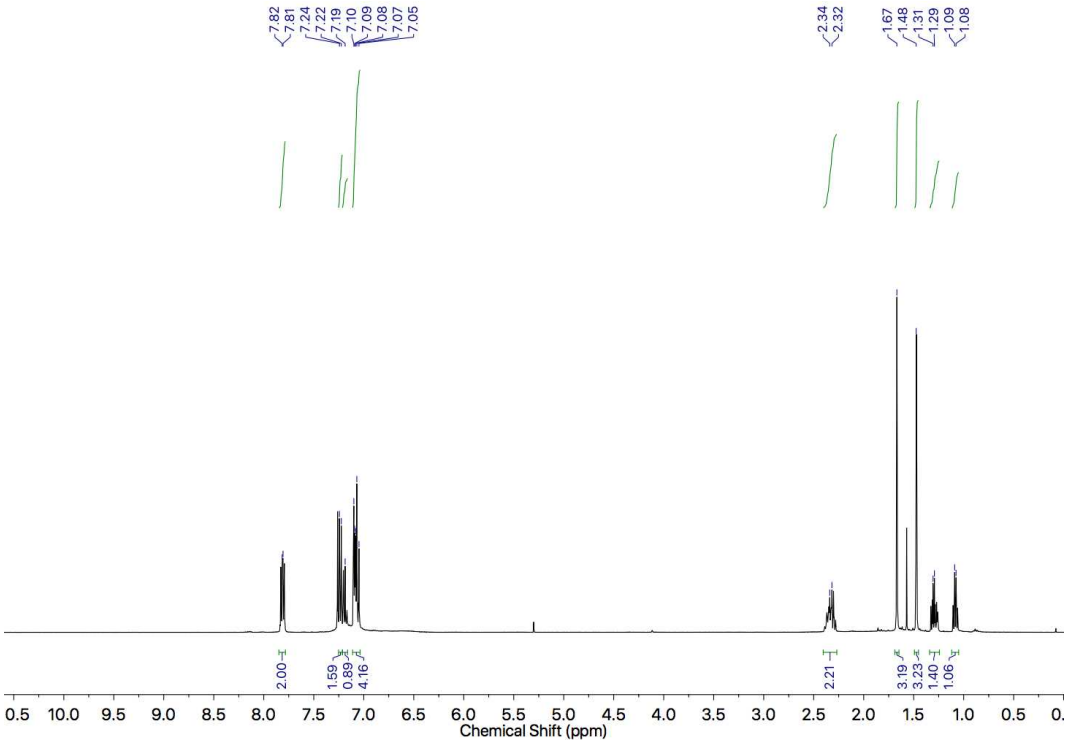

Figure 232: ^{1}H NMR (400 MHz, $CDCl_3$) of *cis*-**74q**.

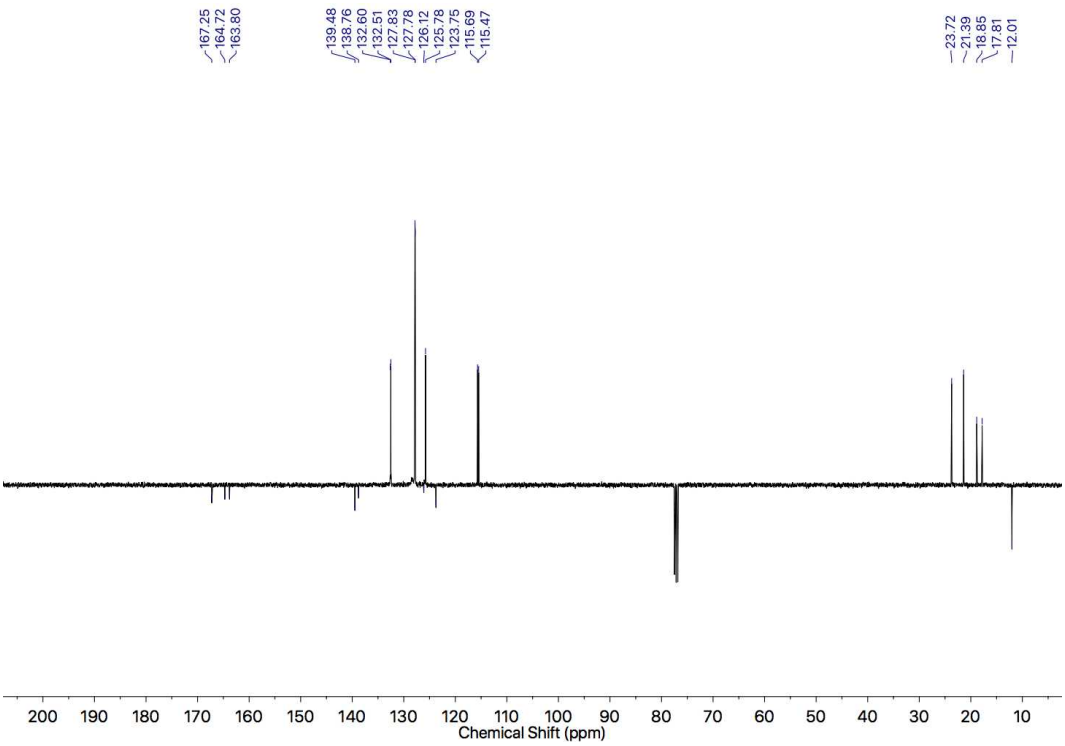

Figure 233: JMOD NMR (101 MHz, $CDCl_3$) of *cis*-**74q**.

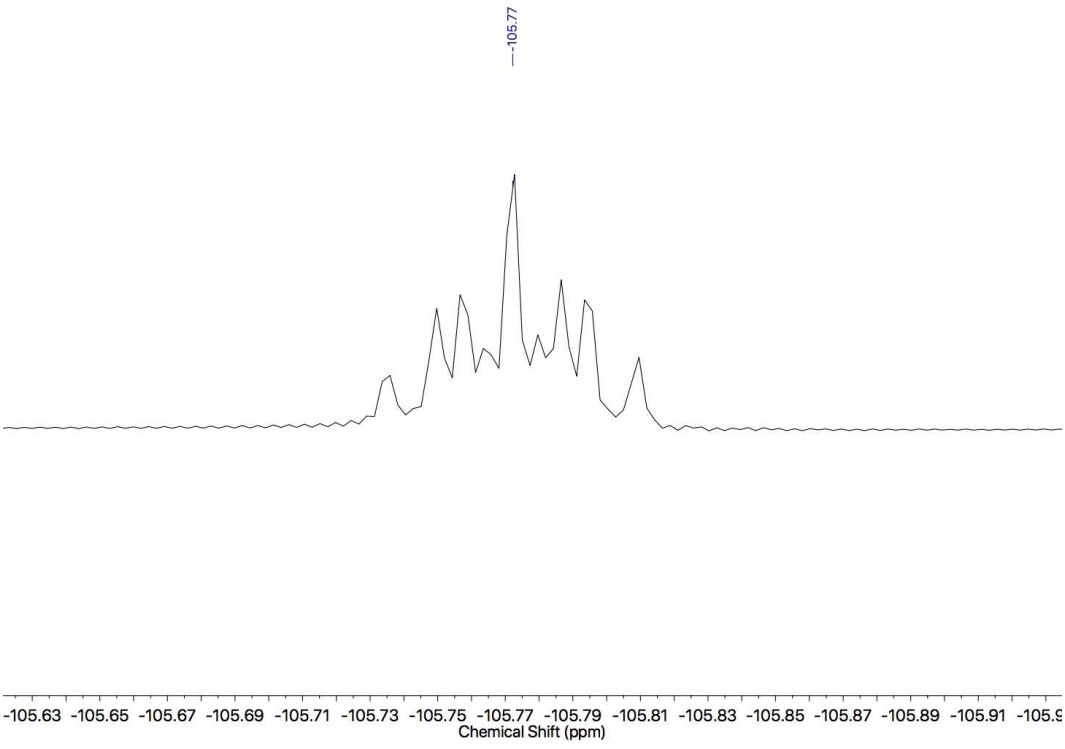

Figure 234: ^{19}F NMR (376 MHz, $CDCl_3$) of *cis*-**74q**.

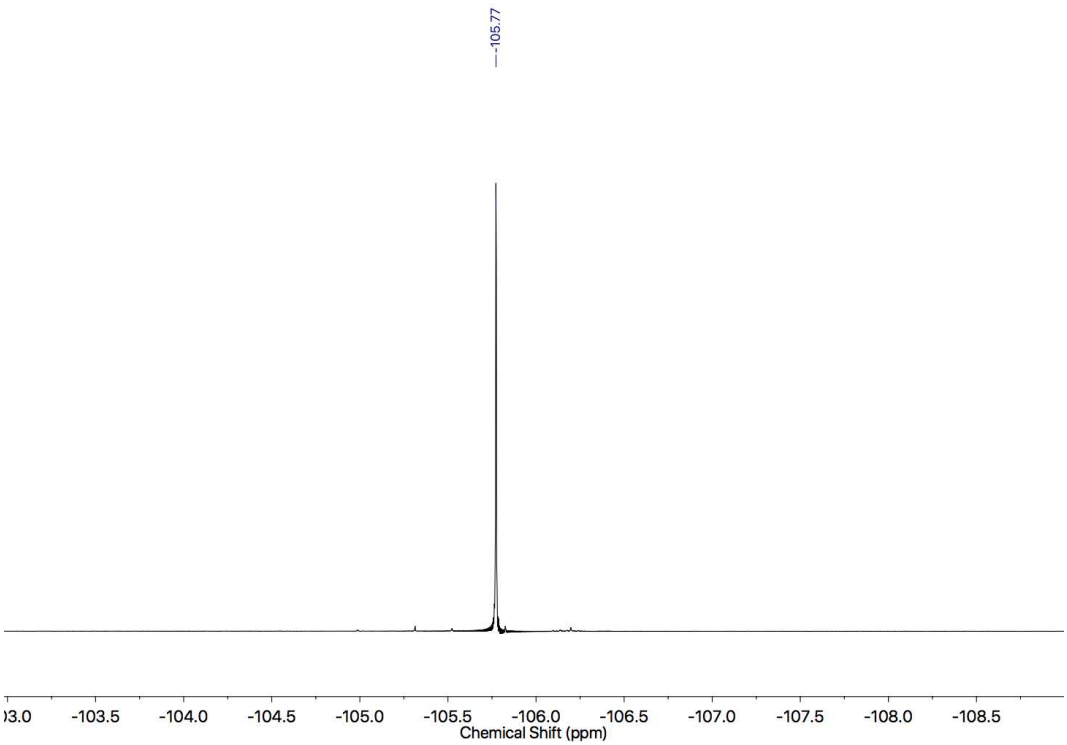

Figure 235: $^{19}F\{^{1}H\}$ NMR (376 MHz, $CDCl_3$) of *cis*-**74q**.

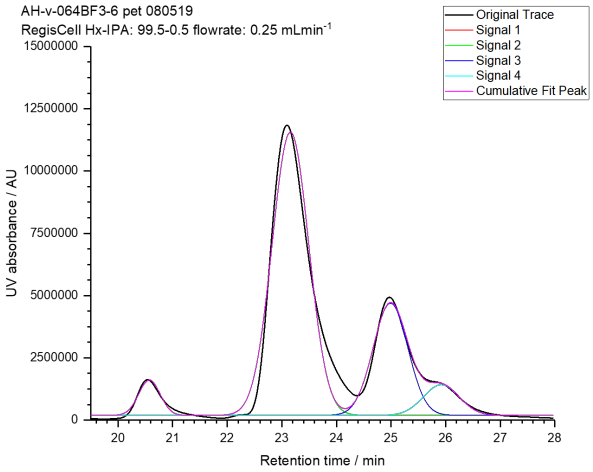

Figure 236: **74q**: (R_{mp})-**296** (77% *ee*), $AgSbF_6$, $[Cu(MeCN)_4]PF_6$, $CDCl_3$, 0.1 M, 0 °C, 6 h. NMR yield 33%, ee_{cis} 33%, ee_{trans} 6%. HPLC conditions *cis*-**74q** (23.2 min, 25.0 min), *trans*-**74q** (20.5 min, 26.0 min). RegisCell, isocratic hexane-isopropanol 99.5-0.5, flowrate 0.25 $mLmin^{-1}$.

Cis-**74r**

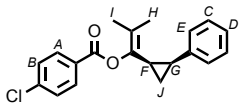

δ$_H$ ($CDCl_3$, 400 MHz) 7.71 (2H, dt, *J* = 8.6, 2.1, ***H***$_A$), 7.37 (2H, dt, *J* = 8.6, 2.1, ***H***$_B$), 7.24 (2H, tt, *J* = 7.4, 1.7, ***H***$_C$), 7.18 (1H, tt, *J* = 7.3, 1.7, ***H***$_D$), 7.08 (2H, dd, *J* = 6.8, 1.8, ***H***$_E$), 2.40-2.26 (2H, m, ***H***$_F$, ***H***$_G$), 1.67 (3H, s, ***H***$_H$), 1.46 (3H, s, ***H***$_I$), 1.30 (1H, td, *J* = 8.8, 5.4, ***H***$_J$), 1.07 (1H, td, *J* = 6.1, 5.5, ***H***$_{J'}$). **δ**$_C$ ($CDCl_3$, 100 MHz) 163.2, 139.7, 139.5, 138.8, 131.4, 128.8, 128.3, 127.9, 127.8, 125.8, 123.8, 23.7, 21.3, 18.9, 17.8, 12.1. HRMS m/z [$M^{+\cdot}$] 327.1144 (calc. for $C_{20}H_{20}ClO_2$ 327.1146)

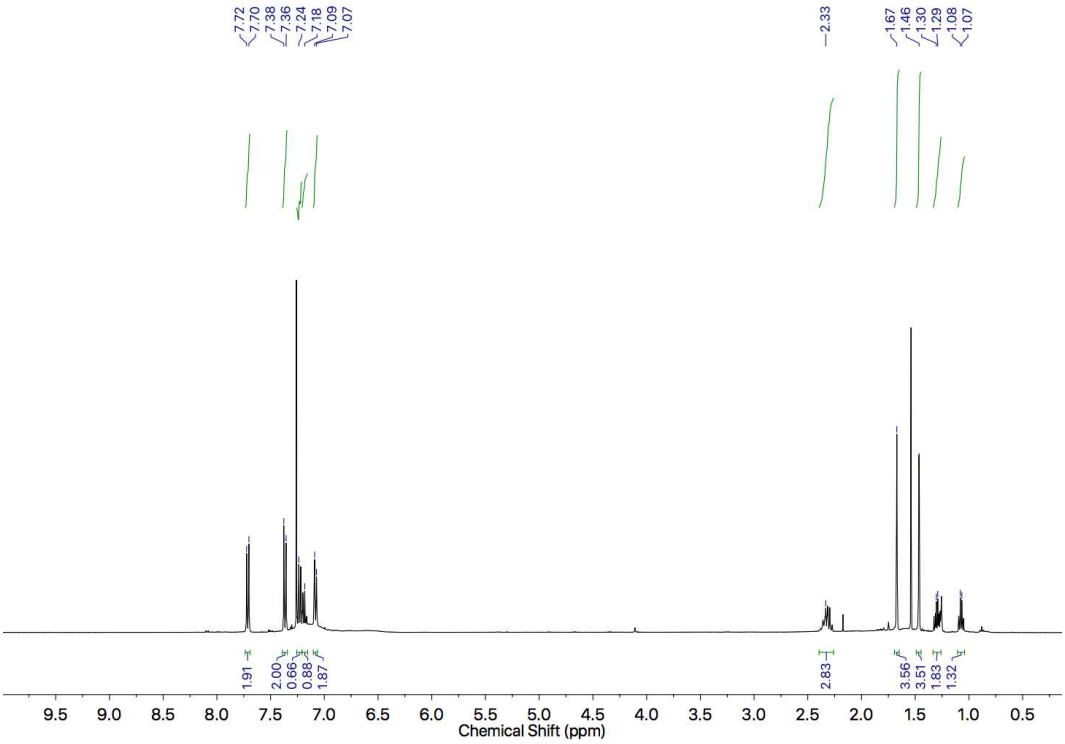

Figure 237: ^{1}H NMR (400 MHz, $CDCl_3$) of *cis*-**74r**.

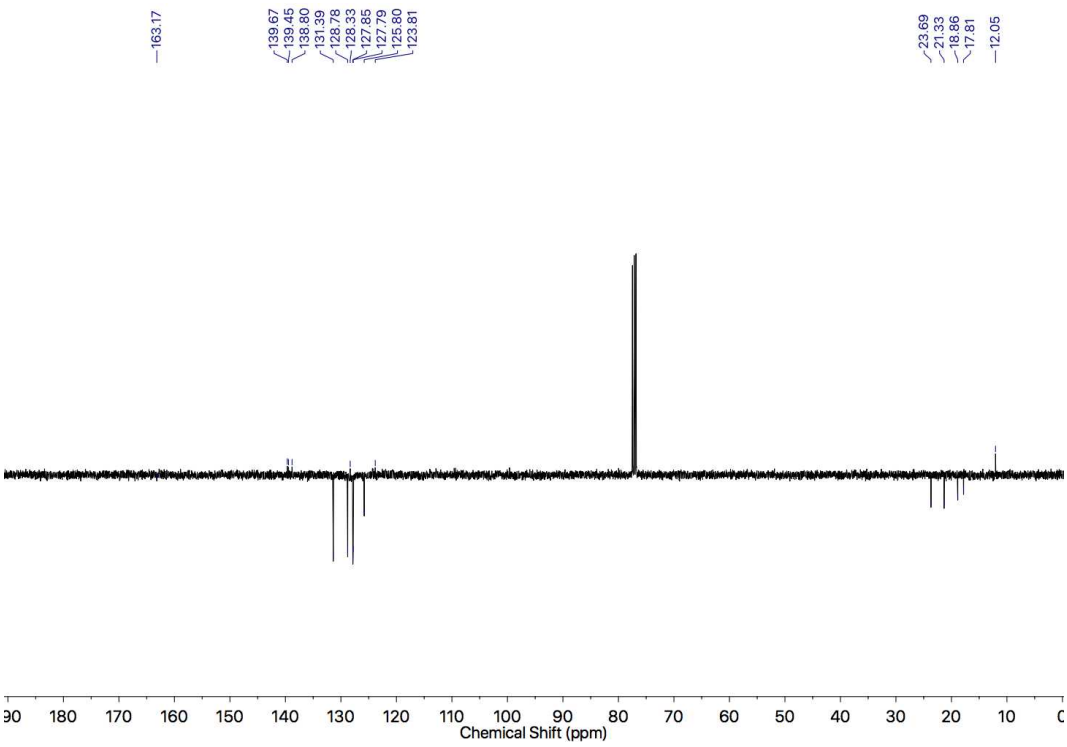

Figure 238: JMOD NMR (101 MHz, $CDCl_3$) of *cis*-**74r**.

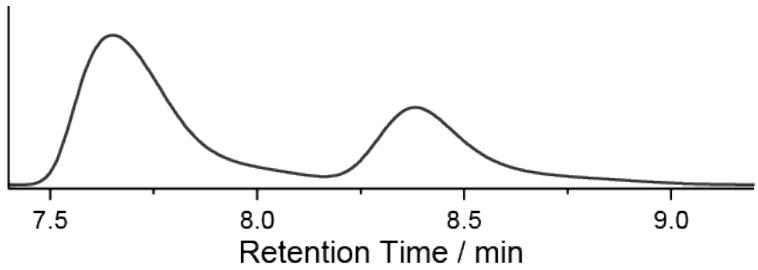

Figure 239: *cis*-**74r** – (R_{mp})-**296** (77% *ee*), $AgSbF_6$, $[Cu(MeCN)_4]PF_6$, $CDCl_3$, 0.1 M, 0 °C, 6 h. NMR yield 20%, *de* 90%, ee_{cis} 10%, ee_{trans} 24%. HPLC conditions *cis*-**74r** 13.6 min (10518392, 67.9%), 15.0 min (4980712, 32.1%). RegisPack, isocratic hexane-isopropanol 99.5-0.5, flowrate 0.50 $mLmin^{-1}$.

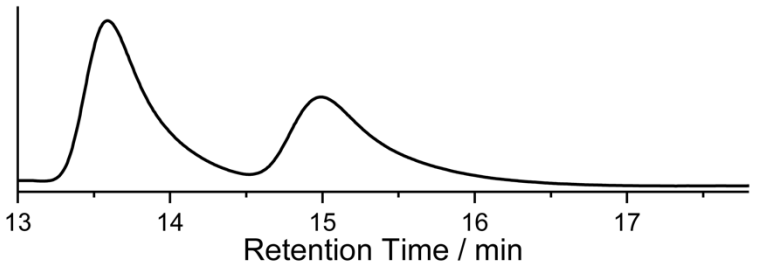

Figure 240: *Trans*-**74r** – (R_{mp})-**296** (77% *ee*), $AgSbF_6$, $[Cu(MeCN)_4]PF_6$, $CDCl_3$, 0.1 M, 0 °C, 6 h. NMR yield 20%, *de* 90%, ee_{cis} 10%, ee_{trans} 24%. 13.6 min (880566, 62.2%), 15.0 min (535870, 37.8%). RegisPack, isocratic hexane-isopropanol 99.5-0.5, flowrate 0.50 $mLmin^{-1}$.

Cyclopropanes **74s**

Catalyst	Yield / %	*dr*	er_{cis}	er_{trans}
$(Ph_3P)AuCl^a$	79	82 : 18	1 : 1	1 : 1
(R_{mp})-**296**	45	96 : 4	73 : 27	-

Cis-**74s**

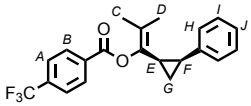

δ_H ($CDCl_3$, 400 MHz) 7.88 (2H, d, *J* = 8.2, H_B), 7.66 (2H, d, *J* = 8.4, H_A), 7.25 (2H, tt, *J* = 6.5, 2.0, H_I), 7.20 (1H, tt, *J* = 7.1, 1.5, H_J), 7.09 (2H, dd, *J* = 8.4, 1.7, H_H), 2.47-2.28 (2H, m, H_E, H_F), 1.70 (3H, s, H_D), 1.48 (3H, s, H_C), 1.33 (1H, ddd, *J* = 14.3, 8.8, 5.4, H_G), 1.09 (1H, q, *J* = 6.0, $H_{G'}$). δ_C ($CDCl_3$, 101 MHz) 163.5, 139.4, 138.9, 134.7 (q, *J* = 32.4), 134.5, 130.4, 127.9, 127.8, 125.9, 125.5 (q, *J* = 3.7), 124.0, 122.4, 23.7, 21.2, 18.9, 17.8, 12.2. δ_F ($CDCl_3$, 376 MHz) -63.4. $\delta_{F\{H\}}$ ($CDCl_3$, 376 MHz) -63.4. HR-EI-MS m/z 360.1325 [$M^{+\cdot}$] (calc. m/z for $C_{21}H_{19}O_2F_3$ 360.1332).

Trans-**74s**

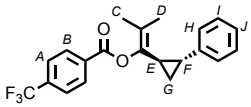

δ_H ($CDCl_3$, 400 MHz) 8.24 (2H, d, *J* = 8.2, H_B), 7.78 (2H, d, *J* = 8.2, H_A), 7.30-7.23 (2H, m, H_I), 7.17 (1H, tt, *J* = 7.5, 1.3, H_J), 7.09 (2H, dd, *J* = 7.8, 1.5, H_H), 2.13 (1H, ddd, *J* = 9.5, 7.7, 3.2, H_E), 2.03 (1H, d, *J* = 1.2, H_F), 1.87 (3H, s, H_D), 1.62 (3H, s, H_C), 1.20-1.15 (2H, m, H_G, $H_{G'}$). δ_C ($CDCl_3$, 101 MHz) 167.6, 164.5, 141.1, 135.5, 134.5, 130.5, 128.5, 126.1, 126.0, 125.8, 122.7, 121.6, 24.0, 23.3, 19.0, 18.3, 14.9. δ_F ($CDCl_3$, 376 MHz) -63.4. $\delta_{F\{H\}}$ ($CDCl_3$, 376 MHz) -63.4. HR-EI-MS m/z 360.1326 [$M^{+\cdot}$] (calc. m/z for $C_{21}H_{19}O_2F_3$ 360.1332).

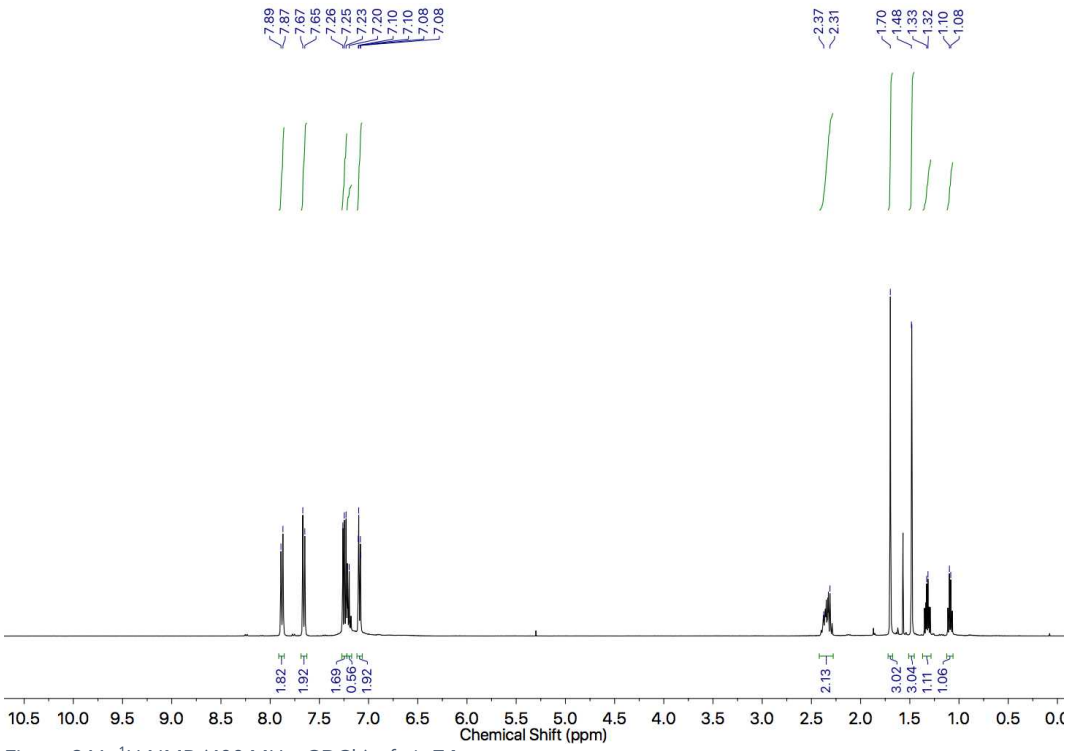

Figure 241: ^{1}H NMR (400 MHz, $CDCl_3$) of *cis*-**74s**.

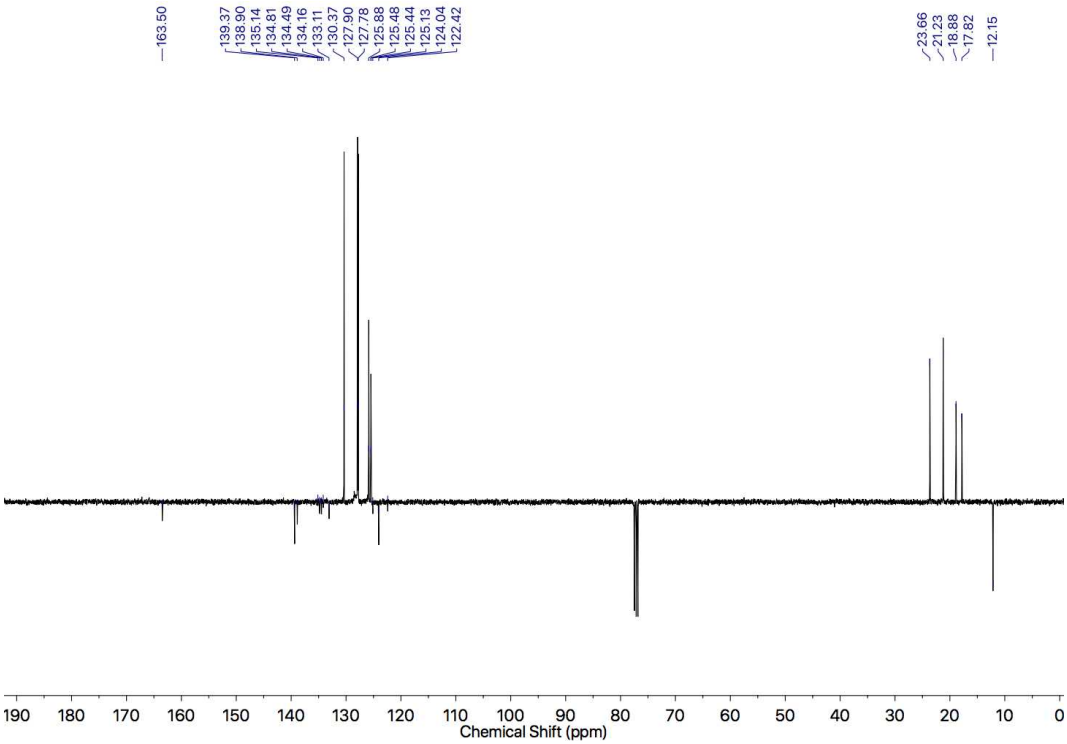

Figure 242: JMOD NMR (101 MHz, $CDCl_3$) of *cis*-**74s**.

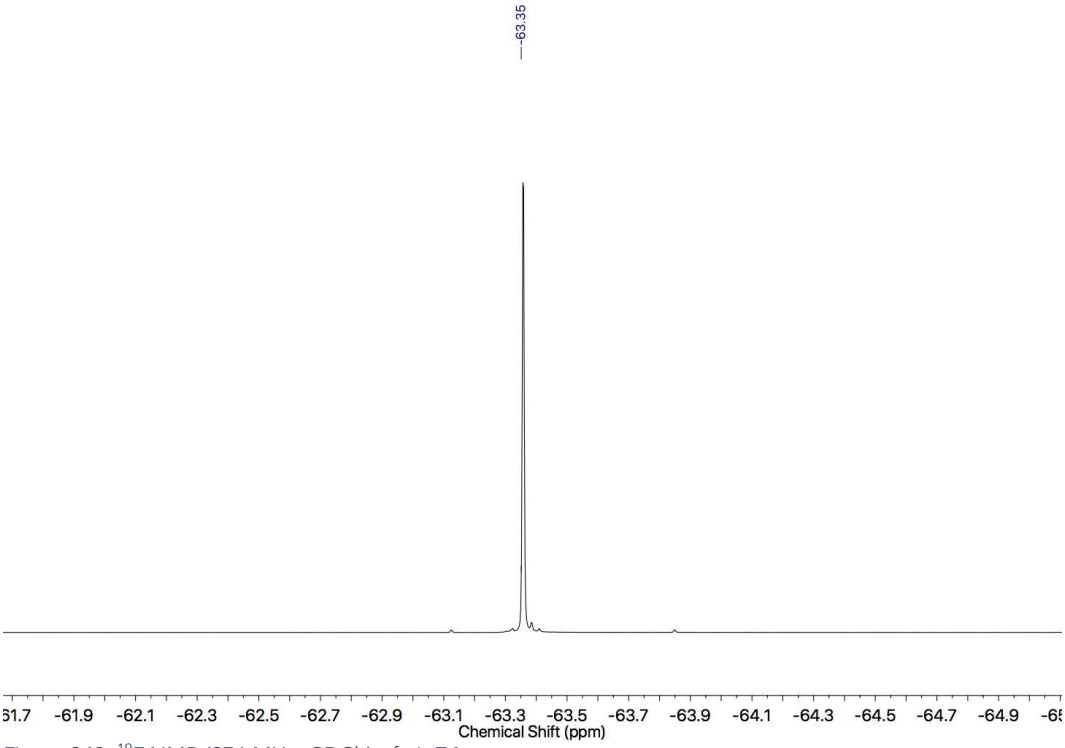

Figure 243: ^{19}F NMR (376 MHz, $CDCl_3$) of *cis*-**74s**.

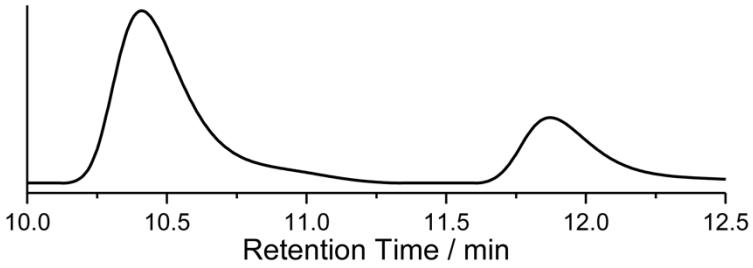

Figure 244: Chiral Stationary Phase HPLC (RegisCell, *n*-hexane-isopropanol 99.9 : 0.1, 303 K, load Et_2O, flowrate 0.75 $mLmin^{-1}$) of 73 : 27 *er cis*-**74s**. Retention times (min): 10.4 (72.6%), 11.9 (27.4%). The absolute stereochemistry of the products was not determined. The (1*S*,2*R*)-**74s** isomer is shown for illustrative purposes only.

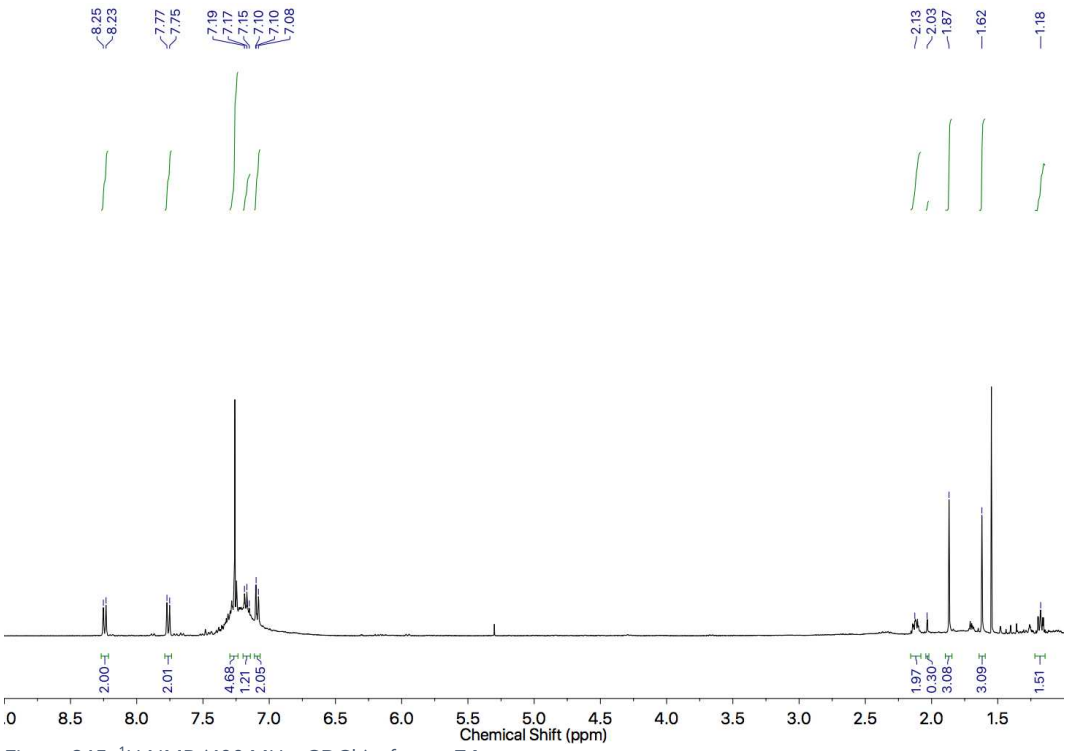

Figure 245: ^{1}H NMR (400 MHz, $CDCl_3$) of *trans*-**74s**.

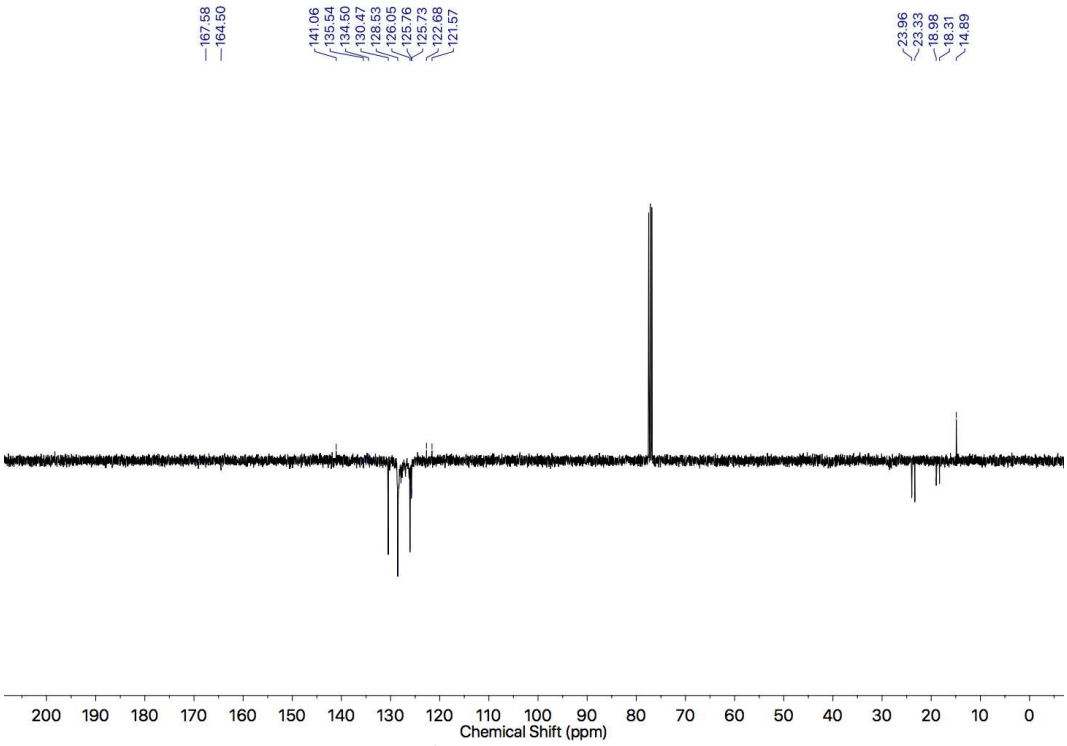

Figure 246: JMOD NMR (101 MHz, $CDCl_3$) of *trans*-**74s**.

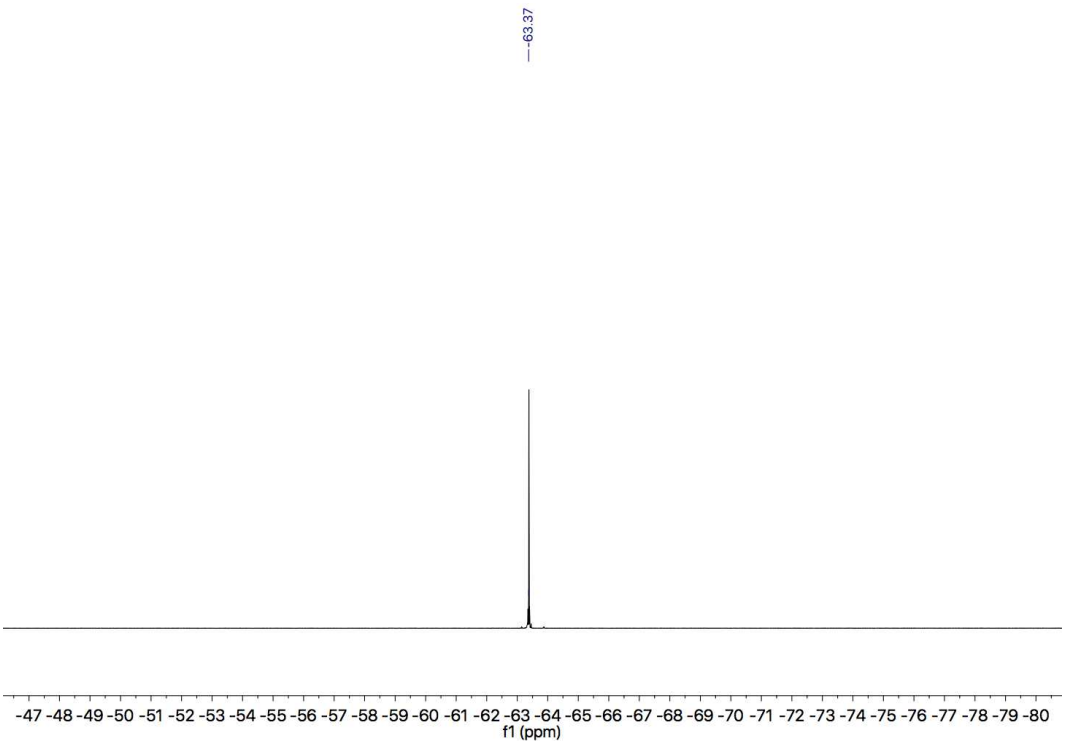

Figure 247: ^{19}F NMR (376 MHz, $CDCl_3$) of *trans*-**74s**.

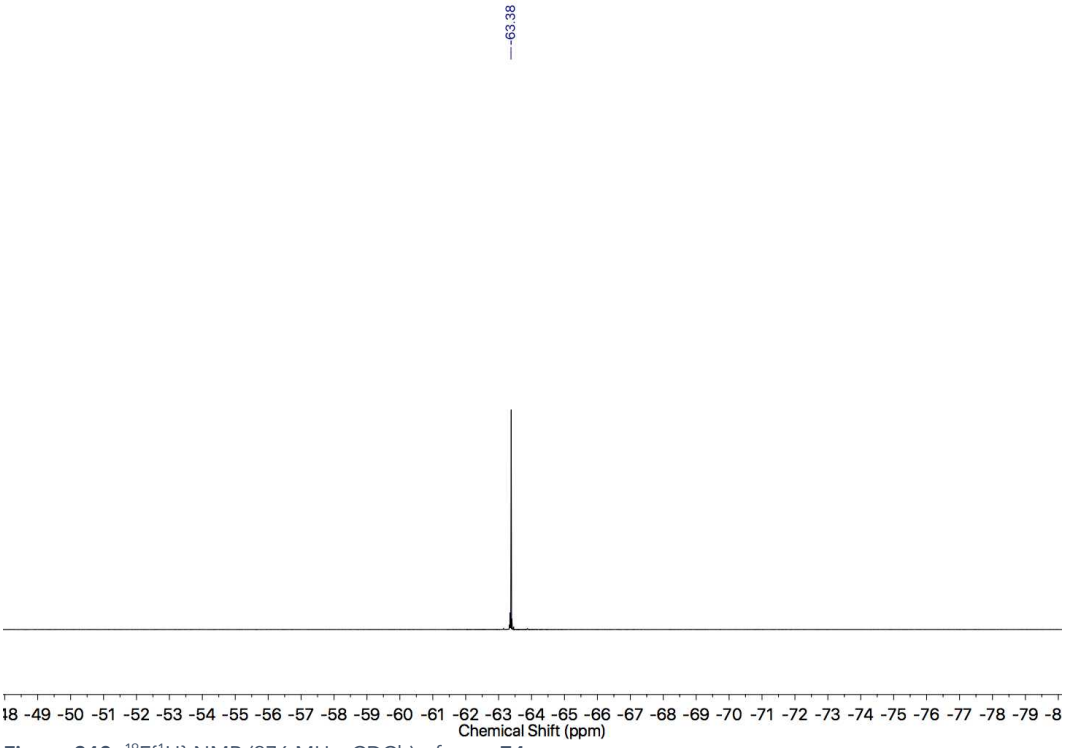

Figure 248: $^{19}F\{^1H\}$ NMR (376 MHz, $CDCl_3$) of *trans*-**74s**.

Cyclopropane *cis*-***74t***

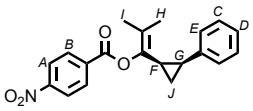

δ$_H$ ($CDCl_3$, 400 MHz) 8.21 (2H, dt, *J* = 9.0, 2.1, ***H***$_A$), 7.86 (2H, dt, *J* = 9.0, 2.1, ***H***$_B$), 7.25-7.19 (3H, m, ***H***$_C$, ***H***$_D$), 7.08 (2H, dd, *J* = 8.1, 1.9, ***H***$_E$), 2.40-2.27 (2H, m, ***H***$_F$, ***H***$_G$), 1.73 (3H, s, ***H***$_H$), 1.49 (3H, s, ***H***$_I$), 1.35 (1H, td, *J* = 8.9, 5.4, ***H***$_J$), 1.09 (1H, td, *J* = 6.3, 5.5, ***H***$_{J'}$). **δ**$_C$ ($CDCl_3$, 100 MHz) 162.7, 150.7, 139.3, 139.1, 135.3, 131.1, 128.0, 127.8, 126.0, 124.3, 123.5, 23.5, 21.1, 18.9, 17.9, 12.5. HRMS m/z [$M^{+\cdot}$] 337.1301 (calc for $C_{20}H_{19}NO_4$ 337.1309)

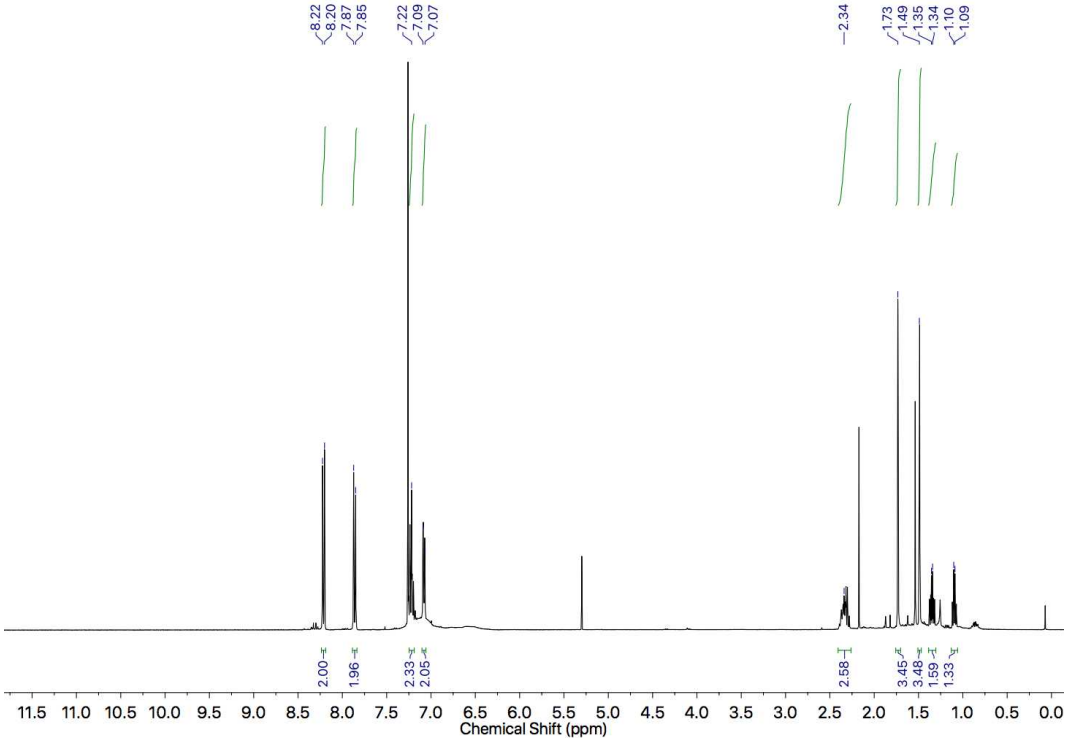

Figure 249: ^{1}H NMR (400 MHz, $CDCl_3$) of *cis*-**74t**.

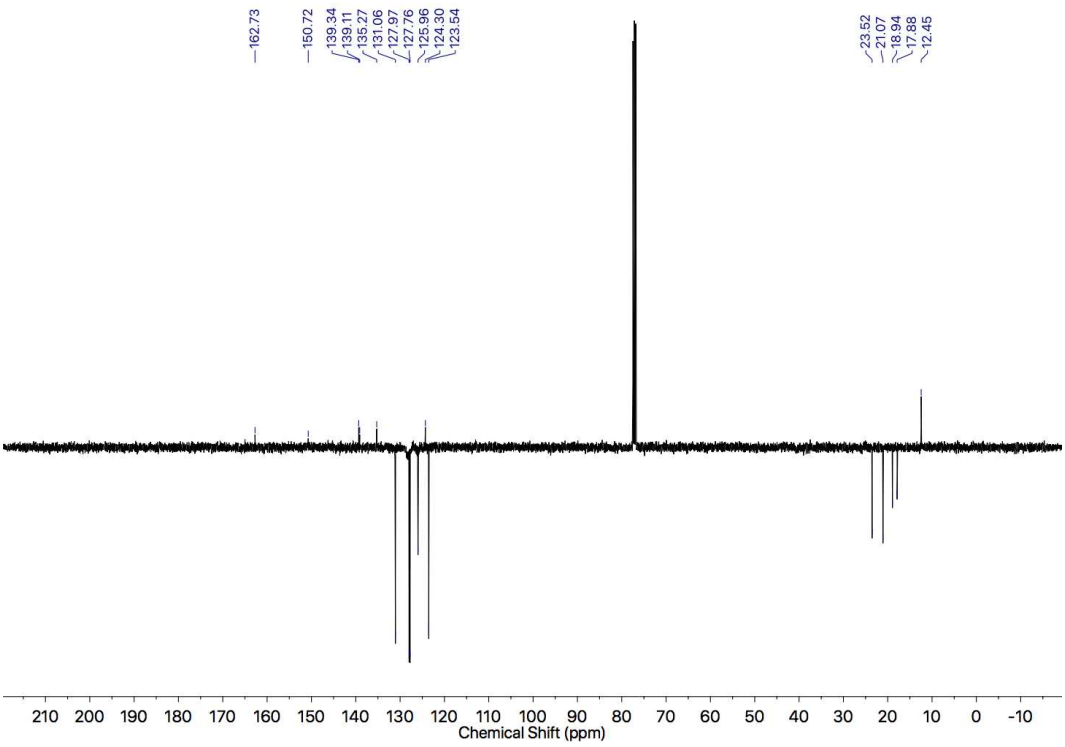

Figure 250: JMOD NMR (101 MHz, $CDCl_3$) of *cis*-**74t**.

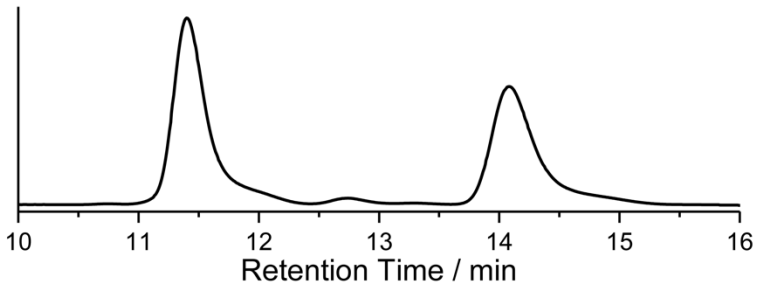

Figure 251: *cis*-**74t** – (R_{mp})-**296** (77% *ee*), $AgSbF_6$, $[Cu(MeCN)_4]PF_6$, $CDCl_3$, 0.1 M, 0 °C, 6 h. NMR yield 1%, ee_{cis} 10%. HPLC conditions *cis*-**74t** 11.4 min (2215721, 54.9%), 14.1 min (1820260, 45.1%). RegisCell, isocratic hexane-isopropanol 99-1, flowrate 0.75 $mLmin^{-1}$.

Cyclopropane **74u**

Catalyst	**Yield / %**	***dr***	***er*$_{cis}$**
$(Ph_3P)AuCl$[a]	86	4.4 : 1	1 : 1
(R_{mp})-**296**	53	92 : 2	75 : 25

Cis-**74u**

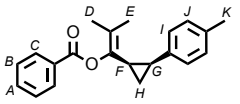

δ$_H$ ($CDCl_3$, 400 MHz) 7.88 (2H, dd, *J* = 7.9, 1.1, ***H***$_C$), 7.57 (1H, tt, *J* = 7.4, 1.3, ***H***$_A$), 7.42 (2H, tt, *J* = 7.8, 1.5, ***H***$_B$), 7.06 (2H, d, *J* = 8.1, ***H***$_J$), 7.00 (2H, d, *J* = 8.1, ***H***$_I$), 2.35 (3H, s, ***H***$_K$), 2.34-2.25 (2H, m, ***H***$_F$, ***H***$_G$), 1.66 (3H, s, ***H***$_E$), 1.49 (3H, s, ***H***$_D$), 1.26 (1H, td, *J* = 8.9, 5.4,

H_H), 1.07 (1H, dt, J = 6.7, 5.9, $H_{H'}$). δ_C ($CDCl_3$, 101 MHz) 164.8, 138.9, 136.3, 135.1, 133.1, 130.0, 130.0, 128.5, 128.4, 127.7, 123.4, 23.6, 21.3, 21.2, 18.8, 17.8, 11.7.

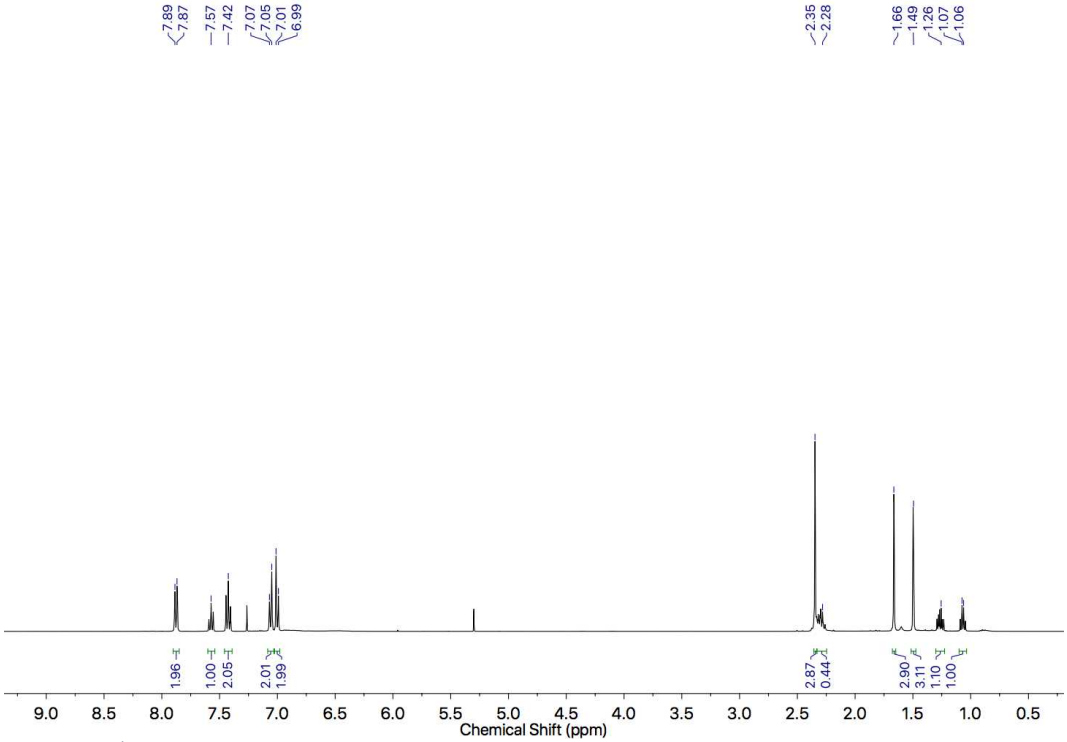

Figure 252: ^{1}H NMR (400 MHz, $CDCl_3$) of *cis*-**74u**.

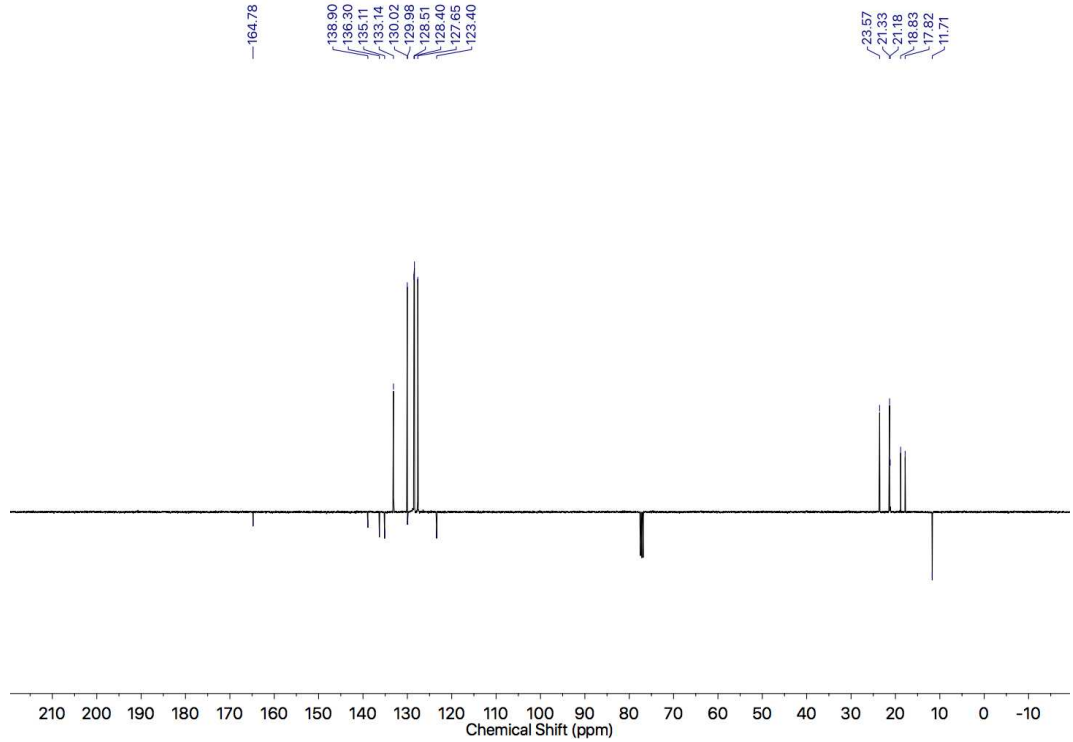

Figure 253: JMOD NMR (101 MHz, $CDCl_3$) of *cis*-**74u**.

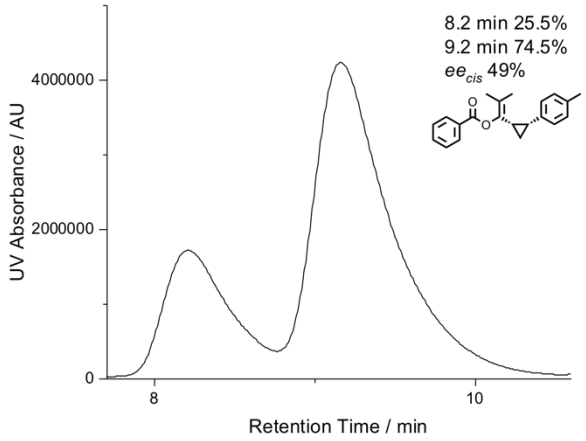

Figure 254: Chiral Stationary Phase HPLC (RegisPack, *n*-hexane-isopropanol 99.5 : 0.5, 303 K, load petrol, flowrate 0.75 mLmin^{-1}) of 25 : 75 *er cis*-**74u**. Retention times (min): 8.2, 9.2. The absolute stereochemistry of the products was not determined. The (1*S*,2*R*)-**74u** isomer is shown for illustrative purposes only.

Cyclopropane **74v**

Catalyst	**Yield / %**	***dr***	**er_{cis}**
$(Ph_3P)AuCl$[a]	66	4.5 : 1	1 : 1
(R_{mp})-**296**	25	25 : 1	73 : 27

Cis-**74v**

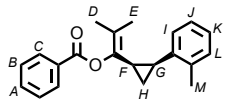

δ$_H$ ($CDCl_3$, 400 MHz) 7.68 (2H, dd, *J* = 8.3, 1.2, ***H***$_C$), 7.54 (1H, tt, *J* = 7.4, 1.2, ***H***$_A$), 7.37 (2H, dd, *J* = 7.9, 7.6, ***H***$_B$), 7.14-7.11 (2H, m, ***H***$_L$, ***H***$_K$), 7.07 (1H, dt, *J* = 8.9, 3.9, ***H***$_J$), 6.96 (2H, d, *J* = 7.4, ***H***$_I$), 2.43 (1H, td, *J* = 8.9, 5.7, ***H***$_F$), 2.34 (3H, s, ***H***$_M$), 2.28 (1H, td, *J* = 8.6, 6.8, ***H***$_G$), 1.83 (3H, s, ***H***$_E$), 1.44 (3H, s, ***H***$_D$), 1.29 (1H, td, *J* = 8.9, 5.4, ***H***$_H$), 1.18 (1H, dt, *J* = 6.2, 5.9, ***H***$_{H'}$). **δ**$_C$ ($CDCl_3$, 101 MHz) 164.4, 139.4, 138.3, 137.2, 133.1, 130.2, 129.7, 129.6, 128.3, 127.1, 125.9, 125.4, 122.1, 21.2, 20.2, 19.8, 19.0, 18.2, 10.3.

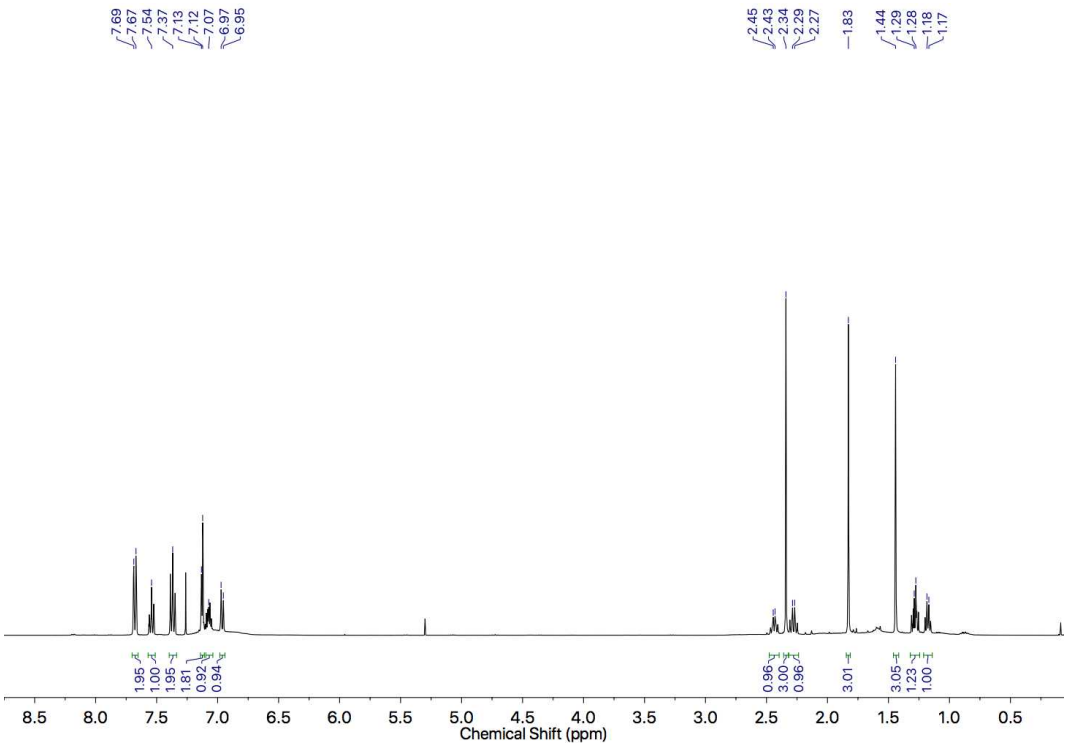

Figure 255: ^{1}H NMR (400 MHz, $CDCl_3$) of *cis*-**74v**.

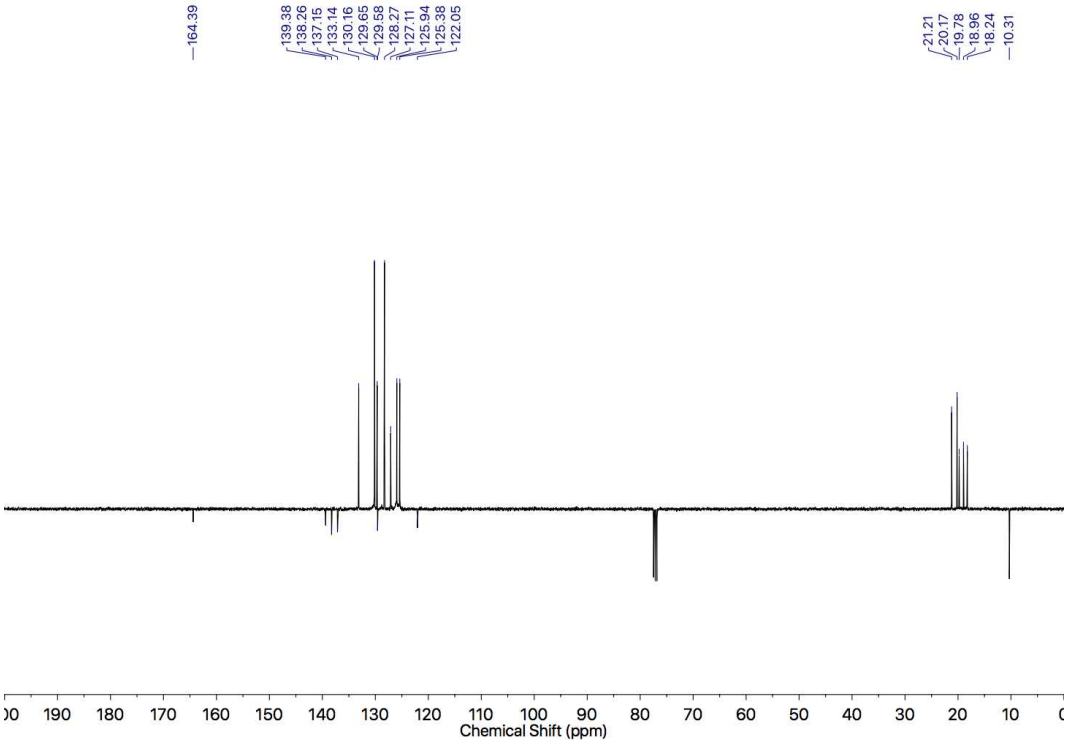

Figure 256: JMOD NMR (101 MHz, $CDCl_3$) of *cis*-**74v**.

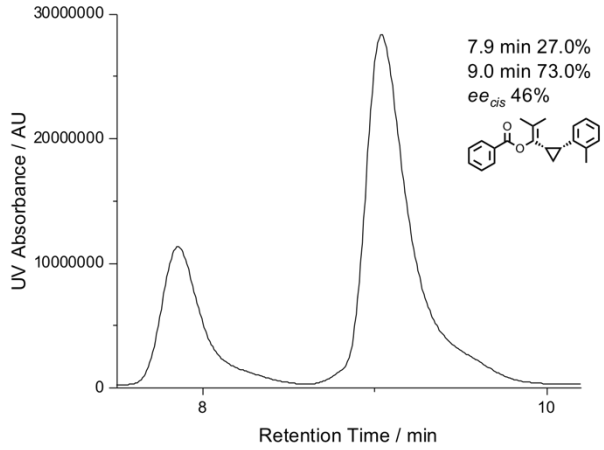

Figure 257: Chiral Stationary Phase HPLC (RegisCell, *n*-hexane-isopropanol 99.5 : 0.5, 303 K, load petrol, flowrate 0.75 mLmin^{-1}) of 27 : 73 *er cis*-**74v**. Retention times (min): 7.9, 9.0. The absolute stereochemistry of the products was not determined. The (1*S*,2*R*)-**74v** isomer is shown for illustrative purposes only.

Cyclopropanes **74w**

Catalyst	**Yield / %**	***dr***	***er*$_{cis}$**	***er*$_{trans}$**
$(Ph_3P)AuCl$	63	90 : 10	1 : 1	1 : 1
(R_{mp})-**296**	40	97 : 3	77 : 23	-

Cis-**74w**

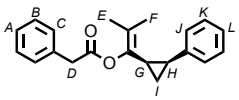

δ_H ($CDCl_3$, 400 MHz) 7.38-7.28 (5H, m, H_A, H_B, H_C), 7.21 (2H, tt, J = 7.2, 1.7, H_K), 7.15 (1H, tt, J = 7.2, 1.5, H_L), 6.95 (2H, dt, J = 6.9, 1.9, H_J), 3.61 (2H, s, H_D), 2.27-2.21 (2H, m, H_G, H_H), 1.47 (3H, s, H_F), 1.34 (3H, s, H_E), 1.13 (1H, td, J = 8.8, 5.4, H_I), 0.82 (1H, td, J = 6.4, 5.4, $H_{I'}$). δ_C ($CDCl_3$, 101 MHz) 169.8, 139.4, 138.4, 134.1, 129.5, 128.7, 127.7, 127.4, 127.3, 125.6, 123.5, 41.5, 24.1, 21.7, 18.6, 17.5, 11.4. HR-EI-MS m/z 306.1607 [$M^{+\cdot}$] (calc. m/z for $C_{21}H_{22}O_2$ 306.1620).

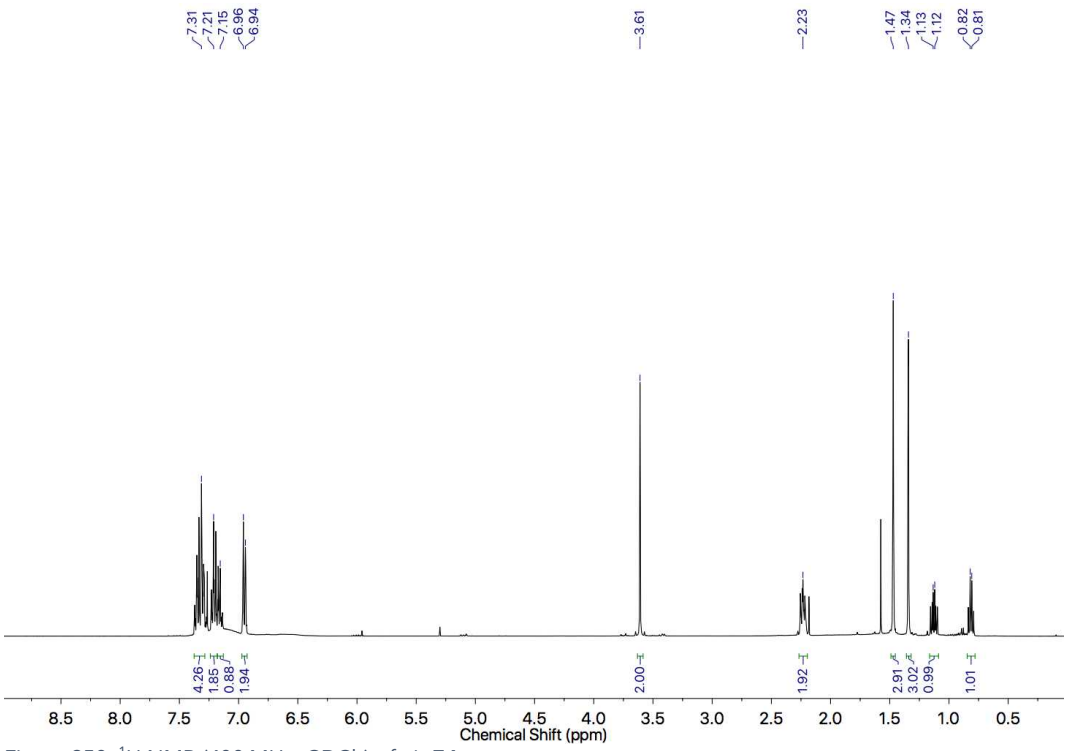

Figure 258: ^{1}H NMR (400 MHz, $CDCl_3$) of *cis*-**74w**.

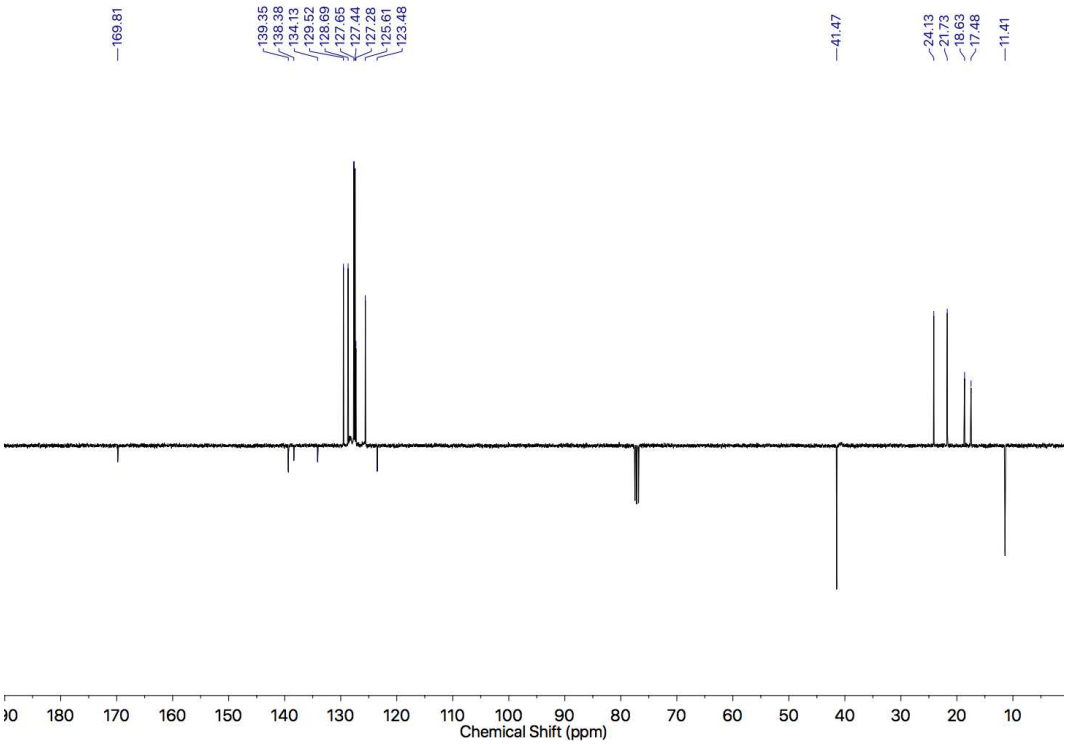

Figure 259: JMOD NMR (101 MHz, $CDCl_3$) of *cis*-**74w**.

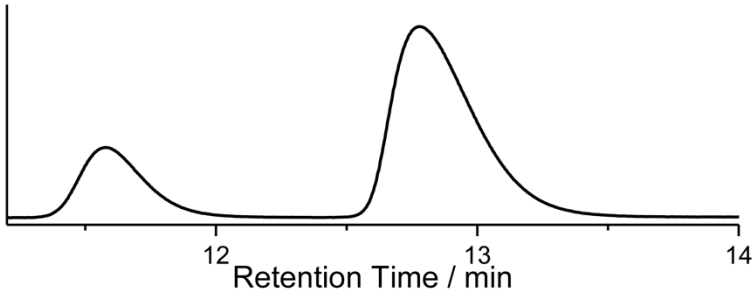

Figure 260: Chiral Stationary Phase HPLC ((*S*,*S*)Whelk, *n*-hexane-isopropanol 99.5 : 0.5, 303 K, load petrol, flowrate 0.50 mLmin^{-1}) of 77 : 23 *er cis*-**74w**. Retention times (min): 11.6 (23.1%), 12.8 (76.9%). The absolute stereochemistry of the products was not determined. The (1*S*,2*R*)-**74w** isomer is shown for illustrative purposes only.

Cyclopropanes ***74x***

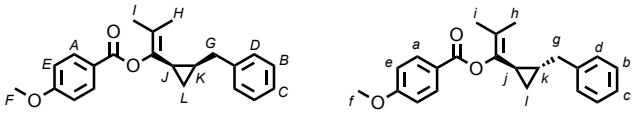

δ_H ($CDCl_3$, 400 MHz) 8.05 (2H, dt, *J* 9.0, 2.5 Hz, H_a), 7.99 (2H, tt, *J* 9.0, 2.5 Hz, H_A), 7.38-7.13 (10H, m, $H_{B\text{-}D}$, $H_{b\text{-}d}$), 6.95 (2H, dt, *J* 9.0, 2.5 Hz, H_e), 6.92 (2H, dt, *J* 9.0, 2.1 Hz, H_E), 3.88 (3H, s, H_f), 3.87 (3H, s, H_F), 2.81 (1H, dd, *J* 15.3, 6.1 Hz, H_g), 2.72 (1H, dd, *J* 14.8, 6.4 Hz, H_G), 2.57 (1H, dd, *J* 14.7, 7.0 Hz, $H_{G'}$), 2.48 (1H, dd, *J* 14.8, 8.6 Hz, H_g), 2.01 (1H, br. ddd, *J* 7.1, 6.9, 6.7 Hz, H_j), 1.80 (3H, s, H_H), 1.78 (3H, s, H_h), 1.71 (1H, br. ddd, *J* 7.9, 5.2, 4.8 Hz, H_J), 1.64 (3H, s, H_i), 1.56 (3H, s, H_I), 1.34 (1H, ddd, *J* 11.6, 5.1, 2.7 Hz, H_k), 1.27-1.23 (1H, m, H_K), 0.93 (1H, ddd, *J* 17.0, 9.2, 5.0 Hz, H_l), 0.82 (1H, ddd (dt), *J* 8.0, 4.9 Hz, H_L), 0.64 (1H, ddd (dt), *J* 8.7, 5.3 Hz, $H_{L'}$), 0.46 (1H, q, *J* 5.7 Hz, $H_{l'}$). δ_C ($CDCl_3$, 100 MHz) 164.6, 163.7, 163.7, 142.1, 141.5, 141.2, 140.1, 132.3, 132.1, 132.1, 128.5, 128.5, 128.4, 128.4, 126.1, 125.9, 122.5, 122.4, 122.2, 119.9, 113.9, 113.8, 55.6, 55.6, 39.6, 35.9, 24.0, 23.6, 19.7, 19.5, 18.9, 18.9, 18.7, 17.4, 12.4, 11.4. HRGCMS [$M^{+\cdot}$] m/z 336.1713 (calc. m/z for $C_{22}H_{24}O_3$ 336.1726).

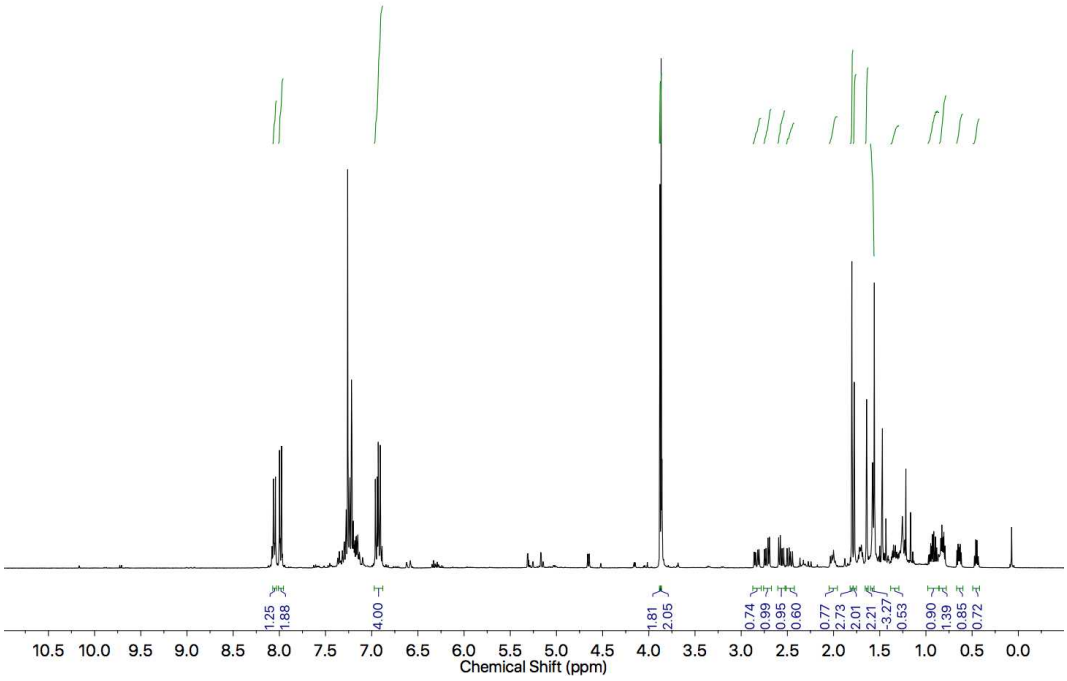

Figure 261: ^{1}H NMR (400 MHz, $CDCl_3$) of **74x**.

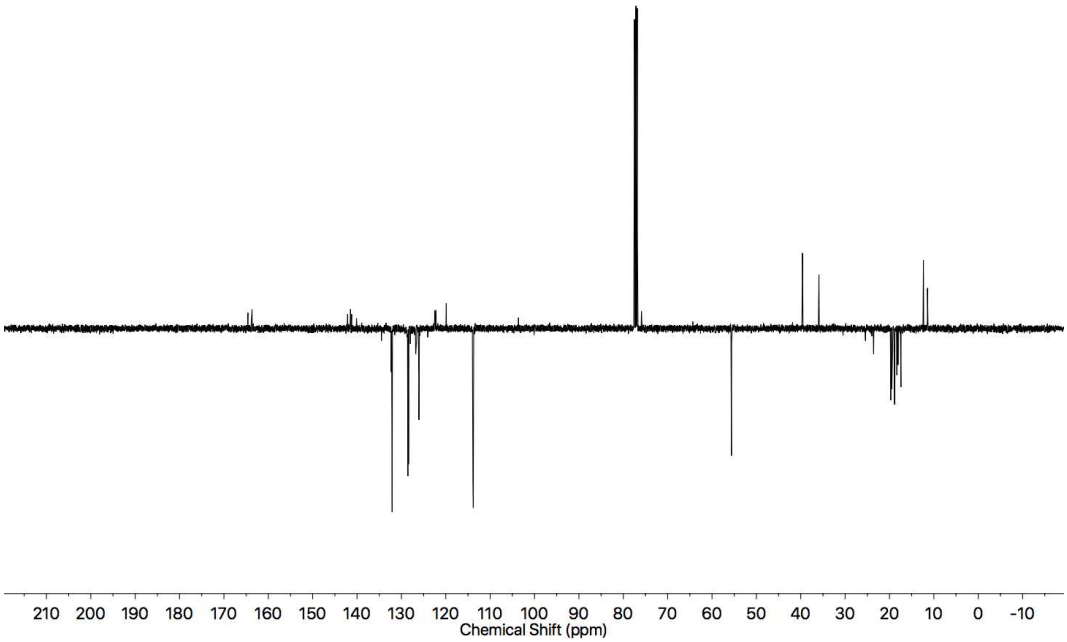

Figure 262: JMOD NMR (101 MHz, $CDCl_3$) of **74x**.

The absolute configuration of *cis*-**297** was determined by comparison to known selectivity of (*R*)-DTBM-SEGPHOS(AuCl)$_2$ by Toste *et al*. *cis*-**74a**, *cis*-**74p**, *cis*-**74s**, *cis*-**74m** were converted to ketone **297** as per the approach to Toste *et al*. Converging

HPLC traces demonstrate the matching absolute stereochemistry for (1*S*,2*R*)-**74a**, (1*S*,2*R*)-**74p**, and (1*S*,2*R*)-**74s**.

Cis-**297**

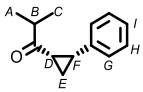

$LiAlH_4$ (50 µL, 50 µmol, 2 eq., 1 M) was added to a solution of *cis*-**74a** (8.7 mg, 25 µmol, 1 eq.) in anhydrous THF (0.2 mL) at 0 °C, then stirred at room temperature for 2 h. The reaction was quenched with MeOH, washed with 5% w/v $LiCl_{aq}$ 2(15 mL) and extracted with CH_2Cl_2 (3 x 15 mL). The combined organic phases were dried ($MgSO_4$) and reduced *in vacuo*. The residue was dissolved in CH_2Cl_2, filtered through a Celite® and the filtrate reduced *in vacuo*, yielding *cis*-**297** as a colourless oil (2.4 mg, 13 µmol, 51%). $\boldsymbol{\delta}_H$ ($CDCl_3$, 400 MHz) 7.27-7.14 (5H, m, $\boldsymbol{H}_G$, $\boldsymbol{H}_H$, $\boldsymbol{H}_I$), 2.68 (1H, ddd (app q), J = 8.3, $\boldsymbol{H}_E$), 2.59 (1H, sept., J = 6.9, $\boldsymbol{H}_B$), 2.50 (1H, ddd, J = 9.2, 7.5, 5.8, $\boldsymbol{H}_D$), 1.87 (1H, ddd, J = 7.6, 5.7, 4.9, $\boldsymbol{H}_F$), 1.31 (1H, ddd, J = 8.5, 7.5, 4.8, $\boldsymbol{H}_{F'}$), 0.99 (3H, d, J = 6.9, $\boldsymbol{H}_A$), 0.93 (3H, d, J = 6.9, $\boldsymbol{H}_C$). $\boldsymbol{\delta}_C$ ($CDCl_3$, 101 MHz) 209.4, 136.2, 129.2, 127.9, 126.7, 41.9, 28.9, 28.3, 17.9, 17.8, 11.7.

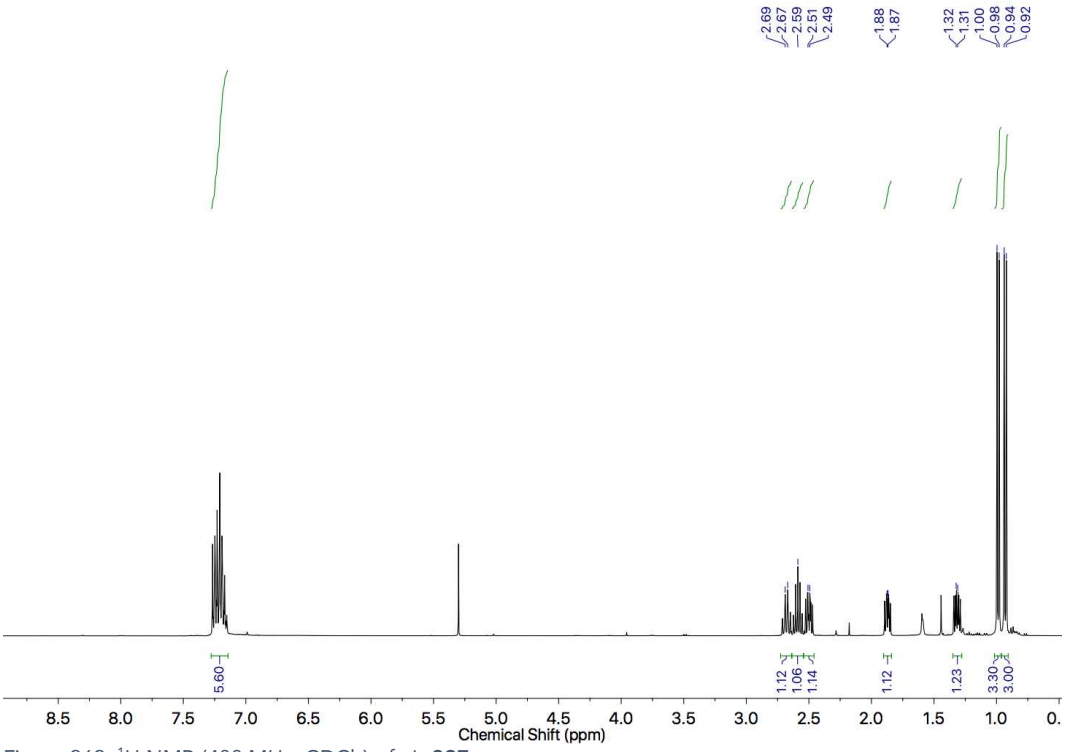

Figure 263: ^{1}H NMR (400 MHz, $CDCl_3$) of *cis*-**297**.

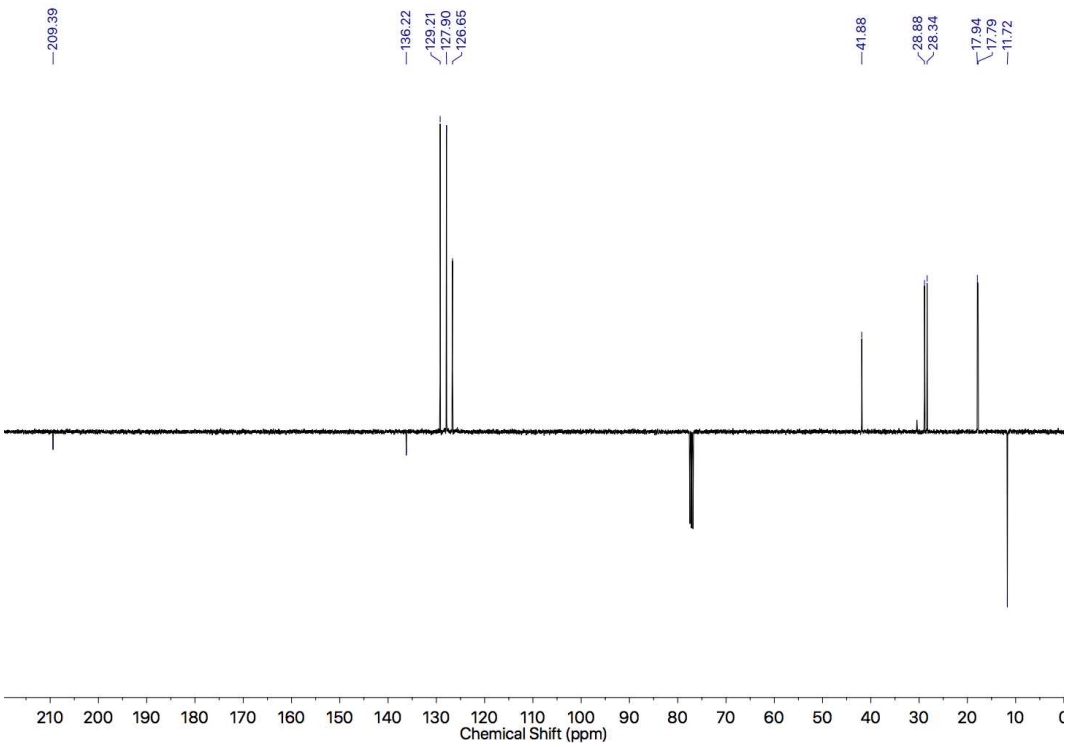

Figure 264: JMOD NMR (101 MHz, $CDCl_3$) of *cis*-**297**.

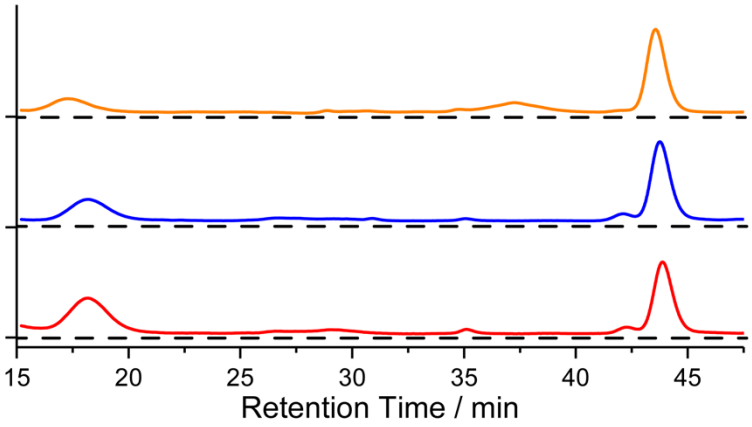

Figure 265: Chiral stationary phase HPLC ((*S*,*S*)Whelk, hexane-isopropanol 99.5 : 0.5, 303 K, load petrol, flowrate 0.25 mLmin^{-1}) of *cis*-**297** crude reaction mixtures. 220 nm UV absorbance shown. Retention times (min): 18.1, 43.7. (1) Reduction of *cis*-**74a** (*er* 22 : 78) to *cis*-**297** (apparent *er* 22 : 78 integrals 22221 (17.3 min) : 81636 (43.6 min)). (2) Reduction of *cis*-**74s** (*er* 27 : 73) to *cis*-**297** (apparent *er* 29 : 71 integrals 36466 (18.2 min) : 90032 (43.7 min)). (3) Reduction of *cis*-**74p** (*er* 30 : 70) to *cis*-**297** (apparent *er* 39 : 61 integrals 32137 (18.2 min) : 50259 (43.9 min)).

Cyclopropane *Cis*-***74y***

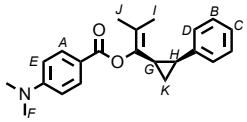

δ$_H$ ($CDCl_3$, 400 MHz) 7.78 (2H, dt, *J* = 9.1, 2.3, ***H***$_A$), 7.25 (2H, tt, *J* = 7.3, 1.4, ***H***$_B$), 7.18 (1H, tt, *J* = 7.3, 1.2, ***H***$_C$), 7.11 (2H, dd, *J* = 7.8, 1.3, ***H***$_D$), 6.64 (2H, dt, *J* = 9.1, 2.3, ***H***$_E$), 3.06 (3H, s, ***H***$_F$), 2.40-2.25 (2H, m, ***H***$_G$, ***H***$_H$), 1.60 (3H, s, ***H***$_I$), 1.46 (3H, s, ***H***$_J$), 1.25 (1H, dt,

J = 5.5, 3.5, $\boldsymbol{H}_K$), 1.09 (1H, td, J = 6.3, 5.5, $\boldsymbol{H}_{K'}$). $\boldsymbol{\delta}_C$ ($CDCl_3$, 100 MHz) 165.3, 153.6, 139.8, 138.5, 131.8, 127.8, 127.7, 125.6, 123.0, 116.7, 110.8, 40.2, 24.0, 21.9, 18.8 , 17.8, 11.7. HRMS m/z [$M^{+\cdot}$] 335.1879 (calc. for $C_{22}H_{25}NO_2$ 335.1880).

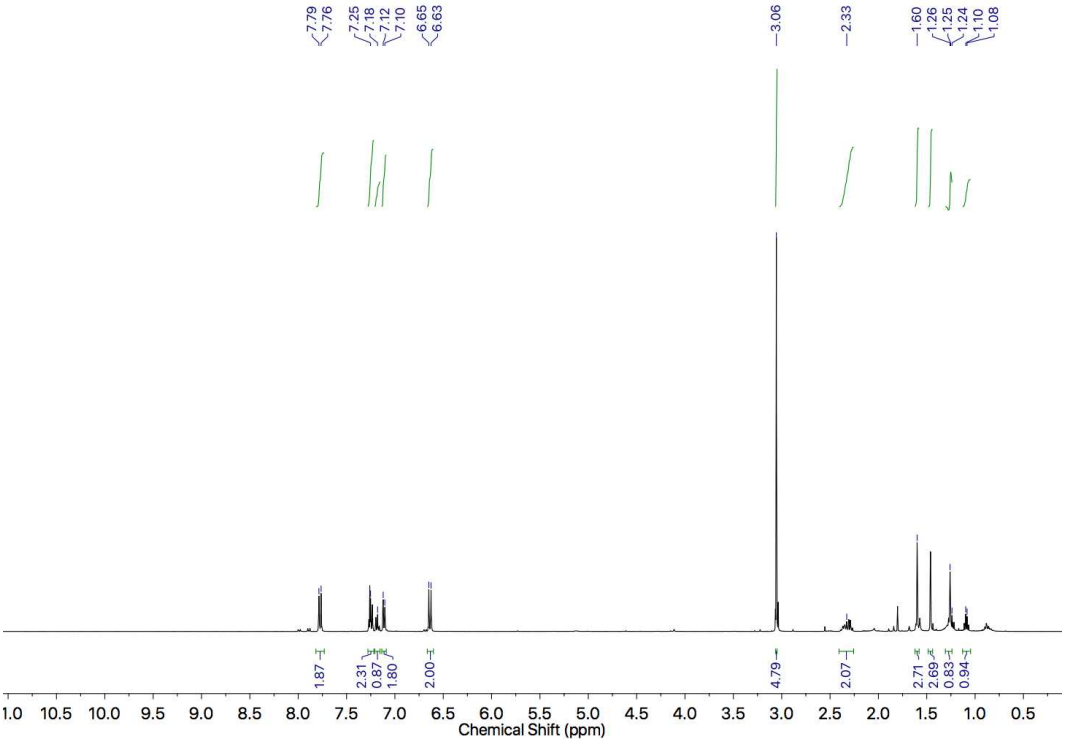

Figure 266: ^{1}H NMR (400 MHz, $CDCl_3$) of *cis*-**74y**.

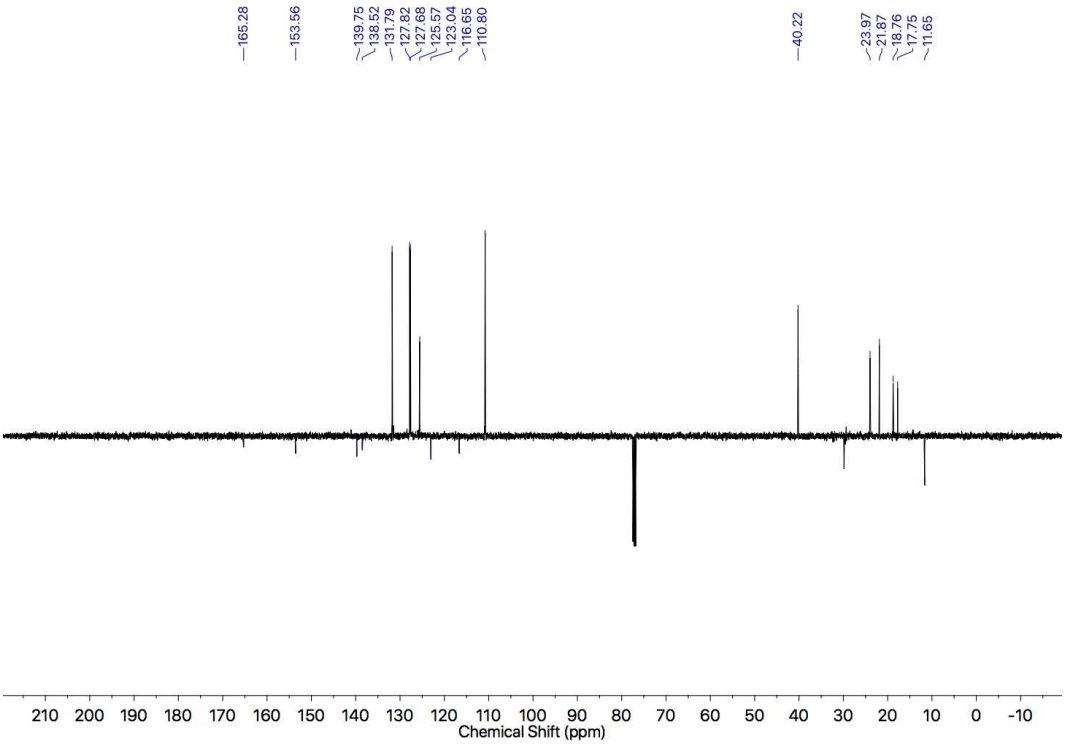

Figure 267: JMOD NMR (101 MHz, $CDCl_3$) of *cis*-**74y**.

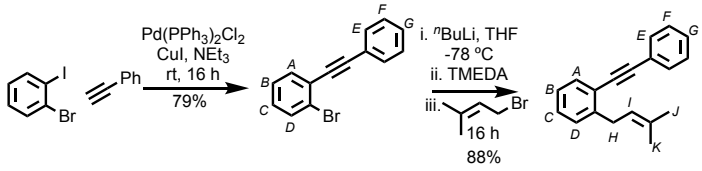

A dry CEM MW vial was charged with $Pd(PPh_3)_2Cl_2$ (31 mg, 0.044 mmol, 0.025 eq.) and CuI (17 mg, 0.088 mmol, 0.050 eq.) and purged with nitrogen. 1-Bromo-2-iodobenzene (500 mg, 1.77 mmol, 1.0 eq.) and phenylacetylene (181 mg, 1.77 mmol, 1.0 eq.) were added in degassed NEt_3 (7 mL), and the reaction stirred at room temperature for 16 h. The reaction was quenched with NH_4Cl (15 mL) and extracted with CH_2Cl_2 (3 x 20 mL). The combined organic phases were dried over $MgSO_4$ and dried in vacuo. The residue was purified by column chromatography (SiO_2, cyclohexane), yielding a pale yellow oil 1-bromo-2-(phenylethynyl)benzene (357 mg, 1.39 mmol, 79%). Spectra match literature.[81] δ_H ($CDCl_3$, 400 MHz) 7.65-7.55 (4H, m, $\mathbf{H}_F$, $\mathbf{H}_A$, $\mathbf{H}_B$), 7.40-7.34 (3H, m, $\mathbf{H}_E$, $\mathbf{H}_G$), 7.30 (1H, td, J = 7.5, 1.2, $\mathbf{H}_{B/C}$), 7.19 (1H, td, J = 8.0, 1.7, $\mathbf{H}_{B/C}$); δ_C ($CDCl_3$, 101 MHz) 133.4, 132.6, 131.8, 129.5, 128.8, 128.5, 127.2, 125.8, 125.6, 123.1, 94.1, 86.2; LRMS [M + H^+] 255.9, 257.9.

A dry CEM MW vial was charged with 1-bromo-2-(phenylethynyl)benzene (100 mg, 0.389 mmol, 1.0 eq.), purged with nitrogen, dissolved in anhydrous THF (2.0 mL), and cooled to -78 °C. ^{n}BuLi in hexanes (0.23 mL, 2.5 M, 0.583 mmol, 1.5 eq.) was added dropwise and the solution stirred for 10 minutes. TMEDA (87 µL, 0.583 mmol, 1,5 eq.) was added, and the solution stirred for a further 10 minutes. 1-bromo-3-methyl-2-butene (45 µL, 0.389 mmol, 1.0 eq.) was added and the reaction stirred at room temperature for 16 h. The reaction was quenched with NH_4Cl (20 mL), extracted in Et_2O (3 x 15 mL), and the combined organic phases dried over $MgSO_4$. The residue was purified by column chromatography (SiO_2, cyclohexane), yielding a colourless oil 1-(3-methylbut-2-en-1-yl)-2-(phenylethynyl)benzene (84.8 mg, 0.344 mmol, 88%). Spectra match literature.[81] δ_H ($CDCl_3$, 400 MHz) 7.56-7.50 (3H, m), 7.39-7.33 (3H, m), 7.28 (1H, td, J = 7.9, 1.4, $\mathbf{H}_{B/C}$), 7.26-7.22 (1H, m), 7.19 (1H, td, J = 7.2, 1.8, $\mathbf{H}_{B/C}$), 5.40 (1H, tqq, J = 7.4, 1.4, $\mathbf{H}_I$), 3.62 (2H, d, J = 7.3, $\mathbf{H}_H$), 1.76 (6H, 2 x s, $\mathbf{H}_J$, $\mathbf{H}_K$); δ_C ($CDCl_3$, 101 MHz) 143.9, 133.0, 132.3, 131.8, 131.6, 128.6, 128.6, 128.5, 128.4, 128.3, 125.9, 123.8, 122.7, 122.6, 93.4, 88.5, 32.2, 25.9, 18.1; LRMS [M + H^+] 247.2.

Compound **214a**[81]

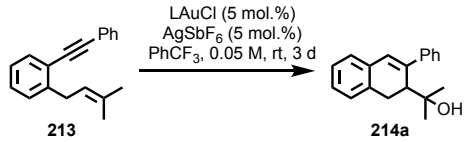

General procedure: A foil covered CEM MW vial was charged with $AgSbF_6$ (1.1 mg, 3.1 µmol, 0.05 eq.) and, in the case of (R_{mp})-**296**, $[Cu(MeCN)_4]PF_6$ (1.2 mg, 3.1 µmol, 0.05 eq.), then purged with N_2. [Au(L)(Cl)] (3.1 µmol, 0.05 eq.) was transferred in $PhCF_3$ (0.50 mL) and stirred for 5 minutes. **213** (15.3 mg, 0.062 mmol, 1 eq.) in $PhCF_3$ (0.2 mL) and H_2O (2.8 mg, 0.155 mmol, 2.5 eq.) were added. The mixture was stirred at rt for 3 days. After 3 days, the reaction was quenched with 1 drop of NEt_3, and concentrated *in vacuo*. **214a** was purified by column chromatography (SiO_2, petrol-EtOAc 0→20%) yielding a white solid. Enantiomeric excess was evaluated by chiral stationary phase HPLC. Spectra match literature.[81] δ_H (CD_2Cl_2, 400 MHz) 7.58 – 7.50 (2H, m), 7.43 – 7.34 (2H, m), 7.33 – 7.25 (1H, m), 7.21 – 7.09 (4H, m), 6.86 (1H, s), 3.32 – 3.19 (2H, m), 3.11 (1H, dd, J = 7.1, 2.3 Hz), 1.18 – 1.12 (1H, m), 0.96 (3H, s), 0.88 (3H, s). δ_C (CD_2Cl_2, 101 MHz) 143.9, 140.9, 136.0, 135.2, 129.1, 128.4, 128.1, 127.8, 127.6, 127.2, 126.9, 126.8, 75.3, 46.0, 31.3, 29.2, 28.1. LRMS [M – $H_2O^{+\cdot}$] 246.1.[81]

Table 11. Summary of reactions leading to **214a**.

	Catalyst	Yield / %	*er*
1	$(Ph_3P)AuCl$	25	50 : 50
2	(R_{mp})-**296**	18	48 : 52
3	(*R*)-DTBM-SEGPHOS®$(AuCl)_2$	9	57 : 43

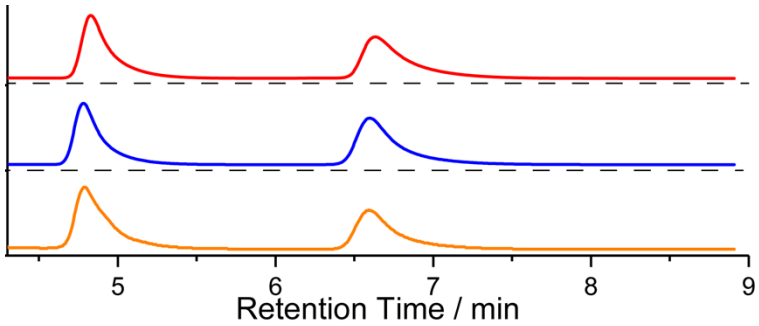

Figure 268: Entry 1 (red). Chiral Stationary Phase HPLC (RegisPack, n-hexane-isopropanol 90 : 10, 303 K, load Et_2O, flowrate 1 $mLmin^{-1}$) of 50 : 50 *er*. Retention times (min): 4.8 (12016368, 50%), 6.6 (12066647, 50%). Entry 2 (blue). Chiral Stationary Phase HPLC (RegisPack, n-hexane-isopropanol 90 : 10, 303 K, load Et_2O, flowrate 1 $mLmin^{-1}$) of 48 : 52 *er*. Retention times (min): 4.8 (2141961, 48%), 6.6 (2349383, 52%). Entry 3 (orange). Chiral Stationary Phase HPLC (RegisPack, n-hexane-isopropanol 90 : 10, 303 K, load Et_2O, flowrate 1 $mLmin^{-1}$) of 57 : 43 *er*. Retention times (min): 4.8 (788670, 57%), 6.6 (597795, 43%).

Enyne cyclisation substrate 2**31b** was synthesised according to a literature route.

Compound **232b**

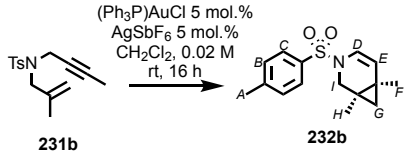

General procedure: A CEM MW vial was charged with [Au(L)(Cl)] (4.4 μmol, 0.05 eq.), $AgSbF_6$ (1.5 mg, 4.4 μmol, 0.05 eq.), and in the case of **296**, $[Cu(MeCN)_4]PF_6$ (1.7 mg, 4.4 μmol, 0.05 eq.), and purged with N_2. Alkyne substrate **231b** (24.4 mg, 0.088 mmol, 1.0 eq.) was added in degassed anhydrous CH_2Cl_2 (4.4 mL, 0.02 M) and the reaction stirred at rt for 16 h. The mixture was filtered through Celite© and concentrated *in vacuo*. The residue was purified by column chromatography (SiO_2, isocratic pet-EtOAc 95 : 5). Spectra match literature.[102] δ_H ($CDCl_3$, 400 MHz) 7.65 (2H, d, *J* = 8.3, H_C), 7.31 (2H, d, *J* = 8.4, H_B), 6.25 (1H, d, *J* = 8.0, H_E), 5.17 (1H, d, *J* = 8.0, H_D), 3.77 (1H, d, *J* = 11.5, H_I), 3.68 (1H, d, *J* = 11.5, $H_{I'}$), 2.42 (3H, s, H_A), 1.11 (6H, s, H_F, H_H), 0.72 (1H, d, *J* = 4.3, H_G), 0.33 (1H, d, *J* = 4.3, $H_{G'}$). δ_C ($CDCl_3$, 101 MHz) 143.7, 135.2, 129.9, 127.2, 120.2, 118.3, 46.8, 29.5, 26.4, 24.0, 21.7, 18.8, 17.6. LRMS [$M^{+\cdot}$] 277.0.

Table 12. Summary of reactions leading to **232b**.

	Catalyst	Yield / %	*er*
1	$(Ph_3P)AuCl$	76	50 : 50
2	(R_{mp})-**296**	37	51 : 49
3	(*R*)-DTBM-SEGPHOS®$(AuCl)_2$	20	50 : 50

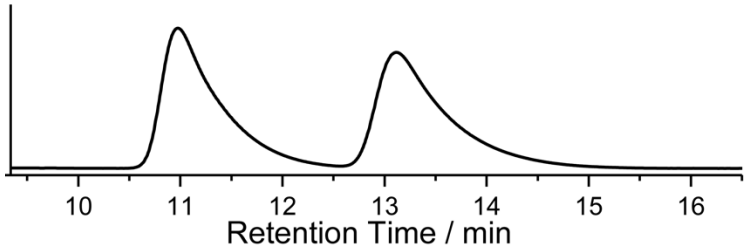

Figure 269: Entry 1. Chiral Stationary Phase HPLC (RegisPack, n-hexane-isopropanol 97 : 3, 303 K, load Et_2O, flowrate 0.75 $mLmin^{-1}$) of 50 : 50 *er*. Retention times (min): 11.0 (50%), 13.1 (50%).

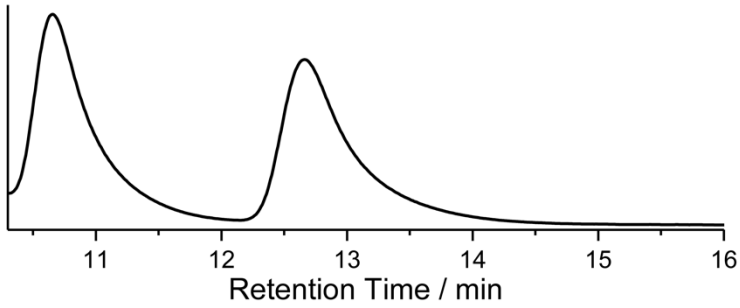

Figure 270: Entry 2. Chiral Stationary Phase HPLC (RegisPack, n-hexane-isopropanol 97 : 3, 303 K, load Et_2O, flowrate 0.75 $mLmin^{-1}$) of 51 : 49 *er*. Retention times (min): 10.7 (677924, 51%), 12.7 (643413, 49%).

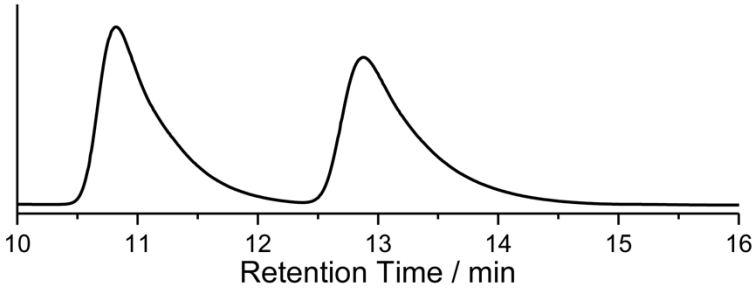

Figure 271: Entry 3. Chiral Stationary Phase HPLC (RegisPack, n-hexane-isopropanol 97 : 3, 303 K, load Et_2O, flowrate 0.75 $mLmin^{-1}$) of 50 : 50 *er*. Retention times (min): 10.8 (9190911, 50%), 12.9 (9063509, 50%).

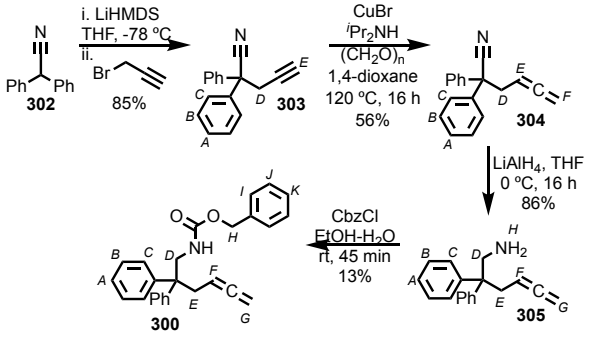

A dry CEM MW vial was charged with diphenylacetonitrile (1.00 g, 5.17 mmol, 1.0 eq.), purged with nitrogen, dissolved in anhydrous THF (5.0 mL) and cooled to -78 °C. LiHMDS (6.7 mL, 1 M, 6.73 mmol, 1.3 eq.) was added dropwise and stirred for 15 minutes. Propargyl bromide (0.86 mL, 80 wt.% in toluene, 7.76 mmol, 1.5 eq.) was added and the solution stirred for 16 h, gradually warming to room temperature. The solution was quenched with NH_4Cl (15 mL) and brine (15 mL), extracted in Et_2O (3 x 20 mL). The combined organic phases were dried over $MgSO_4$ and dried in vacuo. The residue was purified by column chromatography (SiO_2, pet-EtOAc 0→15%), yielding a pale yellow oil **303** (1.02 g, 4.41 mmol, 85%). Spectra match literature.[17] δ_H ($CDCl_3$, 400 MHz) 7.43-7.33 (10H, m, H_A, H_B, H_C), 3.26 (2H, d, J = 2.6, H_D), 2.14 (1H, t, J = 2.6, H_E); δ_C ($CDCl_3$, 101 MHz) 139.0, 129.0, 128.5, 127.2, 121.7, 78.4, 73.4, 51.3, 31.0; LRMS [M + H^+] 232.0.

A dry CEM MW vial was charged with CuBr (0.120 g, 0.834 mmol, 0.4 eq.) and paraformaldehyde (0.125 g, 4.17 mmol, 2.0 eq.) and purged with nitrogen. **303** (0.482 g, 2.08 mmol, 1.0 eq.) was added in degassed 1,4-dioxane (12 mL) and $^{i}Pr_2NH$ (0.59 mL). The suspension was heated at 120 °C for 16 h. The reaction was cooled to room temperature and concentrated in vacuo. The resulting residue was purified by column chromatography (SiO_2, pet-EtOAc 0→15%) yielding a colourless oil **304** (285 mg, 1.16 mmol, 56%). Spectra match literature.[17] δ_H ($CDCl_3$, 400 MHz) 7.43-7.29 (10H, m, H_A, H_B, H_C), 5.05 (1H, tt, J = 7.6, 6.7, H_E), 4.67 (2H, dt, J 6.7, 2.5, H_F), 3.11 (2H, dt, J = 7.6, 2.5, H_D); δ_C ($CDCl_3$, 101 MHz) 210.6, 139.7, 129.0, 128.1, 127.3, 122.0, 84.6, 75.5, 52.2, 39.6; LRMS [M + H^+] 246.2.

A dry flask was charged with **304** (2.06 g, 8.40 mmol, 1.0 eq.), in anhydrous THF (10 mL) under N_2. $LiAlH_4$ (25 mL, 25 mmol, 1M solution THF, 3.0 eq.) was added dropwise at 0 °C. The solution was stirred at room temperature for 16 h. After 16 h, the solution was quenched with EtOAc then 1 M NaOH (20 mL). 6 M HCl was added until neutral and the compound was extracted in Et_2O (3 x 30 mL). The combined organic layers were washed with sat. $NaHCO_3$ (50 mL) and extracted in Et_2O (3 x 30 mL), dried over $MgSO_4$, and concentrated in vacuo, yielding a yellow oil **305** (1.80 g, 7.2 mmol, 86%). Spectra match literature.[17] δ_H ($CDCl_3$, 400 MHz) 7.32-7.15 (10H, m, H_A, H_B, H_C), 4.68-4.60 (1H, m, H_F), 4.58-4.54 (2H, m, H_G), 3.36 (2H, s, H_D), 2.87 (2H, 2H, dt, J = 8.0, 2.4, H_E), 0.82 (2H, br. s, H_H); δ_C ($CDCl_3$, 101 MHz) 209.8, 146.2, 128.5, 128.4, 128.3, 126.5, 85.9, 74.2, 52.1, 49.1, 36.6; LRMS [M + H^+] m/z 250.2.

EtOH-H_2O (1 : 1, 10 mL) was added to amine **305** (0.500 g, 2.0 mmol, 1.0 eq.) and $NaHCO_3$ (0.25 g, 3.0 mmol, 1.5 eq.). Benzyl chloroformate (0.33 mL, 2.4 mmol, 1.2 eq.) was added slowly and the solution stirred at room temperature for 45 minutes. The solution diluted with water (20 mL) and extracted in EtOAc (3 x 15 mL). The combined organic phases were dried over $MgSO_4$ and concentrated in vacuo. The residue was purified by column chromatography (SiO_2, pet-EtOAc 0→5%) then re-purified by column chromatography (SiO_2 pet-Et_2O 0→5%) yielding a colourless oil **306** (103 mg, 0.269 mmol, 13%). Spectra match literature.[17] δ_H ($CDCl_3$, 400 MHz) 7.40-7.15 (15H, m, H_A, H_B, H_C, H_I, H_J, H_K), 5.05 (2H, s, H_H), 4.80-4.68 (1H, m, H_F), 4.54-4.46 (2H, 2H, H_G), 4.35 (1H, br. s, N**H**), 3.98 (2H, d, J = 6.0, H_D), 2.85 (2H, td, J 7.9, 2.4, H_E); δ_C ($CDCl_3$, 101 MHz)

210.0, 156.4, 145.0, 136.6, 128.6, 128.4, 128.2, 126.7, 85.2, 74.0, 66.9, 50.7, 47.9, 37.4; LRMS [M + H^+] m/z 384.4.

Compound **301**

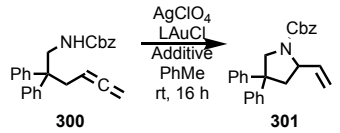

General Procedure: A CEM MW vial was charged with $AgClO_4$ (0.9 mg, 4.5 µmol, 0.05 eq.), LAuCl (4.5 µmol, 0.05 eq.) and in the case of (R_{mp})-**296**, $[Cu(MeCN)_4]PF_6$ (1.7 mg, 4.5 µmol, 0.05 eq.). The flask was purged with N_2, and allene **300** (34.7 mg, 0.091 mmol, 1.0 eq.) was added in degassed anhydrous PhMe (0.60 mL, 0.15 M) and stirred at rt overnight. The mixture was concentrated *in vacuo*. The residue was purified by column chromatography (SiO_2, pet-Et_2O 0→25%) yielding a colourless oil. Spectra match literature.[98]

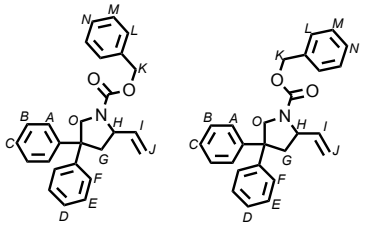

A mixture of carbamate rotamers was observed. δ_H ($CDCl_3$, 400 MHz) 7.48-7.07 (15H, m), [5.78 (td, J = 10.5, 7.1), 5.77 (td, J = 10.5, 7.1), 1:1, 1H], 5.33-5.06 (4H, m), [4.76 (dd, J = 11.6, 1.9), 4.60 (dd, J = 11.5, 1.6) 1:1, 1H], [4.17 (dd, J 16.0, 7.4), 4.11 (dd, J 15.6, 7.3), 1:1, 1H], [3.72 (d, J = 15.6 Hz), 3.71 (d, J = 15.6), 1:1, 1H], 2.88-2.81 (1H, m), [2.47 (dd, J = 12.5, 9.8 Hz), 2.42 (dd, J = 12.5, 9.8 Hz), 1:1, 1 H]. δ_C ($CDCl_3$, 101 MHz) 155.4, 154.8, 145.5, 144.9, 139.3, 138.6, 137.0, 136.8, 128.8, 128.7, 128.4, 128.3, 128.2, 127.8, 127.7, 126.9, 126.7, 126.6, 115.8, 115.2, 67.0, 59.6, 59.1, 56.3, 53.2, 52.8, 45.8, 44.7. LRMS [M + H^+] m/z 384.3286 (calc. $C_{26}H_{26}N_1O_2$ m/z 384.1964).

Table 13. Summary of reactions leading to **301**.

	Catalyst	Yield / %	*er*
1	$(Ph_3P)AuCl$	5	50 : 50
2	(R_{mp})-**296**	51	50 : 50
3	(*R*)-DTBM-SEGPHOS®$(AuCl)_2$	38	67 : 33

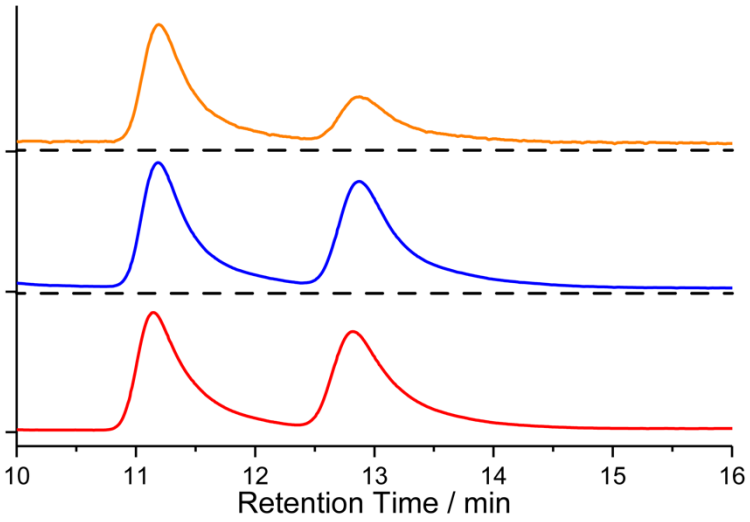

Figure 272: Chiral Stationary Phase HPLC (RegisPack, n-hexane-isopropanol 75 : 25, 303 K, load pet, flowrate 0.50 $mLmin^{-1}$). Retention times (min): 11.2, 12.9. Top (entry 3) *er* 67 : 33, Middle (entry 2) *er* 50 : 50, Bottom (entry 1) *er* 50 : 50.

Appendix 1: Molecular Modelling

*Models of the reaction of ester **71a** and styrene (**72a**) mediated by [Au(PPh$_3$)(Cl)]*

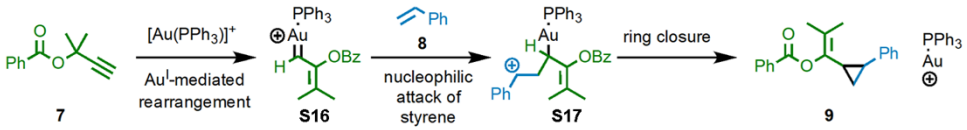

Figure 273. Proposed pathway for the reaction of 7 and 8 mediated by [Au(PPh$_3$)(Cl)]

We initially investigated the reaction of ester **71a** with styrene (**72a**) mediated by [Au(PPh$_3$)(Cl)] (**Figure 273**) to determine a reasonable transition state for the same reaction mediated by rotaxane complex **296**. Models of the transition states for the reaction of presumed carbene intermediate **S16** with styrene were constructed based on transition state structures reported by Echavarren and co-workers in a related reaction by modifying the substituents of the phosphine and carbene. Scanning of the distance between the carbenic carbon and the β-position of styrene, followed by

transition state optimisation of the structures that corresponded to energetic maxima on the scanned coordinate yielded four transition states **TSI** (**Figure 274**), two leading to *cis*-**74a**, two leading to *trans*-**74a**, of which *cis*-**TSIb** was found to be more stable by 10.3 kJmol^{-1} than the nearest alternative pathway. All transition states were determined to be first order saddle points with a single imaginary frequency mode.

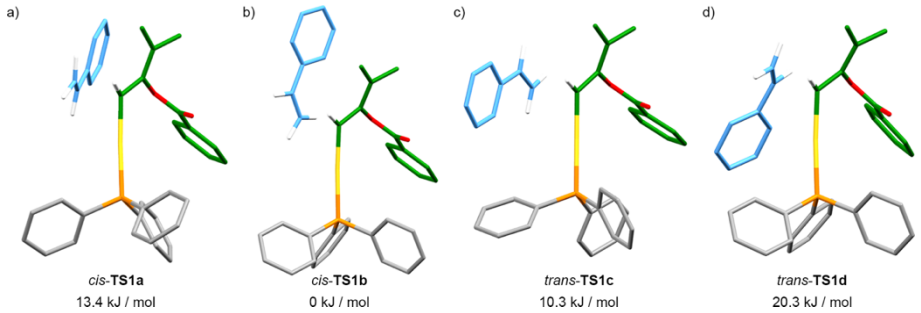

Figure 274. Transition states and their relative energies for the reaction S16→S17 determined by DFT (CAM-B3LYP, 6-31G*(C,H,O,P)/SDD(Au)). For structures see "Model_AuPPh3Cl_TS1.cif" submitted as electronic supporting information.

It should be noted that, in accordance with Echavarren and co-workers' previous report, in all cases IRC calculations indicate that transition states **TSI** correspond to a stepwise mechanism as shown in **Figure 273**, in which the styrene acts as a nucleophile on the electrophilic carbene to generate aryl cations **S17**, that then undergo ring closure with extremely low barrier to give the observed cyclopropane product. Specifically, in the case of *cis*-**TSIb** (**Figure 274**), the reaction of **S16** to produce **S17** was found to proceed with a barrier of 3.0 kJmol^{-1} and to be extremely favourable (-45.2 kJmol^{-1}). Subsequent ring closure was essentially barrierless, passing through *cis*-**TSIIb** (first order saddle point, single imaginary frequency mode) to generate cyclopropane *cis*-**74a** initially with the Au^{I} catalyst associated with the carbonyl of the ester. (Note: although **S17** and **TSIIb** were found to be minima and maxima respectively on the potential energy surface by frequency analysis, their structures are related by an extremely small atomic reorganisation and were energetically indistinguishable at this level of theory).

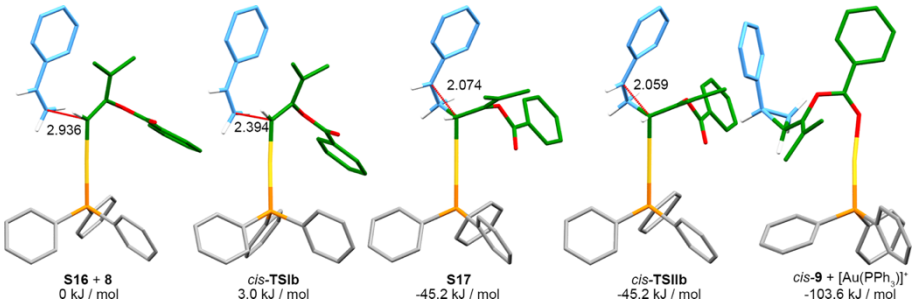

Figure 275. Intermediates and transition states and their relative energies for the reaction from **S16** → cyclopropane **74a** determined by DFT (CAM-B3LYP, 6-31G*(C,H,O,P)/SDD(Au)). For structures see "Model_DFT_AuPPh3Cl_full_reaction.cif" submitted as electronic supporting information.

Diastereomeric transition states for the reaction of **71a** with **72a**

A model of the transition state for the reaction of 7 with 8 mediated by [Au(6)(Cl)] was constructed by joining *cis*-TSIb with a model of [Cu((R_{mp})-5]$^+$ by replacing one of the Ph substituents of *cis*-TSIb (highlighted) with the rotaxane framework with the highlighted atoms removed (**Figure 276**). The diastereomeric model was generated by using the same rotaxane framework with the enantiomer of *cis*-TSIb.

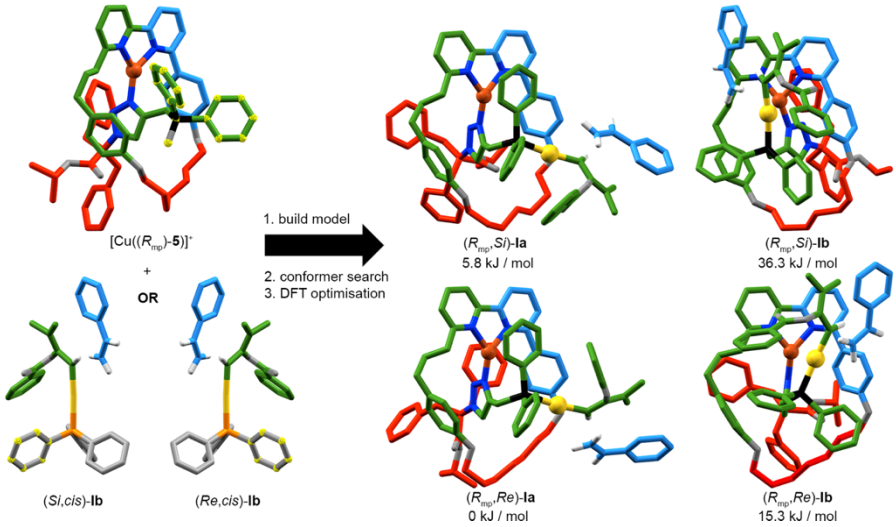

Figure 276. Procedure for the construction of candidate conformations of the transition state for the reaction mediated by **296**, the four lowest energy conformations found and their energies as evaluated using DFT (CAM-B3LYP, 6-31G(C,H,O,P,N)/SDD(Au,Cu)). For structures of Ia and Ib see "Model_Rmp_confs_I.cif" submitted as electronic supporting information.

A conformational search was performed using these models of (R_{mp},*Re*)-**Ia** and (R_{mp},*Si*)-**Ia**, where Re and Si refer to the face of the carbene approached by styrene (Note: (R_{mp},*Si*)-**Ia** gives rise to the observed major product (1*S*,2*R*)-**74a**). The transition state fragment (carbene unit, styrene moiety, Au and P atoms) was frozen, the Cu ion was restricted to a trigonal planar configuration, and a conformational search was performed

(Spartan '10, MMF) by rotating triazole-N^1-C, and the single bonds of the C-C-P fragment in 60 degree increments followed by re-optimisation using the same model with no restriction on these bond angles. This search was repeated several times starting from different initial states and yielded reproducible results; for both diastereomeric structures, two families of low energy conformations were identified, one in which the P-Au bond was projected parallel or nearly parallel to the triazole-N-Cu bond and the other in which the P-Au bond is projected towards the same O substituent of the macrocycle. The two lowest energy conformations included one of each family and were predicted to be more stable than the next lowest energy conformation by > 10 kJ / mol. These conformations were then reoptimized with the transition state fragment frozen using DFT (CAM-B3LYP, 631-G(C,H,O,P,N)/SDD(Au, Cu)) with the result that conformers **Ia** were found to be more stable by >15 kJ / mol (**Figure 276**).

Conformers (R_{mp},*Re*)-**Ia** and (R_{mp},*Si*)-**Ia** were taken forward for transition state optimisations and the results of these calculations are summarised in **Table 14** A transition state search using an ONIOM method was carried out initially with the transition state fragment (including the Ph substituents of the P atom), in the high level (CAM-B3LYP, 631-G(C,H,O,P)/SDD(Au)) and the rest of the molecule in the low level (UFF) and frozen, except for the methylene linking the different fragments. The outputs of the ONIOM calculations were then subjected to a transition state search using DFT (CAM-B3LYP, 631-G(C,H,O,P,N)/SDD(Au,Cu)) with no frozen or restricted atoms. This yielded two diastereomeric transition state structures **TS1** with a single imaginary mode. These structures were re-optimized in the gas phase (entry 5, CAM-B3LYP, 631-G*(C,H,O,P,N)/SDD(Au,Cu)) and in $CHCl_3$ (entry 4, PCM($CHCl_3$), CAM-B3LYP, 631-G(C,H,O,P,N)/SDD(Au,Cu)), the latter of which was subjected to a single point energy calculation (entry 6, $CHCl_3$, CAM-B3LYP, 631-G*(C,H,O,P,N)/SDD(Au,Cu)). Attempts to directly locate a transition state with these latter parameters proved prohibitively computationally expensive. The structures of Re/Si **TS1-Oniom** (**Table 14**, entry 2), **TS1-631G** (entry 3), **TS1-631GCHCl3** (entry 4) and **TS1-631GG** (entry 5) are provided as supporting information (.xyz).

Examining the computed relative energies of **TS1**, the outcome is strongly dependent on the method used. When evaluated using an Oniom method (entry 2), the calculations predict a very large preference for the (1*S*,2*R*)-**74a** major product observed

experimentally. Optimisation of the entire structure using DFT with a 6-31G basis set in the gas phase (entry 3) predicts the opposite enantiomer. When solvent is included ($CHCl_3$, entry 4), or a larger basis set employed in the gas phase (entry 5) the correct product is predicted, both with reasonable agreement to the experimental value. Re-subjecting the output of entry 4 to a single point energy calculation with a larger basis set (6-31G*, entry 6) results in an even higher predicted preference for the experimentally observed major product. The results in **Table 14** suggest that although the structures of **TS1** determined using DFT are useful from an illustrative point of view, the relative energies determined are not particularly reliable, especially given the relatively small difference (~3 kJ / mol) predicted from experiment.

Table 14. Comparison of the outcomes of different calculations for **TS1**

Entry	Method	Basis Set	Solvent	Imaginary modes (cm^{-1})	ΔE[*Si* – *Re*] (kJ / mol)	(1*S*,2*R*)-74a : (1*R*,2*S*)-74a
1	Experiment	-	$CHCl_3$	-	–3.0	79 : 21
2	Oniom (CAM-B3LYP:UFF)	6-31G/SDD(Au)	-	–175.19 (*Si*), –51.23 (*Re*)	–25.4	100 : 0
3	CAM-B3LYP	6-31G/SDD(Au,Cu)	-	–159.89 (*Si*), –118.84 (*Re*)	1.7	32 : 68
4	CAM-B3LYP	6-31G/SDD(Au,Cu)	$CHCl_3$	–176.85 (*Si*), –175.54 (*Re*)	–2.3	74 : 26
5	CAM-B3LYP	6-31G*/SDD(Au,Cu)	-	–149.80 (*Si*), –120.42 (*Re*)	–4.9	90 : 10
6	CAM-B3LYP (single point)	6-31G*/SDD(Au,Cu)	$CHCl_3$	-	–6.4	94 : 6

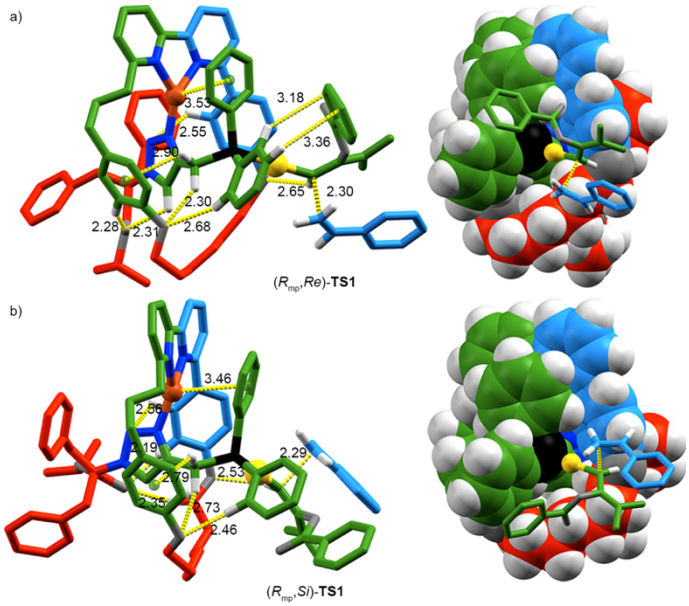

Figure 277. Transition states TS1 determined for the reaction mediated by [Au(6)(Cl)] using DFT (CAM-B3LYP, 6-31G(C,H,O,P,N)/SDD(Au,Cu), PCM(CHCl3)) with selected intercomponent interactions and distances indicated. For structures see "Model_Table_S17_structures.cif" submitted as electronic supporting information.

Transition states for the formation of cyclopropanes **74c**, **74s** and **74p**

Transition states for the reactions leading to cyclopropanes **74c**, **74s** and **74p** were constructed by modification of diastereomeric transition states TS1 (Table 14, entry 4), followed by repeating the transition state search, first in the gas phase then in $CHCl_3$ (PCM). The structures obtained are shown in **Figure 278** and the results are summarized in Table 10.

Table 15. Comparison of the outcomes of different calculations of **TS1**

Entry	Method	Basis Set	Solvent	Imaginary modes (cm^{-1})	ΔE[*Si* – *Re*] (kJ / mol)	(1*S*,2*R*)-*9* : (1*R*,2*S*)-*9*
			Cyclopropanes **74c**			
1	Experiment	-	$CHCl_3$	-	0.4	55 : 45
2	CAM-B3LYP	6-31G/SDD(Au,Cu)	$CHCl_3$	–190.27 (*Si*), –175.54 (*Re*)	3.1	16 : 84
			Cyclopropanes **74s**			
3	Experiment	-	$CHCl_3$	-	–2.2	73 : 27
4	CAM-B3LYP	6-31G/SDD(Au,Cu)	$CHCl_3$	–177.19 (*Si*), –160.62 (*Re*)	–3.1	80 : 20
			Cyclopropanes **74p**			
5	Experiment	-	$CHCl_3$	-	–2.0	70 : 30
6	CAM-B3LYP	6-31G/SDD(Au,Cu)	$CHCl_3$	–194.11 (*Si*), –170.46 (*Re*)	–3.0	79 : 21

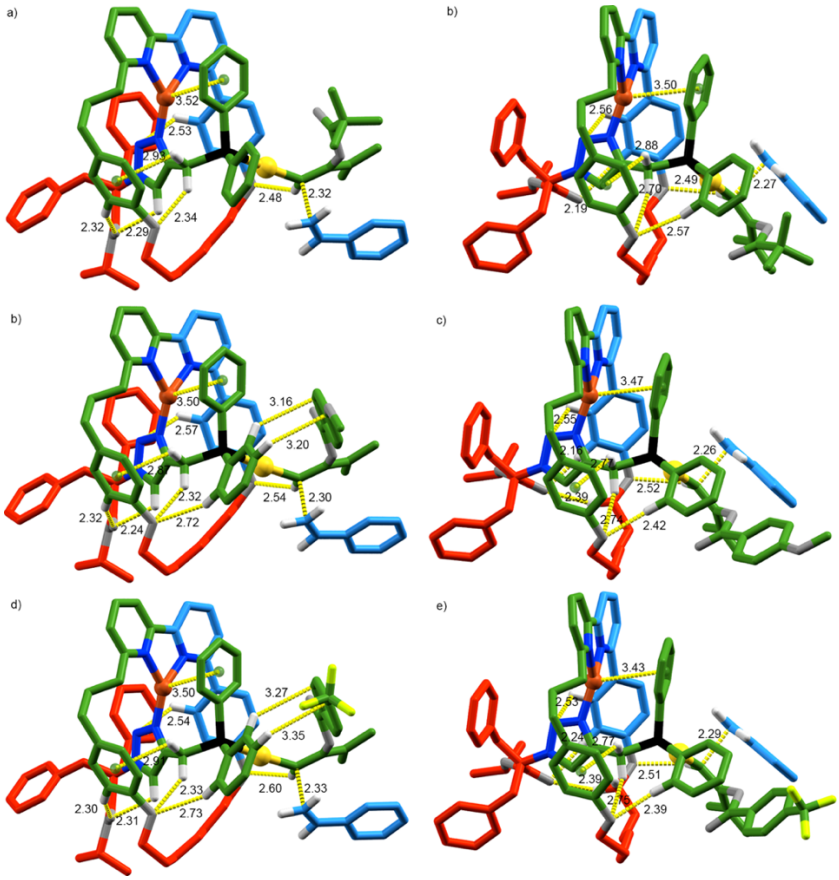

Figure 278. Transition states determined (DFT (CAM-B3LYP, 6-31G(C,H,O,P,N)/SDD(Au,Cu), PCM(CHCl3)) for reactions leading to cyclopropanes a) (1R,2S)-**74c**, b) (1S,2R)-**74c**, c) (1R,2S)-**74s**, d) (1S,2R)-**74s**, e) (1R,2S)-**74p**, f) (1S,2R)-**74p**. with selected intercomponent interactions and distances indicated. For structures see "Model_Table_S18_structures.cif" submitted as electronic supporting information.

The results obtained for cyclopropanes **74s** and **74p** are in reasonable agreement with experiment. The fact that modelling does not predict the correct ranking of *ee* for **74a**, **74s**, and **74p**, is not surprising, given the small difference between the experimental values (~1 kJ / mol). The large discrepancy between the experimental and modelled data for cyclopropanes **74c** may indicate that, in the case of pivolyl esters, different/additional conformations of the catalyst-substrate complex may be important in product formation. Indeed, given the potential for other catalytically relevant conformations, further detailed studies are required to assess their relevance and provide a more detailed framework for discussing the selectivity induced by the mechanically planar chiral stereogenic unit.

Chapter 3: A Simplified Approach to Mechanically Planar Chiral Rotaxane Ligands

Abstract: Having demonstrated the potential for MPC rotaxane ligands (Chapter 2), the synthesis of these ligands remained a limiting aspect. The necessity of separable MPC diastereoisomers, poor selectivity, and limited modifications, reduce the potential of MPC ligands beyond initial proof-of-principle.

This chapter details efforts to simplify the synthetic process, to attain a broader library of MPC catalysts. The first approach details post-synthetic modifications of rotaxanes formed in high diastereoselectivity, enabling facile diversification without reliance upon lengthy diastereoisomeric separations. Finally this chapter describes a general, molecular-shuttle methodology to allow the synthesis of enantiopure MPC rotaxanes with any axle. This work will allow a more systematic investigation of MPC in the future.

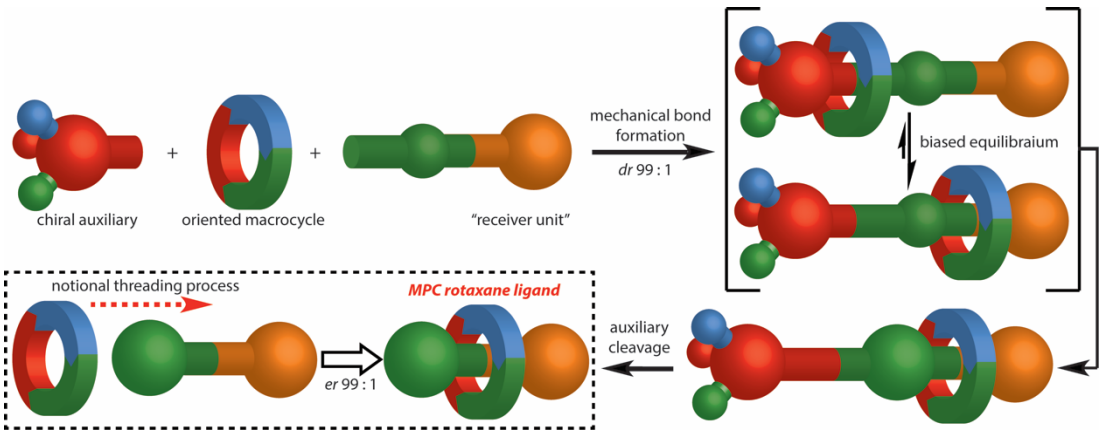

Partial Prior Publication: "*Simplicity in the Design, Operation, and Applications of Mechanically Interlocked Molecular Machines*" – A. W. Heard, S. M. Goldup, *ACS Cent. Sci.*, **2020**, *6*, 117-128. "*A Chiral Interlocking Auxiliary Strategy for the Synthesis of Mechanically Planar Chiral Rotaxanes*" – A. de Juan, D. Lozano, A. W. Heard, M. A. Jinks, J. Meijide Suarez, S. M. Goldup, *ChemRxiv*, **2021**.

3.1. Introduction

Chapter 2 detailed the challenging development of the first application of MPC (Figure 279).[1] This was a significant break-through in the application of mechanically interlocked molecules and a new class of chiral ligand. However, there are several weaknesses to this approach which limit the general applicability of MPC ligands. Overcoming these design weaknesses could develop MPC into a field of interest to general chemistry and the catalysis community, rather than being limited to the groups with expertise in the synthesis of interlocked molecules.

The previous MPC catalyst [Au((R_{mp})-**6**)(Cl)] synthesis was long and required a difficult diastereoisomeric separation (Figure 279a). The reliance on separable diastereoisomers is the major drawback of this approach, as obvious structural variations to modify catalyst behaviour do not always translate into similarly separable diastereoisomers. Furthermore, the screening of separation conditions is time consuming and doing this for each new ligand structure vastly reduces the appeal of this ligand class. Finally, even though both diastereoisomers ((S,R_{mp})-**4** and (S,S_{mp})-**4**) were carried forward to a final catalyst, low diastereoselectivity in the AT-CuAAC step leads to significantly lower atom economy. A highly selective AT-CuAAC step would make the investigation of MPC more facile and increase atom economy.

Another limitation of this work is the absence of stimuli-regulated behaviour. The first Au^{I}-catalyst developed by Goldup and co-workers displayed tuneable diastereoselectivity in response to each co-factor that was bound within the rotaxane.[2] The work of the previous chapter was not active for co-factors other than Cu^{I}, this was attributed to the inverted triazole orientation and the geometry of the metallo-rotaxane resulting from this. Therefore, investigation of otherwise identical catalysts with opposite triazole orientations would increase the understanding of this ligand class.[1] Stimuli-regulated enantioselectivity would increase catalyst scope, as was recently achieved by Berná and co-workers with an organic co-factor (Chapter 2, Figure 9).[3]

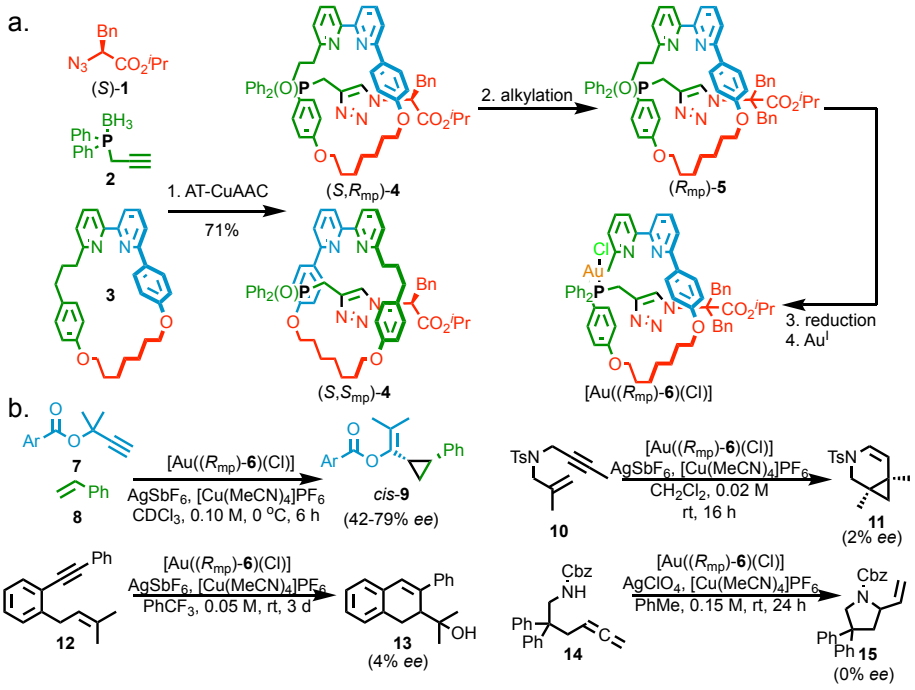

Figure 279: Goldup and co-workers first MPC rotaxane ligand (a) synthesis and (b) catalytic scope.

Finally, the generality of this first generation catalyst was low (Figure 279b).[1] Despite approaching the best literature selectivities for some Au^{I}-catalysed cyclopropanations (*cis*-**9**), the substrate scope was poor and the catalyst did not show significant selectivity for other Au^{I}-catalysed reactions. Although the low generality is not uncommon in enantioselective Au^{I}-catalysis,[4] it is still a disappointing result limiting the catalyst applicability.

This chapter details attempts to streamline the catalyst synthesis, targeting higher selectivity in the AT-CuAAC step, and an easily modified catalyst structure to allow faster access to structural analogues tuned to the desired application. If the challenges listed above are overcome, MPC ligands could become more generally useful in catalysis.

3.1.1. Introduction to Molecular Shuttles

The ability of interlocked molecules to undergo large amplitude positional changes on application of a stimulus, suits them ideally to molecular machines. Although we are accustomed to viewing the world on a macroscopic scale, with machines and motors playing a key part in our lives, it is first important to note that Brownian motion dominates at low Reynolds numbers; where viscosity dominates over inertia.[5] Macroscopic ideas of machines involving momentum, inertia, gravity, and friction are not applicable on the molecular scale.[5,6]

In the last 30 years, chemists have applied many stimuli (light, temperature, redox potentials, pH, heat, solvent polarity, ion-binding, chemical stimuli and more)[7] to drive large amplitude motion of molecules to complete tasks. This culminated in the 2016 Nobel Prize in Chemistry.[8–10]

The first stimuli responsive molecular shuttle was reported by Stoddart and co-workers.[11] By changing the solution pH, the affinity of the cationic macrocycle for the two stations changed, causing movement of the macrocycle to occupy the most thermodynamically preferable station (Figure 280a).[11] In shuttles, both co-conformations are occupied, with a Boltzmann distribution between states. At high pH, the macrocycle prefers to occupy the bisaniline station (**16**), as the π-donor interaction is most stabilising here. At low pH, the protonated amines repel the positively charged macrocycle, so the ether station becomes preferable (**16**-2H$^+$). The same behaviour was developed for [2]catenane **17** (Figure 280b) in response to oxidation of the tetrathiafulvalene station.[12]

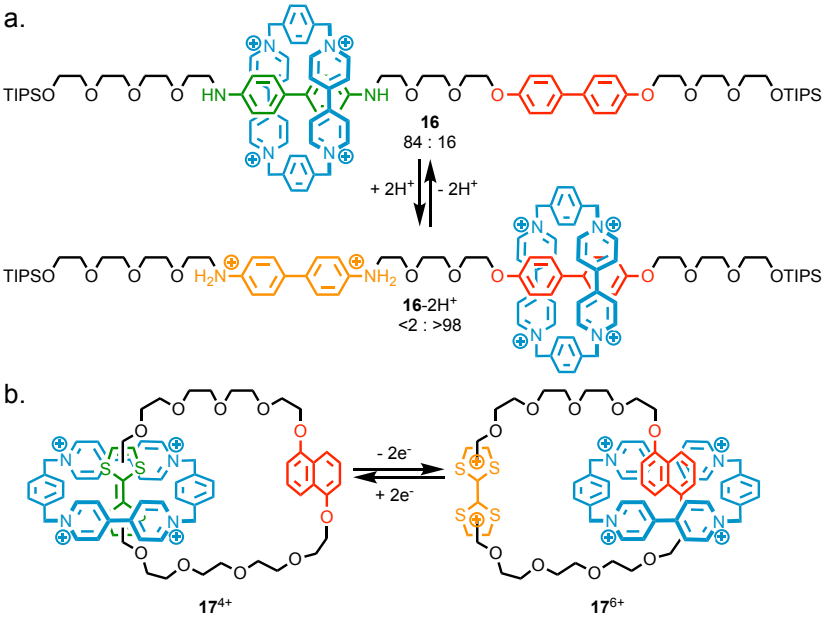

Figure 280: Stoddart and co-workers' (a) [2]rotaxane shuttle **16**[11] and (b) [2]catenane shuttle **17**.[12] Counter-ions omitted for clarity.

With a chemical (Figure 280a)[11] or electrochemical stimuli (Figure 280b),[12] the affinity of the macrocycle for each station can be changed, resulting in Brownian motion mediated shuttling from one station to the new thermodynamic minimum. On application of the stimulus, the system is by definition out of equilibrium, however rapidly adjusts to find the new minimum. Changing the thermodynamic minimum through a chemical stimulus results in net movement of the macrocycle.

Sauvage and co-workers developed electrochemical shuttle **18**, in which the driving force is the different coordination geometries of Cu^{I} and Cu^{II} (Figure 281).[13,14] When bound to Cu^{I}, requiring a tetrahedral 4-coordinate geometry, the macrocycle lies occupying the phenanthroline station. Upon oxidation of Cu^{I} to Cu^{II}, the macrocycle shuttles to the terpyridine station to accommodate the metal ion in a 5-coordinate trigonal bipyramidal geometry.[13,14]

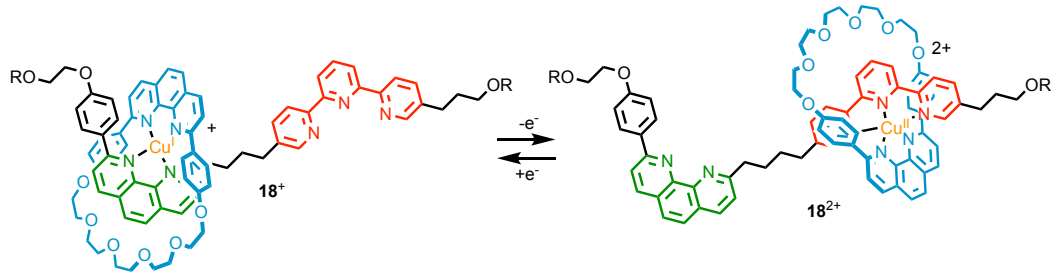

Figure 281: Sauvage and co-workers' electrochemically driven shuttle **18**.[13] Counter-ions omitted for clarity. R = $C_6H_4C(C_6H_4$-*t*-Bu$)_3$.

Stoddart and co-workers reported a pH responsive nanoscale molecular elevator **22**.[15,16] The [4]rotaxane was synthesised from the inclusion complex of tritopic D_{3h}-host **20** with trifurcated guest **19a**.[17] Upon application of acid or base stimuli, the macrocycle component moves between two defined stations 0.7 nm apart. The estimated force exerted on descending the elevator was 200 pN.[15] These molecular shuttles have been applied to [c2]daisy chains to make stimuli responsive molecular muscles.

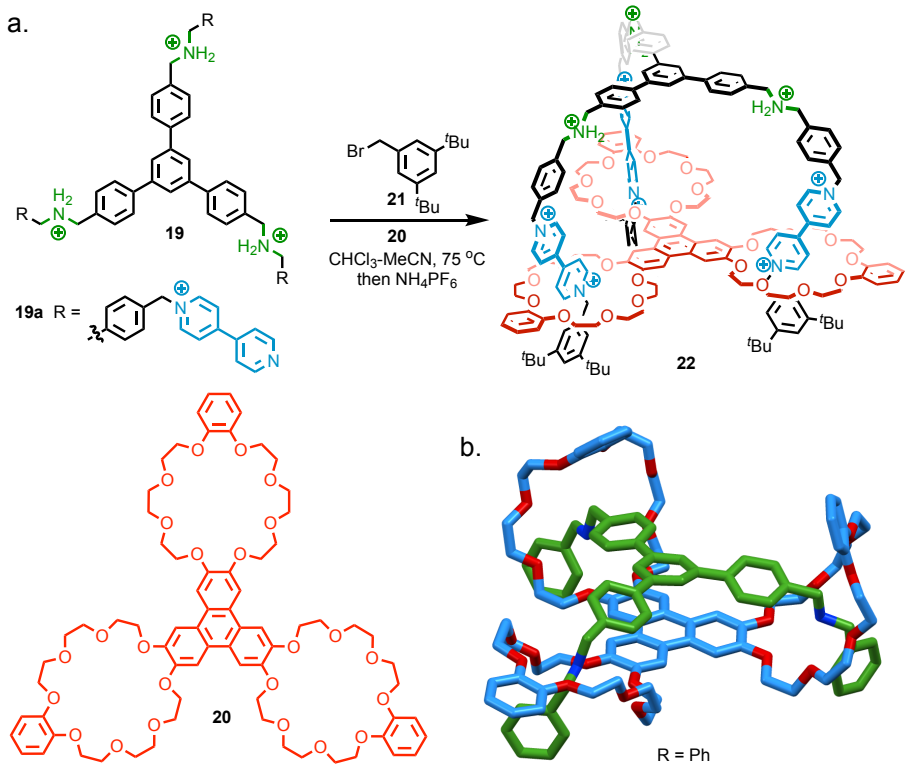

Figure 282: (a) Stoddart and co-workers' molecular elevator **22**,[15] and (b) Single crystal X-ray structure of Stoddart and co-workers' pseudorotaxane tritopic host-guest complex from macrocycle **20** and guest **19b** (R = Ph) (solvent molecules and counter-ions omitted for clarity).[17]

Recently Loeb and co-workers have developed [3]rotaxane **23**, where a large macrocycle can shuttle over a smaller macrocycle, thereby creating a molecular switch with no empty recognition sites (Figure 283).[18–20] Evidence for this shuttle process came from

the observation of two distinct proton environments at -42 °C, which coalesce above room temperature when the shuttling occurs faster than the NMR timescale.[18] Simple shuttles have even been developed where the stimulus is solvent polarity, disturbing the H-bond network and disfavouring a specific binding site.[19]

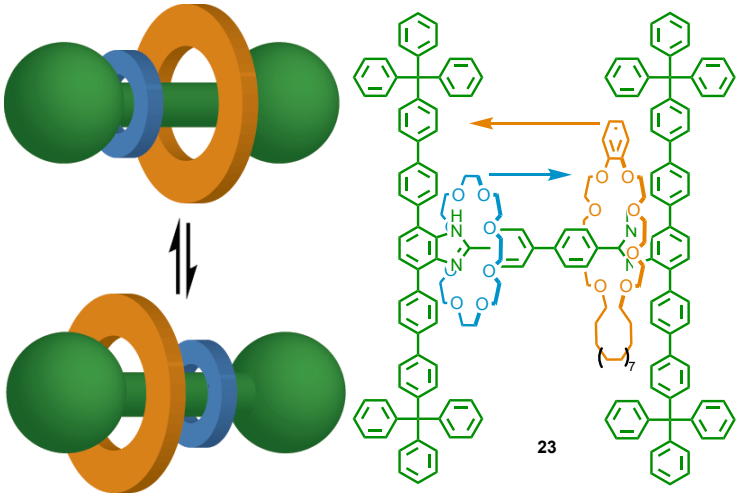

Figure 283: Loeb and co-workers' ring-through-ring [3]rotaxane shuttle **23**.[18] Variable Temperature NMR study of [3]rotaxane ***** revealed $\Delta H^{\ddagger}$ = 11.6 kcal.mol^{-1}, $\Delta S^{\ddagger}$ = -3.0 cal.mol^{-1}K^{-1}, $\Delta G^{\ddagger}_{298\ K}$ = 12.5 kcal.mol^{-1} (d^8-PhMe, $\Delta G^{\ddagger}$ = -RTln(kh/k_BT) = $\Delta H^{\ddagger}$ - T $\Delta S^{\ddagger}$, ln(k/T) = -$\Delta H^{\ddagger}$/RT + $\Delta S^{\ddagger}$/R + ln(k_B/h),).

Balzani, Credi, Stoddart and co-workers have demonstrated a molecular shuttle, that operates continuously and autonomously under irradiation through a photoelectron transfer process (Figure 284).[21] Upon absorption of the photon by **24**, an electron is transferred from the ruthenium-based stopper to the distal viologen unit **25**, reducing the affinity of the macrocycle for this station. As the affinity is reduced, the macrocycle relaxes to the new thermodynamically favoured station **26**. Spontaneous back electron transfer regenerates the original stations **27** and the macrocycle then returns to its original equilibrium position **24**. Thus, over one cycle of photon absorption, electron transfer and back electron transfer, the macrocycle undergoes net displacement from one station to the other and back again.[21]

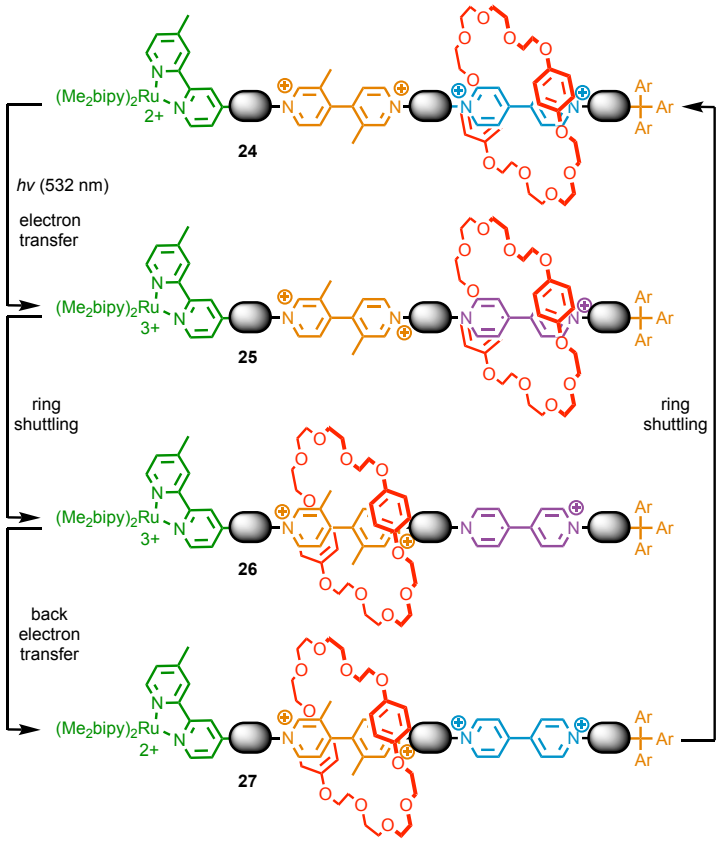

Figure 284: Balzani, Credi and Stoddart's continuous shuttle **24**.[21] Ar = 4-*t*-Bu-C_6H_4. Irradiation at 532 nm causes internal electron transfer, which in-turn induces macrocycle shuttling. Back electron transfer and shuttling restores the system to the ground state.

Di Stefano and co-workers have incorporated time dependent relaxation into shuttling, by using 2-cyano-2-arylpropanoic acids **29** as a chemical fuel to drive pulsed conformational switching of a [2]catenane **28** (Figure 285).[22] Addition of the acidic fuel causes a conformational change to the protonated state **30**. Once the 2-cyano-2-arylpropanoate anion **31** decarboxylates, the system returns to the neutral conformational state **28**. Decarboxylation of **31** to **32** is the rate limiting step. It was demonstrated that the substituent of the 2-cyano-2-arylpropanoic acid **29** allows control of the reversion kinetics (Hammett parameter ρ = +5.2). When X = OMe, the decarboxylation of **31** occurs slowly over several days, whereas over a few minutes when X = Cl. The variation in fuel structure enables tuning of the switch kinetics.

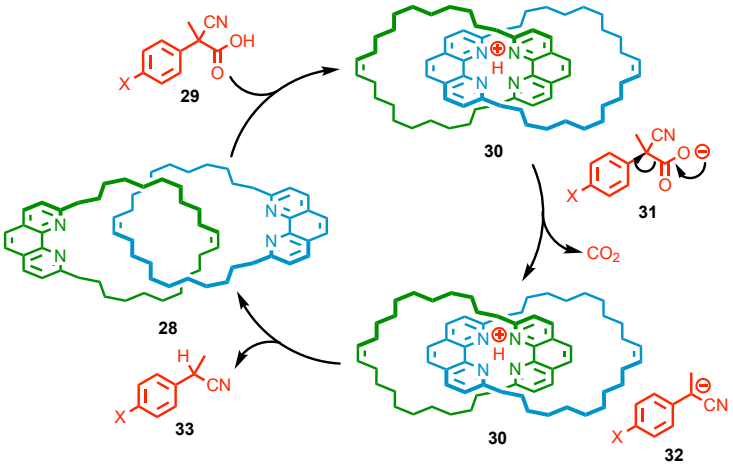

Figure 285: Di Stefano and co-workers fluxional conformational [2]catenane **28** switch.[22] Addition of acid **29** causes shuttling and circum-rotation to catenane **30**. As **31** decarboxylates it deprotonates **30**, causing reversion to the initial co-conformation **28**.

3.1.1.1. Unidirectional Rotors

Di Stefano's work was subsequently elaborated into an autonomous molecular motor by Leigh and co-workers, by combining acid/base switchable stations with complementary acid/base labile gates (Figure 286).[23]

Catenane **34** is an example of an energy ratchet-based motor. In an energy ratchet mechanism, the potential energy maxima and minima are varied periodically, resulting in an asymmetric potential energy surface. The controlled protonation of the amine to give an ammonium unit with higher affinity for the macrocycle is synchronized with removal/reintroduction of the hydrazone and disulfide gates to generate a 360° rotation.[23]

At high pH, the amine station remains unprotonated and the macrocycle preferentially occupies the triazolium station **34**. Under these conditions the disulfide "gate" is under dynamic exchange between open and closed states through disulfide exchange.[23] At low pH, the ammonium station is the preferential station for the macrocycle. Under these conditions the acylhydrazone "gate" is under dynamic exchange between open and closed states.

Addition of trichloroacetic acid (TCA) causes a reduction of pH, stopping the disulfide exchange and initiating the dynamic exchange of the hydrazone gate.[23] As the TCA decomposes, the pH rises until the hydrazone exchange stops and the disulfide exchange recommences. The elegance of the operation mechanism developed is that

all these steps are achieved by a simple change in pH that synchronizes both pairs of events.

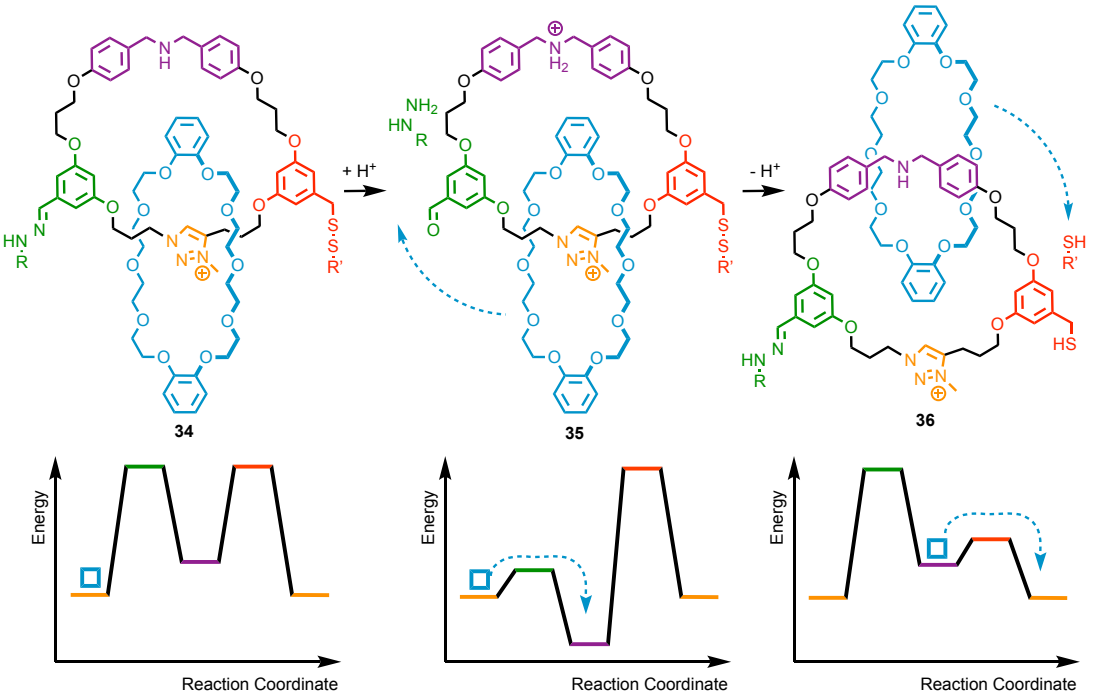

Figure 286: Leigh and co-workers' energy ratchet automated catenane motor **34**, and energy profiles to display the energy ratchet mechanism.[23] R = CO(3,5-di-*t*-Bu-C_6H_3). R' = CH_2(2,5-di-Me-C_6H_3).

Another class of molecular machine mechanism is the information ratchet. Information ratchets change the relative maxima of the potential surface in relation to the position of the particle on the potential surface. Leigh and co-workers have developed the automated catenane motor **37**, operating *via* an information ratchet mechanism (Figure 287).[24] The macrocycle has the same affinity for both stations, and the rate of un-gating both stoppers is the same regardless of the position of the macrocycle. However, when the macrocycle occupies the station closer to a free alcohol, the stoppering process is slower than if it were to occupy the distant station (**38** and **40**). Because of this kinetic bias dependent upon the macrocycle position, the macrocycle undergoes net unidirectional motion around the larger ring.[24]

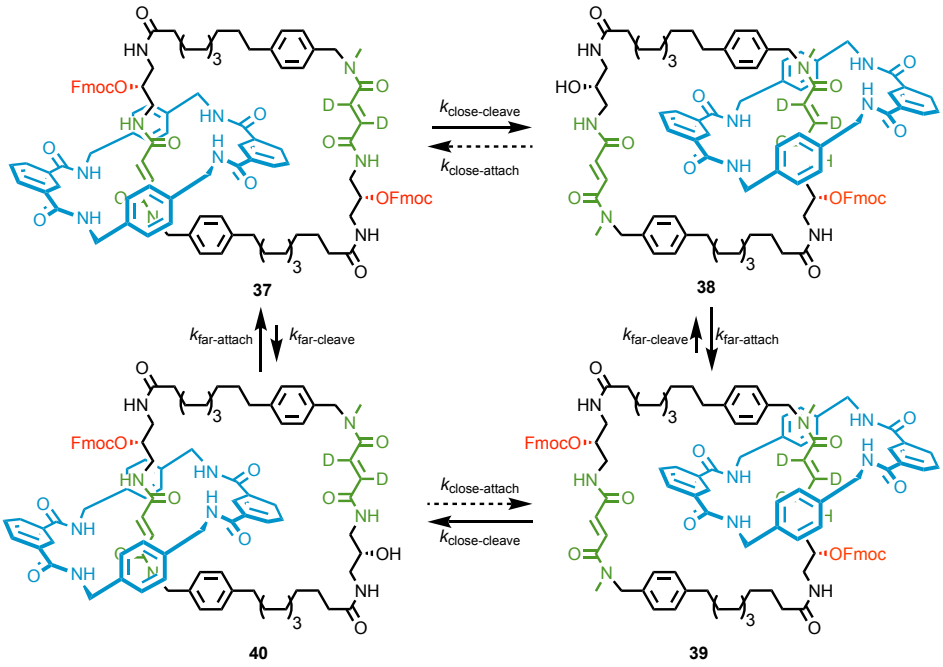

Figure 287: Leigh and co-workers' information ratchet automated catenane motor **37**.[24] The rate of reaction of the hydroxyl group further away from the macrocycle ($k_{far\text{-}attach}$) is greater than for the hydroxyl group hindered by the nearby macrocycle ($k_{close\text{-}attach}$).

3.1.1.2. Molecular Pumps

Stoddart and co-workers have synthesised rotaxanes by pumping macrocycles against the thermodynamic gradient by using an electrochemical, energy ratchet approach (Figure 288).[25,26] Electrochemical reduction of viologen units in the macrocycle and axle, creates a favourable radical-cation interaction,[27,28] which leads to the formation of *pseudo*rotaxane **43**. The attractive interaction is removed by re-oxidizing the system, causing the positively charged macrocycle to move either towards the pyridinium end of the axle (red), or towards the neutral aromatic group (orange).[25,26,29] Stoddart and co-workers were able to kinetically bias this motion towards the neutral aromatic unit, due to charge-charge repulsion between the macrocycle and the pyridinium stopper. The macrocycle becomes trapped between the viologen station and the ^{i}Pr group, as the dicationic viologen unit blocks its path electrostatically (**44**). The cycle completes *via* a slow, thermally activated slippage of the macrocycle over the neutral aromatic group to give co-conformation **45**. Repeating a further complete cycle allows additional rings to be pumped onto the axle, yielding [3]rotaxane **46**.[25,26] Stoddart and co-workers have since used this approach to synthesise interlocked daisy-chain polymers from a *'blue box'* macrocycle bearing the redox pump moiety.[30]

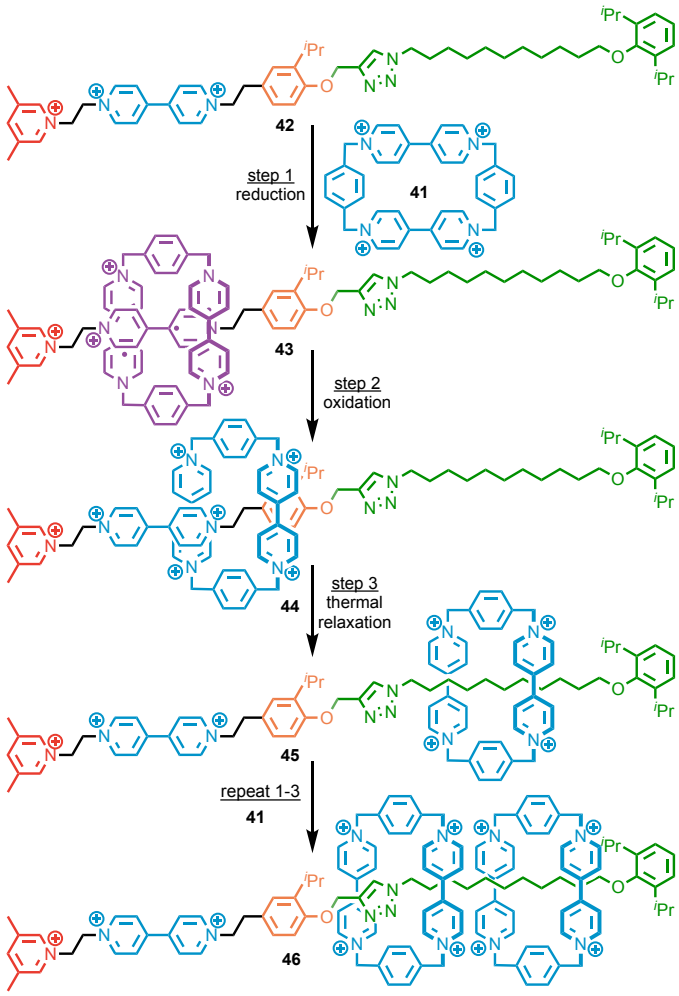

Figure 288: Stoddart and co-workers' macrocycle pump.[25,26,31] (Counter-ions omitted for clarity). Electrochemical reduction causes threading of **41** onto the favourable radical-cation station (purple). Reoxidation causes the macrocycle to occupy the ethylene group (**44**) further away from the positive pyridinium units (red and blue). Thermal relaxation over the isopropyl group (orange) traps the macrocycle onto the axle (green) forming rotaxanes **45** and **46**.

This same pump-moiety has been utilised to thread up to 10 macrocycles (**47**, carrying 40^{+} charge) onto a polyethyleneglycol chain through sequential redox cycles (Figure 289a).[32] Furthermore, Stoddart and co-workers have combined this electrochemical energy ratchet mechanism with a photocleavable nitrobenzyl stopper (Figure 289b).[33] This enabled the threading of macrocycles onto an axle with electrochemical stimuli, and then controlled release of them with an orthogonal stimuli (365 nm radiation).[33]

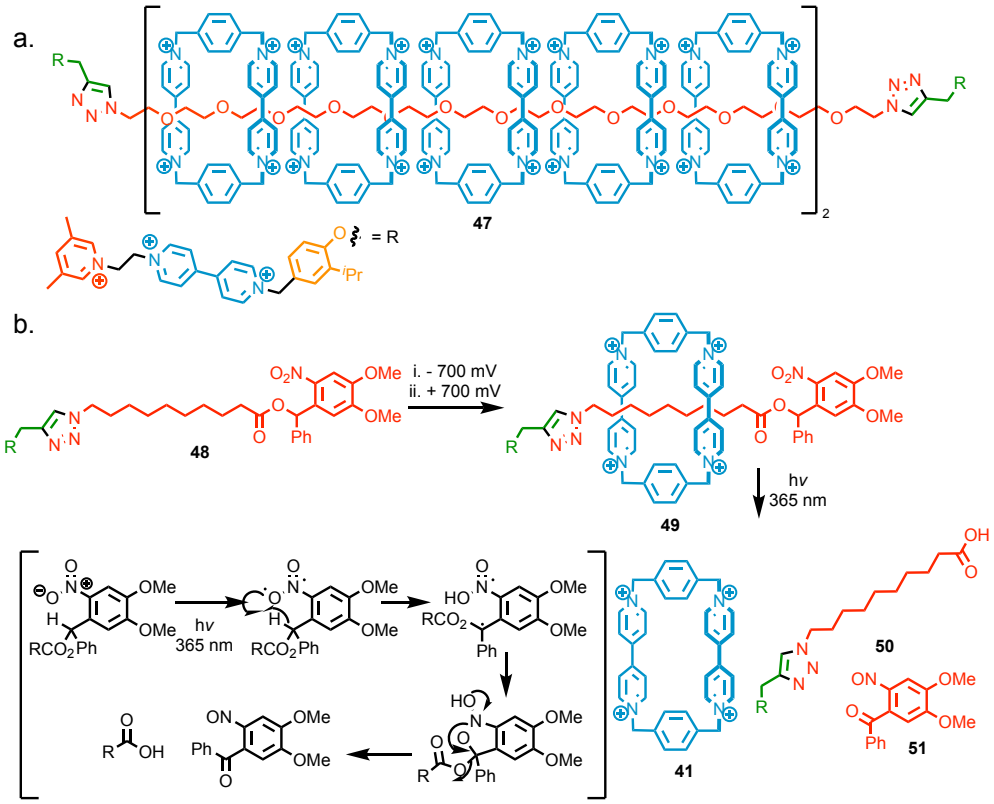

Figure 289: Stoddart and co-workers' (a) polyrotaxane synthesiser **47**,[32] and (b) photocleavable macrocycle release.[33] (Counter-ions omitted for clarity).

Molecular shuttles have allowed chemists to create switchable activity,[34] synthesise otherwise challenging interlocked structures,[35] and to carry out complex procedures for molecular motion[24,36,37] or molecular assembly.[38–40] Molecular shuttles mediate complex behaviour through information or energy ratchet mechanisms.[41] The shuttling of a macrocycle from one station to another is commonplace, however no applications of this approach to retain mechanical chirality have been reported before. The aim of this work is to utilise molecular shuttles to synthesise a library of MPC ligands to further explore the properties of this type of chirality.

3.1.2. Non-Interlocked Molecular Machines

The most iconic molecular motor is Feringa's unidirectional rotor **52**, operating in a pulsed energy ratchet mechanism.[42–44] This example uses light to drive the motor to a higher energy state, **53**, which is followed by thermal relaxation to a local thermodynamic minimum, **54**. A second pulse of light pushes the switch to another higher energy state, **55**, which then thermally relaxes to the beginning conformation **52**. The favourable conformational equilibria results in minimal back rotation and a net flux

of material around the cyclic reaction network.[42–44] The utilisation of light in this system switches the molecule between two complimentary potential surfaces which re-equilibrate to the (*P*,*P*) ground states before being switched to the other potential surface.

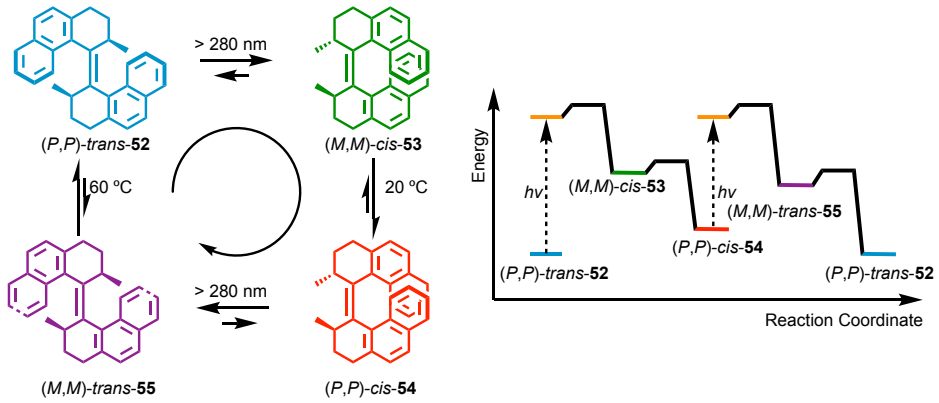

Figure 290: Feringa's unidirectional motor (*P*,*P*)-*trans*-**52**.[42,44,45] *Cis-Trans* photoisomerization promotes the switch to a higher energy (*M*,*M*)-helicity. Thermal relaxation to (*P*,*P*)-helicity and subsequent photoisomerization result in unidirectional rotation.

The molecular walker of Leigh and co-workers operates by an information ratchet mechanism (Figure 291). Lipase AS selectively hydrolyses the rear foot of the walker **57**, resulting in $k_{iiR} > k_{iiS}$ and net-flux of the walker across the track (**57** to **58**).[46] Upon macrocyclization to **59**, the rear foot creates an (*R*)-stereocentre, which has a kinetic preference for hydrolysis by Lipase AS, thus enabling progression of the walker along the track to **60** by an information ratchet mechanism. Upon macrocyclization (**57** or **59**), the front foot creates an (*S*)-stereocentre which is inert to Lipase AS hydrolysis.[46] 68% of bipedal walkers take two steps along the track upon iterative cycles, despite no thermodynamic preference for doing so.

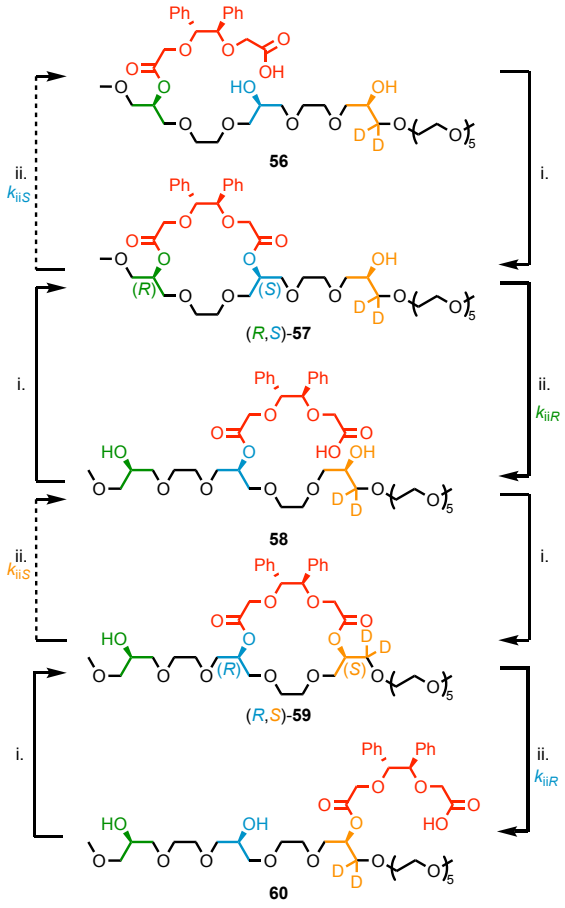

Figure 291: Leigh and co-workers' unidirectional molecular walker **56**.[46] (i) 2,4,6-$Cl_3C_6H_2COCl$, DMAP, Et_3N, $CHCl_3$, 0.05 mM, rt, 20 h and (ii) lipase AS (3.0 equiv w/w), H_2O, 18 mM, 40 °C, 40−64 h. Note: The (S)-stereogenic centre in **59** and **60** has been labelled such as in the initial publication, however by CIP rules it is in fact (*R*) due to D>H priority. Labelling this stereocentre (*S*) follows general structure rule in **56**-**58** and is not hydrolysed by the enzyme.

3.2. Results and Discussion

3.2.1. The Synthesis of Enantioenriched Ligands by Post-Synthetic Modifications

The low diastereoselectivity of the AT-CuAAC reaction was deemed to be the major limiting factor in the synthesis of the first generation MPC catalyst [Au((R_{mp})-**6**)(Cl)] (Figure 279a).

It has previously been observed that bulky aromatic alkynes react with azide (*S*)-**62** to give high diastereoselectivities in the AT-CuAAC step. Thus, alkyne **61** was designed to enable the synthesis of a modifiable rotaxane with high diastereoisomeric excess in the mechanical bond forming step (Figure 292). There are two major benefits to this approach. Firstly, the aromatic alkyne reduces the necessity of challenging diastereoisomer separations, and secondly, a late stage functionalisation would enable facile and systematic modification of the catalyst structure, through choice of the phosphine substituents.

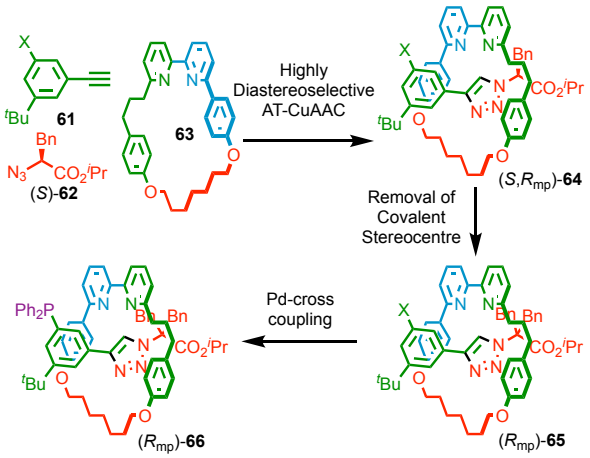

Figure 292: Proposed route to functionable rotaxanes with high enantiomeric excesses, where X = Br, I.

3.2.2. Synthesis of a Functionable Mechanically Planar Chiral Rotaxane

Bromo- and Iodo- stoppers **61a** and **61b** were synthesised in good yields by modified literature procedures. The 1,3,5-trisubstituted arenes were chosen to begin with due to accessibility and the expected low conversion from other substitution patterns. The AT-CuAAC reaction with bromo-stopper **61a** yielded only axle (*S*)-**71a**, due to the interlocked intermediate dissociating upon proto-demetallation of the Cu^{I}-triazolide intermediate. Modification to the iodide substituted arene **61b** resulted in a bulkier stopper.

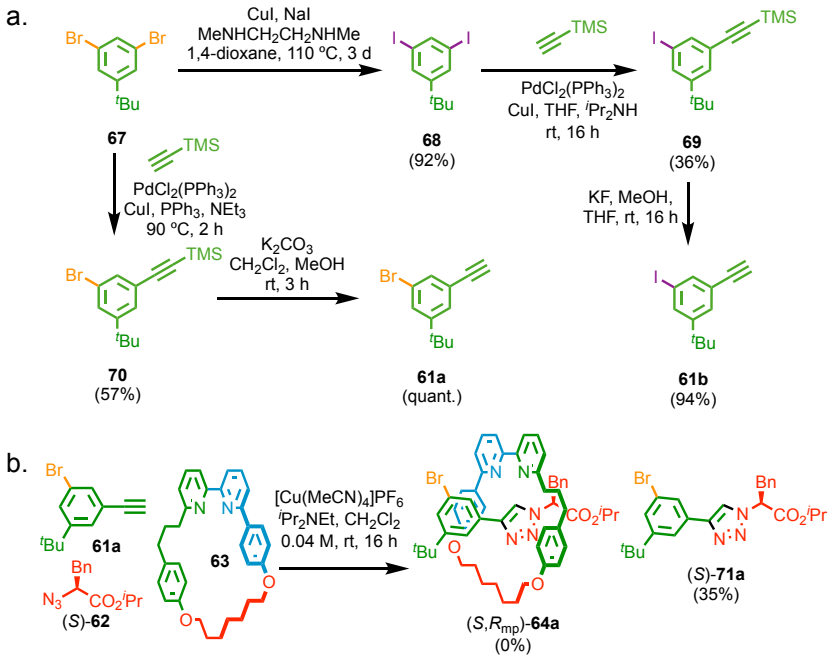

Figure 293: (a) Synthesis of stoppers **61a** and **61b**. (b) Attempted AT-CuAAC synthesis of (*S*,R_{mp})-**64a**, yielding only (*S*)-**71a**.

The AT-CuAAC reaction with **61b** yielded rotaxane (*S*,R_{mp})-**64b** in 86% yield and an excellent *dr* of 95 : 5. Alkylation gave (R_{mp})-**65b** leaving only the MPC stereogenic element with *er* 95 : 5 (Figure 294). Pd cross-coupling gave phosphine oxide (S_{mp})-**72**. Subsequent reduction and complexation to Au^{I} gave (S_{mp})-**73** in excellent enantiomeric excess. This approach was significantly less synthetically challenging, and provided a good scaffold to modify phosphine substituents with ease. The Ph_2PH-coupling reaction was not optimised, hence the lower yield. However, 50% of the starting material (R_{mp})-**65b** was recovered reducing the waste of this low yield reaction.

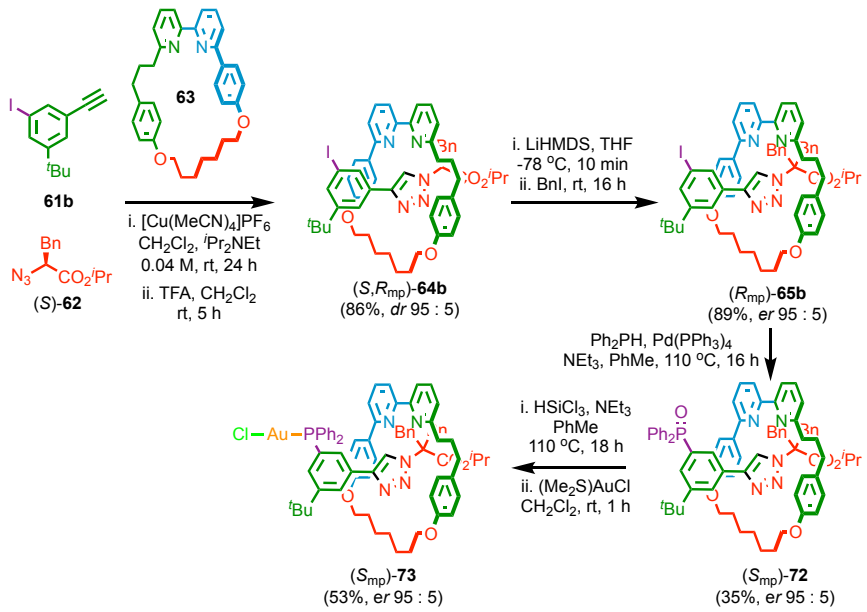

Figure 294: Synthesis of MPC Au^{I}-complex (S_{mp})-**73**.

With interlocked catalyst (S_{mp})-**73** in hand in 90% *ee*, a range of Au^{I}-catalysed reactions were screened to test this post-synthetic modification approach of catalyst generation. Unfortunately this catalyst did not achieve significant enantioselectivity in any of the tested Au^{I}-catalysed reactions (Figure 295), most likely a result of the large distance between the mechanical stereogenic centre and the Au^{I} atom. Furthermore, the largest *P*-substituent (AuCl) can orient freely to point away from the mechanical bond. This catalyst showed some slightly improved enantioselectivity, compared to the original catalyst [Au((R_{mp})-**6**)(Cl)], for Echavarren's cycloisomerization of **12** to **13** (*er* 45 : 55).[4] However, generally the enantioselectivity was poor.

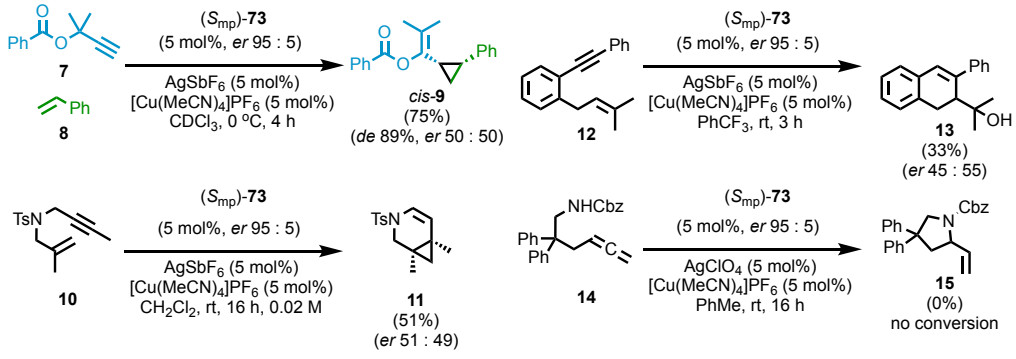

Figure 295: Results from a range of (S_{mp})-**73**-mediated Au^{I} catalytic reactions.

The aryl-stopper approach was redesigned to project the Au^{I} atom closer to the stereogenic mechanical bond (Figure 296a). Furthermore, by placing the P-ligand *ortho* to the triazole, we hoped to produce an environment more similar to Echavarren and co-workers' distant C_2-symmetric John-Phos ligands.[4] Unfortunately the active template

step was inefficient with the extremely bulky alkyne **79**, resulting in recovery of the macrocycle, no rotaxane, and 65% isolated yield of the axle (*S*)-**81** (Figure 296b).

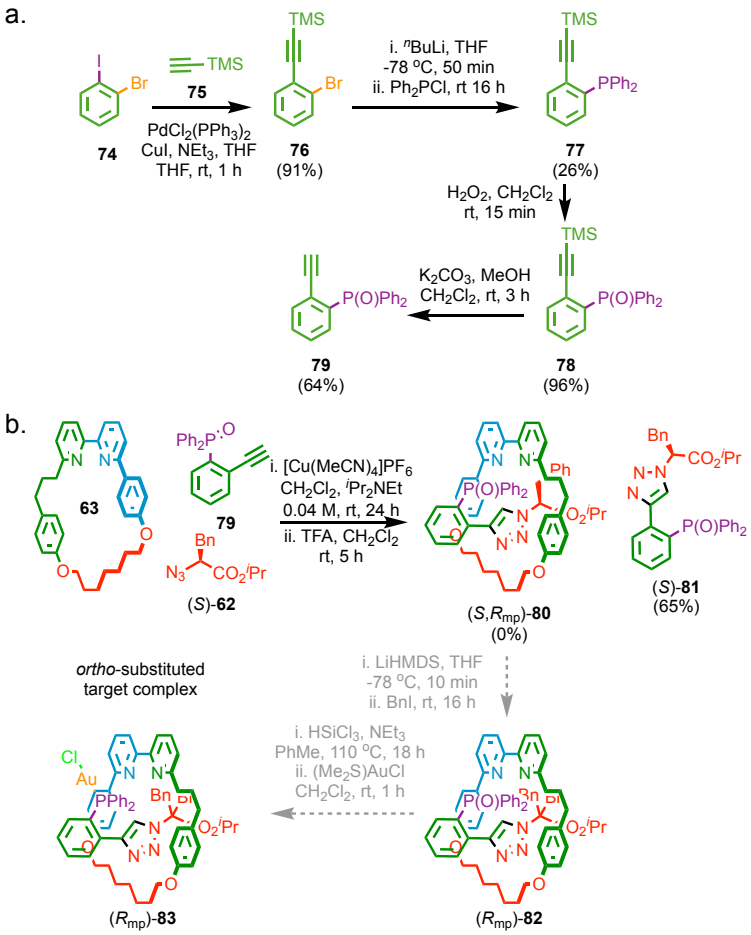

Figure 296: (a) Synthesis of *ortho*-substituted stopper **79**, and (b) proposed catalyst synthesis (R_{mp})-**83**.

Attempts at redesigning the approach *via* the 1-ethynyl-2-iodobenzene stopper yielded the Cu^{I}-triazolide intermediate from the AT-CuAAC step. However, axle and macrocycle dissociated upon demetallation, yielding only axle (*S*)-**87**. Furthermore, the AT-CuAAC was inefficient due to the size of the iodide bearing stopper **85**, requiring 10 equivalents of stopper to convert the macrocycle to the interlocked intermediate.

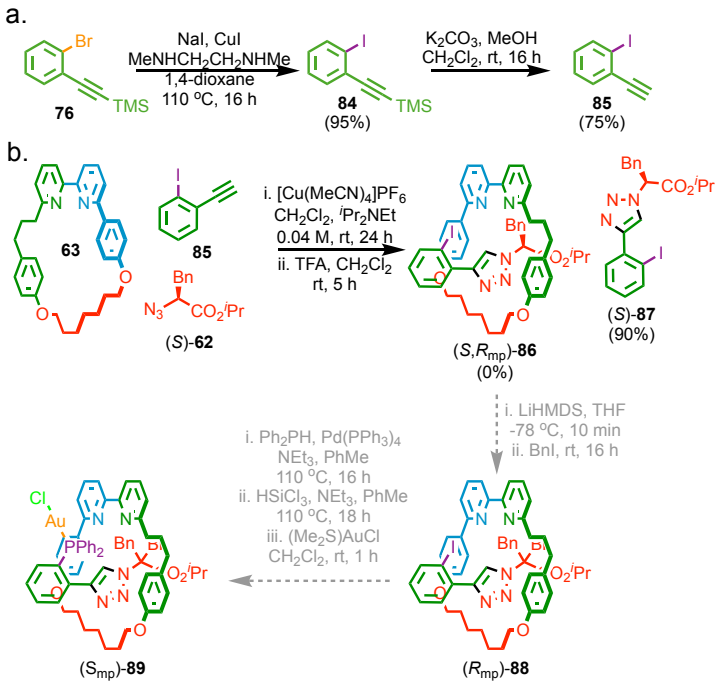

Figure 297: (a) Synthesis of *ortho*-substituted stopper **85**, and (b) proposed catalyst synthesis (S_{mp})-**88**.

It was concluded that a post-synthetic modification approach was likely to be more challenging than expected. Also, a new methodology was developed in the group with potential to be applied to MPC ligands. This recent work by de Juan, Lozano and Jinks is described here as an introduction to my new approach to MPC ligands.

3.2.3. Stereodirecting Auxiliary with Co-Conformational Bias

***90** was synthesised by Dr Mike Jinks, rotaxane (S,S_{mp})-**92** was synthesised by Dr Alberto de Juan. Dr David Lozano acquired and solved the single crystal X-ray structure of (S,S_{mp})-**92**.*

Subsequent to Goldup and co-workers' diastereoselective synthesis of MPC rotaxanes in up to 96% *ee*,[48] it was discovered that *ortho*-methyl alkyne **90** gave high *dr* with distant bulky stoppering units (Figure 298). Furthermore, the ^{1}H NMR of this compound had a reduced chemical shift for the triazole proton, and increased chemical shift of the benzylic ether protons implying H-bonding. This implied that the methyl group destabilises the H-bonding environment between the macrocycle and the triazole proton. The conclusion drawn from this data was that the methyl group both reliably increased the *dr* of the AT-CuAAC to predictable and repeatable levels, and that the methyl group destabilises the triazole station, encouraging shuttling of the macrocycle away from this environment.

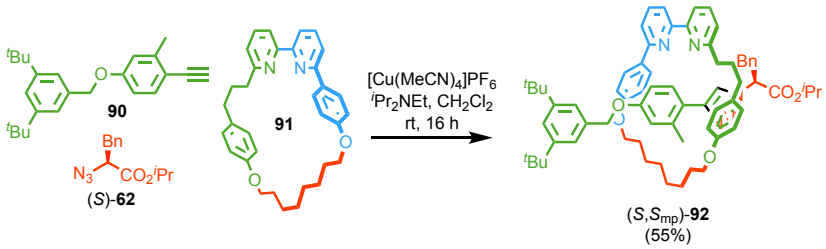

Figure 298: Synthesis of rotaxane (S,S_{mp})-**92** in > 99 : 1 *dr* (Synthesis of **90** was completed by Dr Mike Jinks, and the synthesis of (S,S_{mp})-**92** was completed by Dr Alberto de Juan).

A crystal structure of a racemic mixture of (S,S_{mp})-**92** and (R,R_{mp})-**92** allowed absolute assignment of the MPC stereogenic element (Figure 299). Pleasingly, this crystal structure proved that the MPC stereogenic element is the same orientation as in (S,S_{mp})-**156** (chapter 1).

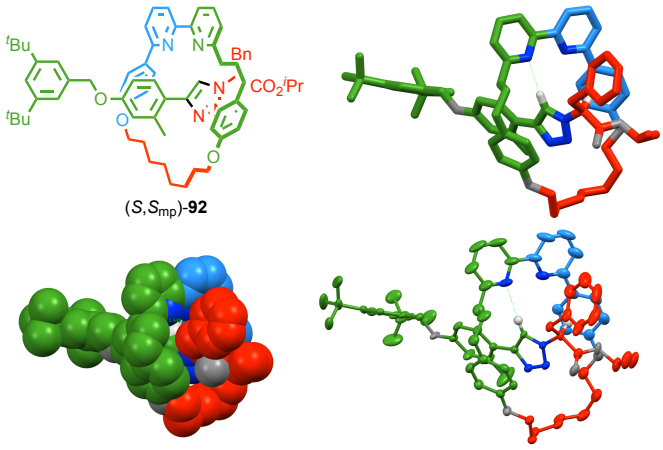

Figure 299: Single crystal X-ray structure of a racemic mixture of (*S*,*S*$_{mp}$)-**92** and (*R*,*R*$_{mp}$)-**92** [$C_{69}H_{81}N_5O_5$]. Solvent molecules omitted for clarity. Crystal structure acquired and solved by Dr David Lozano.

As high diastereoselectivities for the AT-CuAAC step were now reliably accessible, we devised a general shuttle-based approach for synthesising enantiopure MPC ligands. In summary, the *ortho*-methyl substituent on alkyne **90** was large enough to give high diastereoselectivities (*dr* > 99 : 1) in the AT-CuAAC step, and to destabilise the binding of the macrocycle to the triazole station. However this substituent was also small enough for the macrocycle to shuttle over it and occupy the less hindered distant station. The *ortho*-methyl alkyne **90** was compatible with azide (*S*)-**62** resulting in highly diastereoselective AT-CuAAC reactions.

3.2.4. A Molecular Shuttle Approach to the Synthesis of MPC Rotaxanes

The work described in Figure 300 was completed by Drs Alberto de Juan, David Lozano and Mike Jinks.

After discovering that the *ortho*-methyl alkyne **90** gave high *dr* for the AT-CuAAC step, and biased the co-conformation of the product, alkynes **93** were synthesised with a receiving station and cleavable ester link (Figure 300). Both **93a** (R = H) and **93b** (R = PMB) gave (*S*,*S*$_{mp}$)-**94** in high diastereoselectivity. After cleavage with TFA (in the case of **93b**), the macrocycle was trapped on the receiver unit by forming the methyl ester (*S*,*S*$_{mp}$)-**95**. Transesterification cleaved the auxiliary, yielding the MPC rotaxane (*S*$_{mp}$)-**96** in 52% yield over 4 steps and in 97% *ee*. This approach proved applicable for a range of receiving units, enabling access to MPC rotaxanes (*S*$_{mp}$)-**97**-**99** (in > 94% *ee*) with no traceable templating units in the axle.

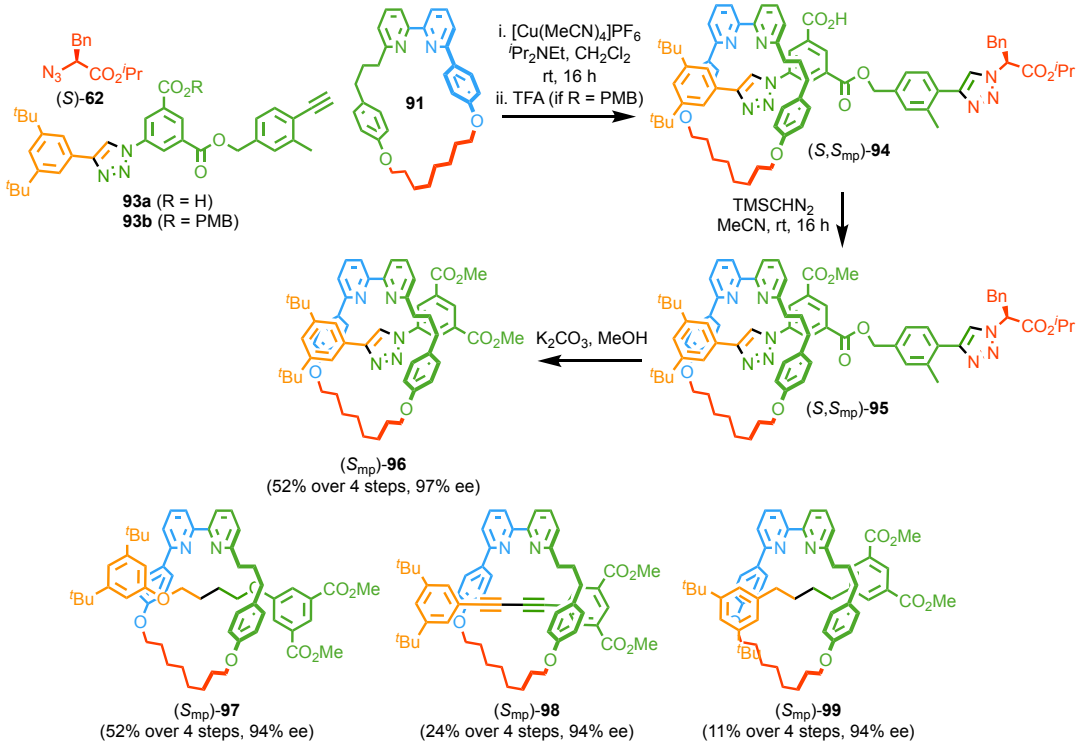

Figure 300: A first generation molecular shuttle. This work is currently unpublished and was completed by Drs Alberto de Juan, David Lozano and Mike Jinks. The rest of this chapter builds on this methodology.

3.2.5. A Proposed MPC Molecular Shuttle Approach to Chiral Phosphines

This optimised second generation shuttle approach was designed in collaboration with Dr Jorge Meijide Suarez from key discoveries earlier in this chapter, and completed by the author.

Earlier in this chapter, the 3-bromo-5-ethynylbenzoate moiety was found to be an ineffective stopper, as it was observed that macrocycle **63** dissociated from the Cu^{I}-triazolide intermediate upon proto-demetallation. This group (green, Figure 301) was used as a spacer between the AT-CuAAC compatible alkyne unit, and the final receiving unit (orange, Figure 301). Aryl bromide moieties are easily functionalised by Pd cross-coupling, providing a facile approach to trap the macrocycle in the preferable co-conformation as well as allowing effective variation of the receiving station.

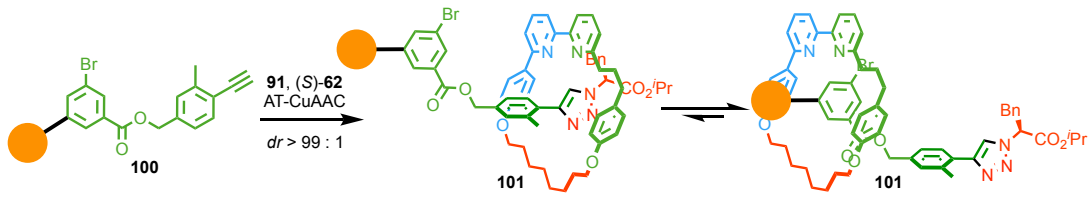

Figure 301: General approach to synthesising *dr* > 99 : 1 rotaxanes.

3.2.6. Synthesis of the Molecular Shuttles

Figure 302 shows the synthesis of the molecular shuttle. Each reaction was a moderate to high yielding, simple transformation from commercially available starting materials. Alkyne **108** could be loaded with the final stoppering unit by a facile CuAAC reaction, however any other linking reaction type would also be appropriate. Once the end group had been loaded onto the central unit, the terminal alkyne was deprotected, yielding alkyne **110** as the final building block before the AT-CuAAC step.

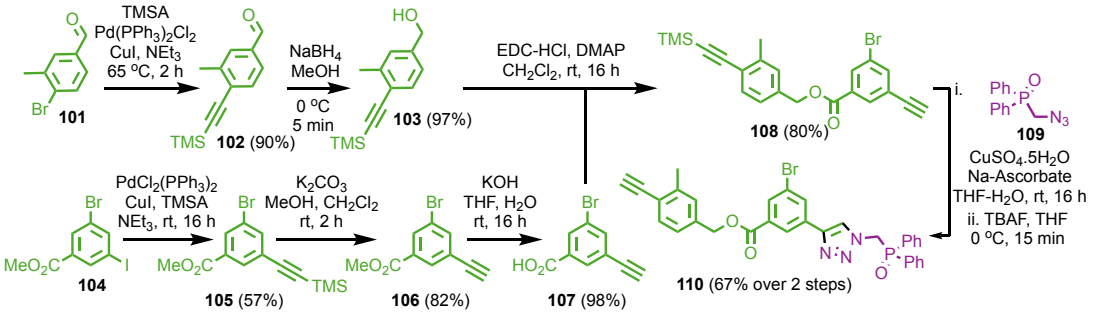

Figure 302: Synthesis of molecular shuttle building blocks.

Azide (*S*)-**62**, alkyne **110** and macrocycle **91** were reacted in 1 : 1 : 1 ratio, yielding the interlocked product (*S*,R_{mp})-**111** in excellent 85% yield (Figure 303). Only one diastereoisomer was observed by LCMS, ^{1}H and ^{31}P NMR. The diastereoselectivity of the AT-CuAAC step was ultimately determined by enantiomeric excess of the final rotaxane. It is worth noting that the Br-substituent led to slow exchange between co-conformations, which were observed by LCMS and ^{1}H NMR at a ratio of 80 : 20 in the favourable receiving station. An investigation of solvents showed that in polar protic solvents such as CD_3OD, a lower selectivity of 60 : 40 was achieved. However, in most other solvents ($CDCl_3$, CD_3CN, d^8-PhMe, and d^8-THF) greater than 80 : 20 ratio was observed and no higher shuttling efficiency could be achieved.

Suzuki-Miyaura cross-coupling of (*S*,R_{mp})-**111** with $PhB(OH)_2$ was completed in 93% yield, giving an 80 : 20 ratio of co-conformational isomers of (*S*,R_{mp})-**112** by ^{1}H NMR. Transesterification yielded the final rotaxane in 70% yield and 99 : 1 *er*. Furthermore, the macrocycle **91** released from the minor co-conformational isomer was recovered, reducing any wasted synthetic effort.

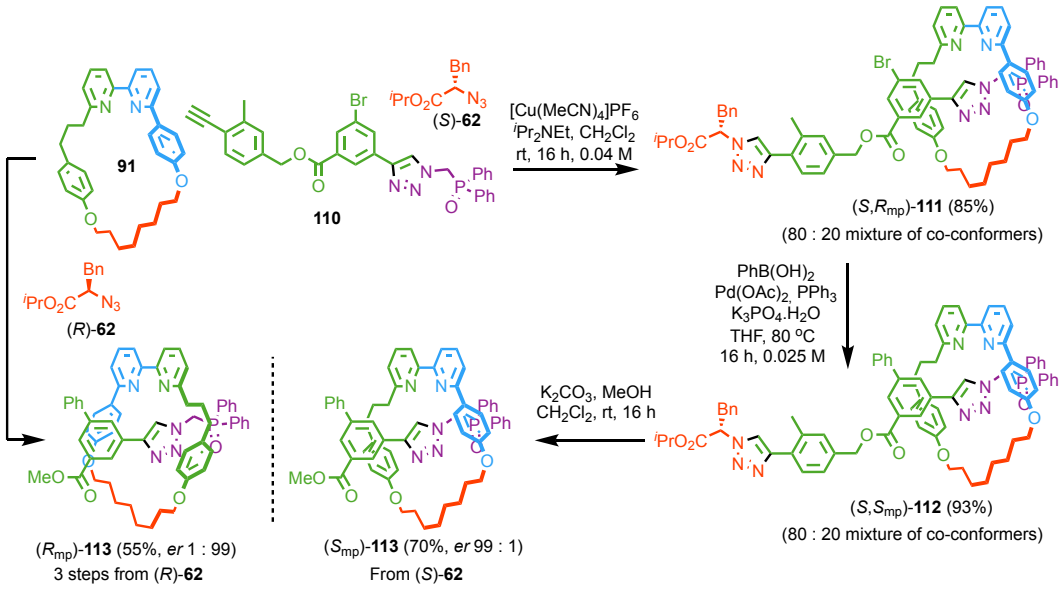

Figure 303: of (S_{mp})-**113** and (R_{mp})-**113** by a molecular shuttle approach.

As shown in Figure 303, the central 1,3,5-trisubstituted aryl bromide allowed facile gating. The 3-methyl-4-ethynylbenzyl alcohol motif gave an efficient route to high *dr* MPC rotaxanes. The ester linkage between these two motifs allows facile cleavage of the chiral directing group subsequent to Pd-catalysed gating. From the AT-CuAAC step, there are 3 steps to the synthesis of enantiopure phosphine oxide (S_{mp})-**113**. Furthermore, both enantiomers are accessible using naturally occurring (*S*)- or (*R*)-phenylalanine. The ability to synthesise enantiopure (S_{mp})-**113** in such high yields (55% over 3 steps is a significant improvement in the synthesis of MPC ligands.

This shuttle approach was used to synthesise (S_{mp})-**113** and (R_{mp})-**113**, both in 98% *ee* as confirmed by CSP-HPLC (Figure 304a). The circular dichroism spectra of these rotaxanes are mirror images of each other (Figure 304b), as would be expected from two opposite enantiomers.

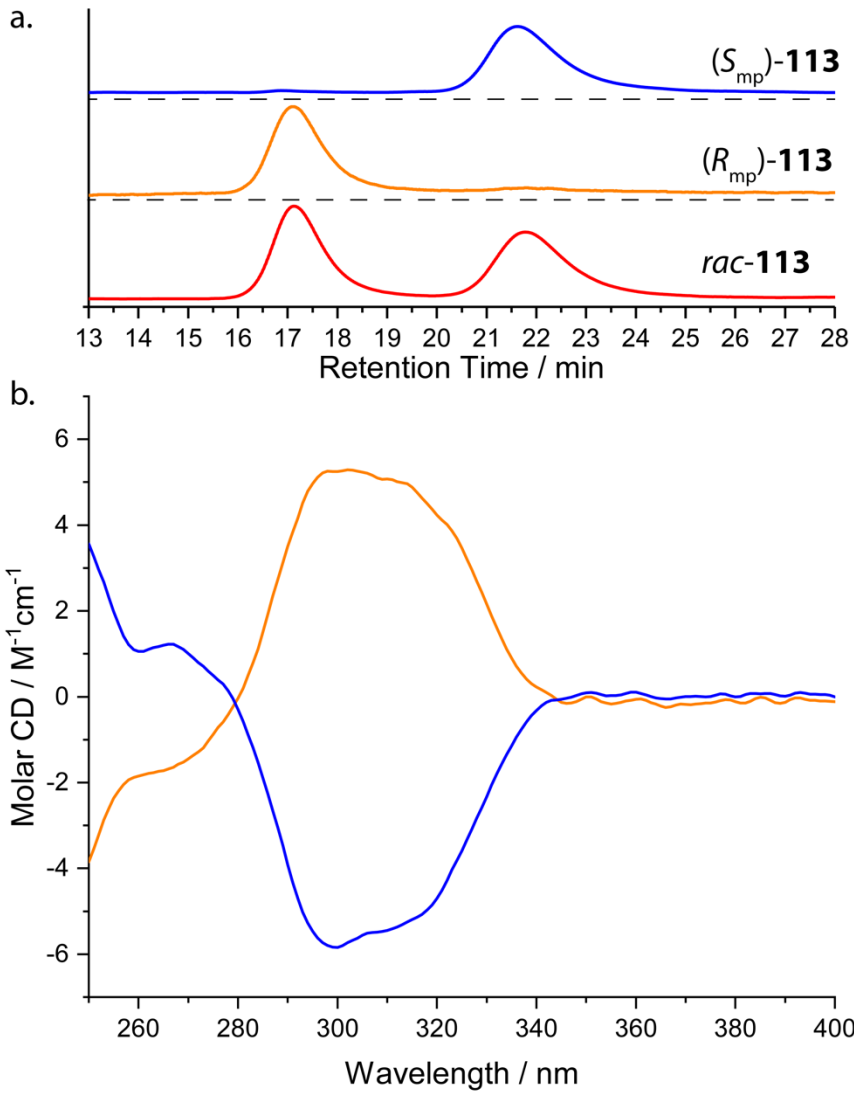

Figure 304: (a) CSP-HPLC of **113** (loaded in EtOAc). RegisPackCLA, n-hexane-ethanol 80 : 20, flowrate 1.0 mLmin-1. Top (blue) (S_{mp})-**113**, (R_{mp})-**113** (16.9 min, 13038, 0.6%), (S_{mp})-**113** (21.6 min, 2350108, 99.4%). Middle (orange) (R_{mp})- **113**, (R_{mp})- **113** (17.1 min, 327587, 98.3%), (S_{mp})-**113** (21.8 min, 5820, 1.7%). Bottom (red) *rac*-**113** (R_{mp})-**113** (17.1 min, 1110899, 50.2%), (S_{mp})-**113** (21.8 min, 1102314, 49.8%). (b) Circular Dichroism Spectra of (R_{mp})-**113** (24.1 µM, *er* 99 : 1, orange) and (S_{mp})-**113** (22.3 µM, *er* 1 : 99, blue) at 293 K in $CHCl_3$.

3.2.7. Investigation of Triazole Orientation

The advantage of the molecular shuttle approach, is that the phosphine component can be loaded in either orientation. To demonstrate this, shuttle precursor **118** was synthesised from 3-amino-5-bromobenzoic acid **114** in good yield by simple transformations (Figure 305).

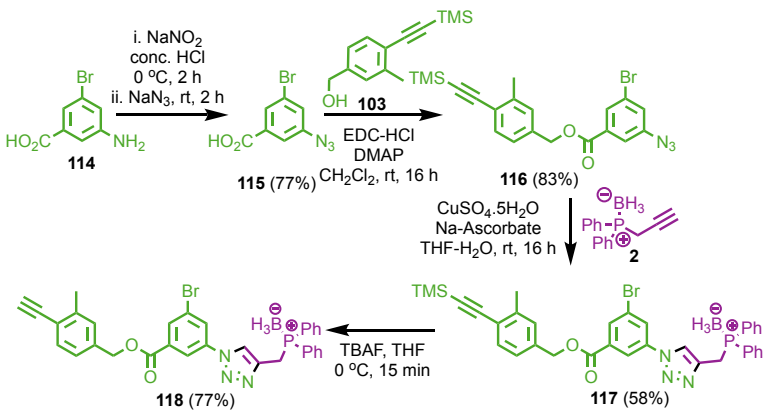

Figure 305: Synthesis of a molecular shuttle building block **118** with the opposite triazole configuration.

Azide (*S*)-**62**, alkyne **118** and macrocycle **91** were reacted in 1 : 1 : 1 ratio, yielding the interlocked product (S,S_{mp})-**119** in 46% yield over two steps (Figure 306). Only one diastereoisomer was observed by ^{1}H NMR, and so the diastereoselectivity of the AT-CuAAC step was determined by enantiomeric excess of the final rotaxane. Suzuki-Miyaura cross-coupling of (S,S_{mp})-**119** with $PhB(OH)_2$ was completed in 93% yield, giving an 80 : 20 ratio of co-conformational isomers of (S,S_{mp})-**120** by ^{1}H NMR. Transesterification yielded the final rotaxane (S_{mp})-**121** in 99 : 1 *er*.

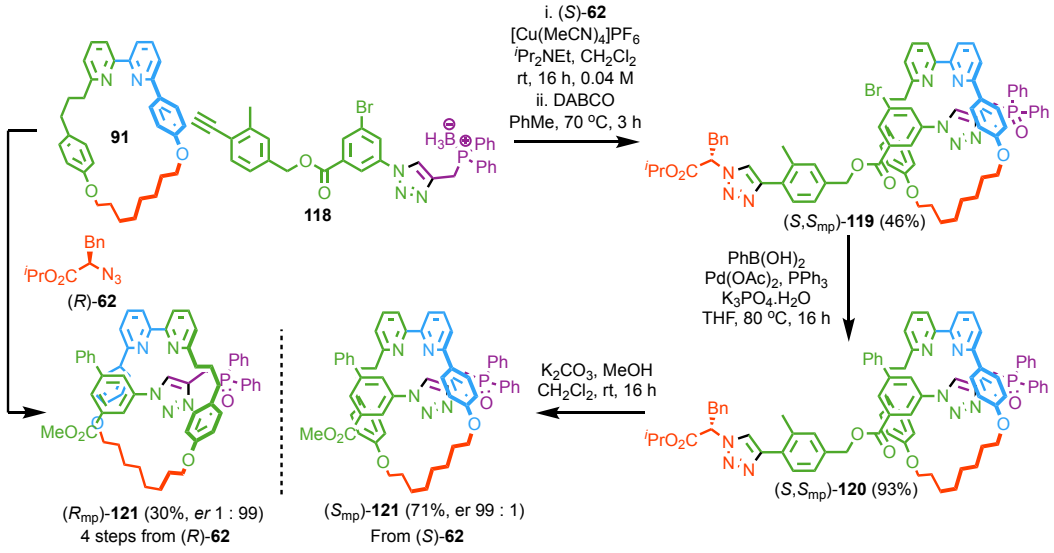

Figure 306: Molecular shuttle approach to the synthesis of (S_{mp})-**121** and (R_{mp})-**121** in 98% *ee*.

3.2.8. Synthesis of the Enantiopure Au^{I}-Complexes for Catalysis

Enantiopure rotaxanes (S_{mp})-**113** and (S_{mp})-**121** were reduced and complexed to Au^{I}, forming (S_{mp})-**122** and (S_{mp})-**123** in 79% and 98% yield respectively (Figure 307). Unfortunately, neither of these catalysts showed enantioselectivity for the cyclopropanation of alkynes with styrene. The metallo-rotaxane active catalysts, with Cu^{I} bound to three *N*-atoms, gave the same enantioselectivity despite a presumed large difference in orientation of the axle in the coordination product.

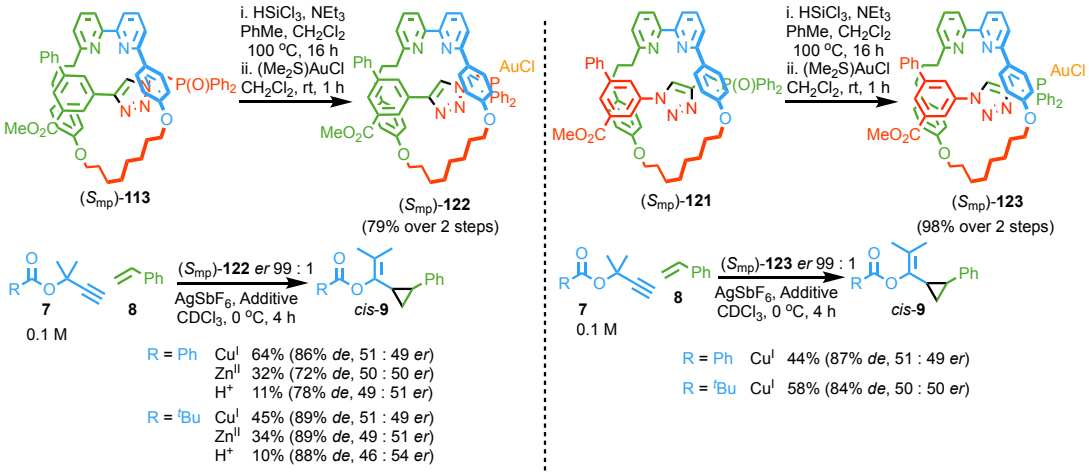

Figure 307: Synthesis of MPC Au^{I}-complexes (S_{mp})-**122** and (S_{mp})-**123** and their mediation of Au^{I}-catalysed cyclopropanation reactions.

When compared to catalyst [((R_{mp})-**6**)AuCl], one notable difference is the size of the stopper. We had already observed an increase in *ee* from 13% to 60% upon alkylation of the stereocentre in (*S*,R_{mp})-**4** to (R_{mp})-**5**. The 3-Ph-5-CO_2Me stopper is significantly smaller, and crucially, does not contain a bulky quaternary carbon adjacent to the triazole. Modification of the shuttle methodology to allow a quaternary carbon centre may increase the efficiency of chiral induction between the mechanical bond and the catalytic active site. Alternatively, Suzuki-Miyaura cross-coupling with 3,5-*di*-tert-butyl phenylboronic acid or other bulky boronic acids could result in sufficient bulk to increase the chiral induction.

3.3. Conclusions and Future Designs

In conclusion, building upon the first example of enantioselective catalysis with an MPC stereogenic element, we have achieved a general methodology to make an MPC ligand with any axle in 99 : 1 *er*. The synthesis of the two enantiopure MPC ligands developed in this chapter was significantly faster than in chapter 2, potentially allowing a much

more systematic investigation of the properties of MPC. Unfortunately the ligands synthesised with this MPC shuttle methodology did not show any enantioselectivity for Au^{I}-catalysed cyclopropanation reactions. However, this methodology provides many opportunities for modification which will be completed in the future.

Future work on this project will include investigation of a bulky quaternary carbon stopper more analogous to the stopper in chapter 2. It will also include investigation of different linkers between the shuttling moiety and the phosphine ligand, such as (diphenylphosphino)acetate esters. Furthermore variation of the phosphine substituents (including *ortho*-tolyl and naphthyl groups) should be investigated.

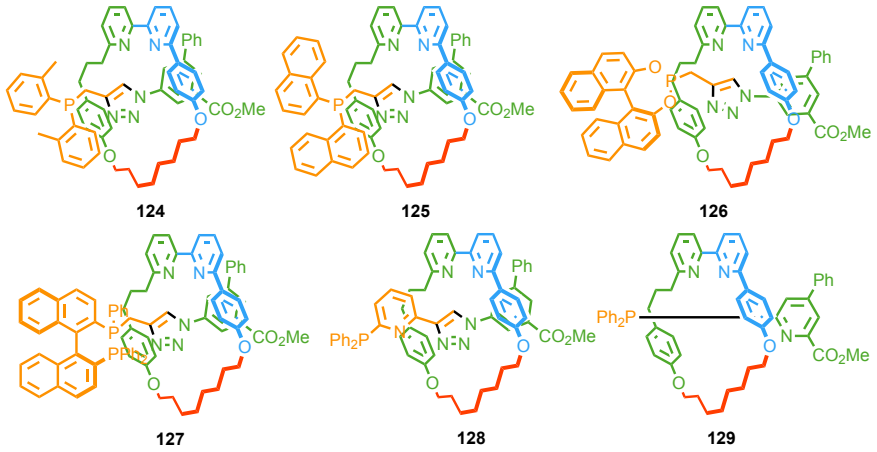

Figure 308: Future target MPC ligands using a molecular shuttle approach. Work is currently underway to synthesise these MPC ligands. These will allow further optimisation and exploration of new transition metal catalysed reactions.

3.4. Final Remarks

Although this thesis ends on a somewhat anticlimactic result, it is important to stress that this is the first demonstration of this new type of chirality for enantioselective catalysis (chapter 2), as well as reporting a new methodology to synthesise MPC rotaxanes with high enantiopurity (chapter 3). The next generation of these MPC catalysts will hopefully be highly selective and much faster to investigate, building on this work.

3.5. Bibliography

[1] A. W. Heard, S. M. Goldup, *Chem* **2020**, *6*, 994–1006.

[2] M. Galli, J. E. M. Lewis, S. M. Goldup, *Angew. Chem. Int. Ed.* **2015**, *54*, 13545–13549.

[3] M. Calles, J. Puigcerver, D. A. Alonso, M. Alajarin, A. Martinez-Cuezva, J. Berna, *Chem Sci* **2020**, *11*, 3629–3635.

[4] G. Zuccarello, J. G. Mayans, I. Escofet, D. Scharnagel, M. S. Kirillova, P. Calleja, J. R. Boothe, A. M. Echavarren, A. H. Pe, *J. Am. Chem. Soc.* **2019**, *141*, 11858–11863.

[5] E. M. Purcell, *Am. J. Phys.* **1977**, *45*, 3–11.

[6] R. D. Astumian, *Phys. Chem. Chem. Phys.* **2007**, *9*, 5067–5083.

[7] A. W. Heard, S. M. Goldup, *ACS Cent. Sci.* **2020**, *6*, 117–128.

[8] J. F. Stoddart, *Angew. Chem. Int. Ed.* **2017**, *56*, 11094–11125.

[9] J. P. Sauvage, *Angew. Chem. Int. Ed.* **2017**, *56*, 11080–11093.

[10] D. A. Leigh, *Angew. Chem. Int. Ed.* **2016**, *55*, 14506–14508.

[11] R. A. Bissell, E. Cordova, A. E. Kaifer, J. F. Stoddart, *Nature* **1994**, *369*, 133–137.

[12] V. Balzani, A. Credi, G. Mattersteig, O. A. Matthews, M. Raymo, J. F. Stoddart, M. Venturi, A. J. P. White, D. J. Williams, *J. Org. Chem.* **2000**, *65*, 1924–1936.

[13] J. Collin, C. Dietrich-buchecker, M. C. Jimenez-molero, J. Sauvage, *Acc. Chem. Res.* **2001**, *34*, 477–487.

[14] J.-P. Collin, A. P. Gavin, J.-P. Sauvage, *New J. Chem.* **1997**, *21*, 525–528.

[15] J. D. Badjic, V. Balzani, A. Credi, S. Silvi, J. F. Stoddart, *Science* **2004**, *303*, 1845–1849.

[16] S. Silvi, M. Venturi, A. Credi, *J. Mater. Chem.* **2009**, *19*, 2279–2294.

[17] V. Balzani, M. Clemente-León, A. Credi, J. N. Lowe, J. D. Badjić, J. F. Stoddart, D. J. Williams, *Chem. Eur. J.* **2003**, *9*, 5348–5360.

[18] K. Zhu, G. Baggi, S. J. Loeb, *Nat. Chem.* **2018**, *10*, 625–630.

[19] H. Tian, Q.-C. Wang, *Chem. Soc. Rev.* **2006**, *35*, 361–374.

[20] S. M. Goldup, *Nature* **2018**, *557*, 39–40.

[21] V. Balzani, M. Clemente-leon, A. Credi, B. Ferrer, M. Venturi, A. H. Flood, J. F. Stoddart, *Proc. Natl. Acad. Sci.* **2006**, *103*, 1178–1183.

[22] C. Biagini, S. Albano, R. Caruso, L. Mandolini, J. A. Berrocal, S. Di Stefano, *Chem. Sci.* **2018**, *9*, 181–188.

[23] S. Erbas-Cakmak, S. D. P. Fielden, U. Karaca, D. A. Leigh, C. T. Mcternan, D. J. Tetlow, M. R. Wilson, *Science* **2017**, *358*, 340–343.

[24] M. R. Wilson, J. Solà, A. Carlone, S. M. Goldup, N. Lebrasseur, D. A. Leigh, *Nature* **2016**, *534*, 235–240.

[25] C. Cheng, P. R. Mcgonigal, S. T. Schneebeli, H. Li, N. A. Vermeulen, C. Ke, J. F.

Stoddart, *Nat. Nanotechnol.* **2015**, *10*, 547–553.

[26] S. Goldup, *Nat. Nanot* **2015**, *10*, 488–489.

[27] I. Aprahamian, J. Olsen, A. Trabolsi, J. F. Stoddart, *Chem. Eur. J.* **2008**, *14*, 3889–3895.

[28] Y. Wang, M. Frasconi, J. F. Stoddart, *ACS Cent. Sci.* **2017**, *3*, 927–935.

[29] I. Aprahamian, *ACS Cent. Sci.* **2020**, *6*, 347–358.

[30] K. Cai, Y. Shi, G. Zhuang, L. Zhang, Y. Qiu, D. Shen, H. Chen, Y. Jiao, H. Wu, C. Cheng, *J. Am. Chem. Soc.* **2020**, *142*, 10308–10313.

[31] Y. Qiu, Y. Feng, Q. H. Guo, R. D. Astumian, J. F. Stoddart, *Chem* **2020**, *6*, 1952–1977.

[32] Y. Qiu, B. Song, C. Pezzato, D. Shen, W. Liu, L. Zhang, Y. Feng, Q. Guo, K. Cai, W. Li, *Science* **2020**, *368*, 1247–1253.

[33] Q. H. Guo, Y. Qiu, X. Kuang, J. Liang, Y. Feng, L. Zhang, Y. Jiao, D. Shen, R. D. Astumian, J. F. Stoddart, *J. Am. Chem. Soc.* **2020**, *142*, 14443–14449.

[34] V. Blanco, A. Carlone, K. D. Hänni, D. A. Leigh, B. Lewandowski, *Angew. Chem. Int. Ed.* **2012**, *51*, 5166–5169.

[35] Y. Qiu, B. Song, C. Pezzato, D. Shen, W. Liu, L. Zhang, Y. Feng, Q. H. Guo, K. Cai, W. Li, *Science.* **2020**, *368*, 1247–1253.

[36] M. Alvarez-Perez, S. M. Goldup, D. A. Leigh, A. M. Z. Slawin, *J. Am. Chem. Soc.* **2008**, *130*, 1836–1838.

[37] V. Serreli, C. Lee, E. R. Kay, D. A. Leigh, *Nature* **2007**, *445*, 523–527.

[38] B. Lewandowski, G. De Bo, J. W. Ward, M. Papmeyer, S. Kuschel, M. J. Aldegunde, P. M. E. Gramlich, D. Heckmann, S. M. Goldup, D. M. D'Souza, *Science* **2013**, *339*, 189–193.

[39] G. De Bo, S. Kuschel, D. A. Leigh, B. Lewandowski, M. Papmeyer, J. W. Ward, *J. Am. Chem. Soc.* **2014**, *136*, 5811–5814.

[40] G. de Bo, M. A. Y. Gall, S. Kuschel, J. de Winter, P. Gerbaux, D. A. Leigh, *Nat. Nanotech.* **2018**, *13*, 381–385.

[41] E. R. Kay, D. A. Leigh, F. Zerbetto, *Angew. Chem. Int. Ed.* **2007**, *46*, 72–191.

[42] D. Roke, S. J. Wezenberg, B. L. Feringa, *Proc. Natl. Acad. Sci.* **2018**, *115*, 9423–9431.

[43] W. R. Browne, B. L. Feringa, *Mol. Switch. Second Ed.* **2011**, *1*, 121–179.

[44] W. R. Browne, B. L. Feringa, *Nat. Nanotechnol.* **2006**, *1*, 25–35.

[45] N. Koumura, R. W. J. Zijlstra, R. A. van Delden, N. Harada, B. L. Feringa, *Nature* **1999**, *401*, 152–155.

[46] C. J. Martin, A. T. L. Lee, R. W. Adams, D. A. Leigh, *J. Am. Chem. Soc.* **2017**, *139*, 11998–12002.

[47] R. J. Bordoli, S. M. Goldup, *J. Am. Chem. Soc.* **2014**, *136*, 4817–4820.

[48] M. A. Jinks, A. De Juan, M. Denis, C. J. Fletcher, M. Galli, E. M. G. Jamieson, F. Modicom, Z. Zhang, S. M. Goldup, *Angew. Chem. Int. Ed.* **2018**, *57*, 14806–14810.

[49] J. E. M. Lewis, J. Winn, L. Cera, S. M. Goldup, *J. Am. Chem. Soc.* **2016**, *138*, 16329–16336.

[50] Y. Li, A. H. Flood, *Angew. Chem. Int. Ed.* **2008**, *47*, 2649–2652.

[51] Y. Li, A. H. Flood, *J. Am. Chem. Soc.* **2008**, *130*, 12111–12122.

[52] G. D. Probst, S. Bowers, J. M. Sealy, B. Stupi, D. Dressen, B. M. Jagodzinska, J. Aquino, A. Gailunas, A. P. Truong, L. Tso, *Bioorganic Med. Chem. Lett.* **2010**, *20*, 6034–6039.

[53] A. J. Martínez-Martínez, A. R. Kennedy, R. E. Mulvey, C. T. O'Hara, *Science* **2014**, *346*, 834–837.

[54] Y. Tobe, N. Utsumi, K. Kawabata, K. Naemura, *Tetrahedron Lett.* **1996**, *37*, 9325–9328.

[55] Y. Tobe, N. Utsumi, A. Nagano, M. Sonoda, K. Naemura, *Tetrahedron* **2001**, *57*, 8075–8083.

[56] X. Cheng, J. Ma, J. Zhi, X. Yang, A. Hu, *Macromolecules* **2010**, *43*, 909–913.

[57] Y. Suzuki, S. Naoe, S. Oishi, N. Fujii, H. Ohno, *Org. Lett.* **2012**, *14*, 326–329.

[58] T. Ishida, S. Kikuchi, T. Tsubo, T. Yamada, *Org. Lett.* **2013**, *15*, 848–851.

[59] H. Kinoshita, N. Hirai, K. Miura, *J. Org. Chem.* **2014**, *79*, 8171–8181.

[60] P. N. W. Baxter, *J. Org. Chem.* **2001**, *66*, 4170–4179.

[61] H. Yuan, M. Wang, Z. Xu, H. Gao, *Adv. Synth. Catal.* **2019**, *361*, 4386–4392.

[62] Y. H. Jung, J. Yu, Z. Wen, V. Salmaso, T. P. Karcz, N. B. Phung, Z. Chen, S. Duca, J. M. Bennett, S. Dudas, *J. Med. Chem.* **2020**, *63*, 9563–9589.

[63] Y. Akae, H. Sogawa, T. Takata, *European J. Org. Chem.* **2019**, *2019*, 3605–3613.

[64] S. Das, D. Hong, Z. Chen, Z. She, W. H. Hersh, G. Subramaniam, Y. Chen, *Org. Lett.* **2015**, *17*, 5578–5581.

[65] A. Odedra, C. J. Wu, T. B. Pratap, C. W. Huang, Y. F. Ran, R. S. Liu, *J. Am. Chem. Soc.* **2005**, *127*, 3406–3412.

[66] I. V. Alabugin, K. Gilmore, S. Patil, M. Manoharan, S. V. Kovalenko, R. J. Clark, I. Ghiviriga, *J. Am. Chem. Soc.* **2008**, *130*, 11535–11545.

[67] J. E. M. Lewis, R. J. Bordoli, M. Denis, C. J. Fletcher, M. Galli, E. A. Neal, *Chem. Sci.* **2016**, *7*, 3154–3161.

[68] J. Yu, A. Ciancetta, S. Dudas, S. Duca, J. Lottermoser, K. A. Jacobson, *J. Med. Chem.* **2018**, *61*, 4860–4882.

[69] M. J. Johansson, D. J. Gorin, S. T. Staben, F. D. Toste, *J. Am. Chem. Soc.* **2005**, *127*, 18002–18003.

3.6. General Experimental Information

Unless otherwise stated, all reagents were purchased from commercial sources (Acros Organics, Alfa Aesar, Fisher Scientific, FluoroChem, Sigma Aldrich and VWR) and used without further purification. Styrene was purified by vacuum distillation prior to usage and stored under inert N_2 atmosphere. $[Cu(MeCN)_4]PF_6$ was prepared as described by Pigorsch and Köckerling. Anhydrous solvents were purchased from Acros Organics. Petrol refers to the fraction of petroleum ether boiling in the range 40-60 °C. IPA refers to isopropanol. THF refers to tetrahydrofuran. EDTA-NH_3 solution refers to an aqueous solution of NH_3 (17% w/w) saturated with sodium-ethylenediaminetetraacetate. $CDCl_3$ (without stabilising agent) was distilled over $CaCl_2$ and K_2CO_3 prior to use. Unless otherwise stated, all reactions were performed in oven dried glassware under an inert N_2 atmosphere with purchased anhydrous solvents. Unless otherwise stated experiments carried out in sealed vessels were performed in CEM microwave vials, with crimped aluminium caps, with PTFE septa. Young's tap vessels and Schlenk techniques were used where specified.

Flash column chromatography was performed using Biotage Isolera-4 or Isolera-1 automated chromatography system. SiO_2 cartridges were purchased commercially from Teledyne Technologies, or Biotage (SNAP or ZIP, 50 μm irregular silica, default flow rates). Neutralised SiO_2 refers to ZIP cartridges which were eluted with petrol-NEt_3 (99 : 1, 5 column volumes), followed by petrol (5 column volumes). Analytical TLC was performed on pre-coated silica gel plates on aluminum (0.25 mm thick, 60F254, Merck, Germany) and observed under UV light (254 nm) or visualised with $KMnO_4$ stain.

All melting points were determined using a Griffin apparatus and are uncorrected. NMR spectra were recorded on Bruker AV400 or AV500 instrument, at a constant temperature of 298 K. Chemical shifts are reported in parts per million from low to high field and referenced to residual solvent. Coupling constants (*J*) are reported in Hertz (Hz). Standard abbreviations indicating multiplicity were used as follows: m = multiplet, quint = quintet, q = quartet, t = triplet, d = doublet, s = singlet, app. = apparent, br = broad, sept = septet. Signal assignment was carried out using 2D NMR methods (COSY, NOESY, TOCSY, HSQC, HMBC or ^{31}P-^{1}H HMBC) where necessary. In some

cases, complex multiplets with multiple contributing proton signals, exact assignment was not possible. In interlocked compounds, all proton signals corresponding to axle components are in lower case, and all proton signals corresponding to the macrocycle components are in upper case. For mixtures of diastereomeric cyclopropanes, upper case is used to denote the major diastereoisomer, and lower case is used to denote the minor diastereoisomer.

Low resolution mass spectrometry was carried out by the mass spectrometry services at University of Southampton (Waters TQD mass spectrometer equipped with a triple quadrupole analyser with UHPLC injection [BEH C18 column; MeCN-H_2O gradient {0.2% formic acid}]). High resolution mass spectrometry was carried out either by the mass spectrometry service at the University of Edinburgh (ThermoElectron MAT 900) or by the mass spectrometry services at the University of Southampton (MaXis, Bruker Daltonics, with a Time of Flight (TOF) analyser; samples were introduced to the mass spectrometer via a Dionex Ultimate 3000 autosampler and UHPLC pump in a gradient of 20% MeCN in hexane to 100% acetonitrile (0.2% formic acid) over 5-10 min at 0.6 mL/min; column: Acquity UPLC BEH C18 (Waters) 1.7 micron 50 × 2.1mm). In HR-MS, the most abundant isotope is quoted. Where 1 Br atom is present, the HR-MS signal quotes corresponds to ^{79}Br. When m/z < 1000, HR-MS is quoted to 4 dp (within 5 ppm of calculated m/z). When m/z > 1000, HR-MS is quoted to 1 dp.

Circular dichroism spectra were acquired on an Applied Photo-physics Chirascan spectropolarimeter, recorded using Applied Photophysics software Ver. 4.2.0 in dried spectroscopic grade $CHCl_3$, following overnight desiccation of the sample, at a concentration range of 0.1-1 10^{-4} M, in a quartz cell of 1 cm path length, at a temperature of 293 K.

Stereochemical purity was determined by Chiral Stationary Phase HPLC on a Waters Acquity Arc Instrument at 303 K, with *n*-hexane-isopropanol isocratic eluents. Regis Technologies (*S*,*S*)-Whelk-O1 (1-(3,5-dinitrobenzamido)-1,2,3,4-tetrahydrophenanthrene stationary phase), RegisPack (tris-(3,5-dimethylphenyl) carbamoyl amylose stationary phase) and RegisCell (tris-(3,5-dimethylphenyl) carbamoyl cellulose stationary phase) columns were used throughout (5 micron, column dimensions 25 cm x 4.6 mm).

Compounds **61a**,[49] **61b**,[50,51] **68**,[52,53] **69**,[50,51] **70**,[54,55] **76**,[56–58] **84**,[59–61] **85**,[61] **104-1106**,[62] **107**,[63] **130**,[64–66] **132**,[67] **134**,[67] **138**,[68] were made by modified literature procedures and matched literature characterisation. Procedures have been included where they differ from the literature.

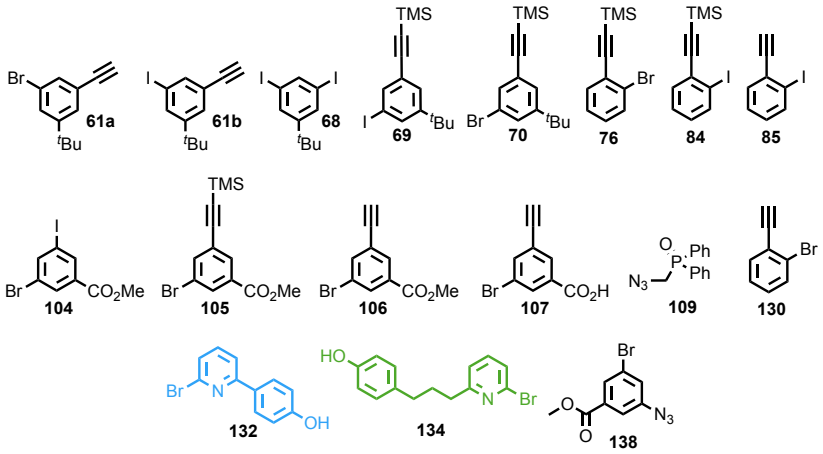

Compound **70**[54,55]

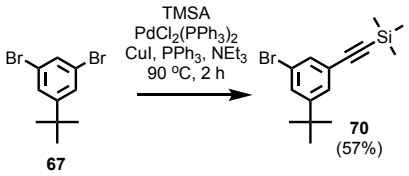

1,3-dibromo-5-tert-butylbenzene (1.50 g, 5.13 mmol, 1.0 eq.), TMS acetylene (504 mg, 5.13 mmol, 1.0 eq.), $PdCl_2(PPh_3)_2$ (90 mg, 0.129 mmol, 0.025 eq.), CuI (48.9 mg, 0.258 mmol, 0.050 eq.) and PPh_3 (67.5 mg, 0.258 mmol, 0.050 eq.) were stirred at 90 °C in NEt_3 (22.5 mL) for 2 h. The reaction mixture was quenched with NH_4Cl (50 mL), washed with brine (50 mL), and extracted in CH_2Cl_2 (3 x 50 mL) and Et_2O (3 x 50 mL). The combined organic layers were dried over $MgSO_4$, concentrated *in vacuo*. The residue was purified by column chromatography (SiO_2, pet) yielding a colourless oil **70** (908 mg, 2.94 mmol, 57%). δ_H ($CDCl_3$, 400 MHz) 7.45 (1H, app. t, *J* = 1.8), 7.43 (1H, app. t, *J* = 1.8), 7.39 (1H, app. t, *J* = 1.5), 1.29 (9H, s), 0.24 (9H, s). δ_C ($CDCl_3$, 101 MHz) 153.5, 131.9, 129.2, 127.9, 124.7, 122.1, 104.1, 95.2, 35.0, 31.2, 0.06. HR-APPI-MS $[M]^{\cdot+}$ m/z 308.0584 (calc. for $C_{15}H_{21}BrSi$ m/z 308.0590).[54,55]

Compound **61a**[49]

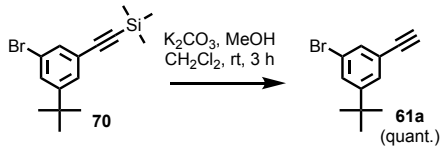

70 (700 mg, 2.26 mmol, 1.0 eq.) was stirred at room temperature with K_2CO_3 (1.56 g, 11.3 mmol, 5.0 eq.) in CH_2Cl_2 (22 mL) and MeOH (22 mL) for 3 h. The product was washed with H_2O (50 mL) and extracted in CH_2Cl_2 (3 x 30 mL). The combined organic layer was dried over $MgSO_4$ and concentrated *in vacuo*, yielding an orange oil **61a** (537 mg, 2.26 mmol, quantitative). δ_H ($CDCl_3$, 400 MHz) 7.50 (1H, app. t, *J* = 1.6), 7.46 (1H, app. t, *J* = 1.6), 7.44 (1H, app. t, *J* = 1.6), 3.09 (1H, s), 1.30 (9H, s). δ_C ($CDCl_3$, 101 MHz) 153.6, 132.0, 129.6, 128.2, 123.7, 122.1, 82.8, 77.9, 35.0, 31.2. HR-APPI-MS $[M]^{+\cdot}$ m/z 236.0190 (calc. for $C_{12}H_{13}Br$ m/z 236.0195).[49]

Compound **68**[52,53]

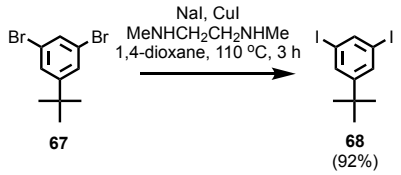

A dry CEM MW vial was charged with 1,3-dibromo-t-*tert*-butylbenzene (2.14 g, 7.33 mmol, 1.0 eq.), CuI (140 mg, 0.733 mmol, 0.1 eq.) and NaI (4.39 g, 29.3 mmol, 4.0 eq.) and purged with N_2. Anhydrous degassed 1,4-dioxane (7.3 mL) and *N*,*N*′-dimethylethane-1,2-diamine (0.158 mL, 129 mg, 1.47 mmol, 0.20 eq.). The suspension was heated at 110 °C for 3 d. The reaction was cooled to room temperature diluted in CH_2Cl_2 (50 mL), washed with H_2O (3 x 25 mL) and extracted in CH_2Cl_2 (3 x 30 mL). The combined organic layers were dried over $MgSO_4$ and concentrated *in vacuo*. The organic residue was purified by column chromatography (SiO_2, petrol) yielding a colourless oil **68** (2.61 g, 6.76 mmol, 92%). δ_H ($CDCl_3$, 400 MHz) 7.86 (1H, t, *J* = 1.5), 7.64 (1H, t, *J* = 1.5), 7.65 (2H, d, *J* = 1.6), 1.27 (9H, s). δ_C ($CDCl_3$, 101 MHz) 155.7, 142.3, 134.2, 95.1, 35.0, 31.2. HR-APPI-MS [$M^{+\cdot}$] m/z 385.9028 (calc. for $C_{10}H_{12}I_2$ 385.9029).[52,53]

Compound **69**[50,51]

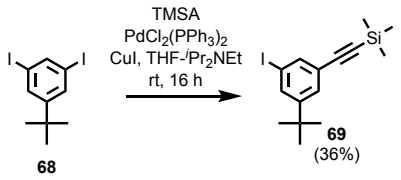

A dry CEM MW vial was charged with CuI (26 mg, 0.137 mmol, 0.02 eq.) and $Pd(PPh_3)_2Cl_2$ (94 mg, 0.134 mmol, 0.02 eq.) and purged with N_2. **68** (2.59 g, 6.70 mmol, 1.0 eq.) was transferred in degassed anhydrous THF-^{i}Pr$_2$NH (67 mL : 13 mL) and trimethylsilylacetylene (0.96 mL, 0.662 g, 6.74 mmol, 1.0 eq.) was added dropwise. The solution was stirred at room temperature for 16 h. After 16 h, the reaction was concentrated under reduced pressure, diluted in CH_2Cl_2 and washed with H_2O (3 x 50 mL). The residue was extracted in CH_2Cl_2 (3 x 30 mL) and the combined organic layers dried over $MgSO_4$ and concentrated *in vacuo*. The residue was purified by column chromatography (SiO_2, hexane) yielding a white solid **69** (0.861 g, 2.42 mmol, 36%). δ_H ($CDCl_3$, 400 MHz) 7.65 (1H, app. t, *J* = 1.6), 7.64 (1H, app. t, *J* = 1.5), 7.43 (1H, app. t, *J* = 1.6), 1.28 (9H, s), 0.25 (9H, s). δ_C ($CDCl_3$, 101 MHz) 153.4, 137.8, 135.1, 128.5, 124.8,

103.9, 95.2, 93.9, 34.9, 31.2, 0.06. HR-ESI-MS [M+H$^+$] m/z 357.0707 (calc. for $C_{15}H_{22}SiI$ m/z 357.0536).[50,51]

Compound **61b**[50,51]

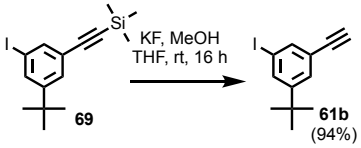

69 (0.861 g, 2.42 mmol, 1.0 eq.) was stirred with KF (0.70 g, 12.1 mmol, 5.0 eq.) in THF (9 mL) and MeOH (9 mL) for 16 h. The reaction was concentrated *in vacuo*, washed with H_2O (30 mL) and extracted in CH_2Cl_2 (3 x 30 mL). The combined organic layers were dried over $MgSO_4$ and solvent removed *in vacuo*. The residue was purified by column chromatography (SiO_2, petrol-CH_2Cl_2 1 : 1) yielding a colourless oil **61b** (0.645 g, 2.27 mmol, 94%). δ_H ($CDCl_3$, 400 MHz) 7.70 (1H, app. t, *J* = 1.7), 7.66 (1H, app. t, *J* = 1.6), 7.47 (1H, app. t, *J* = 1.6), 3.09 (1H, s), 1.29 (9H, s). δ_C ($CDCl_3$, 101 MHz) 153.6, 137.9, 135.5, 128.8, 123.8, 93.9, 82.6, 78.0, 34.9, 31.2. HR-APPI-MS [M$^{+\cdot}$] m/z 284.0062 (calc. for $C_{12}H_{13}I$ 284.0056).[50,51]

Rotaxane (*S*,R_{mp})-**72b**

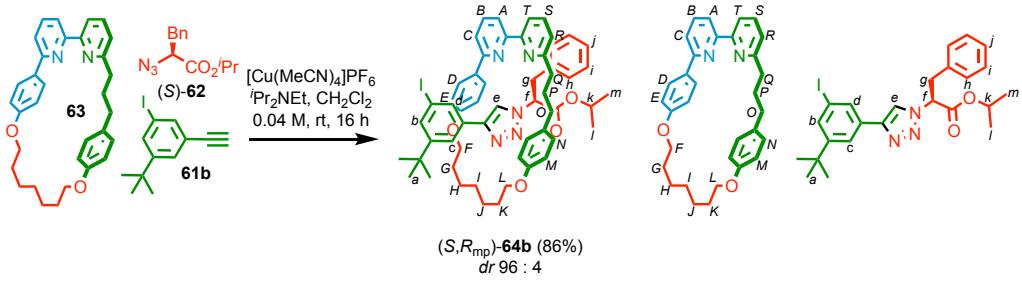

A dry CEM MW vial was charged with macrocycle **63** (120 mg, 0.251 mmol, 1.0 eq.) and $[Cu(MeCN)_4]PF_6$ (89.7 mg, 0.241 mmol, 0.96 eq.), then purged with N_2. Alkyne **61b** (71.2 mg, 0.251 mmol, 1.0 eq.) and azide (*S*)-**62** (58.5 mg, 0.251 mmol, 1.0 eq.) were transferred in anhydrous degassed CH_2Cl_2 (6.3 mL, [**63**] = 0.04 M). $^iPr_2NEt$ (175 µL, 130 mg, 1.00 mmol, 4.0 eq.) was added and the solution stirred at room temperature for 16 h. TFA (1.25 mL, 16.3 mmol, 65 eq.) was added and the solution stirred for 5 h. After 5 h, the solution was washed with saturated EDTA-NH_3 solution (25 mL, 17 w/w%), and extracted in CH_2Cl_2 (3 x 25 mL). The combined organic layers were washed with brine (30 mL) and extracted in CH_2Cl_2 (3 x 50 mL). The combined organic layers were dried over $MgSO_4$ and concentrated *in vacuo*. The residue was purified by column

chromatography (SiO_2, petrol-EtOAc 0→20%) yielding a white foam (*S*,R_{mp})-**64b** (215 mg, 0.216 mmol, 86%, *dr* 96 : 4). δ_H ($CDCl_3$, 400 MHz) 9.88 (1H, s, H_e, 96%), 9.81 (1H, s, H_e, 4%), 8.07 (1H, t, *J* = 1.5, H_d), 7.81 (1H, t, *J* = 1.5, H_c), 7.79 (1H, t, *J* = 7.7, H_S), 7.72 (1H, t, *J* = 7.8, H_B), 7.62 (1H, dd, *J* = 7.9, 0.8, H_T), 7.56 (1H, dd, *J* = 7.7, 0.8, H_A), 7.46 (1H, t, *J* = 1.7, H_b), 7.43 (1H, dd, *J* = 7.9, 0.8, H_C), 7.33 (1H, dd, *J* = 7.8, 0.8, H_R), 7.19-7.05 (3H, m, H_i, H_j), 7.09 (2H, dt, *J* = 8.8, 2.5, H_D), 6.82 (2H, dd, *J* = 7.5, 2.0, H_h), 6.39 (2H, dt, *J* = 8.6, 2.5, H_N), 6.28 (2H, dt, *J* = 8.8, 2.5, H_E), 6.16 (2H, dt, *J* = 8.6, 2.5, H_M), 4.90 (1H, dd, *J* = 11.5, 5.1, H_f), 4.80 (1H, sept., *J* = 6.3, H_k), 4.32 (1H, td, *J* = 9.3, 3.8, $H_{F \text{ or } L}$), 4.12-4.05 (1H, ddd, *J* = 7.9, 7.1, 2.7, $H_{L \text{ or } F}$), 4.02-3.95 (1H, dt, *J* = 10.7, 5.5, $H_{L' \text{ or } F'}$), 3.82 (1H, dt, *J* = 8.5, 4.4, $H_{F' \text{ or } L'}$), 2.83-2.66 (4H, m, H_g, H_O), 2.45 (2H, dd, *J* = 6.2, 6.2, H_Q), 2.40-2.17 (1H, m, H_X), 2.17-2.05 (2H, m, H_X), 2.04-1.90 (1H, m, H_X), 1.90-1.63 (7H, m, H_P, 6H_X), 1.12 (3H, d, *J* = 6.3, H_l), 1.05 (9H, s, H_a), 0.79 (3H, d, *J* = 6.3, H_m). 2.40-1.90 (4H) and 1.90-1.63 (6H) correspond to $H_{G\text{-}K}$. δ_C ($CDCl_3$, 101 MHz) 167.9, 163.9, 159.3, 158.1, 157.7, 157.0, 152.5, 145.6, 137.2 137.2, 135.5, 134.6, 133.5, 132.7, 131.9, 131.8, 131.3, 129.2, 128.6, 128.5, 128.3, 127.1, 123.9, 123.0, 122.7, 120.1, 119.9, 119.6, 114.7, 113.8, 93.9, 69.3, 67.9, 65.3, 63.4, 37.7, 37.6, 35.4, 34.7, 32.5, 31.2, 29.3, 29.0, 28.0, 25.8, 25.6, 21.7, 21.4. HR-ESI-MS $[M+H]^+$ m/z 996.3908 (calc. for $C_{56}H_{63}N_5O_4I$ m/z 996.3919).

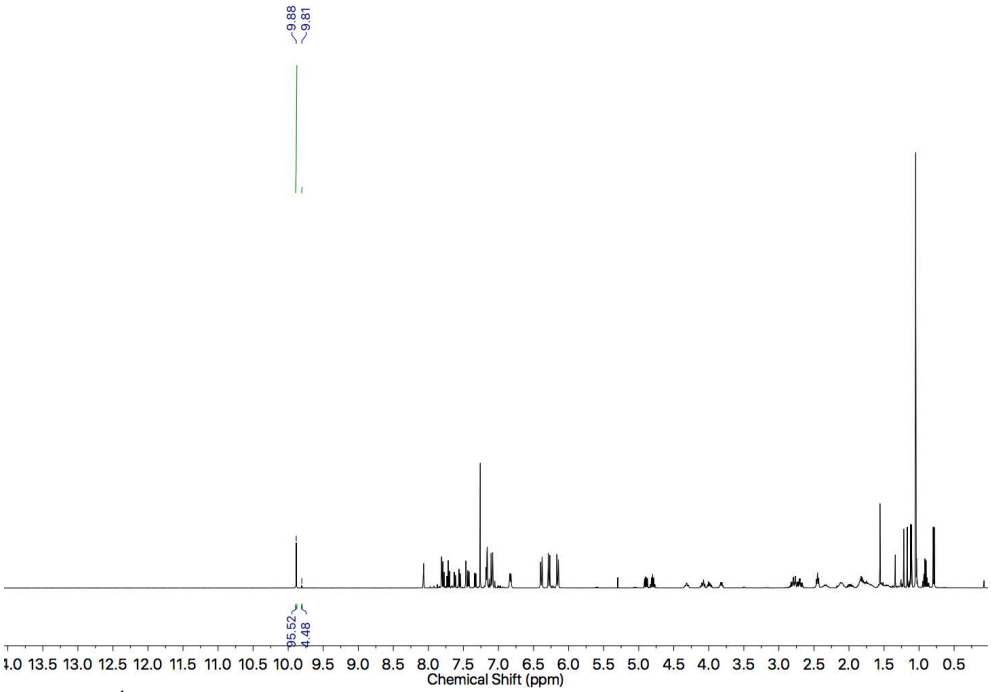

Figure 309: ^1H NMR of (*S*,R_{mp})-**64b** ($CDCl_3$, 400 MHz).

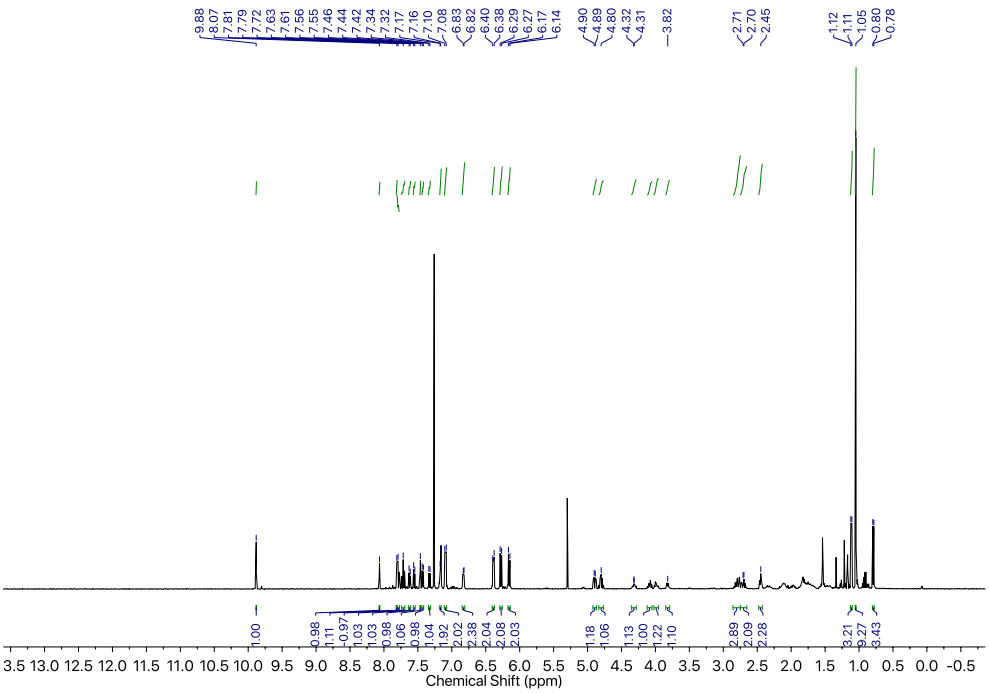

Figure 310: ^{1}H NMR of (*S*,*R*$_{mp}$)-**64b** ($CDCl_3$, 400 MHz).

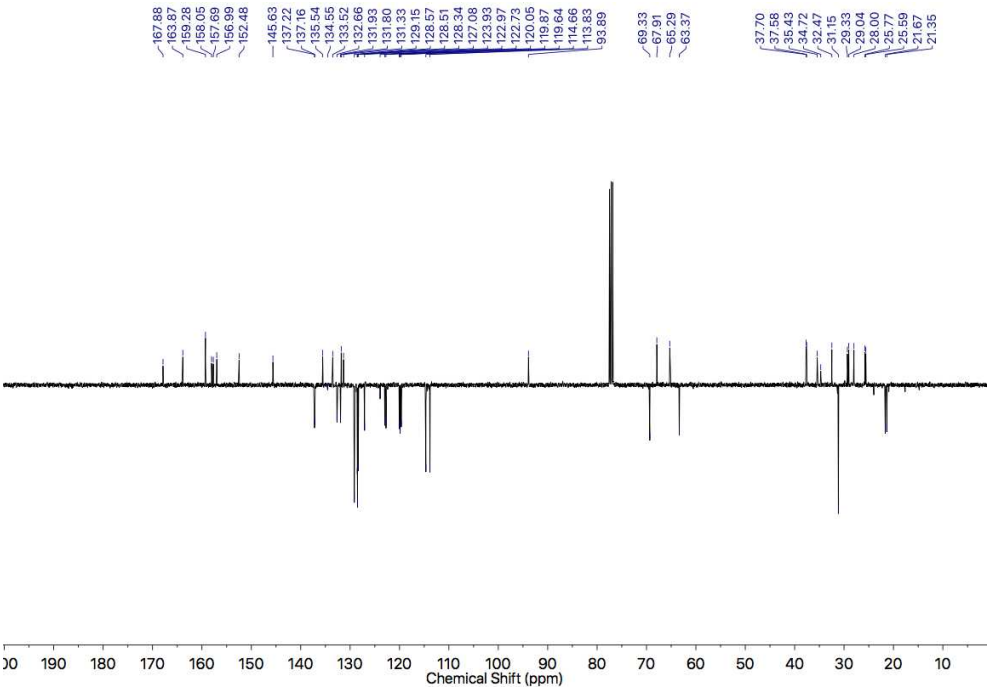

Figure 311: JMOD NMR of (*S*,*R*$_{mp}$)-**64b** ($CDCl_3$, 101 MHz).

Rotaxane (R_{mp})-**65b**

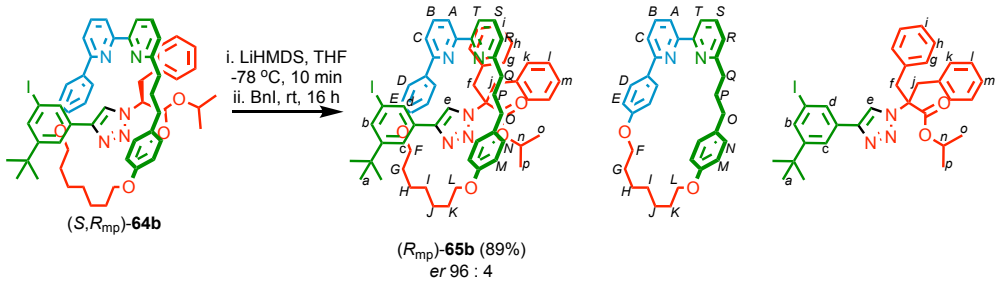

(S,R_{mp})-**64b**

(R_{mp})-**65b** (89%)
er 96 : 4

A dry CEM MW vial was charged with rotaxane (S,R_{mp})-**64b** (182 mg, 0.183 mmol, 1.0 eq., *dr* 96 : 4) and purged with N_2. The solid was dissolved in anhydrous, degassed THF (9.1 mL) and cooled to -78 °C. LiHMDS (0.91 mL, 0.914 mmol, 5.0 eq., 1 M solution in THF) was added and the solution stirred for 10 minutes. Then BnI (1.83 mL, 1.83 mmol, 10.0 eq., 1 M solution in THF) was added and the reaction stirred for 16 h and allowed to warm to room temperature. The reaction was quenched with NH_4Cl (30 mL) and extracted in CH_2Cl_2 (3 x 25 mL). The combined organic layers were dried over $MgSO_4$ and concentrated *in vacuo*. The residue was purified by column chromatography (SiO_2, petrol-EtOAc 0→20%) yielding a white foam (R_{mp})-**65b** (176 mg, 0.162 mmol, 89%, *er* 96 : 4). $\boldsymbol{\delta}_H$ ($CDCl_3$, 400 MHz) 10.12 (1H, s, $\boldsymbol{H}_e$), 8.08 (2H, s, $\boldsymbol{H}_c$, $\boldsymbol{H}_d$), 7.73 (1H, t, J = 7.7, $\boldsymbol{H}_{B\text{ or }S}$), 7.71 (1H, t, J = 7.7, $\boldsymbol{H}_{S\text{ or }B}$), 7.55 (1H, dd, J = 7.9, 0.6, $\boldsymbol{H}_{A\text{ or }T}$), 7.52 (1H, s, $\boldsymbol{H}_b$). 7.52 (1H, dd, J = 7.9, 0.6, $\boldsymbol{H}_{T\text{ or }A}$), 7.44 (1H, dd, J = 7.9, 0.7, $\boldsymbol{H}_{C\text{ or }R}$), 7.29 (1H, dd, J = 7.9, 0.7, $\boldsymbol{H}_{R\text{ or }C}$), 7.27 (2H, d, J = 8.8, $\boldsymbol{H}_D$), 7.16 (1H, tt, J 7.4, 2.6, $\boldsymbol{H}_i$), 7.13-7.04 (5H, m, $\boldsymbol{H}_h$, $\boldsymbol{H}_l$, $\boldsymbol{H}_m$), 6.61 (2H, br. d, J = 7.0, $\boldsymbol{H}_{g\text{ or }k}$), 6.50 (2H, br. d, J = 7.1, $\boldsymbol{H}_{k\text{ or }g}$), 6.37 (2H, dt, J 8.7, 2.3, $\boldsymbol{H}_N$), 6.31 (2H, br. d, J 8.6, $\boldsymbol{H}_M$), 6.16 (2H, dt, J 8.8, 2.5, $\boldsymbol{H}_E$), 4.77 (1H, sept., J = 6.3, $\boldsymbol{H}_n$), 4.70-4.61 (1H, m, $\boldsymbol{H}_{F\text{ or }L}$), 4.15-4.07 (1H, m, $\boldsymbol{H}_{L\text{ or }F}$), 3.99-3.88 (2H, m, $\boldsymbol{H}_{F'}$, $\boldsymbol{H}_{L'}$), 3.16 (1H, d, J = 14.0, $\boldsymbol{H}_{f\text{ or }j}$), 3.08 (1H, d, J = 14.5, $\boldsymbol{H}_{j\text{ or }f}$), 3.03 (1H, d, J = 14.5, $\boldsymbol{H}_{j'\text{ or }f'}$), 2.90 (1H, d, J = 14.0, $\boldsymbol{H}_{f'\text{ or }j'}$), 2.80 (1H, td, J = 13.9, 4.7, $\boldsymbol{H}_Q$), 2.66 (1H, td, J = 13.7, 4.2, $\boldsymbol{H}_{Q'}$), 2.61-2.51 (1H, m, $\boldsymbol{H}_O$), 2.42-2.34 (1H, m, $\boldsymbol{H}_{O'}$), 2.34-2.27 (1H, m, $\boldsymbol{H}_*$), 2.26-2.13 (1H, m, $\boldsymbol{H}_P$), 2.10-1.98 (1H, m, $\boldsymbol{H}_*$), 1.86-1.67 (7H, m, $\boldsymbol{H}_{P'}$, $\boldsymbol{H}_*$), 1.58-1.48 (1H, m, $\boldsymbol{H}_*$), 1.45-1.33 (1H, m, $\boldsymbol{H}_*$), 1.08 (3H, d, J = 6.3, $\boldsymbol{H}_o$), 0.96 (3H, d, J = 6.3, $\boldsymbol{H}_p$), 0.95 (9H, s, $\boldsymbol{H}_a$). *unresolved overlapping 10H $\boldsymbol{H}_{G\text{-}K}$ $\boldsymbol{\delta}_C$ ($CDCl_3$, 101 MHz) 168.6, 163.8, 158.9, 158.7, 157.8, 157.5, 157.0, 152.3, 145.8, 137.2, 137.2, 135.2, 134.8, 133.4, 133.3, 131.6, 130.9, 130.7, 130.6, 130.3, 128.7, 128.7, 128.3, 128.1, 127.8, 126.9, 126.8, 125.2, 124.6, 122.4, 120.0, 119.2, 114.5, 114.4, 94.3, 71.0, 69.9, 67.6, 65.4, 43.2, 41.2, 37.3, 35.4, 31.3, 31.1, 29.9, 29.0,

28.9, 27.6, 25.8, 25.5, 21.7, 21.5. HR-ESI-MS $[M+H]^+$ m/z 1086.4 (calc. for $C_{63}H_{69}N_5O_4I$ m/z 1086.4).

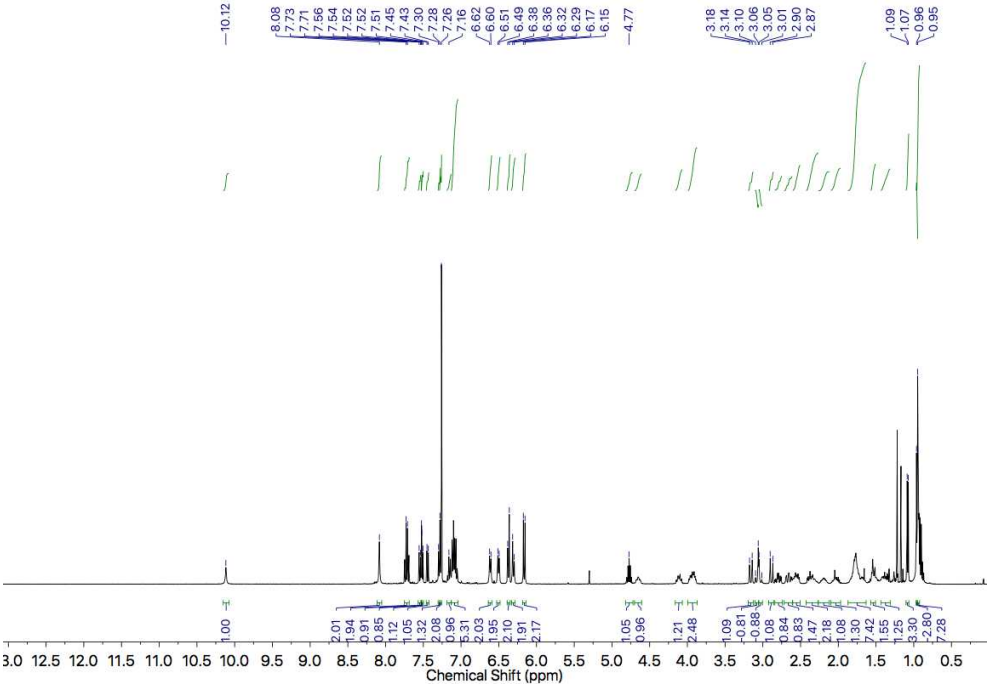

Figure 312: ^{1}H NMR of (R_{mp})-**65b** ($CDCl_3$, 400 MHz).

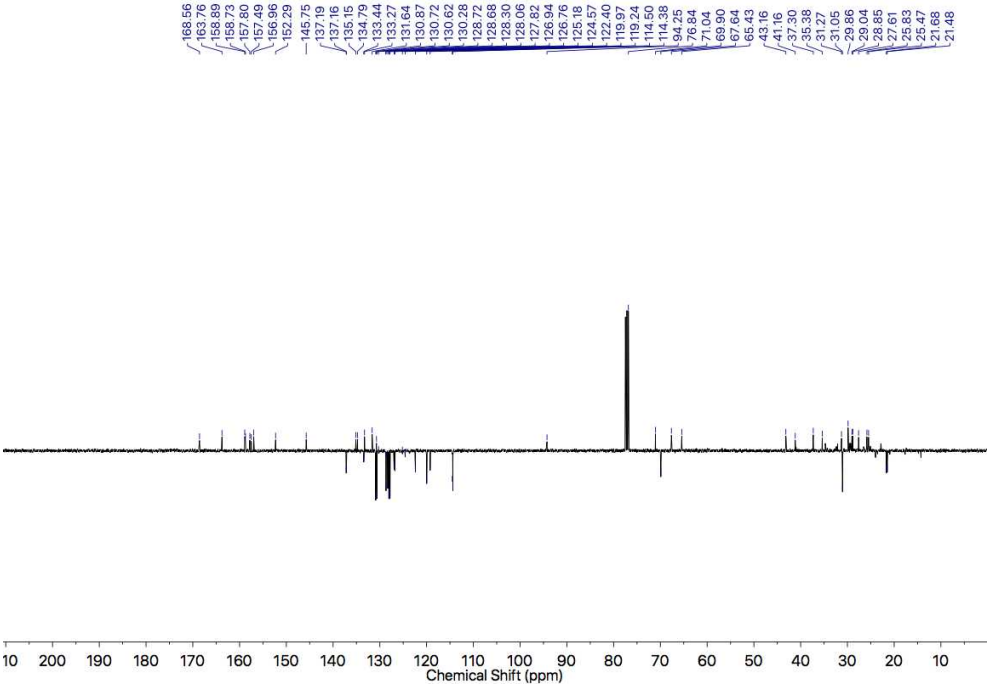

Figure 313: JMOD NMR of (R_{mp})-**65b** ($CDCl_3$, 101 MHz).

Rotaxane (S_{mp})-**72**

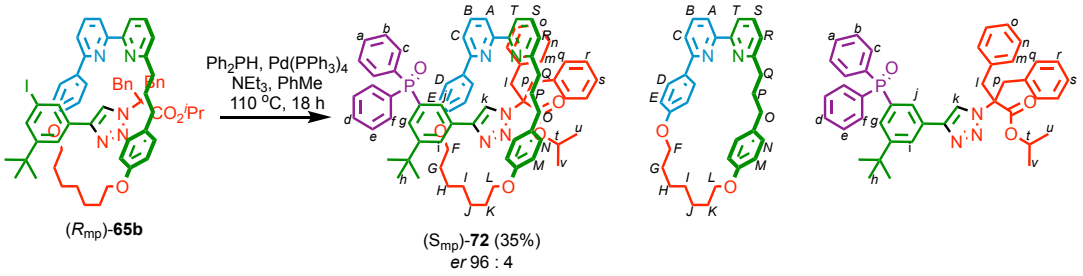

A dry CEM MW vial was charged with rotaxane (R_{mp})-**65b** (50 mg, 0.046 mmol, 1.0 eq.), $Pd(PPh_3)_4$ (2.7 mg, 0.0023 mmol, 0.05 eq.), and purged with N_2. The solid was dissolved in anhydrous, degassed PhMe (0.90 mL, 0.05 M). Ph_2PH (12 µL, 0.069 mmol, 1.5 eq.) and NEt_3 (10 µL, 0.069 mmol, 1.5 eq.). The reaction was refluxed at 110 °C for 18 h. The reaction was quenched with NH_4Cl (30 mL) and extracted in CH_2Cl_2 (3 x 25 mL), washed with H_2O_2 (35 w/w%, 30 mL) and brine, then extracted in CH_2Cl_2 (3 x 25 mL). The combined organic layers were dried over $MgSO_4$ and concentrated *in vacuo*. The residue was purified by column chromatography (SiO_2, petrol-EtOAc 0→100%) yielding a white foam (S_{mp})-**72** (186 mg, 0.016 mmol, 35%). δ_H ($CDCl_3$, 400 MHz) 10.19 (1H, s, H_k), 8.35 (1H, s, H_i), 8.27 (1H, d, J = 12.5, H_j), 7.93 (1H, m, H_d), 7.87-7.76 (2H, m, H_c), 7.76-7.64 (3H, m, H_B, H_S, H_g), 7.59 (1H, d, J = 7.8, H_T), 7.58 (1H, d, J = 7.8, H_R), 7.53 (1H, tdd, J = 7.5, 1.4, 1.4, H_a), 7.50-7.33 (7H, m, H_A, H_e, H_f, H_b), 7.29 (1H, d, J = 7.7, H_C), 7.15 (2H, d, J = 8.6, H_D), 7.10-6.99 (6H, m, H_n, H_o, H_r, H_s), 6.66 (2H, d, J = 7.3, H_m), 6.55 (2H, d, J = 7.2, H_q), 6.36 (2H, d, J = 8.5, H_N), 6.15 (2H, d, J = 8.6, H_E), 6.04 (2H, d, J = 8.5, H_M), 4.70 (1H, sept., J = 6.3, H_t), 4.26-4.14 (1H, m, H_Q), 4.01-3.91 (1H, m, H_O), 3.87-3.73 (2H, m, $H_{Q'}$, $H_{O'}$), 3.16 (1H, d, J = 14.2, $H_{l\ or\ p}$), 3.14 (1H, d, J = 14.6, $H_{p\ or\ l}$), 2.98 (1H, d, J = 14.6, $H_{p'\ or\ l'}$), 2.77-2.67 (2H, m, $H_{F\ or\ L}$), 2.62 (1H, d, J = 14.2, $H_{l'\ or\ p'}$), 2.53-2.39 (2H, m, $H_{L\ or\ F}$), 2.18-1.92 (3H, m, H_*), 1.92-1.57 (5H, m, H_*), 1.55-1.22 (4H, m, H_*), 1.04 (9H, br. s, H_h), 0.98 (3H, d, J = 6.3, H_u), 0.84 (3H, d, J = 6.3, H_v). *12H G, H, I, J, K, P. δ_C ($CDCl_3$, 101 MHz) 168.4, 163.9, 158.8, 157.6, 157.6, 157.5, 157.5, 157.3, 151.1, 151.0, 145.7, 137.1, 135.9, 135.4, 134.3, 133.2, 132.8, 132.7, 132.6, 132.4, 132.3, 132.2, 132.1, 132.0, 132.0,132.0, 131.9, 131.8, 131.8, 131.6, 131.6, 131.5, 131.5, 131.3, 131.2, 130.7, 130.6, 128.8, 128.7, 128.7, 128.7, 128.6, 128.6, 128.5, 127.8, 127.7, 126.6, 126.4, 125.0, 125.0, 122.4, 120.0, 119.9, 119.6, 114.5, 114.2, 71.0, 69.7, 68.2, 66.0, 44.5, 41.8, 37.1, 35.2, 35.0, 31.2, 30.8,

28.8, 28.4, 27.7, 25.8, 25.4, 21.4, 21.3. δ_P ($CDCl_3$, 202 MHz) 29.7. HR-ESI-MS [M+H$^+$] m/z 1160.6 (calc. For $C_{75}H_{79}N_5O_5P$ m/z 1160.6).

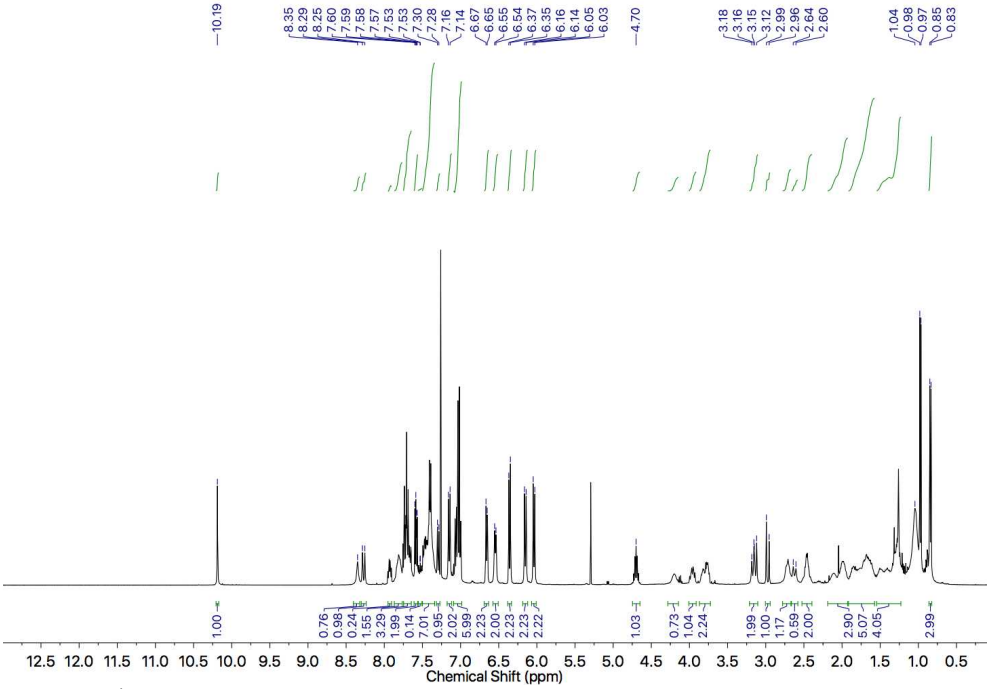

Figure 314: ^{1}H NMR of (S_{mp})-**72** ($CDCl_3$, 400 MHz).

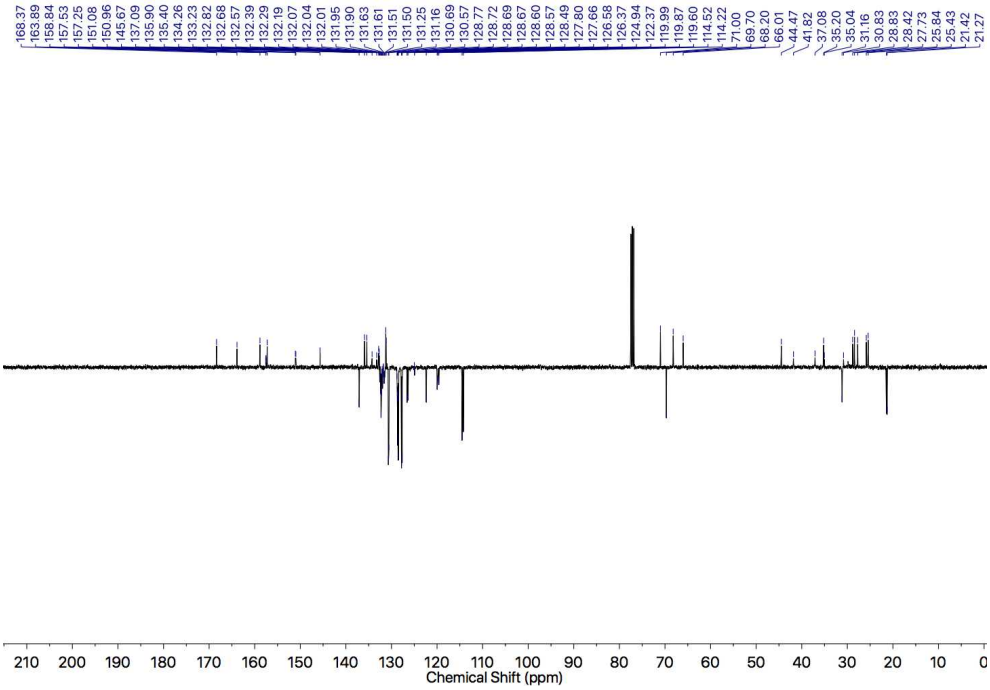

Figure 315: JMOD NMR of (S_{mp})-**72** ($CDCl_3$, 101 MHz).

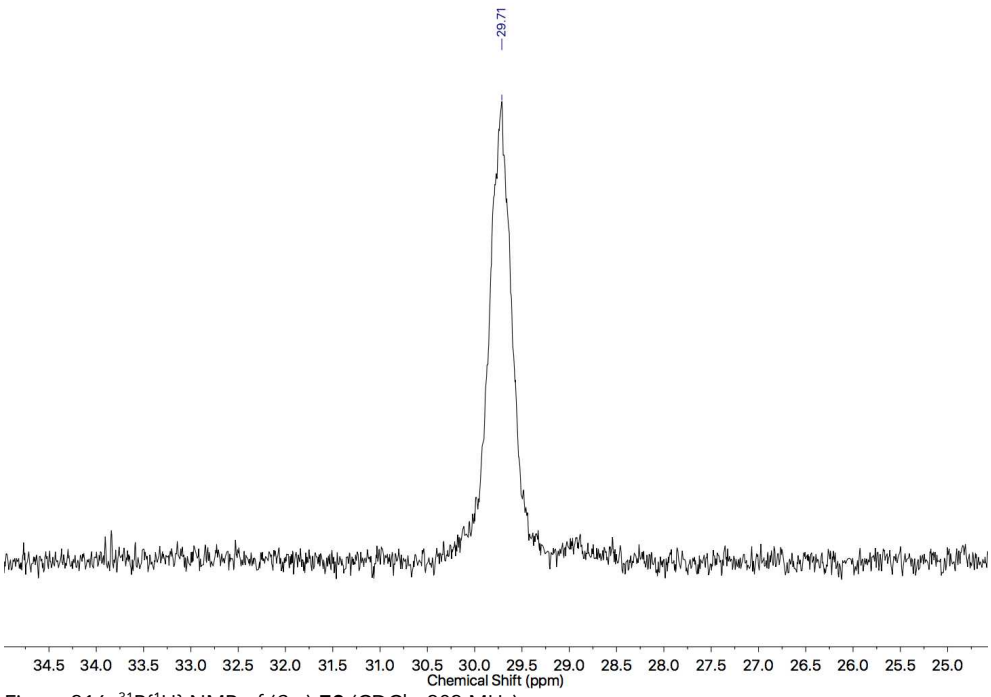

Figure 316: $^{31}P\{^{1}H\}$ NMR of (S_{mp})-**72** ($CDCl_3$, 202 MHz).

Rotaxane (S_{mp})-**73**

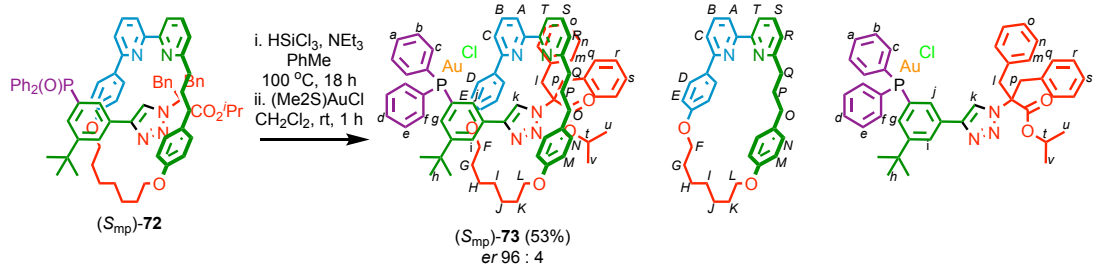

(S_{mp})-**72**

(S_{mp})-**73** (53%)
er 96 : 4

A young's tube flask was dried under reduced pressure and cycled with nitrogen 3 times, as per Schlenk technique. Anhydrous triethylamine (0.23 mL, 162 mg, 1.602 mmol, 100 eq.) and trichlorosilane (81 µL, 109 mg, 0.801 mmol, 50 eq.) were added to the flask. After 5 minutes, rotaxane (S_{mp})-**72** (18.6 mg, 0.0160 mmol, 1.0 eq.) was transferred in anhydrous PhMe (0.8 mL). The young's flask was sealed and refluxed at 100 °C for 18 h. The reaction was then cooled to room temperature, diluted in CH_2Cl_2 (15 mL), and washed with NaOH (1 M, 10 mL) four times. The residue was extracted in CH_2Cl_2 (3 x 15 mL), dried over $MgSO_4$ and concentrated *in vacuo* yielding a yellow oil (18.3 mg, 0.0160 mmol). A dry CEM MW vial was charged with $(Me_2S)AuCl$ (4.7 mg, 0.160 mmol, 1.0 eq.) and the residue was transferred in anhydrous CH_2Cl_2 (0.35 mL). After stirring at rt for 1 h, the reaction was concentrated *in vacuo* and purified by column chromatography (petrol-Et_2O 0→100%) yielding a white solid (S_{mp})-**73** (11.7 mg, 8.50 µmol, 53%). δ_H ($CDCl_3$, 400 MHz) 10.26 (1H, s, H_k), 8.41-8.32 (2H, m, H_g, H_j), 7.76 (1H, t, J = 7.8, $H_{B\ or\ S}$),

7.64 (1H, t, J = 7.8, $\boldsymbol{H}_{\text{S or B}}$), 7.63-7.38 (11H, $\boldsymbol{H}_{\text{a}}$, $\boldsymbol{H}_{\text{b}}$, $\boldsymbol{H}_{\text{c}}$, $\boldsymbol{H}_{\text{d}}$, $\boldsymbol{H}_{\text{e}}$, $\boldsymbol{H}_{\text{f}}$, $\boldsymbol{H}_{\text{i}}$), 7.55-7.51 (2H, m, $\boldsymbol{H}_{\text{A}}$, $\boldsymbol{H}_{\text{T}}$), 7.36 (1H, d, J = 7.8, $\boldsymbol{H}_{\text{C or R}}$), 7.34 (1H, d, J = 7.8, $\boldsymbol{H}_{\text{R or C}}$), 7.19 (2H, d, J = 8.6, $\boldsymbol{H}_{\text{D}}$), 7.10-7.01 (6H, m, $\boldsymbol{H}_{\text{n}}$, $\boldsymbol{H}_{\text{o}}$, $\boldsymbol{H}_{\text{r}}$, $\boldsymbol{H}_{\text{s}}$), 6.72-6.68 (2H, m, $\boldsymbol{H}_{\text{m}}$), 6.58-6.53 (2H, m, $\boldsymbol{H}_{\text{q}}$), 6.39 (2H, d, J = 8.5, $\boldsymbol{H}_{\text{N}}$), 6.19 (2H, d, J = 8.7, $\boldsymbol{H}_{\text{E}}$), 6.08 (2H, d, J = 8.5, $\boldsymbol{H}_{\text{M}}$), 4.70 (1H, sept., J = 6.3, $\boldsymbol{H}_{\text{t}}$), 4.42-4.26 (1H, $\boldsymbol{H}_{\text{Q}}$), 4.08-3.96 (1H, $\boldsymbol{H}_{\text{O}}$), 3.92-3.81 (1H, $\boldsymbol{H}_{\text{O'}}$), 3.79-3.72 (1H, $\boldsymbol{H}_{\text{Q'}}$), 3.14 (1H, d, J = 14.7, $\boldsymbol{H}_{\text{l}}$), 3.13 (1H, d, J = 14.5, $\boldsymbol{H}_{\text{p}}$), 3.04 (1H, d, J = 14.7, $\boldsymbol{H}_{\text{l'}}$), 2.86-2.74 (1H*), 2.71-2.61 (1H*), 2.58 (1H, d, J = 14.5, $\boldsymbol{H}_{\text{p'}}$), 2.52-2.46 (2H*), 2.26-2.16 (1H*), 2.14-1.99 (2H*), 1.95-1.81 (2H*), 1.78-1.62 (1H*), 1.38-1.09 (15H*, $\boldsymbol{H}_{\text{h}}$), 0.97 (3H, d, J = 6.3, $\boldsymbol{H}_{\text{u}}$), 0.82 (3H, d, J = 6.3, $\boldsymbol{H}_{\text{v}}$) *16H F, G, H, I, J, K, L, P. $\boldsymbol{\delta}_{\text{C}}$ ($CDCl_3$, 101 MHz) 168.4, 163.6, 158.7, 157.6, 157.1, 151.4, 145.3, 137.1, 137.0, 135.9, 135.3, 134.8, 134.6, 134.4, 134.4, 134.3, 134.2, 133.8, 133.6, 132.1, 131.6, 131.4, 131.0, 130.8, 130.5, 130.0, 129.7, 129.4, 129.4, 129.3, 129.2, 129.1, 128.9, 128.8, 127.9, 127.7, 127.7 (d, J = 62.7), 126.5 (d, J = 22.7), 125.6, 120.4, 120.0, 114.4, 114.0, 71.1, 69.8, 68.1, 65.8, 44.5, 41.6, 37.2, 35.2, 31.6, 31.3, 29.9, 28.8, 28.4, 27.7, 26.1, 25.8, 21.4, 21.2. $\boldsymbol{\delta}_{\text{P}}$ ($CDCl_3$, 202 MHz) 34.2. HR-ESI-MS $[M\text{-}Cl]^+$ m/z 1340.5 (calc. For $C_{75}H_{78}N_5O_4PAu$ m/z 1340.5457), $[M+H]^+$ m/z 1376.5 (calc. For $C_{75}H_{79}N_5O_4PAuCl$ m/z 1376.5224).

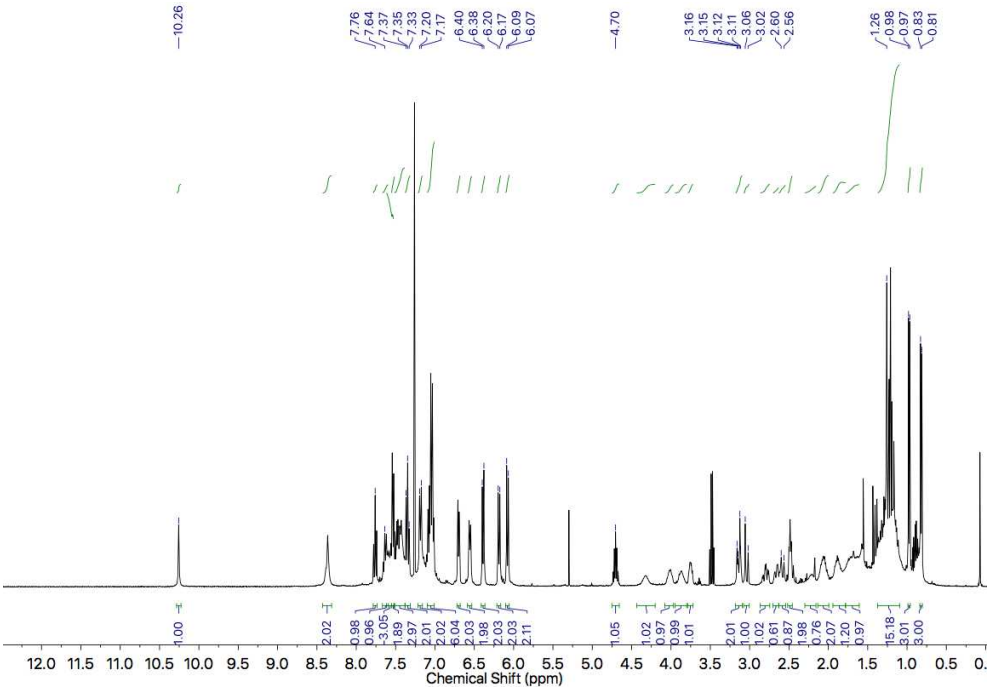

Figure 317: ^{1}H NMR of (S_{mp})-**73** ($CDCl_3$, 400 MHz).

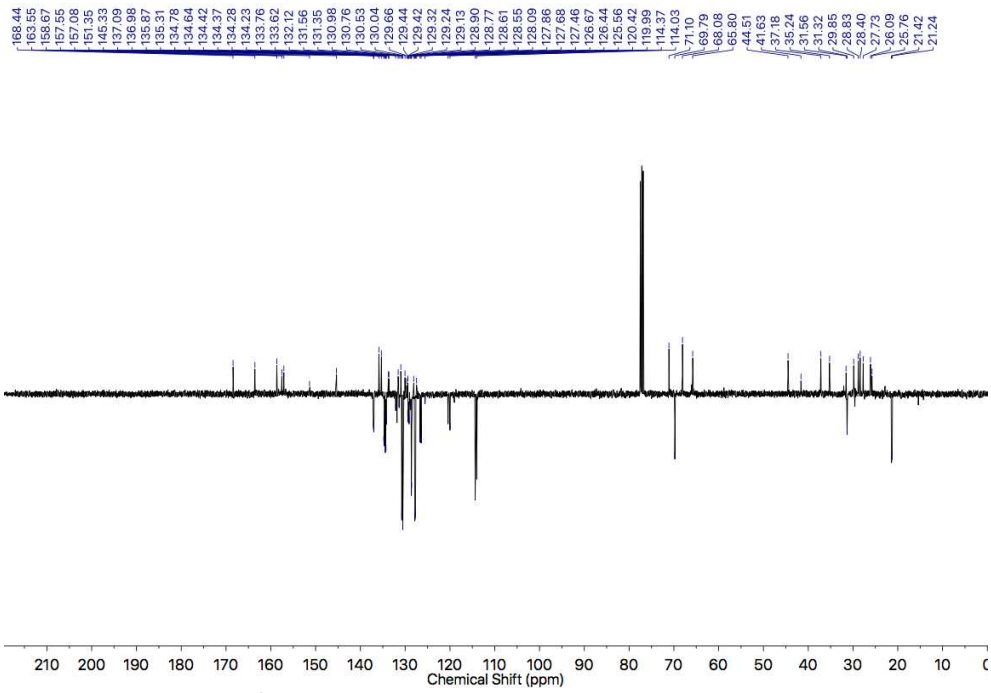

Figure 318: JMOD NMR of (S_{mp})-**73** ($CDCl_3$, 101 MHz).

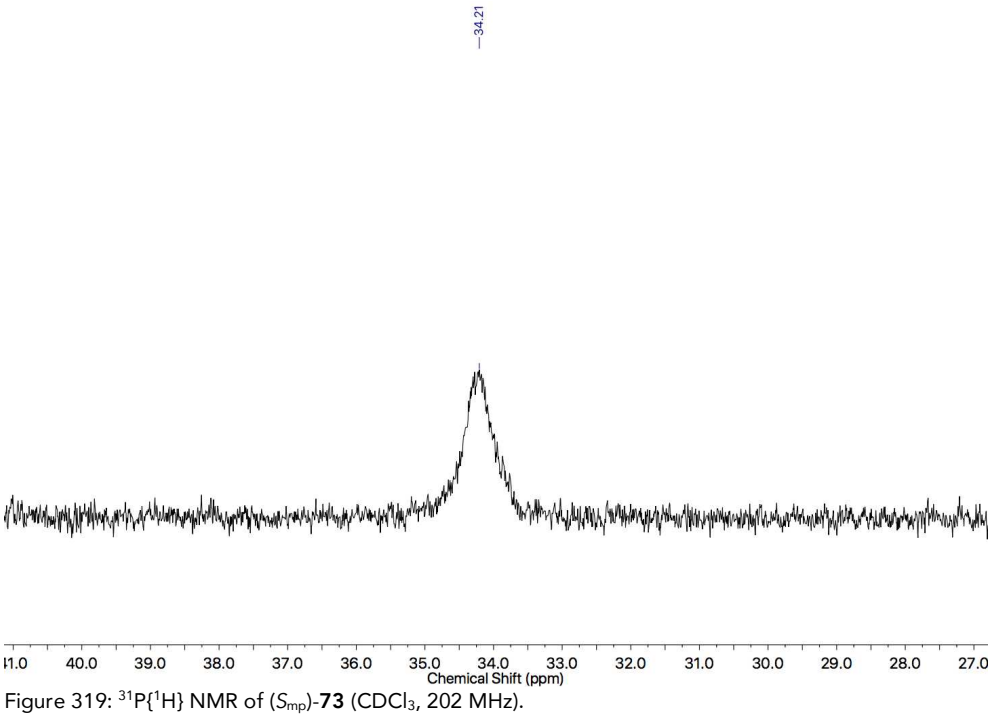

Figure 319: $^{31}P\{^1H\}$ NMR of (S_{mp})-**73** ($CDCl_3$, 202 MHz).

Reactions Catalysed by Rotaxane (S_{mp})-**73**

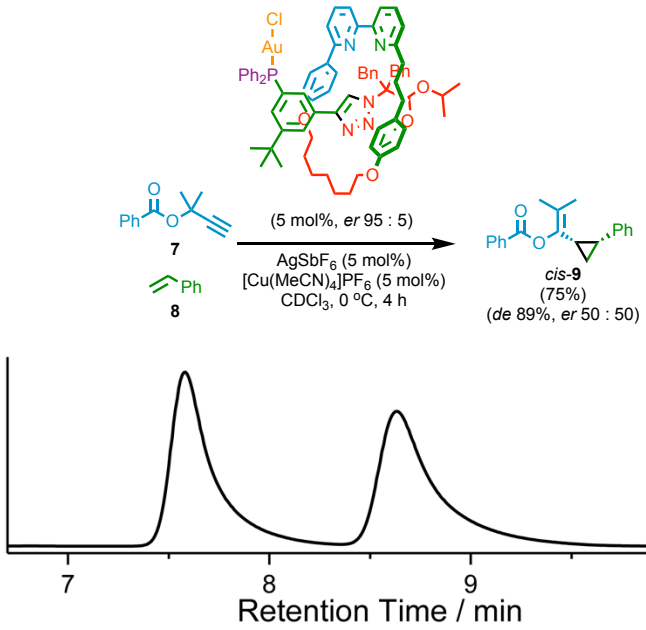

Figure 320: Chiral Stationary Phase HPLC (RegisPack, *n*-hexane-isopropanol 99 : 1, 303 K, load Et_2O, flowrate 0.75 $mLmin^{-1}$) of 50 : 50 *er cis*-**9**. Retention times (min): (1*R*,2*S*)-**9** 6.6 (3885451, 50%), (1*S*,2*R*)-**9** 7.4 (3954197, 50%).

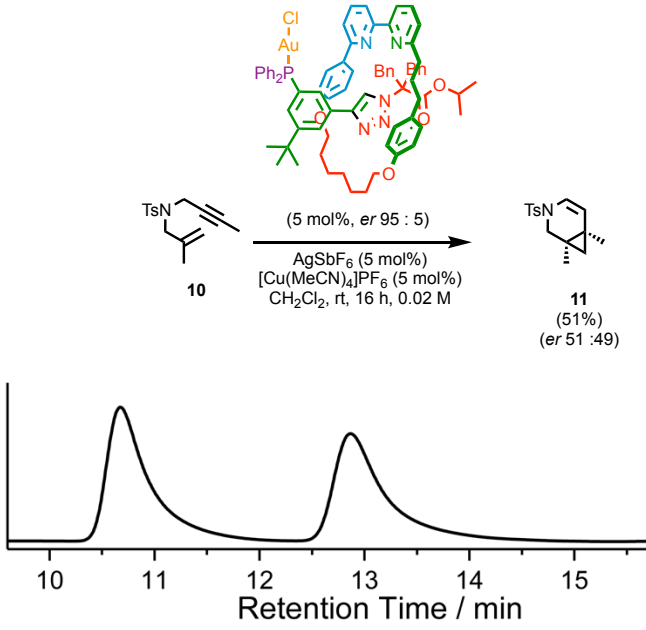

Figure 321: Chiral Stationary Phase HPLC (RegisPack, *n*-hexane-isopropanol 97 : 3, 303 K, load Et_2O, flowrate 0.75 $mLmin^{-1}$) of 51 : 49 *er cis*-**11**. Retention times (min): 10.7 (3600193, 51%), 12.9 (3476852, 49%).

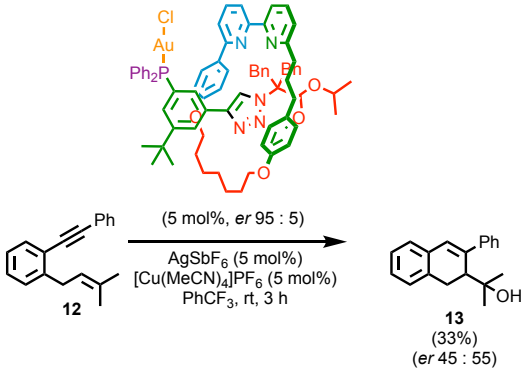

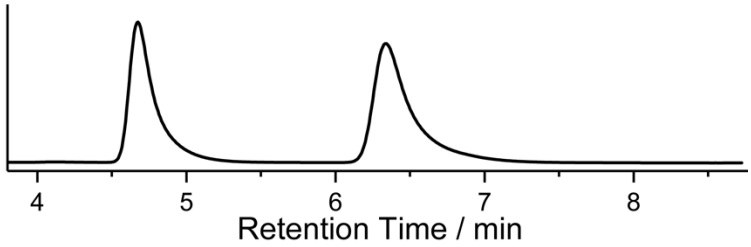

Figure 322: Chiral Stationary Phase HPLC (RegisPack, *n*-hexane-isopropanol 90 : 10, 303 K, load petrol, flowrate 1.0 mLmin^{-1}) of 45 : 55 *er* **13**. Retention times (min): 4.7 (839741, 45%), 6.3 (1034941, 55%).

Compound **76**[56–58]

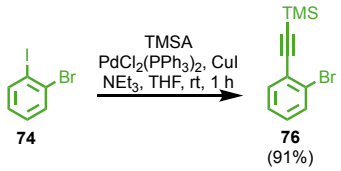

1-bromo-2-iodobenzene (2.20 g, 7.78 mmol, 1.0 eq.), TMS acetylene (916 mg, 9.33 mmol, 1.2 eq.), $PdCl_2(PPh_3)_2$ (137 mg, 0.195 mmol, 0.025 eq.), CuI (37 mg, 0.195 mmol, 0.025 eq.) were stirred under inert atmosphere at rt in NEt_3 (5.4 mL) and THF (15 mL) for 1 h. The reaction concentrated *in vacuo* and the residue was purified by column chromatography (SiO_2, hexane) yielding a colourless oil **76** (1.79 g, 7.07 mmol, 91%). δ_H ($CDCl_3$, 400 MHz) 7.57 (1H, ddd, *J* = 7.9, 1.3, 0.3), 7.49 (1H, ddd, *J* = 7.9, 1.7, 0.3), 7.24 (1H, td, *J* = 7.3, 1.6), 7.15 (1H, ddd, *J* = 7.5, 1.7), 0.28 (9H, s). δ_C ($CDCl_3$, 101 MHz) 133.7, 132.5, 129.7, 127.0, 125.9, 125.4, 103.2, 99.8, 0.0. HR-MS [$M^{+\cdot}$] 251.9962 (calc. for $C_{11}H_{13}BrSi$ m/z 251.9964).[56–58]

Compound **130**[64–66]

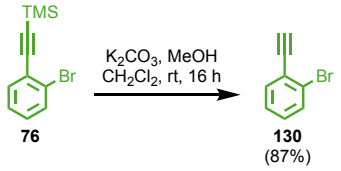

76 (500 mg, 1.97 mmol, 1.0 eq.) was stirred over K_2CO_3 (1.36 g, 9.87 mmol, 5.0 eq.) in CH_2Cl_2 (9 mL) and MeOH (9 mL) for 16 h at room temperature. The crude reaction mixture was washed with water (30 mL) and extracted in CH_2Cl_2 (3 x 15 mL), dried over $MgSO_4$ and concentrated *in vacuo* yielding an orange oil **130** (310 mg, 1.71 mmol, 87%). δ_H ($CDCl_3$, 400 MHz) 7.59 (1H, ddd, *J* = 8.0, 1.3, 0.4), 7.53 (1H, dd, *J* = 7.6, 1.8), 7.27 (1H, td, *J* = 7.5, 1.3), 7.21 (1H, td, *J* = 7.8, 1.8), 3.38 (1H, s). δ_C ($CDCl_3$, 101 MHz) 134.0, 132.4, 129.9, 130.0, 125.5, 124.2, 81.8, 81.7. LR MS [$M^{+\cdot}$] 180.2, 182.2.[64–66]

Compound **84**[59–61]

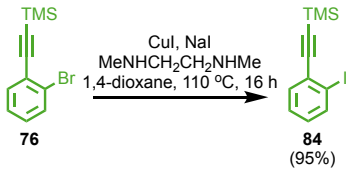

76 (300 mg, 1.18 mmol, 1.0 eq.), CuI (22.6 mg, 0.118 mmol, 0.1 eq.), NaI (710 mg, 4.74 mmol, 4.0 eq.), *N,N'*-dimethylethyl-1,2-diamine (21 mg, 0.237 mmol, 0.2 eq.) was heated at 110 °C in 1,4-dioxane (1.2 mL) for 16 h. The reaction concentrated *in vacuo* and the residue was purified by column chromatography (SiO_2, hexane) yielding a colourless oil **84** (337 mg, 1.12 mmol, 95%). δ_H ($CDCl_3$, 400 MHz) 7.84 (1H, ddd, *J* = 8.0, 1.2, 0.4), 7.47 (1H, dd, *J* = 7.8, 1.7), 7.28 (1H, td, *J* = 7.5, 1.3), 7.00 (1H, ddd, *J* 9.2, 8.0, 1.7), 0.29 (9H, s). δ_C ($CDCl_3$, 101 MHz) 138.8, 132.9, 129.8, 129.7, 127.8, 106.7, 101.4, 89.0, 0.03. LR MS [$M^{+\cdot}$] 300.2.[59–61]

Compound **85**[61]

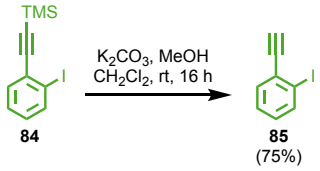

84 (362 mg, 1.43 mmol, 1.0 eq.) was stirred over K_2CO_3 (988 mg, 7.15 mmol, 5.0 eq.) in CH_2Cl_2 (9 mL) and MeOH (9 mL) for 16 h at room temperature. The crude reaction mixture was washed with water (30 mL) and extracted in CH_2Cl_2 (3 x 15 mL), dried over $MgSO_4$ and concentrated *in vacuo* yielding a yellow oil **85** (244 mg, 1.07 mmol, 75%).δ_H ($CDCl_3$, 400 MHz) 7.86 (1H, ddd, *J* = 8.1, 1.2, 0.4), 7.51 (1H, dd, *J* = 7.7, 1.6), 7.31 (1H, td, *J* = 7.6, 1.2), 7.04 (1H, td, *J* = 7.8, 1.7), 3.40 (1H, s). δ_C ($CDCl_3$, 101 MHz) 138.9, 133.6, 130.1, 128.9, 127.9, 100.6, 85.3, 81.2. LR MS [$M^{+\cdot}$] 228.1.[61]

Compound **79**

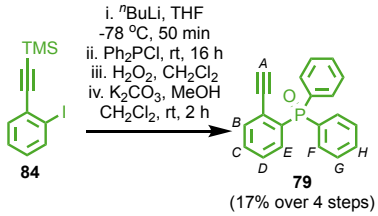

A dry CEM MW vial was charged with **84** (500 mg, 1.97 mmol, 1.0 eq.) and purged with N_2. The compound was dissolved in anhydrous THF (8 mL) and cooled to -78 °C. ^{n}BuLi (0.87 mL, 2.17 mmol, 1.1 eq., 2.5 M in hexanes) was added slowly over 5 minutes. The solution was stirred at -78 °C for 50 minutes. Ph_2PCl (0.43 mL, 2.37 mmol, 1.2 eq.) was added and the reaction was allowed to warm to room temperature over 18 h. The reaction was concentrated onto SiO_2 and purified by column chromatography (SiO_2, petrol-EtOAc 0→5%) yielding a yellow oil (179 mg, 0.499 mmol, 26%). The oil was dissolved in CH_2Cl_2 (2 mL) and stirred with H_2O_2 (2 mL, 35 w/w%) for 15 minutes. The reaction mixture was then washed with brine (10 mL) and extracted in CH_2Cl_2 (3 x 15 mL). The combined organic phases were dried over $MgSO_4$ and concentrated *in vacuo*. The residue was then dissolved in CH_2Cl_2 (2 mL) and MeOH (2 mL), and stirred over K_2CO_3 (332 mg, 2.40 mmol, 5.0 eq.) for 2 h. The reside was washed with $NaHCO_3$ (15 mL) and extracted in CH_2Cl_2 (3 x 15 mL). The combined organic phases were dried over $MgSO_4$ and concentrated *in vacuo*. The residue was purified by column chromatography (SiO_2, petrol-EtOAc 0→100%) yielding a white foam **79** (93 mg, 0.308 mmol, 64%). δ_H ($CDCl_3$, 400 MHz) 7.75 (4H, ddt, J = 12.3, 6.9, 1.4, $\boldsymbol{H}_F$), 7.69 (1H, dddd, J = 13.0, 7.7, 1.5, 0.5, $\boldsymbol{H}_E$), 7.63 (1H, ddd, J = 7.7, 3.9, 1.0, $\boldsymbol{H}_B$), 7.58-7.50 (3H, m, $\boldsymbol{H}_H$, $\boldsymbol{H}_{D\text{ or }C}$), 7.50-7.40 (5H, m, $\boldsymbol{H}_G$, $\boldsymbol{H}_{C\text{ or }D}$), 2.99 (1H, s, $\boldsymbol{H}_A$). δ_C ($CDCl_3$, 101 MHz) 135.1 (d, J_{CP} = 8.9), 134.8 (d, J_{CP} = 101.0), 133.9 (d, J_{CP} = 9.4), 132.3 (d, J_{CP} = 10.0), 132.3 (d, J_{CP} = 106.4), 131.9 (d, J_{CP} = 2.8), 131.8 (d, J_{CP} = 2.4), 128.5 (d, J_{CP} = 11.9), 128.4 (d, J_{CP} = 12.5), 125.4 (d, J_{CP} = 6.7), 85.2, 81.7 (d, J_{CP} = 5.6). $\delta_{P\{1H\}}$ ($CDCl_3$, 202 MHz) 29.0. HR-ESI-MS $[M+H]^+$ m/z 303.0932 (calc. for $C_{20}H_{16}OP$ m/z 303.0933).

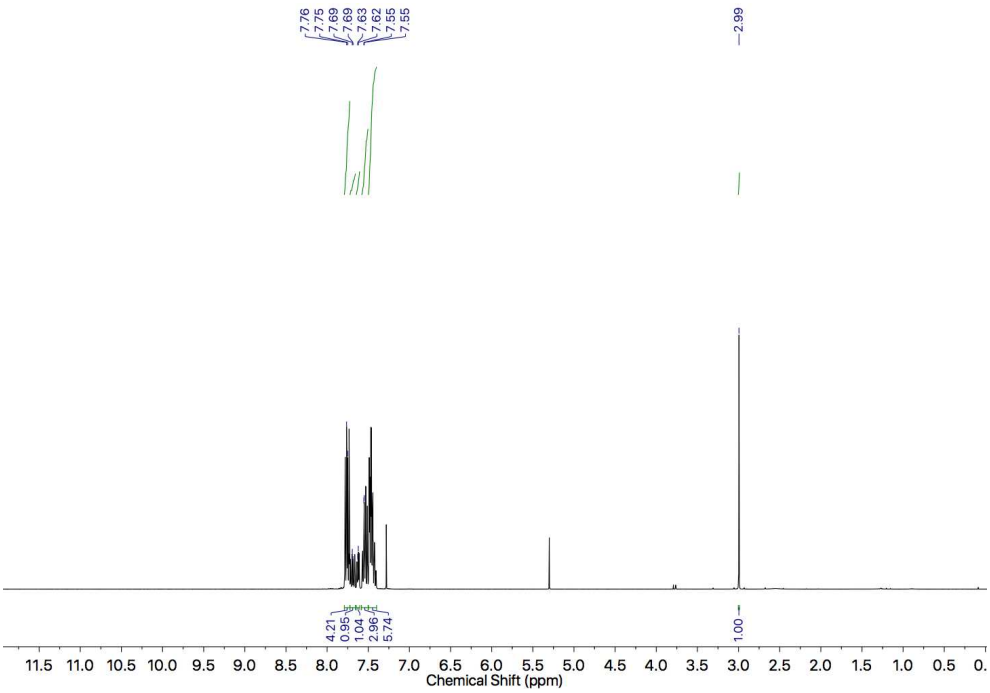

Figure 323: ^{1}H NMR of **79** ($CDCl_3$, 400 MHz).

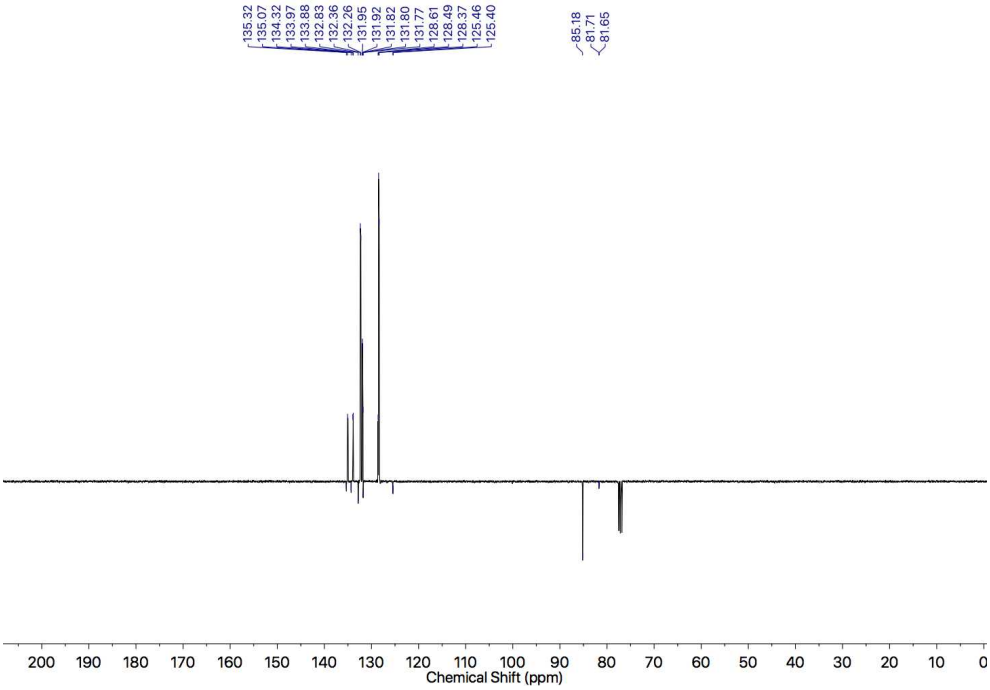

Figure 324: JMOD NMR of **79** ($CDCl_3$, 101 MHz).

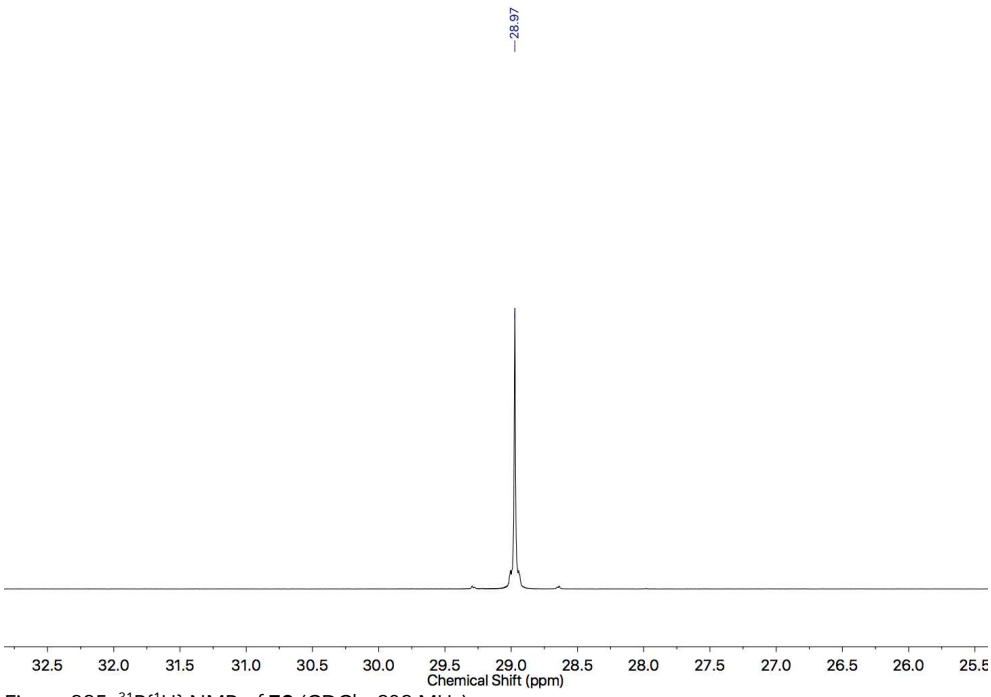

Figure 325: $^{31}P\{^{1}H\}$ NMR of **79** ($CDCl_3$, 202 MHz).

Compound (*S*)-**81**

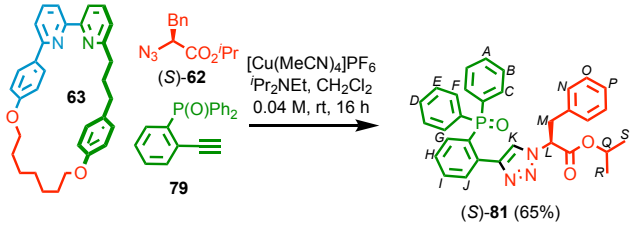

A dry CEM MW vial was charged with macrocycle **63** (12 mg, 0.0251 mmol, 1.0 eq.) and $[Cu(MeCN)_4]PF_6$ (9.0 mg, 0.0241 mmol, 0.96 eq.), then purged with N_2. Alkyne **79** (7.6 mg, 0.0251 mmol, 1.0 eq.) and azide (*S*)-**62** (5.8 mg, 0.0251 mmol, 1.0 eq.) were transferred in anhydrous degassed CH_2Cl_2 (0.63 mL, [**63**] = 0.04 M). $^{i}Pr_2NEt$ (17 µL, 13 mg, 0.100 mmol, 4.0 eq.) was added and the solution stirred at room temperature for 16 h. The residue was concentrated *in vacuo*. No rotaxane was observed in the crude NMR or MS spectra. The residue was purified by column chromatography (SiO_2, petrol-EtOAc 0→100%) yielding recovered macrocycle **63** (8.0 mg, 0.017 mmol, 68%), and axle (*S*)-**81** white foam (8.7 mg, 0.0162 mmol, 65%). δ_H ($CDCl_3$, 400 MHz) 8.90 (1H, s, H_K), 8.08-8.01 (1H, m, H_G), 7.68-7.54 (5H, m, H_C, H_F, H_H), 7.49-7.42 (2H, m, H_I, H_J), 7.42-7.29 (5H, m, H_B, H_D, H_E), 7.26-7.21 (3H, m, H_O, H_P), 7.16 (1H, ddd, J = 14.5, 7.8, 1.1, H_A), 7.09-7.05 (2H, m, H_N), 5.31 (1H, dd, J 7.8, 7.8, H_L), 4.92 (1H, sept., J = 6.3, H_Q), 3.39 (1H, dd, J = 13.8, 8.7, H_M), 3.11 (1H, dd, J = 13.8, 7.2, $H_{M'}$), 1.14 (3H, d, J = 6.3, H_R), 1.02 (3H, d, J = 6.3, H_S). δ_C ($CDCl_3$, 101 MHz) 167.3, 145.4, 145.4, 135.7, 135.2, 134.3 (d, J_{CP} = 12.3),

132.7 (d, J_{CP} = 2.2), 132.0 (d, J_{CP} = 9.6), 131.9 (d, J_{CP} = 2.5), 131.8, 131.7, 131.7 (d, J_{CP} = 9.8), 130.7, 129.7, 129.2, 128.8, 128.6 (d, J_{CP} = 4.2), 128.5 (d, J_{CP} = 4.1), 127.7 (d, J_{CP} = 12.4), 127.4, 125.8, 70.2, 64.2, 39.1, 21.7, 21.5. $\delta_{P\{1H\}}$ ($CDCl_3$, 202 MHz) 32.6. HR-ESI-MS $[M+H]^+$ m/z 536.2103 (calc. for $C_{32}H_{31}N_3O_3P$ 536.2908), 558.1915 (calc. for $C_{32}H_{30}N_3O_3PNa$ 558.1917).

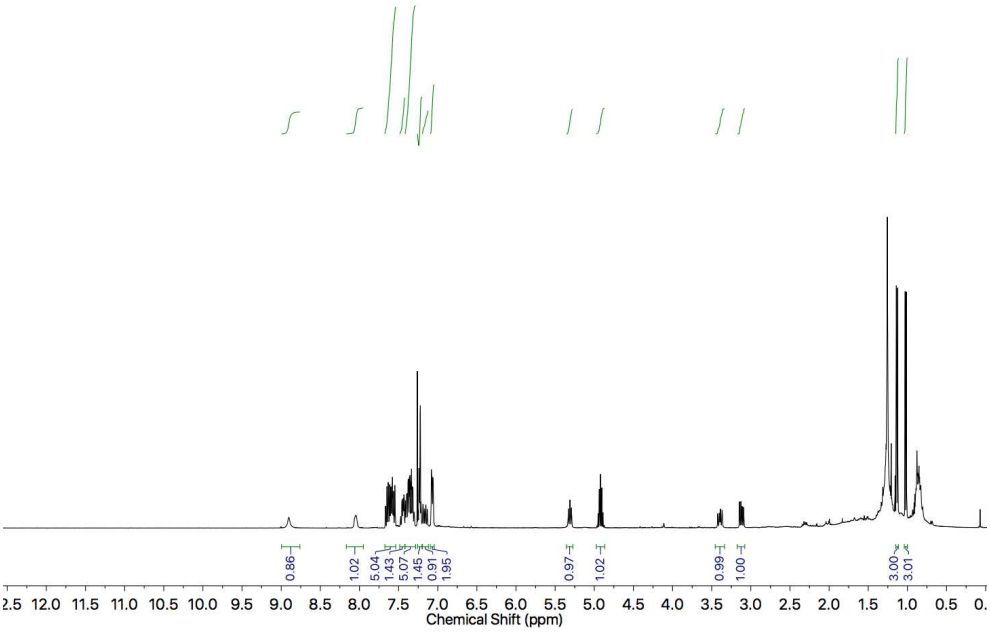

Figure 326: ^1H NMR of (*S*)-**81** ($CDCl_3$, 400 MHz).

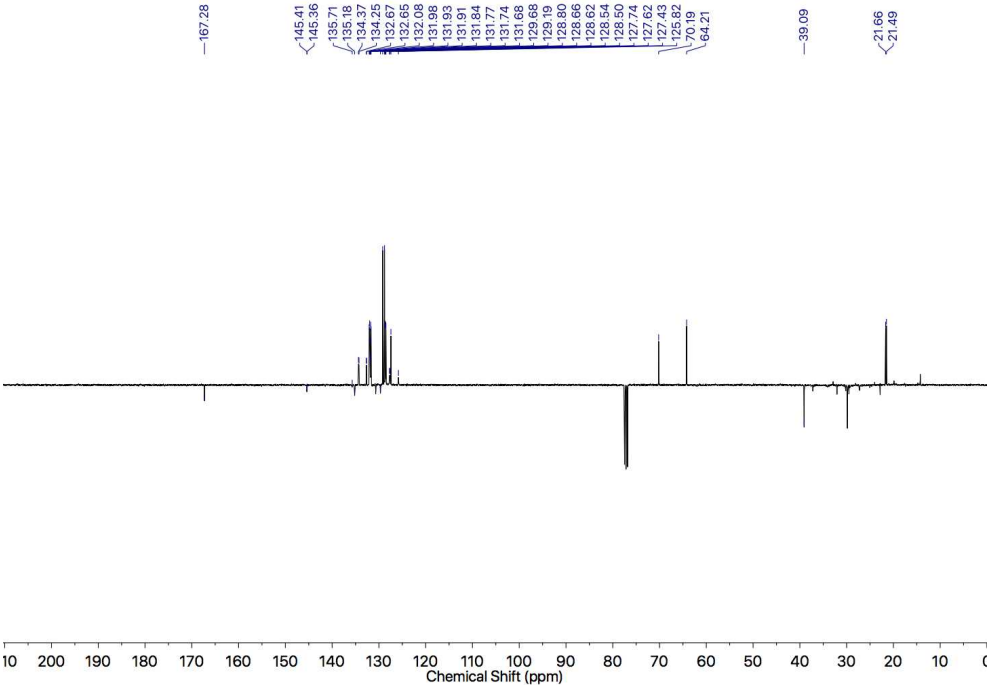

Figure 327: JMOD NMR of (*S*)-**81** ($CDCl_3$, 101 MHz).

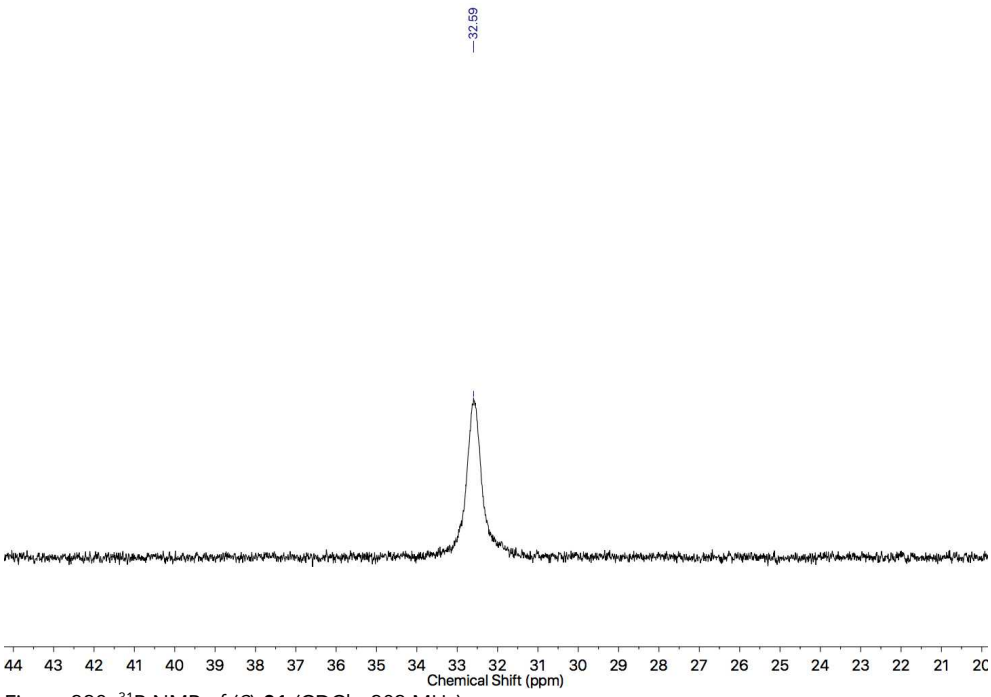

Figure 328: ^{31}P NMR of (*S*)-**81** ($CDCl_3$, 202 MHz).

Compound (*S*)-**131**

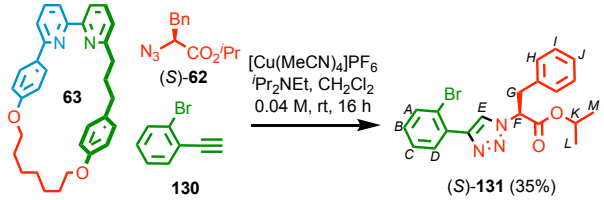

A dry CEM MW vial was charged with macrocycle **63** (12 mg, 0.0251 mmol, 1.0 eq.) and $[Cu(MeCN)_4]PF_6$ (9.0 mg, 0.0241 mmol, 0.96 eq.), then purged with N_2. Alkyne **130** (13.6 mg, 0.0752 mmol, 3.0 eq.) and azide (*S*)-**62** (17.5 mg, 0.0752 mmol, 3.0 eq.) were transferred in anhydrous degassed CH_2Cl_2 (0.63 mL, [**63**] = 0.04 M). $^{i}Pr_2NEt$ (22 µL, 16.2 mg, 0.125 mmol, 5.0 eq.) was added and the solution stirred at room temperature for 16 h. The residue was concentrated *in vacuo*. The residue was purified by column chromatography (SiO_2, petrol-EtOAc 0→100%) yielding recovered macrocycle (10 mg, 0.0209 mmol, 83%), and axle white foam (*S*)-**131** (11.0 mg, 0.027 mmol, 35%). δ_H ($CDCl_3$, 400 MHz) 8.31 (1H, s, H_E), 8.07 (1H, dd, *J* = 7.9, 1.7, H_A), 7.65 (1H, dd, *J* = 8.1, 1.2, H_D), 7.40 (1H, td, *J* = 7.6, 1.3, H_B), 7.29-7.22 (3H, m, H_I, H_J), 7.20-7.17 (1H, m, H_C), 7.14-7.10 (2H, m, H_H), 5.63 (1H, dd, *J* = 8.3, 6.8, H_F), 5.08 (1H, sept., *J* = 6.3, H_K), 3.59-3.48 (2H, m, H_G, $H_{G'}$), 1.25 (3H, d, *J* = 6.3, H_L), 1.20 (3H, d, *J* = 6.3, H_M). δ_C ($CDCl_3$, 101 MHz) 167.8, 145.4, 134.8, 133.6, 131.4, 130.8, 129.5, 129.2, 128.9, 127.8, 127.7, 123.2, 121.4, 70.7,

64.4, 39.2, 21.8, 21.7. HR-ESI-MS $[M+H]^+$ m/z 414.0821 (calc. for $C_{20}H_{21}N_3O_2Br$ 414.0812), $[M+Na]^+$ m/z 436.0633 (calc. for $C_{20}H_{20}N_3O_2BrNa$ 436.00631).

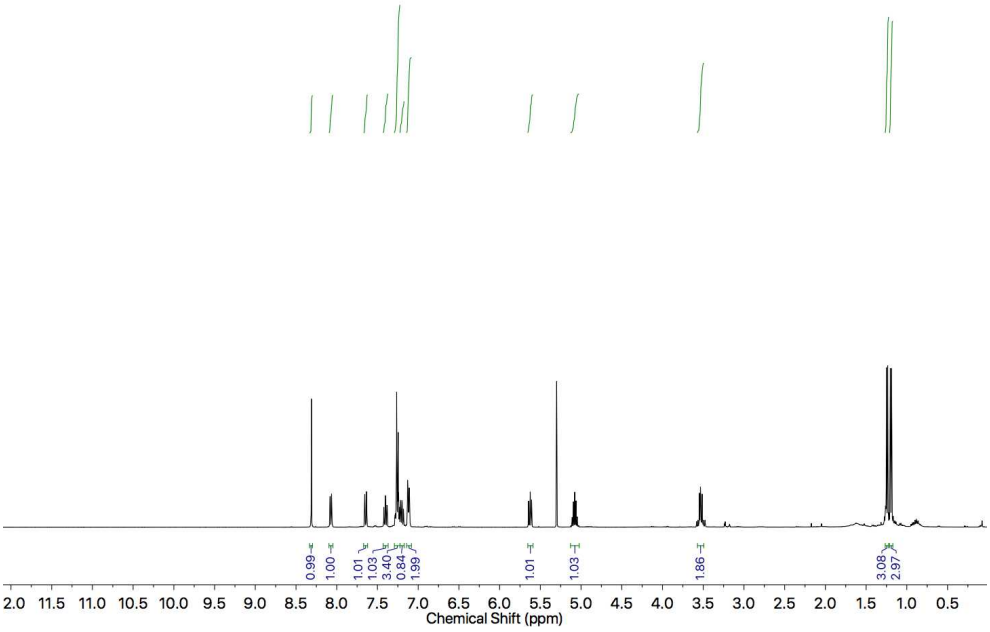

Figure 329: ^1H NMR of (*S*)-**131** ($CDCl_3$, 400 MHz).

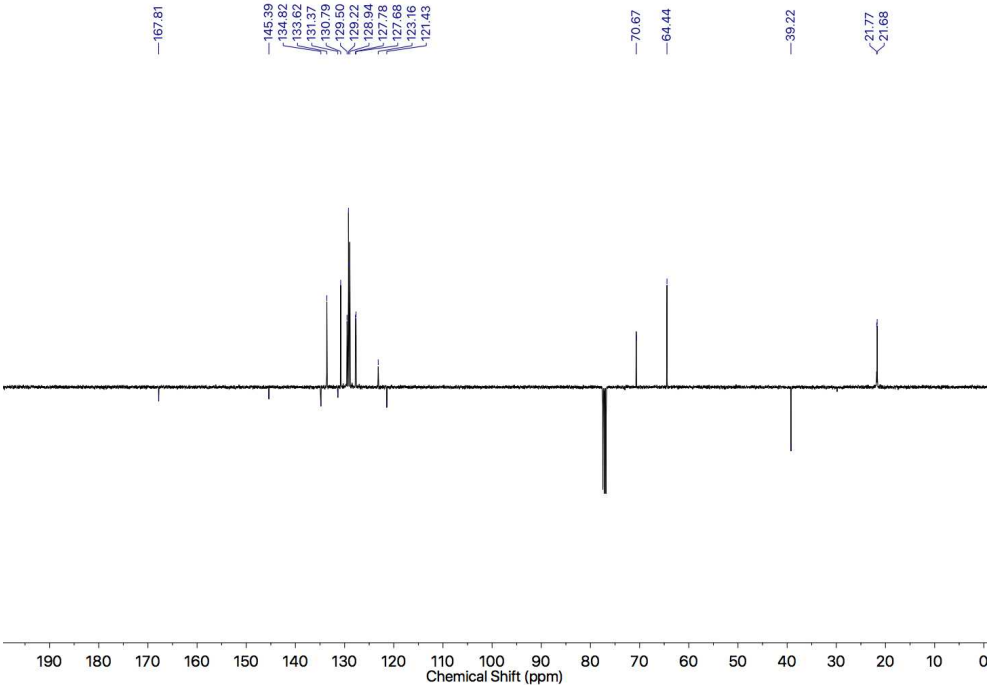

Figure 330: JMOD NMR of (*S*)-**131** ($CDCl_3$, 101 MHz).

Compound (*S*)-**87**

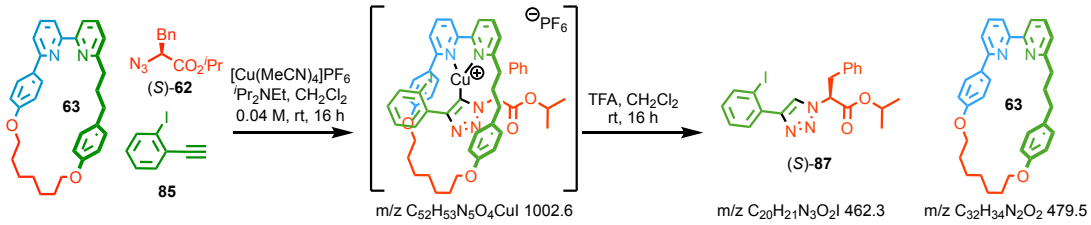

A dry CEM MW vial was charged with macrocycle **63** (24 mg, 0.0502 mmol, 1.0 eq.) and $[Cu(MeCN)_4]PF_6$ (17.9 mg, 0.0482 mmol, 0.96 eq.), then purged with N_2. Alkyne **85** (90.8 mg, 0.501 mmol, 10.0 eq.) and azide (*S*)-**62** (117 mg, 0.501 mmol, 10.0 eq.) were transferred in anhydrous degassed CH_2Cl_2 (1.25 mL, [**63**] = 0.04 M). $^iPr_2NEt$ (84 µL, 62 mg, 0.501 mmol, 10.0 eq.) was added and the solution stirred at room temperature for 16 h. The reaction was concentrated *in vacuo* and monitored by ^1H NMR and LCMS. After 16 h, the residue was stirred with TFA (77 µL, 114 mg, 1.0 mmol, 20.0 eq.) in CH_2Cl_2 (2.5 mL) for 16 h. The reaction was washed with EDTA-NH_3 (10 mL) and brine (10 mL), extracted in CH_2Cl_2 (3 x 15 mL). The combined organic layers were dried over $MgSO_4$, and concentrated *in vacuo*. LCMS and ^1H NMR showed that the Cu^I-triazolide complex (m/z 1002.6) formed during the CuAAC, however once demetallated the *pseudo*rotaxane dissociated yielding axle (*S*)-**87** (m/z 462.3) and macrocycle **63** (m/z 479.5).

Compound **133**

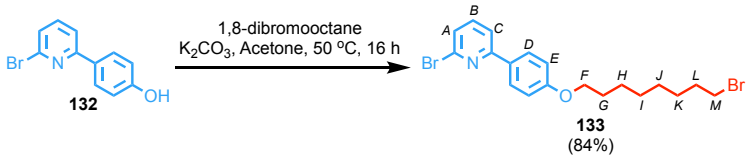

132 (1.79 g, 7.15 mmol, 1.0 eq.),1,8-dibromoctatane (4.00 mL, 21.5 mmol, 3.0 eq.), and K_2CO_3 (6.97 mg, 50.4 mmol, 7.0 eq.) were heated in acetone (100 mL) at 50 °C for 16 h. The reaction mixture was cooled to rt and concentrated *in vacuo*. The residue was suspended in CH_2Cl_2 (200 mL), dried over $MgSO_4$, filtered through a silica plug, and had the solvent removed *in vacuo*. The residue was purified by flash pad (SiO_2, petrol-CH_2Cl_2 0→50%) yielding a white solid **133** (2.66 g, 6.03 mmol, 84%). δ_H ($CDCl_3$, 400 MHz) 7.94 (2H, d, J = 8.9, H_E), 7.61 (1H, dd, J = 7.8, 0.9, H_C), 7.54 (1H, app. t, J = 7.7, H_B), 7.33 (1H, dd, J = 7.6, 0.9, H_A), 6.96 (2H, d, J = 8.9, H_E), 4.01 (2H, t, J = 6.5, H_F), 3.42 (2H, t, J = 6.8, H_M), 1.92-1.84 (2H, m, H_L), 1.84-1.76 (2H, m, H_G), 1.52-1.32 (8H, m, H_H, H_I, H_J, H_K);

δ_C ($CDCl_3$, 101 MHz) 160.7, 158.4, 142.2, 139.0, 130.1, 128.4, 125.5, 118.2, 114.8, 68.2, 34.1, 32.9, 29.8, 29.3, 28.8, 28.2, 26.1. HR-ESI-MS (+ve) $[M+H]^+$ m/z 440.0217 (calc. for $C_{19}H_{20}Br_2NO$ m/z 440.0219). Melting Point 64-66 °C.

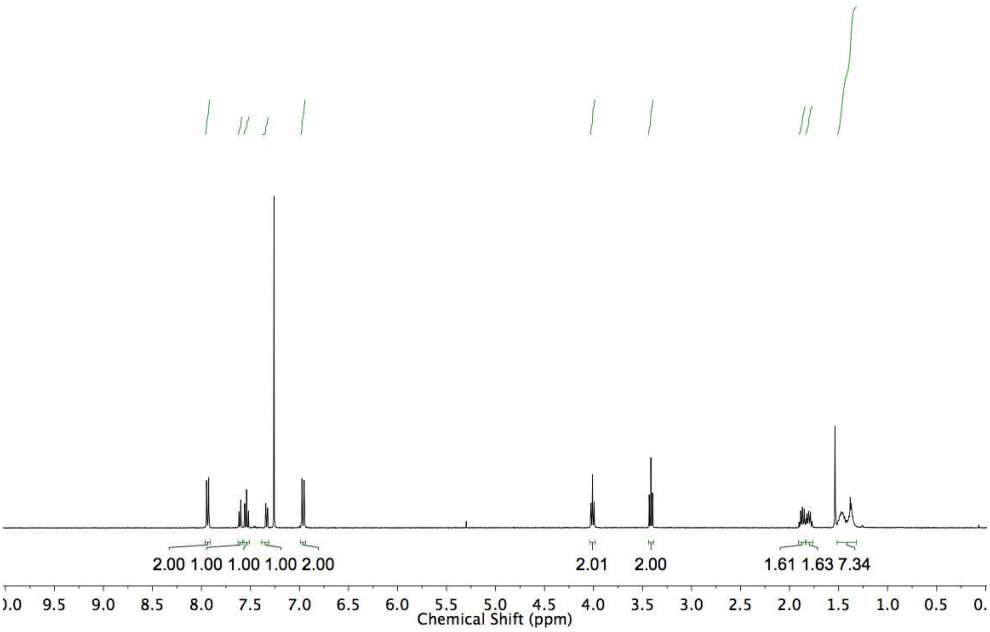

Figure 331: ^1H NMR of **133** ($CDCl_3$, 400 MHz).

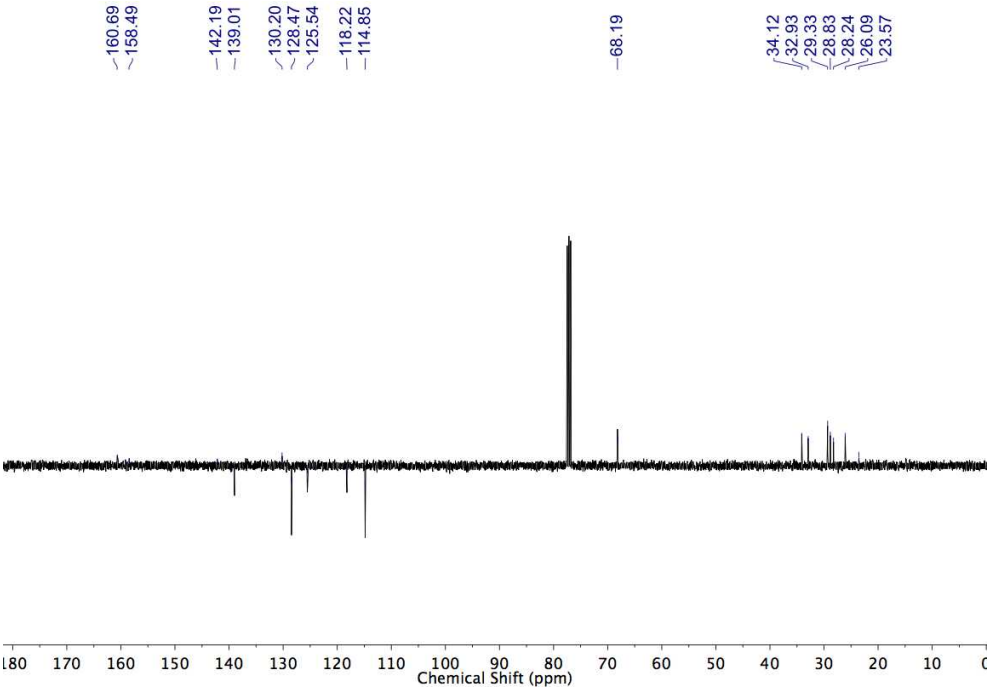

Figure 332: JMOD NMR of **133** ($CDCl_3$, 101 MHz).

Compound **135**

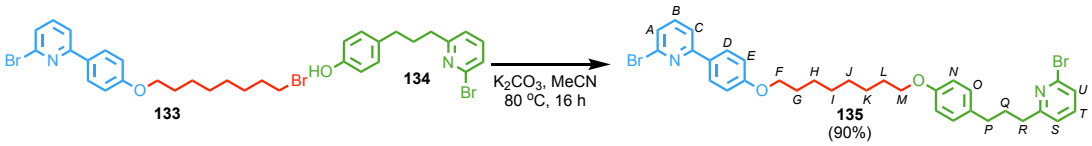

134 (760 mg, 2.61 mmol, 1.0 eq.), **133** (1.23 g, 2.78 mmol, 1.1 eq.), and K_2CO_3 (2.35 g, 17.0 mmol, 6.5 eq.), dissolved in MeCN (30 mL) and heated under reflux for 16 h. The reaction mixture was cooled to rt and concentrated *in vacuo*. The residue was suspended in CH_2Cl_2 (100 mL), dried over $MgSO_4$, filtered through a silica plug, and concentrated *in vacuo*. The residue was purified by column chromatography (SiO_2, petrol-CH_2Cl_2 0→90%) yielding a white solid **135** (1.53 g, 2.34 mmol, 90%). δ_H ($CDCl_3$, 400 MHz) 7.93 (2H, d, J = 8.9, H_D), 7.60 (1H, dd, J = 7.8, 1.0, H_C), 7.52 (1H, app. t, J = 7.7, H_B), 7.42 (1H, app. t, J = 7.7, H_T), 7.32 (1H, dd, J = 7.7, 1.0, H_A), 7.28 (1H, dd, J = 7.9, 0.9, H_U), 7.12-7.04 (3H, m, H_O, H_S), 6.96 (2H, d, J = 8.9, H_E), 6.82 (2H, d, J = 8.8, H_N), 4.00 (2H, t, J = 6.5, H_F), 3.93 (2H, t, J = 6.5, H_M), 2.83-2.74 (2H, m, H_R), 2.61 (2H, t, J = 7.6, H_P), 2.05-1.96 (2H, m, H_Q), 1.86-1.73 (4H, m, H_G, H_L), 1.55-1.34 (8H, m, H_H, H_I, H_J, H_K); δ_C ($CDCl_3$, 101 MHz) 163.9, 160.7, 158.4, 157.5, 142.1, 141.7, 139.0, 138.7, 133.9, 130.1, 129.4, 128.4, 125.5, 125.4, 121.6, 118.2, 114.8, 114.5, 68.2, 68.1, 37.5, 34.6, 31.6, 29.4 (3C, from HSQC), 29.3, 26.1, 26.1. HR-ESI-MS $[M+H]^+$ m/z 651.1225 (calc. for $C_{33}H_{37}Br_2N_2O_2$ m/z 651.1216). Melting point 80-82 °C.

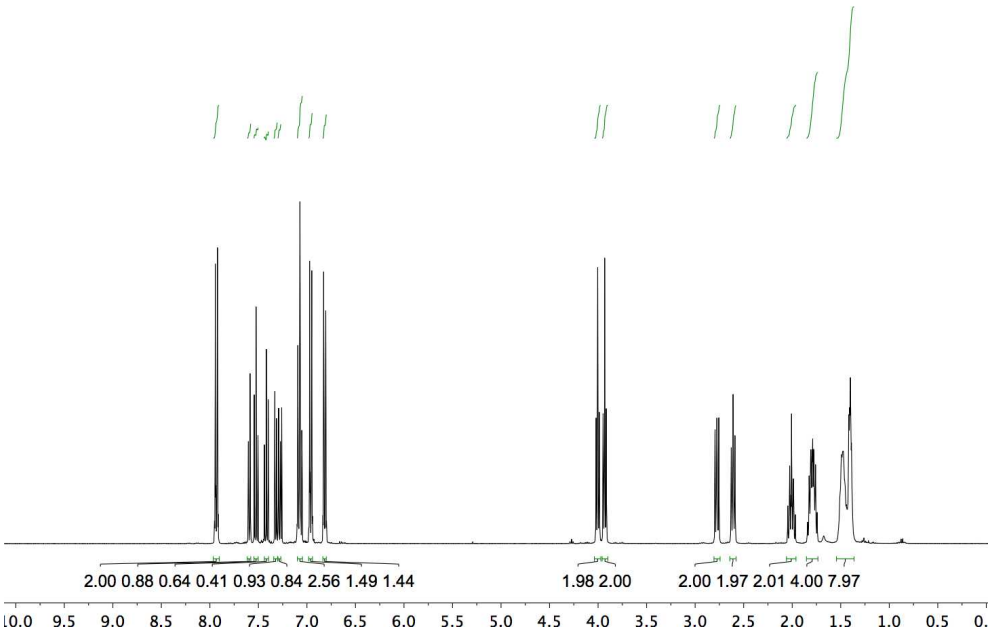

Figure 333: ^{1}H NMR of **135** ($CDCl_3$, 400 MHz).

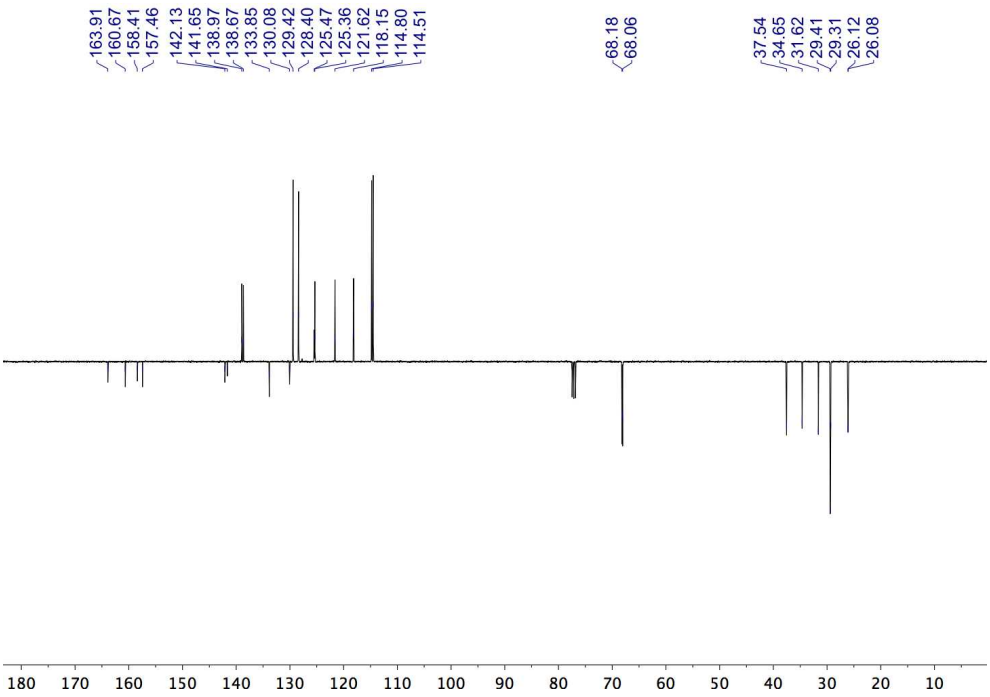

Figure 334: JMOD NMR of **135** ($CDCl_3$, 101 MHz).

Macrocycle **91**

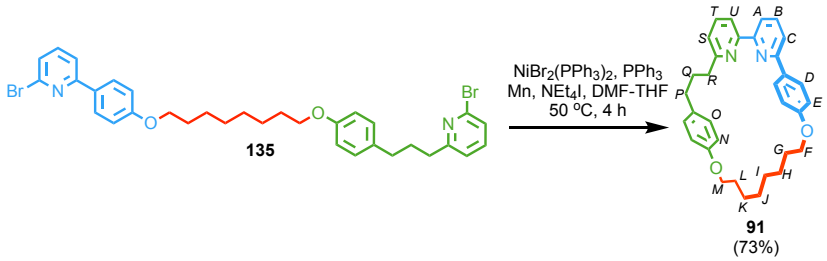

A flask was charged with $[Ni(PPh_3)_2Br_2]$ (2.16 g, 2.91 mmol, 1.0 eq.), PPh_3 (1.52 g, 5.81 mmol, 2.0 eq.), Mn (1.89 g, 29.1 mmol, 10.0 eq.) and NEt_4I (1.49 mg, 5.81 mmol, 2.0 eq.) and DMF (30 mL), protected by a N_2 atmosphere, which was sonicated for 15 minutes, followed by stirring at 50 °C for 10 minutes. To this catalyst mixture was added **135** (1.90 g, 2.91 mmol, 1.0 eq.) dissolved in anhydrous DMF (15 mL) and anhydrous THF (15 mL) via syringe over 4 h at 50 °C, followed by additional stirring of the reaction for 30 minutes, protected by a N_2 atmosphere. The reaction was allowed to cool, was poured onto sat. EDTA-NH_3 solution (100 mL) and the aqueous layer was extracted with EtOAc (2 x 100 mL). The combined organic phases were washed with LiCl 5% v/w (5 x 60 mL), brine (80 mL), dried with $MgSO_4$, filtered and the solvent removed *in vacuo*. The crude product was purified by column chromatography (SiO_2, petrol-EtOAc 0→85%) to yield **91** as an pale yellow solid (1.04 g, 2.11 mmol, 73%). δ_H ($CDCl_3$, 400 MHz) 8.14 (2H, d, J = 8.9, H_D), 7.80 (1H, app. t, J = 7.7, H_B), 7.74-7.63 (4H, m, H_A, H_C, H_T, H_U), 7.23-7.16

(3H, m, $\boldsymbol{H}_O$, $\boldsymbol{H}_S$), 6.95 (2H, d, J = 8.9, $\boldsymbol{H}_E$), 6.75 (2H, d, J = 8.6, $\boldsymbol{H}_N$), 4.10 (2H, t, J = 6.3, $\boldsymbol{H}_F$), 3.89 (2H, t, J = 6.5, $\boldsymbol{H}_M$), 2.99 (2H, t, J = 7.2, $\boldsymbol{H}_R$), 2.72 (2H, t, J = 7.4, $\boldsymbol{H}_P$), 2.34-2.24 (2H, m, $\boldsymbol{H}_Q$), 1.84-1.77 (2H, m, $\boldsymbol{H}_G$), 1.77-1.65 (2H, m, $\boldsymbol{H}_L$), 1.57-1.34 (8H, m, $\boldsymbol{H}_H$, $\boldsymbol{H}_I$, $\boldsymbol{H}_J$, $\boldsymbol{H}_K$); $\boldsymbol{\delta}_C$ ($CDCl_3$, 101 MHz) 162.4, 160.1, 157.2, 157.1, 156.7, 156.5, 137.4, 136.8, 134.7, 132.0, 129.8, 128.5, 122.7, 119.6, 119.4, 118.6, 115.2, 114.6, 68.2, 68.1, 37.5, 34.5, 31.2, 28.9, 28.2, 28.2, 28.0, 25.2, 25.0; HR-ESI-MS $[M+H]^+$ m/z 493.2860 (calc. for $C_{33}H_{37}N_2O_2$ m/z 493.2850).

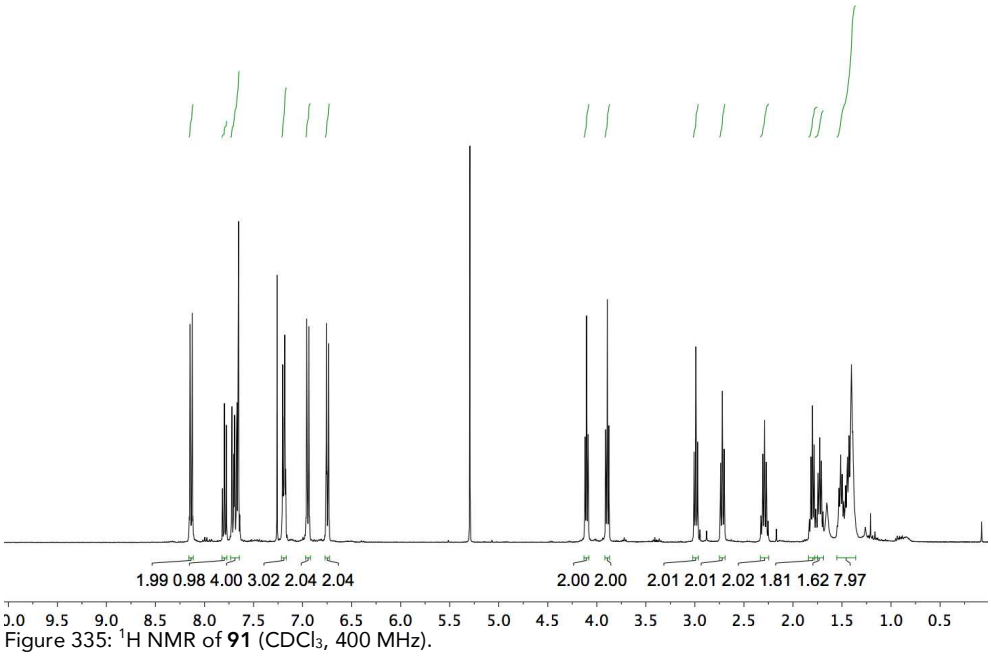

Figure 335: ^1H NMR of **91** ($CDCl_3$, 400 MHz).

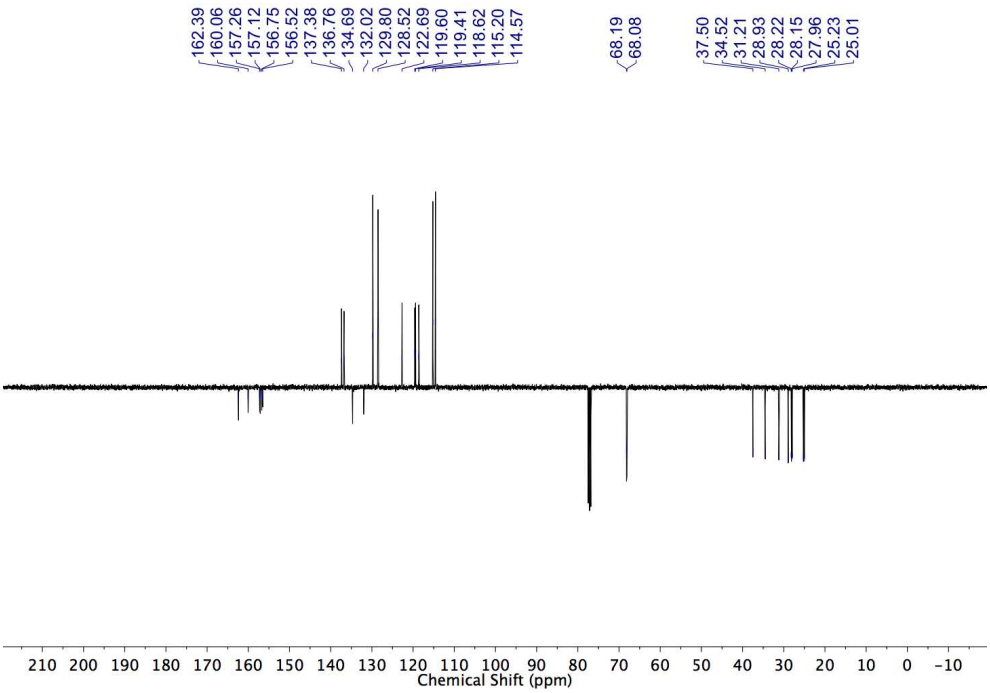

Figure 336: JMOD NMR of **91** ($CDCl_3$, 101 MHz).

Rotaxane (R^*,R_{mp}^*)-**92**

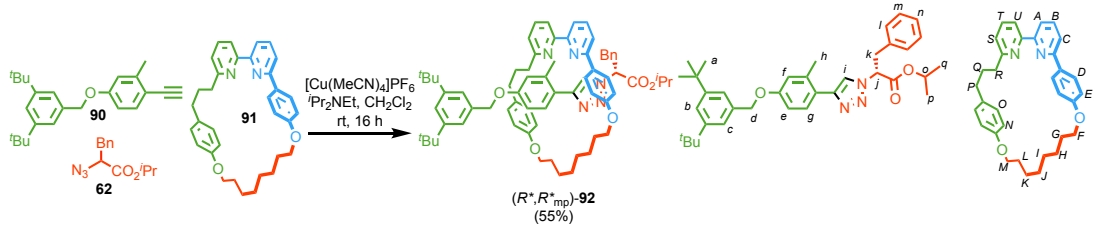

A dry CEM MW vial was charged with **90** (40.8 mg, 0.122 mmol, 2.0 eq.), **62** (28.3 mg, 0.122 mmol, 2.0 eq.), **91** (30 mg, 0.061 mmol, 1.0 eq.) and $[Cu(MeCN)_4]PF_6$ (21.8 mg, 0.059 mmol, 0.96 eq.). Anhydrous CH_2Cl_2 (0.8 mL) and $^iPr_2NEt$ (42.6 µL, 31.6 mg, 0.24 mmol, 4.0 eq.) were added and the solution stirred at rt for 16 h. Formic acid (23.0 µL, 0.61 mmol, 10.0 eq.) was added and the reaction stirred at rt for a further 16 h. Sat. EDTA-NH_3 solution (8 mL) was added, and the aqueous layer was extracted with CH_2Cl_2 (2 x 10 mL), and the combined organic extracts were dried over $MgSO_4$, filtered, and had the solvent removed *in vacuo*. The residue was purified by column chromatography (CH_2Cl_2-MeOH 0→10%) to yield a racemic mixture of rotaxanes (S,S_{mp})/(R,R_{mp})-**92** as a beige foam (42.0 mg, 0.397 mmol, 65%). δ_H ($CDCl_3$, 400 MHz) 8.15 (1H, s, H_j), 7.77-7.70 (3H, m, H_B, H_C, H_T), 7.52-7.45 (3H, m, H_A, H_U, H_g), 7.42 (2H, d, J = 8.7, H_D), 7.30 (1H, t, J = 1.6, H_b), 7.25 (1H, d, J = 7.4, H_S), 7.23-7.19 (3H, m, H_m, H_n), 7.02-6.97 (4H, m, H_c, H_l), 6.90 (1H, d, J = 2.6, H_f), 6.73 (2H, d, J = 8.4, H_O), 6.68 (1H, dd, J = 8.6, 2.6, H_e), 6.54 (2H, d, J = 8.6, H_E), 6.42 (2H, d, J = 8.4, H_N), 5.13-5.07 (1H, m, H_j), 4.99-4.90 (2H, H_d, H_o), 4.16 (1H, d, J = 10.7, $H_{d'}$), 4.03 (2H, dd, J = 6.8, 6.6, H_F), 3.90-3.83 (1H, m, H_M), 3.81-3.75 (1H, m, $H_{M'}$), 3.45 (1H, dd, J = 13.6, 6.9, H_k), 3.36 (1H, dd, J = 13.6, 8.5, $H_{k'}$), 2.90-2.76 (2H, m, H_R), 2.75-2.65 (1H, m, H_P), 2.59-2.51 (1H, m, $H_{P'}$), 2.18 (3H, s, H_h), 2.10-1.93 (2H, m, H_Q), 1.82-1.67 (4H, m, H_G, H_L), 1.51-1.37 (8H, m, H_H, H_I, H_J, H_K), 1.30 (18H, s, H_a), 1.18 (3H, d, J = 6.3, H_p), 1.03 (3H, d, J = 6.3, H_q). δ_C ($CDCl_3$, 101 MHz) 168.1, 163.2, 159.2, 158.7, 158.5, 158.4, 158.3, 157.2, 150.3, 147.2, 136.8, 136.8, 136.8, 136.3, 135.4, 132.5, 131.8, 129.6, 129.3, 129.2, 128.7, 128.5, 127.4, 122.9, 122.0, 122.0, 121.8, 121.5, 120.4, 120.2, 119.4, 117.4, 114.9, 114.6, 112.9, 70.3, 70.0, 67.8, 67.2, 64.0, 38.8, 37.9, 35.2, 34.9, 32.0, 31.7, 31.6, 29.3, 28.7, 28.7, 28.7, 25.9, 21.7, 21.6, 21.4. LR-ESI-MS (+ve) $[M+H]^+$ m/z 1060.6.

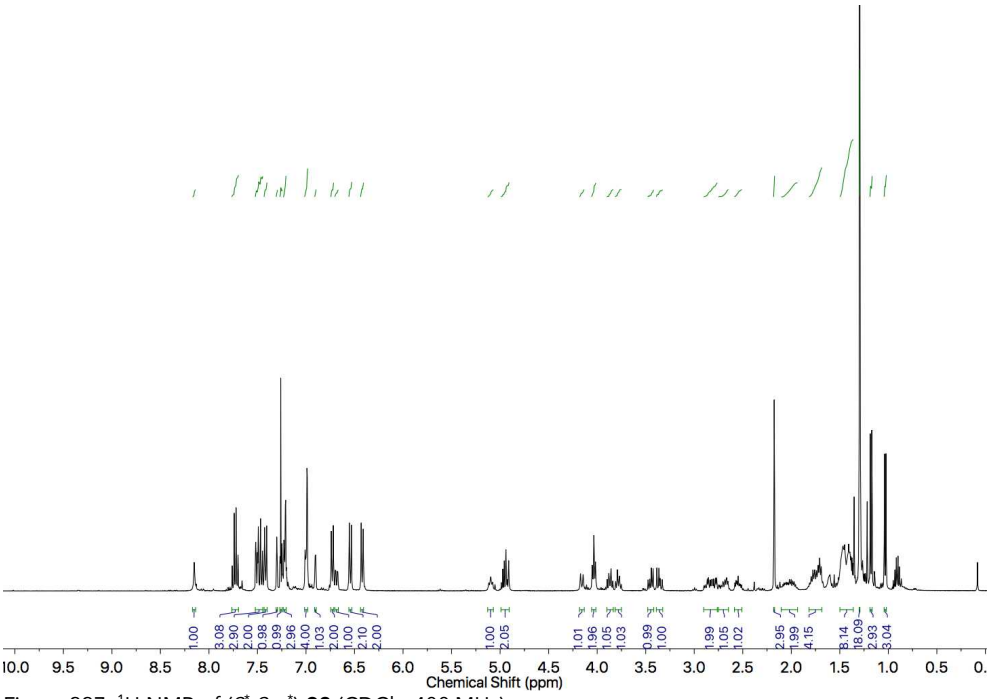

Figure 337: ^{1}H NMR of (S^{*},S_{mp}^{*})-**92** ($CDCl_3$, 400 MHz).

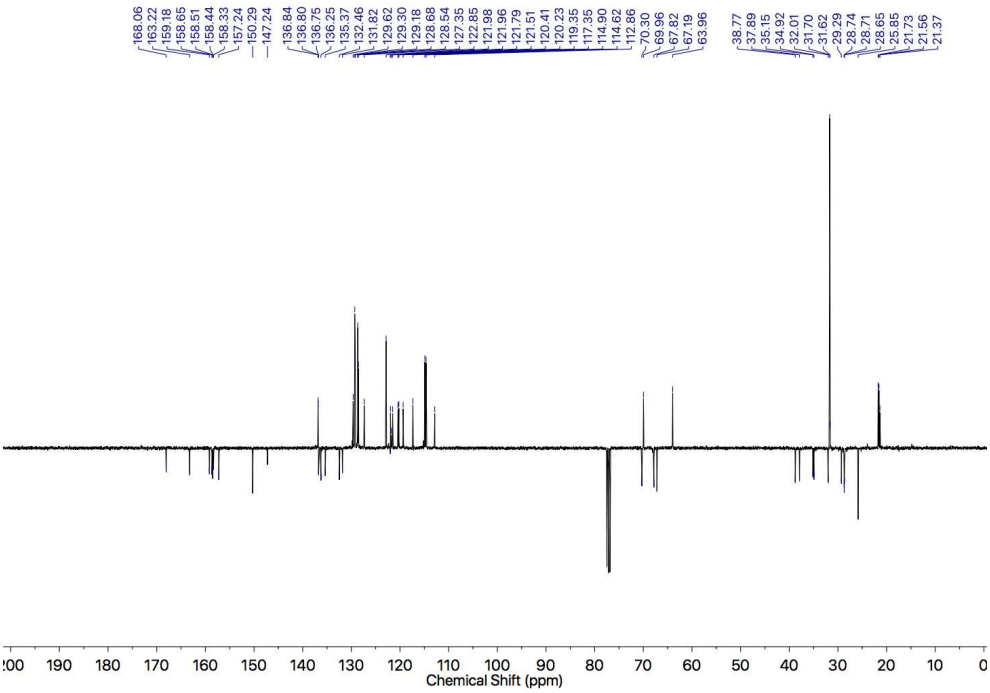

Figure 338: JMOD NMR of (S^{*},S_{mp}^{*})-**92** ($CDCl_3$, 101 MHz).

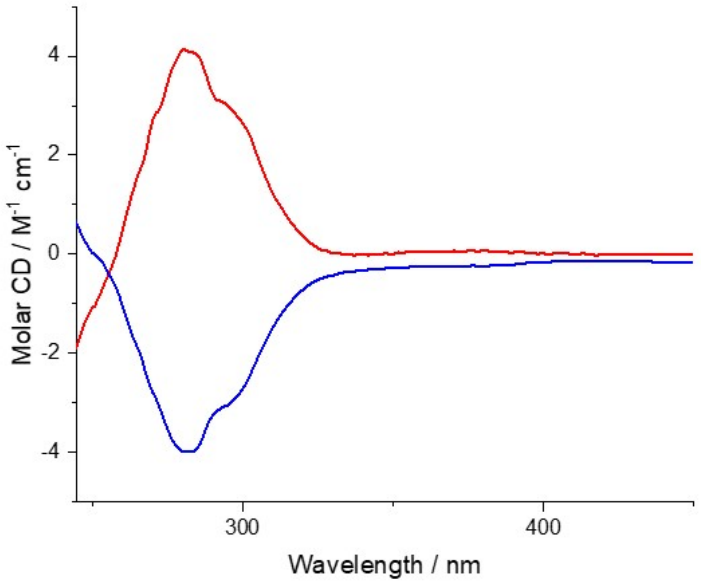

Figure 339: Circular Dichroism Spectra of (S,S_{mp})-**92** (blue 28 μM) and (R,R_{mp})-**92** (red, 26 μM) at 293 K in $CHCl_3$.

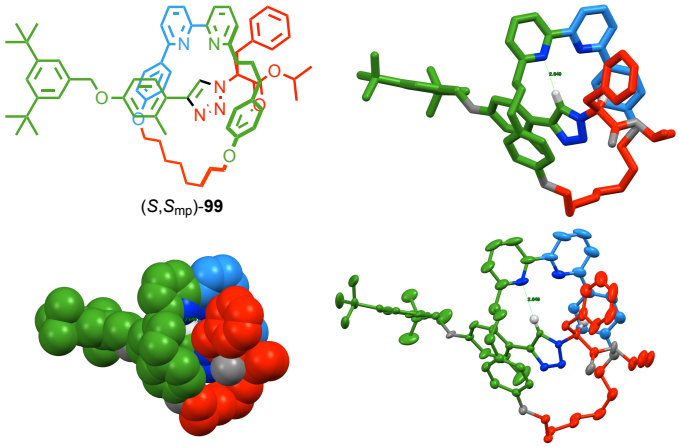

Figure 340: Single crystal X-ray structure of a racemic mixture of (S,S_{mp})-**92** and (R,R_{mp})-**92** [$C_{69}H_{81}N_5O_5$]. Solvent molecules omitted for clarity.

Single crystals of (S^*,S_{mp}^*)-**92** were grown by slow evaporation of *n*-pentane-CH_2Cl_2. Data was collected at 100 K using a Rigaku 007 HF diffractometer equipped with a Saturn724+ enhanced sensitivity detector. Cell determination, data collection, data reduction, cell refinement and absorption correction were performed with CrysalisPro. Using Olex2 the structure was solved with the SHELXT program using charge flipping, and refined with the SHELXL refinement package. H atoms were placed in calculated positions and refined using a riding model.

Figure 341: Capped stick and ellipsoid representation of single crystal X-ray structure of (S^*,S_{mp}^*)-**92** [$C_{69}H_{81}N_5O_5$]. Solvent molecules omitted for clarity.

Figure 342: Space-fill representation of Single crystal X-ray structure of a racemic mixture of (S^*,S_{mp}^*)-**92** [$C_{69}H_{81}N_5O_5$]. Solvent molecules omitted for clarity.

Figure 343: Capped stick and ellipsoid representation of single crystal X-ray structure of (S^*,S_{mp}^*)-**92** [$C_{69}H_{81}N_5O_5$]. Solvent molecules omitted for clarity

Identification code	(S^*,S_{mp}^*)-**92**	ρ_{calc}g/cm^3	1.147
Empirical formula	$C_{69}H_{81}N_5O_5$	μ/mm^{-1}	0.071
Formula weight	1059.6	F(000)	1182.0
Temperature / K	100	Crystal size/mm^3	0.08 × 0.05 × 0.05
Crystal system	triclinic	Radiation	Mo K**α** (**λ** = 0.71073)
Space group	P-1	2**Θ** range for data collection/°	3.328 to 52.848
a/Å	12.9612(5)	Index ranges	-16 ≤ h ≤ 16, -18 ≤ k ≤ 18, -22 ≤ l ≤ 22
b/Å	14.8800(6)	Reflections collected	18924
c/Å	18.2493(6)	Independent reflections	18924 [R_{int} = ?, R_{sigma} = 0.0527]
α/°	107.539(3)	Data/restraints/parameters	18924/54/759
β/°	101.014(3)	Goodness-of-fit on F^2	1.024
γ/°	101.388(4)	Final R indexes [I>=2**σ** (I)]	R_1 = 0.0923, wR_2 = 0.2265
Volume/Å^3	3169.5(2)	Final R indexes [all data]	R_1 = 0.1266, wR_2 = 0.2447
Z	2	Largest diff. peak/hole / e Å^{-3}	0.65/-0.34

Compound **102**

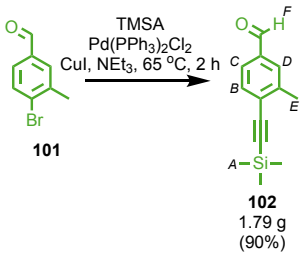

A CEM MW vial was charged with $PdCl_2(PPh_3)_2$ (320 mg, 0.456 mmol, 0.05 eq.), CuI (174 mg, 0.913 mmol, 0.10 eq.) and **101** (1.82 g, 9.13 mmol, 1.0 eq.) and purged with N_2. TMSA (3.8 mL, 2.69 g, 27.4 mmol, 3.0 eq.) in degassed NEt_3 (17 mL). The solution was stirred at 65 °C for 2 h. After 2 h the reaction was cooled to room temperature, concentrated *in vacuo*, washed with brine (50 mL) and extracted in CH_2Cl_2 (3 x 50 mL). The combined organic layers were dried over $MgSO_4$ and concentrated *in vacuo*. The residue was purified by column chromatography (SiO_2, petrol-Et_2O 0→10%) yielding a white solid **102** (1.79 g, 8.27 mmol, 90%). δ_H ($CDCl_3$, 400 MHz) 9.96 (1H, s, H_F), 7.70 (1H, br. s, H_D), 7.63 (1H, d, J = 7.3, H_C), 7.56 (1H, d, J = 7.3, H_B), 2.50 (3H, s, H_E), 0.27 (9H, s, H_A). δ_C ($CDCl_3$, 101 MHz) 191.9, 141.6, 135.7, 132.8, 130.4, 129.3, 127.0, 103.2, 103.0, 20.7, 0.0. HR-APPI-MS [$M^{+\cdot}$] m/z 216.0958 (calc. for $C_{13}H_{16}OSi$ m/z 216.0965). Melting Point 89-91 °C.

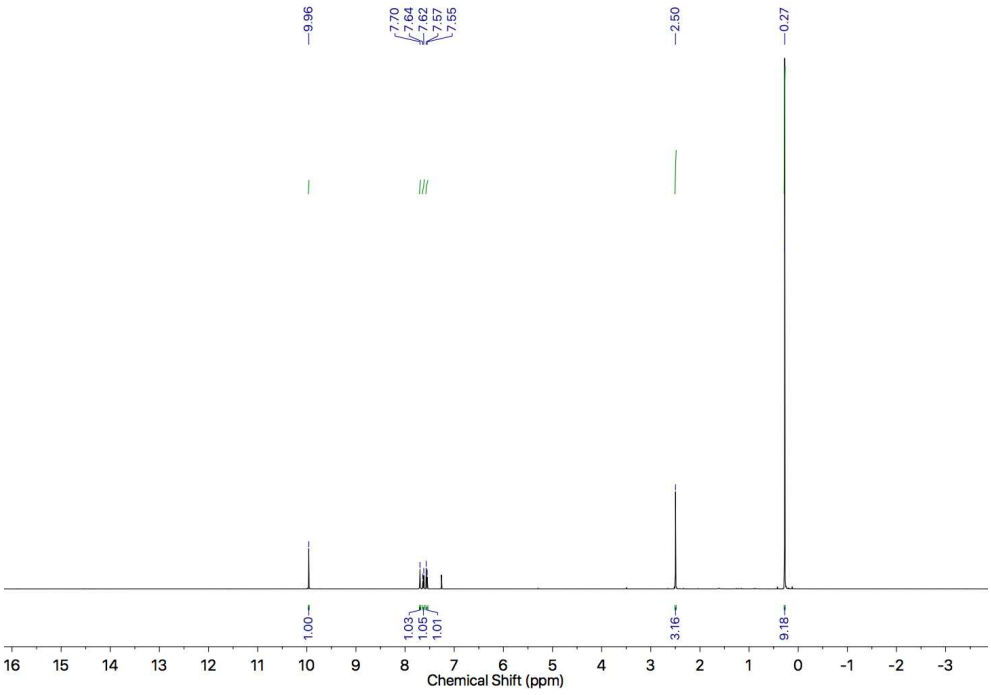

Figure 344: ^1H NMR of **102** ($CDCl_3$, 400 MHz).

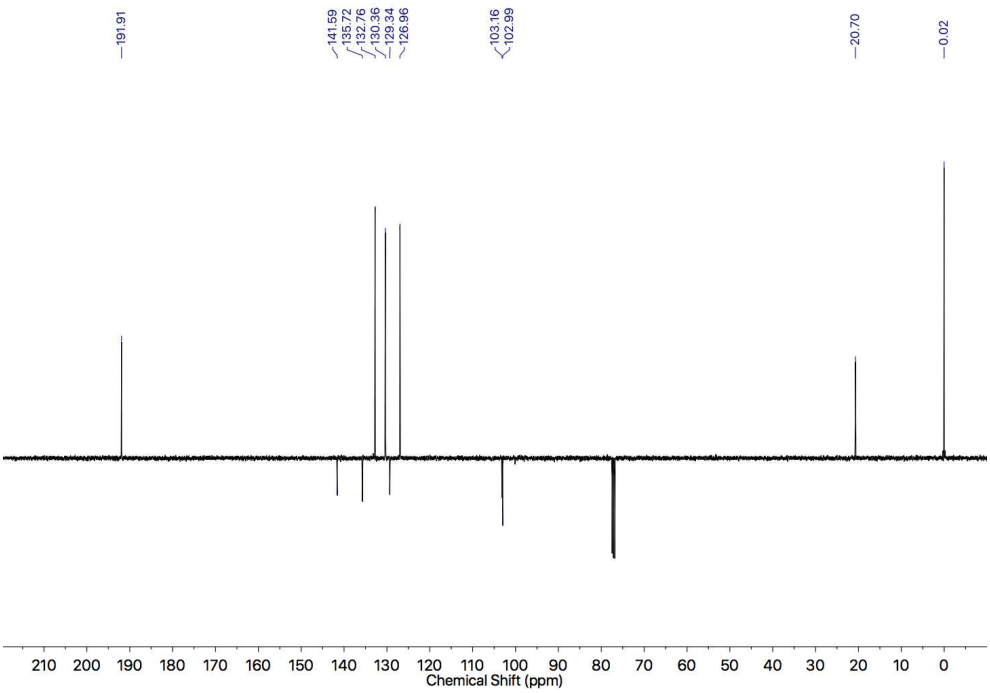

Figure 345: JMOD NMR of **102** ($CDCl_3$, 101 MHz).

Compound **103**

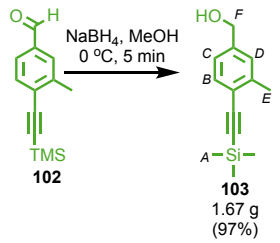

102 (1.71 g, 7.90 mmol, 1.0 eq.) was dissolved in MeOH (15 mL) at 0 °C. $NaBH_4$ (450 mg, 11.9 mmol, 1.5 eq.) was added and the solution stirred for 5 minutes. After 5 minutes, the reaction was quenched with HCl (20 mL, 1 M) and extracted in CH_2Cl_2 (3 x 20 mL), the combined organic layers were dried over $MgSO_4$ and concentrated *in vacuo* yielding a white solid **103** (1.67 g, 7.65 mmol, 97%). δ_H ($CDCl_3$, 400 MHz) 7.42 (1H, d, *J* = 7.8, H_B), 7.20 (1H, br. s, H_D), 7.11 (1H, d, *J* = 7.8, H_C), 4.64 (2H, d, *J* = 5.9, H_F), 2.43 (3H, s, H_E), 1.80-1.60 (1H, br. s, O*H*), 0.26 (9H, s, H_A). δ_C ($CDCl_3$, 101 MHz) 141.3, 141.1, 132.4, 128.0, 124.1, 122.3, 104.0, 98.4, 65.2, 20.8, 0.21. HR-APPI-MS [$M^{+\cdot}$] m/z 218.1114 (calc. for $C_{13}H_{18}OSi$ m/z 218.1122). Melting Point 48-50 °C.

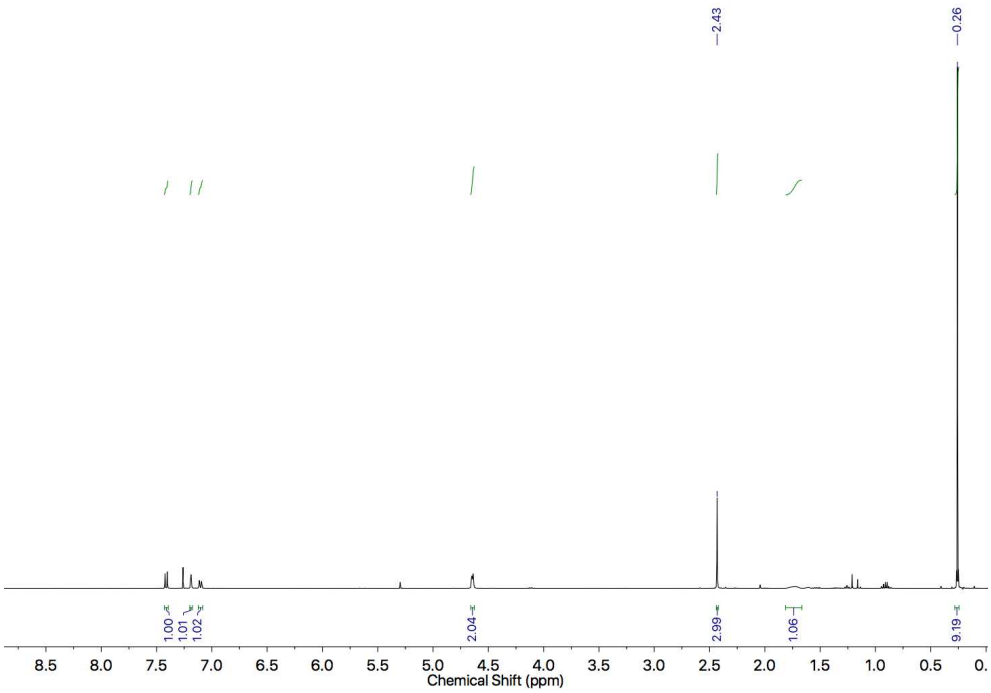

Figure 346: ^{1}H NMR of **103** ($CDCl_3$, 400 MHz).

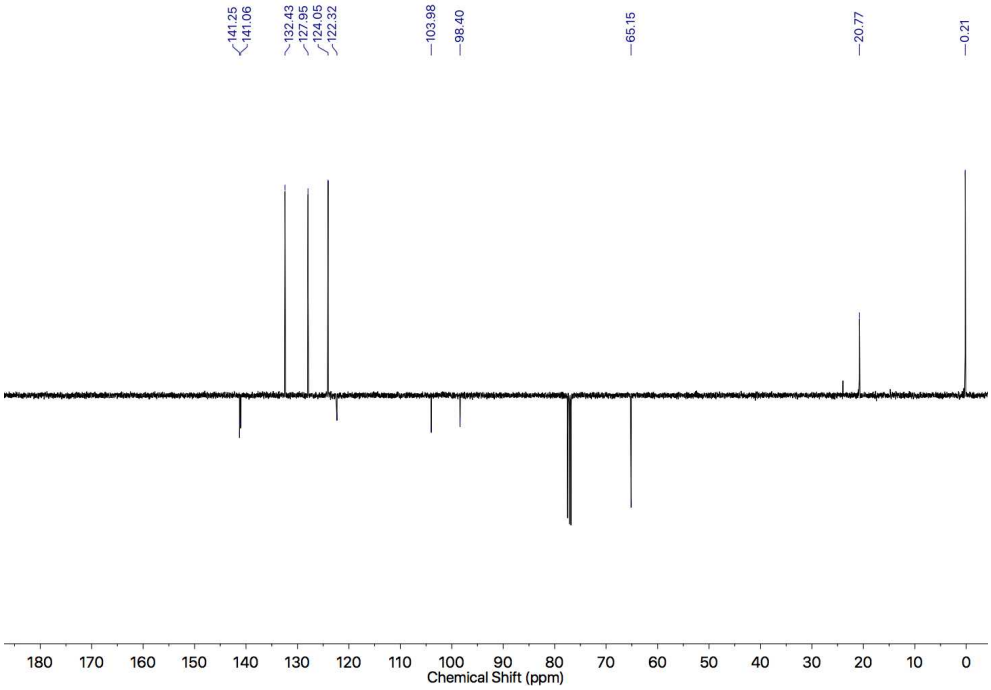

Figure 347: JMOD NMR of **103** ($CDCl_3$, 101 MHz).

Compound **105**[62]

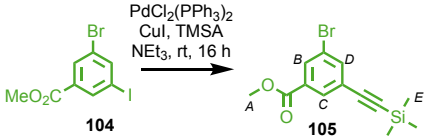

A dry 250 mL round bottom flask was charged with **104** (10.0 g, 29.3 mmol, 1.0 eq.), $PdCl_2(PPh_3)_2$ (412 mg, 0.587 mmol, 0.02 eq.) and CuI (223 mg, 1.17 mmol, 0.04 eq.) and purged with N_2. Anhydrous NEt_3 (70 mL) and trimethylsilylacetylene (3.82 mL, 3.03 g, 30.8 mmol, 1.05 eq.) were added, and the solution stirred at room temperature for 1 h. After 1 h, the reaction was concentrated *in vacuo*, diluted in CH_2Cl_2, washed with brine (2 x 50 mL) and extracted in CH_2Cl_2 (3 x 50 mL). The combined organic layers were dried over $MgSO_4$ and concentrated *in vacuo*. The residue was purified by column chromatography (SiO_2, petrol-EtOAc 0→5%) yielding a white solid **105** (4.98 g, 16.0 mmol, 57%). δ_H ($CDCl_3$, 400 MHz) 8.10 (1H, dd, *J* = 1.9, 1.5, H_B), 8.04 (1H, dd, *J* = 1.5, 1.5, H_C), 7.77 (1H, dd, *J* = 1.9, 1.5, H_D), 3.92 (3H, s, H_A), 0.25 (9H, s, H_E). δ_C ($CDCl_3$, 101 MHz) 165.2, 138.7, 132.6, 132.1, 131.8, 125.6, 122.2, 102.3, 97.3, 52.7, -0.1. HR-APPI-MS $[M]^{+\cdot}$ m/z 311.0100 (calc. for $C_{13}H_{16}O_2BrSi$ m/z 311.0097). Melting Point 58-59 °C.[62]

Compound **106**[62]

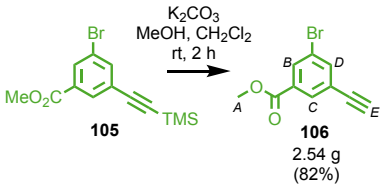

105 (4.00 g, 12.9 mmol, 1.0 eq.) was stirred over K_2CO_3 (5.00 g, 36.2 mmol, 2.8 eq.) in CH_2Cl_2 (7 mL) and MeOH (7 mL) for 16 h. After 16 h, the reaction was washed with water (20 mL) and extracted in CH_2Cl_2 (3 x 20 mL). The combined organic layers were dried over $MgSO_4$ and concentrated *in vacuo*. The residue was purified by column chromatography (SiO_2, petrol-EtOAc 0→10%) yielding a white solid **106** (2.54 g, 10.6 mmol, 82%). δ_H ($CDCl_3$, 400 MHz) 8.13 (1H, dd, *J* = 1.7, 1.7, H_B), 8.06 (1H, dd, *J* = 1.5, 1.5, H_C), 7.78 (1H, dd, *J* = 1.7, 1.7, H_D), 3.92 (3H, s, H_A), 3.17 (1H, s, H_E). δ_C ($CDCl_3$, 101 MHz) 165.1, 138.9, 133.0, 132.2, 131.9, 124.5, 122.3, 81.2, 79.7, 52.7. HR-APPI-MS $[M]^{+\cdot}$ m/z 238.9701 (calc. for $C_{10}H_8O_2Br$ m/z 238.9702). Melting Point 56-57 °C.[62]

Compound **107**[63]

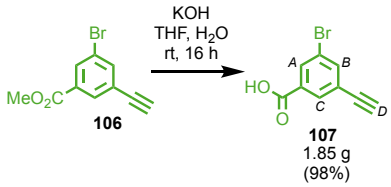

106 (2.00 g, 8.37 mmol, 1.0 eq.) and KOH (4.70 g, 83.7 mmol, 10.0 eq.) were stirred in THF (20 mL) and water (20 mL) at room temperature for 16 h. The reaction was washed with HCl (2 M, 100 mL) and extracted in EtOAc (3 x 50 mL). The combined organic layers were dried over $MgSO_4$ and concentrated *in vacuo* yielding an off-white solid **107** (1.85 g, 8.22 mmol, 98%). $\boldsymbol{\delta}_H$ (d^6-acetone, 400 MHz) 8.15 (1H, app. t, *J* = 1.7, $\boldsymbol{H}_A$), 8.08 (1H, app. t, *J* = 1.7, $\boldsymbol{H}_C$), 7.90 (1H, app. t, *J* = 1.7, $\boldsymbol{H}_B$), 3.90 (1H, s, $\boldsymbol{H}_D$). $\boldsymbol{\delta}_C$ (d^6-acetone, 101 MHz) 165.5, 139.2, 134.0, 133.6, 132.6, 125.7, 122.9, 81.9, 81.7. HR-APPI-MS $[M-H]^-$ m/z 222.9405, 224.9388 (calc. for $C_9H_4O_2Br$ m/z 222.9400). Melting Point 207-209 °C.[63]

Compound **136**

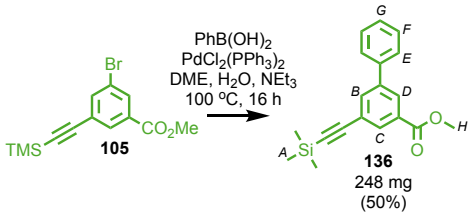

105 (500 mg, 1.61 mmol, 1.0 eq.), $PhB(OH)_2$ (215 mg, 1.77 mmol, 1.1 eq) and $PdCl_2(PPh_3)_2$ (56 mg, 0.080 mmol, 0.05 eq.) were heated at 100 °C for 16 h in DME (3.2 mL), water (3.2 mL) with NEt_3 (0.45 mL, 3.21 mmol, 2.0 eq.). After 16 h, the reaction was quenched with sat. NH_4Cl (20 mL) and extracted in CH_2Cl_2 (3 x 20 mL). The combined organic layers were dried over $MgSO_4$, concentrated *in vacuo*, and the residue purified by column chromatography (SiO_2, petrol-EtOAc 0→5%) yielding a colourless oil **136** (248 mg, 0.804 mmol, 50%). $\boldsymbol{\delta}_H$ ($CDCl_3$, 400 MHz) 8.21 (1H, app. t, *J* = 1.7, $\boldsymbol{H}_D$), 8.11 (1H, app. t, *J* = 1.5, $\boldsymbol{H}_C$), 7.87 (1H, app. t, *J* = 1.7, $\boldsymbol{H}_B$), 7.63-7.60 (2H, m, $\boldsymbol{H}_E$), 7.48-7.44 (2H, m, $\boldsymbol{H}_F$), 7.39 (1H, tt, *J* = 7.4, 1.3, $\boldsymbol{H}_G$), 3.95 (3H, s, $\boldsymbol{H}_H$), 0.27 (9H, s, $\boldsymbol{H}_A$). $\boldsymbol{\delta}_C$ ($CDCl_3$, 101 MHz) 166.5, 141.8, 139.4, 134.8, 131.9, 131.0, 129.1, 128.3, 128.2, 127.3, 124.2, 104.0, 95.6, 52.5, 0.05. HR-ESI-MS $[M+Na]^+$ m/z 331.1126 (calc. for $C_{19}H_{20}O_2SiNa$ m/z 331.1125).

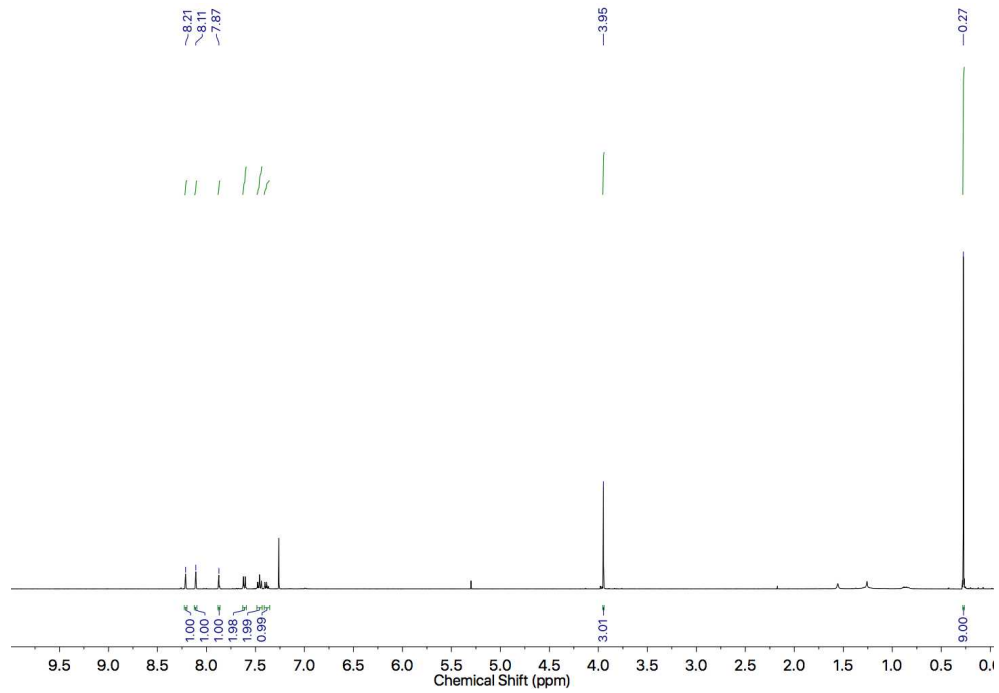

Figure 348: ^{1}H NMR of **136** ($CDCl_3$, 400 MHz).

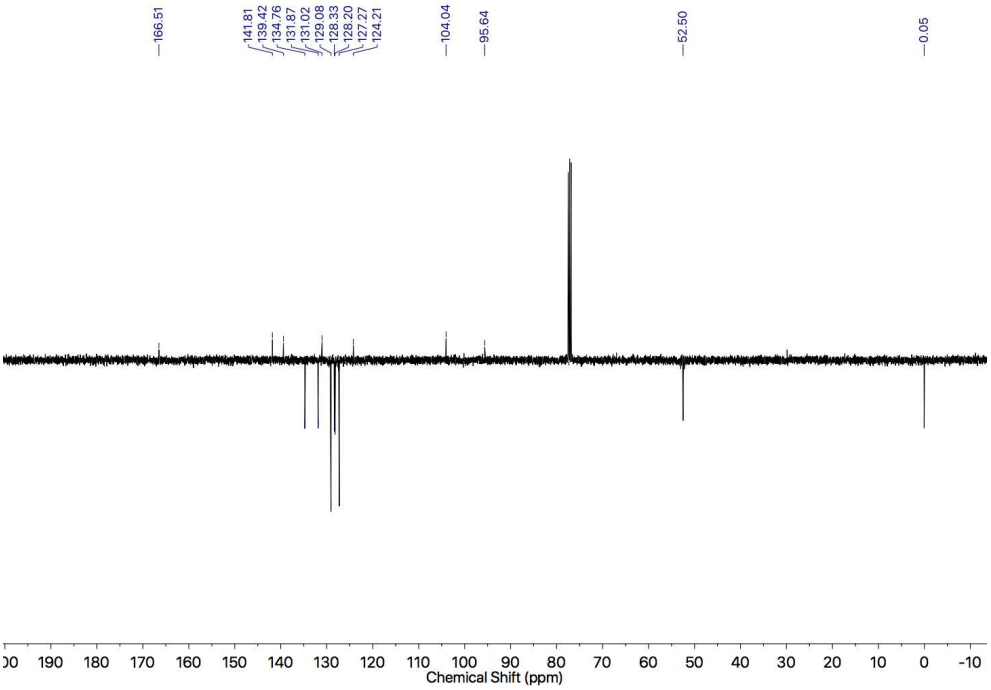

Figure 349: JMOD NMR of **136** ($CDCl_3$, 101 MHz).

Compound **137**

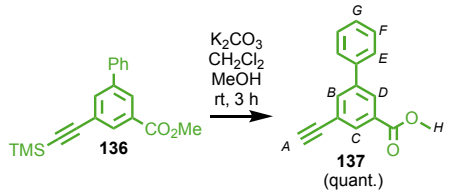

136 (248 mg, 0.804 mmol, 1.0 eq.) was stirred over K_2CO_3 (333 mg, 2.41 mmol, 3.0 eq.) in CH_2Cl_2 (2 mL) and MeOH (2 mL) for 3 h. The solution was washed with brine (20 mL), extracted in CH_2Cl_2 (3 x 15 mL). The combined organic layers were dried over $MgSO_4$, concentrated *in vacuo*, and the residue purified by column chromatography (SiO_2, petrol-EtOAc 0→10%) yielding a white solid **137** (190 mg, 0.804 mmol, quantitative). δ_H ($CDCl_3$, 400 MHz) 8.25 (1H, app. t, J = 1.7, $\boldsymbol{H}_D$), 8.14 (1H, app. t, J = 1.5, $\boldsymbol{H}_C$), 7.90 (1H, app. t, J = 1.7, $\boldsymbol{H}_B$), 7.63-7.59 (2H, m, $\boldsymbol{H}_E$), 7.49-7.44 (2H, m, $\boldsymbol{H}_F$), 7.40 (1H, tt, J = 7.3, 1.3, $\boldsymbol{H}_G$), 3.95 (3H, s, $\boldsymbol{H}_H$), 3.15 (1H, s, $\boldsymbol{H}_A$). δ_C ($CDCl_3$, 101 MHz) 166.4, 141.9, 139.3, 134.9, 132.0, 131.1, 129.1, 128.7, 128.3, 127.3, 123.2, 82.7, 78.3, 52.5. HR-ESI-MS $[M+H]^+$ m/z 237.0992 (calc. for $C_{16}H_{13}O_2$ m/z 237.0916). Melting Point 89-90 °C.

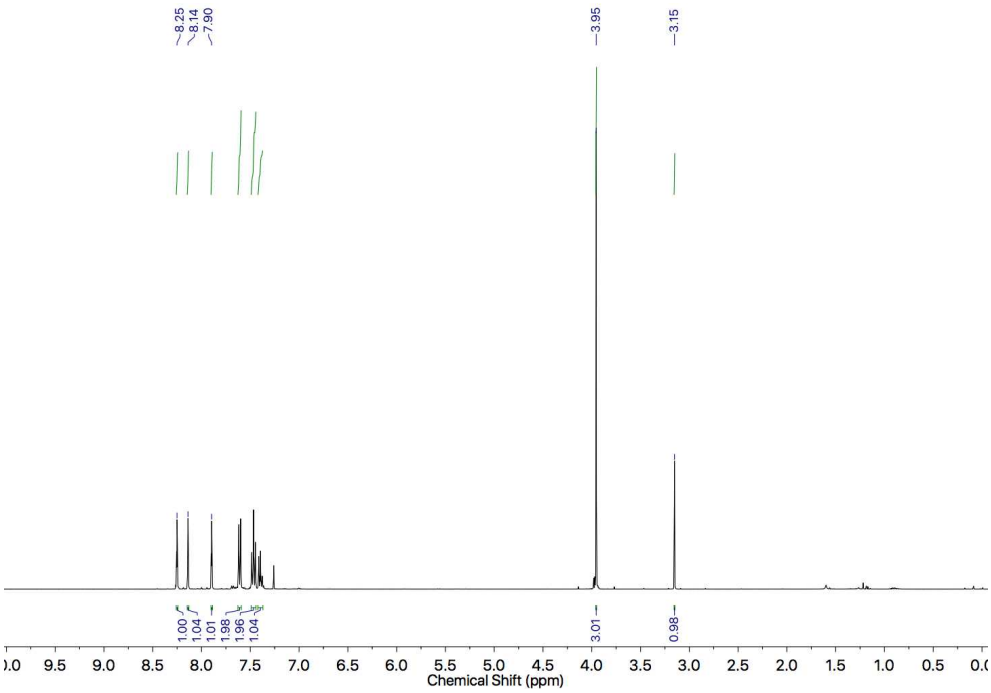

Figure 350: ^{1}H NMR of **137** ($CDCl_3$, 400 MHz).

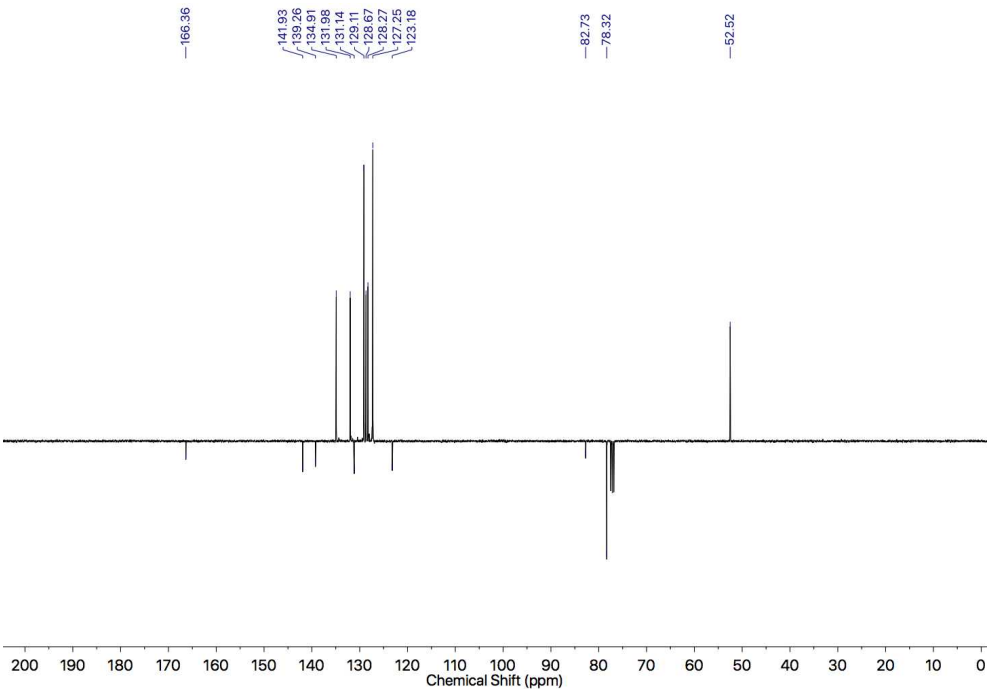

Figure 351: JMOD NMR of **137** ($CDCl_3$, 101 MHz).

Compound **115**

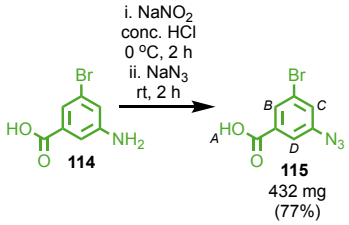

114 (500 mg, 2.31 mmol, 1.0 eq.) was dissolved in conc. HCl (11.7 M, 5.3 mL) and cooled to 0 °C. $NaNO_2$ (192 mg, 2.78 mmol, 1.2 eq.) was added slowly and the solution stirred at 0 °C for 2 h. After 2 h, NaN_3 (451 mg, 6.94 mmol, 3.0 eq.) was added portionwise and the solution was stirred for 2 h at 0 °C. The crude reaction mixture was diluted in brine (30 mL) and extracted in EtOAc (3 x 30 mL). The combined organic layers were dried over $MgSO_4$, and concentrated *in vacuo*. The residue was purified by column chromatography (SiO_2, pet-EtOH 9:1) yielding a white solid **115** (432 mg, 1.78 mmol, 77%). δ_H (CD_3OD, 400 MHz) 7.87 (1H, dd, *J* = 1.7, 1.3, $\boldsymbol{H}_B$), 7.59 (1H, dd, *J* = 2.2, 1.3, $\boldsymbol{H}_D$), 7.41 (1H, dd, *J* = 2.2, 1.8, $\boldsymbol{H}_C$). δ_C (CD_3OD, 101 MHz) 167.2, 143.6, 135.5, 129.8, 127.0, 124.1, 119.9. HR-APPI-MS $[M\text{-}H]^-$ m/z 239.9414, 241.9394 (calc. for $C_7H_3N_3O_2Br$ m/z 239.9414). Decomposes 157-159 °C.

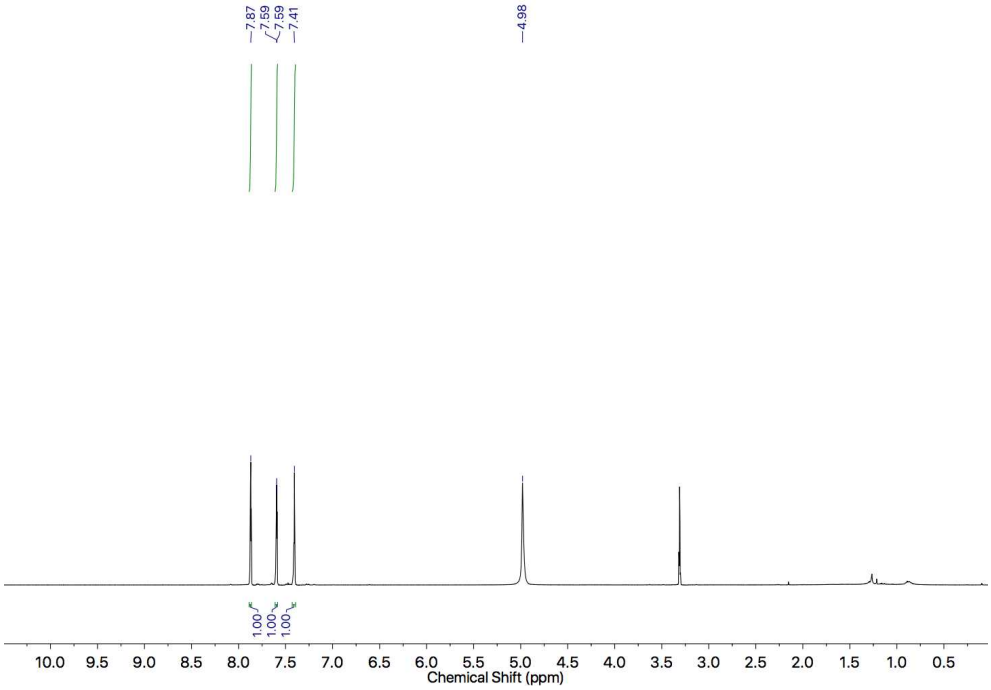

Figure 352: ^{1}H NMR of **115** (CD_3OD, 400 MHz).

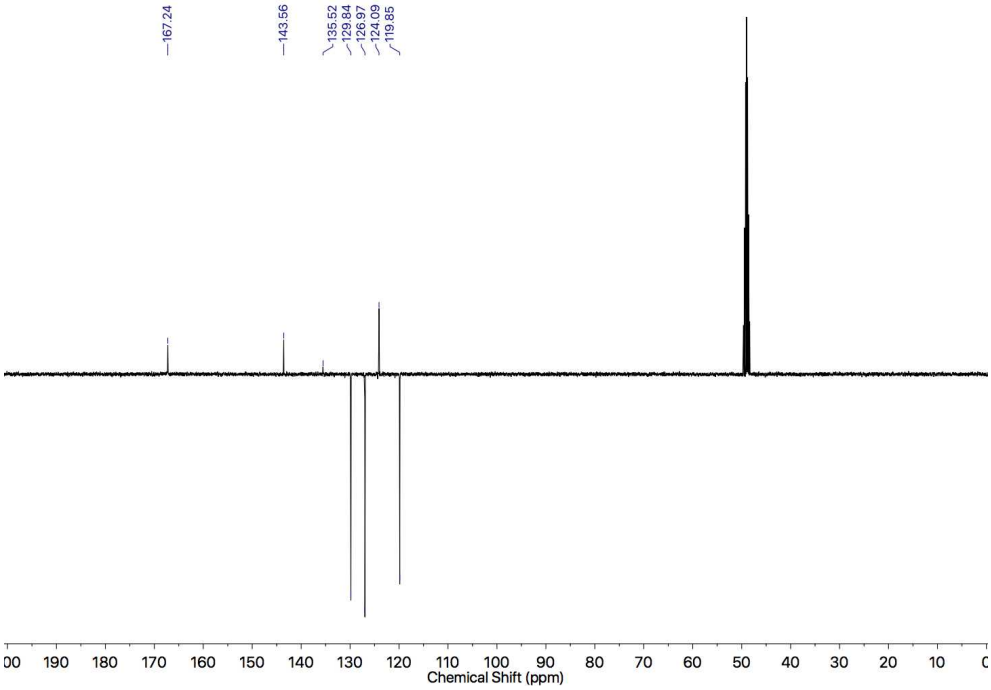

Figure 353: JMOD NMR of **115** (CD_3OD, 101 MHz).

Compound **138**[68]

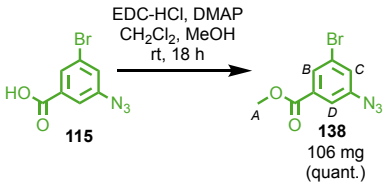

A dry flask was charged with **115** (100 mg, 0.413 mmol, 1.0 eq.), EDC-HCl (158 mg, 0.826 mmol, 2.0 eq.) and DMAP (10.1 mg, 0.0826 mmol, 0.2 eq.), then purged with N_2. Anhydrous CH_2Cl_2 (3 mL) and anhydrous MeOH (3 mL) were added at 0 °C, then the reaction was stirred at room temperature for 18 h. The crude reaction mixture was concentrated *in vacuo*, diluted in CH_2Cl_2 (30 mL), and washed with HCl (1 M, 30 mL) and brine (30 mL) before being extracted in CH_2Cl_2 (3 x 25 mL). The combined organic layers were dried over $MgSO_4$, and concentrated *in vacuo*. The residue was purified by column chromatography (SiO_2, pet-EtOAc 0→10%) yielding a white solid **138** (106 mg, 0.413 mmol, quantitative). δ_H ($CDCl_3$, 400 MHz) 7.92 (1H, app. t, J = 1.6, H_B), 7.62 (1H, dd, J = 2.1, 1.3, H_D), 7.33 (1H, app. t, J = 2.0, H_C), 3.93 (3H, s, H_A). δ_C ($CDCl_3$, 101 MHz) 165.0, 142.1, 133.3, 129.1, 126.3, 123.4, 118.9, 52.8. LR-ESI-MS $[M+H-N_2]^+$ m/z 228.9733 (calc. for $C_8H_8BrNO_2$ m/z 228.9733). Melting Point 48-50 °C.[68]

Compound **139**

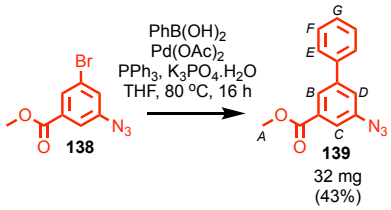

A dry CEM MW vial was charged with **138** (75 mg, 0.293 mmol, 1.0 eq.), $PhB(OH)_2$ (107 mg, 0.879 mmol, 3.0 eq.), $K_3PO_4.H_2O$ (202 mg, 0.879 mmol, 3.0 eq.), $Pd(OAc)_2$ (3.3 mg, 0.0146 mmol, 0.05 eq.) and PPh_3 (7.7 mg, 0.0293 mmol, 0.10 eq.), then purged with N_2. The mixture was dissolved in anhydrous THF (11.7 mL) and stirred at 80 °C for 16 h. The reaction was cooled to rt, concentrated *in vacuo*, washed with brine (15 mL), and extracted in CH_2Cl_2 (3 x 20 mL). The combined organic layers were dried over $MgSO_4$, then concentrated *in vacuo*. The residue was purified by column chromatography (SiO_2, petrol-EtOAc 0→10%) yielding a yellow oil **139** (32 mg, 0.126 mmol, 43%). δ_H ($CDCl_3$, 400 MHz) 8.05 (1H, app. t, J = 1.5, H_B), 7.69 (1H, dd, J = 2.2, 1.4, H_C), 7.61-7.58 (2H, m, H_E), 7.49-7.44 (2H, m, H_F), 7.43-7.40 (1H, m, H_G), 7.39 (1H, dd, J = 2.2, 1.7, H_D), 3.96 (3H,

s, H_A). δ_C ($CDCl_3$, 101 MHz) 166.3, 143.4, 141.2, 139.3, 132.4, 129.1, 128.4, 127.3, 125.0, 122.0, 118.7, 52.6. HR-ESI-MS $[M-N_2+H]^+$ m/z 227.0940 (calc. for $C_{14}H_{13}NO_2$ m/z 227.0941).

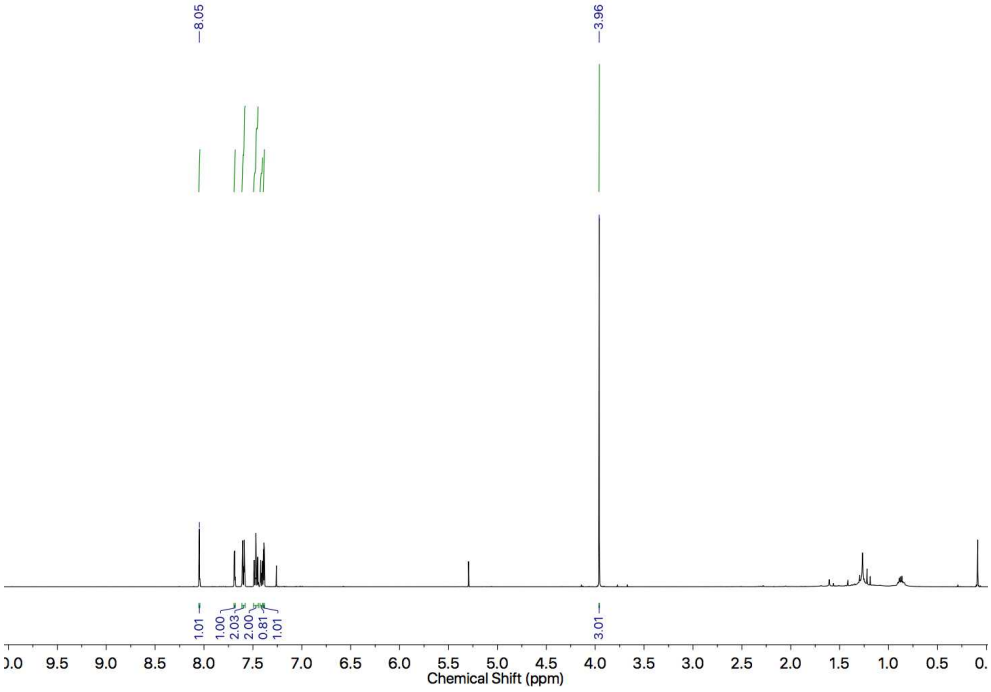

Figure 354: ^1H NMR of **139** ($CDCl_3$, 400 MHz).

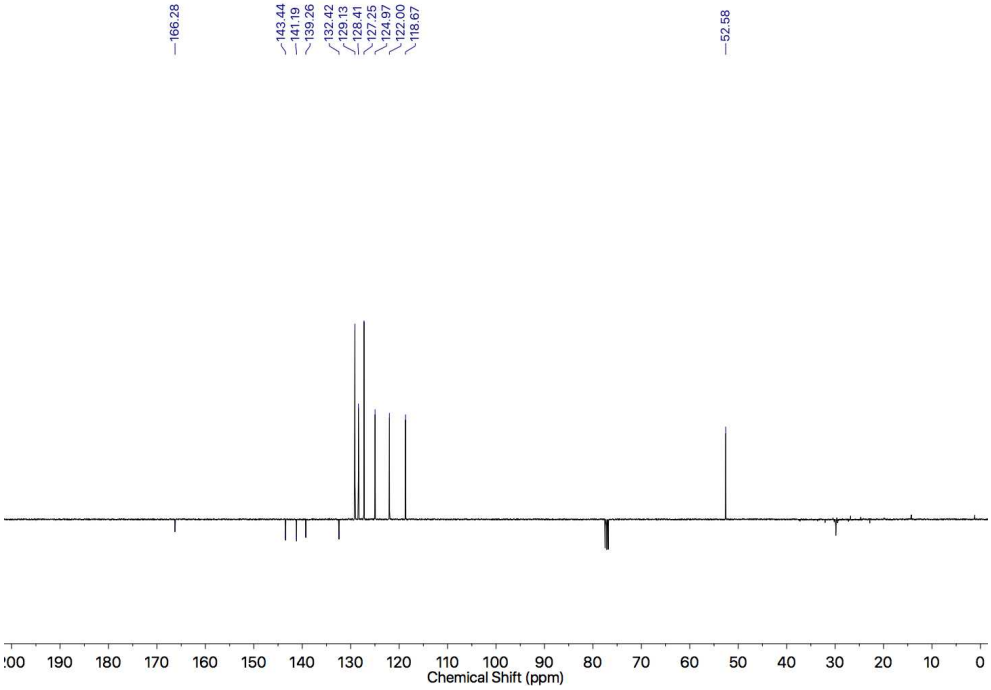

Figure 355: JMOD NMR of **139** ($CDCl_3$, 101 MHz).

Compound **108**

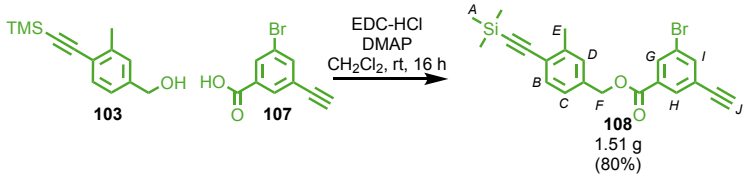

107 (1.00 g, 4.44 mmol, 1.0 eq.), **103** (970 mg, 4.44 mmol, 1.0 eq.), EDC-HCl (937 mg, 4.89 mmol, 1.1 eq.) and DMAP (109 mg, 0.89 mmol, 0.2 eq.) were dissolved in CH_2Cl_2 (44 mL) at 0 °C and stirred at room temperature for 16 h. The solution was washed with HCl (1 M, 2 x 50 mL) and extracted in CH_2Cl_2 (3 x 50 mL). The combined organic layers were dried over $MgSO_4$ and concentrated *in vacuo*. The residue was purified by column chromatography (SiO_2, petrol-EtOAc 0→5%) yielding a yellow oil **108** (1.51 g, 3.56 mmol, 80%). $\boldsymbol{\delta}_H$ ($CDCl_3$, 400 MHz) 8.15 (1H, app. t, J = 1.7, $\boldsymbol{H}_G$), 8.08 (1H, app. t, J = 1.5, $\boldsymbol{H}_H$), 7.79 (1H, app. t, J = 1.7, $\boldsymbol{H}_I$), 7.45, (1H, d, J =7.9, $\boldsymbol{H}_B$), 7.24 (1H, br. s, $\boldsymbol{H}_D$), 7.19 (1H, br. d, J = 7.9, $\boldsymbol{H}_C$), 5.30 (2H, s, $\boldsymbol{H}_F$), 3.17 (1H, s, $\boldsymbol{H}_J$), 2.45 (3H, s, $\boldsymbol{H}_E$), 0.26 (9H, s, $\boldsymbol{H}_A$). $\boldsymbol{\delta}_C$ ($CDCl_3$, 101 MHz) 164.4, 141.2, 139.1, 135.6, 133.1, 132.5, 132.1, 132.0, 129.5, 125.6, 124.5, 123.4, 122.4, 103.6, 99.2, 81.2, 79.8, 67.2, 20.8, 0.17. HR-ESI-MS $[M+H]^+$ m/z 447.0389, 449.0372 (calc. for $C_{22}H_{21}BrNaO_2Si$ m/z 447.0386).

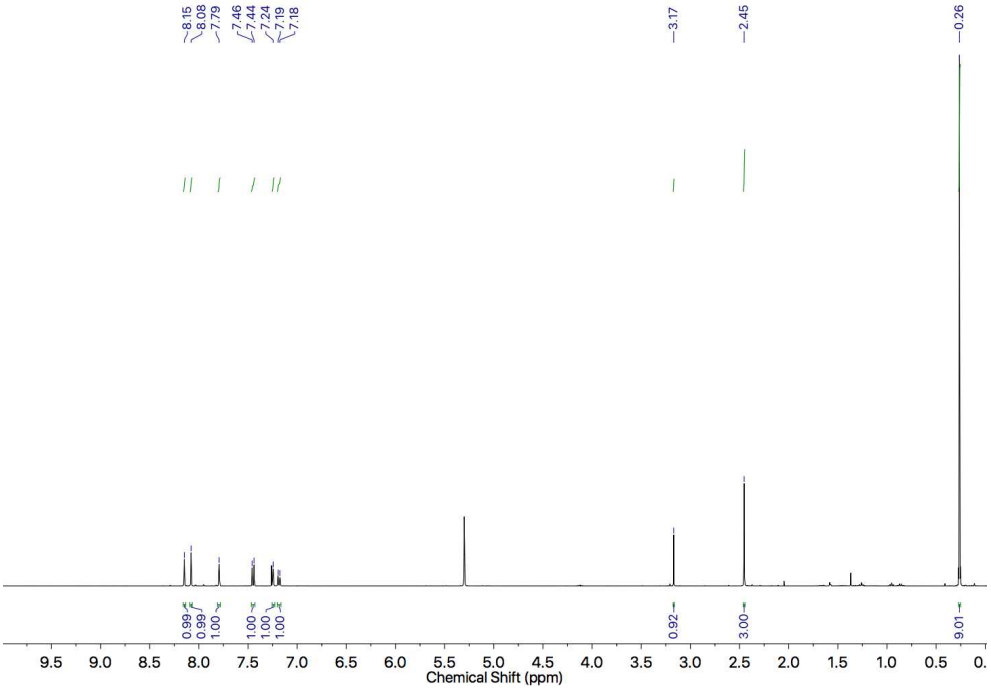

Figure 356: ^{1}H NMR of **108** ($CDCl_3$, 400 MHz).

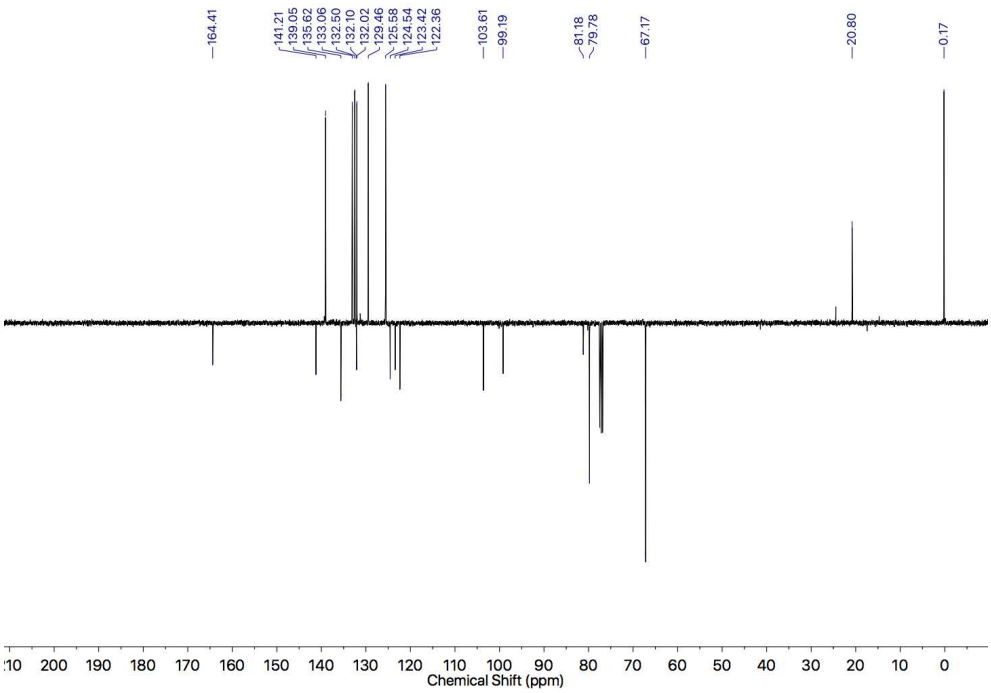

Figure 357: JMOD NMR of **108** ($CDCl_3$, 101 MHz).

Compound **116**

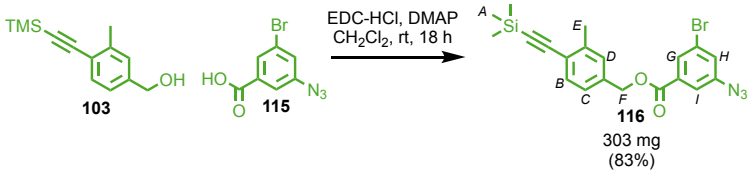

A dry flask was charged with **115** (200 mg, 0.826 mmol, 1.0 eq.), EDC-HCl (317 mg, 1.65 mmol, 2.0 eq.), **103** (217 mg, 0.992 mmol, 1.2 eq.) and DMAP (20.1 mg, 0.165 mmol, 0.2 eq.), then purged with N_2. Anhydrous CH_2Cl_2 (8.3 mL) was added at 0 °C, then the reaction was stirred at room temperature for 18 h. The crude reaction mixture was concentrated *in vacuo*, diluted in CH_2Cl_2 (30 mL), and washed with HCl (1 M, 30 mL) and brine (30 mL) before being extracted in CH_2Cl_2 (3 x 25 mL). The combined organic layers were dried over $MgSO_4$, and concentrated *in vacuo*. The residue was purified by column chromatography (SiO_2, pet-EtOAc 0→10%) yielding a yellow oil **116** (303 mg, 0.683 mmol, 83%). δ_H ($CDCl_3$, 400 MHz) 7.93 (1H, dd, *J* = 1.7, 1.4, H_G), 7,64 (1H, dd, *J* = 2.2, 1.4, H_I), 7.45 (1H, d, *J* = 7.8, H_B), 7.34 (1H, app. t, *J* = 1.5, H_H), 7.24 (1H, br. s, H_D), 7.18 (1H, br. d, *J* = 7.9, H_C), 5.30 (2H, s, H_F), 2.45 (3H, s, H_E), 0.26 (9H, s, H_A). δ_C ($CDCl_3$, 101 MHz) 164.4, 142.2, 141.2, 135.6, 133.3, 132.5, 129.5, 129.1, 126.5, 125.6, 123.5, 123.4, 119.1, 103.6, 99.2, 67.2, 20.8, 0.2. HR-ESI-MS $[M+Na]^+$ m/z 464.0401, 466.0384 (calc. for $C_{20}H_{20}BrN_3NaO_2Si$ m/z 464.0400).

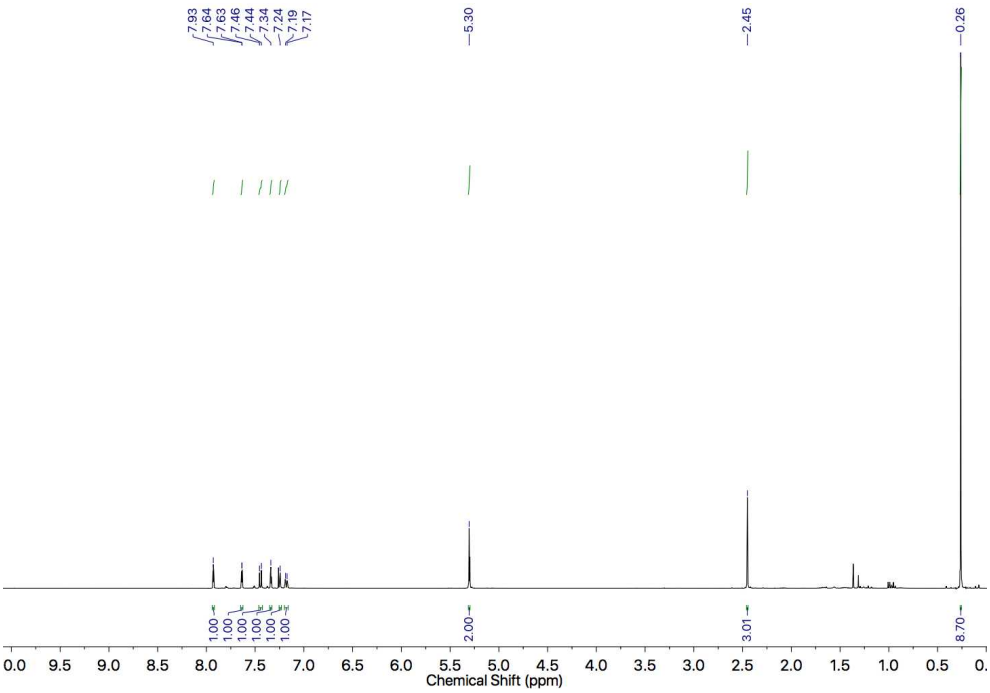

Figure 358: ^{1}H NMR of **116** ($CDCl_3$, 400 MHz).

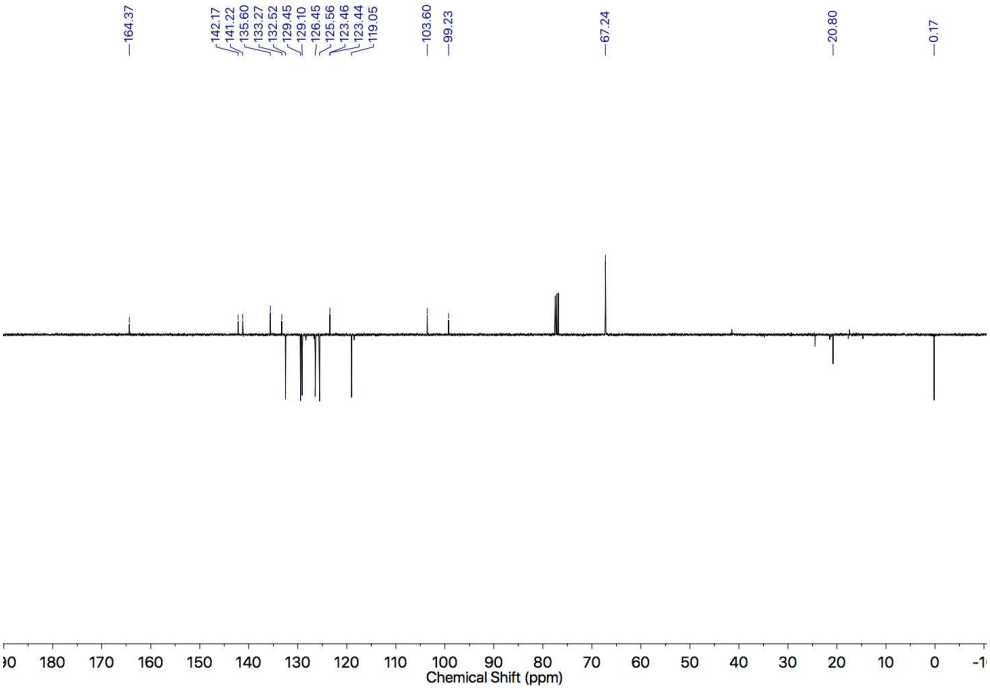

Figure 359: JMOD NMR of **116** ($CDCl_3$, 101 MHz).

Compound **140**

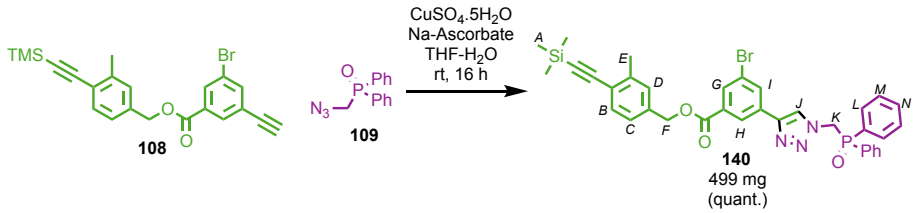

108 (311 mg, 0.732 mmol, 1.0 eq.) and **109** (188 mg, 0.732 mmol, 1.0 eq.) were stirred with $CuSO_4.5H_2O$ (18.2 mg, 0.073 mmol, 0.10 eq.) and sodium ascorbate (21.7 mg, 0.110 mmol, 0.15 eq.) at room temperature in THF (3.6 mL) and water (3.6 mL) for 16 h. The reaction was concentrated *in vacuo*, diluted in CH_2Cl_2, washed with brine (20 mL) and extracted in CH_2Cl_2 (3 x 20 mL). The combined organic layers were dried over $MgSO_4$ and concentrated *in vacuo*. The residue was purified by column chromatography (SiO_2, petrol-EtOAc 0→60%) yielding a white foam **140** (499 mg, 0.732 mmol, quantitative). $\boldsymbol{\delta}_H$ ($CDCl_3$, 400 MHz) 8.32-8.30 (2H, m, $\boldsymbol{H}_J$, $\boldsymbol{H}_H$), 8.19 (1H, app. t, J = 1.7, $\boldsymbol{H}_I$), 8.10 (1H, app. t, J = 1.7, $\boldsymbol{H}_G$), 7.76 (4H, br. ddd, J = 12.1, 7.0, 1.4, $\boldsymbol{H}_L$), 7.58 (2H, ttd, J = 7.5, 2.8, 1.4, $\boldsymbol{H}_N$), 7.50 (4H, app. td, J = 7.4, 3.2, $\boldsymbol{H}_M$), 7.44 (1H, d, J = 7.9, $\boldsymbol{H}_B$), 7.25 (1H, br. s, $\boldsymbol{H}_D$), 7.20 (1H, dd, J = 7.9, 1.3, $\boldsymbol{H}_C$), 5.30 (2H, s, $\boldsymbol{H}_F$), 5.30 (2H, d, J = 8.0, $\boldsymbol{H}_K$), 2.45 (3H, s, $\boldsymbol{H}_E$), 0.25 (9H, s, $\boldsymbol{H}_A$). $\boldsymbol{\delta}_C$ ($CDCl_3$, 101 MHz) 164.9, 146.1, 141.2, 135.8, 133.3 (d, J_{CP} = 2.7), 132.5, 131.3 (d, J_{CP} = 9.8), 133.0, 132.5 (d, J_{CP} = 12.8), 132.5, 132.2, 129.6, 129.3 (d, J_{CP} = 12.4), 128.2, 125.7, 125.5, 123.3, 123.1, 121.9, 103.7, 99.0, 67.0, 50.4 (d, J_{CP} = 69.8), 20.8, 0.16. $\boldsymbol{\delta}_P$ ($CDCl_3$, 202 MHz) 27.1. HR-ESI-MS $[M+H]^+$ m/z 682.1279 (calc. for $C_{35}H_{34}BrN_3O_3PSi$ m/z 682.1285), $[M+Na]^+$ m/z 704.1094 (calc. for $C_{35}H_{33}BrN_3O_3PSiNa$ m/z 704.1104).

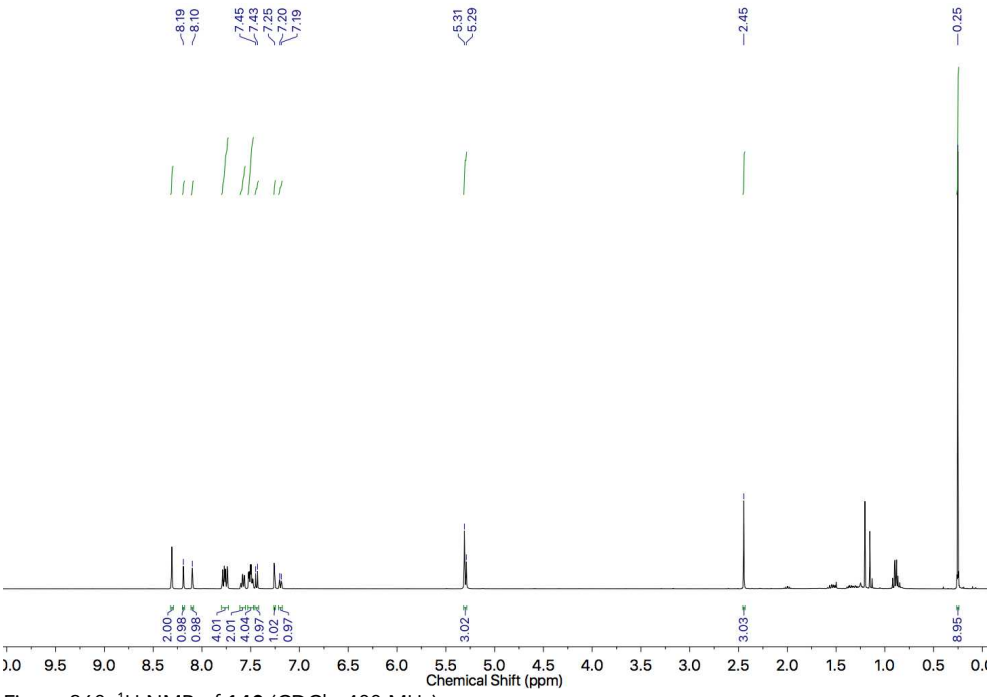

Figure 360: ^{1}H NMR of **140** ($CDCl_3$, 400 MHz).

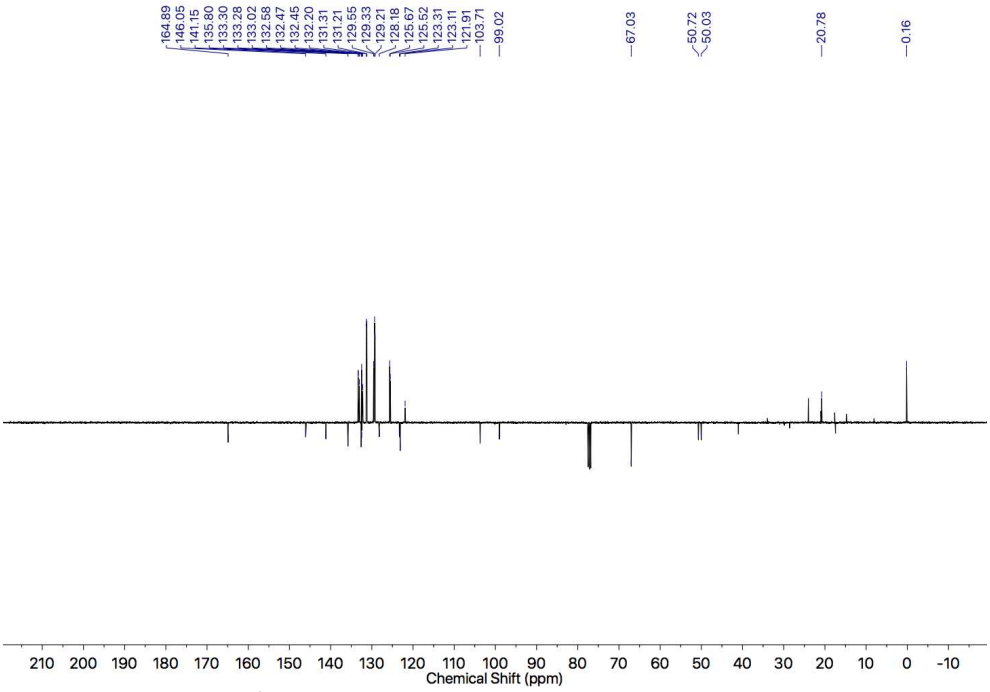

Figure 361: JMOD NMR of **140** ($CDCl_3$, 101 MHz).

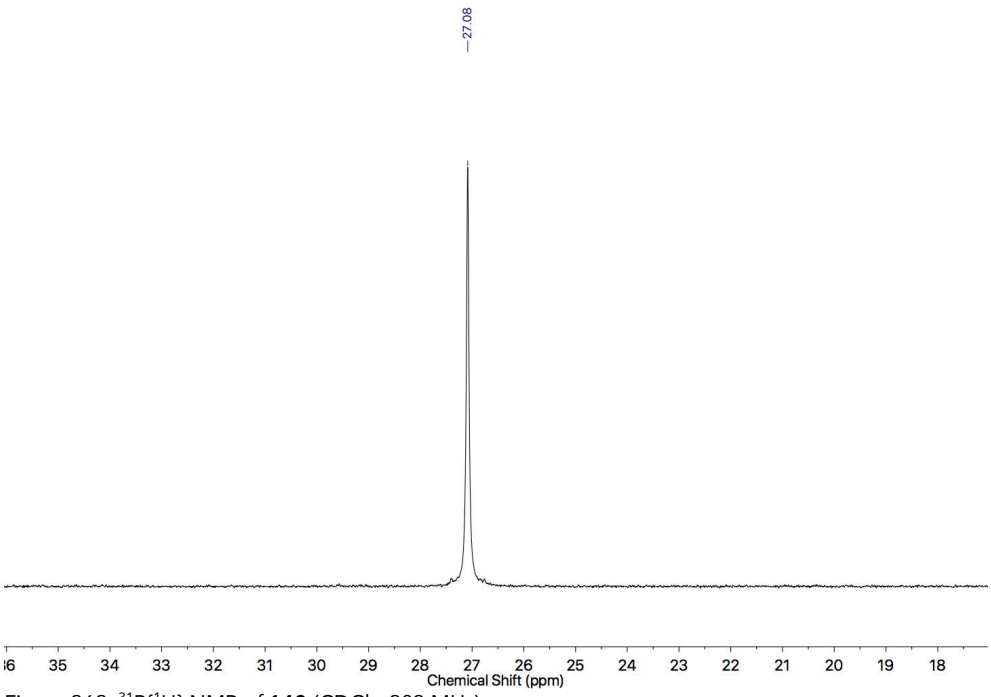

Figure 362: $^{31}P\{^{1}H\}$ NMR of **140** ($CDCl_3$, 202 MHz).

Compound **110**

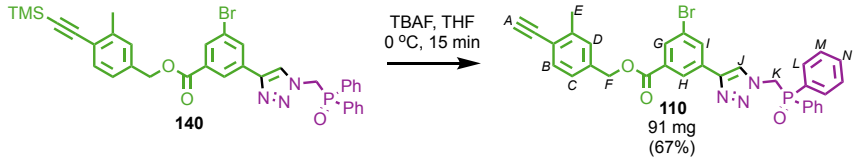

140 (314 mg, 0.460 mmol, 1.0 eq.) was dissolved in THF (4.6 mL) and cooled to 0 °C. TBAF (1 M in THF, 1.4 mL, 1.4 mmol, 3.0 eq.) was added and the solution stirred for 15 minutes. The reaction was washed with brine (3 x 20 mL) and extracted in Et_2O (3 x 20 mL). The combined organic layers were dried over $MgSO_4$ and concentrated *in vacuo*. The residue was purified by column chromatography (SiO_2, petrol-EtOAc 50→60%) yielding a white foam **110** (238 mg, 0.390 mmol, 85%). δ_H ($CDCl_3$, 400 MHz) 8.32 (1H, app. t, J = 1.5, $\boldsymbol{H}_H$), 8.30 (1H, br. s, $\boldsymbol{H}_J$), 8.20 (1H, app. t, J = 1.7, $\boldsymbol{H}_I$), 8.11 (1H, dd, J = 1.9, 1.5, $\boldsymbol{H}_G$), 7.79-7.73 (4H, m, $\boldsymbol{H}_L$), 7.62-7.56 (2H, m, $\boldsymbol{H}_N$), 7.53-7.46 (5H, m, $\boldsymbol{H}_M$, $\boldsymbol{H}_B$), 7.28 (1H, br. s, $\boldsymbol{H}_D$), 7.23 (1H, br. d, J = 8.0, $\boldsymbol{H}_C$), 5.32 (2H, s, $\boldsymbol{H}_F$), 5.28 (2H, d, J = 6.8, $\boldsymbol{H}_K$), 3.30 (1H, s, $\boldsymbol{H}_A$), 2.47 (3H, s, $\boldsymbol{H}_E$). δ_C ($CDCl_3$, 101 MHz) 164.9, 146.1, 141.3, 136.2, 133.3 (d, J_{CP} = 2.9), 133.1, 132.9, 132.5 (d, J_{CP} = 16.9), 132.2, 131.3 (d, J_{CP} = 9.6), 129.7, 129.3, 129.3 (d, J_{CP} = 12.3), 128.3, 125.8, 125.5, 123.1, 122.3, 121.9, 82.3, 81.6, 67.0, 50.4 (d, J_{CP} = 70.0), 20.8. δ_P ($CDCl_3$, 202 MHz) 26.8. HR-ESI-MS $[M+H]^+$ m/z 610.0891 (calc. for $C_{32}H_{26}BrN_3O_3P$ m/z 610.0890).

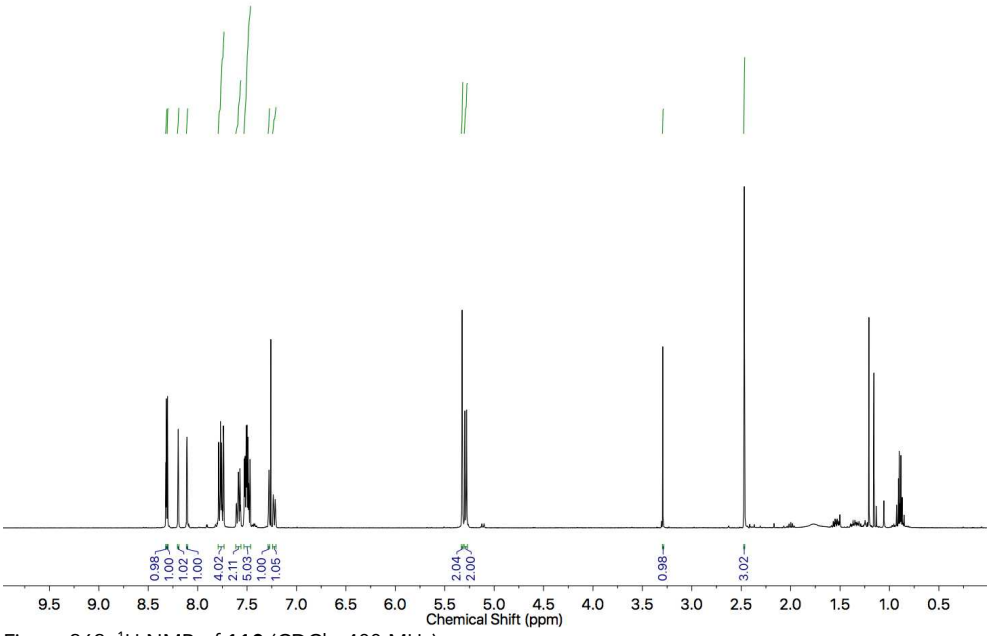

Figure 363: ^{1}H NMR of **110** ($CDCl_3$, 400 MHz).

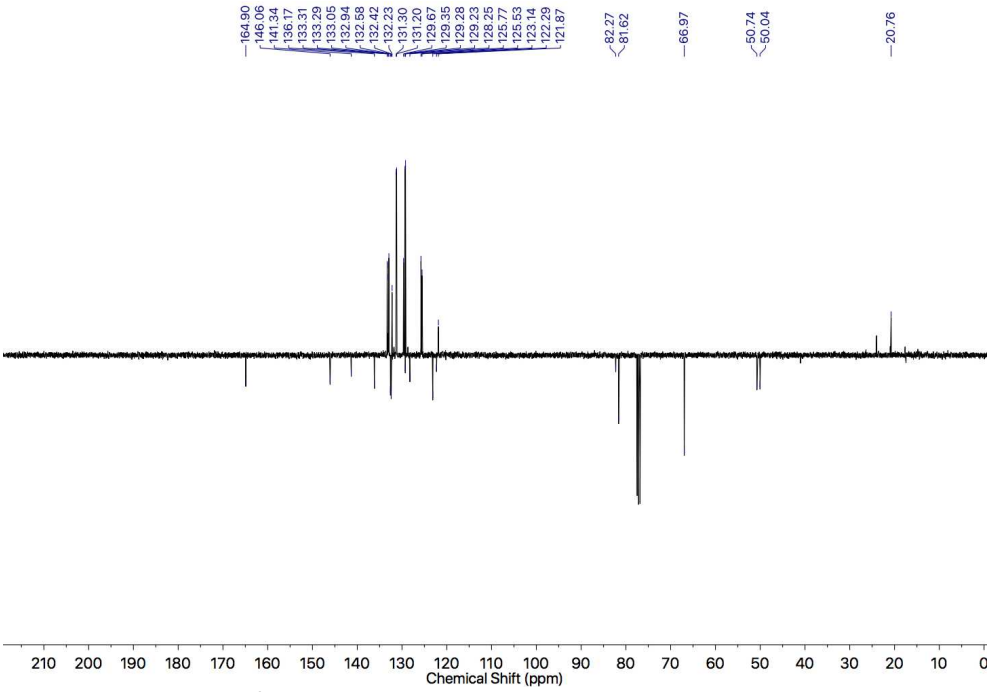

Figure 364: JMOD NMR of **110** ($CDCl_3$, 101 MHz).

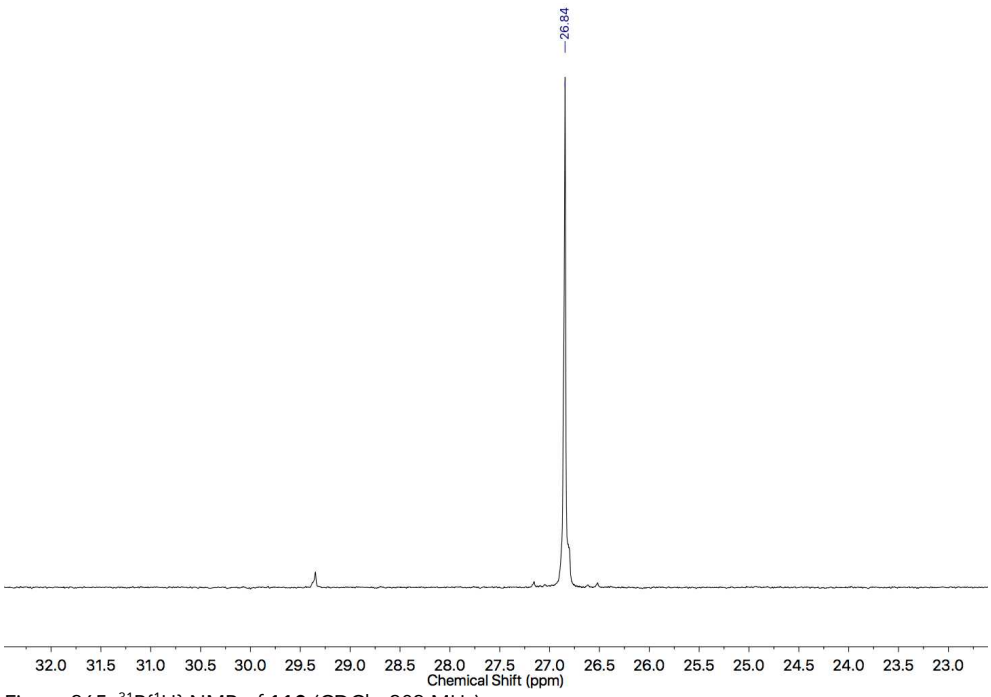

Figure 365: $^{31}P\{^{1}H\}$ NMR of **110** ($CDCl_3$, 202 MHz).

Compound **117**

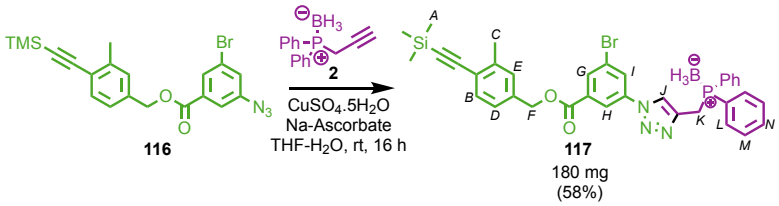

116 (200 mg, 0.452 mmol, 1.0 eq.) and **2** (108 mg, 0.452 mmol, 1.0 eq.) were stirred with $CuSO_4.5H_2O$ (11.2 mg, 0.0452 mmol, 0.10 eq.) and sodium ascorbate (13.4 mg, 0.0678 mmol, 0.15 eq.) at room temperature in THF (2.3 mL) and water (2.3 mL) for 16 h. The reaction was concentrated *in vacuo*, diluted in CH_2Cl_2, washed with brine (20 mL), then H_2O_2 (35 wt.%, 15 mL) and extracted in CH_2Cl_2 (3 x 20 mL). The combined organic layers were dried over $MgSO_4$ and concentrated *in vacuo*. The residue was purified by column chromatography (SiO_2, petrol-EtOAc 0→20%) yielding a white foam **117** (180 mg, 0.262 mmol, 58%). δ_H ($CDCl_3$, 400 MHz) 8.21-8.20 (2H, m, H_G, H_H), 8.10 (1H, app. t, J = 2.0, H_I), 7.97 (1H, d, J = 2.1, H_J), 7.77-7.71 (4H, m, H_L), 7.51-7.42 (7H, m, H_M, H_N, H_D), 7.28 (1H, s, H_E), 7.21 (1H, br. d, J = 7.9, H_B), 5.35 (2H, s, H_F), 3.87 (2H, d, J = 11.2, H_K), 2.47 (3H, s, H_C), 0.28 (9H, s, H_A). δ_C ($CDCl_3$, 101 MHz) 163.90, 141.2, 140.4 (d, J_{CP} = 2.4), 137.90, 135.4, 133.3, 132.6, 132.5 (d, J_{CP} = 9.3), 132.5, 131.8, 129.6, 129.1 (d, J_{CP} = 10.1), 128.1 (d, J_{CP} = 55.3), 127.6, 125.7, 123.6, 123.5, 121.4 (d, J_{CP} = 3.0), 119.8, 103.6,

99.3, 67.5, 24.7 (d, J_{CP} = 36.0), 20.8, 0.1. δ_P ($CDCl_3$, 202 MHz) 17.2. HR-ESI-MS [M-BH_2+O]$^+$ m/z 682.1279 (calc. for $C_{35}H_{34}BrN_3O_3PSi$ m/z 682.1285).

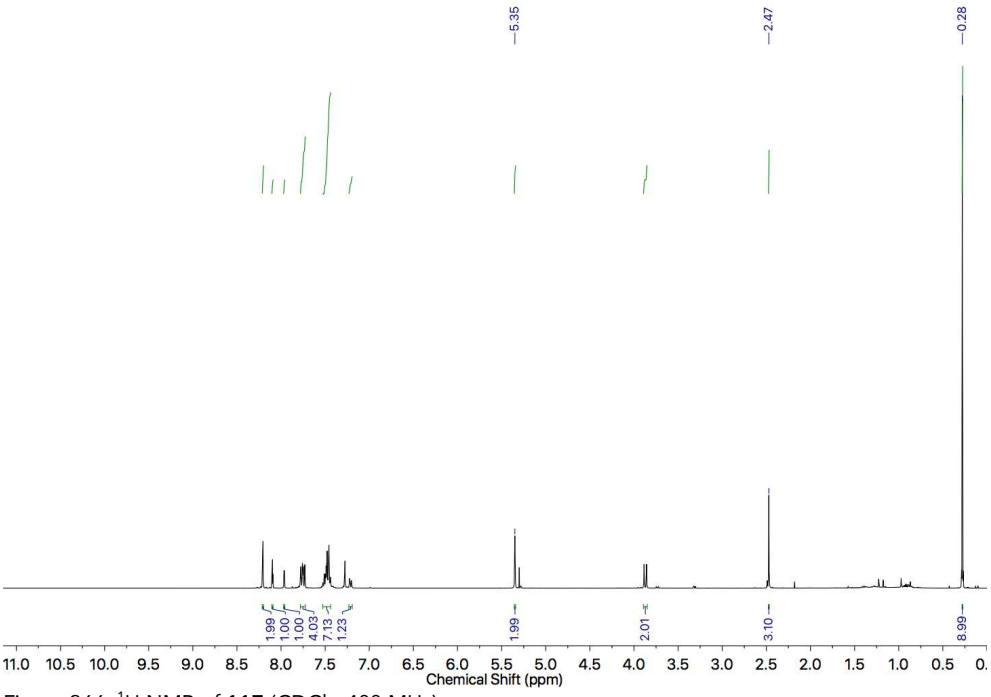

Figure 366: ^{1}H NMR of **117** ($CDCl_3$, 400 MHz).

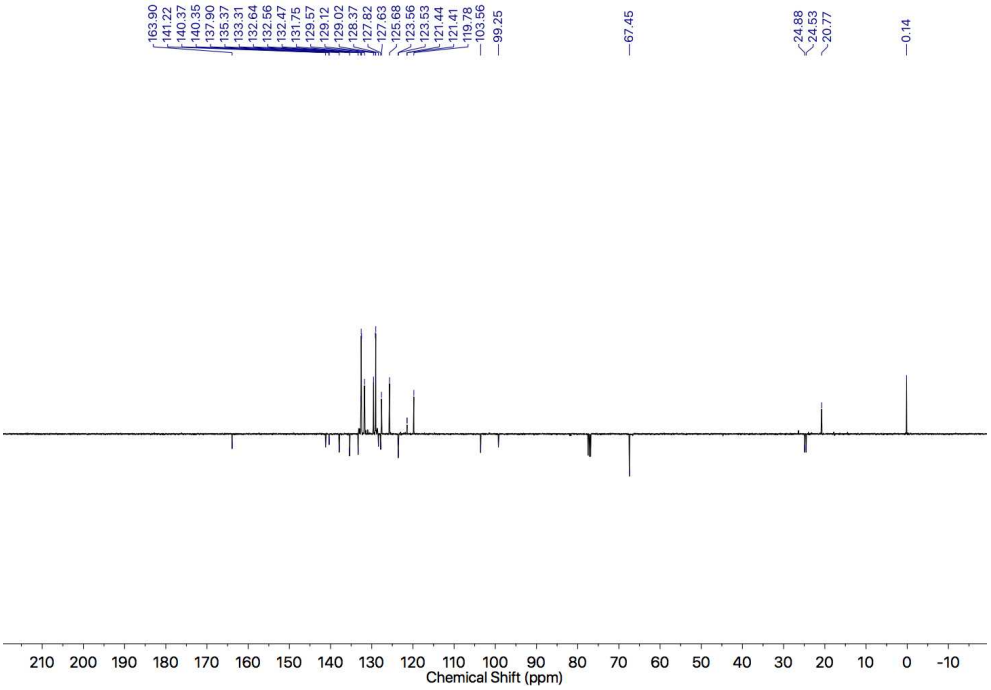

Figure 367: JMOD NMR of **117** ($CDCl_3$, 101 MHz).

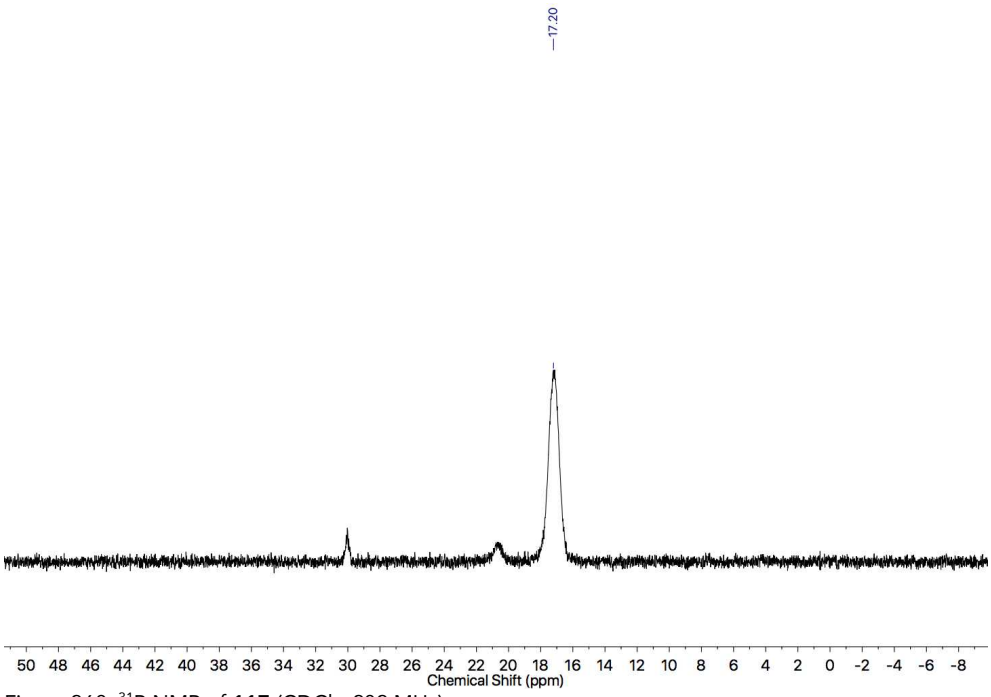

Figure 368: ^{31}P NMR of **117** ($CDCl_3$, 202 MHz).

Compound **118**

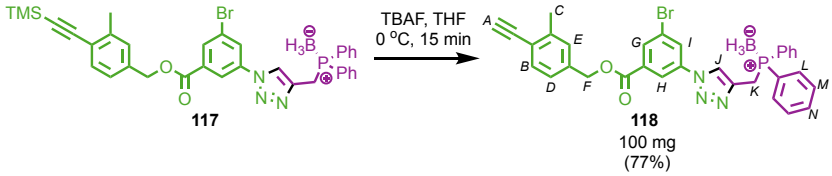

117 (146 mg, 0.215 mmol, 1.0 eq.) was dissolved in anhydrous THF (2.7 mL) and cooled to 0 °C. TBAF (1.0 M in THF, 0.80 mL, 0.80 mmol, 3.7 eq.) was added and the reaction stirred at 0 °C for 15 minutes. The reaction was washed with brine (15 mL), extracted in EtOAc (3 x 15 mL), then the combined organic layers were dried over $MgSO_4$ and concentrated *in vacuo*. The residue was purified by column chromatography (SiO_2, petrol-EtOAc 0→25%) yielding a yellow oil **118** (100 mg, 0.164 mmol, 77%). $\boldsymbol{\delta}_H$ ($CDCl_3$, 400 MHz) 8.21-8.19 (2H, m, $\boldsymbol{H}_G$, $\boldsymbol{H}_H$), 8.08 (1H, t, J = 2.0, $\boldsymbol{H}_I$), 7.96 (1H, d, J = 2.1, $\boldsymbol{H}_J$), 7.77-7.71 (4H, m, $\boldsymbol{H}_L$), 7.52-7.41 (9H, m, $\boldsymbol{H}_M$, $\boldsymbol{H}_N$, $\boldsymbol{H}_B$), 7.28 (1H, br. s, $\boldsymbol{H}_E$), 7.22 (1H, br. d, J = 7.9, $\boldsymbol{H}_D$), 5.34 (2H, s, $\boldsymbol{H}_F$), 3.86 (2H, d, J = 11.2, $\boldsymbol{H}_K$), 3.30 (1H, s, $\boldsymbol{H}_A$), 2.47 (3H, s, $\boldsymbol{H}_C$). $\boldsymbol{\delta}_C$ ($CDCl_3$, 101 MHz) 163.9, 141.4, 140.4 (d, J_{CP} = 2.4), 137.9, 135.8, 133.3, 133.0, 132.7, 132.5 (d, J_{CP} = 9.3), 131.8 (d, J_{CP} = 2.5), 129.6, 129.1 (d, J_{CP} = 10.0), 128.1 (d, J_{CP} = 55.3), 127.7, 125.7, 123.6, 122.5, 121.5 (d, J_{CP} = 3.0), 119.8, 82.1, 81.8, 67.4, 24.7 (d, J_{CP} = 36.0), 20.7. $\boldsymbol{\delta}_P$ ($CDCl_3$, 202 MHz) 17.2. HR-ESI-MS $[M+H]^+$ m/z 606.1136 (calc. for $C_{32}H_{27}BBrN_3O_2P$ m/z 606.1117).

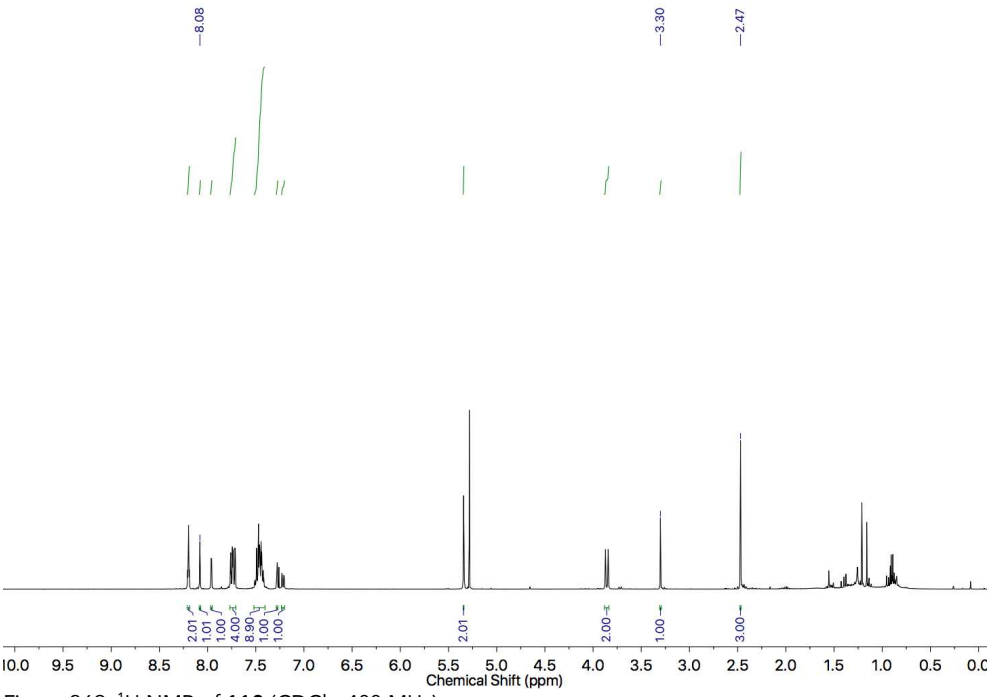

Figure 369: ^{1}H NMR of **118** ($CDCl_3$, 400 MHz).

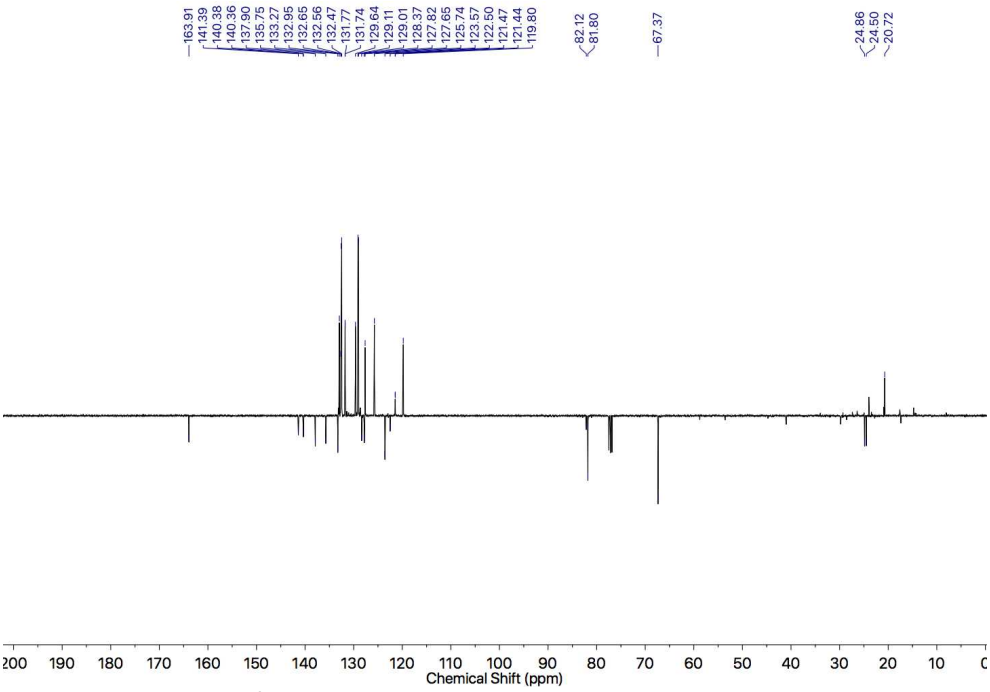

Figure 370: JMOD NMR of **118** ($CDCl_3$, 101 MHz).

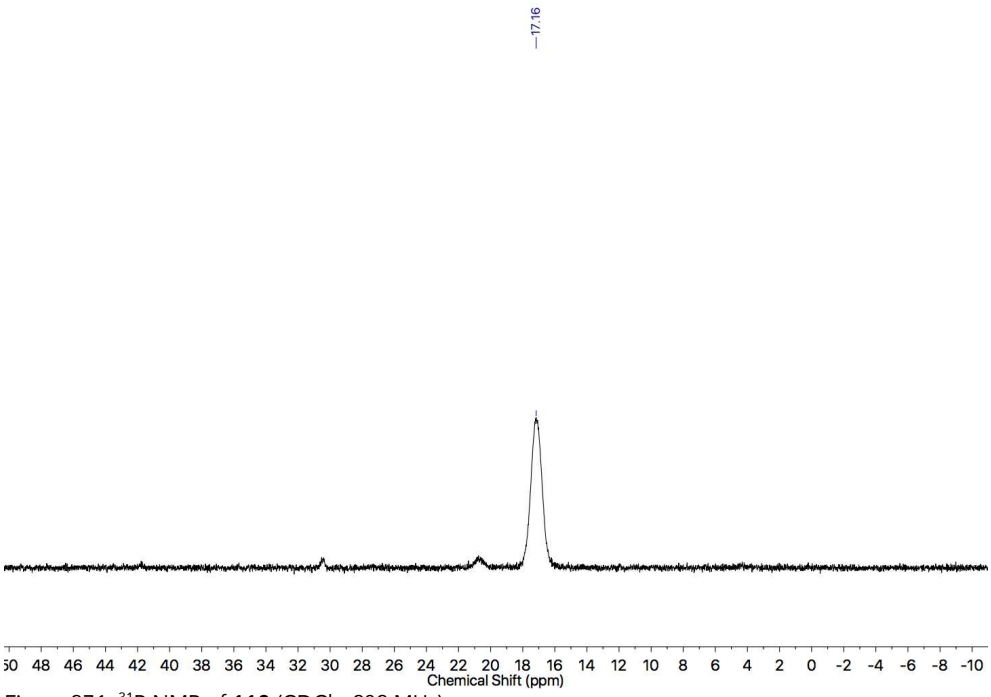

Figure 371: ^{31}P NMR of **118** ($CDCl_3$, 202 MHz).

Compound **141**

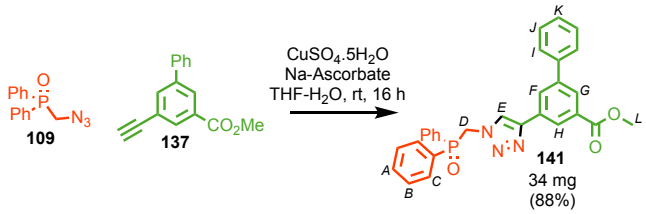

109 (20.0 mg, 0.078 mmol, 1.0 eq.) and **137** (18.4 mg, 0.078 mmol, 1.0 eq.) were stirred over $CuSO_4.5H_2O$ (1.9 mg, 0.0078 mmol, 0.10 eq.) and sodium ascorbate (2.3. mg, 0.0117 mmol, 0.15 eq.) in THF (0.4 mL) and water (0.4 mL) for 16 h, at room temperature. The solution was washed with brine (15 mL) and extracted in CH_2Cl_2 (3 x 15 mL). The combined organic layers were dried over $MgSO_4$ and concentrated *in vacuo*. The residue was purified by column chromatography (SiO_2, petrol-EtOAc 0→80%) yielding a white solid **141** (34 mg, 0.069 mmol, 88%). δ_H (CD_2Cl_2, 400 MHz) 8.39 (1H, br. s, H_E), 8.36 (1H, br. s, H_G), 8.25 (1H, br. s, H_F), 8.20 (1H, br. s, H_H), 7.82-7.73 (4H, br. m, H_C), 7.66 (2H, br. d, J = 7.8, H_I), 7.59 (2H, br. t, J = 7.3, H_A), 7.55-7.48 (4H, m, H_B), 7.46 (2H, br. t, J = 7.4, H_J), 7.38 (1H, tt, J = 7.3, 2.1, H_K), 5.34 (2H, br. s, H_D), 3.92 (3H, s, H_L). δ_C (CD_2Cl_2, 101 MHz) 166.5, 142.0, 139.7, 132.9, 132.7, 132.5, 131.5, 131.2, 129.1, 129.0, 128.9, 128.3, 127.9, 127.6, 127.2, 125.4, 121.7, 52.1, 50.3 (d, J_{CP} = 71.5). δ_P ($CDCl_3$, 202 MHz) 27.0. HR-ESI-MS $[M+H]^+$ m/z 494.1632 (calc. for $C_{29}H_{25}O_3N_3P$ m/z 494.1628).

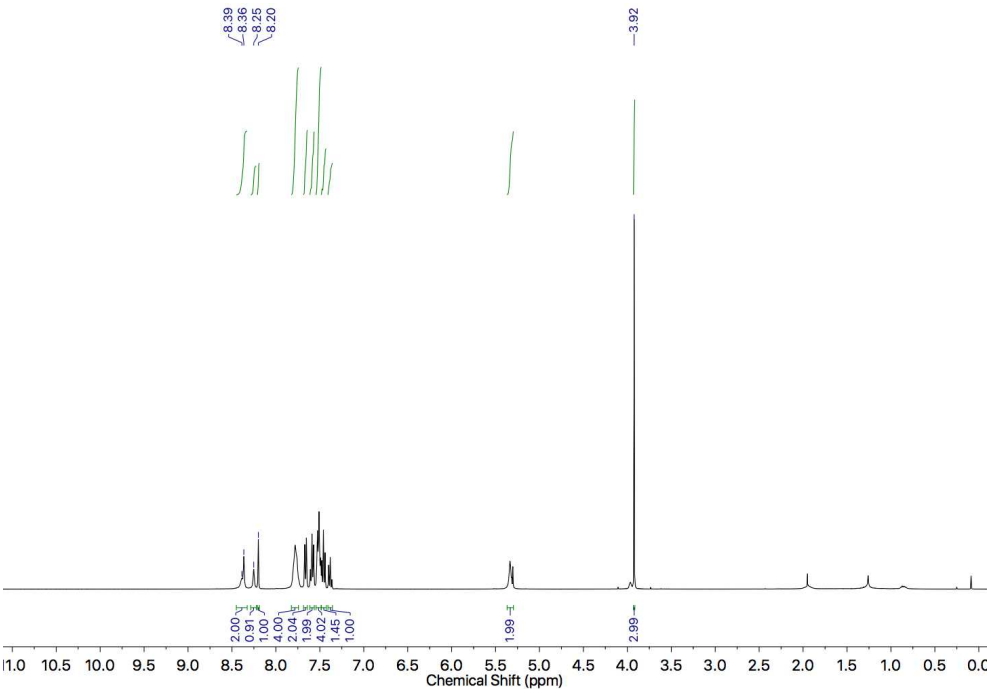

Figure 372: ^{1}H NMR of **141** (CD_2Cl_2, 400 MHz).

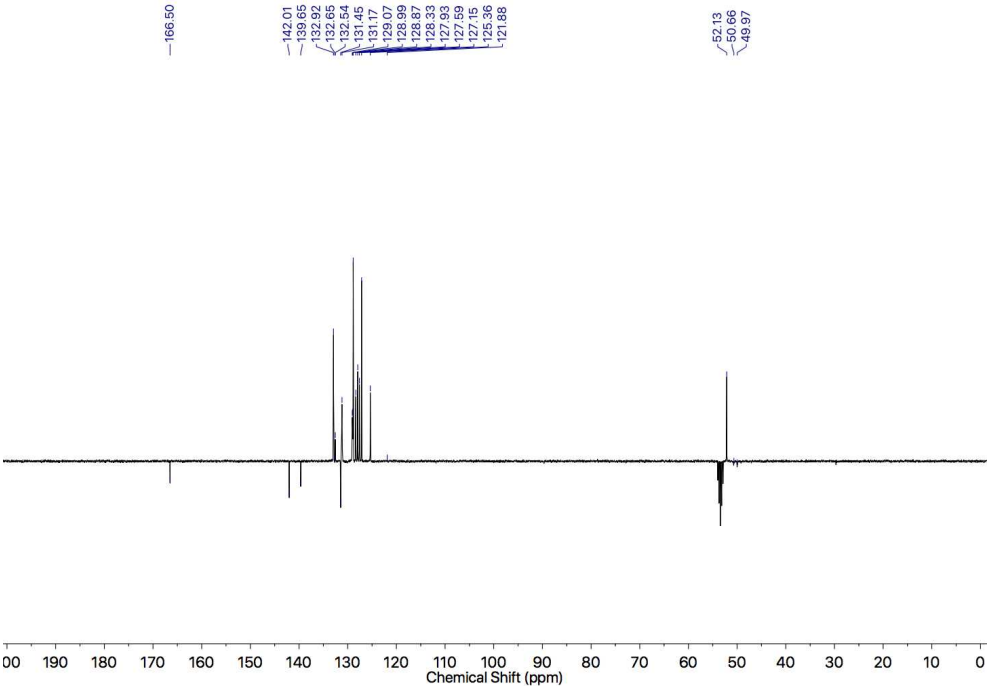

Figure 373: JMOD NMR of **141** (CD_2Cl_2, 101 MHz).

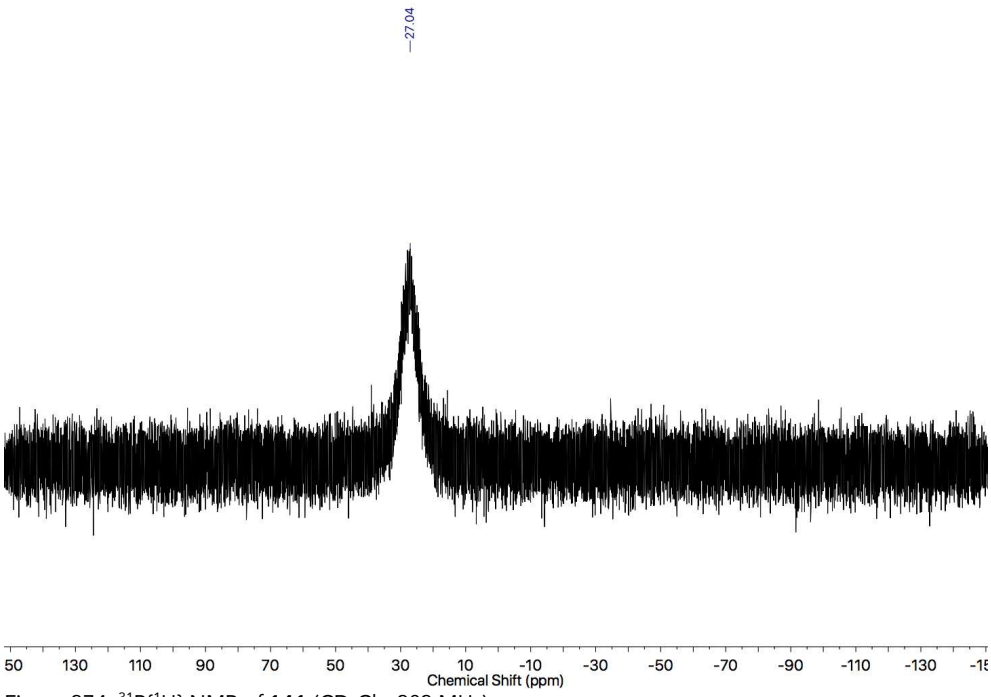

Figure 374: $^{31}P\{^{1}H\}$ NMR of **141** (CD_2Cl_2, 202 MHz).

Rotaxane **113**

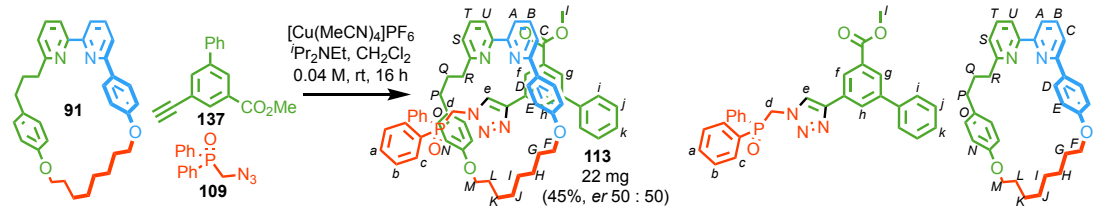

A CEM MW flask was charged with **137** (11.8 mg, 0.0500 mmol, 1.0 eq.), **109** (12.9 mg, 0.0500 mmol, 1.0 eq.), **91** (24.6 mg, 0.0500 mmol, 1.0 eq.) and $[Cu(MeCN)_4]PF_6$ (17.9 mg, 0.0480 mmol, 0.96 eq.) and purged with N_2. Anhydrous CH_2Cl_2 (1.25 mL) and $^{i}Pr_2NEt$ (26 µL, 0.150 mmol, 3.0 eq.) were added and the solution stirred at room temperature for 16 h. The solution was washed with EDTA-NH_3 (15 mL) and extracted in CH_2Cl_2 (3 x 15 mL). The combined organic layers were dried over $MgSO_4$ and concentrated *in vacuo*. The residue was purified by column chromatography (SiO_2, petrol-EtOAc 0→70%) yielding a white solid **113** (22 mg, 0.022 mmol, 45%, *er* 50 : 50). Enantiopurity determined by chiral stationary phase HPLC loaded in EtOAc (RegisPackCLA, *n*-hexane-ethanol 80 : 20, flowrate 1.0 mLmin^{-1}, retention times 17.6 min (50.0%), 22.4 min (50.0%). δ_H ($CDCl_3$, 400 MHz) 9.41 (1H, s, H_e), 8.26 (1H, br. s, H_f), 8.10 (1H, br. s, H_h), 8.03 (1H, br. s, H_g), 7.86-7.80 (2H, m, H_c), 7.75-7.63 (4H, m, H_a, $H_{a'}$, H_B, H_T), 7.62 (1H, d, J = 7.5, H_A), 7.54-7.45 (3H, H_S, H_U, H_k), 7.43-7.36 (8H, m, $H_{c'}$, H_b, $H_{b'}$, H_j), 7.24-7.18 (2H, m, H_i), 7.14 (1H, d, J = 7.6, H_C), 7.09 (2H, d, J = 8.6, H_D), 6.41 (2H, d, J = 8.0, H_O), 6.25 (2H, d, J = 8.6, H_E), 5.94 (2H, d, J = 8.0, H_N), 4.57 (1H, dd, J = 15.9,

5.5, $\boldsymbol{H}_{d}$), 4.45 (1H, dd, J = 15.9, 8.7, $\boldsymbol{H}_{d'}$), 3.93-3.81 (3H, m, $\boldsymbol{H}_{F}$, $\boldsymbol{H}_{F'}$, $\boldsymbol{H}_{M}$), 3.78 (3H, s, $\boldsymbol{H}_{I}$), 3.77-3.70 (1H, m, $\boldsymbol{H}_{M'}$), 2.58-2.49 (2H, m, $\boldsymbol{H}_{R}$), 2.46-2.33 (2H, m, $\boldsymbol{H}_{P}$), 1.97-1.50 (12H, m, $\boldsymbol{H}_{Q}$, 10 of $\boldsymbol{H}_{G}$-$\boldsymbol{H}_{L}$), 0.95-0.85 (2H, m, 2 of $\boldsymbol{H}_{G}$-$\boldsymbol{H}_{L}$). $\boldsymbol{\delta}_{C}$ ($CDCl_3$, 101 MHz) 167.4, 163.4, 159.5, 158.8, 158.1, 157.5, 156.9, 146.2, 140.4, 140.0, 137.0, 137.0, 132.5, 132.0, 131.9, 131.8 (d, J_{CP} = 9.2), 131.4 (d, J_{CP} = 9.6), 131.2, 130.0, 129.5, 129.0, 128.9, 128.8, 128.6, 128.4, 127.2, 127.0, 126.4, 126.1, 122.2, 120.2, 119.9, 119.6, 114.1, 113.6, 67.8, 66.5, 51.9, 48.9 (d, J_{CP} = 72.1), 37.6, 35.1, 31.7, 28.6, 28.4, 25.9, 24.0, 17.4, 14.8. $\boldsymbol{\delta}_{P}$ ($CDCl_3$, 202 MHz) 26.1. HR-ESI-MS $[M+H]^+$ m/z 986.4411 (calc. for $C_{62}H_{61}O_5N_5P$ m/z 986.4405).

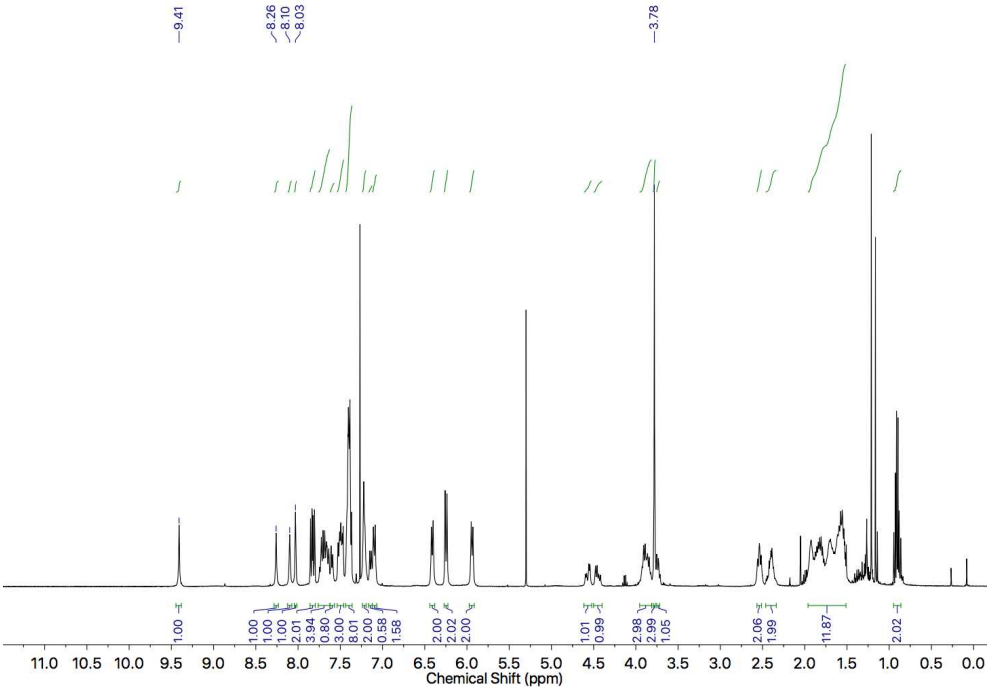

Figure 375: ^{1}H NMR of **113** ($CDCl_3$, 400 MHz).

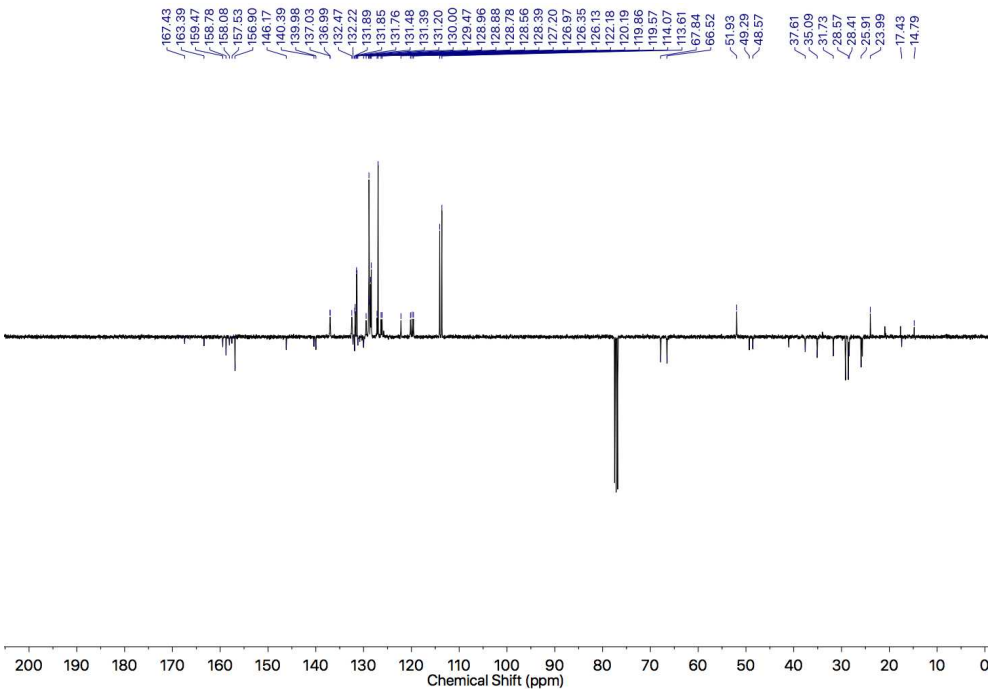

Figure 376: JMOD NMR of **113** ($CDCl_3$, 101 MHz).

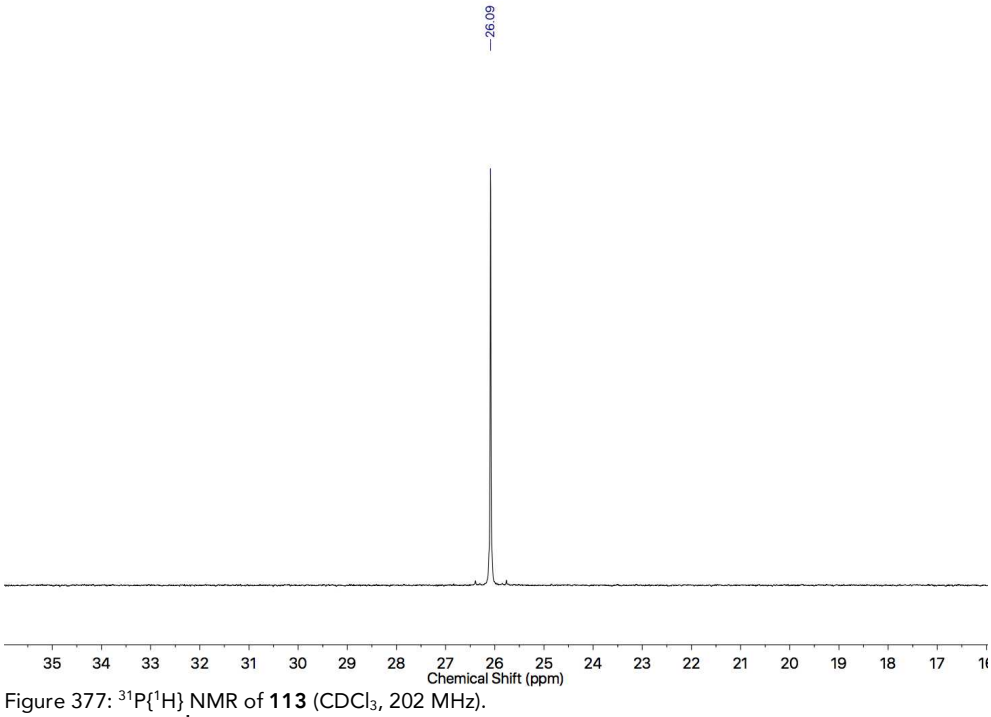

Figure 377: $^{31}P\{^1H\}$ NMR of **113** ($CDCl_3$, 202 MHz).

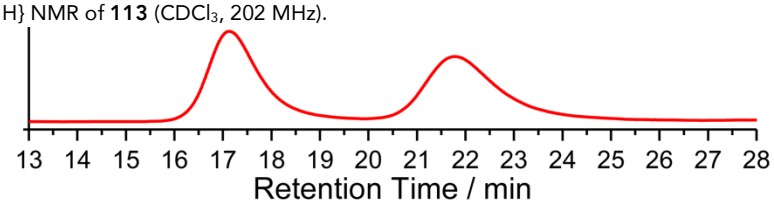

Figure 378: CSP-HPLC of *rac*-**113** (loaded in EtOAc). RegisPackCLA, *n*-hexane-ethanol 80 : 20, flowrate 1.0 mLmin^{-1}, retention times (R_{mp})-**113** (17.6 min, 1172563, 50.0%), (S_{mp})-**113** (22.4 min, 1173155, 50.0%).

(*S*)-**142**

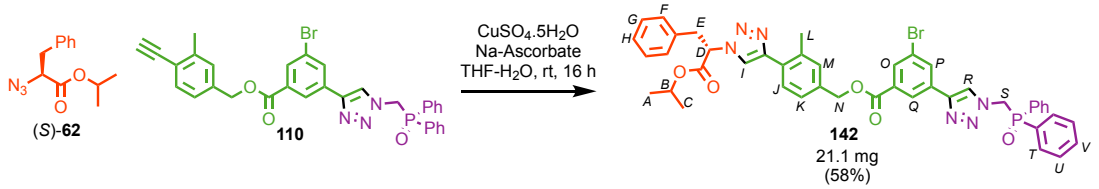

A vial was charged with **110** (26.2 mg, 0.0429 mmol, 1.0 eq.), $CuSO_4.5H_2O$ (1.1 mg, 0.0043 mmol, 0.10 eq.) and sodium ascorbate (1.3 mg, 0.0064 mmol, 0.15 eq.). (*S*)-**62** (10 mg, 0.0429 mmol, 1.0 eq.) was transferred in THF (0.25 mL), followed by water (0.25 mL). The reaction was stirred at room temperature for 16 h. After 16 h, the solution was washed with brine (20 mL) and extracted in CH_2Cl_2 (3 x 20 mL). The combined organic layers were dried over $MgSO_4$ and concentrated *in vacuo*. The residue was purified by column chromatography (SiO_2, petrol-EtOAc 0→60%) yielding a white foam **142** (21.1 mg, 0.0250 mmol, 58%). $\boldsymbol{\delta}_H$ ($CDCl_3$, 400 MHz) 8.33 (1H, app. t, J = 1.5, $\boldsymbol{H}_Q$), 8.29 (1H, s, $\boldsymbol{H}_R$), 8.21 (1H, app. t, J = 1.7, $\boldsymbol{H}_P$), 8.13 (1H, app. t, J = 1.7, $\boldsymbol{H}_O$), 7.80-7.74 (5H, m, $\boldsymbol{H}_T$, $\boldsymbol{H}_J$), 7.73 (1H, s, $\boldsymbol{H}_I$), 7.62-7.56 (2H, m, $\boldsymbol{H}_V$), 7.54-7.48 (4H, m, $\boldsymbol{H}_U$), 7.37-7.33 (2H, m, $\boldsymbol{H}_K$, $\boldsymbol{H}_M$), 7.27-7.22 (3H, m, $\boldsymbol{H}_G$, $\boldsymbol{H}_H$), 7.09 (2H, dd, J = 7.7, 2.2, $\boldsymbol{H}_F$), 5.63 (1H, t, J = 6.4, $\boldsymbol{H}_D$), 5.37 (2H, s, $\boldsymbol{H}_N$), 5.29 (2H, d, J = 6.7, $\boldsymbol{H}_S$), 5.08 (1H, sept., J = 6.3, $\boldsymbol{H}_B$), 3.52 (2H, d, J = 7.5, $\boldsymbol{H}_E$), 2.43 (3H, s, $\boldsymbol{H}_L$), 1.24 (3H, d, J = 6.3, $\boldsymbol{H}_A$), 1.20 (3H, d, J = 6.3, $\boldsymbol{H}_C$). $\boldsymbol{\delta}_C$ ($CDCl_3$, 101 MHz) 167.9, 165.0, 146.5, 146.1, 136.1, 135.5, 134.9, 133.3 (d, J_{CP} = 2.8), 133.0, 132.6, 132.2, 131.3 (d, J_{CP} = 9.8), 131.2, 130.3, 129.4, 129.4, 129.2, 129.2, 128.9, 128.3, 127.7, 126.4, 125.6, 123.1, 122.1, 121.9, 70.6, 67.2, 64.3, 50.4 (d, J_{CP} = 70.1), 39.3, 21.8, 21.7, 21.5. $\boldsymbol{\delta}_P$ ($CDCl_3$, 202 MHz) 26.8. HR-ESI-MS $[M+H]^+$ m/z 843.2059, 845.2049 (calc. for $C_{44}H_{41}BrN_6O_5P$ m/z 843.2054).

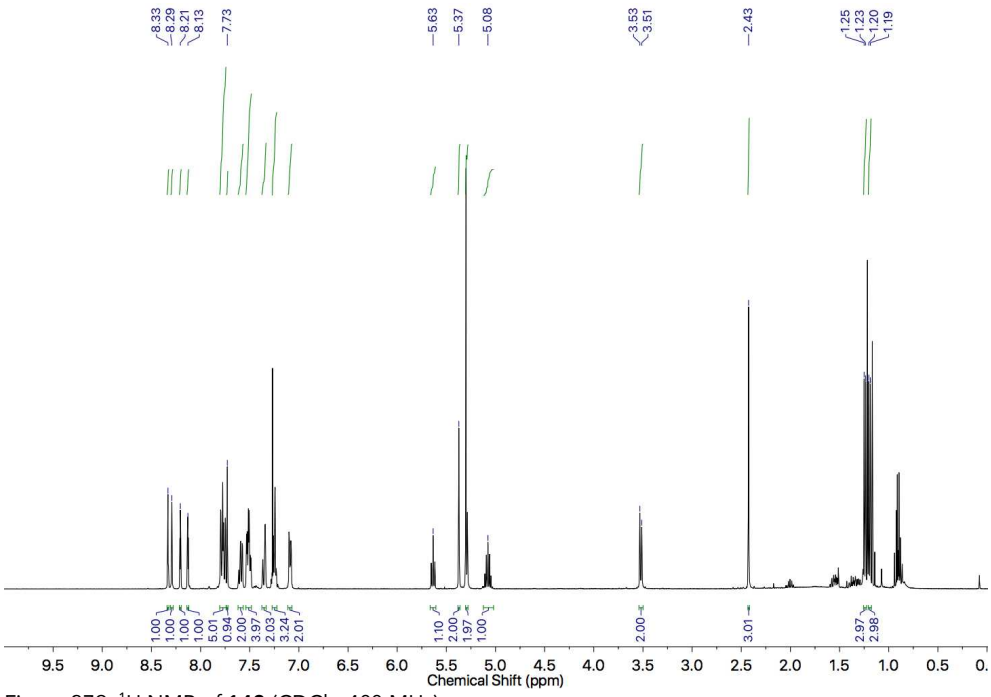

Figure 379: ^{1}H NMR of **142** ($CDCl_3$, 400 MHz).

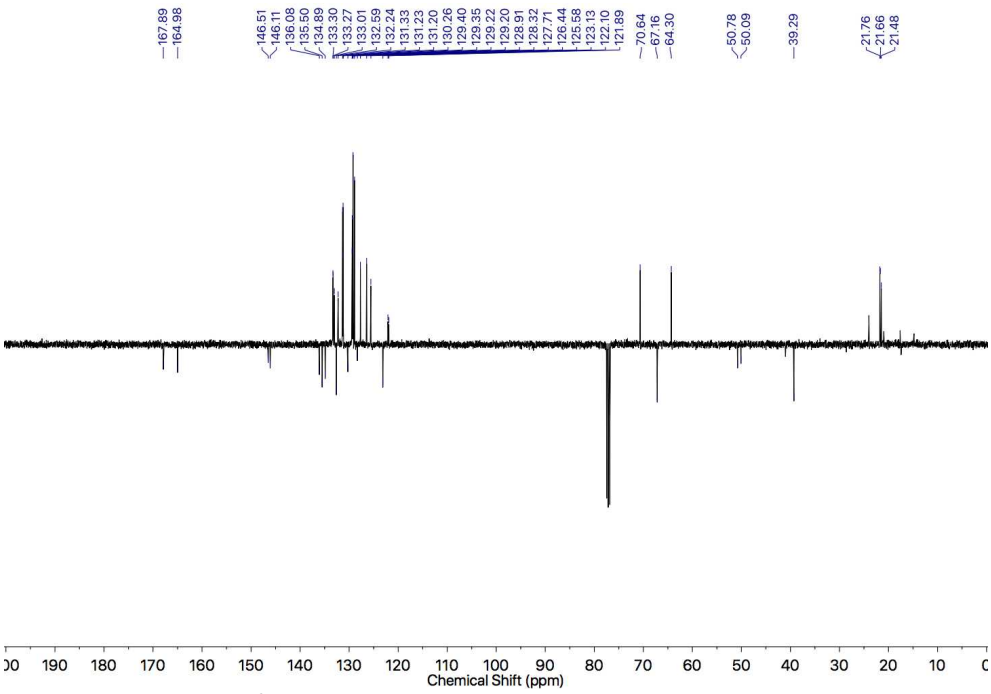

Figure 380: JMOD NMR of **142** ($CDCl_3$, 101 MHz).

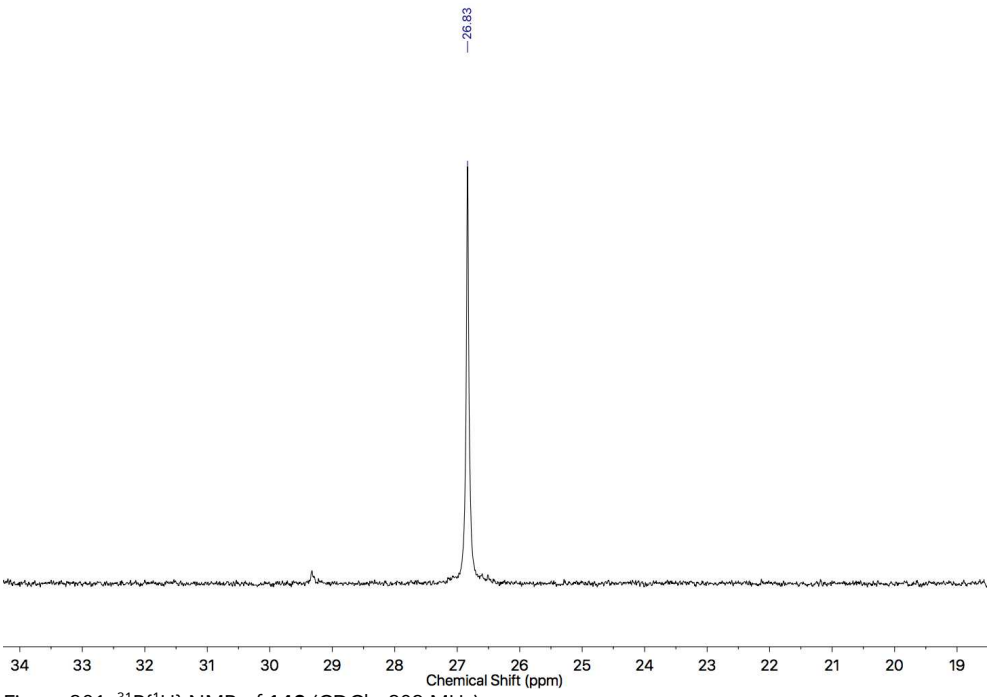

Figure 381: $^{31}P\{^{1}H\}$ NMR of **142** ($CDCl_3$, 202 MHz).

Rotaxane (S,R_{mp})-**111**

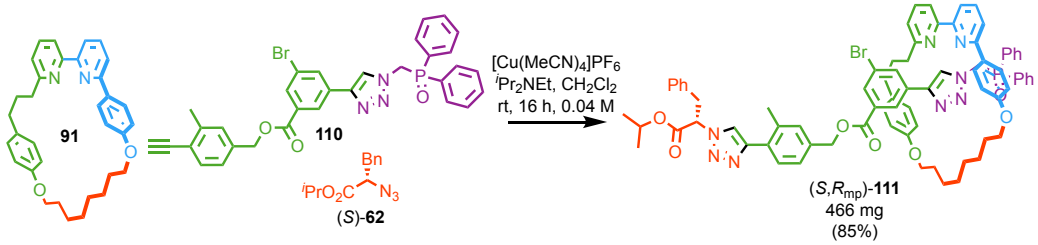

A dry CEM MW vial was charged with **91** (202 mg, 0.410 mmol, 1.0 eq.), **110** (250 mg, 0.410 mmol, 1.0 eq.) and $[Cu(MeCN)_4]PF_6$ (147 mg, 0.393 mmol, 0.96 eq.) and purged with N_2. (*S*)-**62** (96 mg, 0.410 mmol, 1.0 eq.) and $^{i}Pr_2NEt$ (285 µL, 1.64 mmol, 4.0 eq.) were transferred in anhydrous CH_2Cl_2 (10 mL) and the reaction stirred at room temperature for 16 h. After 16 h, the reaction was washed with sat. EDTA-NH_3 (20 mL) and extracted in CH_2Cl_2 (3 x 20 mL). The combined organic layers were dried over $MgSO_4$ and concentrated *in vacuo*. The residue was purified by column chromatography (SiO_2, petrol-EtOAc 0→70%) yielding a yellow foam (S,R_{mp})-**111** (466 mg, 0.349 mmol, 85%). A ratio of co-conformational isomers of 80 : 20 was determined by ^{1}H NMR in $CDCl_3$.

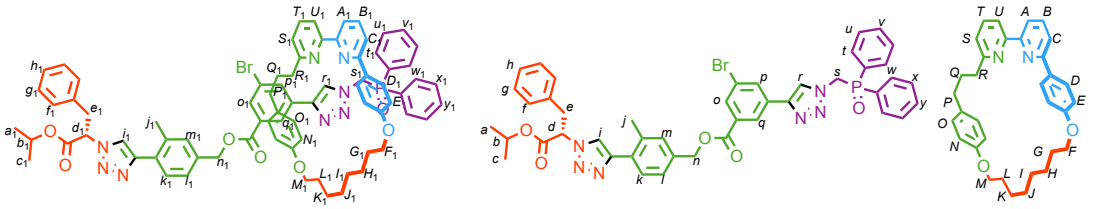

major co-conformation

Major co-conformation (80% occupancy)

δ$_H$ ($CDCl_3$, 400 MHz) 9.26 (1H, s, ***H***$_{r1}$), 8.31-8.28 (1H, m, ***H***$_{i1}$), 8.23 (1H, br. s, ***H***$_{q1}$), 7.95 (1H, br. s, ***H***$_{p1}$), 7.85 (1H, br. s, ***H***$_{o1}$), 7.84-7.69 (5H, m, ***H***$_{t1}$, ***H***$_{w1}$, ***H***$_{B1}$), 7.71-7.56 (4H, m, ***H***$_{v1}$, ***H***$_{y1}$, ***H***$_{S1}$, ***H***$_{k1}$), 7.56-7.46 (2H, m, ***H***$_{x1}$), 7.44-7.35 (6H, m, ***H***$_{u1}$, ***H***$_{C1}$, ***H***$_{T1}$, ***H***$_{m}$, ***H***$_{l1}$), 7.24-7.20 (4H, m, ***H***$_{g1}$, ***H***$_{A1}$), 7.19-7.15 (1H, m, ***H***$_{U1}$), 7.10-7.03 (5H, m, ***H***$_{D1}$, ***H***$_{f1}$, ***H***$_{h1}$) , 6.41 (2H, d, *J* = 8.4, ***H***$_{O1}$), 6.24 (2H, d, *J* = 8.4, ***H***$_{E1}$), 5.93 (2H, d, *J* = 8.4, ***H***$_{N1}$), 5.62 (1H, t, *J* = 7.5, ***H***$_{d1}$), 5.29 (2H, s, ***H***$_{n}$), 5.07 (1H, sept., *J* = 6.3, ***H***$_{b1}$), 4.62 (1H, dd, *J* = 15.9, 5.6, ***H***$_{s1}$), 4.46 (1H, dd, *J* = 15.9, 7.8, ***H***$_{s1'}$), 3.98-3.82 (2H, m, ***H***$_{M1}$), 3.79 (1H, td, *J* = 7.4, 7.3, ***H***$_{F1}$), 3.65 (1H, td, *J* = 7.5, 7.4, ***H***$_{F1'}$), 2.64-2.52 (2H, m, ***H***$_{R1}$), 3.51 (2H, d, *J* = 7.5, ***H***$_{e1}$), 2.44-2.37 (2H, m, ***H***$_{P1}$), 2.31 (3H, s, ***H***$_{j1}$), 1.91-1.45 (10H, m, ***H***$_{G1}$, ***H***$_{H1}$, ***H***$_{K1}$, ***H***$_{L1}$, ***H***$_{Q1}$), 1.24 (3H, d, *J* = 6.3, ***H***$_{a1}$), 1.19 (3H, d, *J* = 6.3, ***H***$_{c1}$), 0.94-0.84 (4H, m, ***H***$_{I1}$, ***H***$_{J1}$). **δ**$_C$ ($CDCl_3$, 101 MHz) 168.0, 167.9, 165.4, 164.3, 163.3, 162.9, 159.4, 159.2, 158.6, 158.1, 157.8, 157.5, 157.0, 156.9, 146.7, 146.5, 145.9, 145.1, 137.0, 136.6, 135.9, 135.8, 135.8, 135.1, 135.0, 134.9, 134.9, 133.7, 133.5, 133.5, 133.3, 133.3, 133.1, 133.0, 132.9, 132.9, 132.9, 132.5, 132.5, 132.5, 132.5, 132.2, 132.1, 132.0, 131.8, 131.7, 131.6, 131.5, 131.4, 131.4, 131.3, 131.3, 131.2, 131.0, 130.6, 130.2, 129.8, 129.3, 129.2, 129.2, 129.2, 129.1, 129.0, 128.9, 128.9, 128.9, 128.8, 128.7, 128.5, 128.3, 128.3, 127.7, 127.6, 127.1, 126.3, 126.1, 126.0, 122.4, 122.3, 122.2, 122.0, 121.9, 121.8, 121.7, 120.3, 120.3, 120.0, 119.9, 119.9, 119.8, 119.6, 119.6, 114.0, 113.8, 113.8, 113.5, 70.6, 70.4, 67.7, 67.0, 66.4, 66.3, 64.2, 64.1, 49.3, 48.6, 39.2, 39.1, 38.0, 37.6, 35.6, 35.0, 32.0, 31.4, 29.2, 29.0, 28.9, 28.8, 28.7, 28.6, 28.5, 28.4, 25.8, 25.6, 25.6, 24.0, 21.8, 21.7, 21.4, 21.2, 21.0, 17.6, 17.4, 14.8. **δ**$_P$ ($CDCl_3$, 202 MHz) 27.2 (***P***$_2$, 20% occupancy), 26.9 (***P***$_{axle}$), 26.0 (***P***$_1$, 80% occupancy). HR-ESI-MS $[M+H]^+$ m/z 1337.5 (calc. for $C_{77}H_{77}BrN_8O_7P$ m/z 1337.5).

Solvent	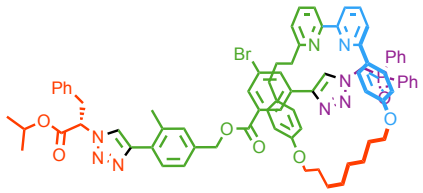	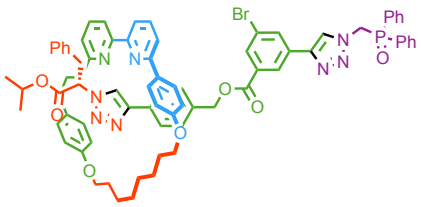
$CDCl_3$	80	20
d^8-THF	83	17
d^4-CD_3OD	66	34
d^6-acetone	80	20
d^8-PhMe	81	19

Table 16: Co-conformational occupancy of the molecular shuttle in different solvents, subsequent to 30 minutes annealing at 60 °C, determined by ^{1}H NMR.

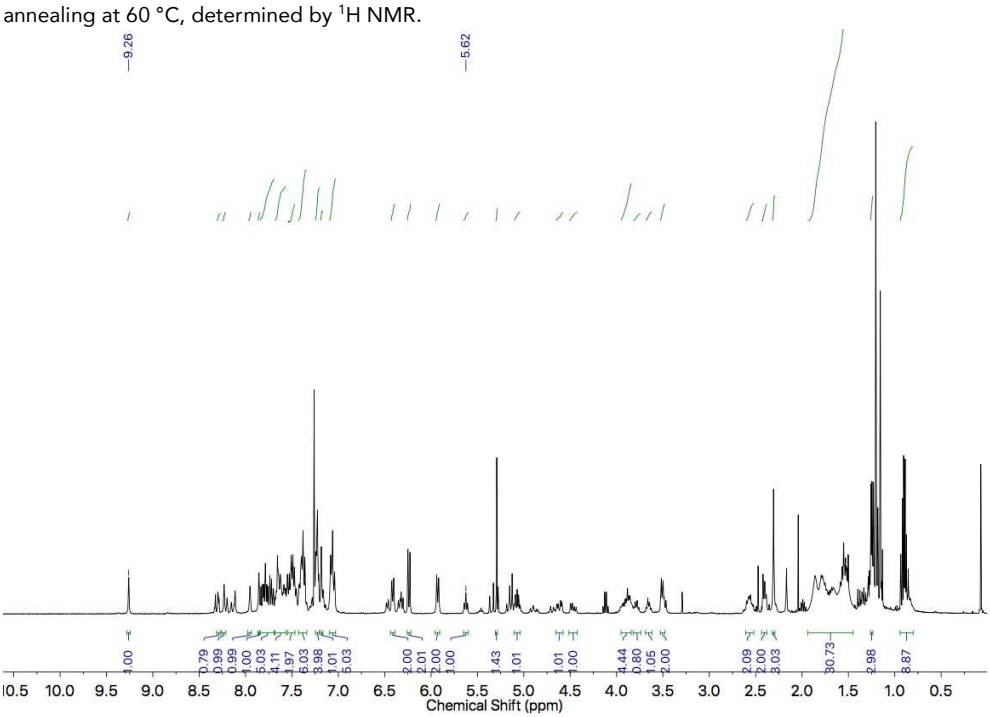

Figure 382: ^{1}H NMR of (S,R_{mp})-**111** ($CDCl_3$, 400 MHz).

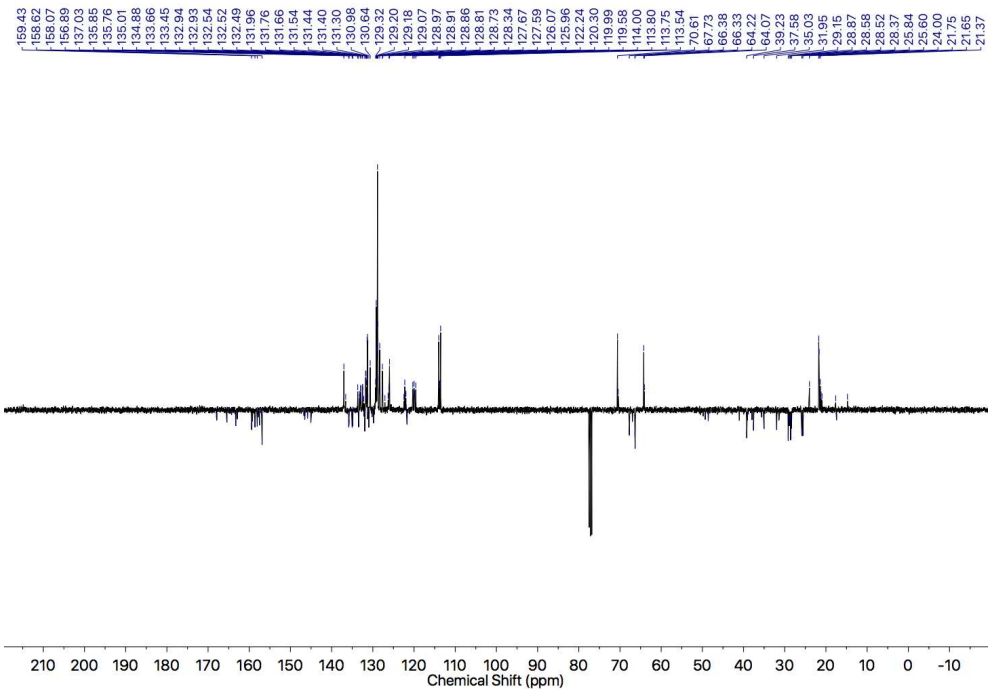

Figure 383: JMOD NMR of (S,R_{mp})-**111** ($CDCl_3$, 101 MHz).

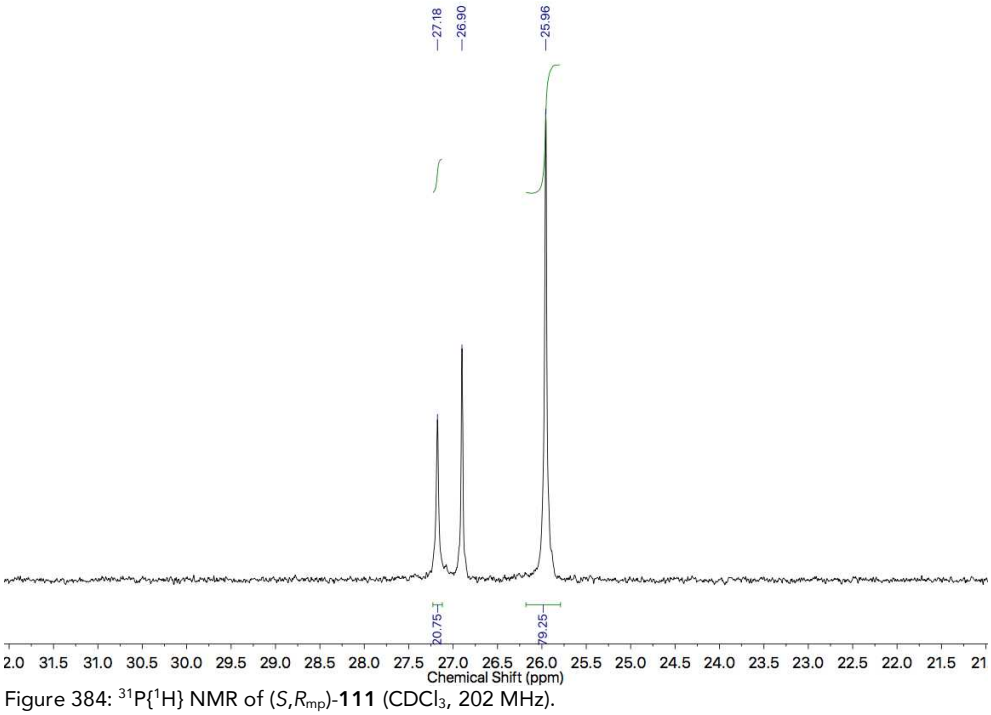

Figure 384: $^{31}P\{^1H\}$ NMR of (S,R_{mp})-**111** ($CDCl_3$, 202 MHz).

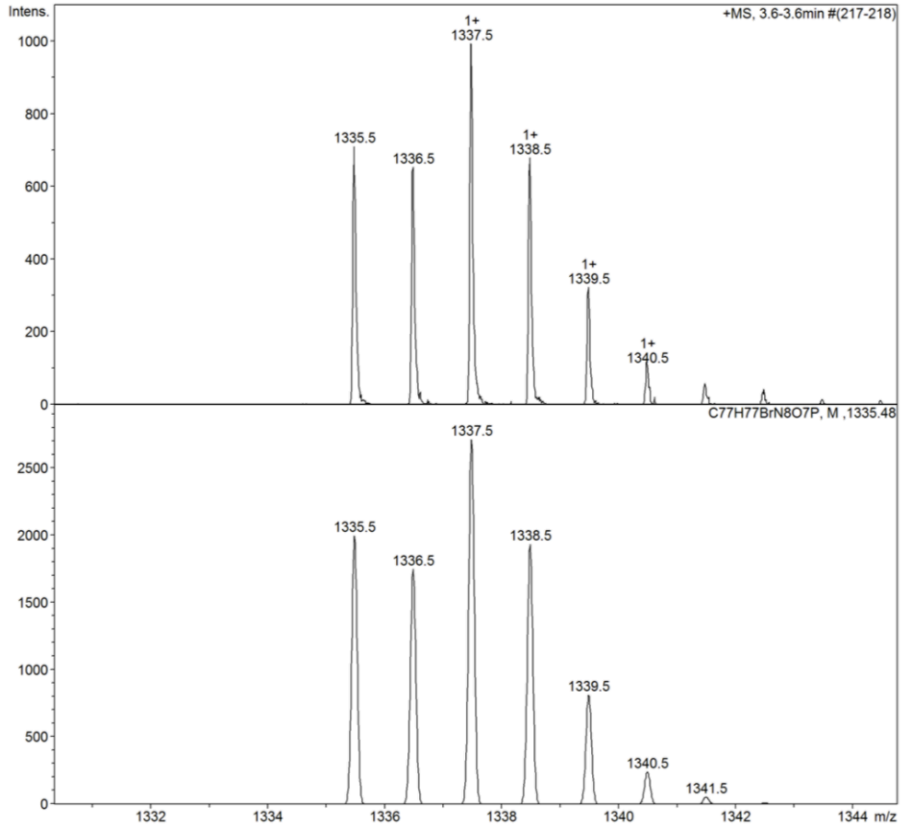

Figure 385: Isotope pattern of (S,R_{mp})-**111** $C_{77}H_{77}BrN_8O_7P$.

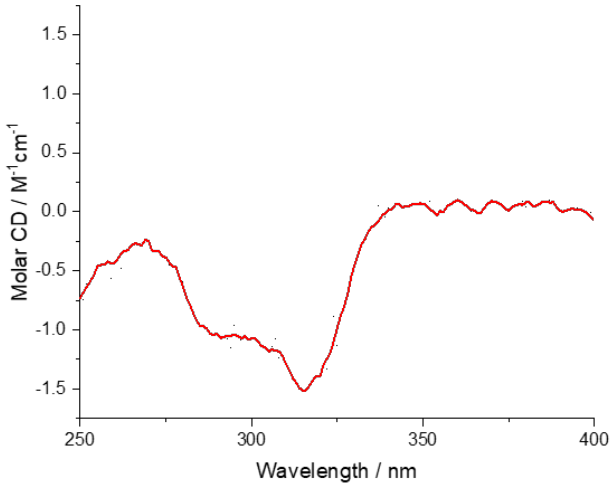

Figure 386: Circular Dichroism Spectra of (S,R_{mp})-**111** (15.2 µM, red) at 293 K in $CHCl_3$.

Rotaxane (S_{mp})-**113**

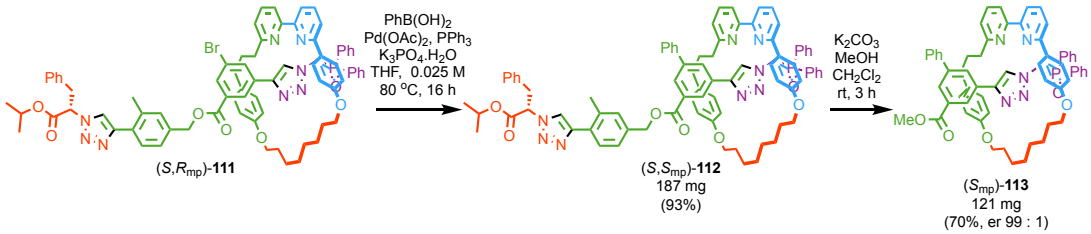

A CEM MW vial was charged with (S,R_{mp})-**111** (200 mg, 0.150 mmol, 1.0 eq.), $PhB(OH)_2$ (54.7 mg, 0.449 mmol, 3.0 eq.), $Pd(OAc)_2$ (1.7 mg, 0.0075 mmol, 0.05 eq.), PPh_3 (3.9 mg, 0.015 mmol, 0.10 eq.) and $K_3PO_4.H_2O$ (103 mg, 0.449 mmol, 3.0 eq.) and purged with N_2. Anhydrous THF (6.0 mL) was added and the solution refluxed at 80 °C for 16 h. The reaction was diluted in CH_2Cl_2 (15 mL), washed with brine (20 mL) and extracted in CH_2Cl_2 (3 x 20 mL). The combined organic layers were dried over $MgSO_4$ and concentrated *in vacuo*. The residue was purified by column chromatography (SiO_2, petrol-EtOAc 30→70%) yielding a yellow foam (S,S_{mp})-**112** (187 mg, 0.140 mmol, 93%, co-conformational ratio 79 : 21). A CEM MW flask was charged with (S,S_{mp})-**112** (232 mg, 0.174 mmol, 1.0 eq.) and K_2CO_3 (48.1 mg, 0.348 mmol, 1.0 eq.) and purged with N_2. Anhydrous CH_2Cl_2 (5.8 mL) and anhydrous MeOH (9.3 mL). were added and the solution stirred at room temperature for 16 h. The solution was diluted with CH_2Cl_2, dried over Na_2SO_4, and concentrated *in vacuo*. The residue was purified by column chromatography (SiO_2, petrol-EtOAc 50→70%) yielding a white solid (S_{mp})-**113** (121 mg, 0.123 mmol, 70%, *er* 99 : 1). NMR spectroscopic data for the pure product matched that of the racemate obtained above. Enantiopurity determined by chiral stationary phase HPLC loaded in EtOAc (RegisPackCLA, *n*-hexane-ethanol 80 : 20, flowrate 1.0 $mLmin^{-1}$, retention times 17.6 min (98.5%), 22.4 min (1.5%).

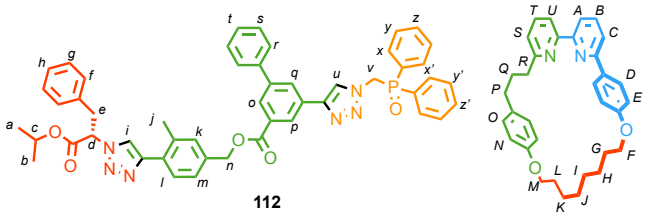

112

δ_H ($CDCl_3$, 400 MHz) 9.42 (1H, s, H_u), 8.30 (1H, s, H_i), 8.08-8.04 (2H, m, H_o, H_p), 7.84-7.75 (4H, m, H_x, $H_{x'}$), 7.70-7.63 (8H, m, H_B, H_C, H_T, H_y, $H_{y'}$, H_q), 7.57-7.33 (11H, m, H_A, H_S, H_U, H_g, H_h, H_k, H_l, H_m, H_z, $H_{z'}$), 7.26-7.20 (5H, m, H_f, H_s, H_t), 7.15-7.06 (4H, m, H_r, H_D), 6.40

(2H, d, J = 7.9, $\boldsymbol{H}_O$), 6.26-20 (2H, m, $\boldsymbol{H}_E$), 5.95 (2H, d, J = 7.9, $\boldsymbol{H}_N$), 5.63 (1H, t, J = 7.0, $\boldsymbol{H}_d$), 5.29 (2H, s, $\boldsymbol{H}_n$), 5.26-5.18 (2H, m, $\boldsymbol{H}_v$), 5.11-5.04 (1H, m, $\boldsymbol{H}_c$), 4.61-4.37 (2H, m, $\boldsymbol{H}_R$), 3.93-3.77 (5H, m, $\boldsymbol{H}_F$, $\boldsymbol{H}_M$, $\boldsymbol{H}_P$) 3.75-3.68 (1H, m, $\boldsymbol{H}_{P'}$), 3.55-3.49 (2H, m, $\boldsymbol{H}_e$), 2.33 (3H, s, $\boldsymbol{H}_j$), 1.93-1.48 (14H, m, $\boldsymbol{H}_G$, $\boldsymbol{H}_H$, $\boldsymbol{H}_I$, $\boldsymbol{H}_J$, $\boldsymbol{H}_K$, $\boldsymbol{H}_L$, $\boldsymbol{H}_Q$), 1.26-1.23 (3H, m, $\boldsymbol{H}_a$), 1.21-1.18 (3H, m, $\boldsymbol{H}_b$). $\boldsymbol{\delta}_C$ ($CDCl_3$, 101 MHz) 167.9, 166.8, 159.4, 158.7, 146.1, 140.5, 139.9, 137.0, 137.0, 136.9, 136.2, 135.8, 134.9, 132.6, 132.5, 132.5, 132.4, 132.3, 132.2, 132.1, 132.1, 132.0, 131.8, 131.8, 131.8, 131.7, 131.5, 131.4, 131.3, 130.6, 130.0, 129.7, 129.2, 129.1, 129.1, 129.0, 128.9, 128.8, 128.7, 128.6, 128.4, 127.7, 127.3, 127.2, 127.0, 126.1, 125.9, 122.5, 120.2, 114.0, 114.0, 113.6, 70.6, 67.2 (d, J_{CP} = 126.3), 66.2, 66.2, 64.2, 41.0, 39.2, 35.0, 29.1, 28.6, 28.5, 25.9, 24.0, 21.7, 21.7, 21.4, 20.9, 17.6, 17.4. $\boldsymbol{\delta}_P$ ($CDCl_3$, 202 MHz) 30.1 ($\boldsymbol{P}_{min}$), 26.4 ($\boldsymbol{P}_{maj}$).

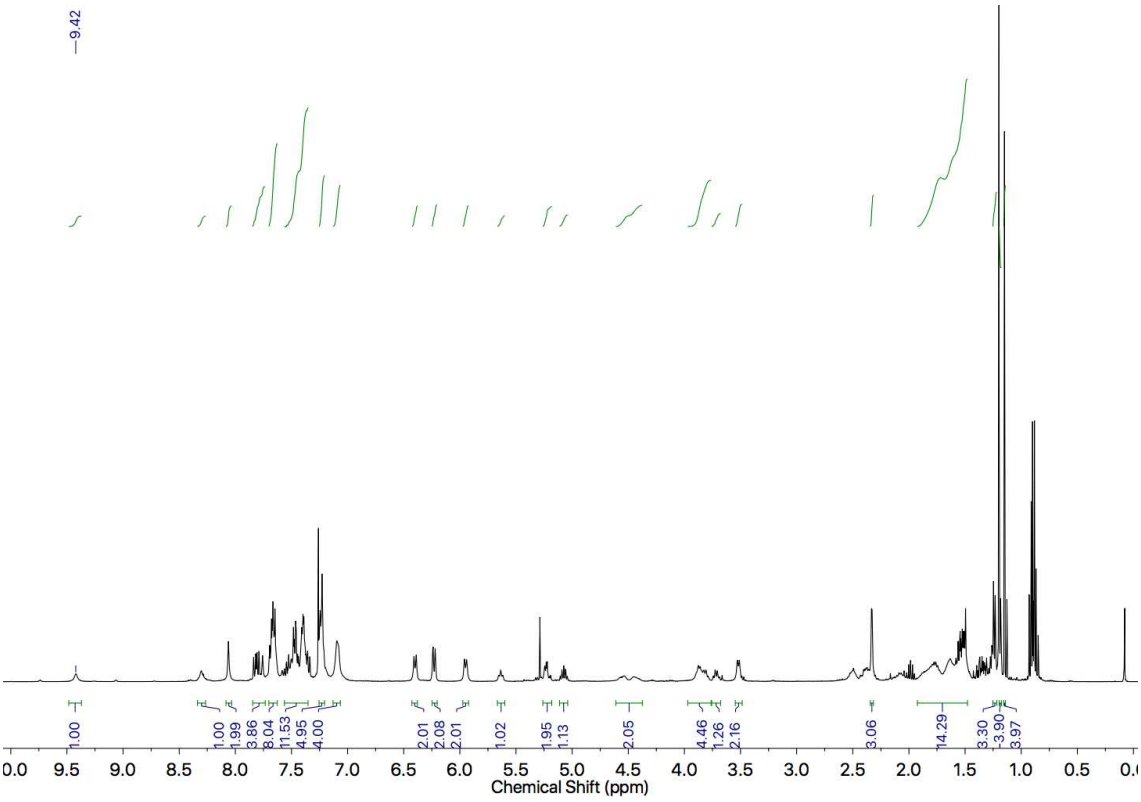

Figure 387: ^{1}H NMR of **112** ($CDCl_3$, 400 MHz).

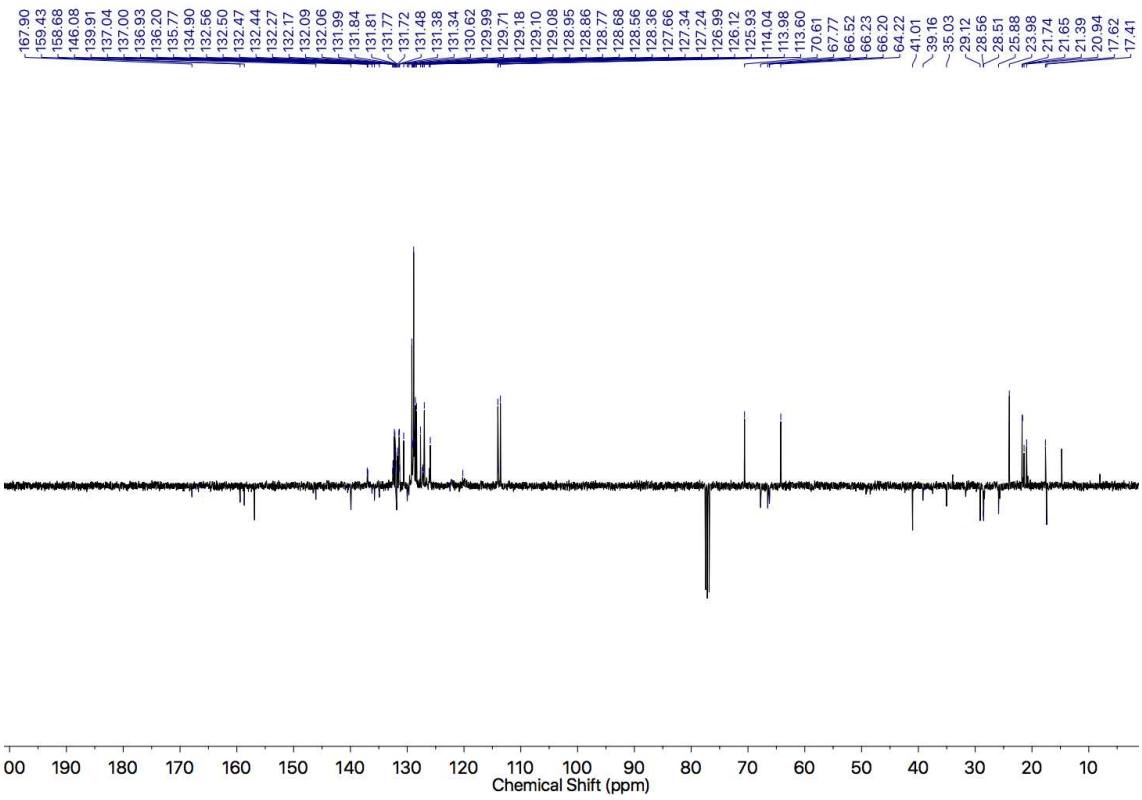

Figure 388: JMOD NMR of **112** ($CDCl_3$, 101 MHz).

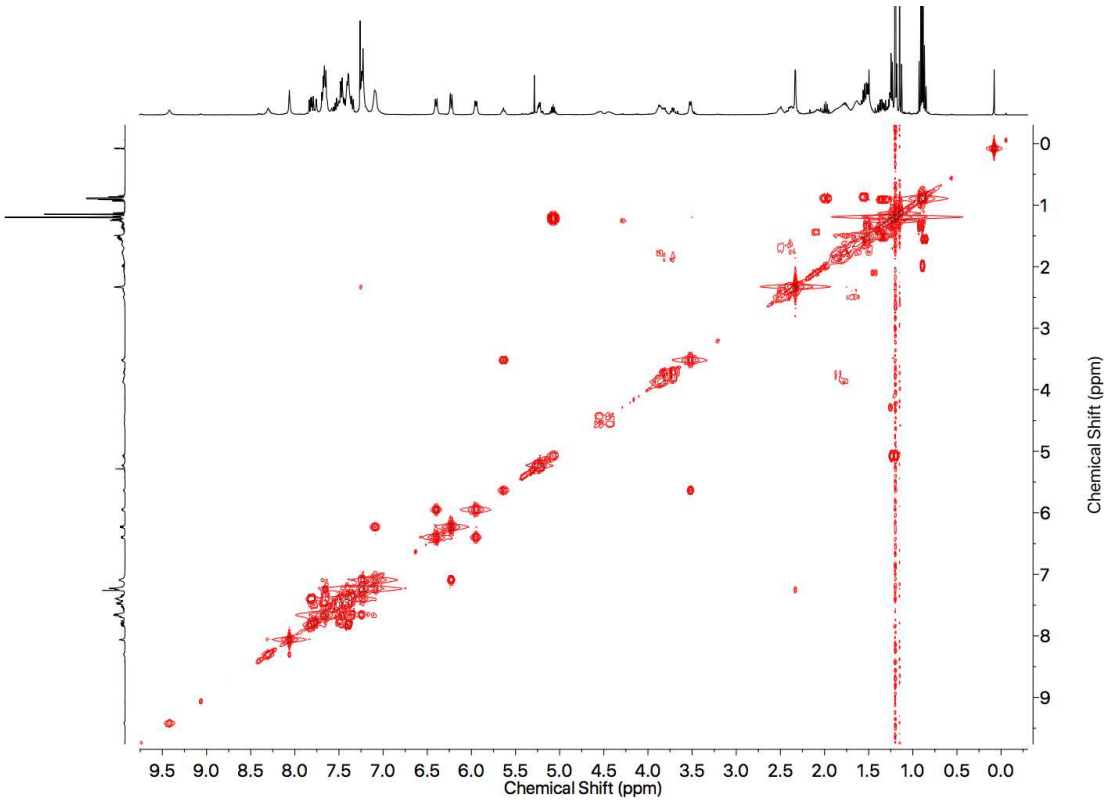

Figure 389: COSY NMR of **112** ($CDCl_3$).

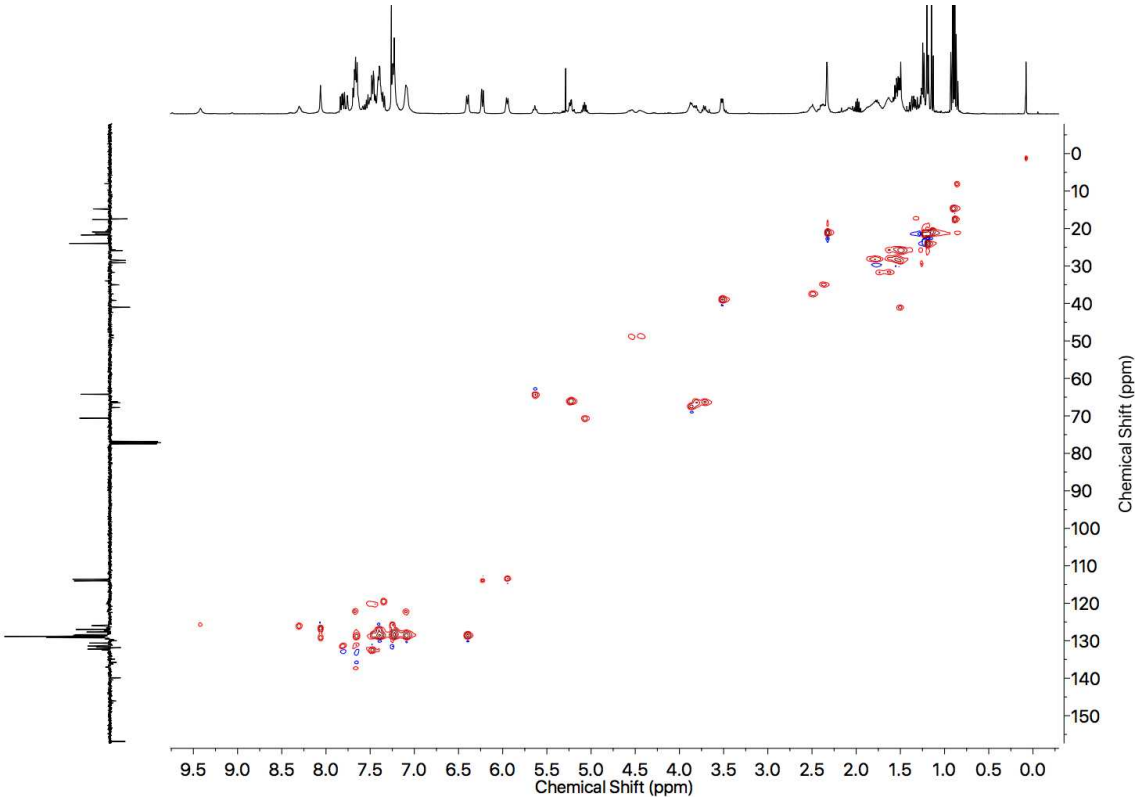

Figure 390: HSQC NMR of **112** ($CDCl_3$).

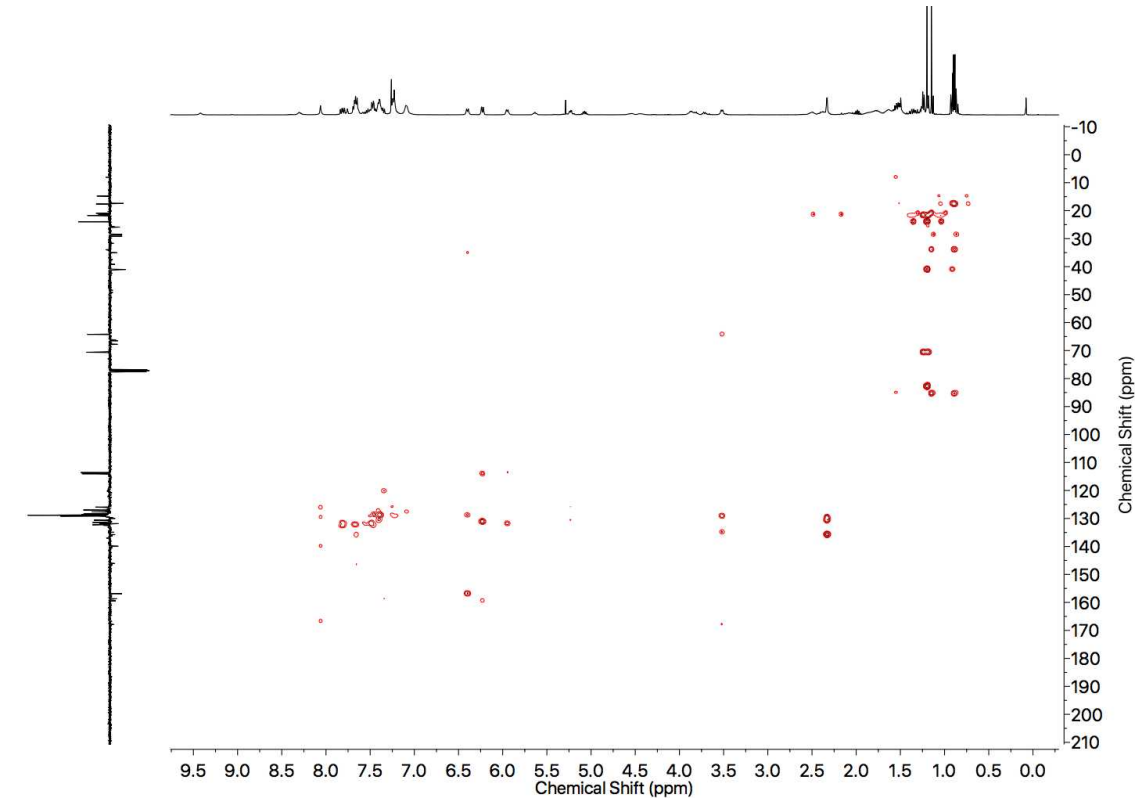

Figure 391: HMBC NMR of **112** ($CDCl_3$).

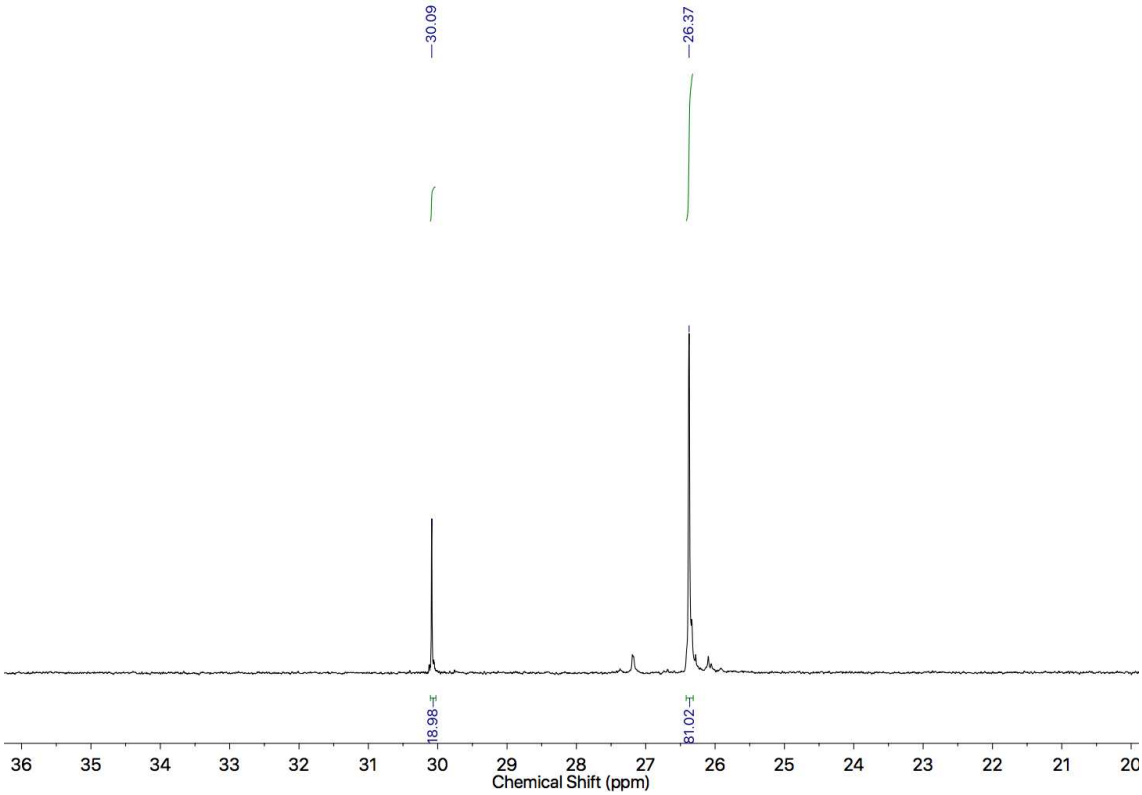

Figure 392: $^{31}P\{^{1}H\}$ NMR of **112** ($CDCl_3$, 202 MHz).

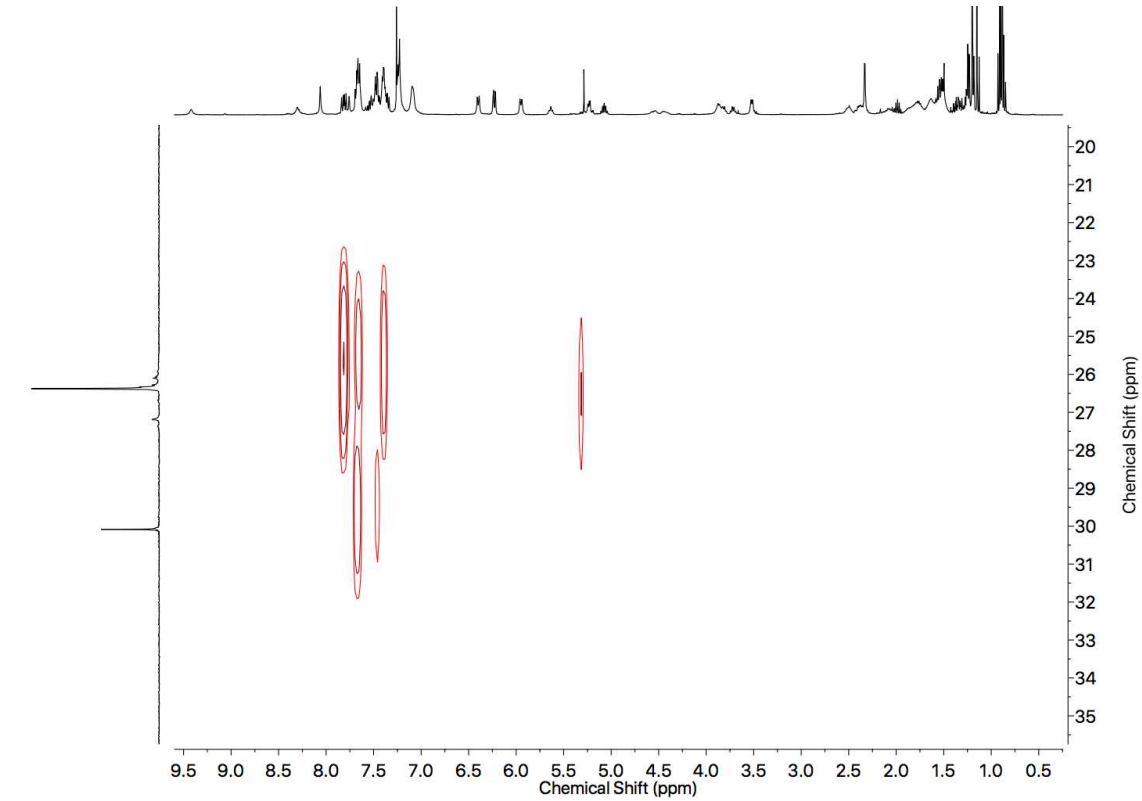

Figure 393: ^{1}H-^{31}P HMBC NMR of **112** ($CDCl_3$).

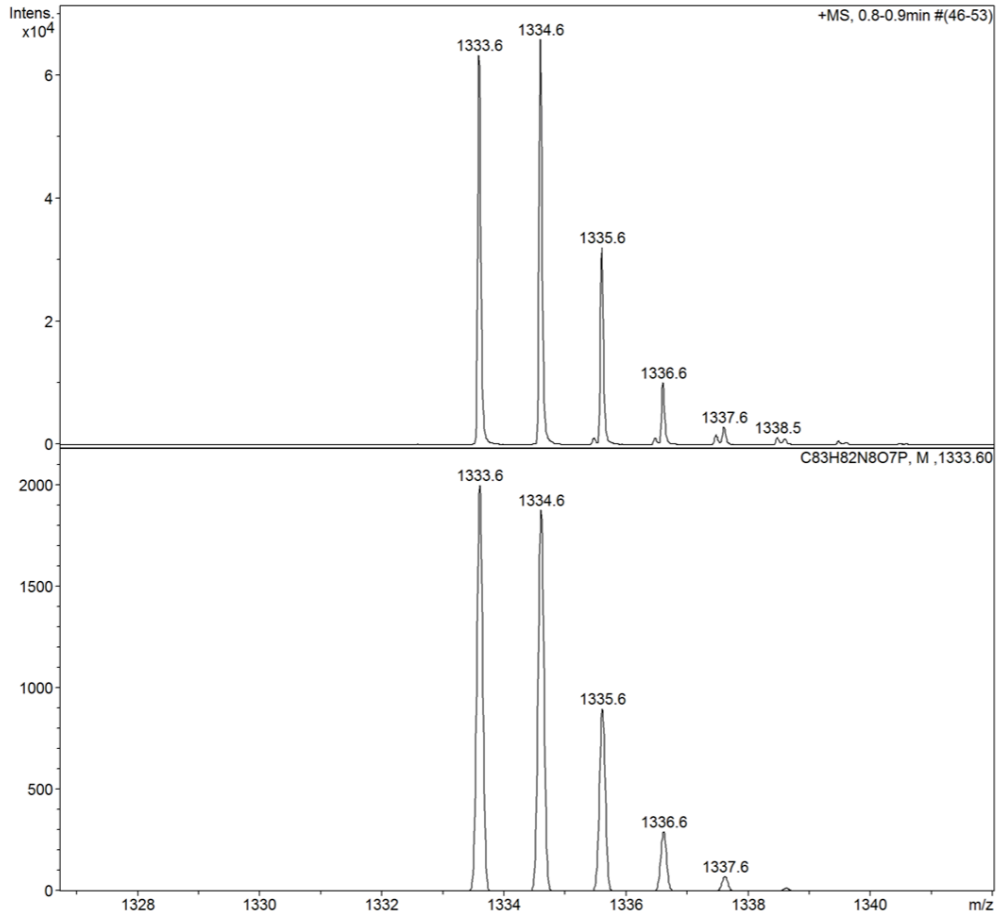

Figure 394: HR-ESI-MS isotope pattern of **112** C83H82N8O7P.

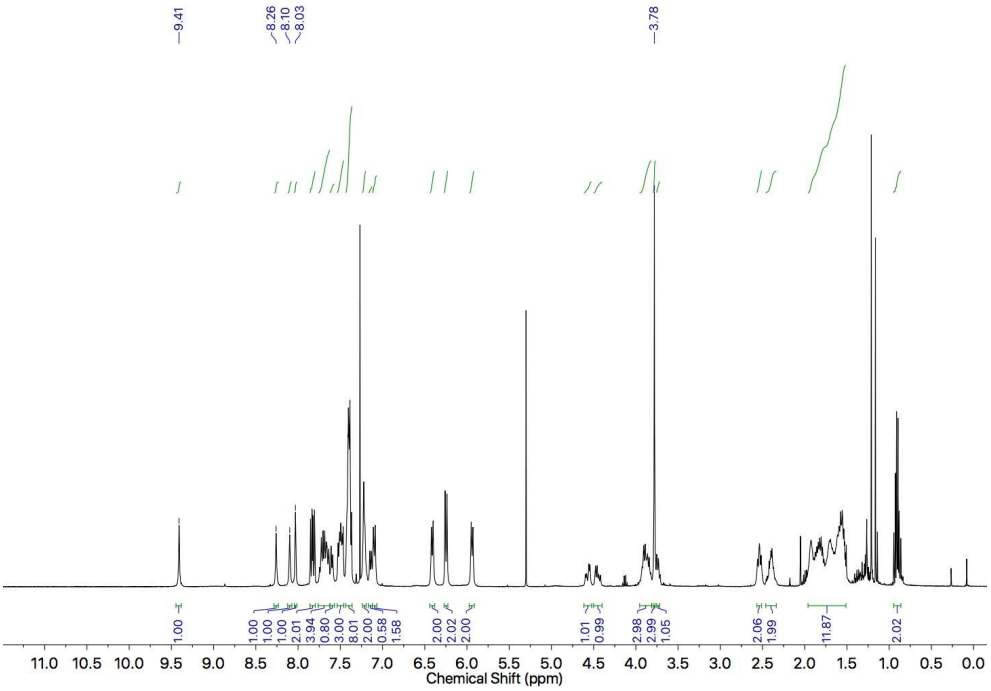

Figure 395: ^{1}H NMR of (S_{mp})-**113** ($CDCl_3$, 400 MHz).

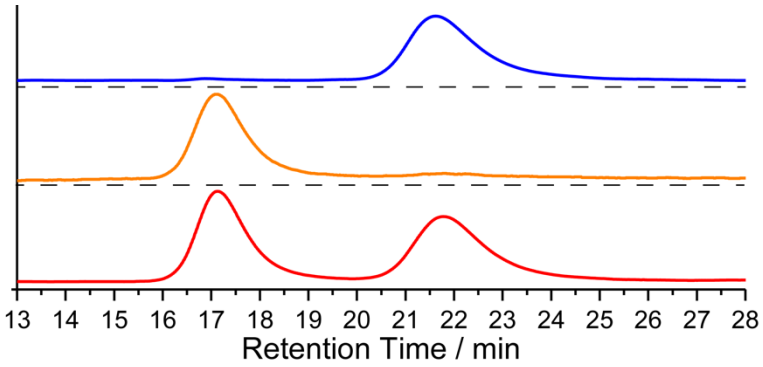

Figure 396: CSP-HPLC of **113** (loaded in EtOAc). RegisPackCLA, n-hexane-ethanol 80 : 20, flowrate 1.0 mLmin-1. Top (blue) (S_{mp})-**113**, (R_{mp})-**113** (16.9 min, 13038, 0.6%), (S_{mp})-**113** (21.6 min, 2350108, 99.4%). Middle (orange) (R_{mp})-**113**, (R_{mp})- **113** (17.1 min, 327587, 98.3%), (S_{mp})-**113** (21.8 min, 5820, 1.7%). Bottom (red) *rac*-**113** (R_{mp})-**113** (17.1 min, 1110899, 50.2%), (S_{mp})- **113** (21.8 min, 1102314, 49.8%).

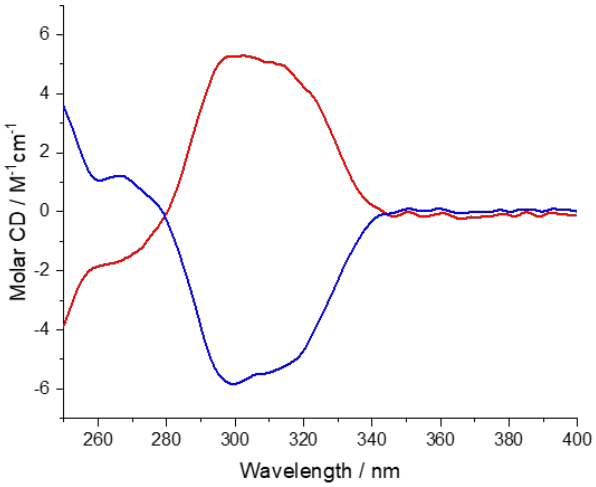

Figure 397: Circular Dichroism Spectra of (R_{mp})-**113** (24.1 µM, *er* 99 : 1, red) and (S_{mp})-**113** (22.3 µM, *er* 1 : 99, blue) at 293 K in $CHCl_3$.

Rotaxane **143**

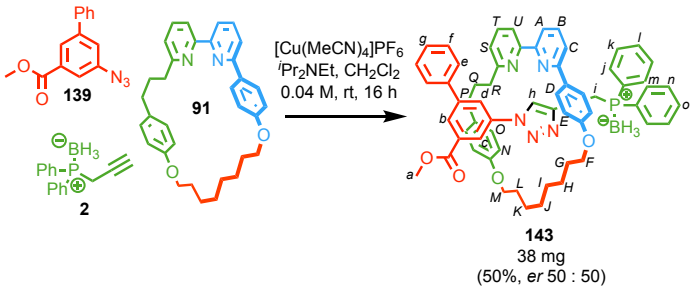

A dry CEM MW vial was charged with **139** (20.0 mg, 0.0790 mmol, 1.0 eq.), **2** (18.8 mg, 0.0790 mmol, 1.0 eq.), **91** (38.9 mg, 0.0790 mmol, 1.0 eq.) and $[Cu(MeCN)_4]PF_6$ (28.3 mg, 0.0758 mmol, 0.96 eq.), then purged with N_2. The mixture was dissolved in anhydrous CH_2Cl_2 (2.0 mL) and $^iPr_2NEt$ (55 µL, 0.316 mmol, 4.0 eq.) was added. The solution stirred at room temperature for 16 h. The solution was washed with EDTA-NH_3 (15 mL), H_2O_2 (35 wt.%, 15 mL), brine (30 mL) and extracted in CH_2Cl_2 (3 x 15 mL). The combined organic layers were dried over $MgSO_4$ and concentrated *in vacuo*. The residue was purified by column chromatography (SiO_2, petrol-EtOAc 0→20%) yielding a yellow foam **143** (38.2 mg, 0.0387 mmol, 50%). δ_H ($CDCl_3$, 400 MHz) 9.46 (1H, d, J = 1.8, H_h), 8.26 (1H, br. s, H_d), 8.24 (1H, br. s, H_c), 8.00 (1H, br. s, H_b), 7.80-7.69 (7H, m, H_B, H_j, H_l, H_m, H_o), 7.62-7.57 (2H, m, H_A, H_T), 7.42-7.29 (7H, m, H_U, H_h, H_k, H_n), 7.24 (1H, br. d, J = 7.7, H_S), 7.22-7.14 (4H, m, H_C, H_e, H_g), 6.88 (2H, d, J = 8.7, H_D), 6.40 (2H, d, J = 8.5, H_O), 5.93 (2H, d, J = 8.6, H_E), 5.88 (2H, d, J = 8.5, H_N), 3.92-3.86 (1H, m, H_R), 3.83-3.77 (2H, m, $H_{R'}$, H_P), 3.76 (3H, s, H_a), 3.73-3.67 (1H, m, $H_{P'}$), 3.49 (1H, br. d, J = 11.3, H_i), 3.47 (1H, br. d, J = 10.4, $H_{i'}$), 2.65-2.49 (2H, m, H_F), 2.47-2.32 (2H, m, H_M), 1.52-1.92 (14H, m, H_Q, H_G, H_H, H_I, H_J, H_K, H_L). δ_C ($CDCl_3$, 101 MHz) 166.6, 163.2, 159.2, 158.3, 157.9, 157.8, 156.8, 141.1, 138.9,137.7 (2C, d, J_{CP} = 3.4), 137.2, 137.1, 136.8, 132.8 (2C, d, J_{CP} = 6.6), 132.7 (2C, J_{CP} = 6.7), 132.0, 131.4, 131.2, 130.5, 128.9, 128.8, 128.7, 128.5 (2C), 127.8, 127.6, 127.0, 126.1, 123.0, 122.4, 120.0, 119.9, 119.7, 119.14, 113.84, 113.34, 67.5, 66.2, 52.0, 37.4, 34.9, 32.5, 29.1, 28.7, 28.7, 28.5, 25.8, 25.5, 24.7 (d, J_{CP} = 36.6). δ_P ($CDCl_3$, 202 MHz) 17.2.

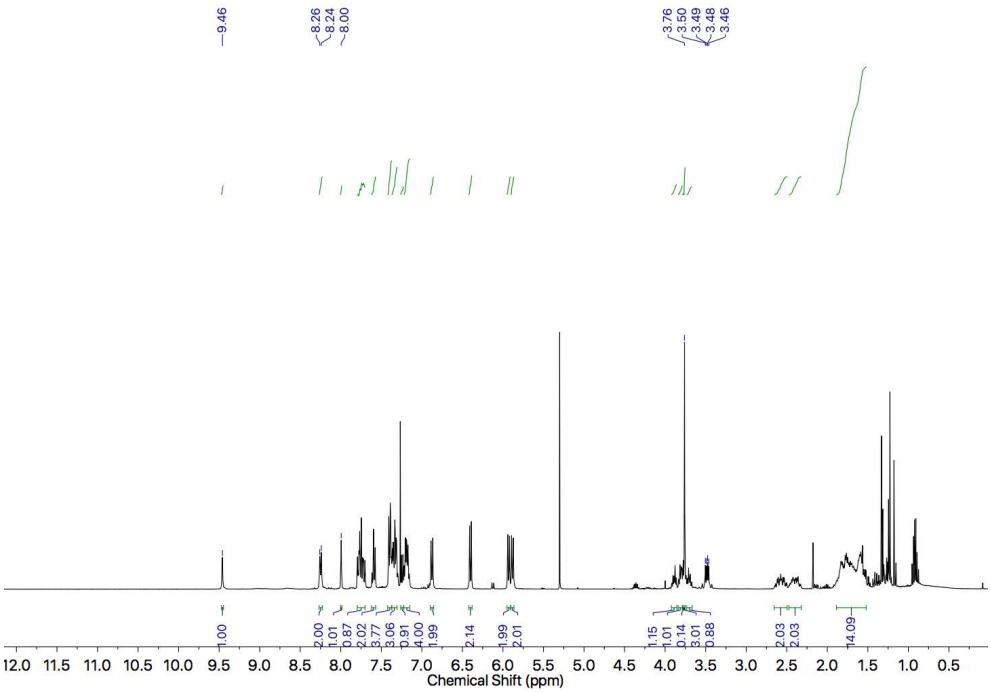

Figure 398: ^{1}H NMR of **143** ($CDCl_3$, 400 MHz).

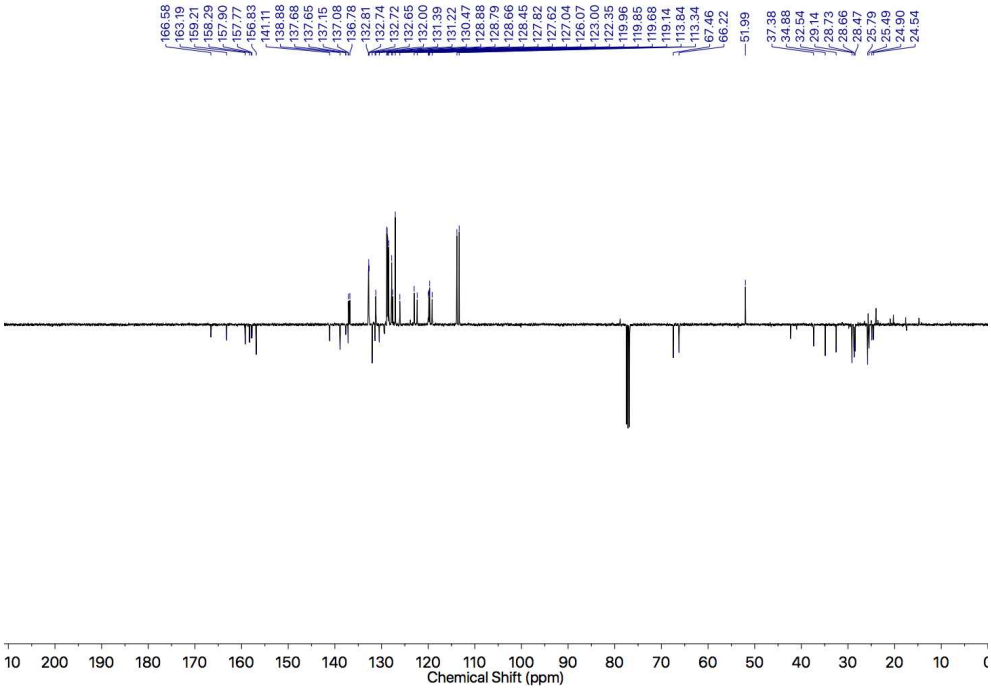

Figure 399: JMOD NMR of **143** ($CDCl_3$, 101 MHz).

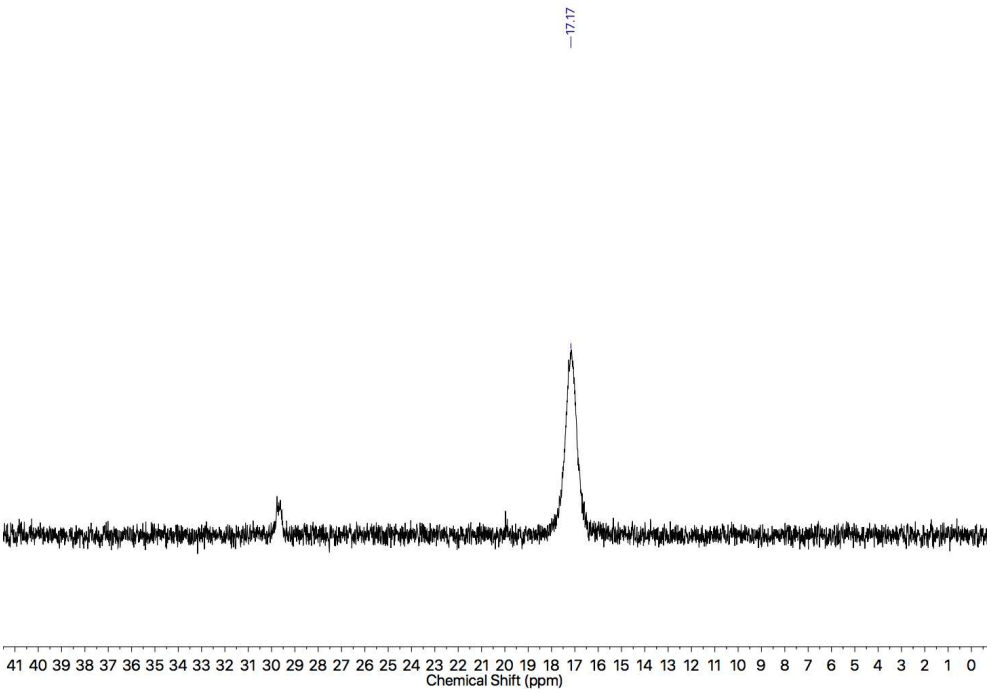

Figure 400: ^{31}P NMR of **143** ($CDCl_3$, 202 MHz).

Rotaxane **121**

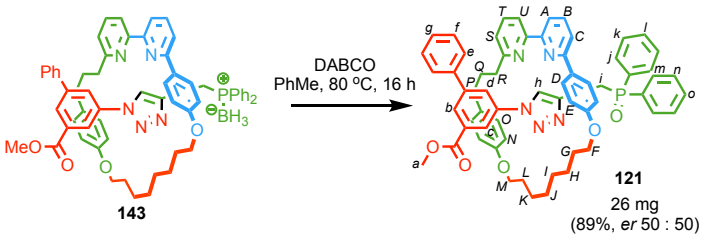

A dry CEM MW vial was charged with **143** (30.0 mg, 0.0305 mmol, 1.0 eq.) and DABCO (4.1 mg, 0.0366 mmol, 1.2 eq.), purged with N_2. Anhydrous PhMe (0.6 mL) was added, and the solution was refluxed at 70 °C for 16 h. The reaction was concentrated *in vacuo*, diluted in EtOAc and filtered through a short plug of SiO_2, then concentrated *in vacuo*. The residue was purified by column chromatography (SiO_2, petrol-EtOAc 40→100%) yielding a white foam **121** (26.2 mg, 0.0270 mmol, 89%, *er* 50 : 50). Enantiopurity determined by chiral stationary phase HPLC loaded in EtOAc ((*S*,*S*)-Whelk, *n*-hexane-EtOH 70 : 30, flowrate 1.0 mLmin^{-1}, retention times 31.1 min (50.1%), 36.2 min (49.9%)). $\boldsymbol{\delta}_H$ ($CDCl_3$, 400 MHz) 9.43 (1H, d, *J* = 1.9, $\boldsymbol{H}_h$), 8.24 (1H, br. app. t, *J* = 1.5, $\boldsymbol{H}_b$), 8.19 (1H, br. app. t, *J* = 1.6, $\boldsymbol{H}_d$), 7.98 (1H, app. t, *J* = 1.6, $\boldsymbol{H}_c$), 7.89-7.83 (2H, m, $\boldsymbol{H}_j$), 7.77-7.69 (3H, m, $\boldsymbol{H}_m$, $\boldsymbol{H}_B$), 7.61 (1H, t, *J* = 7.8, $\boldsymbol{H}_T$), 7.59 (1H, br. d, *J* = 7.6, $\boldsymbol{H}_A$), 7.41 (1H, br. d, *J* = 7.6, $\boldsymbol{H}_U$), 7.39-7.28 (7H, m, $\boldsymbol{H}_g$, $\boldsymbol{H}_k$, $\boldsymbol{H}_l$, $\boldsymbol{H}_n$, $\boldsymbol{H}_o$), 7.26 (1H, br. d, *J* = 7.7, $\boldsymbol{H}_S$), 7.22-7.14 (5H, m, $\boldsymbol{H}_C$, $\boldsymbol{H}_e$, $\boldsymbol{H}_f$), 6.91 (2H, d, *J* = 8.6, $\boldsymbol{H}_D$), 6.42 (2H, d, *J* = 8.4, $\boldsymbol{H}_O$), 6.12 (2H, dt, *J* = 8.7, 2.4, $\boldsymbol{H}_E$), 5.86 (2H, d, *J* = 8.4, $\boldsymbol{H}_N$), 3.91-3.76 (3H, m, $\boldsymbol{H}_F$, $\boldsymbol{H}_{F'}$, $\boldsymbol{H}_M$), 3.73 (3H, s, $\boldsymbol{H}_a$), 3.67-3.61 (1H, m, $\boldsymbol{H}_{M'}$), 3.56 (1H, dd, *J* = 15.5, 13.0, $\boldsymbol{H}_i$), 3.45 (1H, dd, *J* = 15.2, 15.2, $\boldsymbol{H}_{i'}$), 2.57 (1H, ddd, *J* = 25.7, 12.9, 4.9, $\boldsymbol{H}_R$), 2.52 (1H, ddd, *J* = 25.6, 12.9, 4.9, $\boldsymbol{H}_{R'}$), 2.39 (2H, app. t, *J* = 6.0, $\boldsymbol{H}_P$), 1.86-1.67 (6H, m, $\boldsymbol{H}_Q$, $\boldsymbol{H}_G$, $\boldsymbol{H}_L$), 0.98-0.77 (8H, m, $\boldsymbol{H}_H$, $\boldsymbol{H}_I$, $\boldsymbol{H}_J$, $\boldsymbol{H}_K$). $\boldsymbol{\delta}_C$ ($CDCl_3$, 101 MHz) 166.6, 163.5, 159.4, 158.6, 157.7, 157.7, 156.8, 141.2, 139.0, 137.3, 137.0 (d, J_{CP} = 24.8), 137.0, 136.9, 131.9, 131.7, 130.7, 130.7 (2C), 131.6 (d, J_{CP} = 9.4), 131.2 (d, J_{CP} = 9.3), 130.5, 128.8, 128.7 (d, J_{CP} = 4.1), 128.6 (d, J_{CP} = 4.4), 128.5 (2C), 127.9, 127.6, 127.0, 126.2, 124.0, 122.9, 122.4, 119.9, 119.8, 119.8, 119.4, 114.0, 113.4, 66.8 (d, J_{CP} = 127.3), 52.0, 37.4, 34.9, 32.8, 29.9, 29.5, 29.1, 28.7, 28.4, 25.8, 25.5, 22.9. $\boldsymbol{\delta}_P$ ($CDCl_3$, 202 MHz) 29.2. HR-ESI-MS $[M+H]^+$ m/z 986.4382 (calc. for $C_{62}H_{61}N_5O_5P$ m/z 986.4405).

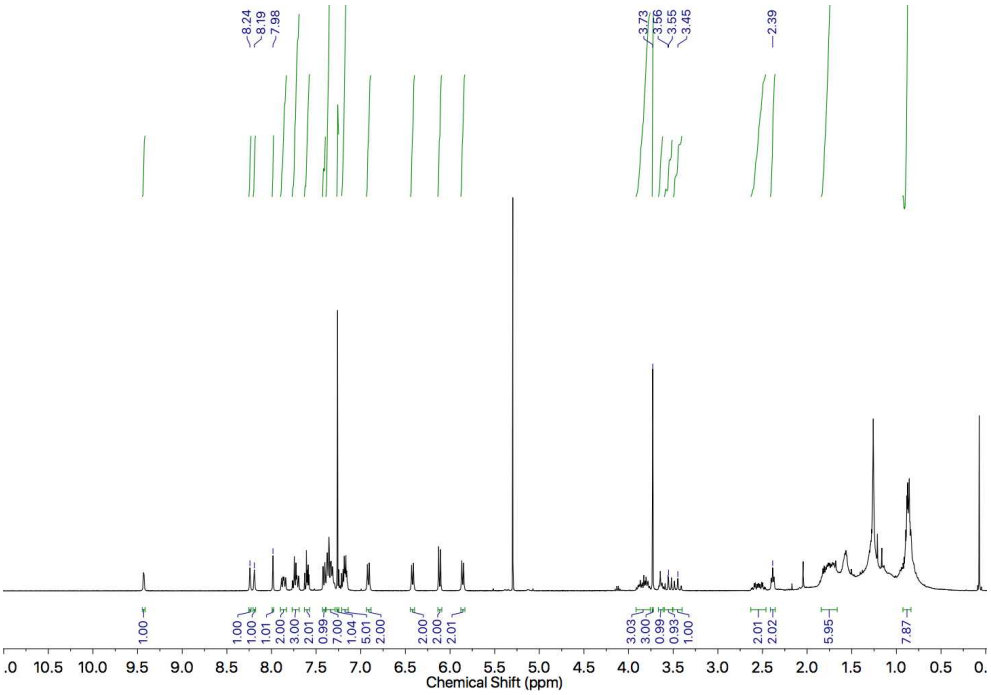

Figure 401: ^{1}H NMR of **121** ($CDCl_3$, 400 MHz).

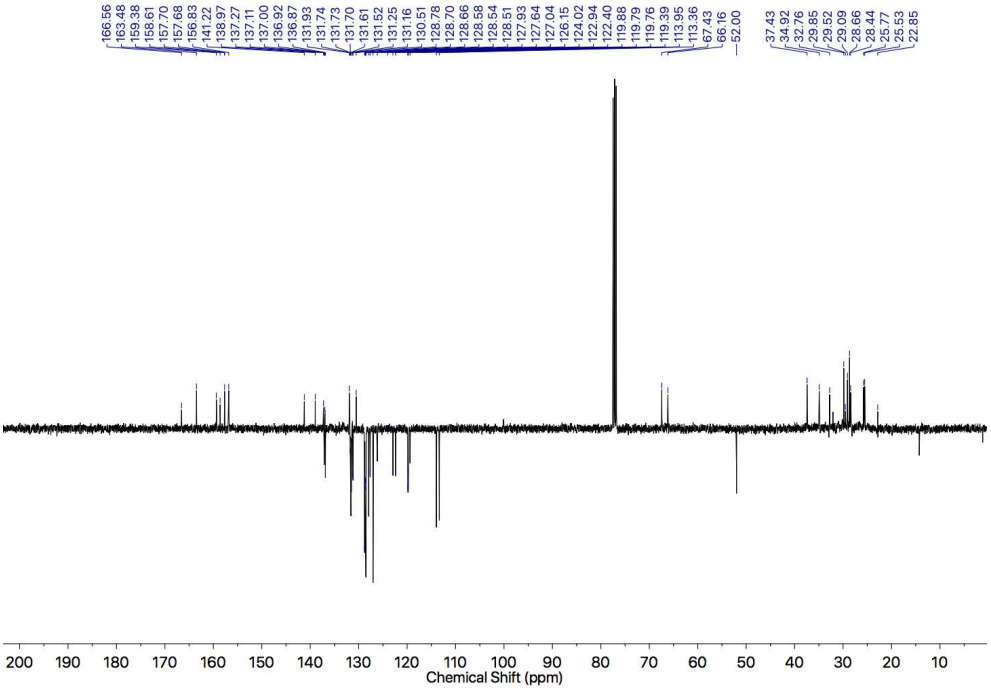

Figure 402: JMOD NMR of **121** ($CDCl_3$, 101 MHz).

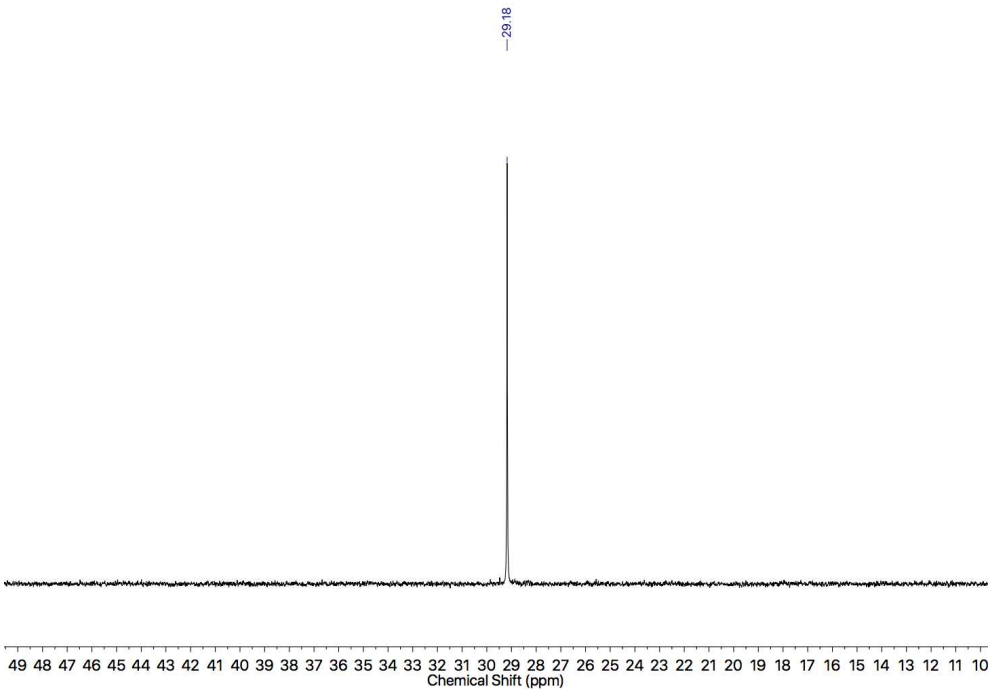

Figure 403: $^{31}P\{1H\}$ NMR of **121** ($CDCl_3$, 202 MHz).

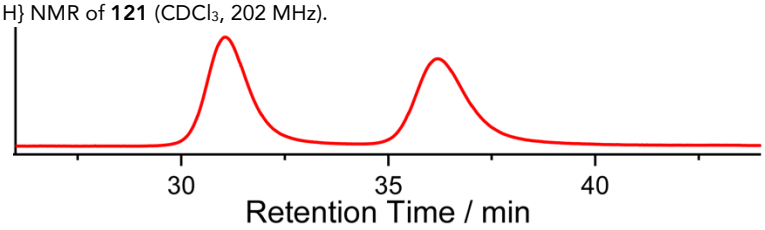

Figure 404: CSP-HPLC of *rac*-**121** (loaded in EtOAc). (*S*,*S*)-Whelk, *n*-hexane-ethanol 70 : 30, flowrate 1.0 $mLmin^{-1}$, retention times (R_{mp})-**121** (31.1 min, 1421174, 50.1%), (S_{mp})-**121** (36.2 min, 1415154, 49.9%).

Rotaxane (S,S_{mp})-**144**

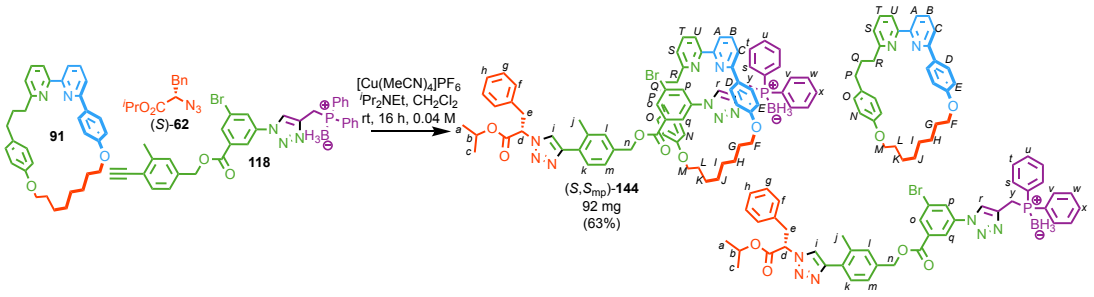

A dry CEM MW vial was charged with **91** (53.5 mg, 0.109 mmol, 1.0 eq.), **118** (66.0 mg, 0.109 mmol, 1.0 eq.), (*S*)-**62** (25.3 mg, 0.109 mmol, 1.0 eq.) and $[Cu(MeCN)_4]PF_6$ (39.0 mg, 0.104 mmol, 0.96 eq.), then purged with N_2. Anhydrous CH_2Cl_2 (2.7 mL) and $^iPr_2NEt$ (76 µL, 56 mg, 0.434 mmol, 4.0 eq.) was added and the reaction stirred at room temperature for 16 h. The reaction was washed with EDTA-NH_3 (0.1 M, 20 mL), brine (30 mL), and extracted in CH_2Cl_2 (3 x 30 mL). The combined organic layers were dried over $MgSO_4$ and concentrated *in vacuo*. The residue was purified by column chromatography (SiO_2, petrol-EtOAc 0→25%) yielding a yellow foam (S,S_{mp})-**144** (91.8 mg, 0.0688 mmol, 63%). Mixture of two co-conformations in dynamic exchange. δ_H ($CDCl_3$, 400 MHz) 9.35 (1H, d, J = 2.1, H_r), 8.25 (1H, app. t, J = 1.6, H_q), 8.14 (1H, app. t, J = 1.7, H_p), 7.81 (1H, br. dd, J = 1.6, 1.4, H_o), 7.79 (1H, t, J = 7.8, H_B), 7.77-7.70 (4H, m, H_s, H_v), 7.67 (1H, br. s, H_k), 7.65 (1H, t, J = 7.8, H_T), 7.57 (1H, dd, J = 7.8, 0.9, H_A), 7.45 (1H, dd, J = 7.8, 0.8, H_U), 7.37-7.32 (2H, m, H_u, H_x), 7.32-7.29 (2H, m, H_t), 7.29 (1H, dd, J = 7.9, 0.9, H_C), 7.27 (1H, dd, J = 7.9, 0.9, H_S), 7.25-7.19 (4H, m, H_h, H_i, H_w), 7.17 (1H, br. s, H_l), 7.14 (1H, br. dd, J = 7.8, 1.6, H_m), 7.10-7.06 (4H, m, H_f, H_g), 6.80 (2H, dt, J = 8.8, 2.4, H_D), 6.42 (2H, br. d, J = 8.5, H_O), 5.94 (2H, dt, J = 8.8, 2.5, H_E), 5.91 (2H, br. d, J = 8.5, H_N), 5.64 (1H, app. t, J = 7.5, H_d), 5.14 (1H, d, J = 12.1, H_n), 5.08 (1H, sept., J = 6.2, H_b), 5.05 (1H, d, J = 12.2, $H_{n'}$), 3.89-3.76 (4H, m, H_F, H_M), 3.63 (1H, dd, J = 15.0, 11.7, H_y), 3.52 (2H, d, J = 7.3, H_e), 3.45 (1H, dd, J = 15.1, 10.3, $H_{y'}$), 2.70-2.46 (4H, m, H_P, H_R), 2.34 (3H, s, H_j), 1.86-1.52 (10H, m, H_G, H_H, H_K, H_L, H_Q),1.24 (3H, d, J = 6.2, H_a), 1.19 (3H, d, J = 6.2, H_c), 0.95-0.86 (4H, m, H_I, H_J). δ_C ($CDCl_3$, 101 MHz) 167.9, 164.6, 163.2, 159.3, 158.1, 157.8, 157.8, 156.8, 146.4, 137.9, 137.9, 137.3, 137.2, 136.8, 135.7, 135.5, 134.8, 132.7 (d, J_{CP} = 9.5), 132.6 (d, J_{CP} = 9.5), 132.1, 131.4, 131.3, 131.3, 131.2, 131.0, 130.6, 130.0, 129.4 (d, J_{CP} = 7.4), 129.2, 129.1, 128.9 (d, J_{CP} = 8.1), 128.8 (d, J_{CP} = 8.3), 128.8, 128.7, 128.6, 127.7 (d, J_{CP} = 5.4), 127.3, 126.3, 122.4, 122.0, 121.6, 120.1, 119.9, 119.9, 119.3, 113.7, 113.2, 70.6, 67.2, 66.6, 66.1, 64.2, 39.2, 37.3, 34.8, 33.1,

29.1, 28.8, 28.6, 28.5, 25.6 (d, J_{CP} = 18.7), 24.9, 24.5, 24.0, 17.4. δ_P ($CDCl_3$, 202 MHz) 17.2. HR-ESI-MS $[M+H]^+$ m/z 1335.5 (calc. for $C_{77}H_{80}BBrN_8O_6P$ m/z 1335.5).

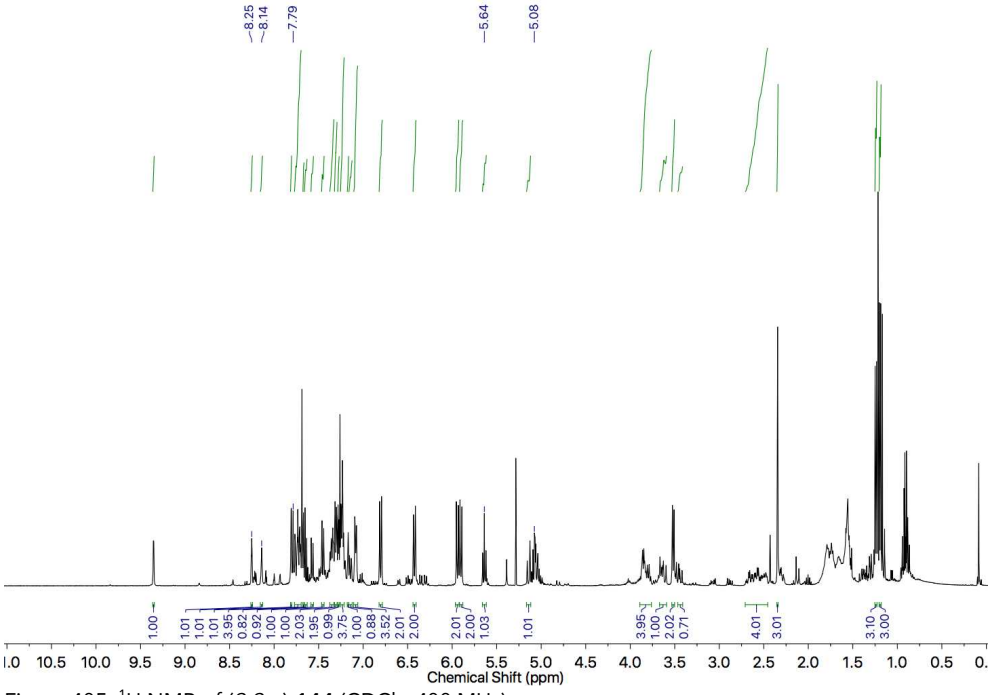

Figure 405: ^1H NMR of (S,S_{mp})-**144** ($CDCl_3$, 400 MHz).

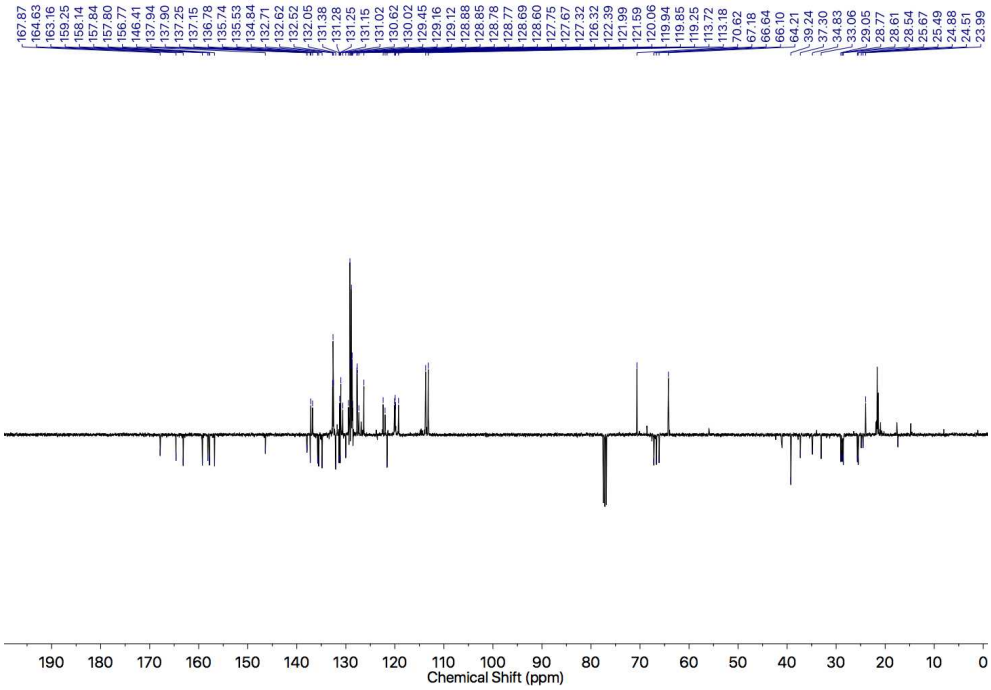

Figure 406: JMOD NMR of (S,S_{mp})-**144** ($CDCl_3$, 101 MHz).

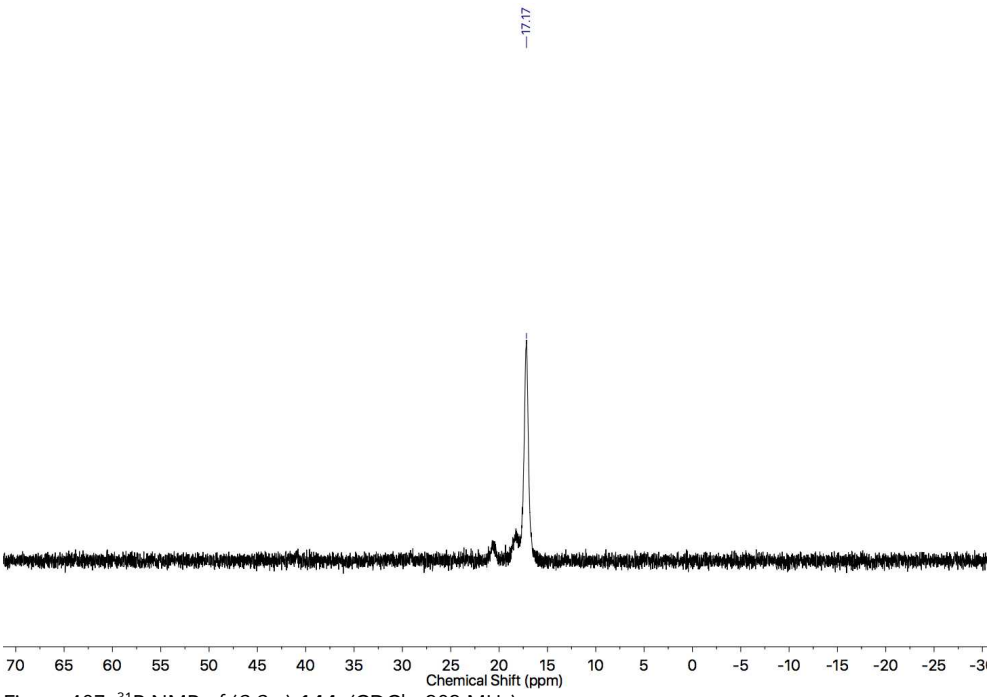

Figure 407: ^{31}P NMR of (S,S_{mp})-**144** ($CDCl_3$, 202 MHz).

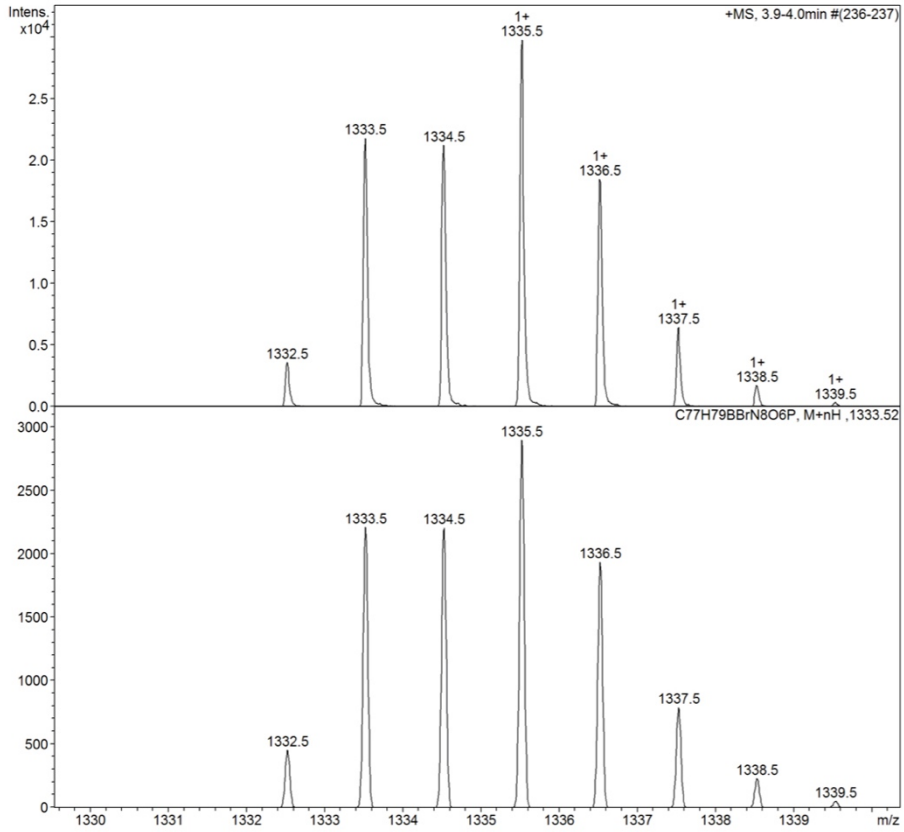

Figure 408: Isotope pattern of (S,S_{mp})-**144** $C_{77}H_{80}BBrN_8O_6P$.

Rotaxane (S,S_{mp})-**119**

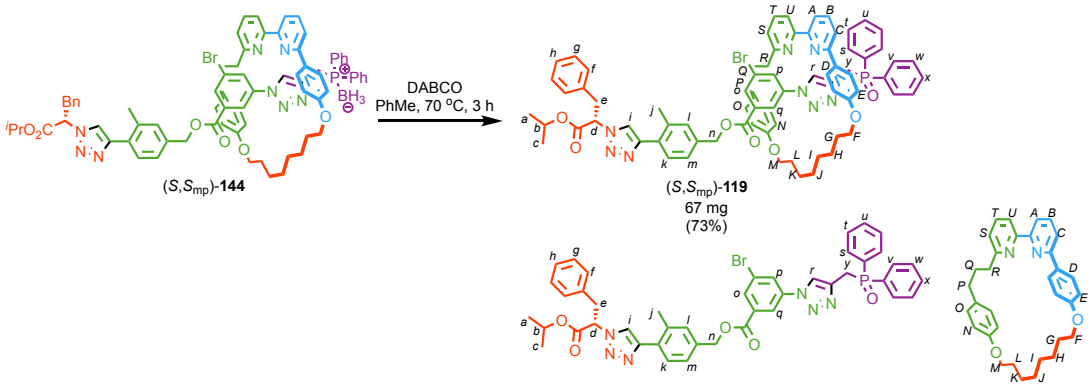

(S,S_{mp})-**144** (91.8 mg, 0.0688 mmol, 1.0 eq.) was refluxed at 70 °C under inert atmosphere with DABCO (23.2 mg, 0.206 mmol, 3.0 eq.) in anhydrous PhMe (1.4 mL) for 3 h. The reaction was concentrated *in vacuo* onto SiO_2, and purified by column chromatography (SiO_2, petrol-EtOAc 0→70%) yielding a white foam (S,S_{mp})-**119** (67 mg, 0.0502 mmol, 73%). Mixture of two co-conformations in dynamic exchange. δ_H ($CDCl_3$, 400 MHz) 9.28 (1H, d, J = 2.1, H_r), 8.22 (1H, br. app. t, J = 1.7, H_q), 8.14 (1H, br. app. t, J = 1.7, H_p), 7.87-7.79 (3H, m, H_s, H_o), 7.78 (1H, t, J = 7.7, H_B), 7.73-7.66 (4H, m, H_v, H_x, H_k), 7.65 (1H, t, J = 7.7, H_T), 7.58 (1H, d, J = 7.7, H_A), 7.46 (1H, d, J = 7.7, H_U), 7.42-7.29 (5H, m, H_t, H_u, H_w, H_), 7.29-7.25 (2H, m, H_C, H_S), 7.25-7.19 (4H, m, H_g, H_h, H_i), 7.17 (1H, br. s, H_l), 7.15 (1H, br. dd, J = 7.9, 1.7, H_m), 7.08 (2H, dd, J = 7.7, 2.2, H_f), 6.84 (2H, dt, J = 8.7, 1.8, H_D), 6.42 (2H, br. d, J = 8.5, H_O), 6.13 (2H, br. d, J = 8.7, H_E), 5.84 (2H, dt, J = 8.5, 2.5, H_N), 5.63 (1H, app. t, J = 7.4, H_d), 5.16-5.04 (3H, m, H_b, H_n, $H_{n'}$), 3.86 (2H, t, J = 5.9, H_M), 3.82-3.75 (1H, m, H_F), 3.61-3.55 (3H, m, H_y, $H_{F'}$), 3.51 (2H, d, J = 7.5, H_e), 2.67 (1H, td, J = 12.8, 4.6, H_R), 2.56 (1H, td, J = 12.8, 5.0, $H_{R'}$), 2.50-2.41 (1H, m, H_P), 2.37-2.29 (1H, m, $H_{P'}$), 2.34 (3H, s, H_j), 1.84-1.46 (10H, m, H_G, H_H, H_K, H_L, H_Q), 1.24 (3H, d, J = 6.3, H_a), 1.19 (3H, d, J = 6.3, H_c), 0.94-0.82 (4H, m, H_I, H_J). δ_C ($CDCl_3$, 101 MHz) 167.88, 164.63, 163.52, 159.40, 158.43, 157.67 (2C), 156.74, 146.43, 137.34, 137.27, 137.18, 136.86, 135.7 (d, J_{CP} = 21.7), 134.85, 133.74, 132.8 (d, J_{CP} = 21.7), 132.04, 131.80 (d, J_{CP} = 2.5),131.7 (d, J_{CP} = 2.5), 131.5 (d, J_{CP} = 9.5), 131.31, 131.18, 131.1 (d, J_{CP} = 9.5), 130.96, 130.67, 130.04, 129.46, 129.17, 129.14, 128.87, 128.81, 128.7 (d, J_{CP} = 5.0), 128.60 (d, J_{CP} = 5.0), 127.84, 127.68, 127.42, 126.26, 123.8, 122.47, 122.00, 121.61, 120.02, 119.85, 119.82, 119.48, 113.83, 113.16, 70.63, 67.14, 66.65, 66.03, 64.22, 41.05, 39.25, 37.38, 34.85, 33.26, 29.01, 28.6 (d, J_{CP} = 20.2), 28.64, 25.64, 25.52,

24.01, 21.74, 21.64, 17.42. δ_P ($CDCl_3$, 202 MHz) 30.2 ($P_{minor\ co\text{-}conf}$), 29.1 ($P_{major\ co\text{-}conf}$). HR-ESI-MS $[M+H]^+$ m/z 1337.5 (calc. for $C_{77}H_{76}BrN_8O_7P$ m/z 1337.5).

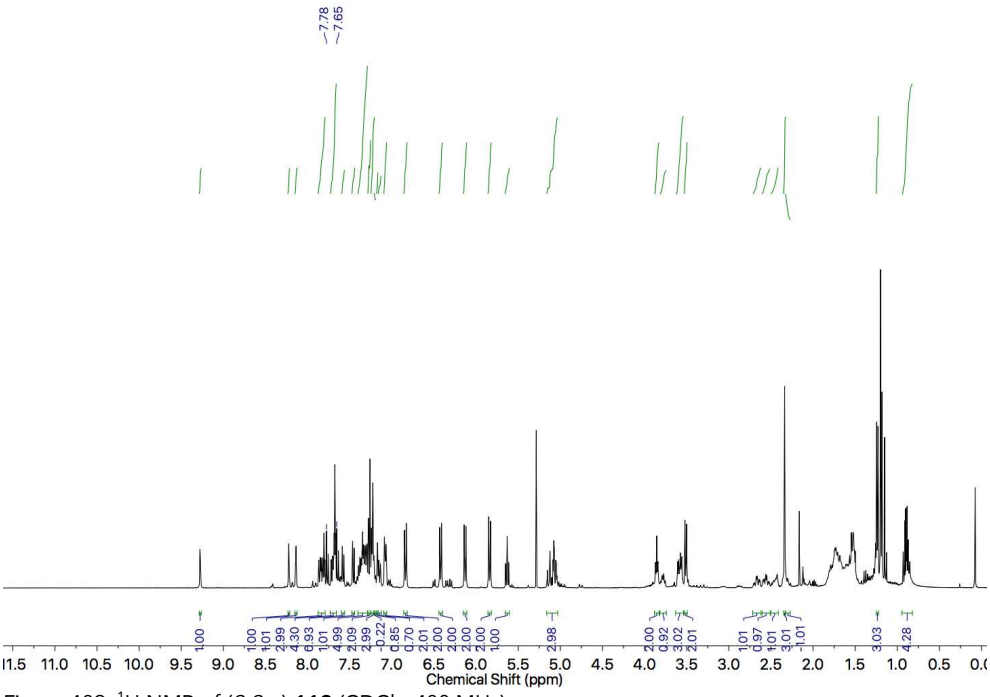

Figure 409: ^1H NMR of (S,S_{mp})-**119** ($CDCl_3$, 400 MHz).

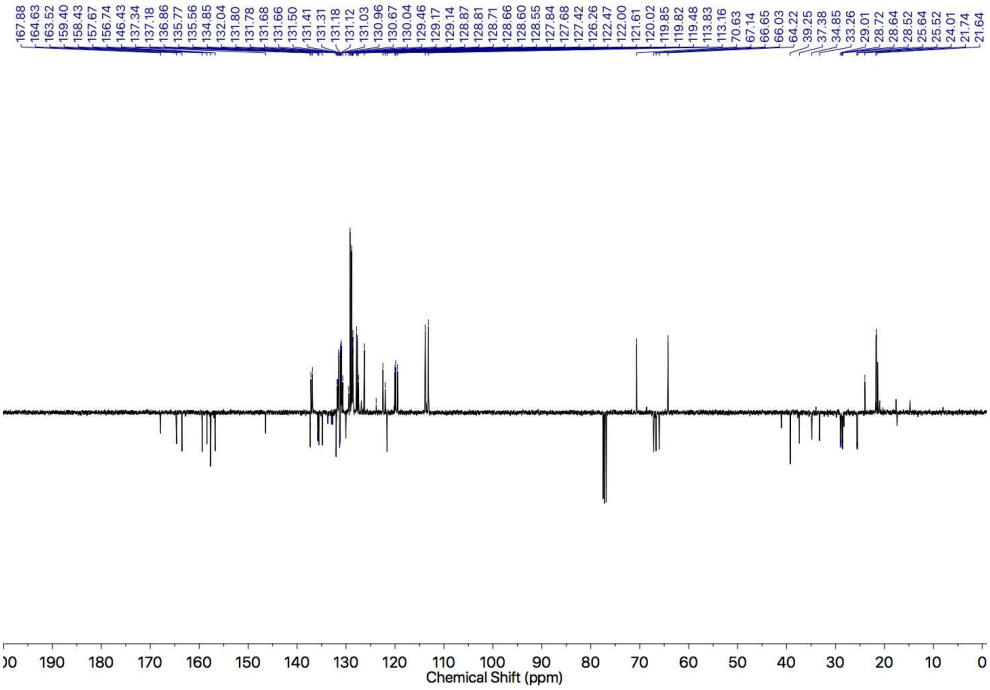

Figure 410: JMOD NMR of (S,S_{mp})-**119** ($CDCl_3$, 101 MHz).

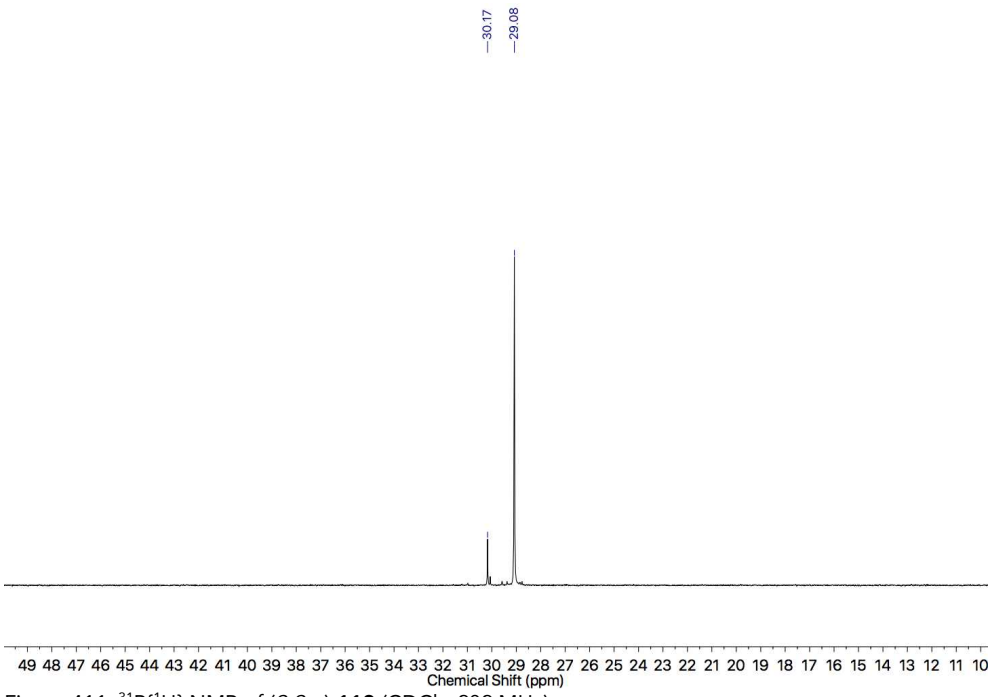

Figure 411: $^{31}P\{^{1}H\}$ NMR of (S,S_{mp})-**119** ($CDCl_3$, 202 MHz).

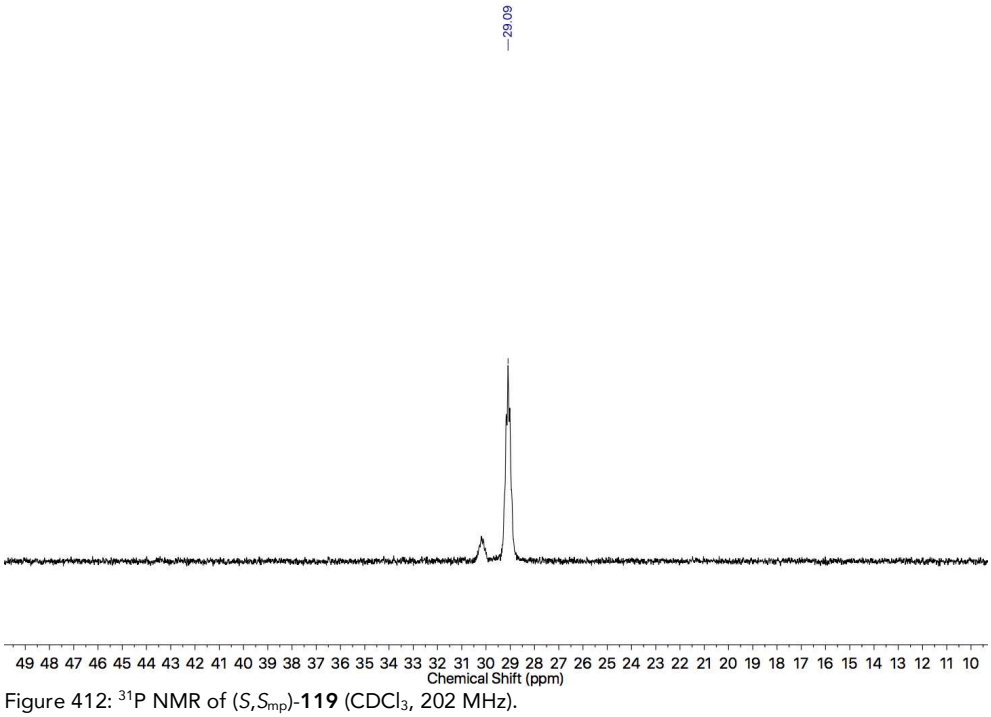

Figure 412: ^{31}P NMR of (S,S_{mp})-**119** ($CDCl_3$, 202 MHz).

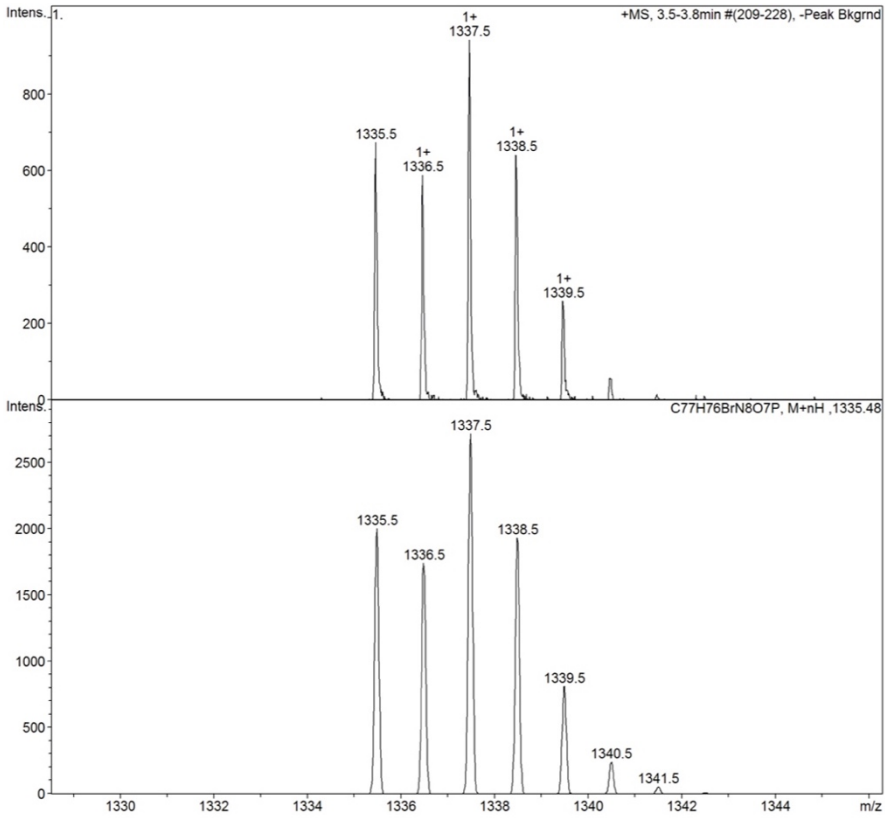

Figure 413: Isotope pattern of (*S*,*S*$_{mp}$)-**119** $C_{77}H_{76}BrN_8O_7P$.

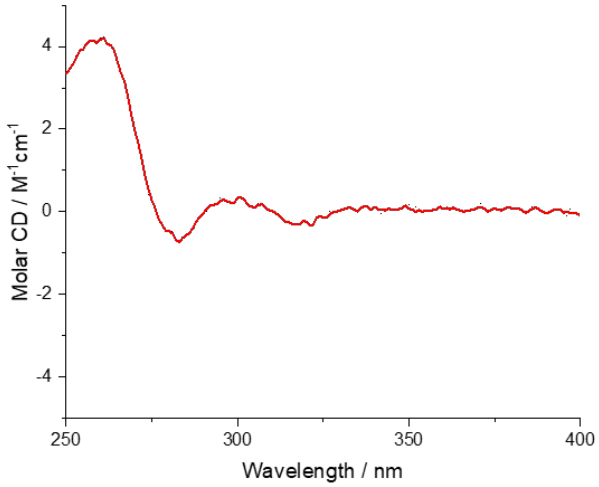

Figure 414: Circular Dichroism Spectra of (*S*,*S*$_{mp}$)-**119** (22.1 µM, red) at 293 K in $CHCl_3$.

Rotaxane (*S*$_{mp}$)-**121**

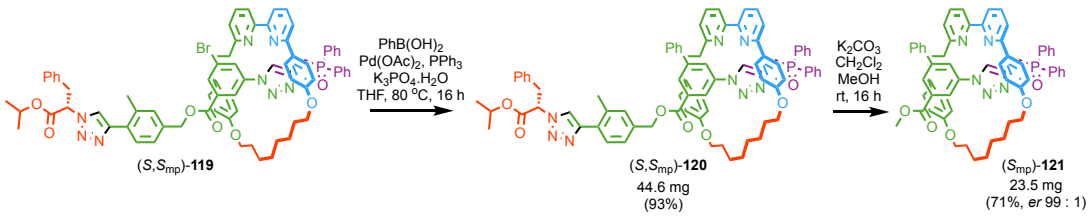

A CEM MW vial was charged with (S,S_{mp})-**119** (48 mg, 0.0359 mmol, 1.0 eq.), $PhB(OH)_2$ (13.1 mg, 0.108 mmol, 3.0 eq.), $Pd(OAc)_2$ (0.81 mg, 0.0036 mmol, 0.10 eq.), PPh_3 (1.9 mg, 0.0072 mmol, 0.20 eq.) and $K_3PO_4.H_2O$ (24.8 mg, 0.108 mmol, 3.0 eq.) and purged with N_2. Anhydrous THF (1.4 mL) was added and the solution refluxed at 80 °C for 16 h. The reaction was diluted in CH_2Cl_2 (15 mL), washed with brine (20 mL) and extracted in CH_2Cl_2 (3 x 20 mL). The combined organic layers were dried over $MgSO_4$ and concentrated *in vacuo*. The residue was purified by column chromatography (SiO_2, petrol-EtOAc 30→70%) yielding a yellow foam (S,S_{mp})-**120** (44.6 mg, 0.0334 mmol, 93%, co-conformational ratio 86 : 14). A CEM MW flask was charged with (S,S_{mp})-**120** (44.6 mg, 0.0334 mmol, 1.0 eq.) and K_2CO_3 (23.1 mg, 0.167 mmol, 5.0 eq.) and purged with N_2. Anhydrous CH_2Cl_2 (0.5 mL) and anhydrous MeOH (1.0 mL). were added and the solution stirred at room temperature for 16 h. The solution was diluted with CH_2Cl_2, dried over Na_2SO_4, and concentrated *in vacuo*. The residue was purified by column chromatography (SiO_2, petrol-EtOAc 50→70%) yielding a white foam (S_{mp})-**121** (23.5 mg, 0.0238 mmol, 71%, *er* 99 : 1). NMR spectroscopic data for the pure product matched that of the racemate obtained above. Enantiopurity determined by chiral stationary phase HPLC loaded in EtOAc ((S,S)-Whelk, *n*-hexane-ethanol 70 : 30, flowrate 1.0 $mLmin^{-1}$, retention times 31.4 min (1.1%), 36.4 min (98.9%).

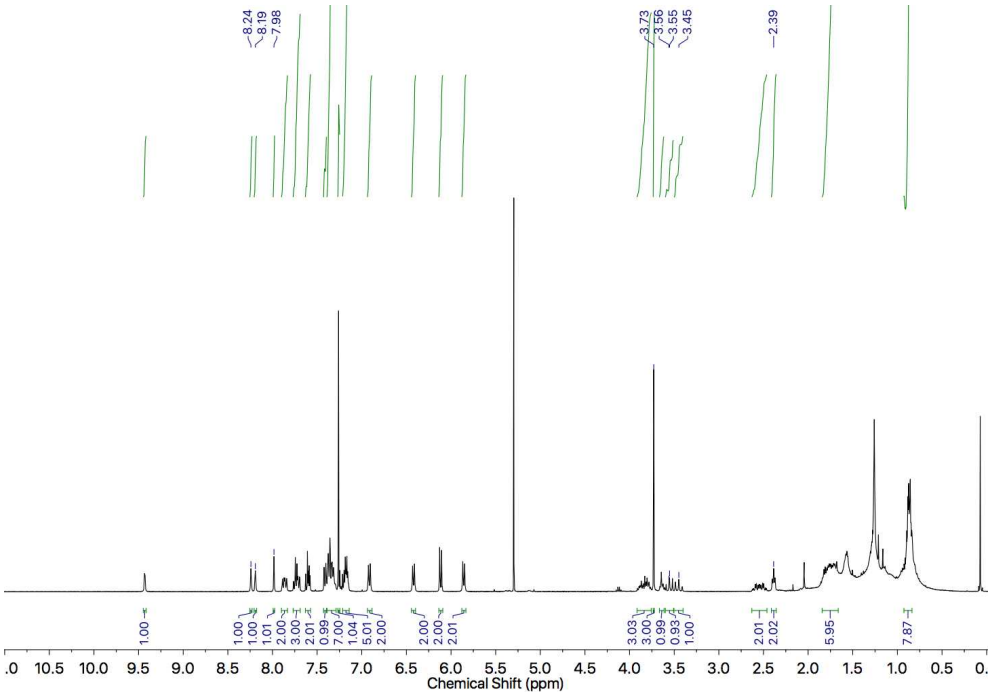

Figure 415: ^1H NMR of (S_{mp})-**121** ($CDCl_3$, 400 MHz).

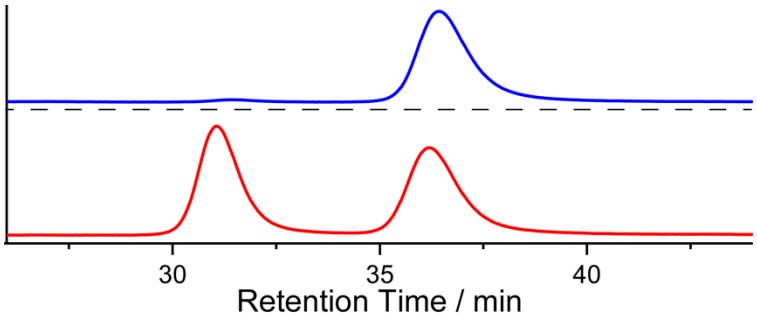

Figure 416: CSP-HPLC of (S_{mp})-**121** (loaded in EtOAc). (*S*,*S*)-Whelk, *n*-hexane-ethanol 70 : 30, flowrate 1.0 mLmin^{-1}. Top (blue) (S_{mp})-**121**, (R_{mp})-**121** (31.4 min, 27824, 1.1%), (S_{mp})-**121** (36.4 min, 2604380, 98.9%). Bottom (red) (*rac*)-**121**, (R_{mp})-**121** (31.1 min, 1429645, 50.1%), (S_{mp})-**121** (36.2 min, 1422629, 49.9%).

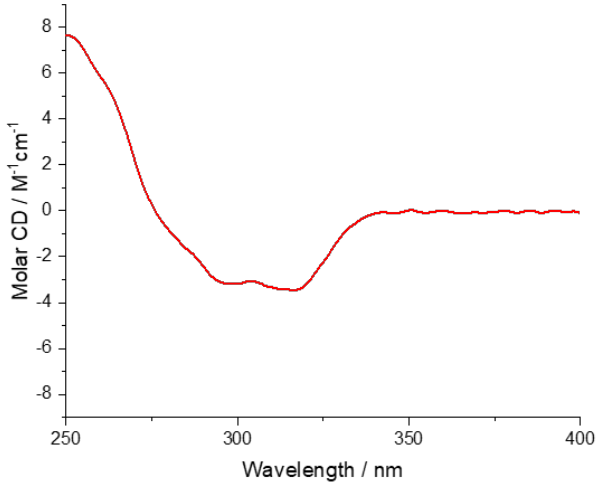

Figure 417: Circular Dichroism Spectra of (S_{mp})-**121** (25.1 µM, *er* 99 : 1, red) at 293 K in $CHCl_3$.

Rotaxane (S_{mp})-**122**

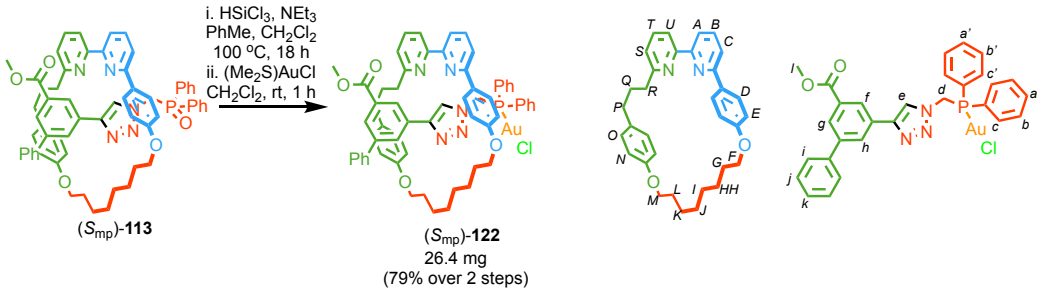

A Young's tap Schlenk tube was dried under vacuum and nitrogen three times. Anhydrous NEt_3 (194 µL, 141 mg, 1.39 mmol, 50 eq.) and $HSiCl_3$ (70 µL, 94 mg, 0.695 mmol, 25 eq.) were added. Subsequently (S_{mp})-**113** (27.4 mg, 0.0278 mmol, 1.0 eq.) was transferred in anhydrous PhMe (1.5 mL) and anhydrous CH_2Cl_2 (0.3 mL). The solution was heated at 100 °C for 18 h. The reaction was cooled to room temperature, diluted in CH_2Cl_2 (20 mL) and washed with NaOH (1 M, 5 x 20 mL). The combined organic layers were dried over $MgSO_4$ and concentrated *in vacuo* yielding a yellow oil. This was dissolved in anhydrous CH_2Cl_2 (0.6 mL) and stirred with (Me_2S)AuCl (9.0 mg, 0.0306, 1.1

eq.) for 1 h. The crude reaction was concentrated directly onto SiO_2 and purified by column chromatography (SiO_2, petrol-EtOAc 20→80%) yielding a white foam (S_{mp})-**122** (26.4 mg, 0.0220 mmol, 79%, *er* 99 : 1). δ_H ($CDCl_3$, 400 MHz) 9.62 (1H, s, H_e), 8.27 (1H, t, J = 1.6, H_f), 8.09 (1H, t, J = 1.7, H_h), 8.08 (1H, t, J = 1.7, H_g), 7.77 (1H, t, J = 7.8, H_B), 7.77 (1H, t, J = 7.8, H_T), 7.66 (1H, d, J = 7.5, H_A), 7.64-7.59 (3H, m, H_U, H_c), 7.57-7.51 (2H, m, $H_{c'}$), 7.49-7.43 (3H, m, H_a, $H_{a'}$, H_C), 7.43-7.33 (7H, m, H_b, $H_{b'}$, H_j, H_k), 7.24 (2H, dd, J = 5.2, 2.2, H_i), 7.17 (1H, dd, J = 7.7, 0.8, H_S), 7.05 (2H, dt, J = 8.7, 2.5, H_D), 6.31 (2H, dt, J = 8.5, 2.4, H_O), 6.26 (2H, dt, J = 8.8, 2.5, H_E), 6.07 (2H, dt, J = 8.6, 2.5, H_N), 4.61 (1H, dd, J = 15.3, 5.6, H_d), 4.54 (1H, dd, J = 15.3, 4.2, $H_{d'}$), 3.97-3.84 (4H, m, H_F, H_M), 3.81 (3H, s, H_l), 2.59-2.42 (2H, m, H_R), 2.36 (2H, t, J = 6.2, H_P), 1.96-1.50 (10H, m, H_G, H_H, H_K, H_L, H_Q), 0.92-0.83 (4H, H_I, H_J). δ_C ($CDCl_3$, 101 MHz) 167.34, 163.28, 159.67, 158.79, 158.17, 157.46, 157.05, 146.32, 140.62, 139.92, 137.34, 137.21, 133.9 (d, J_{CP} = 13.8), 133.6 (d, J_{CP} = 13.7), 132.6 (d, J_{CP} = 2.6), 132.6 (d, J_{CP} = 2.5), 131.94, 131.72, 130.99, 130.26, 129.7 (d, J_{CP} = 10.1), 129.6 (d, J_{CP} = 10.2), 129.26, 128.68, 128.32, 127.36, 127.28, 126.96, 126.69, 126.64, 126.39, 126.06, 125.42, 122.32, 120.42, 120.17, 119.75, 114.30, 113.93, 68.11, 66.74, 52.05, 47.3 (d, J_{CP} = 38.9), 37.53, 34.92, 31.63, 29.32, 28.66, 28.57, 28.46, 25.95, 25.68. δ_P ($CDCl_3$, 202 MHz) 28.2. HR-ESI-MS $[M\text{-}Cl]^+$ m/z 1166.4 (calc. for $C_{62}H_{60}O_4N_5PAu$ m/z 1166.4).

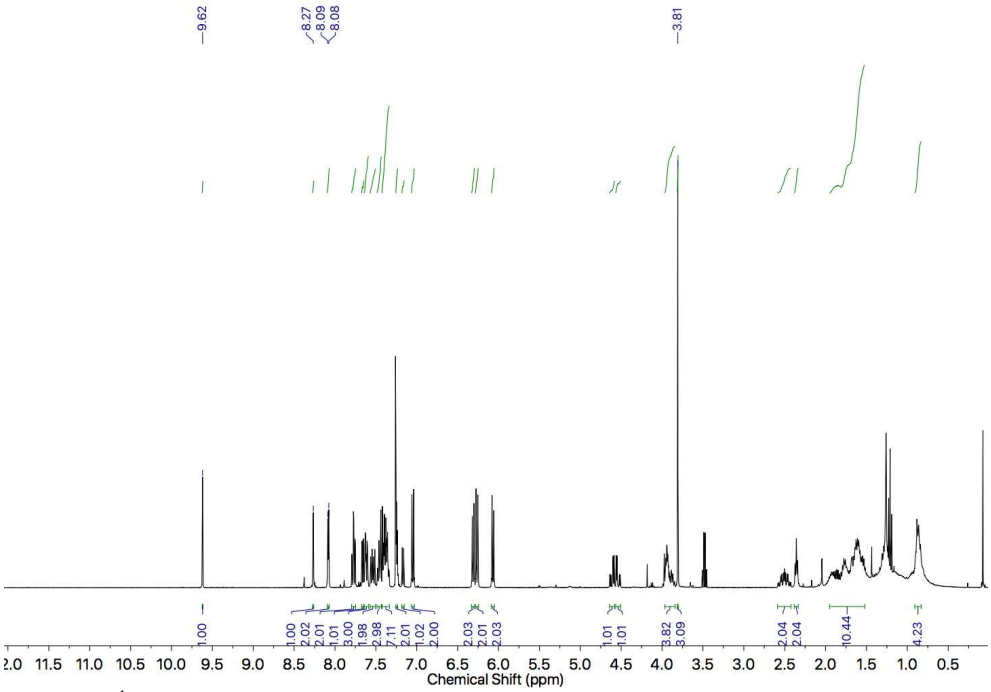

Figure 418: ^1H NMR of (S_{mp})-**122** ($CDCl_3$, 400 MHz).

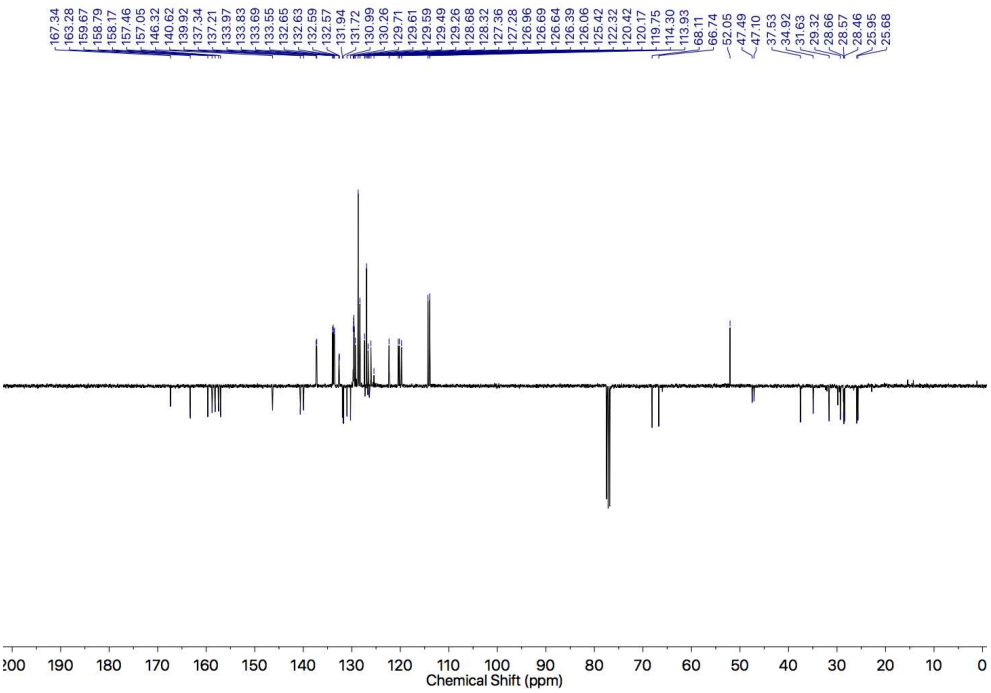

Figure 419: JMOD NMR of (S_{mp})-**122** ($CDCl_3$, 101 MHz).

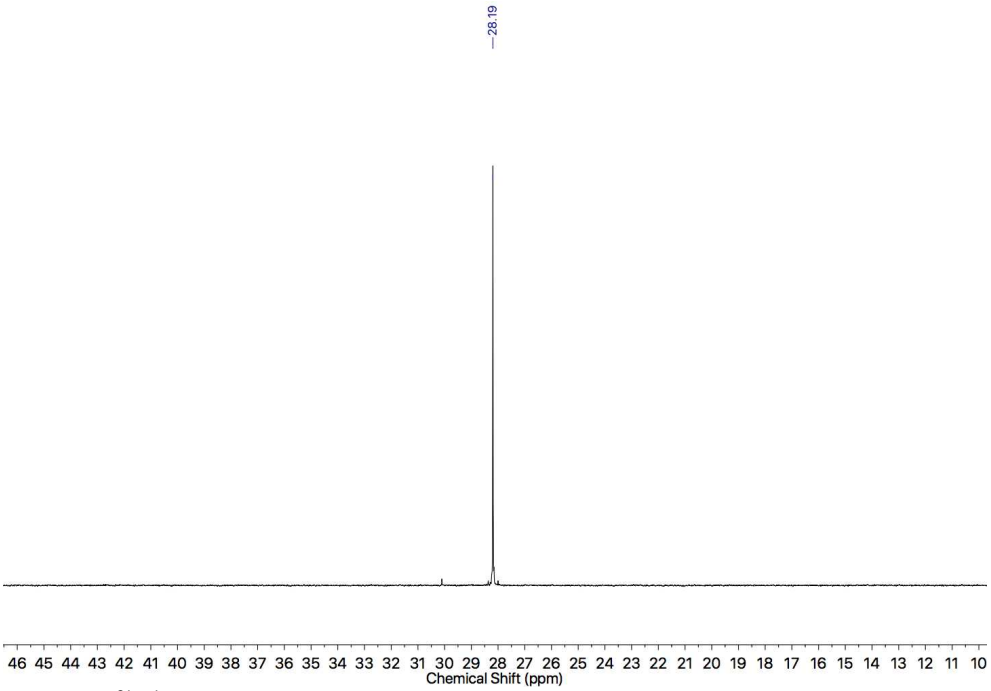

Figure 420: $^{31}P\{^1H\}$ NMR of (S_{mp})-**122** ($CDCl_3$, 202 MHz).

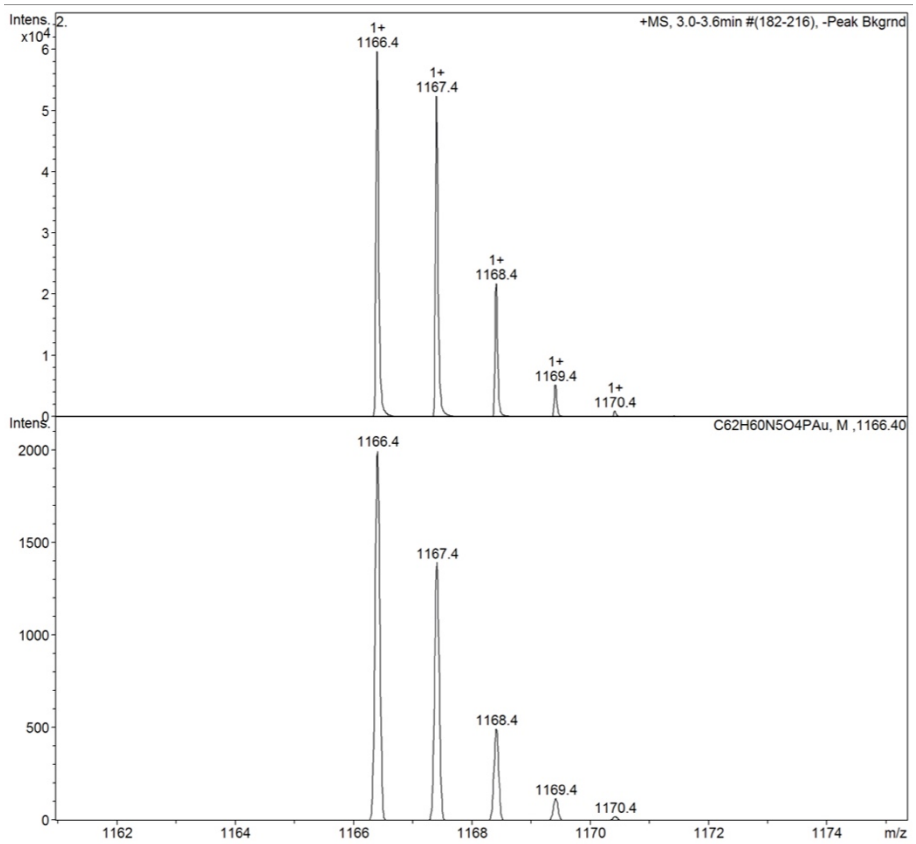

Figure 421: High resolution MS isotope pattern of (S_{mp})-**122** $[M\text{-}Cl]^+$ $C_{62}H_{60}N_5O_4PAu$.

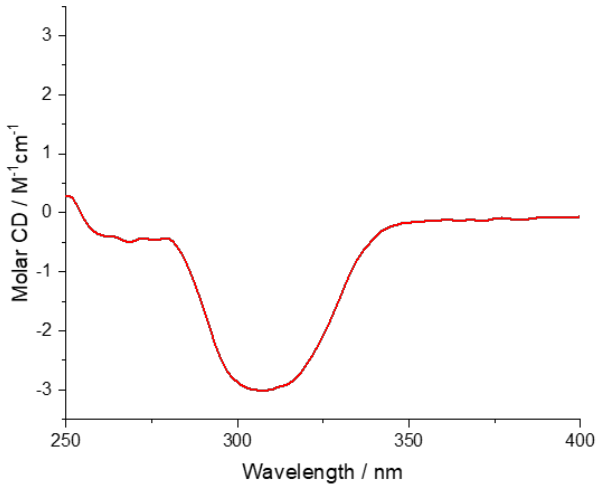

Figure 422: Circular Dichroism Spectra of (S_{mp})-**122** (17.0 μM, red) at 293 K in $CHCl_3$.

Reactions Catalysed by Rotaxane (S_{mp})-**122**

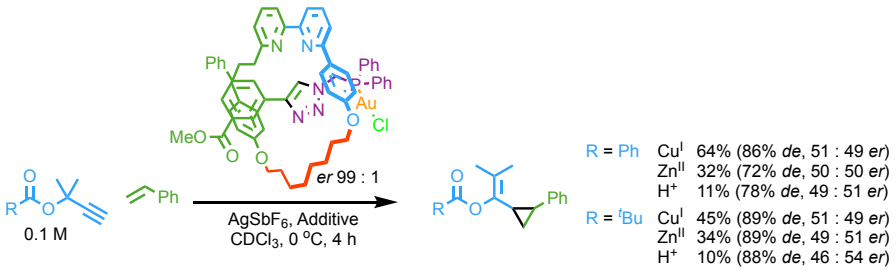

Cu^{I} refers to $[Cu(MeCN)_4]PF_6$. Zn^{II} refers to $Zn(OTf)_2$. H^+ refers to $TsOH.H_2O$.

A dry, foil covered, CEM MW vial was charged with $AgSbF_6$ (1.3 mg, 0.00369 mmol, 5 mol.%), and $[Cu(MeCN)_4]PF_6$ (1.4 mg, 0.00369 mmol, 5 mol.%), then purged with N_2 and cooled to 0 °C. (S_{mp})-**122** (4.4 mg, 0.00369 mmol, 5 mol.%) was added in $CDCl_3$ (200 µL), followed alkyne (0.0732 mmol, 1.0 eq.), and styrene (34 µL, 30.5 mg, 0.293 mmol, 4.0 eq.) in $CDCl_3$ (500 µL). The solution was stirred for 4 h at 0 °C. NMR yield and diastereoselectivity were determined by ^1H NMR against CH_2Cl_2 (20 µL). The reaction was filtered through Celite® and concentrated *in vacuo*. The residue was purified by column chromatography (SiO_2, petrol-Et_2O 0→5%). R = Ph. δ_H ($CDCl_3$, 400 MHz) 7.88 (2H, d, *J* = 7.5), 7.58 (1H, tt, *J* = 7.5, 1.5), 7.43 (2H, tt, *J* = 7.5, 1.0), 7.26 (2H, dd, *J* = 7.0, 6.5), 7.20 (1H, tt, *J* = 7.0, 1.5), 7.12 (2H, dd, *J* = 7.5, 1.5), 2.43-2.28 (2H, m), 1.65 (3H, s), 1.49 (3H, s), 1.29 (1H, ddd (td), *J* = 9.0, 5.5), 1.11 (1H, dt (ddd), *J* = 5.5, 5.5). δ_C (CDCl3, 101 MHz) 164.8, 139.5, 138.7, 133.2, 130.0, 129.9, 128.5, 127.8, 127.8, 125.7, 123.6, 23.9, 21.6, 18.8, 17.8, 11.9. HR-EI-MS m/z 292.1455 [$M^{+\cdot}$] (calc. m/z for $C_{20}H_{20}O_2$ 292.1458).[69] R = ^{t}Bu. δ_H ($CDCl_3$, 400 MHz) 7.21 (2H, tt, *J* = 7.5, 1.6), 7.14 (1H, tt, *J* = 7.4, 1.3), 7.03 (2H, dd, *J* = 7.5, 1.3), 2.28 (1H, d, *J* = 6.5), 2.26 (1H, d, *J* = 6.5), 1.48 (3H, s), 1.41 (3H, s), 1.26 (1H, m), 1.22 (9H, s), 1.00 (1H, dt, *J* = 6.0, 6.0). δ_C ($CDCl_3$, 101 MHz) 176.9, 139.6, 138.2, 127.6, 127.4, 125.6, 123.2, 39.0, 27.4, 24.1, 21.9, 18.7, 17.4, 11.9. HR-EI-MS m/z 272.1766 [$M^{+\cdot}$] (calc. m/z for $C_{18}H_{24}O_2$ 272.1771).[69]

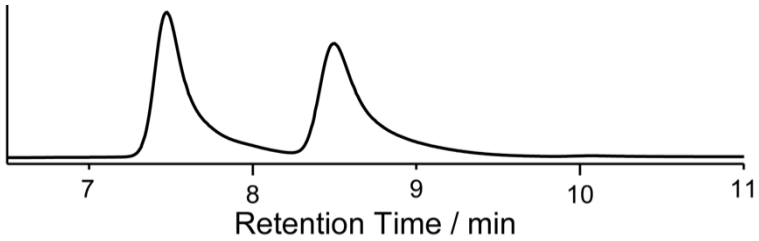

Figure 423: CSP-HPLC of *cis*-**9** (R = Ph, loaded in petrol). RegisPack, *n*-hexane-isopropanol 99 : 1, flowrate 0.75 $mLmin^{-1}$. (7.7 min, 35873, 50%), (9.0 min, 35054, 50%).

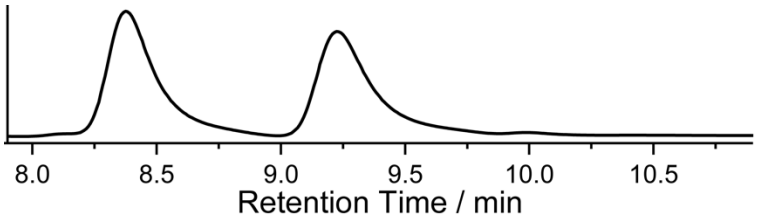

Figure 424: CSP-HPLC of *cis*-**9** (R = ^{t}Bu, loaded in petrol). RegisCell, *n*-hexane-isopropanol 99.5 : 0.5, flowrate 0.50 mLmin^{-1}. (8.4 min, 65249, 50%), (9.2 min, 61331, 50%).

Rotaxane (S_{mp})-**123**

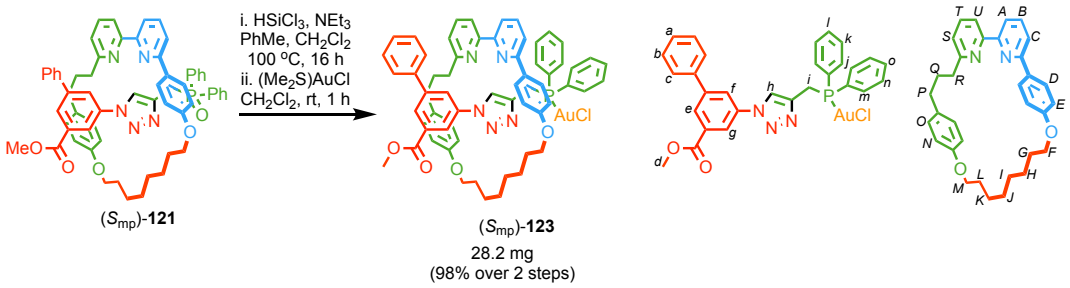

A Young's tap Schlenk tube was dried under vacuum and nitrogen three times. Anhydrous NEt_3 (166 µL, 121 mg, 1.19 mmol, 50 eq.) and $HSiCl_3$ (60 µL, 81 mg, 0.596 mmol, 25 eq.) were added. Subsequently (S_{mp})-**121** (23.5 mg, 0.0238 mmol, 1.0 eq.) was transferred in anhydrous PhMe (1.0 mL) and anhydrous CH_2Cl_2 (0.3 mL). The solution was heated at 100 °C for 18 h. The reaction was cooled to room temperature, diluted in CH_2Cl_2 (20 mL) and washed with NaOH (1 M, 5 x 20 mL). The combined organic layers were dried over $MgSO_4$ and concentrated *in vacuo* yielding a yellow oil. This was dissolved in anhydrous CH_2Cl_2 (0.6 mL) and stirred with (Me_2S)AuCl (7.7 mg, 0.0262, 1.1 eq.) for 1 h. The crude reaction was concentrated directly onto SiO_2 and purified by column chromatography (SiO_2, petrol-EtOAc 20→80%) yielding a white foam (S_{mp})-**123** (28.2 mg, 0.0234 mmol, 98%, *er* 99 : 1). δ_H ($CDCl_3$, 400 MHz) 10.4 (1H, d, J = 2.5, H_h), 8.23 (1H, dd, J = 1.9, 1.5, H_e), 8.18 (1H, t, J = 1.5, H_g), 8.12 (1H, t, J = 1.9, H_f), 7.90 (1H, t, J = 7.7, H_T), 7.76 (1H, dd, J = 7.8, 0.8, H_S), 7.70 (1H, t, J = 7.8, H_B), 7.62-7.54 (6H, m, H_A, H_a, H_j, H_m), 7.49-7.44 (1H, m, H_l), 7.39-7.34 (4H, m, H_n, H_b), 7.30-7.25 (4H, m, H_C, H_U, H_c), 7.23-7.19 (1H, m, H_o), 7.15-7.09 (2H, m, H_k), 6.61 (2H, dt, J = 8.7, 2.4, H_D), 6.36 (2H, d, J = 8.7, 2.5, H_E), 6.26 (2H, d, J = 8.6, H_O), 6.13 (2H, d, J = 8.6, 2.5, H_N), 4.25-4.18 (1H, m, H_F), 4.07-3.99 (2H, m, $H_{F'}$, H_M), 3.86-3.79 (1H, m, $H_{M'}$), 3.77 (3H, s, H_d), 3.68 (1H, dd, J = 14.9, 11.7, H_i), 3.49 (1H, dd, J = 15.0, 10.3, $H_{i'}$), 2.47-2.39 (2H, m, H_R), 2.36-2.31 (1H, m, H_P), 2.27-2.19 (1H, m, $H_{P'}$), 1.95-1.49 (10H, H_G, H_H, H_K, H_L, H_Q), 0.90-0.77 (4H, m, H_I, H_J). δ_C ($CDCl_3$, 101 MHz) 165.70, 163.30, 160.08, 158.73, 157.61, 157.16, 157.02,

142.01, 139.5 (d, J_{CP} = 3.2), 137.97, 137.91, 137.47, 135.83, 133.4 (d, J_{CP} = 14.1), 133.0 (d, J_{CP} = 13.7), 132.6 (d, J_{CP} = 2.4), 132.5 (d, J_{CP} = 2.4), 131.70, 131.34, 130.59, 129.9 (d, J_{CP} = 6.5), 129.7 (d, J_{CP} = 6.6), 128.90, 128.58, 128.39, 128.13, 127.8, 127.61, 127.3, 126.80, 126.7, 122.99, 122.52, 120.15, 120.07, 119.97, 119.60, 114.33, 113.72, 68.19, 66.86, 52.39, 37.16, 34.60, 33.30, 29.84, 29.58, 29.06, 28.85, 26.8 (d, J_{CP} = 35.8), 26.21, 25.97. δ_P ($CDCl_3$, 202 MHz) 30.8. HR-ESI-MS $[M\text{-}Cl]^+$ m/z 1166.4 (calc. for $C_{62}H_{60}O_4N_5PAu$ m/z 1166.4).

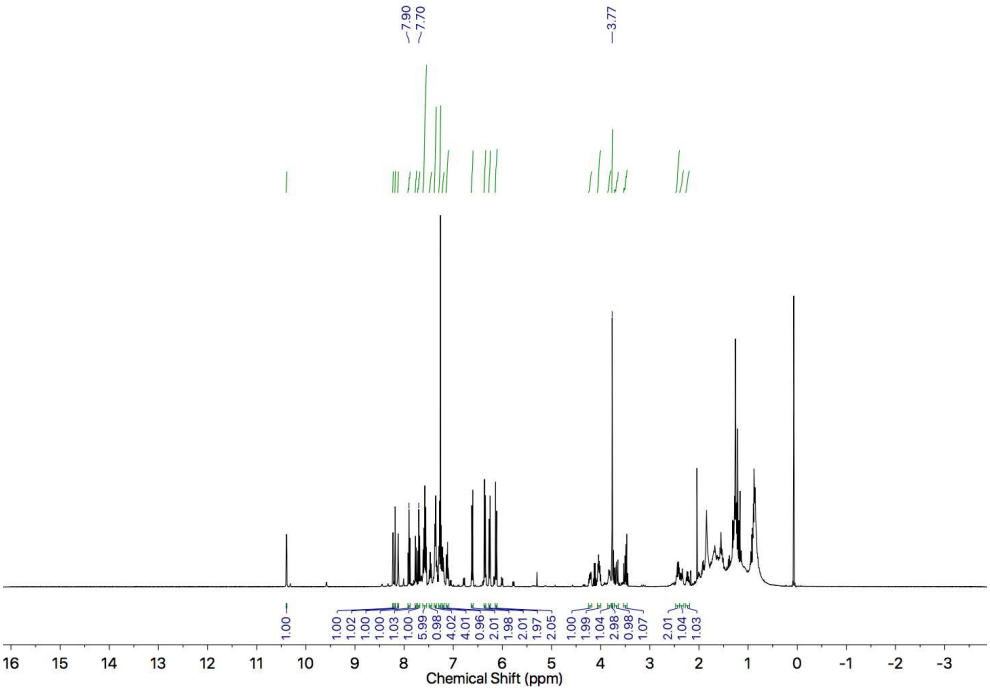

Figure 425: ^1H NMR of (S_{mp})-**123** ($CDCl_3$, 400 MHz).

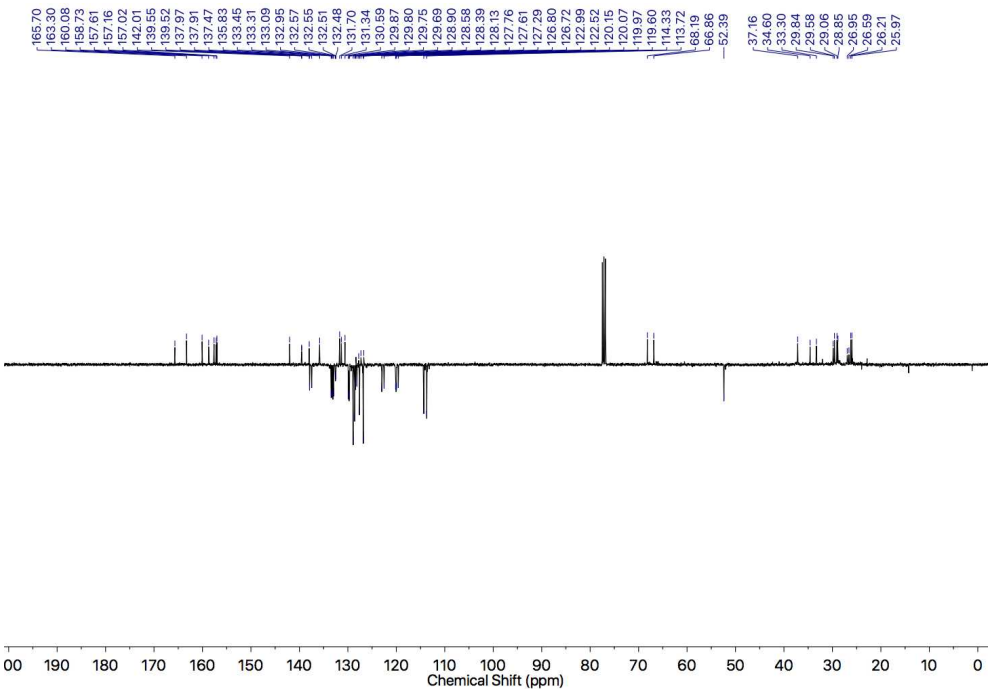

Figure 426: JMOD NMR of (S_{mp})-**123** ($CDCl_3$, 101 MHz).

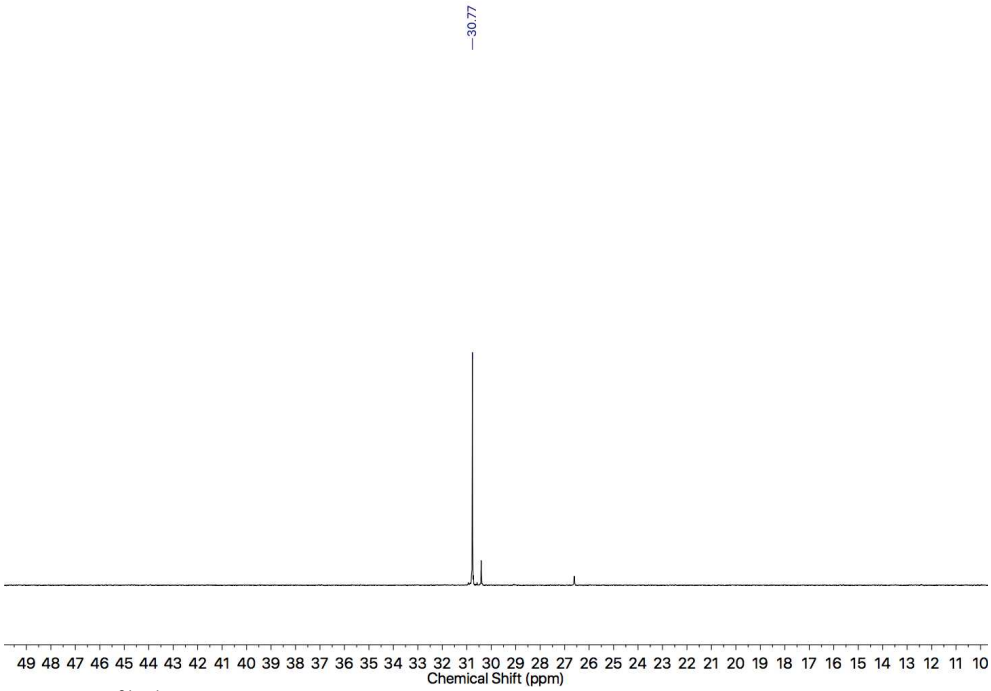

Figure 427: $^{31}P\{^1H\}$ NMR of (S_{mp})-**123** ($CDCl_3$, 202 MHz).

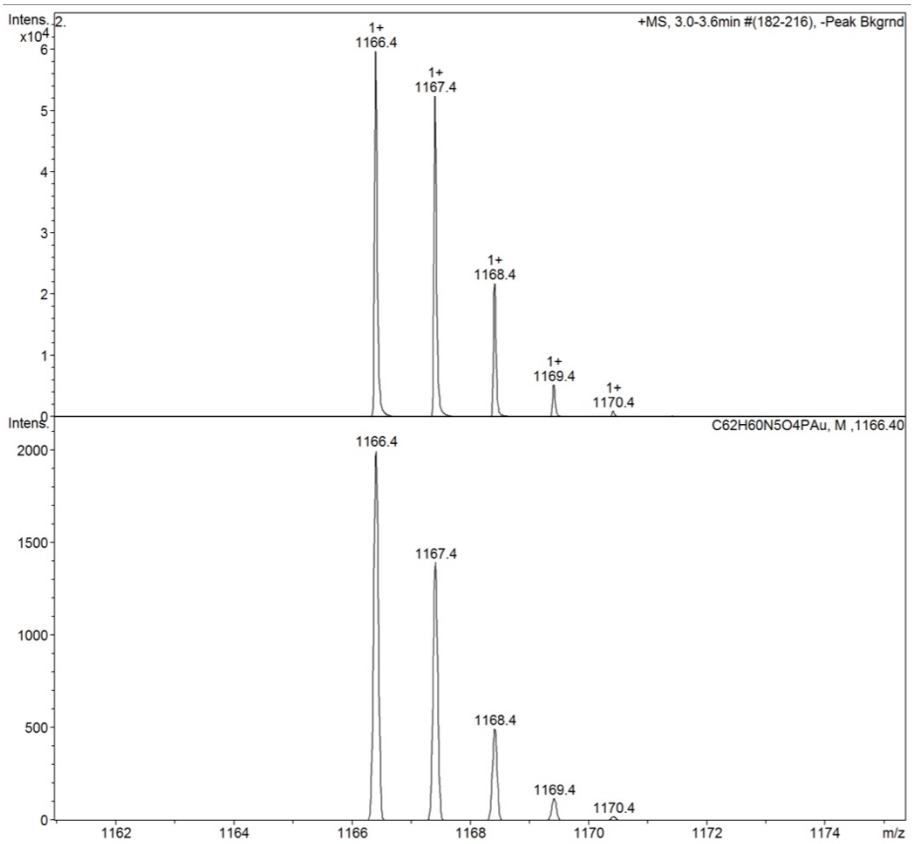

Figure 428: High resolution MS isotope pattern of (S_{mp})-**123** $[M\text{-}Cl]^+$ $C_{62}H_{60}N_5O_4PAu$.

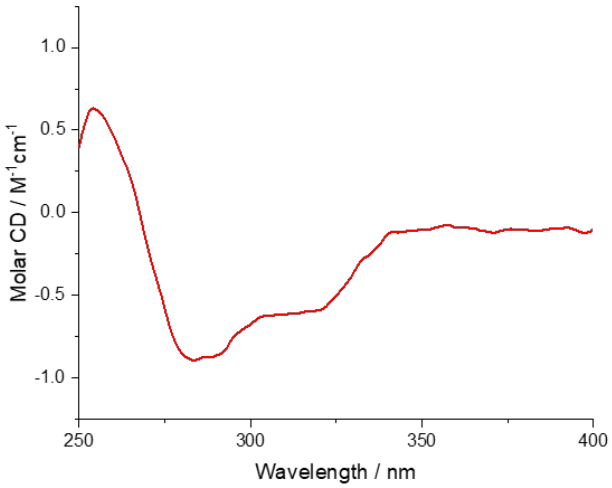

Figure 429: Circular Dichroism Spectra of (S_{mp})-**123** (21.3 µM, red) at 293 K in $CHCl_3$.

Reactions Catalysed by Rotaxane (S_{mp})-**123**

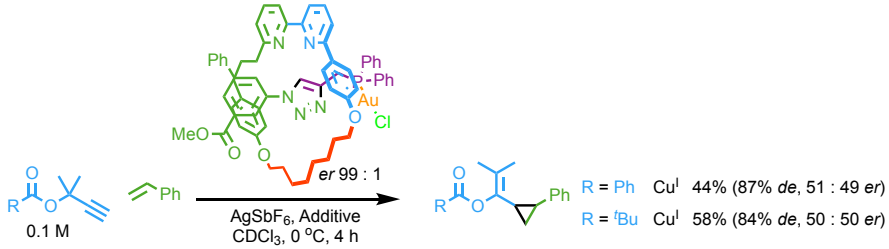

Cu^{I} refers to $[Cu(MeCN)_4]PF_6$.

A dry, foil covered, CEM MW vial was charged with $AgSbF_6$ (1.4 mg, 0.00397 mmol, 5 mol.%), and $[Cu(MeCN)_4]PF_6$ (1.5 mg, 0.00397 mmol, 5 mol.%), then purged with N_2 and cooled to 0 °C. (S_{mp})-**129** (4.8 mg, 0.00397 mmol, 5 mol.%) was added in $CDCl_3$ (200 µL), followed alkyne (0.0795 mmol, 1.0 eq.), and styrene (36 µL, 33.1 mg, 0.318 mmol, 4.0 eq.) in $CDCl_3$ (600 µL). The solution was stirred for 4 h at 0 °C. NMR yield and diastereoselectivity were determined by ^{1}H NMR against CH_2Cl_2 (20 µL). The reaction was filtered through Celite® and concentrated *in vacuo*. The residue was purified by column chromatography (SiO_2, petrol-Et_2O 0→5%). R = Ph. δ_H ($CDCl_3$, 400 MHz) 7.88 (2H, d, *J* = 7.5), 7.58 (1H, tt, *J* = 7.5, 1.5), 7.43 (2H, tt, *J* = 7.5, 1.0), 7.26 (2H, dd, *J* = 7.0, 6.5), 7.20 (1H, tt, *J* = 7.0, 1.5), 7.12 (2H, dd, *J* = 7.5, 1.5), 2.43-2.28 (2H, m), 1.65 (3H, s), 1.49 (3H, s), 1.29 (1H, ddd (td), *J* = 9.0, 5.5), 1.11 (1H, dt (ddd), *J* = 5.5, 5.5). δ_C (CDCl3, 101 MHz) 164.8, 139.5, 138.7, 133.2, 130.0, 129.9, 128.5, 127.8, 127.8, 125.7, 123.6, 23.9, 21.6, 18.8, 17.8, 11.9. HR-EI-MS m/z 292.1455 [$M^{+\cdot}$] (calc. m/z for $C_{20}H_{20}O_2$ 292.1458).[69] R = ^{t}Bu. δ_H ($CDCl_3$, 400 MHz) 7.21 (2H, tt, *J* = 7.5, 1.6), 7.14 (1H, tt, *J* = 7.4, 1.3), 7.03 (2H, dd, *J* = 7.5, 1.3), 2.28 (1H, d, *J* = 6.5), 2.26 (1H, d, *J* = 6.5), 1.48 (3H, s), 1.41 (3H, s), 1.26 (1H, m), 1.22 (9H, s), 1.00 (1H, dt, *J* = 6.0, 6.0). δ_C ($CDCl_3$, 101 MHz) 176.9, 139.6, 138.2, 127.6, 127.4, 125.6, 123.2, 39.0, 27.4, 24.1, 21.9, 18.7, 17.4, 11.9. HR-EI-MS m/z 272.1766 [$M^{+\cdot}$] (calc. m/z for $C_{18}H_{24}O_2$ 272.1771).[69]

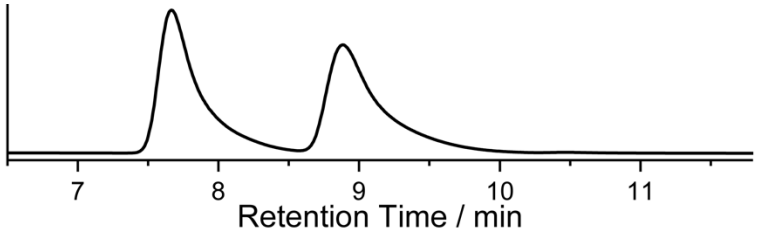

Figure 430: CSP-HPLC of *cis*-**9** (R = Ph, loaded in petrol). RegisPack, *n*-hexane-isopropanol 99 : 1, flowrate 0.75 $mLmin^{-1}$. (7.7 min, 10789922, 50.8%), (8.9 min, 10432050, 49.2%).

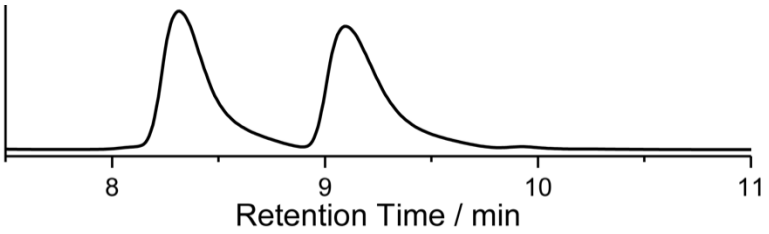

Figure 431: CSP-HPLC of *cis*-**9** (R = ^{t}Bu, loaded in petrol). RegisCell, *n*-hexane-isopropanol 99.5 : 0.5, flowrate 0.50 mLmin^{-1}. (8.3 min, 15689906, 49.8%), (9.1 min, 15788893, 50.2%).